LT+F

74:002

TASK I FINAL REPORT

DESIGN STUDIES OF STEAM GENERATORS FOR MOLTEN SALT REACTORS

REPORT ND/74/66

FWC CONTRACT 8-25-2431

UCC PURCHASE ORDER SUBCONTRACT NO. 91X-88070C

FOSTER WHEELER CORPORATION

NUCLEAR DEPARTMENT

110 South Orange Avenue, Livingston, New Jersey

Best Copy Available

Page 6-92 Missing

CHARGE NO.	DOCUMENT NO.	ISSUE	DATE

TASK I FINAL REPORT

DESIGN STUDIES OF STEAM GENERATORS FOR MOLTEN SALT REACTORS

REPORT ND/74/66

FWC CONTRACT [illegible]

UCC PURCHASE ORDER SUBCONTRACT NO. 91X-88070C

Approved by:

J. F. Cox
Project Manager

W. Wolowodiuk
Program Manager

D. H. Pai
Chief Engineer

FOSTER WHEELER ENERGY CORPORATION
EQUIPMENT DIVISION-NUCLEAR DEPARTMENT
110 SOUTH ORANGE AVENUE
LIVINGSTON, NEW JERSEY 07039

CHARGE NO. 8-25-2431	DOCUMENT NO. ND/74/66	ISSUE 1	DATE 12/16/74

DISTRIBUTION LIST

Union Carbide Corporation

J. L. Crowley (30)

Foster Wheeler Energy Corporation

R. O. Barratt
to J. K. O'Donoghue
to Nuclear Files (Retain)

W. Wolowodiuk
to J. F. Cox (Retain)

D. H. Pai
to C. Nash
to H. Levy (Retain)

S. M. Cho
to H. L. Chou (Retain)

J. Anelli
to C. Holderith (Retain)

W. R. Apblett (2)
to E. D. Montrone (Retain)
to G. V. Amoruso (Retain)

M. J. Kraje
to J. G. Whelley (Retain)

"LEGAL NOTICE"

"This Report was prepared as an account of Government sponsored work. Neither the United States, nor the Commission, nor any person acting on behalf of the Commission:

(a) makes any warranty or representation, express or implied, with respect to the accuracy, completeness or usefulness of the information contained in this report, or that the use of any information apparatus, method or process disclosed in this report may not infringe privately owned rights; or

(b) assumes any liabilities with respect to the use of, or for damages resulting from the use of any information apparatus method, or process disclosed in this report.

"As used in the above, 'person acting on behalf of the Commission' includes any employee or Contractor of the Commission or employee or Subcontractor of such Contractor to the extent that such employee or Contractor of the Commission or employee or Subcontractor of such Contractor prepares, disseminates, or provides access to, any information pursuant to his employment or contract with the Commission or his employment or subcontract with such Contractor."

CHARGE NO. 8-25-2431	DOCUMENT NO. ND/74/66	ISSUE 1	DATE 12/16/74

NOTATIONS IN THIS COLUMN INDICATE WHERE CHANGES HAVE BEEN MADE

FWC FORM 17? - 4

1.0 ABSTRACT

This Task I Final Report of Design Studies of Steam Generators for Molten Salt Reactors presents the work done by Foster Wheeler in accordance with Task I of the Work Plan Detail by Foster Wheeler for Design Studies of Steam Generators for Molten Salt Reactors under Purchase Order Subcontract No. 91X-88070C during the period October 1971 through December 1974. The effort was conducted under two different Foster Wheeler contract numbers due to a termination for the convenience of the government on January 31, 1973. FWC Contract No. 2-25-1352 covered the work performed from October 7, 1971 through January 31, 1973. FWC Contract No. 8-25-2431 covered the work performed from May 17, 1974 through December 31, 1974.

The Foster Wheeler design concept presented in this report is an "L" shaped tube and shell heat exchanger to be used in a steam generator system consisting of four units for a 1000 MW(e) Molten Salt Breader Reactor power plant.

The design utilizes an all welded construction with 100% radiography of all pressure boundry welds. The pressure shell is designed to minimize the annulus between itself and the tube bundle. Where the shell must be of a larger diameter a flow shroud is used to maintain the flow over the bundle. Suitable water, steam and molten salt inlet and outlet nozzles are provided. The mechanical design provisions for the steam generator are covered in Section 3.0.

The design work is supported by thermal/hydraulic and structural analysis as reported herein. The thermal/hydraulic analysis described in Section 4.0 demonstrates that the present unit size is sufficient for the intended service with minimal possibility of the molten salt solidifying on the cold end tubesheet or tubes.

Structural analysis of the proposed design has been conducted and is reported in Section 5.0. An elastic analysis on major components was conducted. Also, simplified inelastic analysis was conducted on the salt inlet nozzle, the outlet tubesheet, the shell and the tubes. Based upon the stress analysis conducted, the design is satisfactory.

Outline versions of a possible manufacturing and inspection plan and maintenance procedures were prepared and may be found in Section 7.0.

References are provided as applicable and supporting calculations are provided in the Appendices.

2.0 INTRODUCTION AND CONCEPT ARRANGEMENT STUDY

2.1 INTRODUCTION

This Task I Final Report presents the work done by Foster Wheeler during the period from October 7, 1971 to December 31, 1974 on Design Studies of Steam Generators for Molten Salt Reactors. This work was performed in two segments due to a termination for the convenience of the government on January 31, 1973. The first segment ran from October 7, 1971 to January 31, 1973. The second segment was begun on May 17, 1974 and ends with this report. This second segment limited the work scope to the completion of Task I.

This document is submitted in compliance with the requirements of Article I - Statement of Work of Purchase Order Subcontract No. 91X-88-70C dated October 7, 1971 as ammended by Supplemental Agreement No. 3 dated May 17, 1974. This Statement of Work is further defined in the Work Plan Detail by Foster Wheeler for Design Studies of Steam Generators for Molten Salt Reactors dated October 7, 1971 and attached to the Subcontract. All codes and standards applicable to this effort have been established by mutual agreement under Sub-Task I of Task I of the work plan defined above.

Portions of the information contained herein have been submitted to Union Carbide in progress reports 1 through 12 which were submitted as required under the subcontract.

2.2 CONCEPT ARRANGEMENT STUDY

A concept arrangement study was performed to arrive at a design concept that offered the most promise. The starting point for this study was to establish the design requirements and criteria through consulting with Union Carbide and then to evaluate posible surface arrangements that might meet these requirements and criteria. For clarity and completeness, the design requirements and criteria established for Task I are presented below.

DESIGN REQUIREMENTS AND CRITERIA

1. The inlet and outlet salt temperatures, the maximum pressure drops, and the total heat transfer capacity of the steam generators must conform with the overall system operating conditions.

a) Full load operating conditions (one of four coolant salt loops - thermal duty = 483 MW):

	Coolant Salt	Water/Steam
Inlet temperature, F	1150	700
Outlet temperature, F	850	1000
Flow rate, Lb/hr	15,280,000	2,517,000
Inlet pressure, psia	235	3800
Outlet pressure, psia	175	3600
Maximum pressure drop, psi	60	200

The design temperatures and pressures are left to the discretion of the designer.

More than one module per coolant salt loop is permissable. If modules are used in parallel, they will share the coolant salt loop duty and flows equally. The maximum water/steam side pressure drop of 200 psi may be relaxed if found to be unnecessarily restrictive.

b) Part load operating range at constant steam generator outlet pressure is defined as any condition between 20 and 100% of full load thermal duty. In this load range the coolant salt flow will be varied linearly from 30% flow at 20% load to 100% flow at 100% load. The feedwater inlet temperature will be maintained constant at 700 F over this load range while the water/steam flow will be varied in proportion to load. The turbine inlet steam temperature must be maintained at 1000 F ± 15 over this load range. If an attemperator is required to maintain the turbine inlet temperature, then the attemperator design becomes a part of the steam generator design.

c) Startup operation of the MSBR power system is defined as zero to 20% of full load. However, the primary fuel salt requires that initial zero power operation must begin with both the fuel and coolant salt systems circulating isothermally at 1050 F.

d) The steam generator must be able to operate at all loads with tolerable thermal stresses and without freezing the coolant salt. Alternately, operation with a frozen salt film may be permissible if desirable and if operation can be shown to be stable.

2. The type of steam generator, the general location of nozzles, the height of the unit, and the minimum tube diameter must be compatible with various design, layout, fabrication, maintenance and inspection considerations.

a) The steam generator shall be a once-through, shell and tube heat exchanger with the coolant salt on the shell side and the water/steam in the tubes.

b) For purposes of the steam generator design, the coolant salt system is assumed to have forced circulation during all expected operation. Natural circulation on the shell side, although a desirable feature, is not a design requirement. The tube side may have forced or natural circulation under decay heat removal conditions.

c) There is no height limit on the steam generator.

d) As a guideline, a minimum tube ID of not less than 0.375 inches shall be used.

e) There are no physical layout limitations.

f) The shell side of the steam generator shall be completely drainable.

g) A tube plugging allowance of 5% but not exceeding 25 tubes shall be used for preliminary sizing purposes.

h) Heat transfer surface may be arranged for vertically up or down tube side flow.

3. The steam generator should be arranged for relatively easy tube bundle replacement or modular replacement. Both seal-welded flanges and cut and weld removal techniques shall be considered for easy tube bundle replacement.

4. The space requirements for the installation of the steam generator should be as small as practical commensurate with economic considerations. It will be necessary to have some data for incremental building and excavation costs.

5. The volumes of both the salt and water/steam in the unit should be kept as low as practical.

6. The use of cover gases to protect structural members should be avoided.

7. The following items shall be considered and accomodated in the design of the steam generator:

   a. Baffle and tube supports, as necessary, to prevent damaging vibration.

   b. Relative expansion between the shell and tube bundle and between individual tubes.

   c. Tube side flow stability under all load conditions.

   d. Protection of nozzles and tubesheets against excessive thermal stress due to transients.

   e. Fabricability of the design including the ability to radiograph all containment welds.

   f. Relief of the salt-steam mixture resulting from a double-ended steam generator tube failure to limit damage to the steam generator. The remainder of the coolant salt system can withstand a continuous pressure of 220 psi without damage.

8. The steam generator shall be designed as a Class 1 vessel in accordance with the applicable portions of Section III of the 1971 ASME Boiler and Pressure Vessel Code with addenda and the other design standards listed in the corrected Appendixes A and D of the Company's RFP, Enclosure 2. The design shall include the Code consideration for operation in excess of 800 F over a 30 year design life at 80% plant factor.

9. The design of all portions of the steam generator in contact with the salt shall be based on Hastelloy N material. The physical properties of this Hastelloy N are listed in the corrected Appendix C of the Comapny's RFP, Enclosure 2.

10. The steam properties on which the steam generator design is based shall be obtained from the 1967 ASME Steam Tables.

11. The steam generator design shall be based on sodium fluoroborate as the coolant salt. The physical properties of sodium fluoroborate are listed in the corrected Appendix B of the Company's RFP, Enclosure 2. The substitution of a different salt with a higher temperature melting point may be the subject of a later study,

12. A corrosion allowance of ½ mill/year on the salt side and ¼ mill/year on the steam side shall be used in selecting material thickness.

13. It will be permissible to divide the steam generator into two subunits in series if the design study indicates an advantage.

14. The design of the steam generator shall be based on a 30 year plant life with the steam generator experiencing 10,000 cycles of 20% or more in power over its life. Normally the load will be changed at a maximum rate of 4%/min. The details of number or reactor scrams etc. and the resulting temperature ramps will be made available.

As an additional requirement not presented above, it was felt that the use of bellows in the shell of the steam generator to accomodate differential thermal expansions was to be avoided.

Within the restrictions set forth above, a large number of surface arrangements were possible. Therefore, a second set of seven basic design areas were setup. These seven areas are, in order of importance:

1. Adequate thermal expansion provision - does this design have sufficient tube flexibility to allow for large temperature difference between tubes and shell or between adjacent tubes?

2. Stratification Problems - are there possible areas within the unit where predicting flow will be difficult?

3. Good Utilization of Volume - does the design allow for all the tubing to be used as active heat transfer surface?

4. Better Mechanical Arrangement - do the mechanical details appear to be difficult?

5. Equal Active Circuit Length - will the tubes have approximately equal heated lengths?

6. Tube Side Inspection - can the tubes be easily nondistructively examined after the unit has been in service?

7. Relative Complexity - do the uncertainties of the design appear to lend themselves to straight forward solutions?

Page 2-7 shows the various possible surface arrangement candidates and how they evaluated against the seven basic design areas. On the chart, no line indicates that the candidate did not affirmatively pass that design area. A solid line indicates that the candidate does pass that design area. A dash line indicates that the candidate may be able to pass that design area with difficulty. When a candidate did not pass a basic design area (no line), it was dropped from further consideration.

The above describe evaluation reduced the possible number of candidates to 7. These seven candidates and some of their more difficult detailed problems are given in on Page 2-8. As Page 2-8 shows the principle problems relate to the fabrication of the U-bend or Elbow shell. Pages 2-9 through 2-12 further outline the fabrication problems of the U-bend shell and the elbow shell.

As can be seen from the foregoing discussion it became apparent that an elbow unit showed the most promise in meeting the design requirements and criteria with the least amount of problems. Thus the elbow unit was selected as the reference design.

MOLTEN SALT STEAMGENERATOR SURFACE ARRANGEMENT

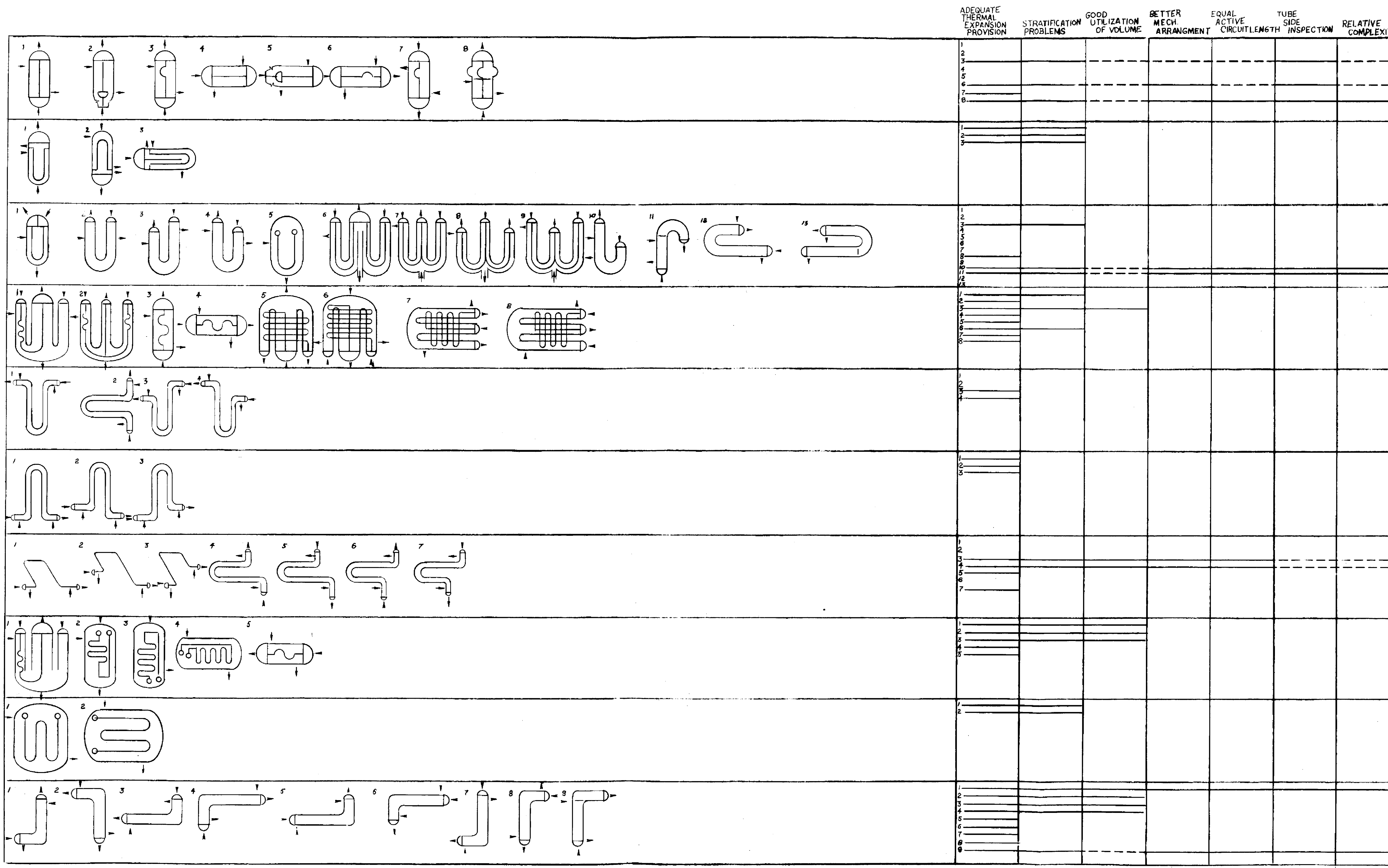

DETAILED PROBLEM AREAS

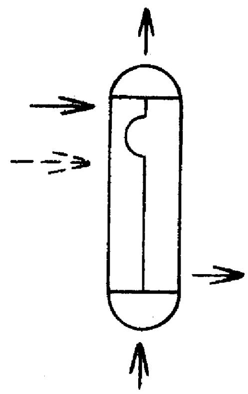

1) The sine wave expansion bend will be excessively large.
2) Complicated tube supports/vibration problems or the introduction of a large ineffective volume.

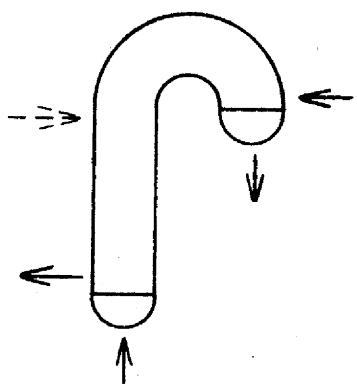

1) The fabrication of the U-bend is very difficult.
2) Complicated tube supports/vibration problems or the introduction of a large ineffective volume.

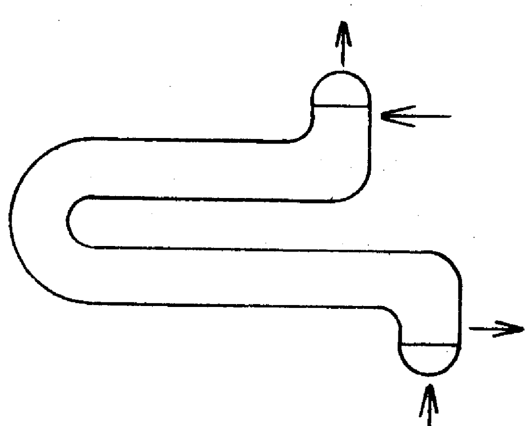

1) The fabrication of the U-bend is twice as difficult as the J tube unit.
2) There is no reasonable way of avoiding the U-bend, vibration, built-up support problems.

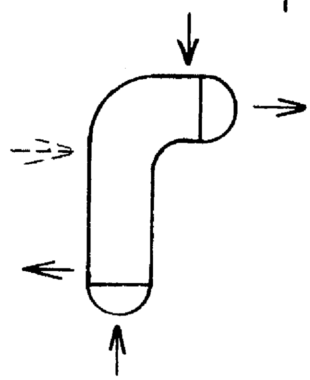

1) The fabrication is simplified compared with the other candidates but is still difficult.

U-BEND SHELL FABRICATION

1. Long shells are longitudinally split members.

2. Long seam welding performed in situ.

3. Weld distortion will cause the shells to go out of round.

4. Subsequent re-preparation of circle seam welds requires special development.

5. Clam shell members for the U-bend will be positioned and the long seam welded in situ. Circle seam welds will require re-preparation using similar special equipment.

6. Final closure at each tubesheet will be done by the addition of transition pieces which are custom machined and include hand holes for completion of NDT procedures and repair if necessary.

7. These problems are somewhat simplified when a small shell diameter are considered.

BY

APPROVED

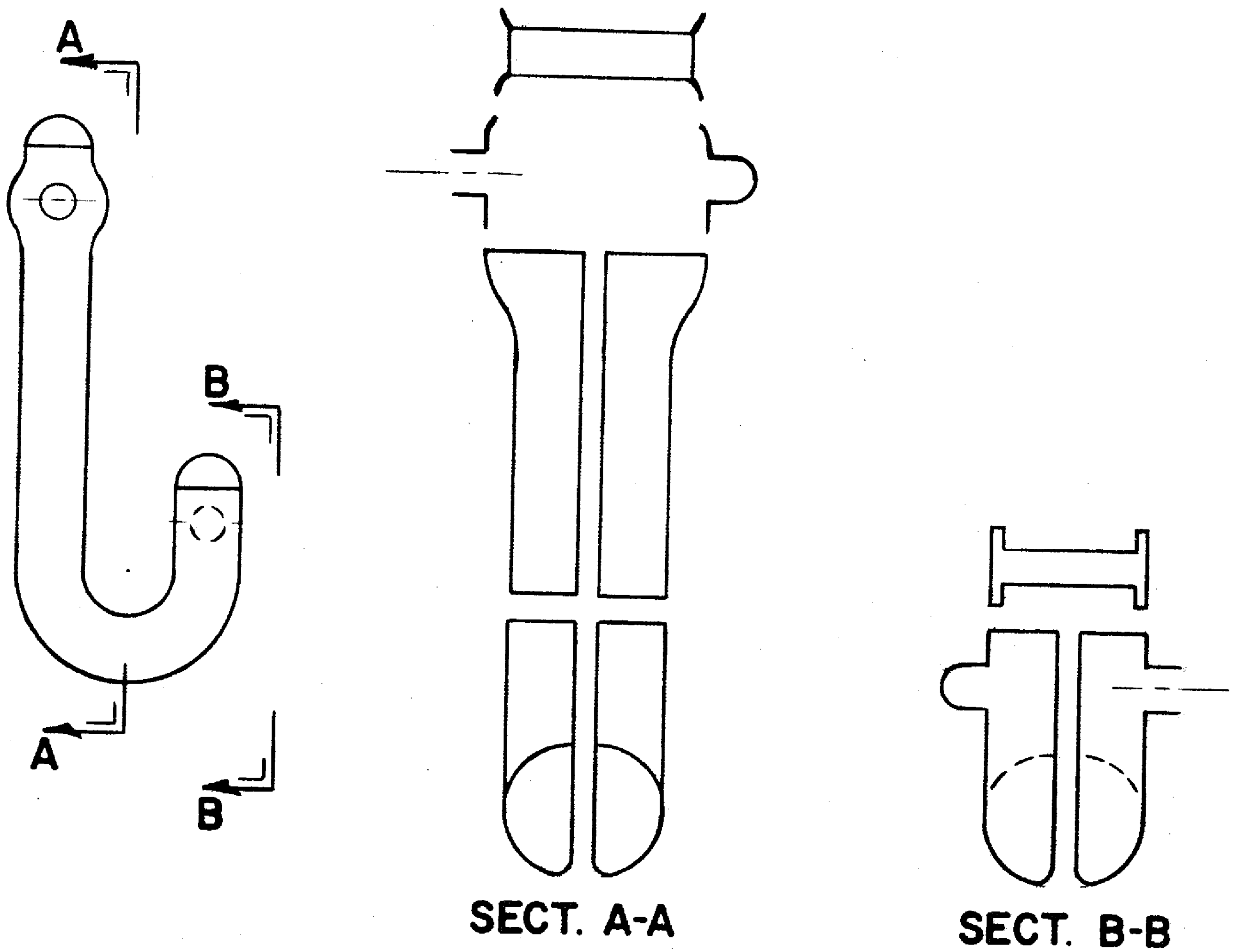

U-SHELL ASSEMBLY

CHARGE NO. 8-25-2431
DOCUMENT NO. ND/74/66
ISSUE 1
DATE 12/16/74

NUCLEAR DEPARTMENT
FOSTER WHEELER ENERGY CORPORATION
LIVINGSTON, N. J.

ELBOW SHELL FABRICATION

1. The fabrication process utilizes shell sections without recourse to clam shells, thereby avoiding the problems of making and inspecting long seam welds in situ.

2. The problems associated with supporting the tubes in the bend area is not considered any more difficult than in the case of the U-bend shell.

3. The installation of the tube bundle will require threading of the tubes through the shell after the supports have been installed.

FWC FORM 172 - 4

NOTATIONS IN THIS COLUMN INDICATE WHERE CHANGES HAVE BEEN MADE

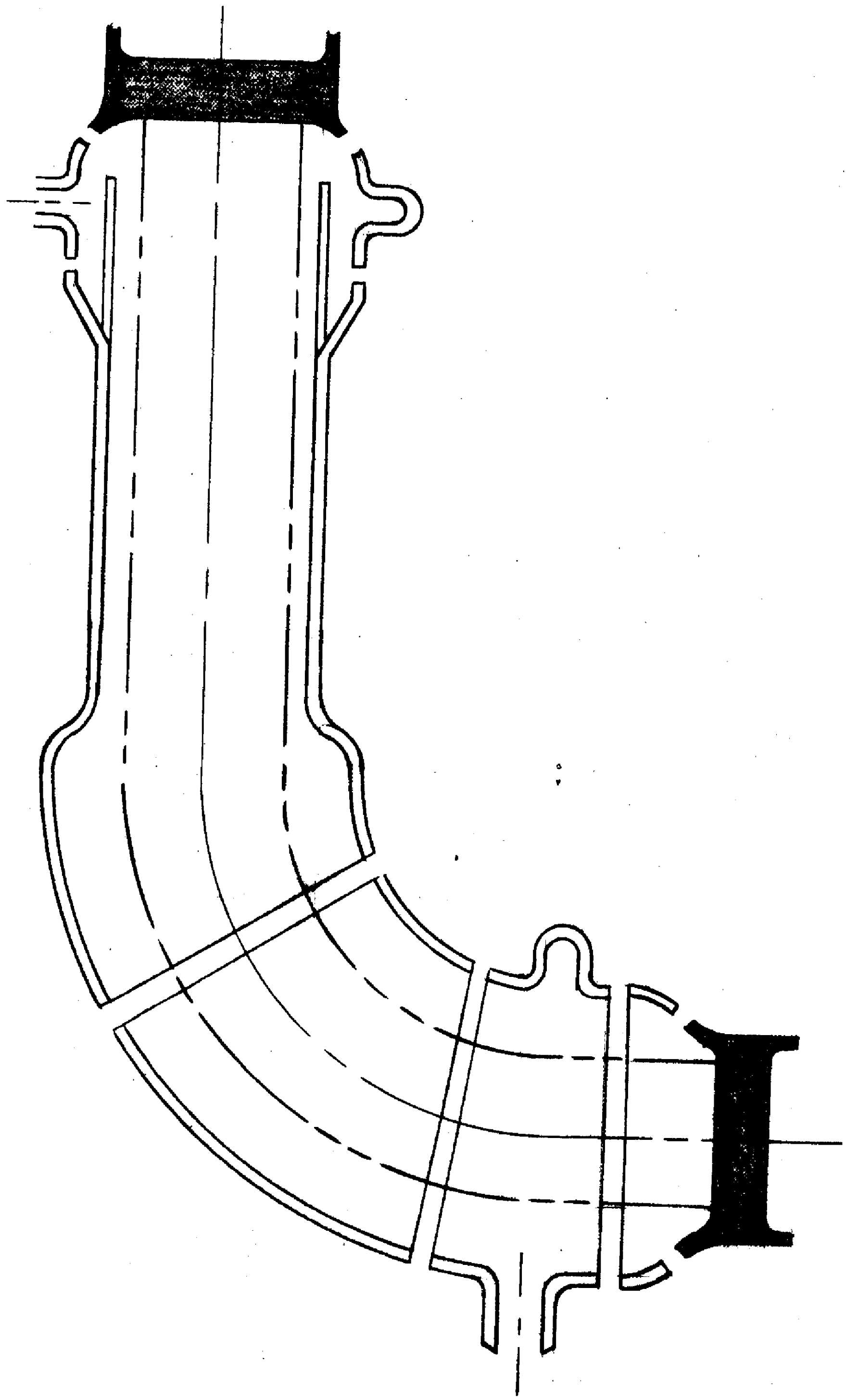

ELBOW SHELL ASSEMBLY

CHARGE NO 8-25-2431	DOCUMENT NO. ND-74-66	ISSUE 1	DATE 12/16/74

SECTION 3.0

MECHANICAL DESIGN REPORT

PRELIMINARY DESIGN

by

Charles H. Holderith

Approved By:

J. Anelli
Supervisor, Mechanical Design

FWC FORM 172 - 4

NOTATIONS IN THIS COLUMN INDICATE WHERE CHANGES HAVE BEEN MADE

TABLE OF CONTENTS

LIST OF FIGURES

3.0 Molten Salt Steam Generator Preliminary Design

3.1 Design Description Summary

The Foster Wheeler Steam Generator is a "L" shaped fixed tubesheet heat exchanger as shown in Figure 3.1. The steam generator design is based on a system of four units per loop. The steam generator has 1014 tubes which are attached at each end to a fixed tubesheet.

The steam generator design is such that the flow of molten salt and super critical fluid through the unit is in the direction of natural circulation. Molten salt enters through an inlet nozzle (Figure 3.4), which is perpendicular to the tube bundle, changes direction 90° and decends approximately 100 feet before exiting through an outlet nozzle (Figure 3.4). Supercritical fluid enters through an inlet nozzle located in the center of the lower head (Figure 3.2) and rises through the heat transfer tubes and exits through an outlet nozzle in the center of the upper head. Vent nozzles are positioned at each tubesheet to shell juncture to prevent the possibility of trapped gases resulting in localized hot spots on the shell (Figures 3.1 and 3.2).

3.2 Molten Salt Steam Generator Design Conditions

A.S.M.E. Section III Class I Pressure Vessel*

Primary Side (Shell)

Design Temperature	1150°F
Design Pressure	300 P.S.I.G.
Joint Efficiency	100%
Allowable Stress	9500 PSI (Primary Membrane)
Shell Material	Hastelloy-"N"
Shell Inside Diameter	39½"

Secondary Side (Tube)

Design Temperature	1120°F
Design Pressure	3800 P.S.I.A.
Joint Efficiency	100%
Allowable Stress	11,600 PSI (Primary Membrane)
Number of Tubes	1014
Tube Pitch	1-1/8" Triangular
Tube Size	3/4" O.D. x .125 min. wall
Effective Length	140 ft.
Tube Material	Hastelloy-"N"
Number of Tie Rods	13

* Designed to A.S.M.E. Section III Class I with Addenda thru Winter, 1973

3.3 Steam Generator Arrangement

The steam generator shown in Figure 3.1 consists of:

1. Upper Shell Assembly
2. Middle Shell Assembly
3. Lower Shell Assembly
4. Bundle Assembly
5. Channel Assembly

The steam generator is installed with the curved short section in the horizontal plane, and the long section in the vertical plane. Support lugs or saddles have not been considered at this time. A functional description of the steam generator can be found in Section 4.0 of this report.

3.4 Shell Assembly

3.4.1 Upper Shell Assembly

The upper shell sub-assembly consists of: expanded shell section, inlet nozzle, intershroud, baffle plate and a shell transition. The upper shell sub-assembly is welded to the tubesheet and the middle shell sub-assembly see Figure 3.1.

The expanded shell section is made from rolled and butt weld Hastelloy - "N" plate. A 20" molten salt inlet nozzle is located midway in this expanded region. This nozzle is a saddle type which was selected so that the nozzle to shell weld is removed from critically stressed shell to nozzle intersection. The use of a saddle type nozzle permits, without the use of special techniques, the radiography of the nozzle welds.

Within the expanded shell section is a second cylinder which is the intershroud, its purpose is to channel the flow of molten salt to the heat transfer tubes. This intershroud has an impingement baffle which protects the heat transfer tubes from excess flow errosion. The shroud is perforated with holes to allow the molten salt to enter from the expanded shell section and decend through the unit as shown on Figure 3.1.

The lower section of the intershroud and the shell transition are of single piece construction as shown in Figure 3.3. A single piece design is recommended to avoid the use of welds in the high stress area of the junction discontinuity.

The upper baffle plate is positioned between the molten salt inlet nozzle and the tubesheet to act as a thermal barrier to prevent the tubesheet and the I. B. W. welds from being thermally shocked.

3.4.2 Middle Shell Sub-Assembly

The middle shell sub-assembly consists of rolled and butt welded sections of Hastelloy - "N" plate. The middle shell acts as a continuation of the intershroud which channels salt flow around the heat transfer tubes.

3.4.3 Lower Shell Sub-Assembly

The lower shell sub-assembly consists of: expanded shell section, outlet nozzle, intershroud, baffle plate and a shell transition. The lower shell sub-assembly is welded to the lower tubesheet and to middle shell sub-assembly.

The expanded shell section is identical with that of the upper shell except the 20" nozzle is used as an outlet for the molten salt.

3.5 Bundle Assembly

The bundle assembly consists of (2) tubesheets, heat transfer tubes, tie-rods, support plates and vibration suppressors. The complete bundle assembly is welded to the shell assembly, for manufacturing sequences see section of this report.

The tubesheets are 15" thick Vacuum Arc or Electroslag Remelt Forgings of Hastelloy - "N" material. The tubesheets are designed to meet the code requirements for stress in perforated plates. The outer rim of the tubesheet is machined to a countour which minimizes the thermal stress by having this rim respond more uniformly to thermal transients with the tube hole ligaments. The lower face of each tubesheet is machined to provide spigots for welding of the heat transfer tubes as shown on Figure 3.2.

The heat transfer tubes are full penetration welded to each tubesheet by using an Internal Bore weld technique. The heat transfer tubes are of Hastelloy - "N" material designed in accordance with A.S.M.E. tubing specifications. Allowances for manufacturing scratches, thinning and corrosion have been included in the tube wall thichness.

The heat transfer tubes are supported in the vertical position by perforated tube support plates commonly used in heat-exchanger equipment. The support plates are of the "Drilled Plate" type as shown on Figure 3.6. This arrangement was chosen in order to provide circulation between the heat transfer tubes, thereby reducing possible stratification problems and preventing solid collection.

The tube support plates and the vibration suppressor grids are supported by (13) 3/4" diameter tie-rods which are located in the tube pattern as shown on Figure 3.6 and 3.7. These tie-rods are threaded into the tube sheets, located at both ends of the unit.

The tie-rods are threaded into the upper tubesheet. The support plates are spaced using sleeves which are 7/8" inside diameter. The sleeves are dimpled to assure the proper location concentric to the tie-rods. This type of assembly is joined in the curved region by a turnbuckle as shown on Figure 3.8. The curved region uses a vibration suppressor grid to properly position the tubes in this area. The function of the grid is to allow expansion of the tubes while restraining them against vibration as shown on Figure 3.7. The tie-rods are secured at the last suppressor grid by means of a heavy hex nut which is seal welded in place.

The vibration suppressor grid is comprised of an outer ring that is rolled thru the "Y" axis and is machined to accept a grid of flat bars as shown on Figure 3.7.

The turnbuckle used to join these grids is shown on Figure 3.8. Each turn buckle is positioned within the grid and accepts at each end a curved tie-rod. This threading assembly is made possible by use of a right and left hand thread within the turn-buckle.

The by-pass of liquid to the outside of the support plates and the suppressor grids is minimized by the manufacturing tolerances that can be maintained. The inside shell diameter can be manufactured to $39\frac{1}{2}$" +3/16" -0" and the supports can be held to an outside diameter of 39 3/8" +1/16 -0.

3.6 Channel Assembly

The channel assembly is comprised of the bundle assembly (described in the preceding section) and the upper and lower hemispherical heads. Each head is joined to the tubesheet by means of a full penetration weld. Located in the center of each head is a 16" nozzle of the saddle type. This type of nozzle allows for full radiography of the closure weld. The 16 nozzle in the lower head serves as the inlet nozzle which carries supercritical fluid into the plenum chamber (lower hemi-head) and then through the heat transfer tubes. Upon exiting the tubes the high pressure steam is collected in the upper plenum (upper hemi-head) and allowed to exit through the 16" outlet nozzle as shown on Figure 3.2.

3.7 Special Design Features

Saddle Nozzle

The saddle type nozzle offers two advantages not found in nozzles of a different design. First, the saddle nozzle permits the radiography of the nozzle to shell weld without the use of special techniques. Secondly, the saddle nozzle removes the weld from the critically stressed nozzle to shell intersection.

Internal Bore Weld

The I.B.W. welding process allows design of a tubesheet that eliminates the crevice created by the standard "through" tubesheet design. The I.B.W. weld is a full penetration weld that can be fully radiographed.

Minimal Flow By-Pass

The close manufacturing tolerances that can be maintained during manufacture of the intershroud, shell cylinder and tube-supports minimizes the by-pass of molten salt to 2 percent of the total flow.

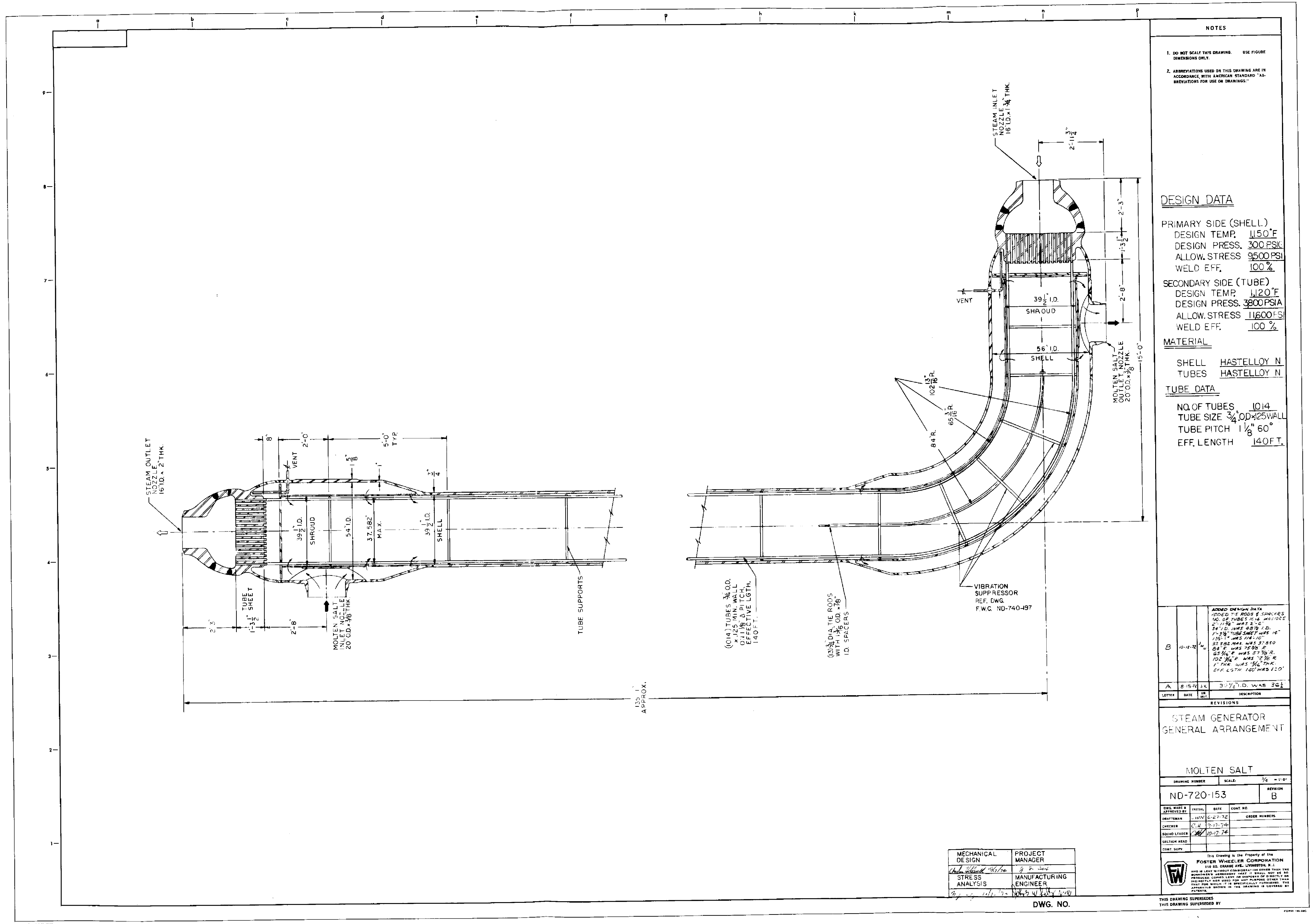
NOTES
1. DO NOT SCALE THIS DRAWING. USE FIGURE DIMENSIONS ONLY.
2. ABBREVIATIONS USED ON THIS DRAWING ARE IN ACCORDANCE WITH AMERICAN STANDARD "ABBREVIATIONS FOR USE ON DRAWINGS."
DESIGN DATA
PRIMARY SIDE (SHELL)
DESIGN TEMP. 1,150°F
DESIGN PRESS. 300 PSIG
ALLOW. STRESS 9,500 PSI
WELD EFF. 100 %
SECONDARY SIDE (TUBE)
DESIGN TEMP. 1,120°F
DESIGN PRESS. 3800 PSIA
ALLOW. STRESS 11,600 PSI
WELD EFF. 100 %
MATERIAL
SHELL HASTELLOY N
TUBES HASTELLOY N
TUBE DATA
NO. OF TUBES 1,014
TUBE SIZE 3/4" O.D. × .125 WALL
TUBE PITCH 1 1/8" 60°
EFF. LENGTH 140 FT.
STEAM INLET NOZZLE 16" I.D. × 1 3/4" THK.
STEAM OUTLET NOZZLE 16" I.D. × 2" THK.
MOLTEN SALT OUTLET NOZZLE 20" O.D. × 3/8" THK.
MOLTEN SALT INLET NOZZLE 20" O.D. × 3/8" THK.
VENT
39 1/2" I.D. SHROUD
56" I.D. SHELL
54" I.D.
37.582" MAX.
TUBE SHEET
TUBE SUPPORTS
(1014) TUBES 3/4" O.D. × .125 MIN. WALL ON 1 1/8 Δ PITCH. EFFECTIVE LGTH. 140 FT.
(13) 3/4" DIA. TIE RODS WITH 1 3/16 O.D. × 7/8" I.D. SPACERS
VIBRATION SUPPRESSOR REF. DWG. F.W.C. ND-740-497
84" R.
65 3/16" R.
102 13/16" R.
2'-11 3/4"
2'-3"
1'-3 1/2"
2'-8"
15'-0"
2'-3"
1'-3 1/2"
2'-0"
5'-0" TYP.
135'-1" APPROX.
LETTER	DATE	DR. INIT.	DESCRIPTION
B	10-12-72	JWN	ADDED DESIGN DATA; ADDED TIE RODS & SPACERS; NO. OF TUBES 1014 WAS 1025; 2'-11 3/4" WAS 2'-6"; 54" I.D. WAS 48 1/2 I.D.; 1'-3 1/2" TUBE SHEET WAS 14"; 135'-1" WAS 114'-10"; 37.582 MAX. WAS 37.850; 84" R. WAS 75 3/8" R.; 65 3/16" R. WAS 57 7/8" R.; 102 13/16" R. WAS 92 7/8" R.; 1" THK. WAS 15/16" THK.; EFF. LGTH. 140' WAS 120'
A	8-15-72	JK	39 1/2" I.D. WAS 36 1/2
REVISIONS
STEAM GENERATOR GENERAL ARRANGEMENT
MOLTEN SALT
DRAWING NUMBER ND-720-153 SCALE: 3/4" = 1'-0" REVISION B
DRAFTSMAN JWN 6-27-72
CHECKER C.H. 9-17-74
SQUAD LEADER 10-17-74
SECTION HEAD
CONT. SUPV.
CONT. NO.
ORDER NUMBERS
This Drawing is the Property of the FOSTER WHEELER CORPORATION 110 SO. ORANGE AVE. LIVINGSTON, N.J. AND IS LENT WITHOUT CONSIDERATION OTHER THAN THE BORROWER'S AGREEMENT THAT IT SHALL NOT BE REPRODUCED, COPIED, LENT, OR DISPOSED OF DIRECTLY OR INDIRECTLY NOR USED FOR ANY PURPOSE OTHER THAN THAT FOR WHICH IT IS SPECIFICALLY FURNISHED. THE APPARATUS SHOWN IN THE DRAWING IS COVERED BY PATENTS.
THIS DRAWING SUPERSEDES
THIS DRAWING SUPERSEDED BY
MECHANICAL DESIGN
PROJECT MANAGER
STRESS ANALYSIS
MANUFACTURING ENGINEER
DWG. NO.
FORM 199-98C

Fig. 3.1

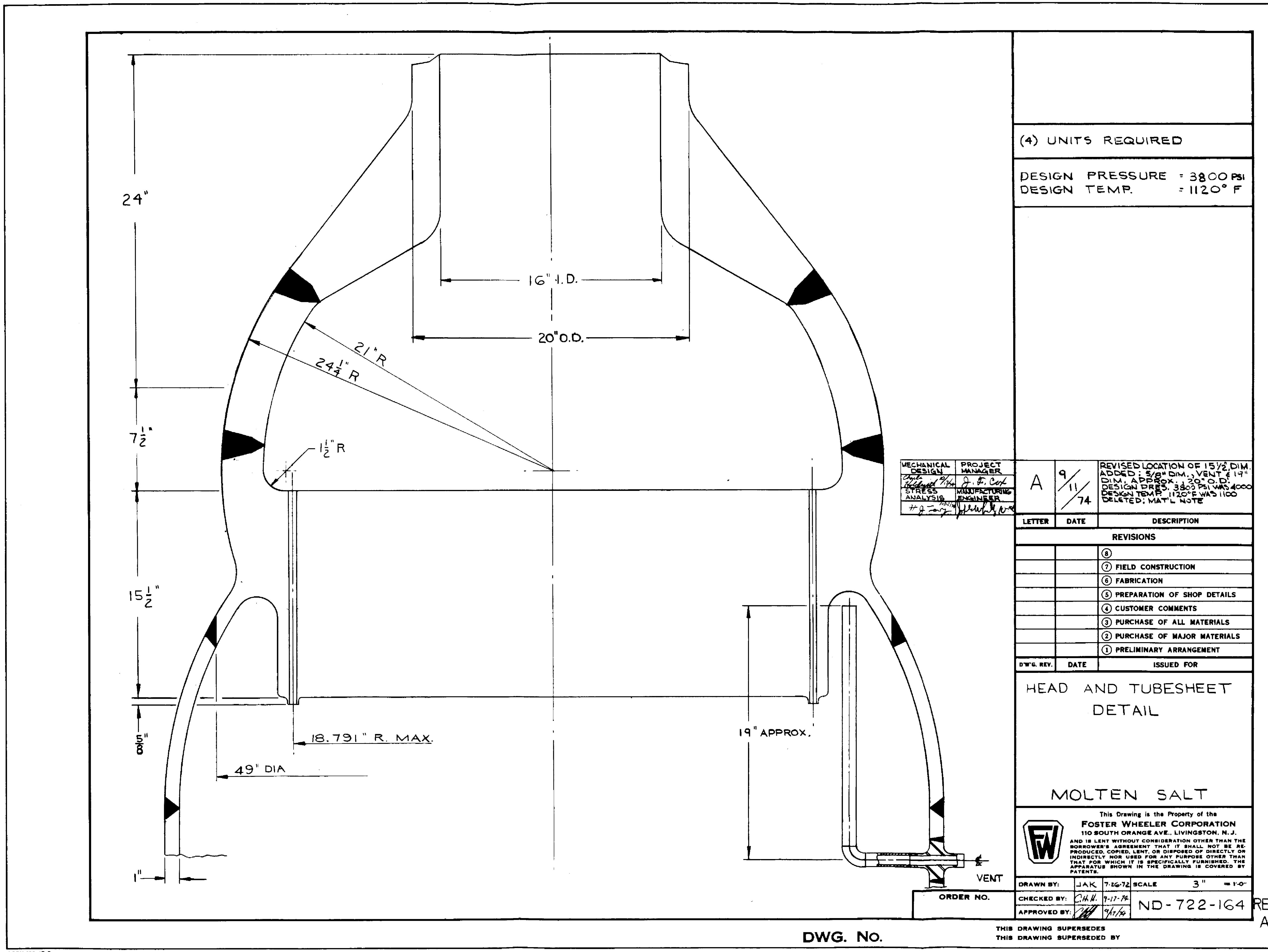

24"
7 1/2"
15 1/2"
5/8"
1"
16" I.D.
20" O.D.
21" R
24 1/4" R
1 1/2" R
18.791" R. MAX.
49" DIA
19" APPROX.
VENT
(4) UNITS REQUIRED
DESIGN PRESSURE = 3800 PSI
DESIGN TEMP. = 1120° F
MECHANICAL DESIGN
PROJECT MANAGER
STRESS ANALYSIS
MANUFACTURING ENGINEER
A
9/11/74
REVISED LOCATION OF 15 1/2" DIM.
ADDED: 5/8" DIM., VENT & 19" DIM. APPROX., 20" O.D.
DESIGN PRES. 3800 PSI WAS 4000
DESIGN TEMP. 1120°F WAS 1100
DELETED: MAT'L NOTE
LETTER
DATE
DESCRIPTION
REVISIONS
8
7 FIELD CONSTRUCTION
6 FABRICATION
5 PREPARATION OF SHOP DETAILS
4 CUSTOMER COMMENTS
3 PURCHASE OF ALL MATERIALS
2 PURCHASE OF MAJOR MATERIALS
1 PRELIMINARY ARRANGEMENT
DWG. REV.
DATE
ISSUED FOR
HEAD AND TUBESHEET DETAIL
MOLTEN SALT
This Drawing is the Property of the
FOSTER WHEELER CORPORATION
110 SOUTH ORANGE AVE., LIVINGSTON, N. J.
AND IS LENT WITHOUT CONSIDERATION OTHER THAN THE BORROWER'S AGREEMENT THAT IT SHALL NOT BE REPRODUCED, COPIED, LENT, OR DISPOSED OF DIRECTLY OR INDIRECTLY NOR USED FOR ANY PURPOSE OTHER THAN THAT FOR WHICH IT IS SPECIFICALLY FURNISHED. THE APPARATUS SHOWN IN THE DRAWING IS COVERED BY PATENTS.
ORDER NO.
DRAWN BY: JAK 7-26-72
SCALE 3" = 1'-0"
CHECKED BY: C.H.H. 9-17-74
APPROVED BY: 9/17/74
ND-722-164
REV. A
DWG. No.
THIS DRAWING SUPERSEDES
THIS DRAWING SUPERSEDED BY
FORM 136-47-C

Fig. 3.2

DESIGN PRESSURE = 300 PSI
DESIGN TEMP = 1150° F

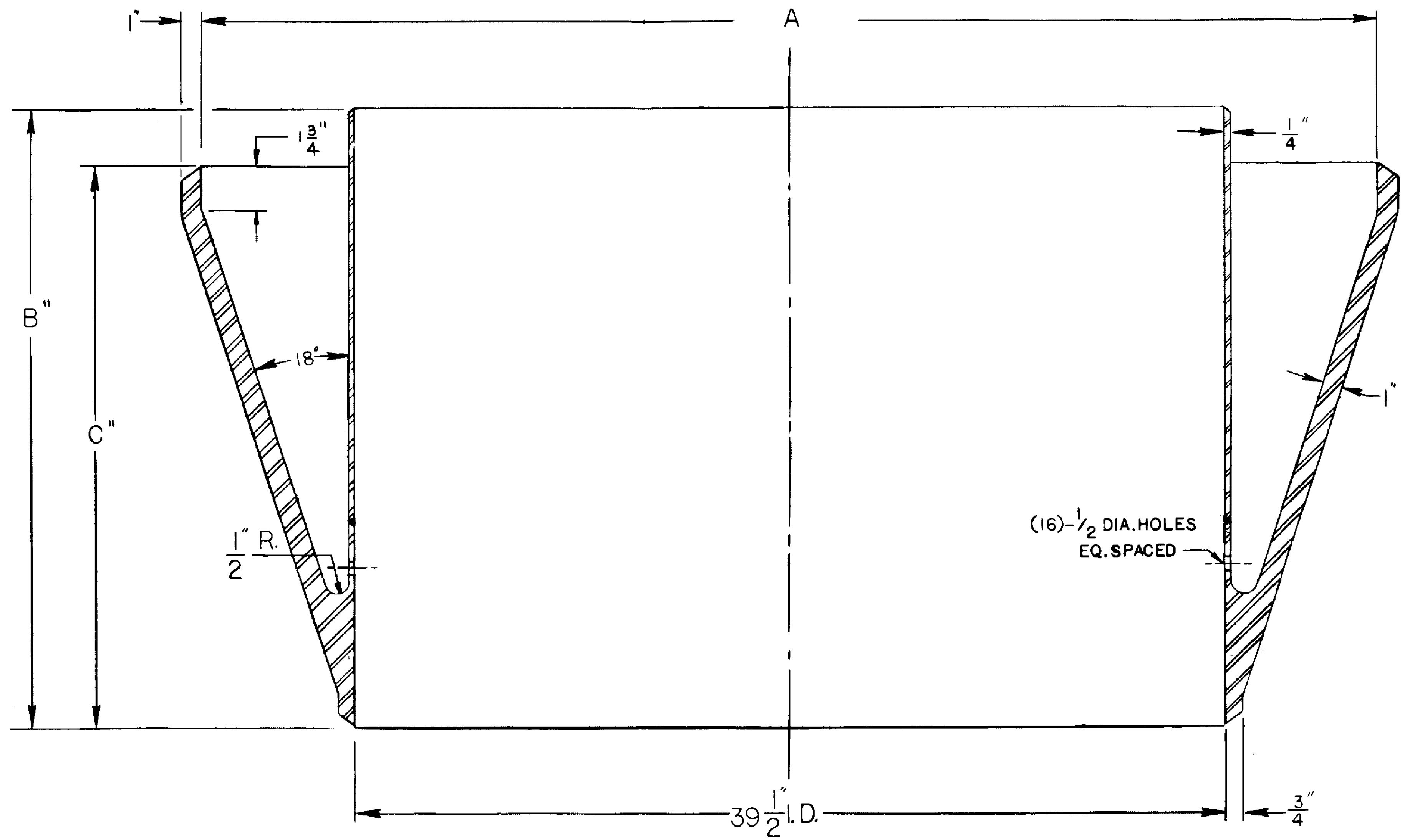

DIM	TOP TRANSITION	BOTTOM TRANSITION
A	54" I.D.	56" I.D.
B	28 1/2"	29 1/2"
C	26"	27"
NO. REQ'D	4	4

LETTER	DATE	DESCRIPTION
B	9-18-74 LRS	REMOVED: MAT'L ADDED: DIM. TABLE & 1 3/4" DIM. DESIGN TEMP 1150°F WAS 1100
A	10-12-72 J.W.N.	39 1/2" I.D. WAS 40" I.D. 1" THK. WAS 15/16" THK. 1/2" R. WAS 1 1/2 R.

REVISIONS

DWG. REV.	DATE	ISSUED FOR
		⑧
		⑦ FIELD CONSTRUCTION
		⑥ FABRICATION
		⑤ PREPARATION OF SHOP DETAILS
		④ CUSTOMER COMMENTS
		③ PURCHASE OF ALL MATERIALS
		② PURCHASE OF MAJOR MATERIALS
		① PRELIMINARY ARRANGEMENT

MECHANICAL DESIGN | PROJECT MANAGER | STRESS ANALYSIS | MANUFACT'RING ENGINEER

SHELL TRANSITION

MOLTEN SALT

DRAWN BY: | SCALE 3" = 1'-0"
CHECKED BY: C.H.H. 9/10/74
APPROVED BY: 9/10/74
ORDER NO.
ND-722-167 REV B

DWG. No.

THIS DRAWING SUPERSEDES
THIS DRAWING SUPERSEDED BY

FORM 196-47-C

Fig. 3.3

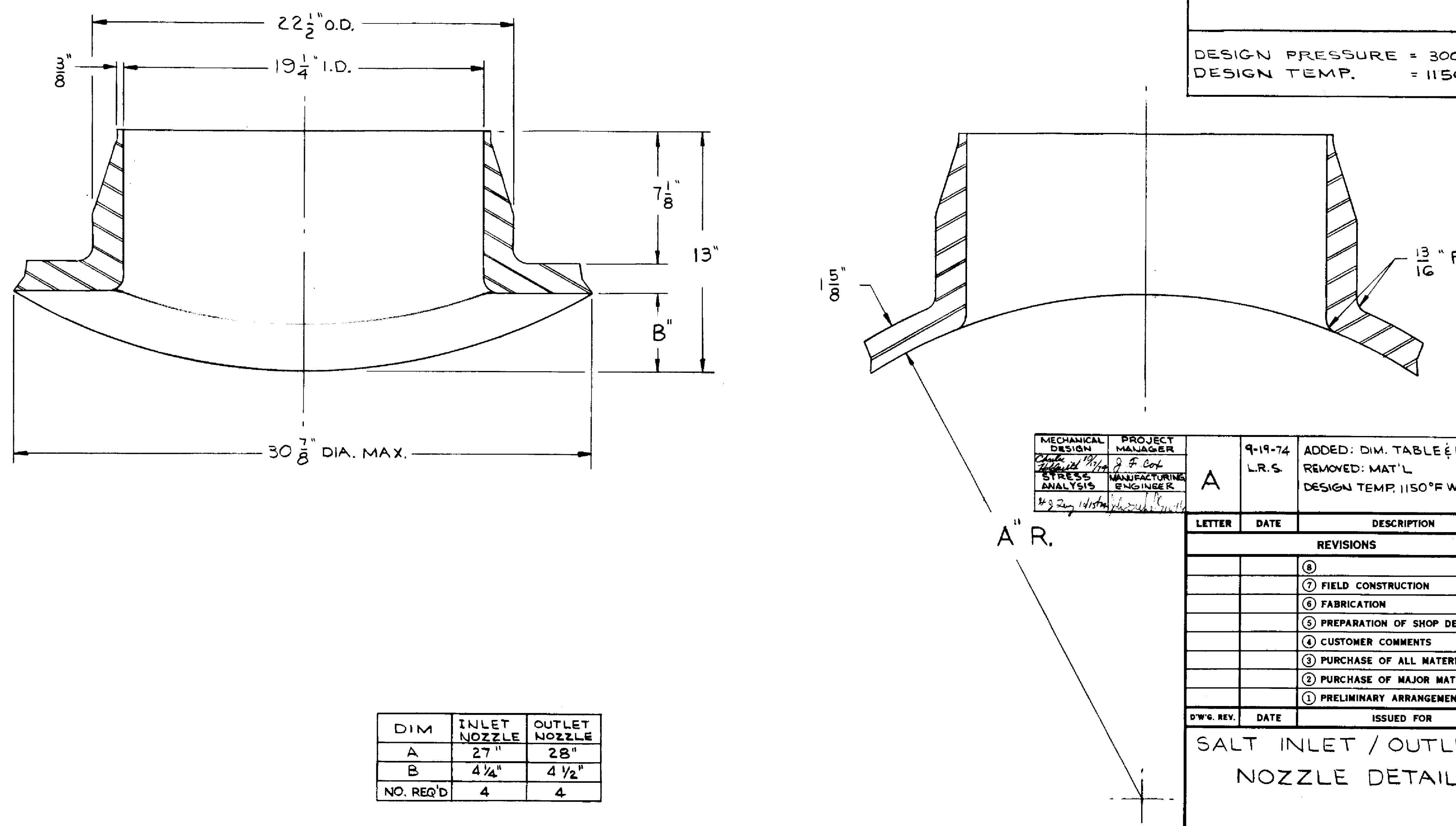

DIM	INLET NOZZLE	OUTLET NOZZLE
A	27"	28"
B	4 1/4"	4 1/2"
NO. REQ'D	4	4

DESIGN PRESSURE = 300 PSI
DESIGN TEMP. = 1150°F

MECHANICAL DESIGN	PROJECT MANAGER
[illegible signature]	J. F. Cox
STRESS ANALYSIS	MANUFACTURING ENGINEER
[illegible signature]	[illegible signature]

LETTER	DATE	DESCRIPTION
A	9-19-74 L.R.S.	ADDED: DIM. TABLE & LETTERS REMOVED: MAT'L DESIGN TEMP. 1150°F WAS 1100

REVISIONS

D'W'G. REV.	DATE	ISSUED FOR
		⑧
		⑦ FIELD CONSTRUCTION
		⑥ FABRICATION
		⑤ PREPARATION OF SHOP DETAILS
		④ CUSTOMER COMMENTS
		③ PURCHASE OF ALL MATERIALS
		② PURCHASE OF MAJOR MATERIALS
		① PRELIMINARY ARRANGEMENT

SALT INLET / OUTLET NOZZLE DETAIL

MOLTEN SALT

DRAWN BY:	JAK	8-1-72	SCALE	3" = 1'-0"
CHECKED BY:	C.H.H.	9-17-74		
APPROVED BY:	[illegible]	9-17-74	ND-722-165	REV A

ORDER NO.

DWG. NO.

THIS DRAWING SUPERSEDES
THIS DRAWING SUPERSEDED BY

FORM 136-47 C

Fig. 3.4

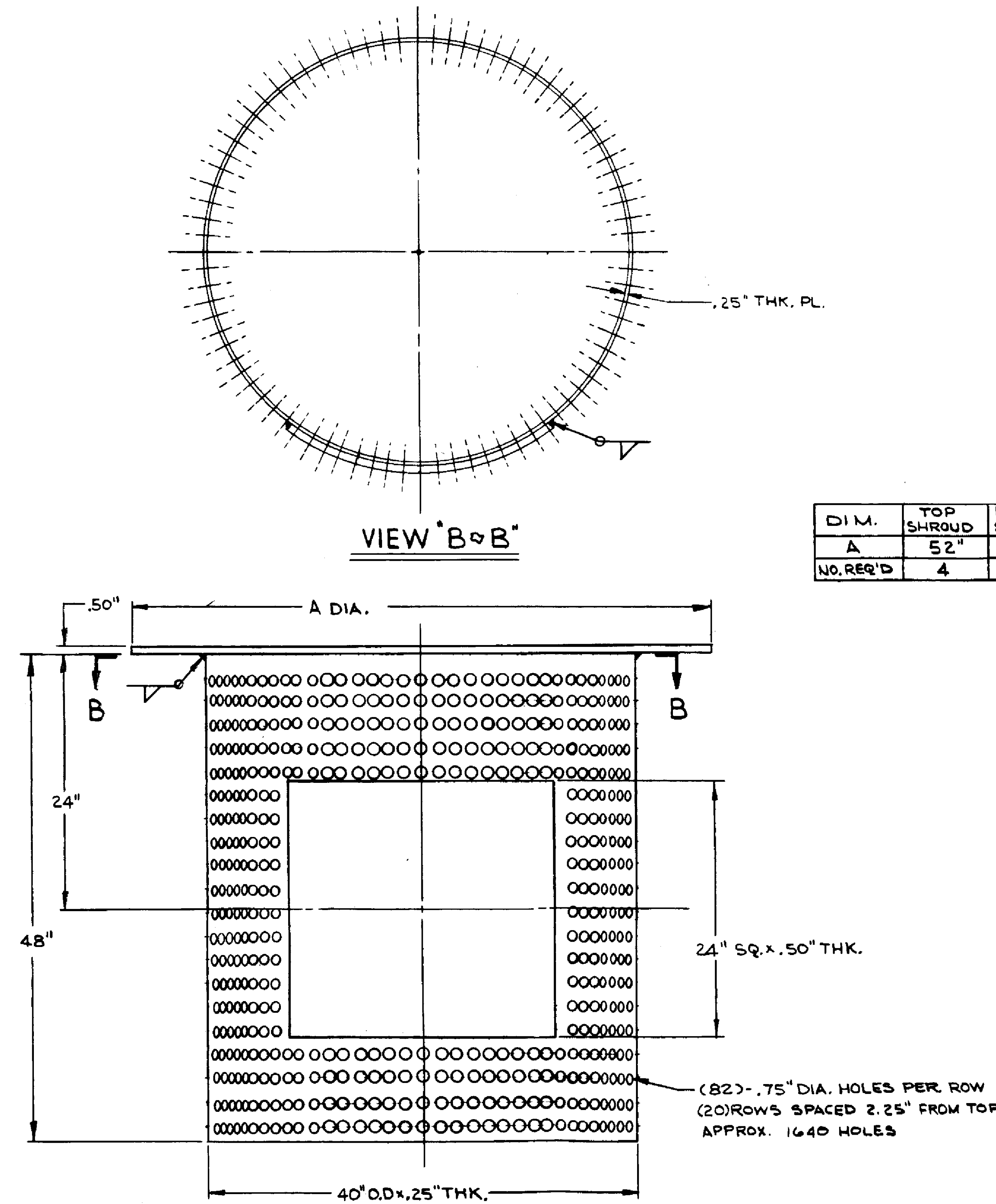

DIM.	TOP SHROUD	BOTTOM SHROUD
A	52"	54"
NO. REQ'D	4	4

MECHANICAL DESIGN	PROJECT MANAGER
STRESS ANALYSIS	MANUFACTURING ENGINEER

LETTER	DATE	DESCRIPTION
		REVISIONS

D'W'G. REV.	DATE	ISSUED FOR
		⑧
		⑦ FIELD CONSTRUCTION
		⑥ FABRICATION
		⑤ PREPARATION OF SHOP DETAILS
		④ CUSTOMER COMMENTS
		③ PURCHASE OF ALL MATERIALS
		② PURCHASE OF MAJOR MATERIALS
		① PRELIMINARY ARRANGEMENT

INTERNAL SHROUD

MOLTEN SALT

DRAWN BY:	L.S.	9/10/74	SCALE 1/2" = 1'-0"
CHECKED BY:	C.H.H.	9/?/74	ND-742-171
APPROVED BY:		9/?/74	

ORDER NO.

REV. 0

DWG. No.

THIS DRAWING SUPERSEDES
THIS DRAWING SUPERSEDED BY

FORM 136-47 C

Fig. 3.5

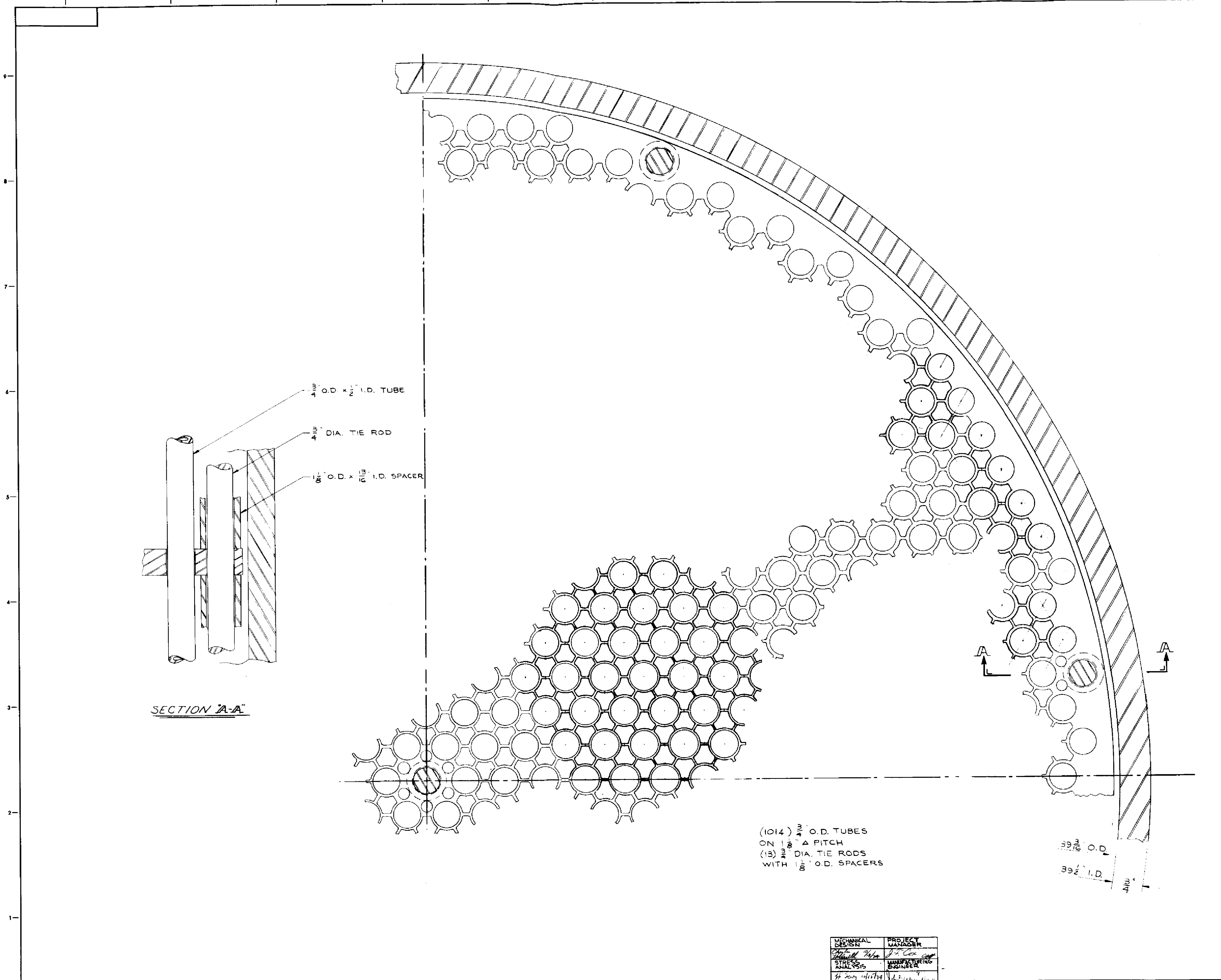

NOTES

1. DO NOT SCALE THIS DRAWING. USE FIGURE DIMENSIONS ONLY.
2. ABBREVIATIONS USED ON THIS DRAWING ARE IN ACCORDANCE WITH AMERICAN STANDARD "ABBREVIATIONS FOR USE ON DRAWINGS."

LETTER	DATE	DR. INIT.	DESCRIPTION

REVISIONS

TUBE SUPPORT PLATE

MOLTEN SALT

DRAWING NUMBER	SCALE: FULL = 1'-0"	REVISION
ND-720-195		

DWG. MADE & APPROVED BY	INITIAL	DATE	CONT. NO. 2-25-1405
DRAFTSMAN	JAK	8-30-72	ORDER NUMBERS
CHECKER	C.H.H	9-17-74	
SQUAD LEADER	[signature]	9-17-74	
SECTION HEAD			
CONT. SUPV.			

DWG. NO.

THIS DRAWING SUPERSEDES
THIS DRAWING SUPERSEDED BY

FORM 1N-44C

Fig. 3.6

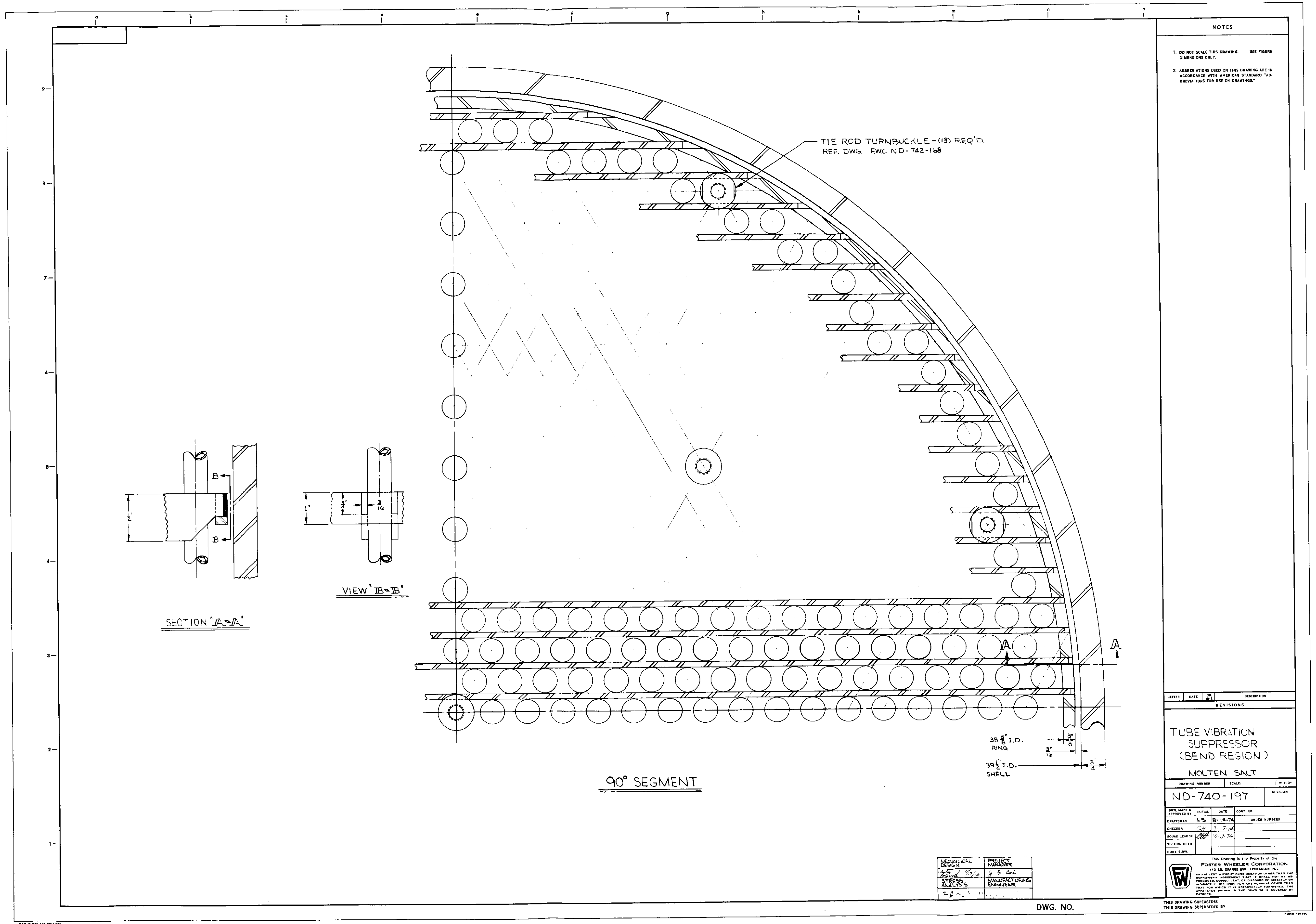
NOTES
1. DO NOT SCALE THIS DRAWING. USE FIGURE DIMENSIONS ONLY.
2. ABBREVIATIONS USED ON THIS DRAWING ARE IN ACCORDANCE WITH AMERICAN STANDARD "ABBREVIATIONS FOR USE ON DRAWINGS."
TIE ROD TURNBUCKLE - (13) REQ'D.
REF. DWG. FWC ND-742-168
SECTION "A-A"
VIEW "B-B"
90° SEGMENT
38 3/8" I.D. RING
39 1/2" I.D. SHELL
LETTER
DATE
DR. INIT.
DESCRIPTION
REVISIONS
TUBE VIBRATION SUPPRESSOR (BEND REGION)
MOLTEN SALT
DRAWING NUMBER
SCALE: 1" = 1'-0"
ND-740-197
REVISION
DWG. MADE & APPROVED BY
INITIAL
DATE
CONT. NO.
DRAFTSMAN LS 8-14-74
ORDER NUMBERS
CHECKER
SQUAD LEADER
SECTION HEAD
CONT. SUPV.
This Drawing is the Property of the
FOSTER WHEELER CORPORATION
110 SO. ORANGE AVE. LIVINGSTON, N. J.
AND IS LENT WITHOUT CONSIDERATION OTHER THAN THE BORROWER'S AGREEMENT THAT IT SHALL NOT BE REPRODUCED, COPIED, LENT, OR DISPOSED OF DIRECTLY OR INDIRECTLY NOR USED FOR ANY PURPOSE OTHER THAN THAT FOR WHICH IT IS SPECIFICALLY FURNISHED. THE APPARATUS SHOWN IN THE DRAWING IS COVERED BY PATENTS.
MECHANICAL DESIGN
PROJECT MANAGER
STRESS ANALYSIS
MANUFACTURING ENGINEER
DWG. NO.
THIS DRAWING SUPERSEDES
THIS DRAWING SUPERSEDED BY

Fig. 3.7

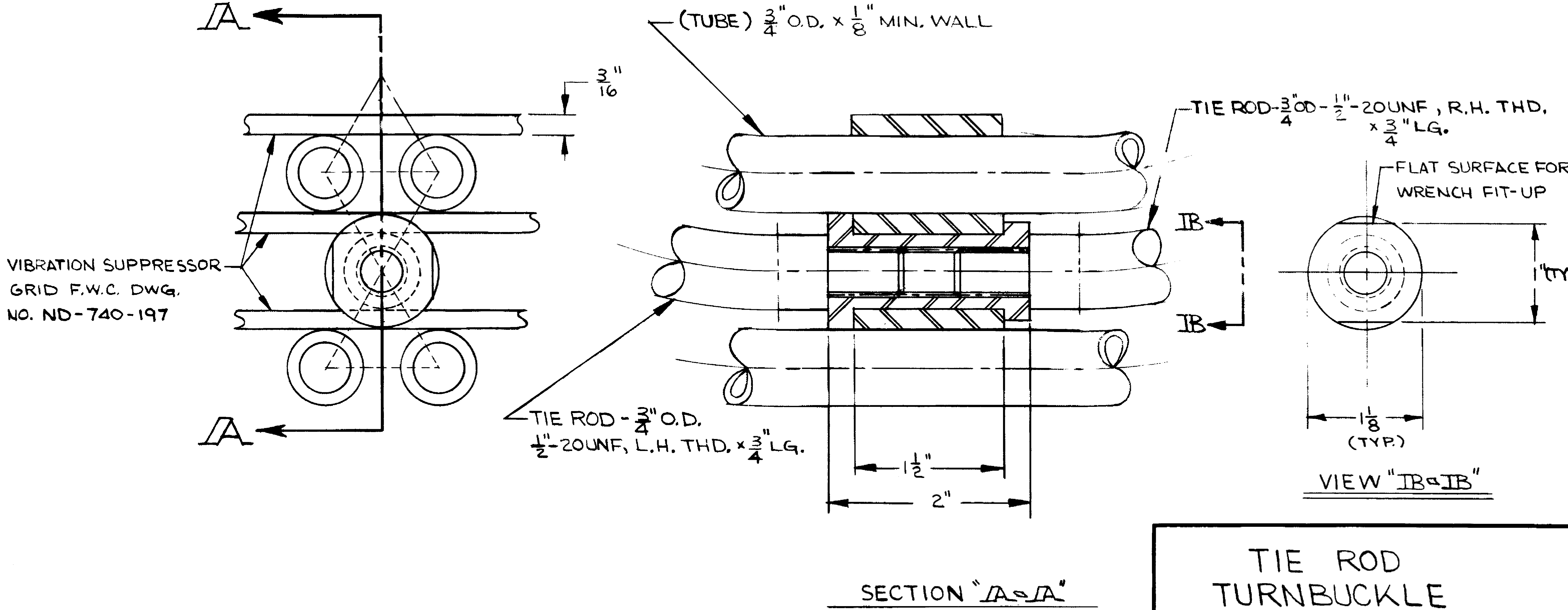

TIE ROD TURNBUCKLE

THIS DRAWING IS THE PROPERTY OF THE
FOSTER WHEELER CORPORATION
110 SO. ORANGE AVE., LIVINGSTON, N.J.
AND IS LENT WITHOUT CONSIDERATION OTHER THAN THE BORROWER'S AGREEMENT THAT IT SHALL NOT BE REPRODUCED, COPIED, LENT, OR DISPOSED OF DIRECTLY OR INDIRECTLY NOR USED FOR ANY PURPOSE OTHER THAN THAT FOR WHICH IT IS SPECIFICALLY FURNISHED. THE APPARATUS SHOWN IN THE DRAWING IS COVERED BY PATENTS.

MECHANICAL DESIGN	Charles Holdsall 10/17/74	
PROJECT MANAGER	J. E. Cox	
STRESS ANALYSIS	[illegible] 10/17/74	
MANUFACTURING ENGINEER	[illegible]	
DRAWN BY:	LRS	8-15-74
CHECKED BY:	C.H.H.	9-17-74
APPROVED BY:	[illegible]	9-17-74
SCALE:	1"=1'-0"	
ORDER NO.		

ND-742-168

REVISION

K&E 17 0253 4-73 TEM 1194•

FORM 285-63-C

Fig. 3.8

SECTION 4

THERMAL/HYDRAULIC DESIGN

BY

H. L. Chou

H. L. CHOU
Thermal/Hydraulic Task Leader

Approved by

S. M. Cho

Dr. S. M. Cho
Manager
Thermal/Hydraulic Engineering

TABLE OF CONTENTS

FWC FORM 172 - 4
NOTATIONS IN THIS COLUMN INDICATE WHERE CHANGES HAVE BEEN MADE

4.0 THERMAL/HYDRAULIC ANALYSIS

It is the intent of this analysis to obtain a conceptual design of a steam generator which will operate with a molten salt system and a supercritical steam-power cycle. The steam generater design is of a once-through, counterflow, shell-and-tube type with salt flowing downward on the shell side and water/steam flowing upward in the tubes. Only one steam generator unit is intended for each of the four heat transport circuits which are connected, in parallel, to the Molten Salt Breeder Reactor.

An axial (or long) flow approach was utilized after several unsuccessful attempts of meeting the design criteria by a cross flow scheme. The difficulty of solving the problems of tube vibration and the excessive pressure drop on the shell side simultanteously, forced the cross flow approach to be abandoned. However, it is noted that the advantage of cross flow approach is not so significant in a supercritical unit, due to the fact that the thick tube wall, necessary for high pressure, becomes a dominant thermal resistance (about 50%) of over-all thermal performance.

The analyses of the basic thermal/hydraulic performances, design uncertainties, flow stabilities, and related systems have been performed and the results are presented in detail in the following sections.

4.1 THERMAL PERFORMANCE

The thermodynamic and transport properties and thermal conductances of all heat transfer media were first determined in order to obtain the steady-state thermal performance of the steam generator.

4.1.1 OVERALL HEAT TRANSFER COEFFICIENT

The heat is transfered from the molten salt on shell side to the steam on tube side. The thermal conductances of molten salt, tube wall, supercritical steam and steam-side fouling were considered.

The molten salt side fouling effect was neglected at the direction of Oak Ridge National Laboratory. The Molten-Salt Reactor Experiment (MSRE) in 1960's denoted no evidence of fouling in the MSRE heat exchanger. However, the coolant mixture chosen for that application was BF_2 with 66 mole % of LiF, and the coolant chosen for MSBR is NaF with 92 mole % of $NaBF_4$.Evidence of the corrosion product, $Na_3C_rF_6$, has been found in loops circulating sodium fluoroborate, and this corrosion/product is expected to deposit on the outside surface of the steam tubes if not removed by some means (Ref.1). The effect of molten salt side fouling on the thermal performance of the steam generator was reported in the FWEC Monthly Progress Report #10 (Ref. 2).

The steam side fouling coefficient of 6667 Btu/hr-ft^2-^{o}F was used and is considered to be a reasonable value for the single-phase flow and the five-year period of tube cleaning.

The design properties of the tube wall material, Hastelloy N (Nickel-Molybdenum-Chromium-Iron Alloy), are tabulated in Reference 3 .

A. Steam Side Coefficient

The correlation by H. S. Swenson (Ref.4) was recommended for super-critical water/steam flowing inside circular tubes exposed to heat flux at the wall. This correlation is expressed by

$$\frac{h_i D_i}{K_i} = 0.00459 \left(\frac{D_i G}{\mu_i} \right)^{0.923} \left(\frac{H_i - H_b}{T_i - T_b} \frac{\mu_i}{K_i} \right)^{0.613} \left(\frac{v_b}{v_i} \right)^{0.231}$$

where

h_i = heat transfer coefficient inside tube, Btu/hr-ft^2-$^\circ$F

D_i = inside diameter of tube, ft

K_i = thermal conductivity of fluid inside tube, Btu/hr-ft-$^\circ$F

G = mass velocity of fluid, lb/hr-ft^2

μ_i = viscosity of fluid at temperature of inside surface of tube, lb/hr-ft

H_i = enthalpy at temperature of inside surface of tube, Btu/lb

H_b = enthalpy at temperature of bulk fluid, Btu/lb

T_i = temperature of fluid at inside surface of tube, $^\circ$F

T_b = temperature of bulk fluid, $^\circ$F

v_b = specific volume of bulk fluid, ft^3/lb, and

v_i = specific volume of fluid at temperature of inside surface of tube ft^3/lb

B. <u>Salt Side Coefficient</u>

The Dittus Boelter correlation was applied to determine the molten salt heat transfer coefficient. The correlation is expressed by

$$Nu = 0.023\,(Re)^{0.8}\,(Pr)^{0.4}$$

where $$Nu = \frac{h_o\,De}{k_b}$$

$$Re = \frac{G\,De}{\mu_b}$$

$$Pr = \frac{Cp_b\,\mu_b}{K_b}$$

h_o = heat transfer coefficient of molten salt, Btu/hr-ft^2-^oF

De = equivalent diameter, ft

K_b = thermal conductivity of molten salt at bulk temperature, Btu/hr-ft-^oF

G = mass velocity of molten salt, lb/hr-ft^2

μ_b = viscosity of molten salt at bulk temperature, lb/hr-ft

Cp_b = specific heat at constant pressure of molten salt at bulk temperature, Btu/lb-^oF

All the conductances of overall, steam side, molten salt side, tube wall, and steam side fouling at full load are plotted versus length of steam generator, as measured from cold end, in Fig. 4.1. The overall conductance was calculated based on outside surface of tube and maximum tube thickness (0.125" + 7%) since the steam is in the supercritical thermodynamic state, special care must be taken to insure that the evaluations of thermodynamic and transport properties are accurate. For given load conditions, the tube length was divided into a sufficient number of sections, so that the specific heat, Cp, of steam in each section could be treated as a constant with negligible error, and the concept of logarithm mean temperature difference could be applied.

The length-averaged mean values were calculated for each conductance to determine the overall performance of the unit as full load conditions and are tabulated below. The method in Ref. 5 was utilized. The attributions to overall resistance of each are also shown.

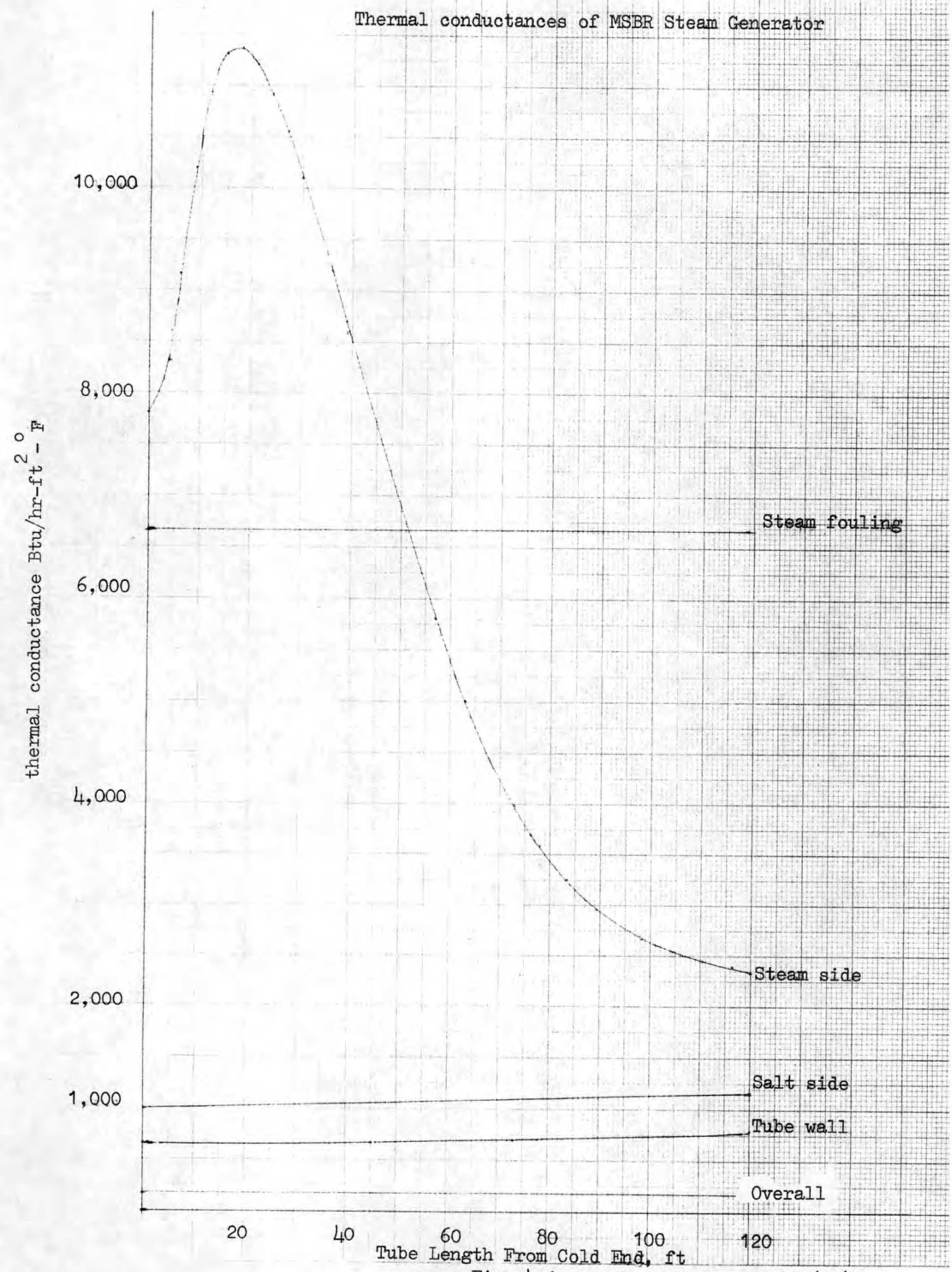
Thermal conductances of MSBR Steam Generator
10,000
8,000
6,000
4,000
2,000
1,000
thermal conductance Btu/hr-ft2 - °F
Steam fouling
Steam side
Salt side
Tube wall
Overall
20
40
60
80
100
120
Tube Length From Cold End, ft

Fig. 4.1

	Conductance Btu/hr-ft^2-^{o}F	% of total resistance
Steam side	4401.41	12.0
Molten salt side	1079.21	31.50
tube wall	499.79	48.58
steam side fouling	6667.0	7.92
overall U	340	100
overall log mean temp. difference	205.67^{o}F	

4.1.2 HEAT TRANSFER SURFACE REQUIREMENTS

The design criteria at full load operating conditions are as follows:

	Salt	Water/Steam
Inlet temperature, ^{o}F	1150	700
Outlet temperature, ^{o}F	850	1000
Flow rate, lb/hr	15,280,000	2,538,000
Inlet pressure, psia	235	---
Outlet pressure, psia	---	3600
Maximum pressure drop, psi	60	200

Thermal duty = 483 MW(t) = 1.65×10^9 Btu/hr.

A basic thermal/hydraulic performance computer program was developed to calculate the sizing of steam generator using the correlations mentioned in Section 4.1.1. This resulted in the basic thermal/hydraulic design of the steam generator as 1000 tubes with length of 120 ft. The specifications of this basic design are summarized below:

No. of tubes per unit		1000
Total length, ft.		120
Tube O. D. in.		0.75
Tube thickness, in.	max. wall	0.13375
Tube I. D. in	min. ID	0.4825
Transverse tube pitch, in		1.125
Longitudinal pitch, in		0.974
Heat transfer rate, Btu/hr		1.646×10^9
Total effective surface area, ft^2 (based on tube OD)		23561.8
Material		Hastelloy N

However, the uncertainties of heat transfer correlations, variation of tube thickness, flow by-pass, and even the flucturations of flow rates will require surface margin to accomodate all the possible deviations from design conditions. This was best accomplished by statistical approach.

4.1.2.1 UNCERTAINTY ANALYSIS OF THERMAL PARAMETERS

In order to obtain an appropriate surface margin to maintain a high confidence level of the design, a statistical computer program, entitled SIMPAK, (Ref. 30), was utilized.

SIMPAK is a package of subroutines which read in the date, draw random numbers, relate data to probability distributions, facilitate the Monte Carlo simulation, compute the mean and standard deviation of resultant probability distributions, and print out details of the probability distributions of a few variables of interest.

Uncertainties were considered for heat transfer correlations used in the thermal sizing of the steam generator. For the steam conductance correlation, Swenson reports a standard deviation of $\pm$ 7.2% which leads to $\pm$ 21.6% for 3σ-deviation. This deviation was used for this study. The steam side fouling conductance was assumed to have a range of $\pm$ 25% (3σ-deviation).

The heat transfer data of molten salt obtained with the forced-convection loop FCL-2 are in good agreement with the empirical correlation of Sieder and Tate (Ref. 1). In Ref. 6, the Seider-Tate type correlation was developed for fuel salt as follows:

$$Nu = 0.0234\ Re^{0.8}\ Pr^{1/3}\ \left(\frac{\mu}{\mu_s}\right)^{0.14}$$

with a standard deviation of 6.2% for Re > 12,000 (18.6% for 3 σ -deviation) and all the properties read at bulk temperature, except μ_s at wall temperature. Since no better information is available, this Sieder-Tate correlation was compared with the Dittus-Boelter correlation, which was used in sizing the steam generator, to predict the uncertainty of coolant salt conductance computed in the performance computer program. It was found, within the temperature range of the shell side fluid, the conductance calculated by Sieder-Tate correlation was about 90.06% of the one calculated by Dittus-Boelter correlation. Therefore, for this uncertainty analysis, the molten salt conductance obtained by Dittus Boelter correlation was first multiplied by 0.9006 and then assumed to have a standard deviation of 8% for more conservation. For thermal conductivity of Hastelloy N, the data obtained from Haynes Stellite were about 4.4% higher than the values used in the performance computer program, (Ref. 7). Therefore, the thermal conductivity of tube wall was first multiplied by 1.022 and then assigned a Standard deviation of 0.7167%. All the above parameters were assumed to have normal distributions to simplify the statistical analysis. The variation of tube wall thickness was limited to the manufacture range of 0.125" $^{+7\%}_{-0\%}$.

The modeling method for overall performance of multi-stage heat exchangers used in Ref. 5 was adopted here to significantly reduce the Monte Carlo computation time. All the heat transfer correlations were included as part of the SIMPAK program so that the inter-dependent variables such as inside diameter of tube, flow rate, mass velocity, heat transfer coefficients, could be related to one another and computed simultaneously. The input data were uncertainties of heat transfer correlations, variation of tube wall thickness, and overall performance parameters of basic design at full load conditions. The SIMPAK did 500 Monte Carlo trials and the cumulative probability of the total surface area of steam generator, based on constant duty and temperature profile, was obtained as shown in Table 4.1 and Fig. 4.2. It is noted that the flow rates of salt and steam were held constant. When one considers the malfunctions of pumps, flow rates of salt and steam may fluctuate. Assuming ± 10% variation of flow rates, a second calculation was made and the results are shown in Table 4.2 and Fig. 4.3. These results are only approximate in the sense that the large fluctuations of flow rates would eventually change the total duty and temperature distribution along the unit.

4.1.2.2 THERMAL DESIGN MARGIN

The above analysis indicates that the confidence level of the basic design of 1000 tubes with length of 120 ft (area = 23562 ft^2) is about 40%. This is considered to be too low a level of design confidence and therefore additional surface must be provided. For the case of constant flow rates (Table 4.1, Figure 4.2), the required surface to give the 99.9% confidence level is 26002 ft^2 which is corresponding to 1014 tubes with length of 131 ft. For the case varying flow rates, the 99.9% confidence level requires a surface area of 26611 ft^2 which corresponds to 1014 tubes with length of 134 ft. The flow by-pass on shell side being 1.2% would require additional 1 ft long.

Therefore the reference design steam generator is designed to contain 1014 tubes, 140 ft. long, plus 13 tie rods. This design gives additional 18% of surface area over the basic design, ang has the highest confidence level (99.9%) to achieve the specified thermal duty and design criteria.

4.1.3 DETAILED PERFORMANCE CALCULATIONS

The heat transfer surface requirements shown in Section 4.1.2 were obtained by a performance computer code. This computer code could be easily modified for all the situations and was extensively used for the thermal hydraulic performances. Simulating the unit by this performance computer code, the unit was divided into 63 sections in length. For each section the thermodynamic properties, transport properties, pressure drops, and heat transfer coefficients were determined by iterations. From 700°F to 750°F of steam temperature in the inlet region, the change in steam enthalpy per section was limited to not more than 10 Btu/lb. From 750°F to final steam outlet temperature, the change in steam enthalpy per section did not exceed 20 Btu/lb. The 1967 ASME steam tables were used for all steam

Table 4.1 Summary Statistics for Overall Surface Area of Steam Generator

Flow Rates of Salt/Water are held constant

Mean 23,756 ft^2

Standard deviation 736

Confidence level	0.0	0.10	0.20	0.30	0.40	0.50	0.60	0.70	0.80	0.90	1.00
Surface area, ft^2	21,958	22,830	23,134	23,374	23,573	23,719	23,889	24,140	24,370	24,729	26,002

NUCLEAR DEPARTMENT
FOSTER WHEELER ENERGY CORPORATION
LIVINGSTON, N. J.

Fig. 4.2 Overall Surface Area of Steam Generator vs. Confidence Level

Flow Rate of Salt and Steam/Water are held constant

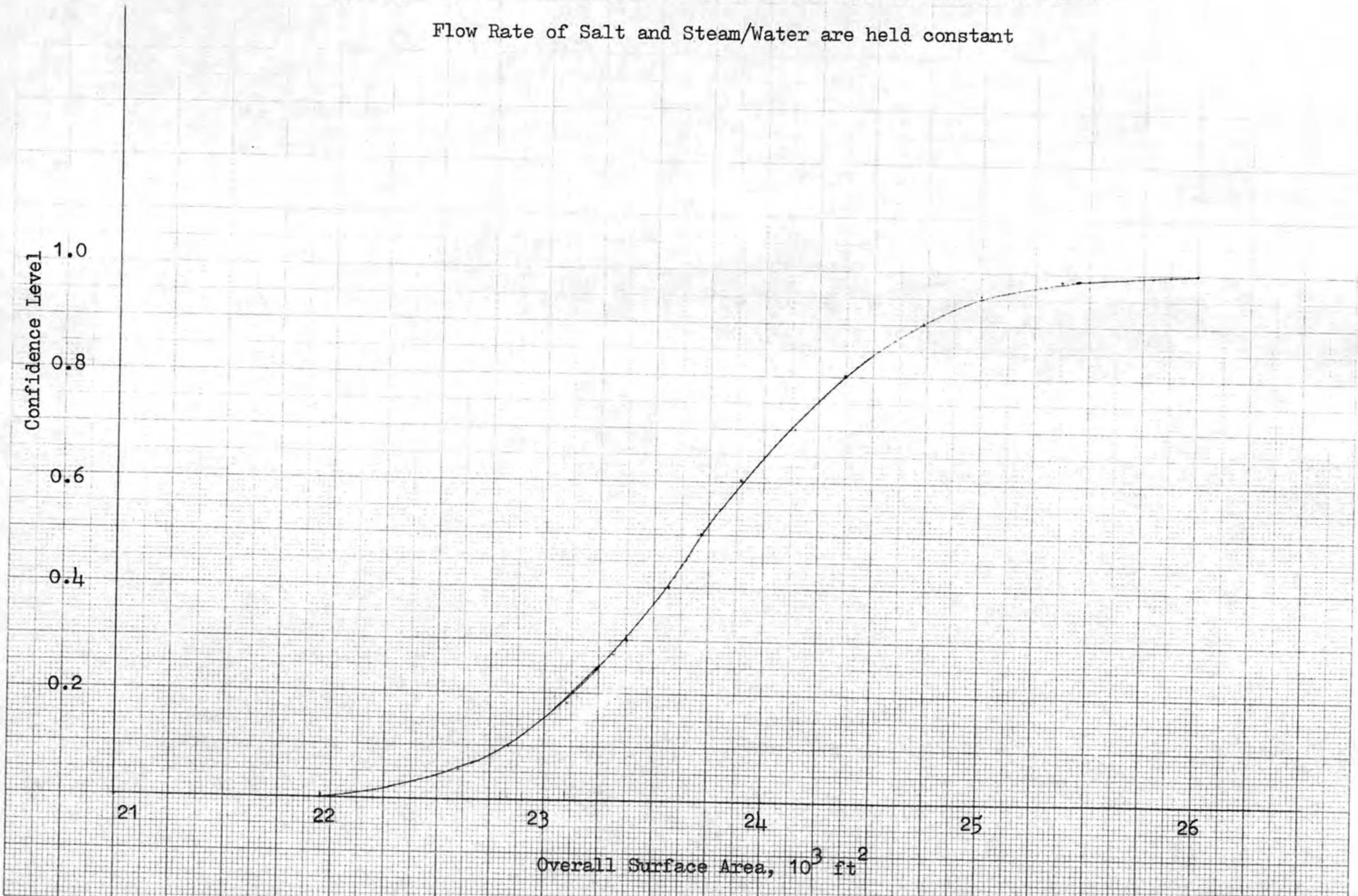

Table 4.2 Summary Statistics for Overall Surface Area of Steam Generator
Each Flow Rate of Salt and Steam/Water entering Unit is Changed

Mean 23762 ft^2

Standard deviation 779

Confidence Level	0.0	0.10	0.20	0.30	0.40	0.50	0.60	0.70	0.80	0.90	1.00
Surface Area, ft^2	21,779	22,789	23,089	23,341	23,568	23,760	23,930	24,147	24,432	24,779	26,611

Fig. 4.3 Overall Surface Area of Steam Generator vs. Confidence Level

Each Flow Rate of Salt and Steam/Water entering Unit is changed

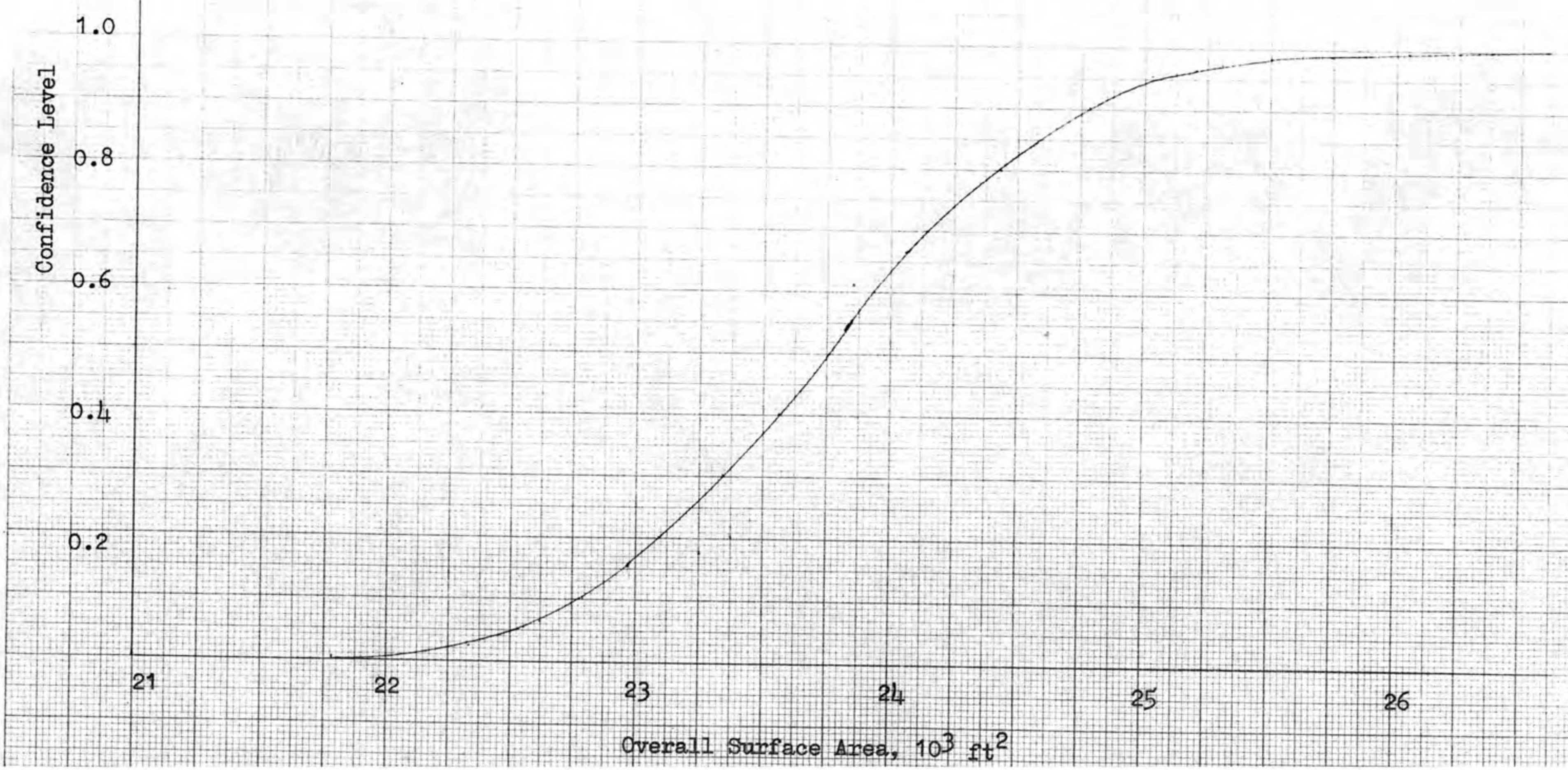

properties.

This detailed performance analysis established the heat transfer surface requirement and pressure drops at full load operating conditions, in accordance with the design criteria (section 4.1.2).

The pressure drops at entrances, exits, tube support plates and vibration suppressors have minor effects on the thermal performance of the steam generator. Temperature and pressure profiles as a function of position in the steam generator for steady state operation at full load are shown in Figures 4.4 to 4.6. The results of the thermal/hydraulic analysis of basic design at full load conditions are also summarized below:

	Salt	Water/Steam
Inlet temperature, ^oF	1150	700
Outlet temperature, ^oF	850.6	1000
Inlet pressure, psia	235	3770.5
Outlet pressure, psia	296	3600
Flow rate, lb/hr	15.28×10^6	2.538×10^6
Mass velocity, lb/hr-ft^2	3.363×10^6	1.999×10^6
Static pressure difference, psi	- 61	+ 170.5
Total net pressure loss, psi	40.2	158.1

Thermal duty = 1.646×10^9 Btu/hr

The pressure drop calculations are presented in Section 4.2.

There are two vent nozzles positioned at each tubesheet-to-shell juncture to vent trapped gases. These vent nozzles will also assist in preventing the salt from freezing at the juncture of the cold leg. The low feedwater temperature of 700^{o}F and stagnation of salt at the corner of cold leg are the possible causes of salt-freezing. For the basic design, the salt temperature at the outside tube surface in the active heat transfer region near the lower tubesheet is about 800^{o}F at full load conditions and is higher than 800^{o}F at part loads. In the stagnant (inactive)

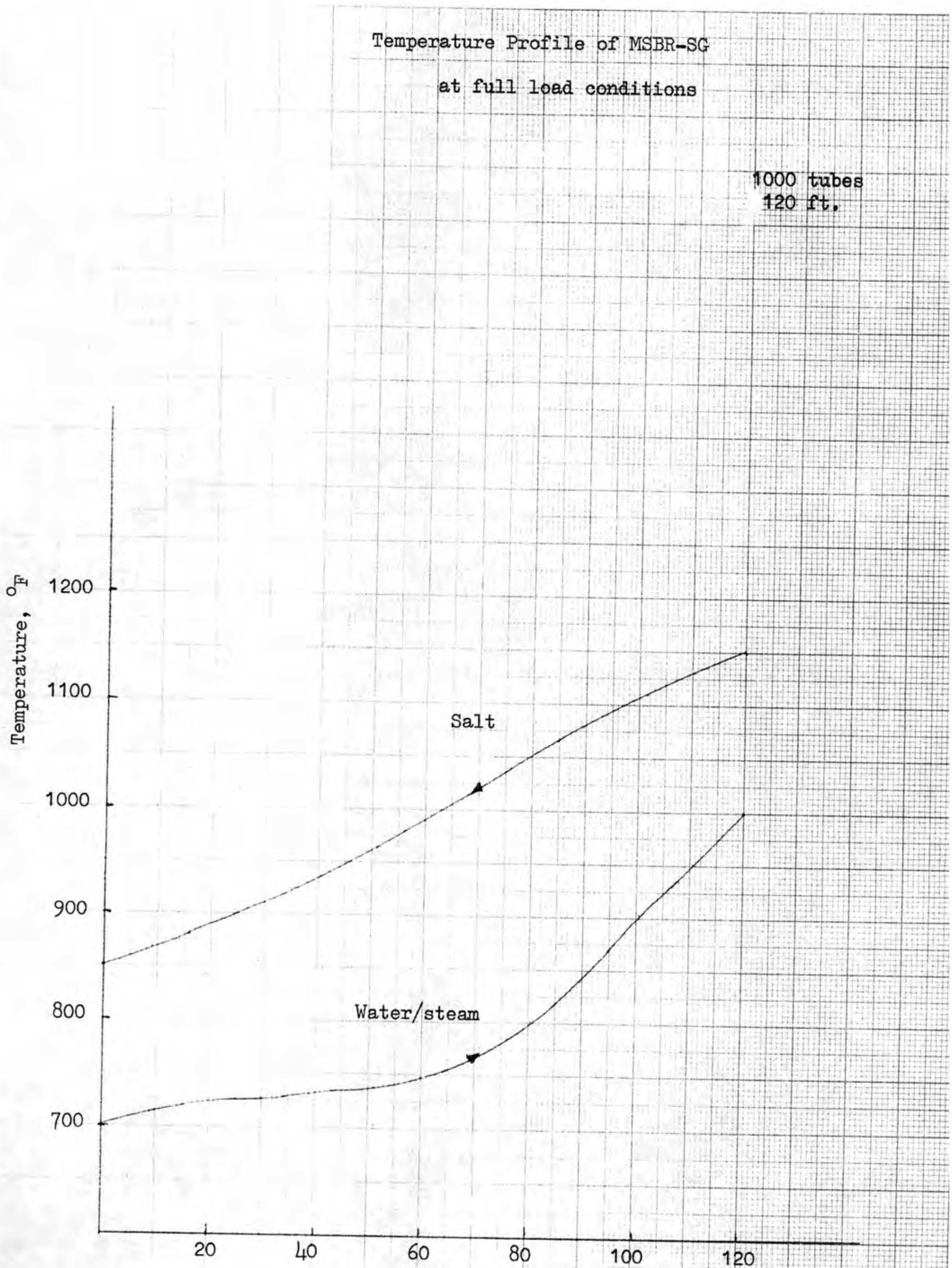
Temperature Profile of MSBR-SG
at full load conditions
1000 tubes
120 ft.
Temperature, °F
1200
1100
1000
900
800
700
Salt
Water/steam
20
40
60
80
100
120
Tube Length from Cold End, ft.

Fig. 4.4

pressure profile of water/steam at full load conditions

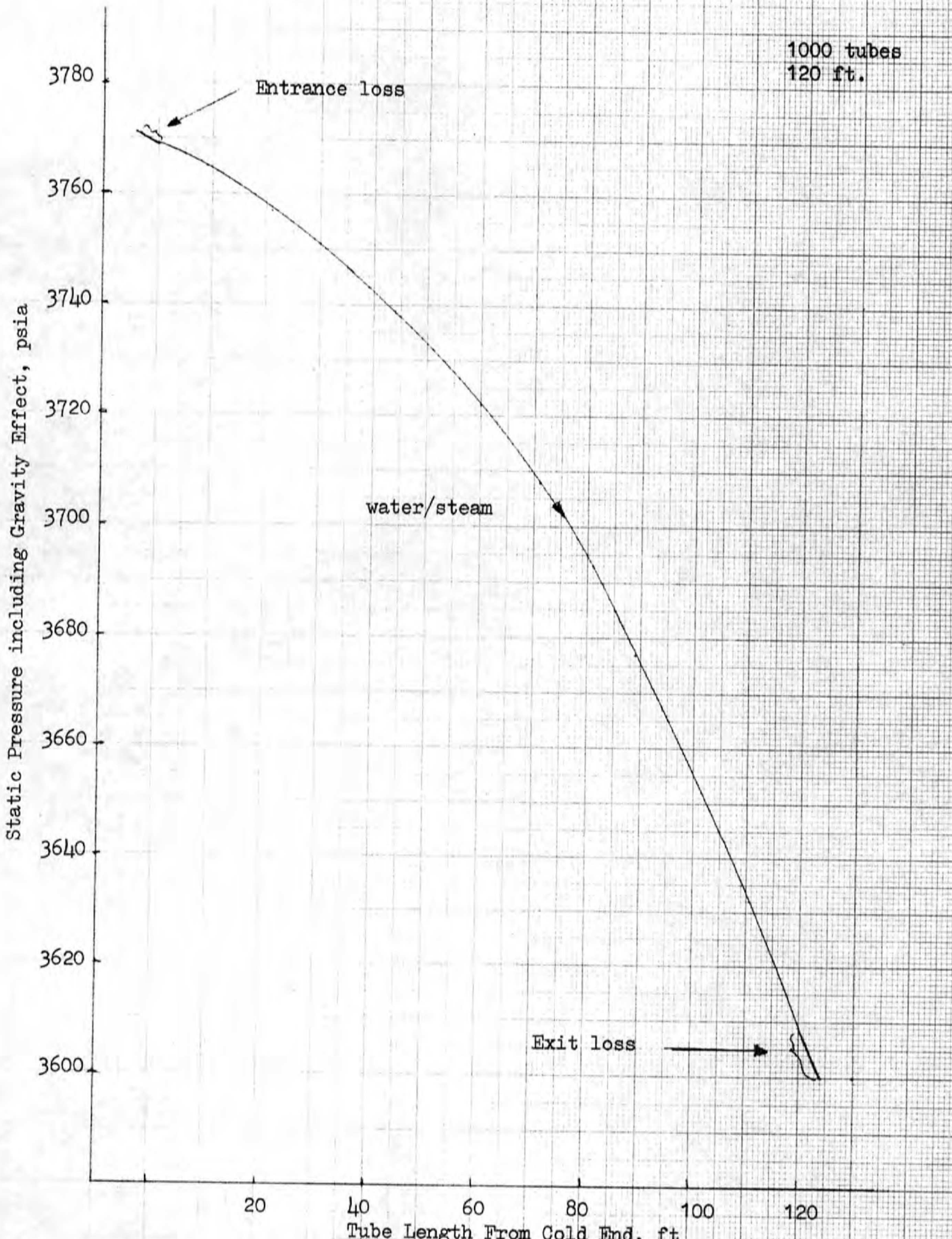

Fig. 4.5

pressure profile of salt at full load conditions

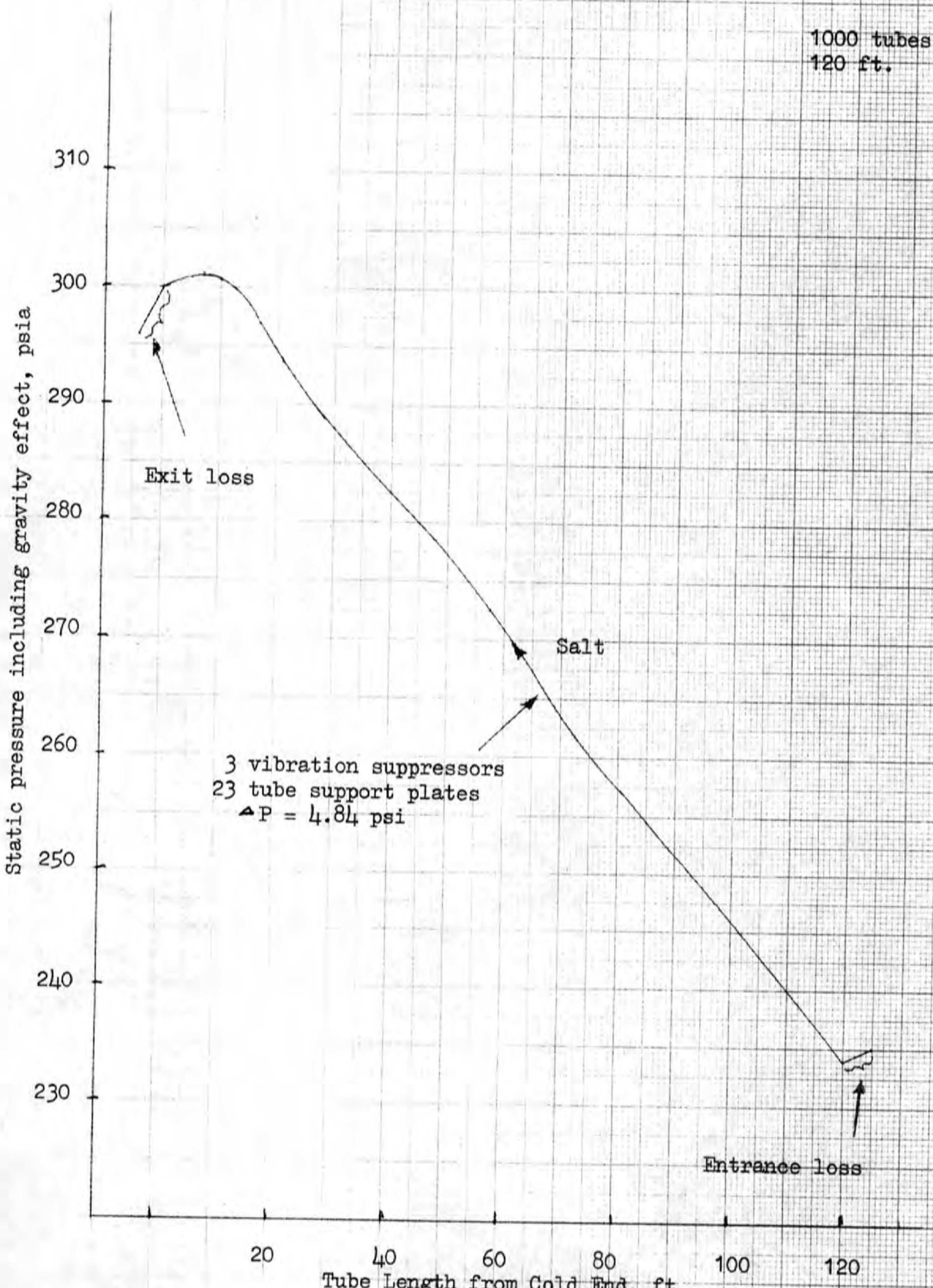

Fig. 4.6

region, the poor heat transfer coefficient on the salt side might create a situation in which the salt-side tube wall temperature could be lowered below the salt freezing point of 725°F. However, the above possibility is remote considering the fact that the steam generator cell of the generating station building is maintained at temperature of 1000°F (Ref. 23) by external heat source. The salt at the tubesheet-to-shell juncture would absorb additional heat through the heat conduction from heated cell to the shell of steam generator. Therefore, the salt temperature near the cold tubesheet would not be below the salt freezing point of 725°F. The vent nozzles will continuously vent out a small amount of salt to keep the salt always in motion (also for higher heat transfer coefficient) instead of stagnant in this region. From the preceding discussions, the unit will be free from a salt freezing problem. Detailed analysis was not undertaken of this problem in the present study but should be a part of future studies.

4.1.4 PART LOAD PERFORMANCE

Partial load operation is defined as any condition between 20 and 100% of full load thermal duty. The operation from zero to 20% load is designated as startup operation.

Two major limitations, of high priority, when the plant undergoes changes in load are: (a) turbine throttle temperature to be held at 1000°F due to turbine limitations, and (b) the coolant salt temperature at steam generator outlet and fuel salt temperature at reactor inlet to be held above the salt freezing points of 725 and 930°F, respectively, at all loads. The primary fuel salt system will operate at constant flow rate and constant reactor inlet temperature of 1050°F, with the reactor outlet temperature controlled as a function of load. It was found that variation of secondary coolant salt flow would be necessary to maintain the fuel salt reactor inlet temperature sufficiently above its freezing point during part load operations. If the coolant salt decreases linearly with load, the reduced coolant salt flow rate would decrease the coolant salt temperature at the steam generator outlet excessively with the danger of being lower than freezing point (Ref. 10). However, if the reduction of the coolant salt flow is less than the reduction of load (percentagewise), there is a chance that the steam outlet temperature might exceed the limitation of 1000°F. This indicates the difficulties of control during the part load operations.

FWC FORM 172 - 4
NOTATIONS IN THIS COLUMN INDICATE WHERE CHANGES HAVE BEEN MADE

Two principal methods for control of part load operation are (1) Varying the coolant salt flow with the flow reduction less than the load reduction (percentagewise) and thus allowing the steam outlet temperature to exceed above the 1000°F design point, with subsequent attemperation of the steam temperature with injected feedwater, (2) Varying the coolant salt flow as method 1 and using a salt throttle valve to bypass some of the coolant salt flow around the primary heat exchanger (from cold to hot legs) to reduce the temperature of the salt entering the steam generator (thus reduce the steam outlet temperature) while keeping coolant salt temperature leaving the steam generator above its full load value of 850°F. These two methods are discussed in detail in the following.

4.1.4.1 METHOD 1

Coolant salt flow was varied linearly from 30% flow at 20% thermal load to 100% flow at 100% load. The associated inlet and outlet temperatures of coolant salt are tabulated in Table 4.3 (Ref. 3). The steam inlet temperature was held constant at 700°F, while the steam flow varied in proportion to load (slight deviation from linearity exists due to water bypass for the attemperator). The steam outlet temperature was allowed to rise above 1,000°F at part loads and was subsequently attemperated with the bypassed feedwater at conditions of 700°F and 3700 psia to maintain 1,000°F turbine inlet temperature.

The results presented in Figures 4.7 to 4.13 indicate that this method is satisfactory. Figure 4.7 shows the uncontrolled and attemperated final steam temperatures versus percent of full load. Figure 4.8 shows the amount of attemperator flow versus percent load. Figure 4.9 shows the amount of salt and water flow rates entering the unit versus percent of full load. Figures 4.10 to 4.13 show the temperature and pressure profiles of salt and water/steam at part loads.

4.1.4.1.1 FEASIBILITY OF USING A SPRAY ATTEMPORATOR AT THE OUTLET OF THE STEAM GENERATOR

It has been Foster Wheeler's experience that utilities do not prefer to use spray attemporation between the final stage of superheat and the turbine. However, such an arrangement is accepted only when there is one stage of superheat.

It has been standard practice at Foster Wheeler that, for large fossil-fired steam generators, two spray attemporator locations are provided between stages of superheat. This arrangement allows the superheaters to be designed with lower alloy steels and lower metal temperatures. Also, this arrangement provides rapid steam temperature control over a wide load range since the steam travel time between point of spraying and point where the temperature is being controlled (the other side of a stage of superheat) is small.

With the present reference design, there are two possible locations for a spray attemporator; (1) at the inlet of the steam generator and (2) at the outlet of the steam generator placing an attemporator at the inlet of the steam generator is not recommended because it would increase the probability of salt freezing at the cold end of the steam generator where the higher pressure (above 3800 psi), colder (below 700°F) water would result.

Locating a spray attemporator at the outlet of the steam generator is quite practical. The inlet feedwater can then be used as a source of spray water with proper pressure head and temperature for this application. The calculations using this approach that are reported herein indicate that the spray flow quantities that would be required over the load range are reasonable and in line with values required on fossil fired steam generator.

It is noted that the change of moisture carry-over to the turbine that could damage the high pressure stages does not exist because of high steam temperatures (1000°F and above) and supercritical pressures (above 3600 psi). Another factor aiding this situation is the long length of piping that will undoubtedly be required between the steam generators and the turbine.

4.1.4.2 METHOD 2

Partial decoupling of the secondary coolant salt loop from the primary fuel salt loop could be accomplished by short-circuiting a fraction of the coolant salt around the primary heat exchanger. This would require a throttling device which is not presently developed. The present steam generator design is not based on this scheme, however, this method would provide useful information for control study.

In this study, the steam inlet and outlet temperatures were held constant at 700 and 1000°F, respectively, during part load operations for which steam flow rate changes linearly with load. The salt flow rate and salt inlet temperature which would maintain the salt outlet temperature at 850°F ± 15° were to be determined.

Table 4.3 Coolant Salt Temperatures and Coolant Salt flow with Varying load.

Load, %	Flow, %	Salt inlet Temperature, °F	Salt outlet Temperature, °F
100	100.00	1150	850
90	91.25	1147	851
80	82.50	1144	853
70	73.75	1139	855
60	65.00	1134	857
50	56.25	1127	860
40	47.50	1117	865
30	38.75	1106	874
20	30.00	1091	891

Base on ORNL Reference Design Heat Exchanger and operation of the fuel salt system at constant reactor inlet temperature of 1050°F.

Uncontrolled and attemperated steam outlet temperatures versus percent load

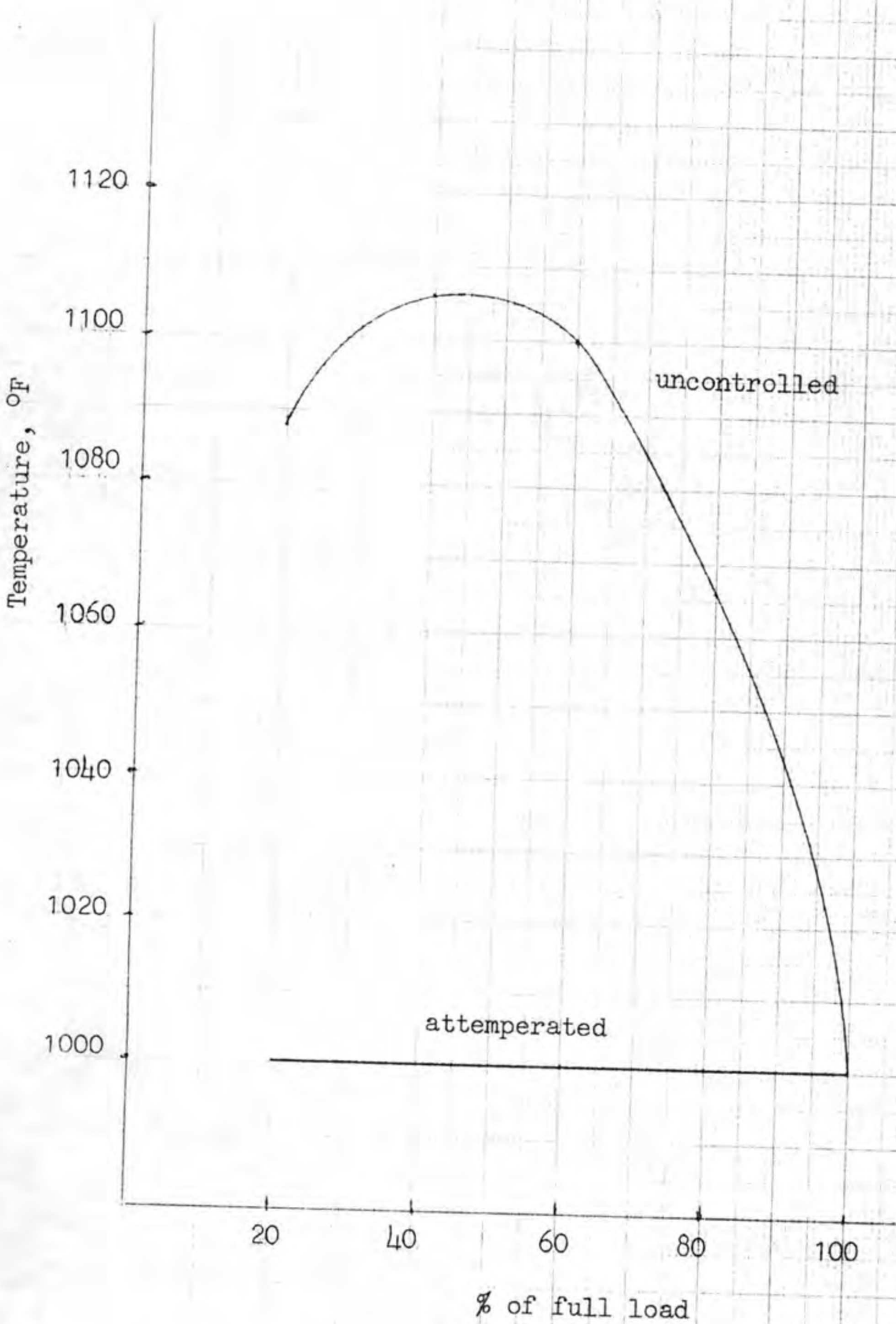

Fig. 4.7

Amount of attemperator flow versus percent load

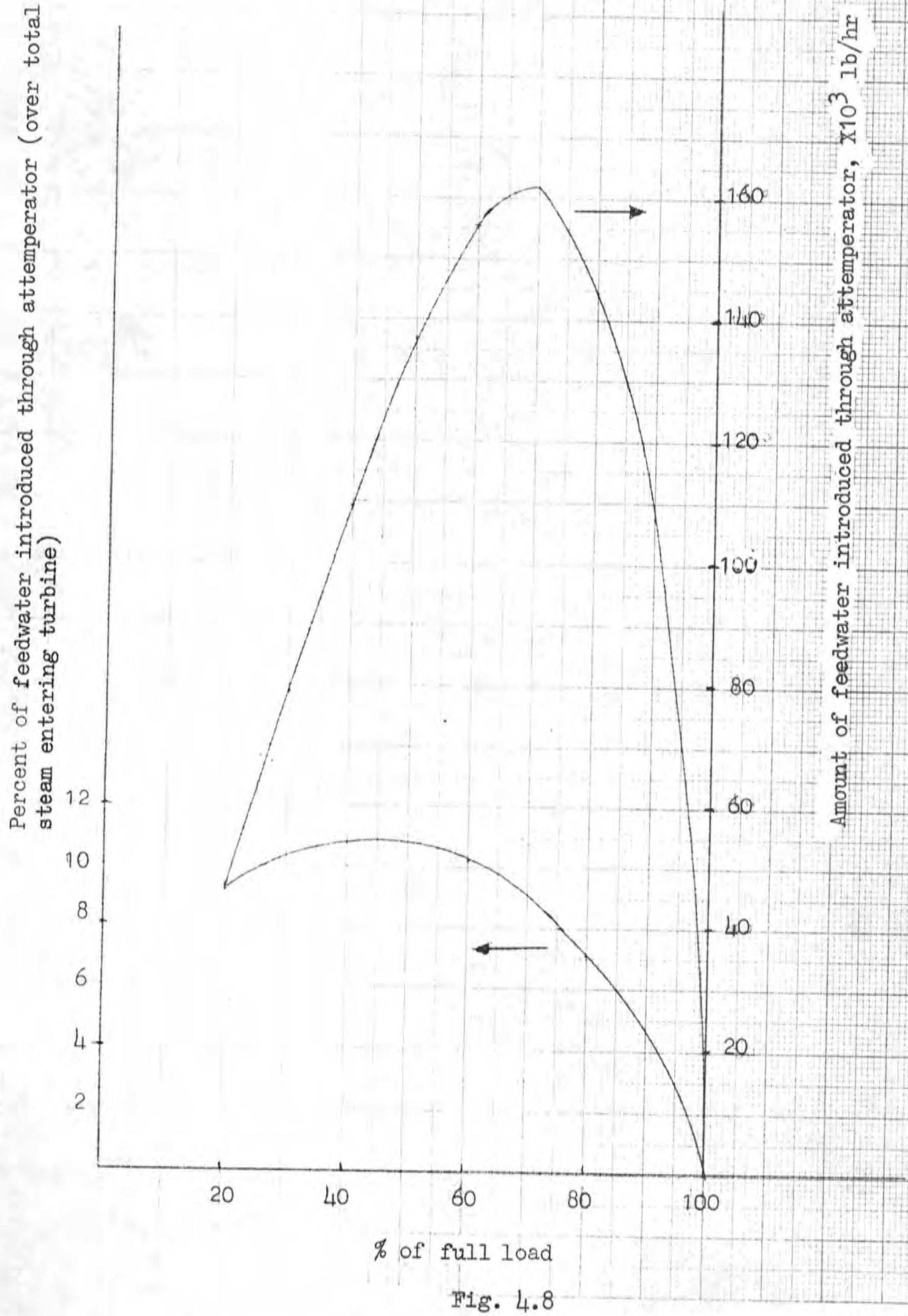

Fig. 4.8

Amount of salt and water/steam entering steam generator versus percent of full load

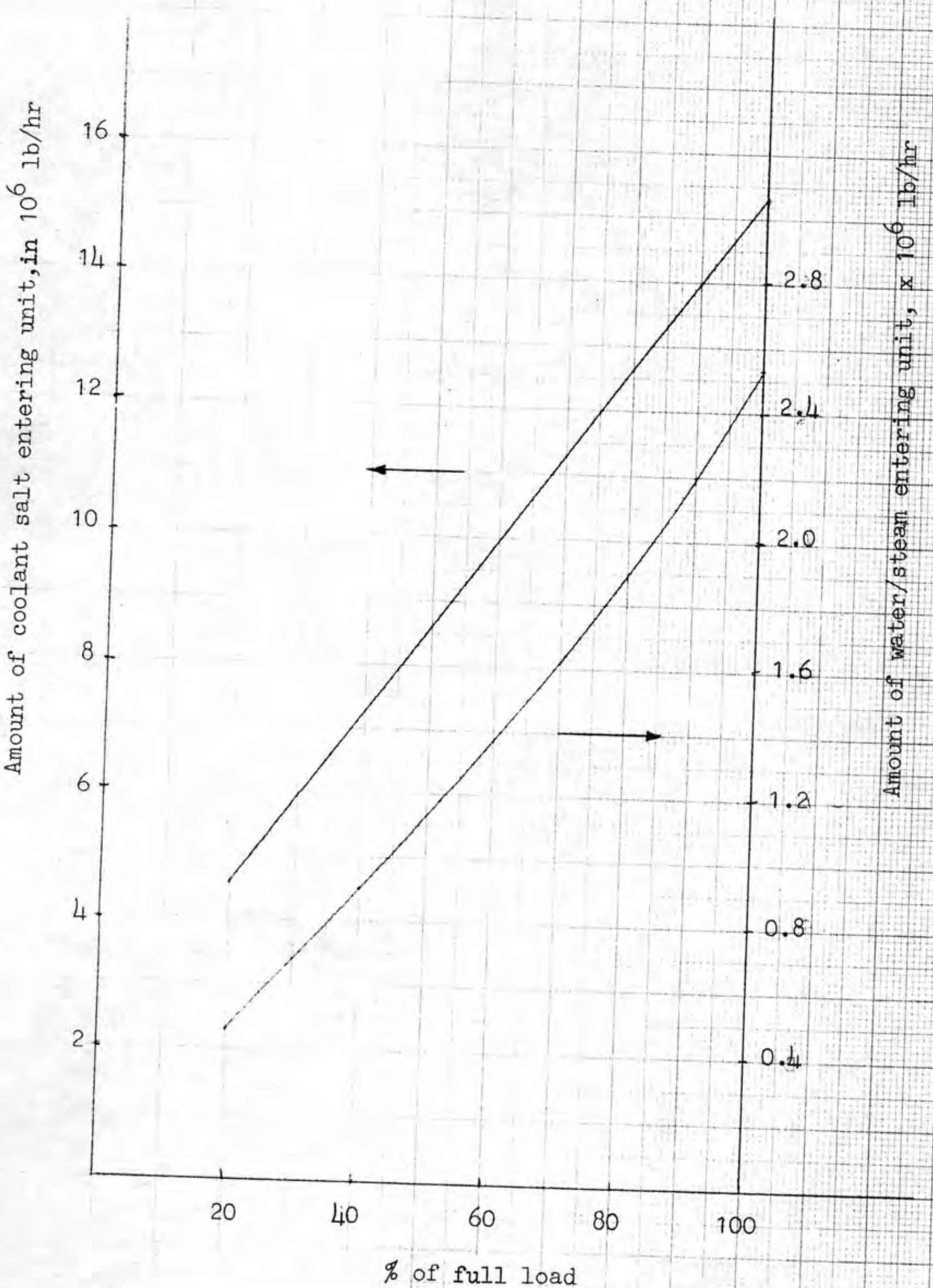

Fig. 4.9

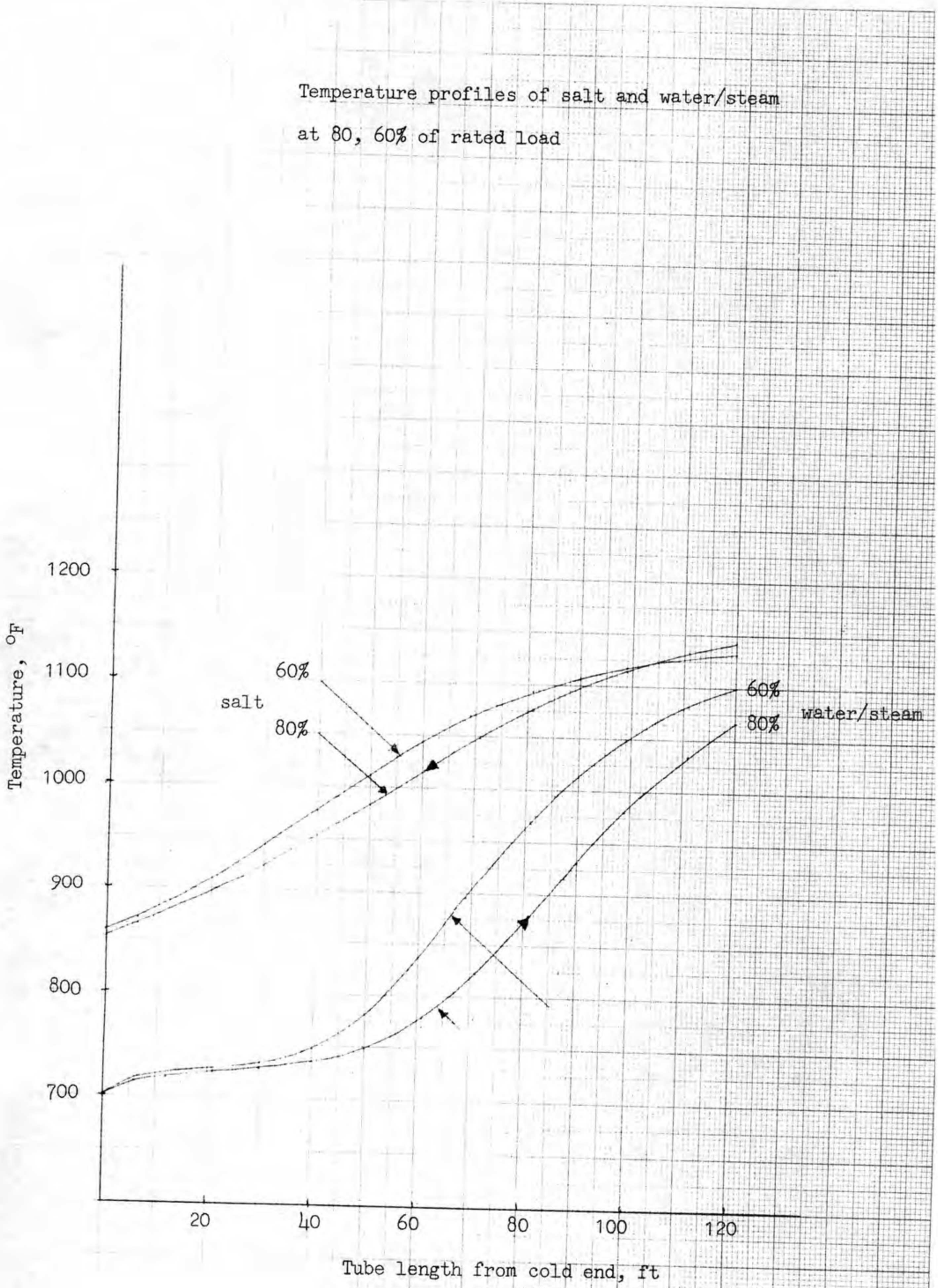

Temperature profiles of salt and water/steam
at 80, 60% of rated load
Temperature, °F
1200
1100
1000
900
800
700
salt
60%
80%
60%
80%
water/steam
20
40
60
80
100
120
Tube length from cold end, ft

Fig. 4.10

Temperature profiles of salt and water/steam

at 40, 20% of rated load

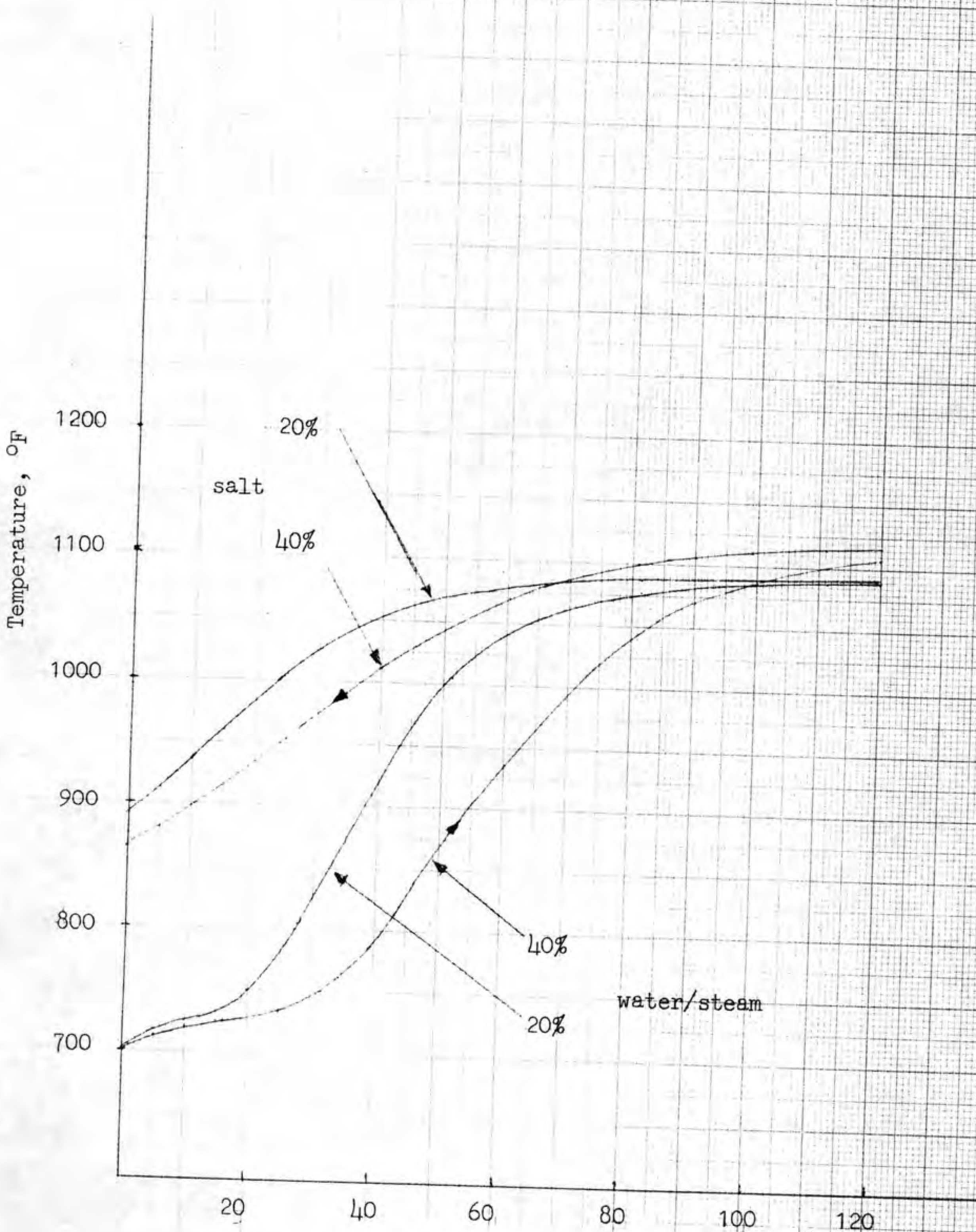

Fig. 4.11

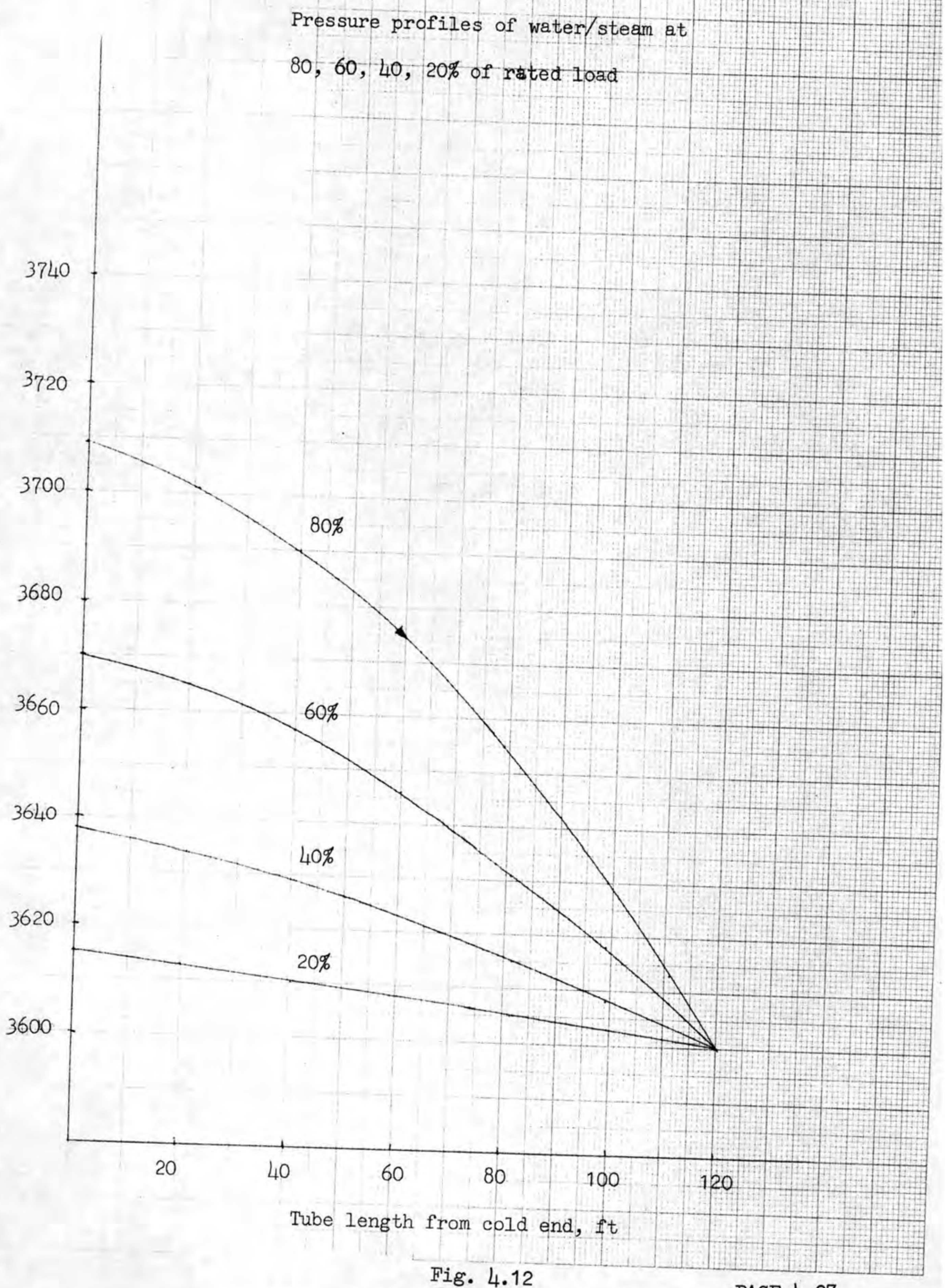
Pressure profiles of water/steam at
80, 60, 40, 20% of rated load
3740
3720
3700
3680
3660
3640
3620
3600
80%
60%
40%
20%
20
40
60
80
100
120
Tube length from cold end, ft

Fig. 4.12

Pressure profiles of salt at 80, 60, 40, 20% of rated load

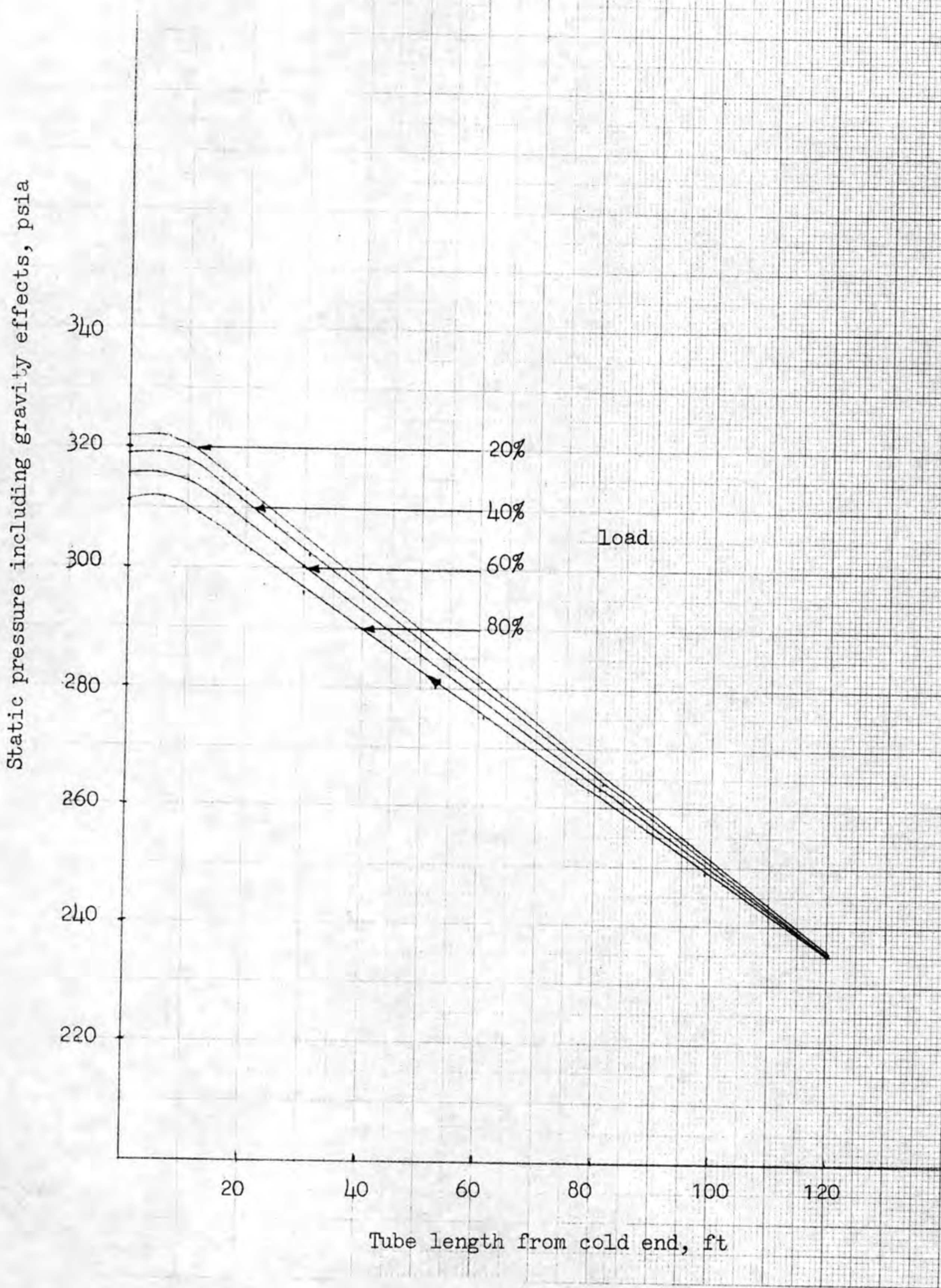

Fig. 4.13

Therefore, for each salt outlet temperature of 835, 850, 865°F, the salt flow rate and salt inlet temperature were computed throughout the range of 20 to 110% of rated load.

The results are summarized in Table 4.4 and plotted in Fig. 4.14 and Fig. 4.15. The constant salt inlet temperature lines presented in Fig. 4.15 were generated from Table 4.4 by using a third order interpolation routine to provide valuable overall information for control analysis. Fig. 4.15, shows that for a part load range of about 64 to 97%, with coolant salt inlet temperature from 1040 to 1140°F, the steam generator would demand more than 100% of coolant salt at full load to maintain the coolant salt outlet temperature above its full load value of 850°F. Therefore this method does not appear to be attractive from a control standpoint.

4.2 PRESSURE DROP CALCULATIONS

The performance computer program used in sizing the steam generator basic design surface requirement also calculated the shell and tube side pressure drops between two tubesheets, which included the effects of elevation head and velocity head, and head losses due to friction and fluid acceleration. The pressure drops between inlet/outlet nozzles, tube support plates and the active heat transfer region were added to estimate the nozzle-to-nozzle overall pressure differences for both shell and tube side fluids.

4.2.1 STEAM/WATER SIDE PRESSURE DROP

The absolute roughness, 0.00006 ft, and minimum inside diameter of tube, 0.4825", were used for tube side pressure drop calculation. Since the flow is in turbulent region ($Re = 1.9 \times 10^7$ to 1.0×10^6), the friction factor was calculated by the Colebrook-White semiemperical formula (Ref. 11) which is expressed as:

$$\frac{1}{\sqrt{f}} + 2 \log\left(\frac{k_s}{D}\right) = 1.14 - 2 \log\left(1 + 9.35 \frac{D}{Re \sqrt{f}\, K_s}\right)$$

where
- f: friction factor
- K_s: absolute roughness, ft
- D: inside diameter of tube, ft
- Re: Reynold number

FWC FORM 172 - 4 — NOTATIONS IN THIS COLUMN INDICATE WHERE CHANGES HAVE BEEN MADE

Table 4.4 Part Load Performance - Method II
Salt Flow Rate and Salt Inlet Temperature

Salt Outlet Temperature, °F	Salt Inlet Temperature °F	Salt Flow Rate, %	Load, %
835°F	1001.8	35.60	19.81
	1005.9	52.18	29.74
	1013.8	66.58	39.68
	1026.3	77.84	49.64
	1045.2	85.08	59.63
	1071.0	88.55	69.64
	1104.1	88.83	79.67
	1145.6	86.69	89.72
	1193.2	83.55	99.78
850°F	1001.3	39.28	19.81
	1004.2	57.86	29.74
	1009.7	74.51	39.68
	1019.1	88.00	49.64
	1033.3	97.57	59.64
	1053.3	102.64	69.64
	1079.8	104.02	79.68
	1113.0	102.39	89.74
	1152.6	98.91	99.81
865°F	1000.9	43.74	19.81
	1002.9	64.69	29.74
	1007.0	83.85	39.69
	1014.1	99.92	49.65
	1025.0	111.87	59.65
	1040.5	119.04	69.66
	1061.6	121.62	79.70
	1088.4	120.50	89.76
	1121.5	116.77	99.85
	1160.2	111.75	109.97

Steam inlet temp. = 700°F

Steam outlet temp. = 1000°F

Steam flow rate = changes linearly with load

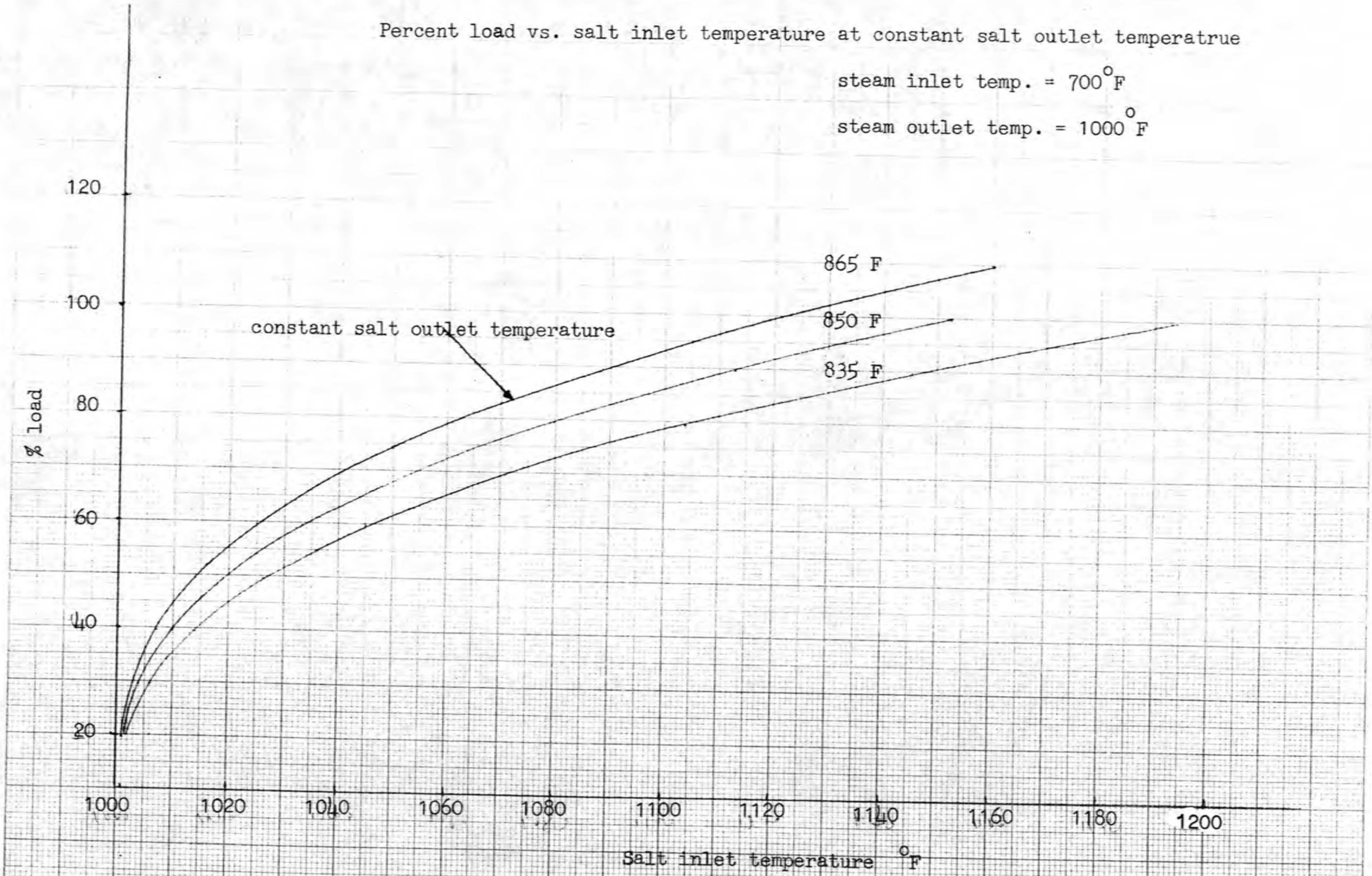

Percent load vs. salt inlet temperature at constant salt outlet temperatrue
steam inlet temp. = 700°F
steam outlet temp. = 1000°F
865 F
850 F
835 F
constant salt outlet temperature
% load
120
100
80
60
40
20
1000
1020
1040
1060
1080
1100
1120
1140
1160
1180
1200
Salt inlet temperature °F

Fig. 4.14

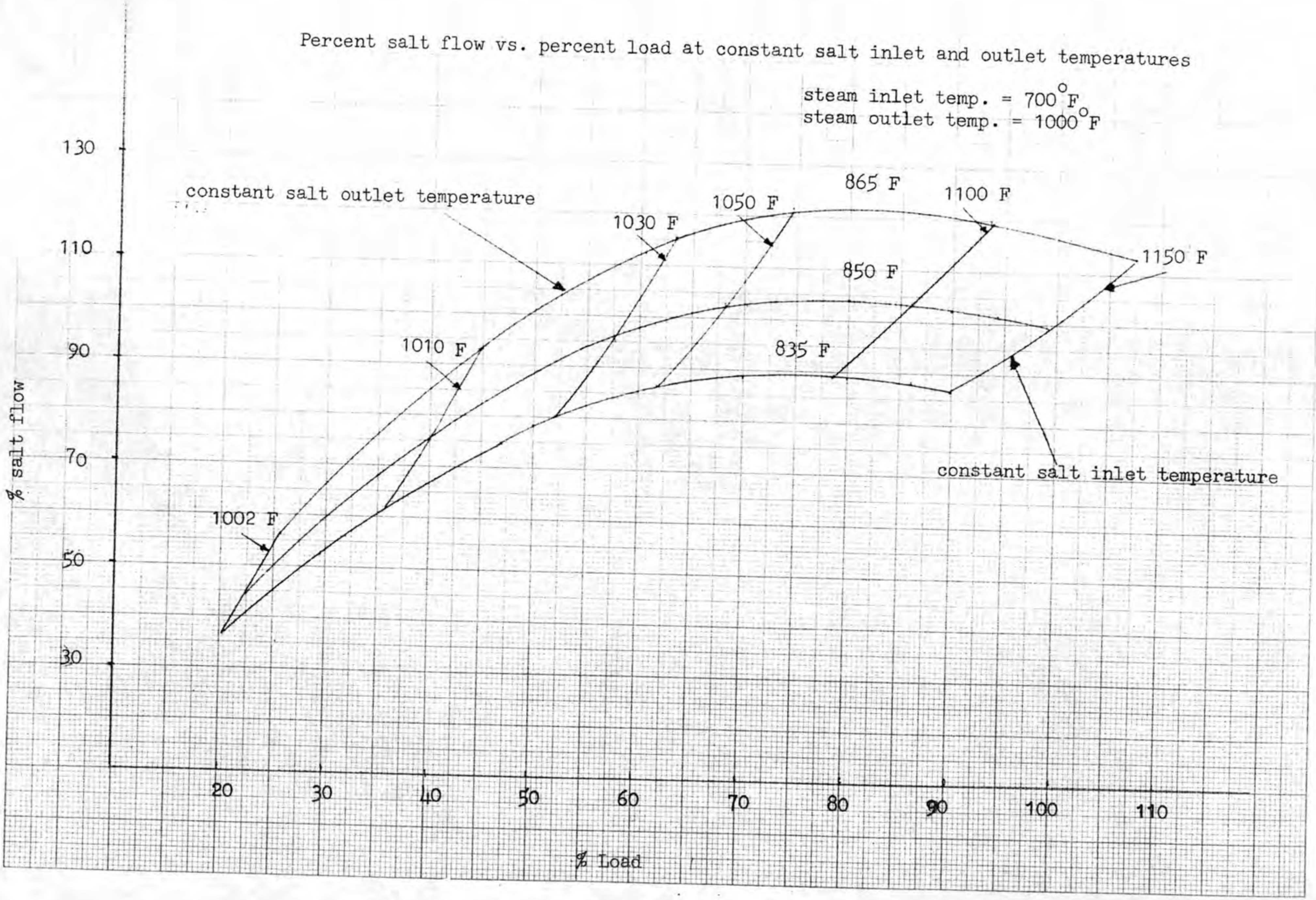
Percent salt flow vs. percent load at constant salt inlet and outlet temperatures
steam inlet temp. = 700°F
steam outlet temp. = 1000°F
constant salt outlet temperature
constant salt inlet temperature
1002 F
1010 F
1030 F
1050 F
865 F
1100 F
1150 F
850 F
835 F
% salt flow
% Load
130
110
90
70
50
30
20
30
40
50
60
70
80
90
100
110

The pressure losses occurred between the inlet nozzle and the lower tubesheet, and between the upper tubesheet and the exit nozzle were calculated per FWEC fluid flow formulas (Ref. 12). The results are summarized in Table 4.5, with hand calculations attached in Appendix B. Pressure profiles of steam generator at full and part loads are also presented in Section 4.1.4.

4.2.2 SALT SIDE PRESSURE DROP

There are 23 tube support plates in vertical and horizontal portions, three vibration suppressors in bend region, one shroud in inlet region and four shrouds in outlet region. The pressure drops occurred at nozzles, shrouds, tube support plates and vibration suppressors were hand-calculated per FWEC Standard Manual (Ref. 12). These values were added to the pressure drops calculated by the active heat transfer region performance code. The results are summarized in Table 4.6. Hand-calculations are attached in Appendix B.

The Colebrook-White formula was used for friction factor calculation. Unit pressure profiles in shell side are shown in Section 4.1.3 and 4.1.4.

4.3 STABILITY

Historically, the early studies of flow instability were developed from operational difficulties with fossil-fired boilers. A number of boiler-tube failures and thermal performance degradation were attributed to water/steam flow instability. Units designed in supercritical pressure region also suffered the same problem as well as in the subcritical region.

In boiling systems, fluctuations are always present because of variations of the rate of bubble formation and population, of flow regimes, of the heat transfer coefficient, etc. Consequently these fluctuations may induce the flow instabilities. In the supercritical region, rapid changes of thermophysical properties are observed in the vicinity of the critical point. The propagations of variations of properties, in particular of the density and of the enthalpy, through the system introduce time and space lags of transformation which under certain conditions can cause unstable flow.

Two major classifications of unstable phenomena are defined as static and dynamic instabilities. Both of them could be analyzed by conservation equations of mass, momentum, energy and the

Table 4.5 Steam-side Pressure and pressure drops

Load	Entrance P. psia	ΔP at nozzle, tubesheet, psi	P. leaving tubesheet, psia	ΔP between tubesheets, psi	P. entering tubesheet, psia	ΔP at nozzle, tubesheet, psi	Exit P. psia
100	3770.5	1.6	3768.9	160	3608.9	8.9	3600
80	3715.5	1.1	3714.4	109	3605.4	5.4	3600
60	3673.7	0.6	3673.1	70	3603.1	3.1	3600
40	3639.7	0.3	3639.4	38	3601.4	1.4	3600
20	3615.5	0.1	3615.4	15	3600.4	0.4	3600

BY
APPROVED

CHARGE NO. 8-25-2431
DOCUMENT NO. ND/74/66
ISSUE 1
DATE 12/16/74

NUCLEAR DEPARTMENT
FOSTER WHEELER ENERGY CORPORATION
LIVINGSTON, N. J.

Table 4.6 Salt-side pressure and pressure drops

Load	Entrance P. psia	ΔP at nozzle, shroud, psi	P entering tube bundle, psi	ΔP at tube support plates, psi	ΔP at tube bundle, psi	P leaving tube bundle, psia	ΔP at shroud, nozzle, psi	Exit P psia
100	235	1.1	233.9	4.8	-70.8	299.9	3.8	296.1
80	235	0.7	234.3	3.3	-76.2	307.2	2.4	304.8
60	235	0.5	234.5	2.1	-80.4	312.9	1.4	311.5
40	235	0.3	234.7	1.1	-84	317.6	0.6	317.0
20	235	0.1	234.9	0.4	-87	321.5	0.2	321.3

proper equation of state. Static instability lies in the steady-state laws, while dynamic instability is time-variant phenomena.

Zuber (Ref. 13) described three mechanisms which could induce thermohydraulic oscillations at supercritical pressure. One is caused by the variation of the heat transfer coefficient at the pseudo critical point, which is defined as the point where C_p reaches its maximum value. The second is caused by the effects of large compressibility and the resultant low velocity of sound in the critical region. The third mechanism is caused by the large variation of flow brought about by density variations of the fluid during the heating process.

Both static and dynamic stabilities for the present steam generator are discussed in detail in the following sections.

4.3.1 STATIC STABILITY

4.3.1.1 INTRODUCTION

Static instability is an amplification of steady state disturbances which encompass tube circuit configuration, heating imbalances, flow rate perturbations, etc. The static instability of primary design importance in steam generators is the excursive instability, which at supercritical pressure, is the equivalent of the "Ledinegg" excursive instability in boiling steam at subcritical pressures. A flow is subjected to a static instability when the flow conditions, changed by a small perturbation, will not return to original steady state conditions (Ref 17).

The significance of the static stability is best analyzed by plotting the pressure drop-flow characteristic as schematically shown in Fig. 4.16. A system of many parallel heated tubes is considered with attention focused on only one tube where various levels of heat input are allowed. The quantity of heat input depends qualitatively on the situation of heating medium distribution among the heated tubes. Demand curves Q1, Q2, and Q3 denote increased levels of heating medium quantity surrounding the concerned heated tube. A constant inlet-to-outlet pressure difference is imposed as indicated by the horizontal line H. Intersections with curve Q1 showing the possible operating points for a constant pressure drop supply system (or any pump characteristics) are indicated by C, D or E. Operation at point D or E will be stable whereas that at point C will be unstable. For example, if at point either D or E the flow is perturbated to increase (decrease), the pressure drop of the heated tube increases (decreases), i.e., the demand of the system is larger (less) than the external supply, and consequently the flow will return to its original value. However, if the flow is perturbated to increase (decrease) at point C, the external system supplies more (less) than that required to maintain the flow. Consequently the flow rate will increase (decrease) until the new operating point E (D) is reached. Therefore, the shape of curve Q1, especially at point C, as shown in Fig. 4.6 should be avoided to insure static stability within the possible range of load operations (Ref. 21). Figure 4.16 also explains the sensitivity of flow maldistribution in the same system. For the sake of argument, assume the operating point is at E. With an increase in heating medium flow around the local tube to Q2, the flow decreases monotonically to point A. Purturbations in any of the system variables can cause a flow excursion or rapid deceleration to a stable point B. Further increase in heating medium surrounding the tube to Q3 results in operation at point F. Therefore, the heating imbalance among circuits will induce flow maldistribution in a system of many parallel heated tubes (Ref. 18).

Another phenomenon which should be considered is the potential of flow reversal (Ref. 18). In a long, vertically-oriented unit, the large hydrostatic head of the steam column may lead to flow reversal. This can occur when the difference in hydraulic heads between two parallel downflow tubes exceed the friction pressure drop. It has been recognized that a superheater with heated downcomers undergoes a potentially critical period during start-up, because at initial low flow the friction pressure drop may be less than the hydrostatic head (Ref. 20). However, the static head can be an important factor in stabilizing upward flow.

4.3.1.2 ANALYSIS METHOD

For a constant pressure drop supply system, the preceding introduction leads to the statement that the operating point is stable if the derivative of the pressure drop - flowrate curve is positive. The mathematical form is (Ref. 22)

$$\frac{\delta \Delta P}{\delta W} > 0$$

where W = flow rate lb/hr.
P = pressure drop psi

This criterion for the flow excursion stability is well known and the prediction techniques have been developed which are based on the solution of the steady-state conservation equations for mass, momentum, energy and the equation of state.

The static stability aspect of the reference design steam generator was analyzed for conditions at 100, 60 and 20% load. At each load, the water/steam and molten salt inlet conditions were kept constant and the flow rate of water/steam was perturbed. The effect of flow maldistribution of molten salt, resulting in the variations of the heat input to the individual tube, was also considered. This investigated the flow sensitivity of water/steam flow maldistribution in a system of parallel heated tubes. The thermal hydraulic performance computer code and the "Steam and Water Pressure Drop Computer Program" (Ref. 14) were used to generate pressure drop-flow characteristics for each load. The potential of flow reversal was also examined. For the calculations of part-load conditions, Method 1 of Section 4.1.4.1 was applied.

4.3.1.3 RESULTS AND DISCUSSION

The results of static stability analysis are presented in Figures 4.17 to 4.20. Used in these figures is the relative flow rate which is the ratio of flow rate under perturbation to that at normal operating condition of a specified load. Curve Q denotes the condition of molten salt surrounding a local tube under the normal flow distribution condition, and curves Q+ and Q- denote the 110% and 90% of the normal molten salt distribution surrounding the tube under consideration respectively. Pressure drop was defined by calculating the pressure difference from normal water/steam inlet (bottom) to outlet (top) plenums regardless of the flow direction. Fig. 4.20 is a continuation of Fig. 4.19, (20% load) to show the peak ΔP of 0.58 psi for the curve Q- of the reverse flow.

4.3.1.4 CONCLUSIONS

Based on the comparison of results with criteria of inception of static instability, the analysis leads to the conclusion that the reference design steam generator is statically stable.

The static stability is insured for the slopes of all the curves are positive ($\delta \Delta P / \delta W > 0$). These curves also indicate the unit is insensitive to the flow maldistribution among the parallel circuits. The onset of flow reversal is limited to very small pressure difference of 0.58 psi (Fig. 4.20). This possiblity may not exist due to the fact that the external pressure supply system is expected to practically always be operating at a much higher range.

4.3.2 DYNAMIC STABILITY

The dynamic stability work was performed by Gulf General Atomic in 1972 under a contract to FWC. The GGA report Ref (15) in its original form is presented in the Appendix B for further reference. An abstract of the GGA report is presented here.

4.3.2.1 INTRODUCTION

Dynamic instability encompasses the possibility of small density perturbations in the steam producing sustained and growing disturbances within the steam generator. In this regard, density wave perturbations are analagous to the velocity perturbations in incompressible flow which can give rise to sustained flow disturbances and eventually produce a transition from laminar to turbulent flow. Since the compressible flow of the steam is already turbulent, unstable density wave perturbations will not lead to a flow transition but will lead to other undesirable effects such as mechanical vibration or thermal cycling of the tubes. Because the perturbations and possible instabilities are time variant phenomena, the instability is classified as dynamic as opposed to static instability.

4.3.2.2 ANALYSIS METHOD

The steam generator for the Molten-Salt Breeder Reactor has been analyzed at approximately 100, 80, 60, 40 and 20 percent of the rated load.

For this investigation an existing code, DYNAM, was modified to permit analysis of the dynamic stability characteristics in the supercritical region. The DYNAM code is based on a method in which the governing equations are derived from conservation principles for mass, momentum, and energy. These time-dependent equations, simplified by considering a single spatial coordinate along the tube axis, are

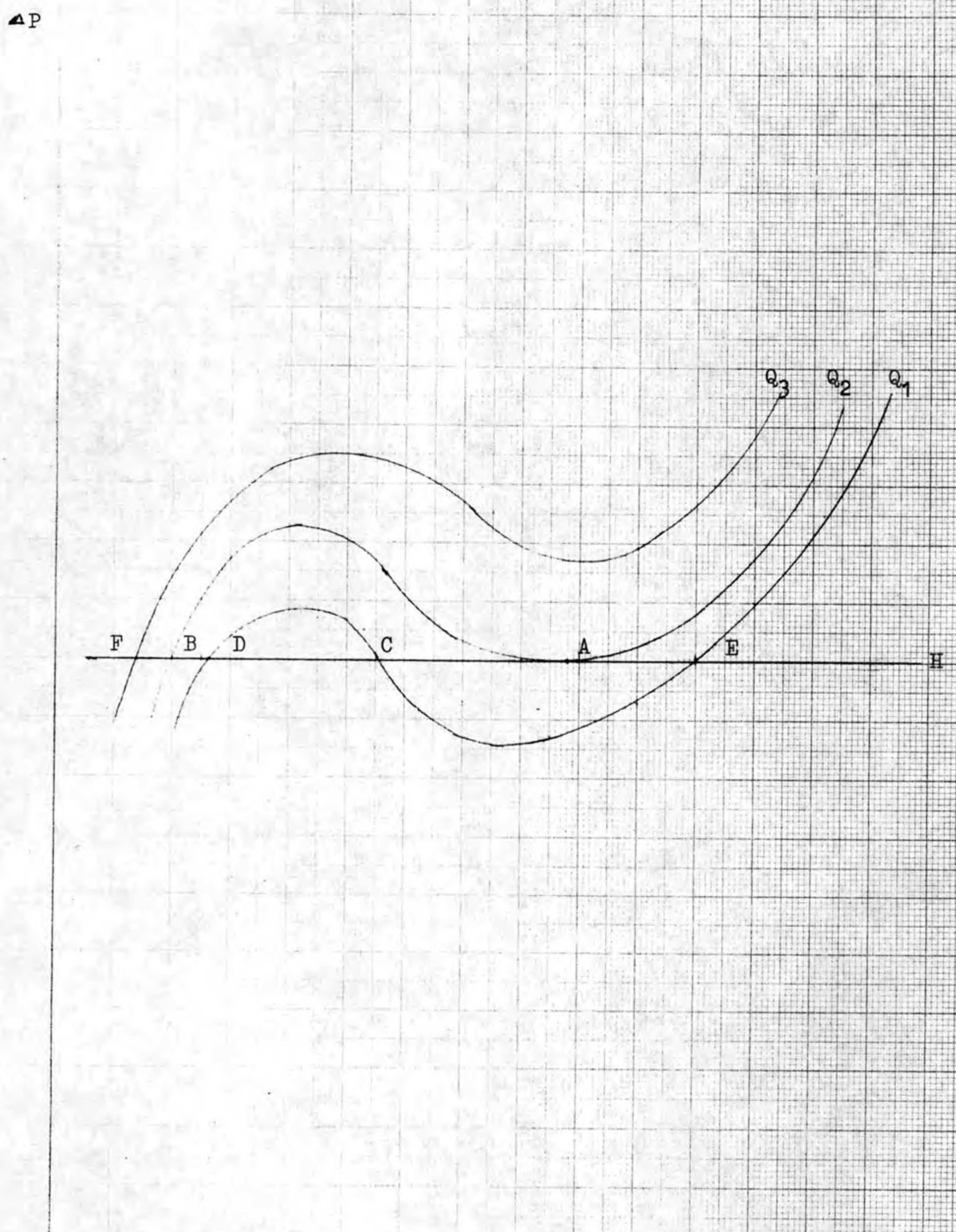

Fig. 4.16 Pressure-Drop Flow Characteristic

Pressure Drop-Flow Characteristic at 100% load

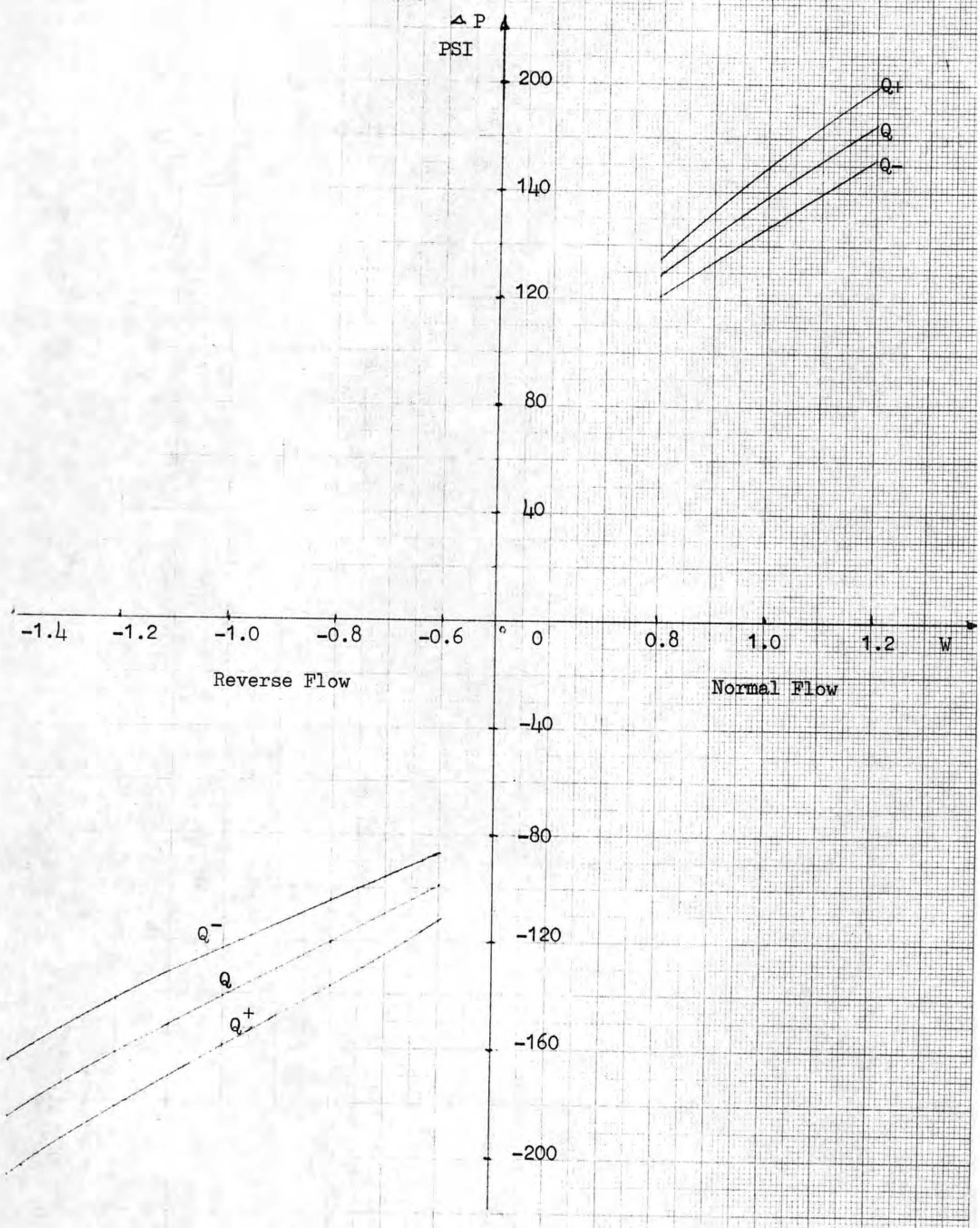

Fig. 4.17

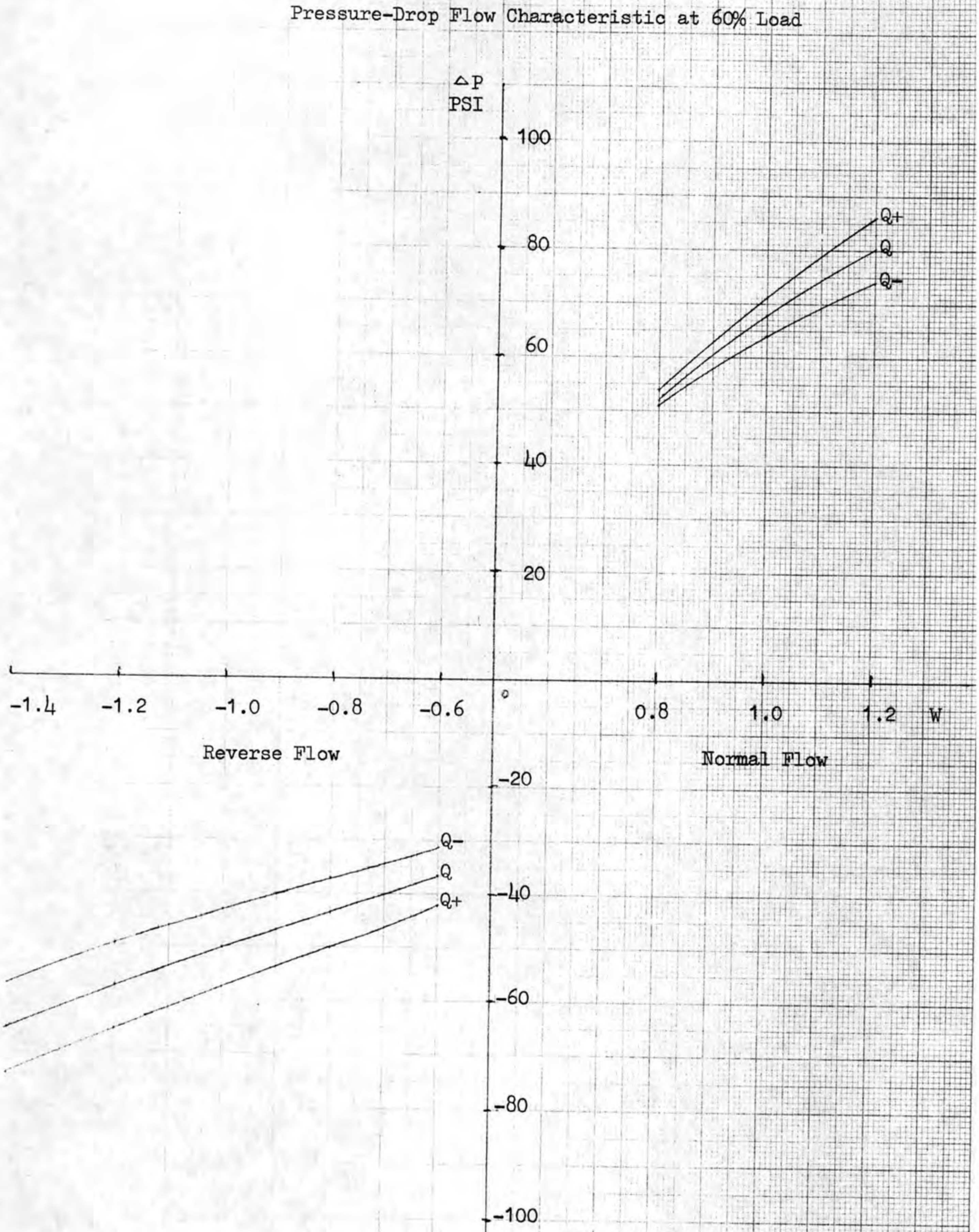
Pressure-Drop Flow Characteristic at 60% Load
△P
PSI
100
80
60
40
20
-20
-40
-60
-80
-100
-1.4
-1.2
-1.0
-0.8
-0.6
0
0.8
1.0
1.2
W
Reverse Flow
Normal Flow
Q+
Q
Q-
Q-
Q
Q+

Fig. 4.18

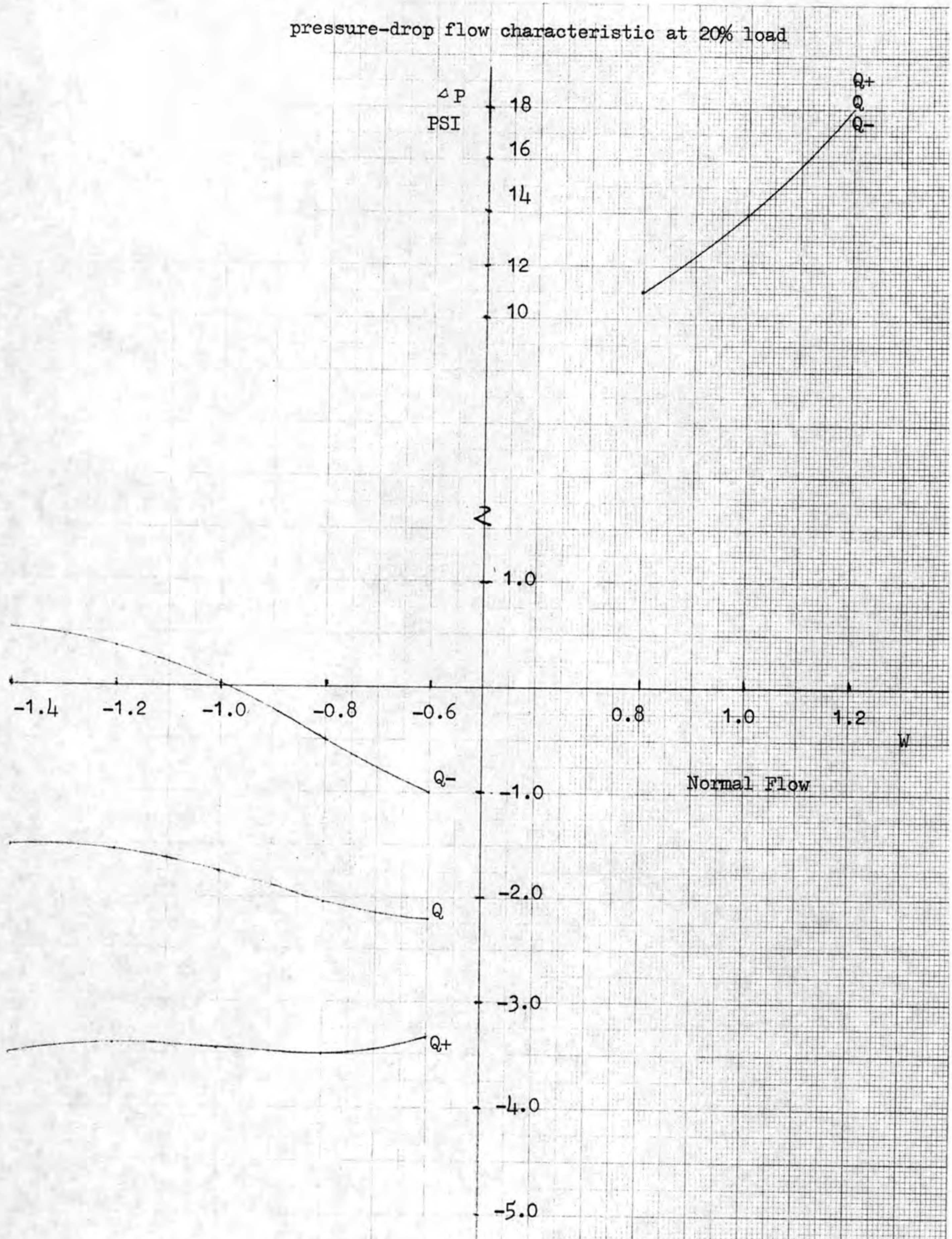
pressure-drop flow characteristic at 20% load
△P
PSI
18
16
14
12
10
1.0
-1.0
-2.0
-3.0
-4.0
-5.0
-1.4
-1.2
-1.0
-0.8
-0.6
0.8
1.0
1.2
W
Normal Flow
Q+
Q
Q-
Q-
Q
Q+

Fig. 4.19

Continuation of Fig. 4.3.IV

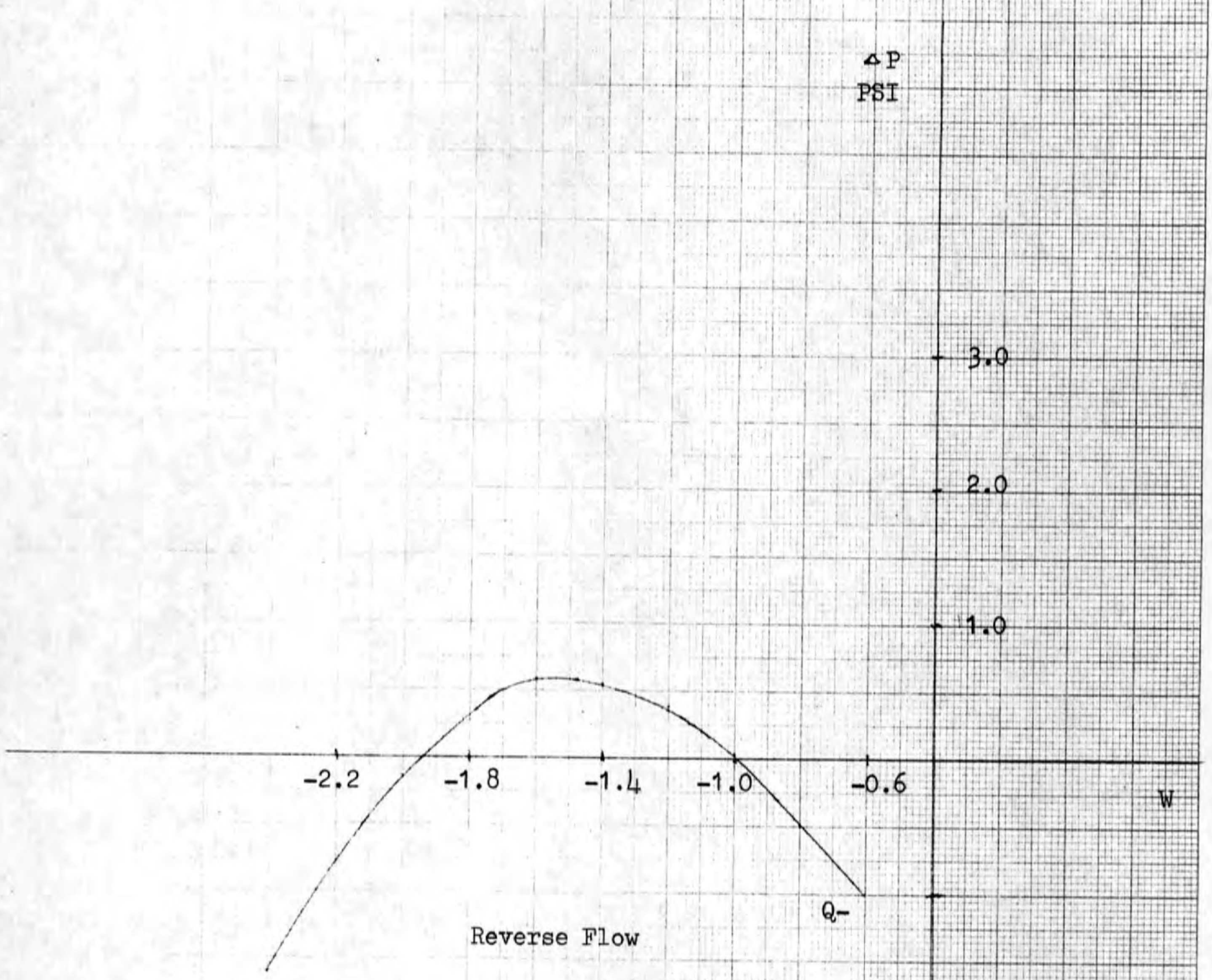

Fig. 4.20

linearized, Laplace-transformed, and integrated over small spatial increments. The resultant linear perturbation equations are examined within the framework of feedback control theory to determine if the design is stable or unstable. Specifically, the Nyquist stability criterion has been used to predict the stability characteristics of the steam generator. The steps in this procedure were discussed fully in GGA report (Ref. 15).

4.3.2.3 CONCLUSIONS AND RECOMMENDATIONS

The results of the GGA report indicate that the system is highly stable and will not amplify naturally occurring small scale perturbations. Analyses of the effects of inlet orificing, exit orificing, and pressure level indicate trends opposite to those observed in subcritical, two-phase systems. Stability is enhanced for this supercritical flow by increasing exit orificing, reducing system pressures toward the critical pressure, reducing flow rates and reducing heating rates. By comparison the stability of subcritical two-phase flows is enhances by increasing inlet orificing and increasing system pressures.

The results of the analysis tend to agree with the idea that stability can be qualitatively checked by considering the density ratio between the inlet and the outlet conditions as a function of the system pressure. In the supercritical region, an increasing density ratio with pressure tends toward instability and a decreasing density ratio toward stability. Below the critical point, the ratio of the density of saturated water at the inlet to the density of the saturated or superheated steam at the outlet decreases with increasing pressure toward the critical point. Above the critical point, the ratio of the density of the supercritical steam at the inlet to the density of supercritical steam at the outlet increases with increasing pressure for a constant heat input. Hence the opposite trend of the effect of pressure on stability above and below the critical point is not surprising. Similar arguments can be made for the effects of other parameters by considering their effect upon the density ratio. Quantitatively, systems with density ratios less than 50, which correspond to the pressures greater than 600 psia for water (Ref. 16), are generally stable. In the present case, the density ratio is much lower than 50 and the system is highly stable.

Although both the quantitative analysis and the qualitative discussion indicate that the system is highly stable, it must be pointed out that experimental tests are required to confirm the system behavior. Test data are available on the behavior of subcritical systems, however data on supercritical systems are quite limited. It is recommended that tests in the supercritical region be performed in order to confirm the stability of the system as determined by the analysis.

4.4 SYSTEMS RELATED TO STEAM GENERATOR

4.4.1 START-UP SYSTEM AND WATER CHEMISTRY

4.4.1.1 START-UP SYSTEM

The freezing temperatures of the fuel and coolant salts are 930°F and 725°F respectively (Ref. 23). The start-up system must therefore provide for the initial coupling of the steam generator to the steam power system without freezing of salt and with a minimum imposition of thermal shock. The salt systems must be filled and circulating isothermally at 1000°F before heat withdrawal can be initiated by decreasing the coolant salt temperature. The temperature of the feedwater must reach 1000°F utilizing a startup boiling before entering the steam generator, and then it will vary between 1000°F at zero load and 700°F in the 5 to 100% load. The 5% initial load operation requires a startup boiler of some 225,000 lb/hr steam capacity and a further increase to a 10% initial load as presently envisioned by ORNL would require a 450,000 lb/hr capacity boiler (Ref. 24).

Additional equipment is necessary to provide the feedwater conditions for starting, hot standby, and shutdown. This includes an auxiliary start-up boiler capable of producing 1000°F supercritical steam, an auxiliary boiler feedpump, a desuperheater and a steam dryer. The overall MSBR steam plant start-up and shutdown system is shown in Figure 4.21. The startup procedures for the salt and steam systems are outlined in the following sections.

4.4.1.1.1 SALT SYSTEMS

The primary and secondary cell electric heaters are turned on, and the primary and secondary circulation pumps are started to circulate helium in the salt systems. When the temperature of the secondary system reaches 850°F, the loop is filled with coolant salt from the heated drain tank, and salt circulation is started. When the primary system reaches 1000°F, it is filled from the fuel salt drain tank, and salt circulation is commenced. Both salt systems will continue to be circulated isothermally at 1000°F until power generation is started. The primary and secondary-salt flow rates are at the levels required for the zero-power level. The reactor is then brought critical at essentially zero power and salt circulating in both systems, including the steam generators at about 1000°F.

4.4.1.1.2 STEAM POWER SYSTEM

Concurrent with the salt systems being electrically heated, the steam system is also being heated. Feedwater is circulated through the mixer, pressure booster pump, attemperator, boiler extraction valve (BE), desuperheater, condenser, demineralizer, low-pressure feedwater heater, and deaerator. A fraction of the feedwater is circulated through the auxiliary boiler, while the remainder is circulated through the high-pressure feedwater heaters before returning to the mixer to complete the cold clean up circuit. Circulation of the feedwater continues in this manner until the chemical requirements of the feedwater for cold cleanup have been met. Cold cleanup of the steam system is accomplished with all four of the steam generators by-passed. When cold clean up is completed, the feedwater flow through the heater string is diverted from the mixer and recirculated back to the hotwell or through the shell side of one of the high pressure heaters before passing to the condenser. Feedwater flow through the auxiliary boiler to the mixer is adjusted to the startup value.

The auxiliary boiler is then started. As the auxiliary boiler load is raised, the steam produced is used to supply the main turbine seals and deaerator. The steam downstream of the boiler extraction valve (BE) passes through the desuperheater. This steam is used for heating the feedwater in the high-pressure feedwater heaters, for warming and rolling the boiler feed pump drive turbine, for warming the steam piping, and for rolling the main turbine.

The steam/feedwater temperature is held below 500°F until feedwater requirements for hot cleanup have been met. When the auxiliary boiler reaches full pressure and temperature, the steam at about 3600 psia and 1000°F at the discharge of the mixer can be admitted to the steam generator. The steam generator bypass flow is then decreased until the full auxiliary boiler flow passes through the steam generator.

When the steam system is ready to take on load, the control of reactor is adjusted as required to maintain the desire salt temperatures as the feedwater flow is increased. While the steam/water flow is being established in the steam generators, the temperature of the feedwater recirculaing to the condenser will be raised to 550°F at the discharge of the last high-pressure heater. The thermal load on the steam generator is then increased by lowering the feedwater inlet temperature from 1000°F to 700°F by mixing this feedwater from last heater and the 1000°F steam from the auxiliary boiler in the mixer. When the 700°F feedwater temperature is reached, the boiler feed booster pumps are started and the feedwater pressure to the steam generator is raised to about 3800 psia, which permits the use of the exit steam from the steam generator passing through reheat steam preheaters to heat the feedwater in the mixer instead of the auxiliary boiler. The auxiliary boiler system is then taken off line making the system self supporting.

The load is gradually increased and the reactor power is adjusted accordingly. At this point in the startup procedure, part of the steam generator output is going to the mixer via the reheat steam preheater, and the remaining steam is going through the boiler extraction valve (BE) to drive the main boiler feed pumps, etc. If the load is about 5%, the main turbines which have previously been warmed, can now be gradually brought up to speed and temperature, first using steam from the hot standby equipment (steam dryer). This steam will give a turbine valve opening equivalent to that at about 20% load with 3600 psia throttling conditions, so that the throttle pressure rise may occur without having to move the turbine control valves.

As the steam load is slowly increased, the reactor power is matched to the load, and salt temperatures are kept at the desired level. The load is held essentially constant until the system comes to equilibrium, at which point the reactor outlet temperature set point is adjusted to meet the requirements for subsequent load-following control.

As the load increases, the main turbines will use steam taken directly from the steam generator. The boiler-turbine valve (BTV), or a control-type bypass is gradually opened while the feedwater flow is increased until, with a wide open boiler-turbine valve, the throttle pressure is 3600 psia and the load is about 20%. At this power level the normal control system regulates the reactor outlet temperature as a function of load, and the steam temperature controller holds the steam temperature at 1000°F.

4.4.1.2 WATER CHEMISTRY

The steam power system of the MSBR plant will not require special water treatment. Aside from the steam generator, material of construction shall not differ from present-day fossil fueled supercritial cycles (Ref. 20) of startup boiler.

The recommended limits for feedwater conditions at the economizer inlet are given in the following table for normal operating conditions and during start-up (Ref. 25).

		Normal Operation	Start-up
Total dissolved solids	- ppb	50	--
Total iron	- ppb	7	50
Total copper	- ppb	5	20
Total silica	- ppb	20	30
Dissolved oxygen	- ppb	5	10
pH		9.3 - 9.7	9.3 - 9.7
Conductivity	- mmhos	0.5	1.0

During the start-up period, there will be variations in the concentrations of the various feedwater contaminants due to changes in temperature and flow conditions and placing into service of cycle components. The feedwater conductivity must be below 1.0 mmho before lighting the burners of the startup boiler. Also after firing has started, the fluid temperature at the roof outlet of the startup boiler must not be permitted to rise above 500°F until the iron content of the feedwater entering the economizer is less than 50 ppb. The limits given in the above table for the startup conditions are for continuous operation. Transient values higher than those given in the table may be tolerated for a short time only, and if they do not decrease, firing rate and temperature may have to be reduced until satisfactory values are obtained.

There are two basic approaches to keep the various constituents to the levels below which they will not cause problems.

a. Minimize the corrosion that takes place within the system: This is accomplished by removal of oxygen and maintaining the pH of the condensate at the specified level. Oxygen is removed by chemical scavenging with hydrazine and mechanical deaeration in the condenser. A nominal hydrazine residual of 0.020 ppm is maintained at the economizer inlet. Feedwater pH is controlled by adding ammonia or a volatile amine such as morpholine or cyclohexylamine.

b. Remove corrosion products and leakage salts from the system: Corrosion products, silicon and salts from condenser leakage are removed by the full flow condensate demineralizer. Both ionized and suspended matter are removed as the unit acts as a highly efficient filter as well as an ion exchanger.

4.4.2 PRESSURE RELIEF SYSTEM

The steam generator was designed to the specifications of the ASME Boiler and Pressure Vessel Code Section III, Nuclear Vessels for class A vessels. The design conditions are: (Ref. 26)

	shell side	tube side
Design temperature, $^{\circ}F$	1150	1120
Design pressure, psia	300	3800
Allowable stress, psi	9500	11600

There is no violent exothermic reaction between the coolant salt and steam, however, the mixture of salt and water is corrosive to the material of steam generator (Hastelloy N) (Ref. 1).

The pressure relief system was designed to protect the steam generator and coolant salt system from the overpressure and

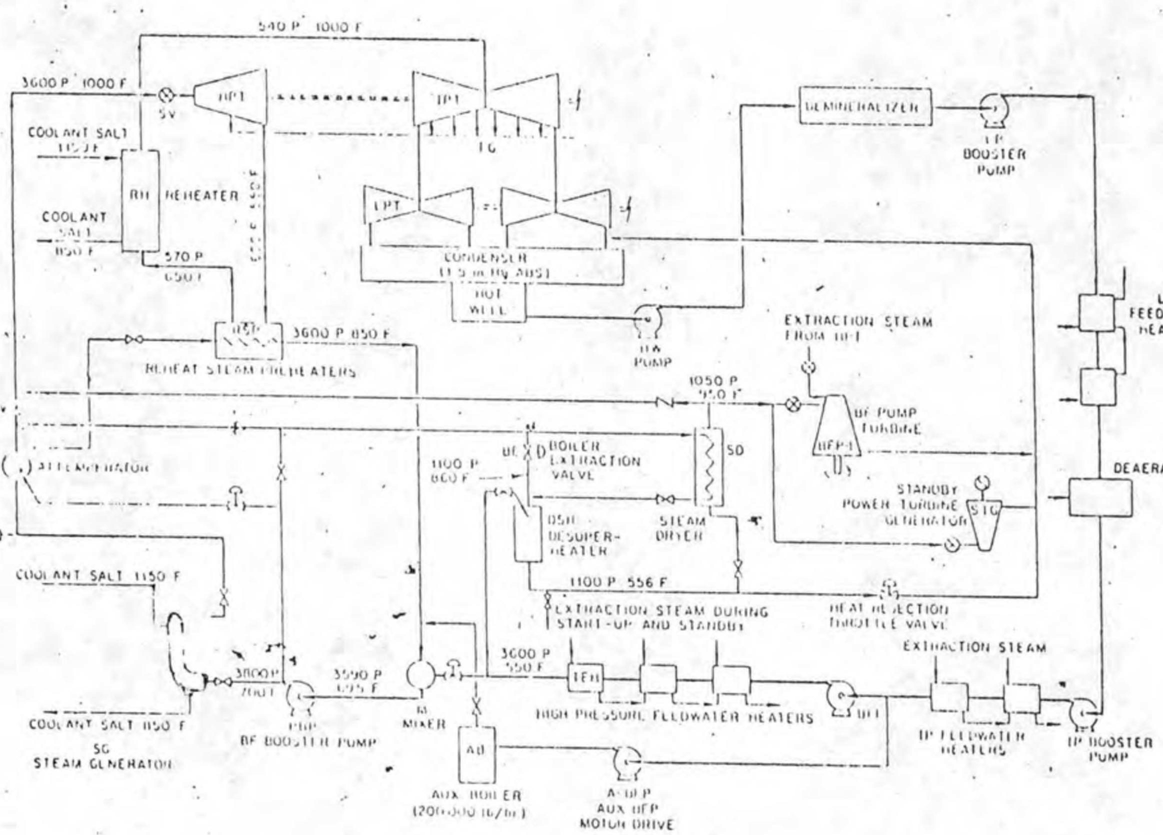

MSBR steam plant startup and shutdown system.

Ref.(23)

Fig. 4.21

highly corrosive mixture, should steam tube suddenly rupture. It was assumed that the coolant salt system could withstand a continuous pressure of 220 psi without damage (Ref. 3).

The present ASME Code Section III, which governs because of emergency cooling consideration, accepts only relief valves as primary relief devices. However, the corrosive property of the mixuure of salt and steam, requirement of rapid pressure relief, are against using relief valves as an appropriate primary relief device. A new subsection NH under Section III is in preparation for inclusion in the new edition of the Code which is expected to recognize rupture disks as primary relief devices for certain types of overpressure conditions (Ref. 27). The Molton-Salt steam generator would be listed as an over pressure condition to which the rupture disk or equivalent device is applicable.

There are three basic types of rupture disks; prebulged disk, reverse buckling assembly and the snap-over assembly. In addition, the rupture disk for the British PFR is a hinged plate supporting a nickel membrane, which serves as the sodium seal; the plate itself is held by a shear pin, designed to fail approximately twice the normal operating pressure (Ref. 28). However, it was learned that response time observed in testing the PFT design was about 10.25 milliseconds slower than with the prebulged disk. All of these four approaches are shown in Fig. 4.22 (Ref. 17). The evaluation and comparison of these four types were discussed in Ref. 27 and Ref. 29. The reverse buckling assembly was recommended and therefore used for this design. The reverse buckling disk has several advantages. It is under compression rather than tension, and the controling factor, elastic modulus, is insensitive to environmental conditions. The reversing pressure can be predicted accurately, and collapse occurs within ± 2% of the normal pressure rating. It has 10 - 15 times the life expectancy of, and is thicker than, the prebulged type. It can be used at system operating pressure up to 90% of the rated burst pressure. It needs no vacuum support and withstands repeated pressure-vacuum cycles.

The reverse buckling disk, for a given geometry buckling, is controlled by elastic modulus of the material. Within the operating range (1150°F - 850°F) the elastic modulus of Hastelloy N varies only about 6%. Therefore the Hastelloy N, which is also, chemically, very compatible with coolant salt, could be suggested be the material for the reverse bulking disk.

There will be no cover gases to protect structure members. The steam generator cell of the generating station building is maintained at about 1000°F to prevent salt from freezing (Ref. 23).

Reversed buckling disks can be used at system operating pressures up to 90% of the rated burst pressure. The rated burst pressure was determined to be 350 psia. A 20 in. diameter disk (thickness = 0.08 in) would provide adequate relief area to dump the mixture of reaction products, thus preventing system from continuous pressure rise. One rupture disk assembly is recommended at each of the inlet and outlet salt piping.

Following a tube rupture, the block valves of water/steam side would be closed. The mixture would be dumped through the rupture disk to a dump tank. The connecting pipes would be of the same size of rupture disk. Each steam generator would have one dump tank of capacity of 2500 ft^3 with ample freeboard to hold the mixture and vent out the steam. The tanks are essentially conventional tanks with internal spiral-guide vanes. These guide vanes cause the mixture to experience centrifugal forces that separate most of the liquid, or solid reaction products from the gaseous reaction products. The gaseous productions are discharged to the separator. The separator is usually installed to remove liquid/solid products from the gaseous discharge, and ensure no reaction products are discharged to the atmosphere.

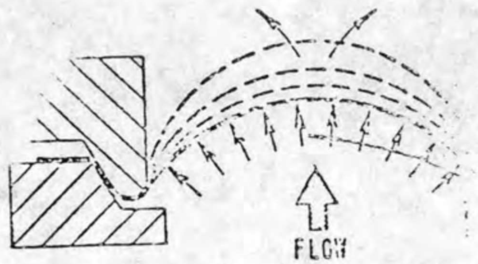

Prebulged Disk Assembly

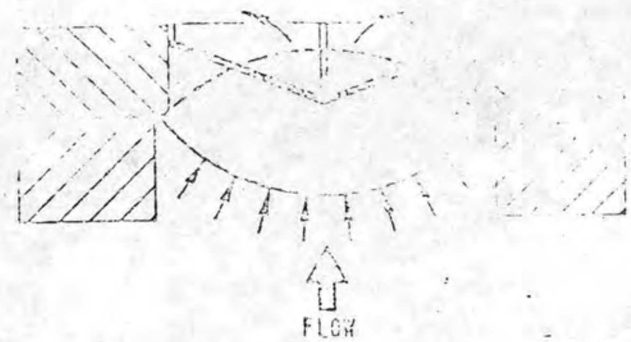

Reverse Buckling Assembly

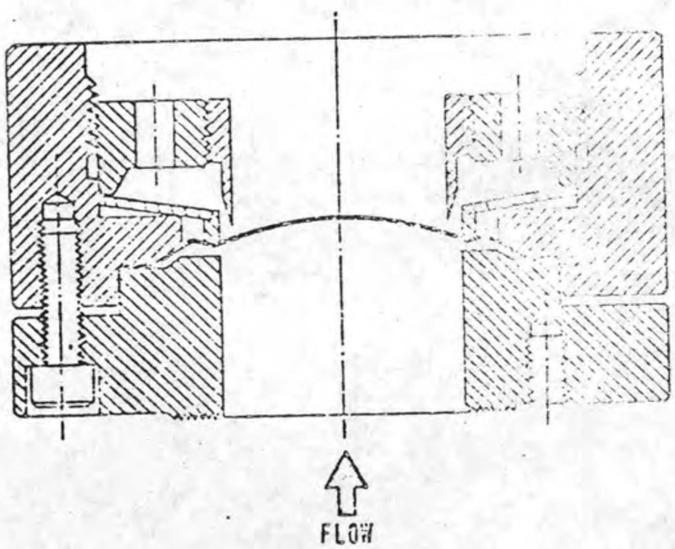

Snap Over Assembly

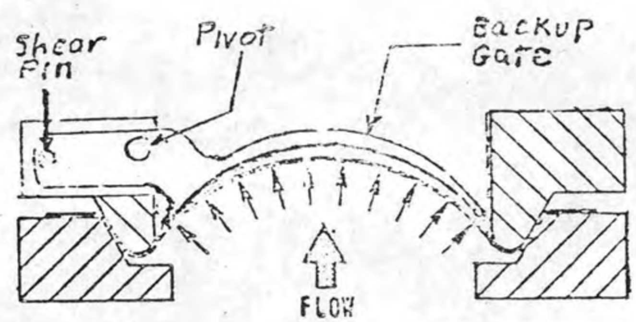

Shear Pin Concept

Fig. 4.22

Various Rupture Disk Concepts

4.5 REFERENCES

1. The Development Status of Molten-Salt Breeder Reactors, ORNL - 4812, August 1972, Oak Ridge National Laboratory.

2. Design Studies of Steam Generator for Molten Salt Reactors Monthly Progress Report #10, August 1 - August 31, Foster Wheeler Corporation.

3. Proposed Scope of Work and Requirements for Design Studies of Steam Generators for Molten Salt Reactors, Enclosure 2, Union Carbide Corporation, March 1971.

4. Heat Transfer to Supercritical Water in Smooth - Bore Tubes, H. S. Swenson, J. R. Carver, C. R. Kakarala, Journal of Heat Transfer, November 1965.

5. GGA - HTGR Steam Generator Evaluation of Surface Mismatch Using Probability Methods, L. Rianhard, R. M. Costello, P. J. Prabhu, W. T. Klamm, Foster Wheeler Corporation, July 1970.

6. Molten-Salt Reactor Program, Semiannual Progress Report, Period ending August 31, 1972, ORNL - 4832, March 1973, Oak Ridge National Laboratory.

7. Private communication from W. Apblett to J. Polcer on thermal conductivity data of Hastelloy N (6/20/74).

8. Design study of steam generators for Molten Salt Reactors Monthly progress Report #8, May 20 - June 30, 1974, Foster Wheeler Corporation.

9. Design study of steam generators for Molten Salt Reactors Monthly Progress Report #10, August 1 - August 31, 1974, Foster Wheeler Corporation.

10. A general summary of the ORNL 1000 MW(e) Molten-Salt Breeder Reactor Reference Design, Enclosure 1, Union Carbide Corporation, November, 1970.

11. Fluid Dynamics, J. W. Daily, D.R.F. Harleman, Addison-Wesley Publishing Company, Inc., 1966.

12. Engineering Department Manual, Volume I, Basic Design, Foster Wheeler Corporation.

13. An Analysis of Thermally Induced Flow Oscillations in the Near-critical and Super-critical Thermodynamic Region, Novak Zuber, General Electric Company, May 25, 1966.

14. Engineering Department Manual, Volume III, Computer Programs, Foster Wheeler Corporation.

15. Analysis of Dynamic Flow Stability in Steam Generators for the Molten-Salt Breeder Reactor, B. E. Boyack, Gulf General Atomic, Gulf-GA - A12416, November, 1972.

16. Lecture Series on Boiling and Two-phase Flow for heat transfer engineers, University of California, Berkeley, California, May 27-28, 1965.P.195

17. Review of Two-Phase Flow Instability, J. A. Boure, A. E. Bergles, L. S. Tong, 71-HT-42, ASME

18. Static and Dynamic Stability of Steam-Water Systems Part 1, Critical Review of the Literature, L. E. Efferding, General Dynamics, GA-5555, October 1964.

19. Supercritical Furnace Design, Foster Wheeler Corporation.

20. Recent Experiences with Radient Superheaters in Central Steam Generators and their Effect on Design Criteria, R. P. Welden, H. H. Pratt, FWC, American Power Conference, Volume XXIV, March, 1962.

21. Test and Evaluation of Alco/BLH Prototype Sodium-Heated Steam Generator, S. M. Cho, etc., LMEC-Memo-70-20, January 1971, Liquid Metal Engineering Center.

22. Performance Changes of a Sodium-Heated Steam Generator, S. M. Cho, K. A. Gardner, etc., 71-HT-15, ASME.

23. Conceptual Design Study of a Single-Fluid Molten-Salt Breeder Reactor ORNL-4541, ORNL.

24. Startup Steam ORNL 1000 MW(e) MSBR, C. R. Clark, Service Department, FWC, Inter Office Correspondence, September 29, 1972.

25. Operating Instructions, Section 3, Feedwater and Cycle Cleanup, FWC.

26. Design studies of Steam Generators for Molten Salt Reactors Monthly Progress Report #11, September 1 - September 30, 1974, FWC.

27. State-of-the-art of Rupture Disks for LMFBR Application, J. P. VerKamp, NEDM-13981, GE, July, 1973.

28. Status of LMFBR Reheat in Western Europe - 1972, WASH-1219, AEC, March 1973.

29. Evaluation and Procurement Guide For Three Types of Metallic Rupture Disk Assemblies, ORNL-TM-4046, ORNL, January, 1973.

30. Computer Programs For The Analysis of Complex Decision Problems, Stanley I. Buchin, 8-171-070, EA-C-905, Harvard University, September, 1970.

SECTION 5

STRUCTURAL FEASIBILITY ANALYSIS

BY

DR. N. J. LEVY

Approved by

C. F. Nash
Structural Analysis Section Manager

TABLE OF CONTENTS

FWC FORM 172 - 4

NOTATIONS IN THIS COLUMN INDICATE WHERE CHANGES HAVE BEEN MADE

5.1 STRESS ANALYSIS OF THE SALT INLET NOZZLE

5.1.1 INTRODUCTION

This report discusses the analysis of the molten salt inlet nozzle of the steam generator. During its service life, it is expected that the nozzle will be subjected to thermal transients which are no worse than those described in ORNL-TM-3767, HYBRID computer simulation of the MSBR. In the interest of conservatism, the transient shown in Figure 2, which is a combination of most severe up and down transient, was assumed for this analysis. Dead weight and thermal expansion loads due to the molten salt feed pipe were not included because they are not available at this time. Internal pressure loadings, however, were considered. Temperature distributions due to the assumed transient condition, and stresses due to these temperature distributions and pressure loads, were obtained by using Foster Wheeler's version of Wilson's Finite Element Program. The finite element model is shown in Figure 1. Inelastic strains were calculated using Bree's method & FWC's simplified elastic-plastic creep computer program.

5.1.2 SUMMARY AND CONCLUSION

The purpose of our analysis was to determine the feasibility of the sodium inlet nozzle under the severe thermal transients and other loads anticipated. Based upon analyses specified in Section III of the ASME Boiler and Pressure Vessel Code, and in Code Case 1331-5, it was concluded that both the nozzle and shell required a thermal liner. With the liner, stresses were calculated to be within the allowable limits. Table I summarizes the results. Based on the table, it is concluded the design is feasible. Final conclusions are dependent on the magnitude of the piping loads (which are presently unavailable).

TABLE 1

STRESS SUMMARY, MSBR MOLTEN SALT INLET NOZZLE WITH LINER

Section (Location)	Stress Category	Calculated Stress Range (psi)	Allowable Stress Limit (psi)
1-1 (Shell)	P_m (design)	4043	S_o = 9500 @ 1150 F
	P_m (operating)	3170	S_{mt} = 7500 @ 1150 F 30 yrs.
	$(P_L+P_L+Q)_R$	19019 (EL.19)	3Sm = 67,500
2-2 (Shell at nozzle)	P_m (design)	5100	9500
	P_m (operating)	4000	7500
	$(P_L+P_b+Q)_R$	26,480 (EL. 158)	67,500
3-3 (Intersect. Shell & Noz.)	P_m (design)	5360	9500
	P_m (operating)	4200	7500
	$(P_L P_b+Q)_R$	33,396 (El. 187)	67,500
4-4 (Nozzle at Shell)	P_m (design)	5236	9500
	P_m (operating)	4100	7500
	$(P_L P_b+Q)_R$	19,108 (El. 215)	67,500
5-5 (Noz. at Start of Reduced Wall)	P_m (design)	2499	9500
	P_m (operating)	1960	7500
	$(P_L P_b+Q)_R$	10,794 (El. 258)	67,500
6-6 (Nozzle at Feed Pipe)	P_m (design)	6415	9500
	P_m (operating)	5025	7500
	$(P_L P_b+Q)_R$	9,278 (El. 336)	67,500

TABLE 1 (CONT'D)

Section (Location)	Stress Category	Calculated stress Range (psi)	Allowable Stress Limit (psi)
7-7 (Feed Pipe)	P_m (design)	7840	9500
	P_m (operating)	6140	7500
	$(P_L P_b + Q)_R$	does not control	----
8-8 (Shell)	P_m (design)	$\frac{pr}{2t}$ = 2700	9500
	P_m (operating)	2100	7500
	$(P_L P_b + Q)_R$	does not control	----

Note: Allowables are at 1150 F

See Section 5.1.6 for creep fatigue interaction and inelastic strain analysis

See Appendix C-2 for material properties and allowables.

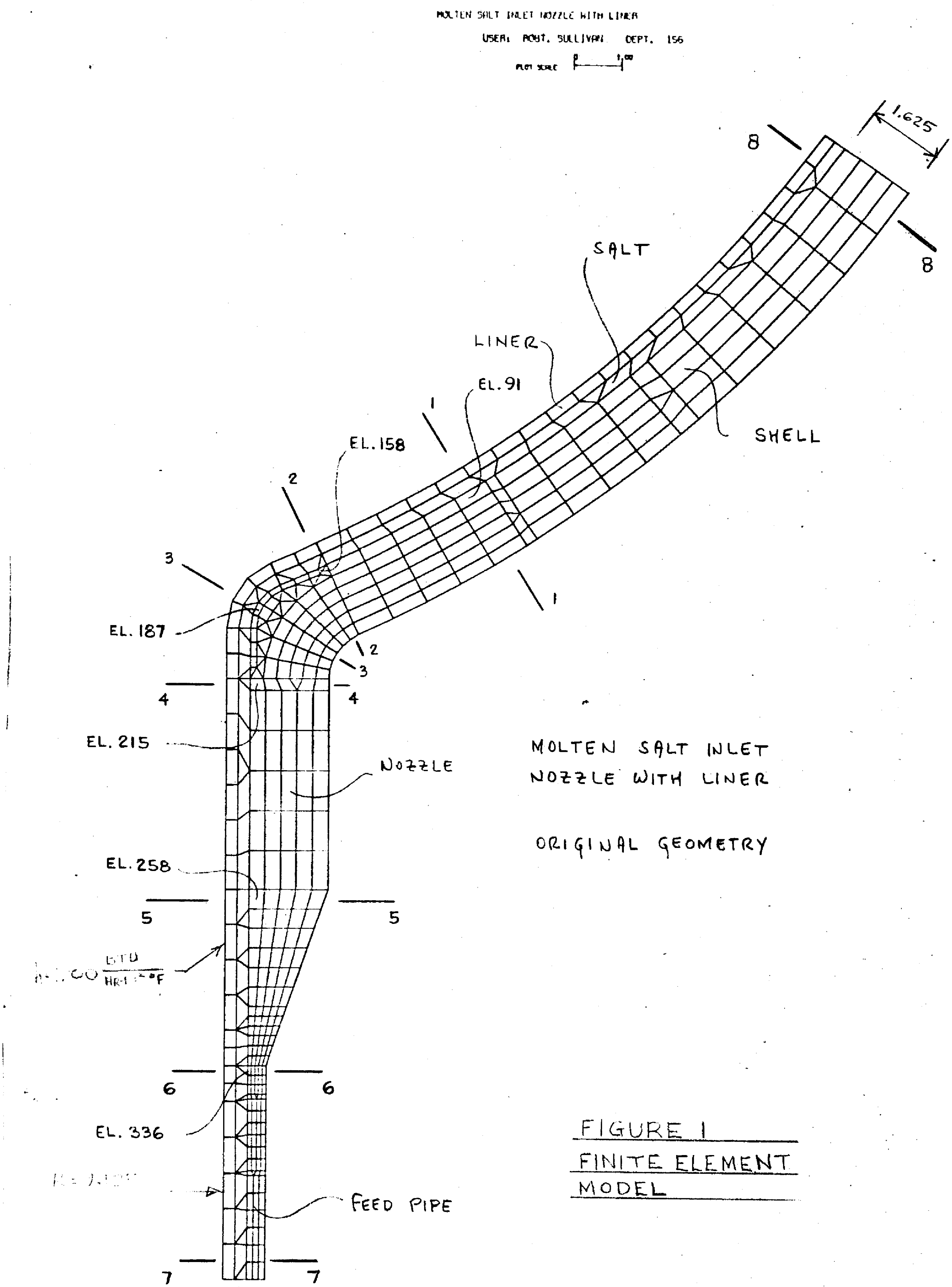

FIGURE 1

FINITE ELEMENT MODEL

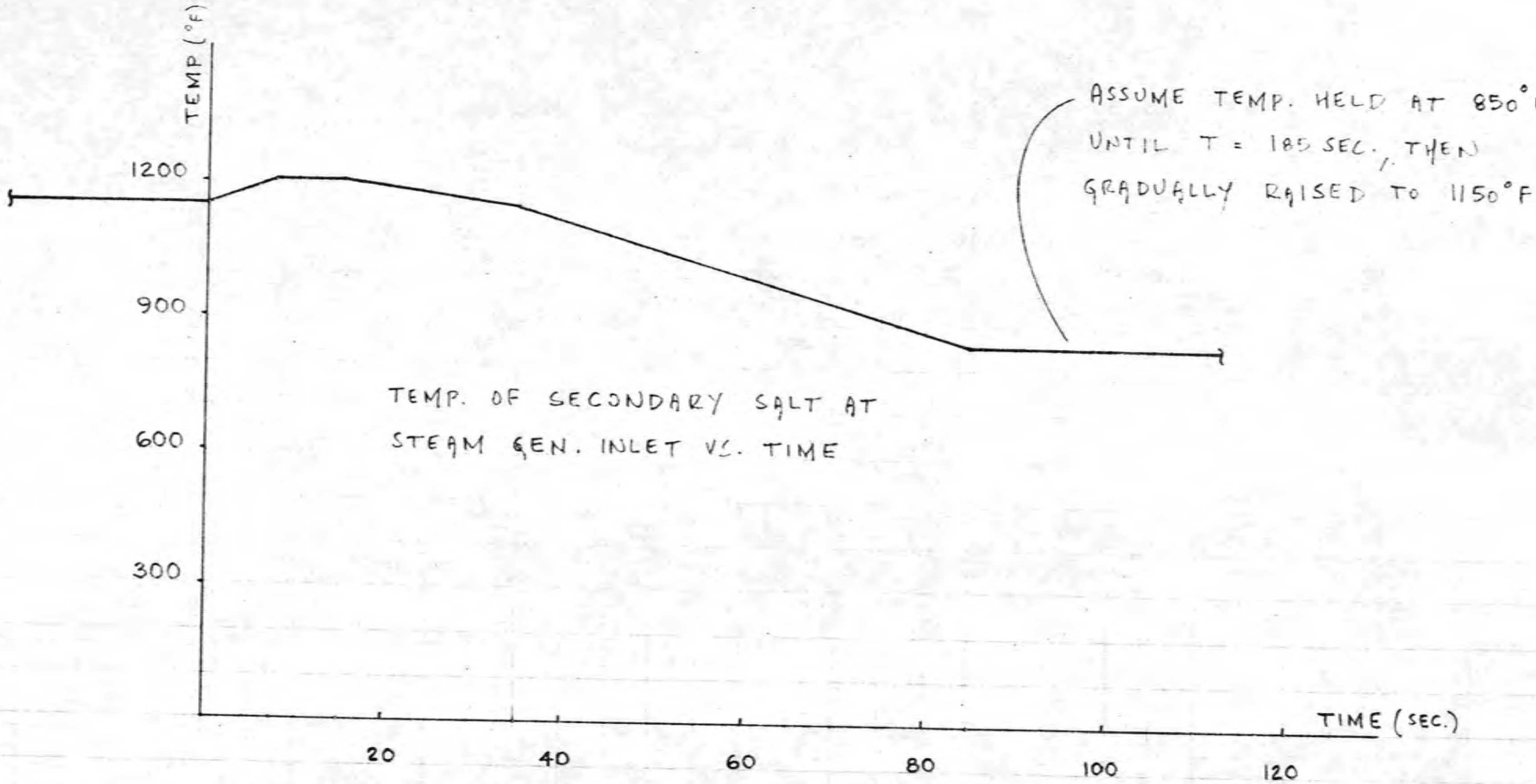

FIGURE 2
ASSUMED TRANSIENT LOAD CONDITION
(STEADY STATE TEMP. = 1150°F)

5.1.3 STRESSES DUE TO PRESSURE

From the finite element computer program, stresses at various locations of the nozzle due to a design pressure of 300 psi were obtained. They are shown below. (Ref. 9)

Section 1-1

Element	σ_r	σ_z	σ_T	σ_{rz}
86	1692	701	4078	1137
87	1584	737	4003	1186
88	1508	740	3928	1209
89	1462	702	3850	1210
90	1459	629	3772	1194
91	1509	511	3693	1164
Avg.	1536	670	3887	1183

Average principal stresses are

$$\left.\begin{aligned}\sigma_1 &= 2362\\ \sigma_2 &= -156\\ \sigma_3 &= 3887\end{aligned}\right\} S = 4043$$

Section 2-2

Element	σ_r	σ_z	σ_T	σ_{rz}
126	3862	2146	6421	2430
127	2149	1594	5813	1443
128	1285	1032	5456	843
129	559	489	5143	396
130	-174	-2	4840	19
156	-701	-571	4547	-88
157	-1002	-773	4321	-583
158	-1683	-667	4198	-657
Avg.	537	405	5092	475

$\sigma_1 = 950$ $\sigma_2 = -8$ $\sigma_3 = 5092$

S = 5100

Section 3-3

Element	σ_r	σ_z	σ_T	σ_{rz}
141	1868	3841	6308	2112
142	1761	1875	5868	1123
143	1354	793	5592	545
144	900	71	5411	132
145	465	-453	5302	-163
184	62	-769	5237	-223
185	236	-812	5322	-448
186	-175	-934	5303	-398
187	-375	-988	5358	-352
Avg.	677	292	5522	259

$\sigma_1 = 808$ $\sigma_2 = 162$ $\sigma_3 = 5522$

S = 5360

Section 4-4

Element	σ_r	σ_z	σ_T	σ_{rz}
210	222	2701	5102	566
211	299	1686	4989	986
212	401	1174	5021	1083
213	146	632	4875	898
214	-47	30	4818	658
215	-253	-722	4725	235
Avg.	128	917	4922	738

$\sigma_1 = 1360$ $\sigma_2 = -314$ $\sigma_3 = 4922$

S = 5236

Section 5-5

Element	σ_r	σ_z	σ_T	σ_{rz}
254	-60	-750	1698	-193
255	-34	26	2008	0
256	-63	948	2361	115
257	-131	1949	2746	137
258	-210	3056	3180	40
Avg.	-100	1046	2399	20

S = 2499

FWC FORM 172 - 4

NOTATIONS IN THIS COLUMN INDICATE WHERE CHANGES HAVE BEEN MADE

Section 6-6

Element	σ_r	σ_z	σ_T	σ_{rz}
332	182	5872	6772	207
333	76	4890	6509	3
334	-43	4223	6336	-120
335	-168	3645	6189	-149
336	-279	3051	6041	-84
Avg.	-46	4336	6369	-29

S = 6415

5.1.4 STRESSES DUE TO TEMPERATURE TRANSIENTS

From the finite element computer program, stresses due to temperature transients at various locations of the nozzle were calculated and are given below. Note that pressure stresses do not enter into the stress intensity range calculation. (Ref. 10)

Section 1-1

	σ_r	σ_z	σ_T	σ_{rz}	
Down Trans	13570	4949	20490	8284	(153 Sec)
Up Trans	247	73	1361	351	(33 Sec)
Range	13323	4876	19129	7933	

σ_1 = 18,090 σ_2 = 110 σ_3 = 19129

S = 19019

Section 2-2

	σ_r	σ_z	σ_T	σ_{rz}	
Down Trans	18390	3625	25200	8870	(153 Sec)
Up Trans	-3016	-829	1351	-1299	(33 Sec)
Range	21406	4454	23849	10,169	

σ_1 = 26,170 σ_2 = -310 σ_3 = 23849

S = 26480

CHARGE NO 8-25-2431	DOCUMENT NO. ND/74/66	ISSUE 1	DATE 12/16/74

SECTION 3-3

	σ_r	σ_z	σ_T	σ_{rz}	
DOWN TRANS	1859	9190	31300	4725	(153 SEC)
UP TRANS	-503	-1852	1787	-822	(33 SEC)
RANGE	2362	1042	29513	5546	

σ =7287 σ_2=3883 σ_3=29513

S =33,396

SECTION 4-4

	σ_r	σ_z	σ_T	σ_{rz}	
DOWN TRANS	-30	17030	21440	-564	(153 SEC)
UP TRANS	-191	-2060	2206	267	(33 SEC)
RANGE	161	19090	19234	-831	

σ_1=19126 σ_2=126 σ_3=19234

S=19108

SECTION 5-5

	σ_r	σ_z	σ_T	σ_{rz}
DOWN TRANS	-167	9300	12180	-27
UP TRANS	-158	1677	1395	35
RANGE	-9	7623	10785	-62

σ_1=7623 σ_2=-9 σ_3=10785

S=10,794

SECTION 6-6

	σ_r	σ_z	σ_T	σ_{rz}
DOWN TRANS	-73	10900	10460	-25
UP TRANS	-218	1478	3867	-52
RANGE	145	9422	6593	27

σ_1=9423
σ_2=145 S=9278
σ_3=9422

FWC FORM 172 - 4

NOTATIONS IN THIS COLUMN INDICATE WHERE CHANGES HAVE BEEN MADE

BY	APPROVED	PAGE 5-9 OF

FWC FORM 172 - 4

NOTATIONS IN THIS COLUMN INDICATE WHERE CHANGES HAVE BEEN MADE

5.1.5 SIMPLIFIED INELASTIC ANALYSIS

Inelastic strains were calculated by Bree's simplfied method (see Chapter VI of the LMFBR Piping Design Guide). In the Bree analysis, it is assumed that there are a total of 200 severe thermal cycles (sum of load scrams and reactor scrams). With a 30-year design life, the time per cycle is 262,800/200 = 1314 hours.

The derivation of the creep law used in the Bree analysis is given in the tubesheet report. The Bree analysis has been computerized by Foster Wheeler, and the following results were obtained:

Location	Total Strain/Cycle	Total Strain
1-1	Negligible	Negligible
2-2	Negligible	Negligible
3-3	1×10^{-4}	0.02%
4-4	Negligible	Negligible
5-5	Negligible	Negligible
6-6	4×10^{-4}	0.08%

Ref.: Computer Run NHJL09F

CHARGE NO 8-25-2431	DOCUMENT NO. ND/74/66	ISSUE 1	DATE 12/16/74

5.1.6 FATIGUE ANALYSIS AND CREEP FATIGUE INTERACTION

A preliminary fatigue analysis was made with the aid of Code Case 1331-4. With a maximum stress range of 33.40 Ksi, or an alternating stress of 16.70 Ksi, the Code Case gives an infinite number of allowable cycles. Thus, fatigue should be no problem.

CREEP FATIGUE INTERACTION

Foster Wheeler has developed a computer program which performs elastic-plastic-creep analysis of a cylinder subjected to time dependent pressure, temperature, and axial loads. To use the program, one constructs a histogram of the loading (see below). The user also supplies subroutines describing the creep, fatigue, and stress to rupture properties of the material. Creep properties were obtained from "Data for Nickel-Molybdenum-Chromium-Iron Alloy, Iron 8", June 1, 1961, while fatigue and stress to rupture properties were obtained from "Bases for Design of MSBR Systems for Temperatures to 1300 F", ORNL Central Files Number 73-1-23. The program automatically computes stresses and strains as a function of time, along with creep and fatigue damage. Creep and fatigue damage are computed in accordance with ASME Code Case 1331-5.

Section 3-3 proved to have the highest loading and only that section was analyzed. The nozzle was idealized as a cylinder with 1.625" wall thickness and approximately 9" inside radius. The loadings and histogram are shown below.

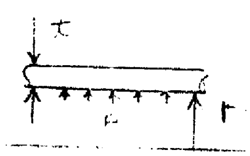

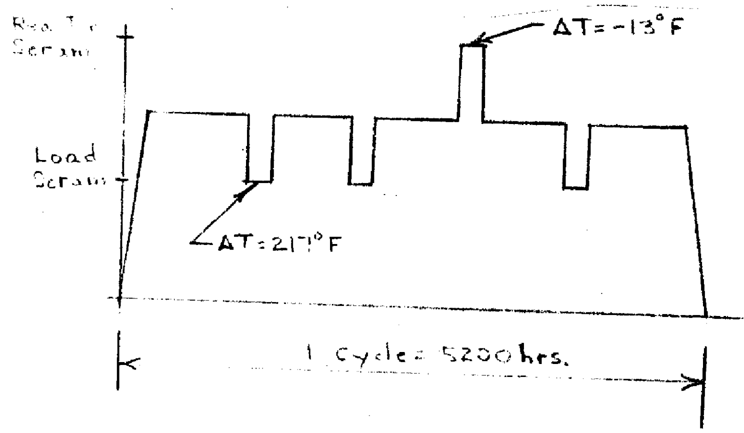

$\frac{pr}{t} = 5360$

solving for p
p = 950 psi

$\frac{E \cdot \Delta T}{2(1-\nu)}$ = 31,300 (up transient)
-1852 (down transient)

$\Delta T = 217^{o}F$
$-13^{o}F$

where $E = 26.2 \times 10^{6}$, $\alpha = 7.72 \times 10^{-6}$

PROGRAM RESULTS

There are a total of 50 cycles, each cycle consisting of 3 load scrams and 1 reactor scram. The program was run for 5 cycles and the strain for each of the remaining cycles was estimated by taking the difference in strain between the fourth and fifth cycles.

Maximum total strain = 0.29 + 45 (0.01) = 0.74%

Creep damage = 0.00222 + 45 (0.048×10^{-2}) = 0.0238

Maximum strain range = 0.248%

Fatigue Damage = $50/10^5 = 5 \times 10^{-4}$ (maximum temperature = 1150 F)

Ref: Computer run EBHJL06C

5.2 STRESS ANALYSIS OF MSBR TUBESHEET-HEADER ASSEMBLY

5.2.1 INTRODUCTION AND SUMMARY

The major tool in analyzing the tubesheet header assembly in Foster Wheeler Corporation's Finite Element Computer Program (Reference 1). A finite element model of the structure was made and is shown in Figure 1. This model was used to determine both pressure and thermal stresses. These stresses were compared to the allowables, using ASME Code Case 1331-5 as a guide.

As seen in Figure 1, the upper (header) side of the tubesheet is in contact with steam, while the lower portion of the tubesheet is in contact with molten salt. The severest thermal stresses occur during transients specified in Reference 2. The severest up and down transients were found to occur during a Ramp Change in Load Demand from 100 to 40% in 3 seconds (Figure 2) and Insertion of Two Safety Rods (Figure 3), respectively. Outlet steam transients were found to be more severe than inlet. Therefore, because inlet and outlet tubesheet geometries are identical, only the outlet tubesheet was analyzed.

Eight locations of possible high stresses were analyzed and are shown in Figure 1. Primary membrane, local membrane plus primary bending, and local membrane plus bending plus secondary stress intensity ranges were obtained at 11 locations. The stress intensities obtained, together with allowables, are shown in Table 1. Except where indicated, primary stresses are due to a design pressure of 4000 psi. Allowables are based on operating (30 year life) conditions. This combination of loading and allowables is conservative.

Although, according to Code Case 1331-5 there is no limit on primary plus secondary stress intensity, the 3Sm limit of Section III of the ASME Code is given for reference purposes.

It is seen that all primary stress intensities are within the allowable limits, Inelastic strains, computed by Bree's simplified method, are also seen to be within allowable limits.

Computer plots of the stresses due to temperature transients are shown in Figures 5 to 13.

TABLE 1

STRESS SUMMARY - MSBR TUBESHEET - HEADER ASSEMBLY

Location (Section)	Stress Category	Allowable Stress Limit (PSI)	Calculated Stress Range (PSI)	Maximu Temper ture,
1-1	P_m	S_{mt} = 13,000	8,570	1075
(Center of T.S.) (Operating Pressure)	P_L+P_b	KS_t = 14,100	13,040	
	$(P_L+P_b+Q)_R$	$3S_m$ = 69,600	23,360	
2-2	P_m	13,000	12,160	1075
(Edge of T.S.)	P_L+P_b	13,200	8,080	
	$(P_L+P_b+Q)_R$	69,600	14,220	
3-3	P_m	8,000	6,150	1150
(T.S. - Shell Juncture)	$(P_L+P_b+Q)_R$	67,500	49,810	
4-4	P_m	19,000	6,550	1000
(T.S. - Header Juncture)	$(P_L+P_b+Q)_R$	71,500	20,310	
5-5 (T.S. Header Juncture)	P_m	19,000	7,150	1000
	$(P_L+P_b+Q)_R$	71,500	60,840	
6-6	P_m	19,000	8,470	1000
(Header Wall)	$(P_L+P_b+Q)_R$	71,500	31,320	
7-7	P_m	19,000	12,970	1000
	$(P_L+P_b+Q)_R$	71,500	37,090	
8-8	P_m	19,000	12,530	1000
	$(P_L+P_b+Q)_R$	71,500	does not control	

NOTE:
1. There are no primary bending stresses at Section 3-3 through 8-8
2. See Section 5.2.5 for creep fatigue interaction.
3. See Appendix C-2 for material properties and allowables.

*Primary plus secondary stress ranges conservatively include peak portions.

FIGURE 1

FINITE ELEMENT MODEL OF TUBESHEET - HEADER ASSEMBLY

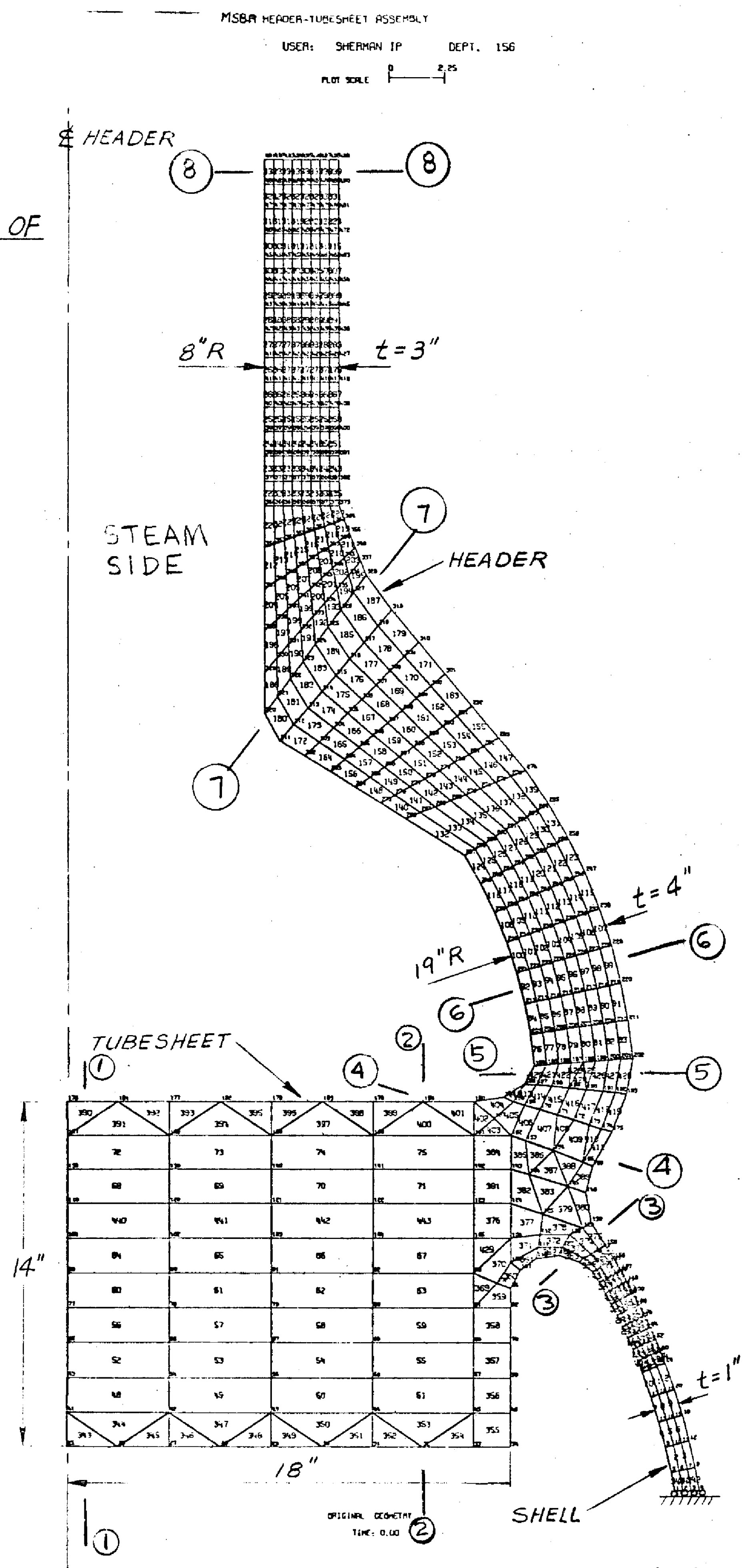

5.2.2 LOADING CONDITIONS

The maximum operating pressure on the steam side of the tubesheet is 3600 psi, while that on the salt side is 175 psi. A design condition of 4000 psi on the steam side with zero pressure on the salt side was conservatively chosen. The primary stresses shown in Table 1 are due to a 4000 psi steam side pressure.

In order to establish the maximum ranges of primary plus secondary stress intensities at the various locations of possible high stress, the thermal transients of Reference 2 were examined. The following transients, shown on Figure 2 and 3, were determined to be the most severe areas:

Severest Up Transient: Ramp Change in Load Damage from 100 to 40% in 3 Seconds (Load Scram)

Severest Down Transient: Insertion of Two Safety Rods (Reactor Scram)

The following load combinations were computed:

1) Pressure + reactor scram + steady state
2) Pressure + load scram + steady state
3) Pressure + reactor scram
4) Pressure + load scram

With pressure always acting, the maximum primary plus secondary stress intensity range is established by one of the following:

A) Condition (1) minus condition (2)
B) Condition (1) alone (or condition (2) alone)
C) Condition (3) alone (or condition (4) alone)

Appendix C-1 includes the calculation for all 3 cases. However, in Table 1, only the highest case is reported.

FIGURE 2 OUTLET STEAM TRANSIENT DUE TO CHANGE OF LOAD FROM 100% TO 40% IN 3 SECONDS, ALL CONTROLS OPERATING

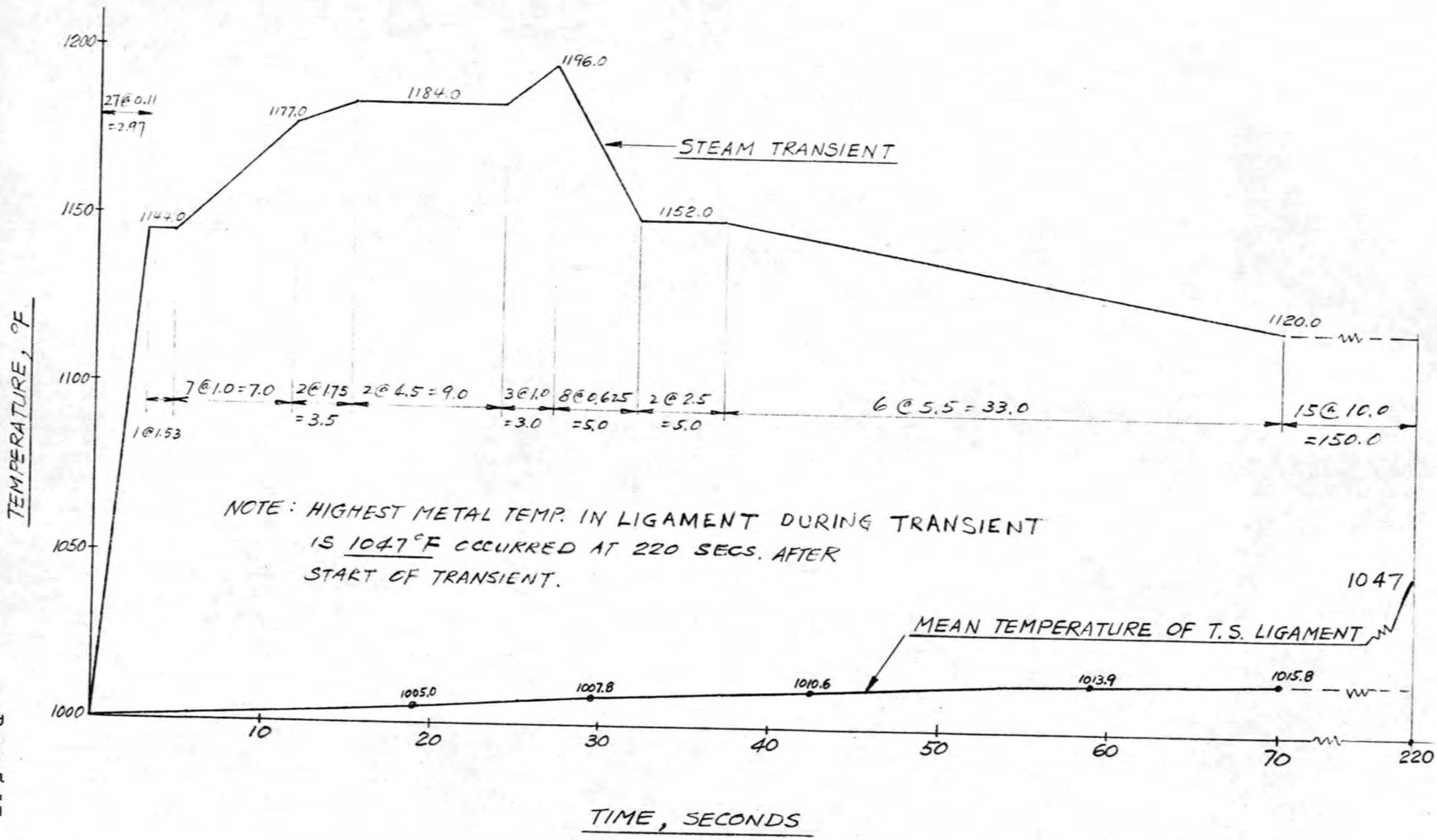

FIGURE 3 OUTLET HEADER STEAM TRANSIENT DUE TO REACTOR SCRAM WITH THERMAL LINER

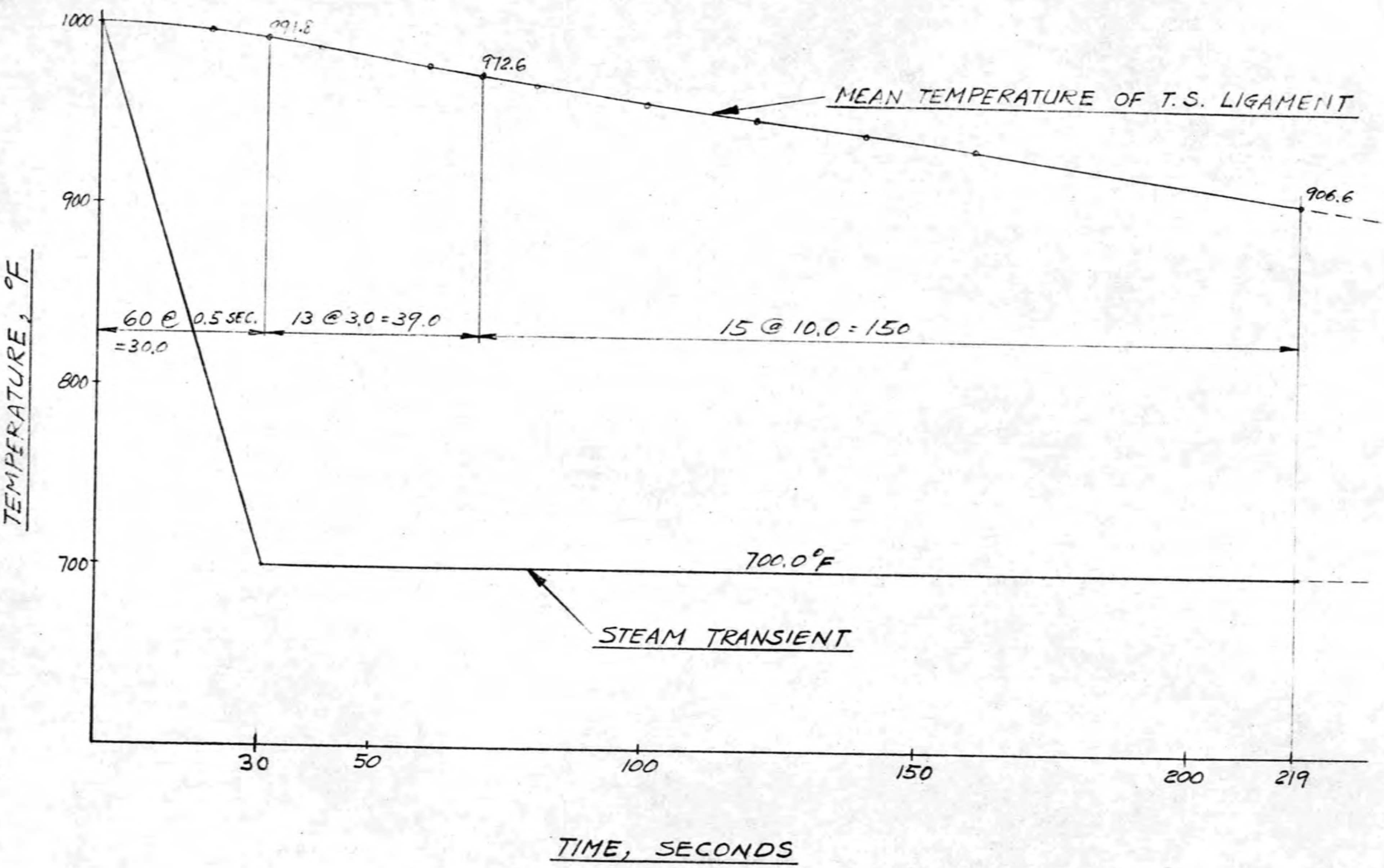

5.2.3 SOME DETAILS OF THE FINITE ELEMENT MODEL

Figure 1 shows the finite element model of the tubesheet-header assembly. The model was used for both pressure and thermal analysis. The liner (see Figure 4) was not modelled, as this would have made the number of elements very large and the model would have become costly to analyze. Instead, an equivalent film coefficient which simulated the thermal resistance of the liner was used.

The average temperature response of the perforated region of the tubesheet was determined from a separate finite element model of the ligament. The average ligament temperatures obtained from this model due to the load scram and reaction scram transients are shown in Figures 2 and 3, respectively. The elements in the perforated region of the complete finite element model (Figure 1) were "forced" to have the above temperature-time histories. Equivalent elastic constants were used (as determined from Section III of the ASME Code) in the perforated region of the tubesheet.

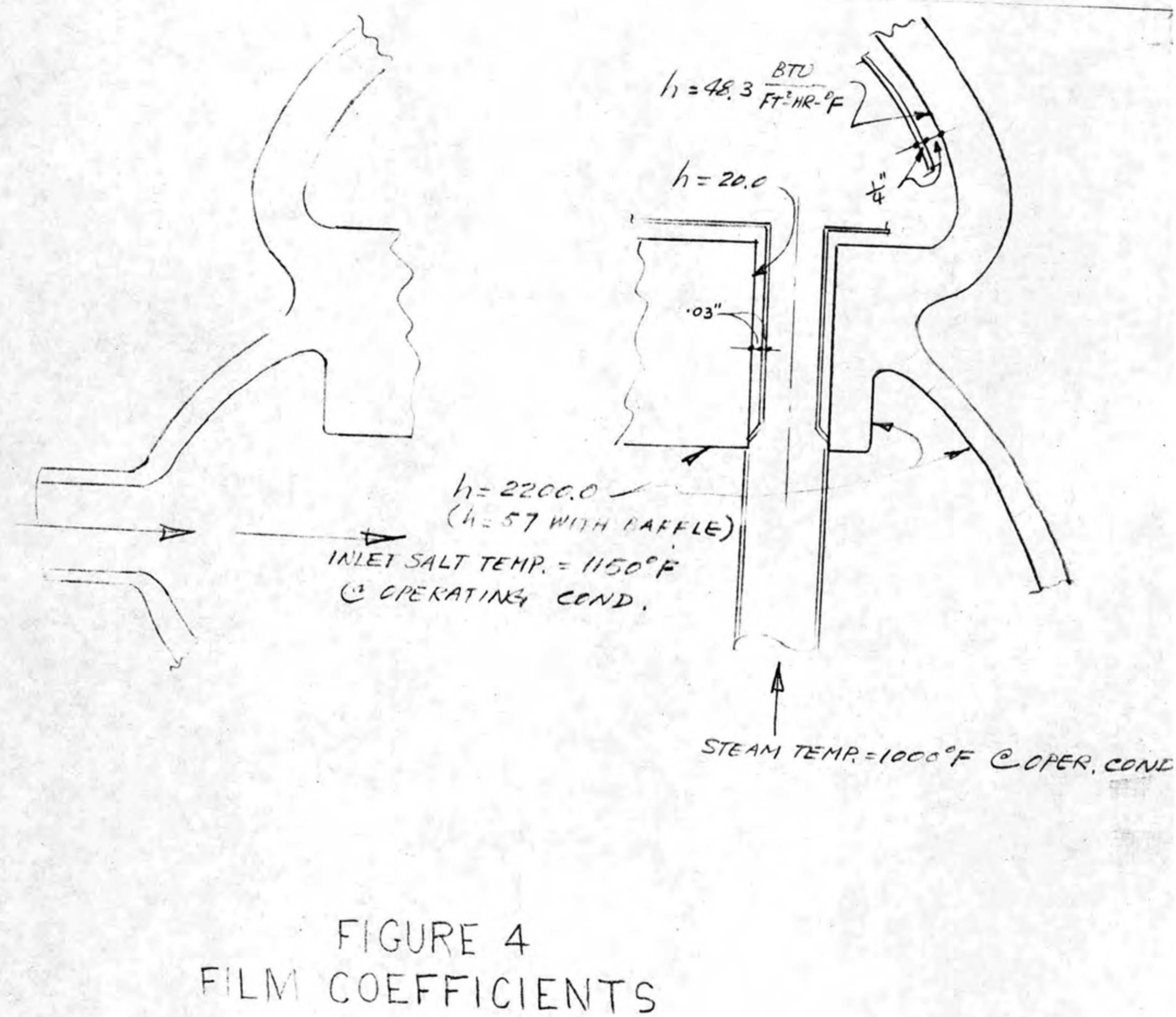

FIGURE 4
FILM COEFFICIENTS

FIGURE 5

DESIGN PRESSURE STRESS INTENSITY

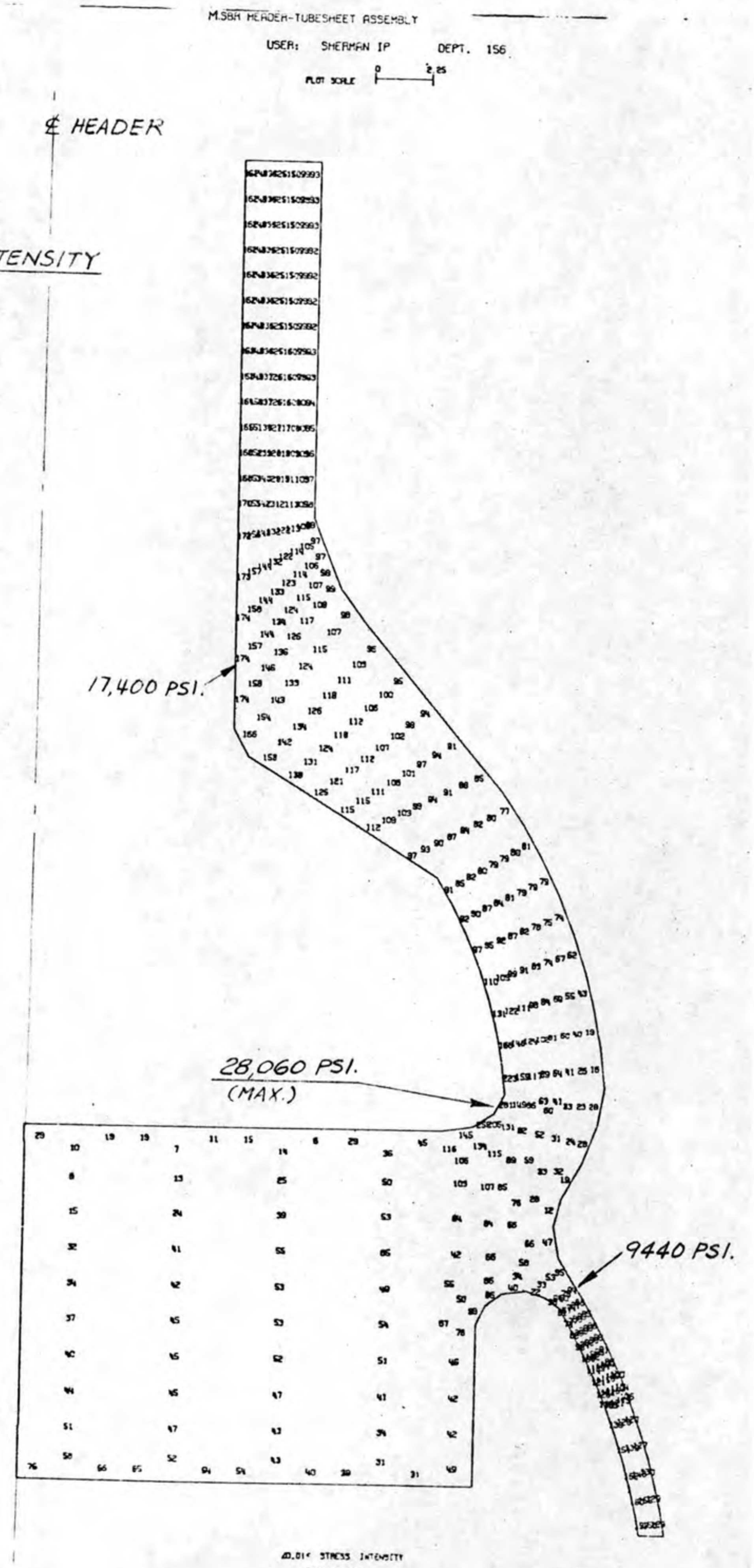

FIGURE 6

DESIGN PRESSURE STRESS INTENSITY CONTOUR

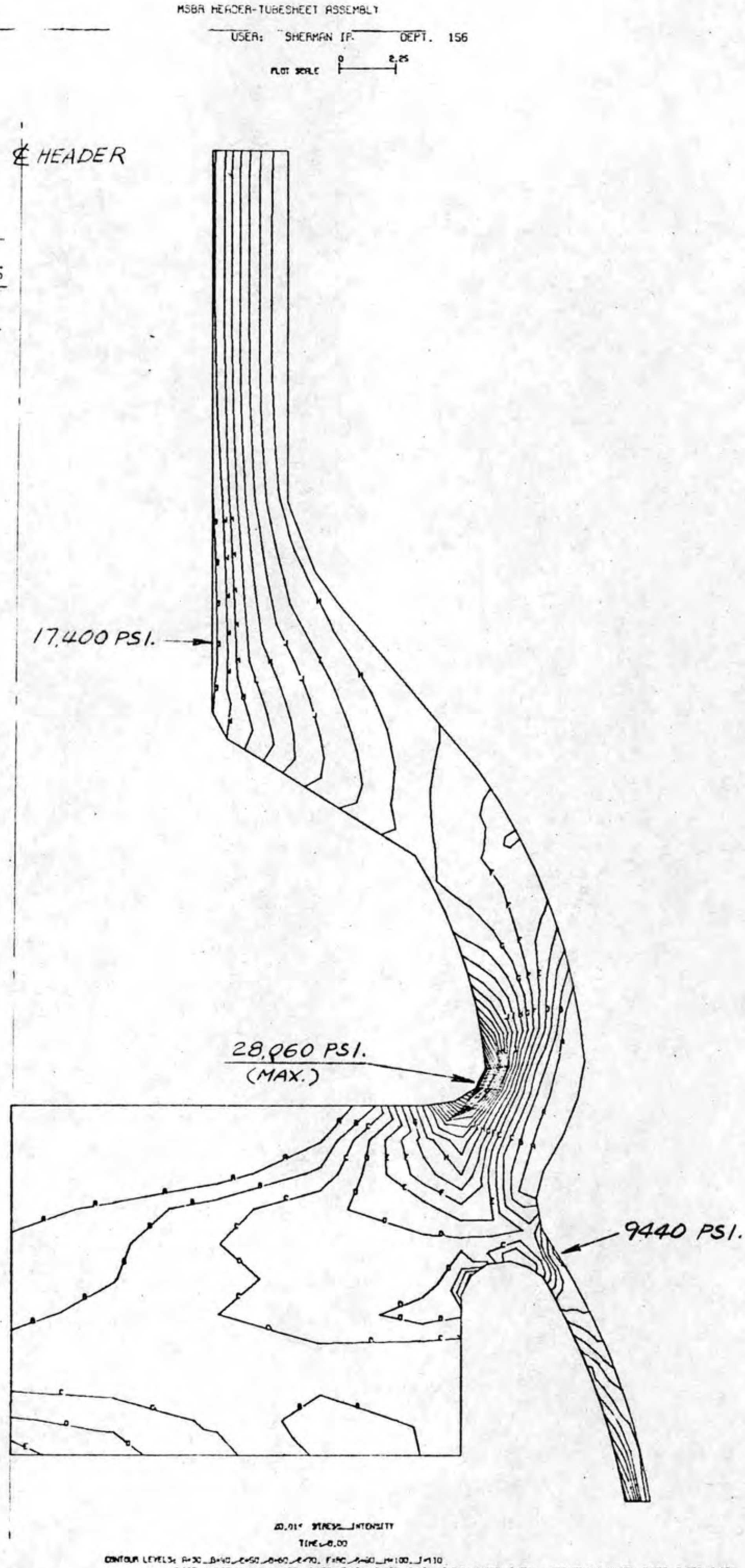

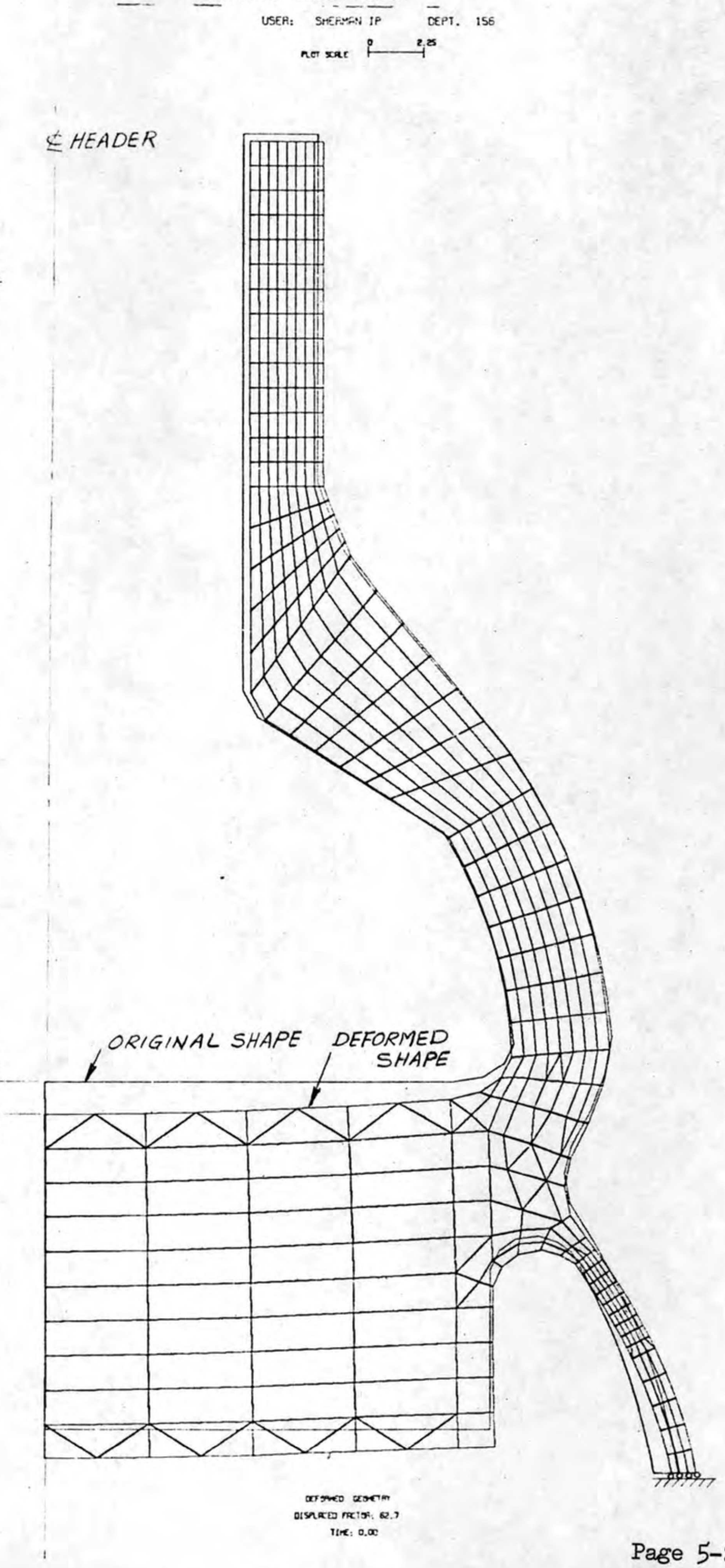

FIGURE 7
DEFORMED SHAPE FOR DESIGN PRESSURE

FIGURE 8

TEMPERATURE CONTOUR AT END OF 220 SEC OF REACTOR SCRAM TRANSIENT

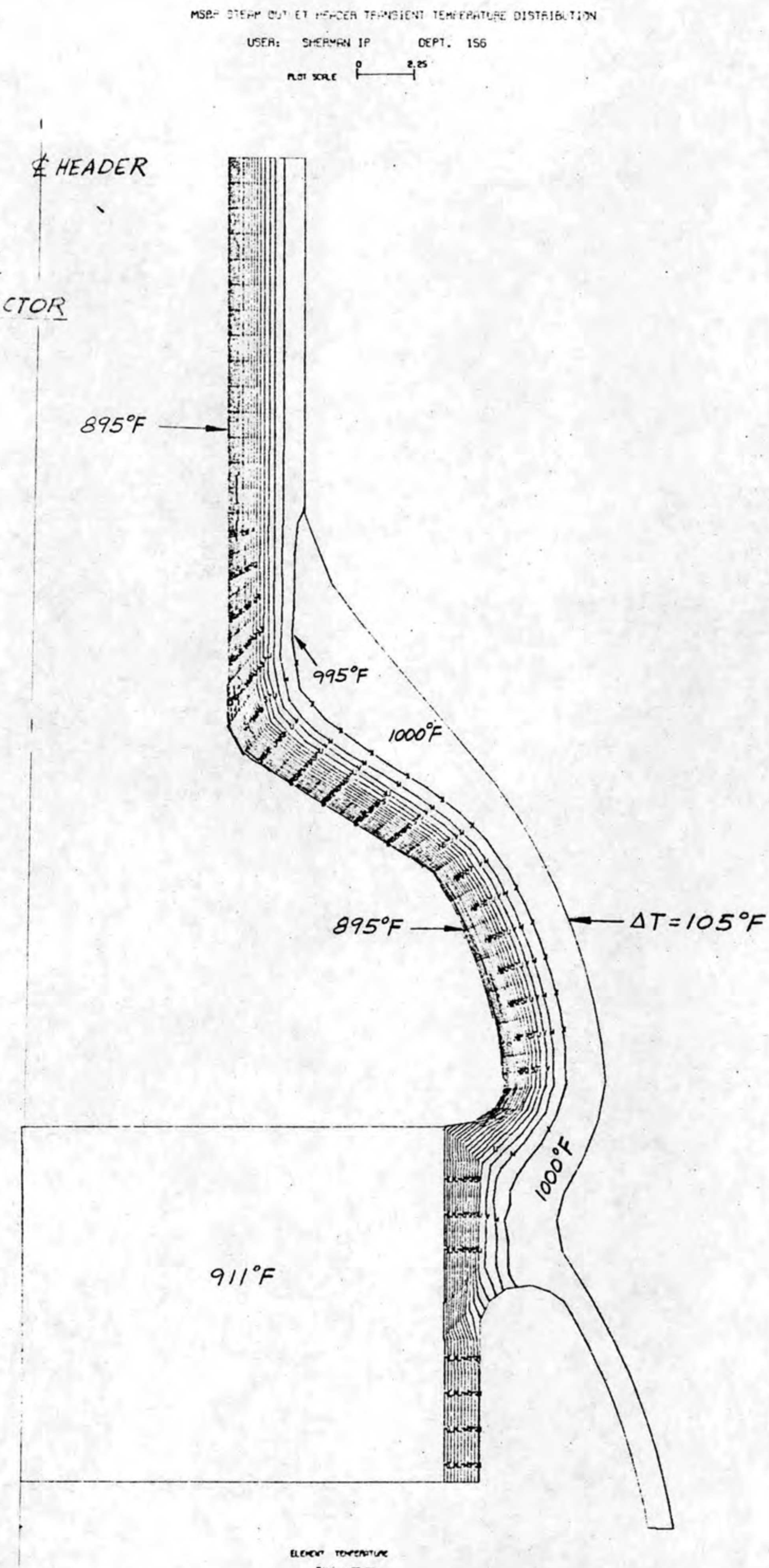

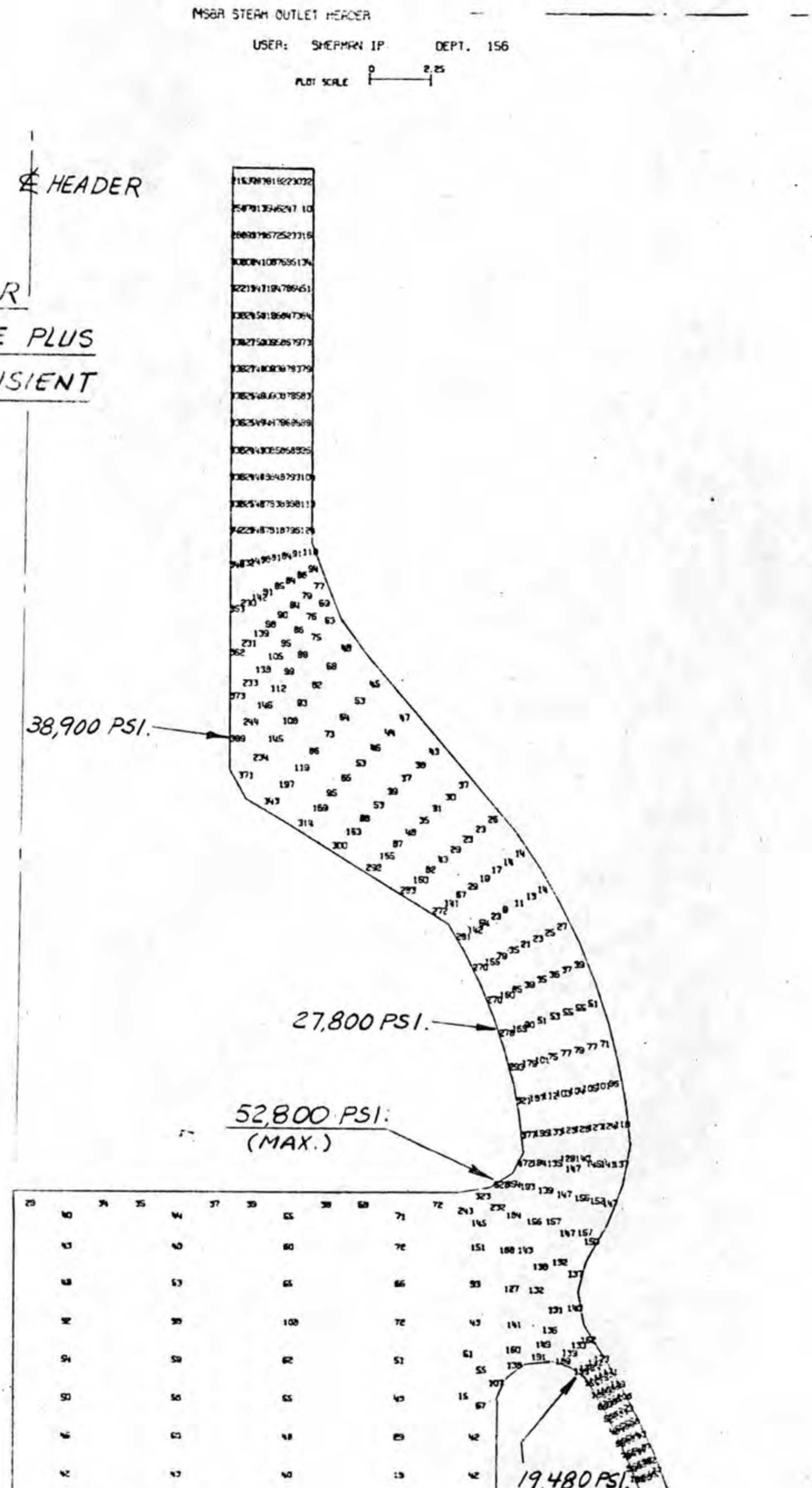

FIGURE 9
STRESS INTENSITY FOR
OPERATING PRESSURE PLUS
REACTOR SCRAM TRANSIENT

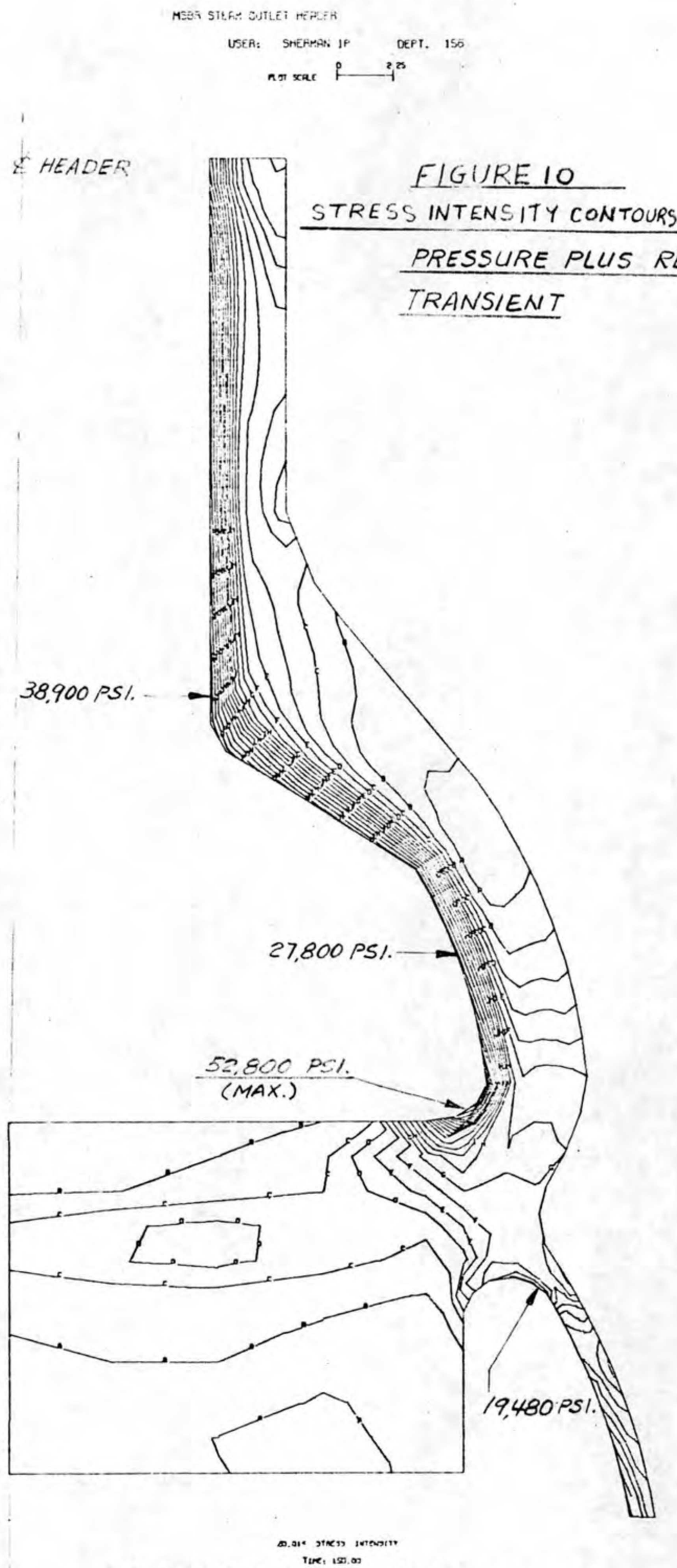

FIGURE 10

STRESS INTENSITY CONTOURS FOR OPERATING PRESSURE PLUS REACTOR SCRAM TRANSIENT

FIGURE 11

TEMPERATURE CONTOUR AT END OF 220 SEC. OF LOAD SCRAM TRANSIENT

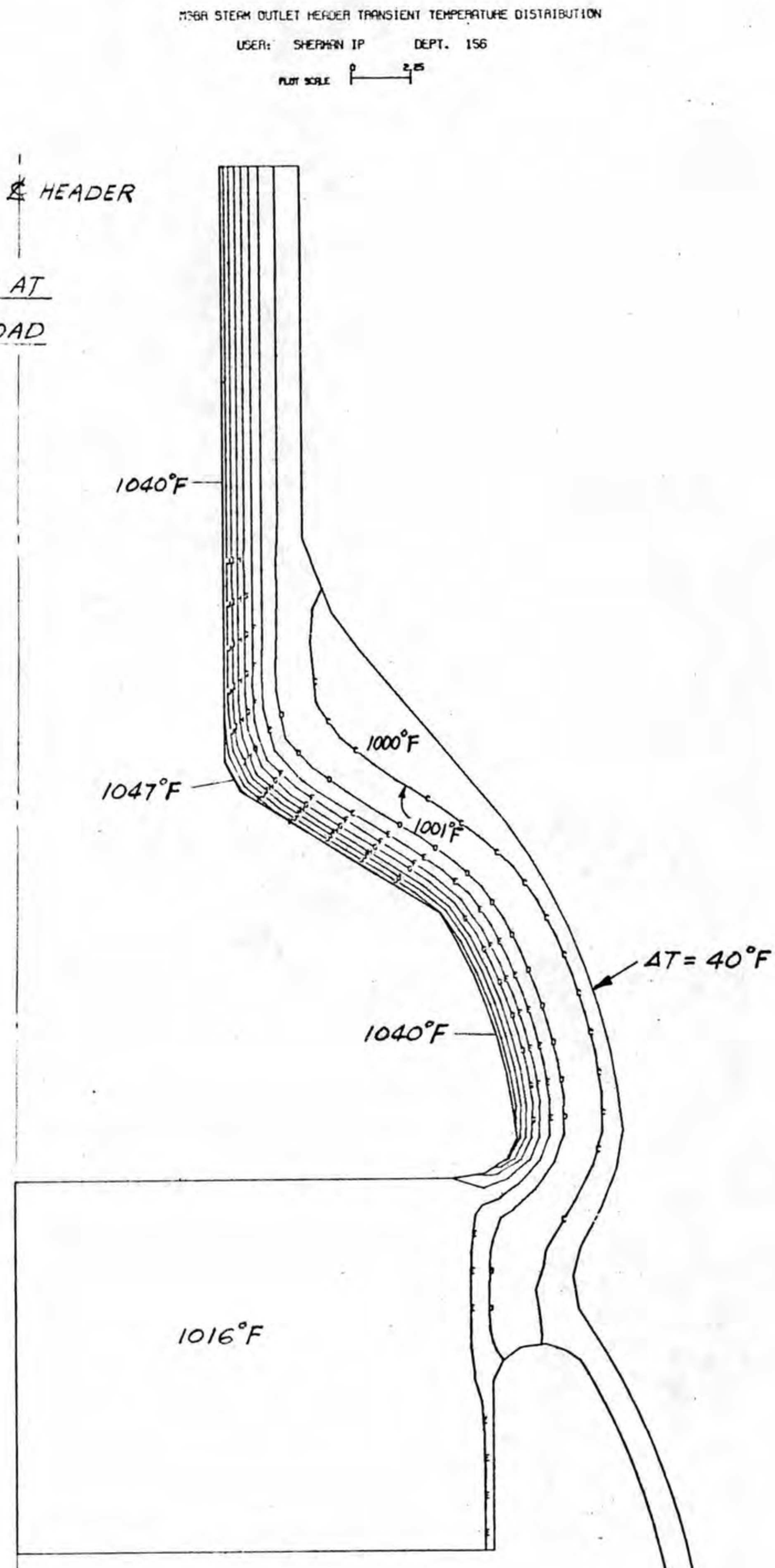

FIGURE 12

STRESS INTENSITY FOR OPERATING PRESSURE PLUS LOAD SCRAM TRANSIENT

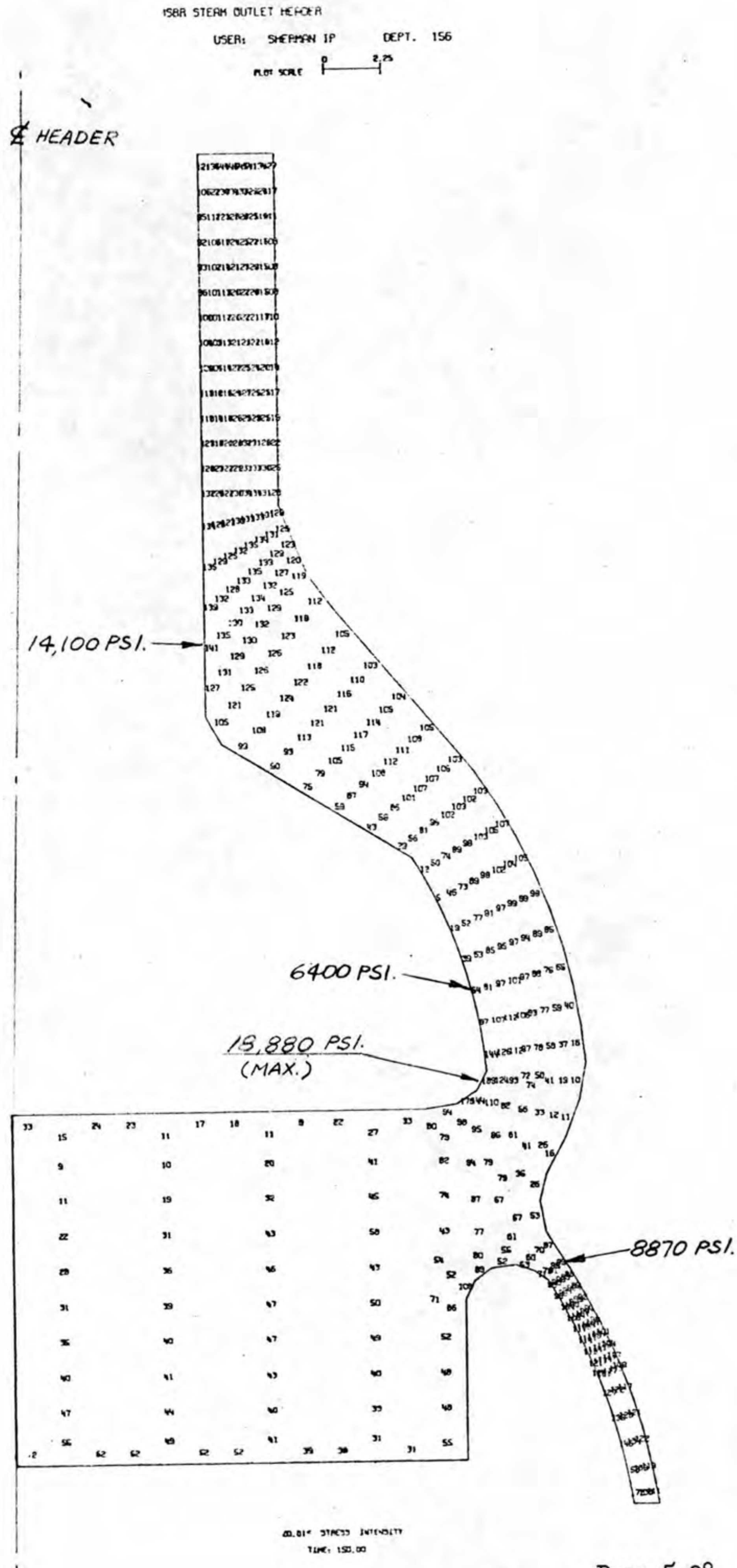

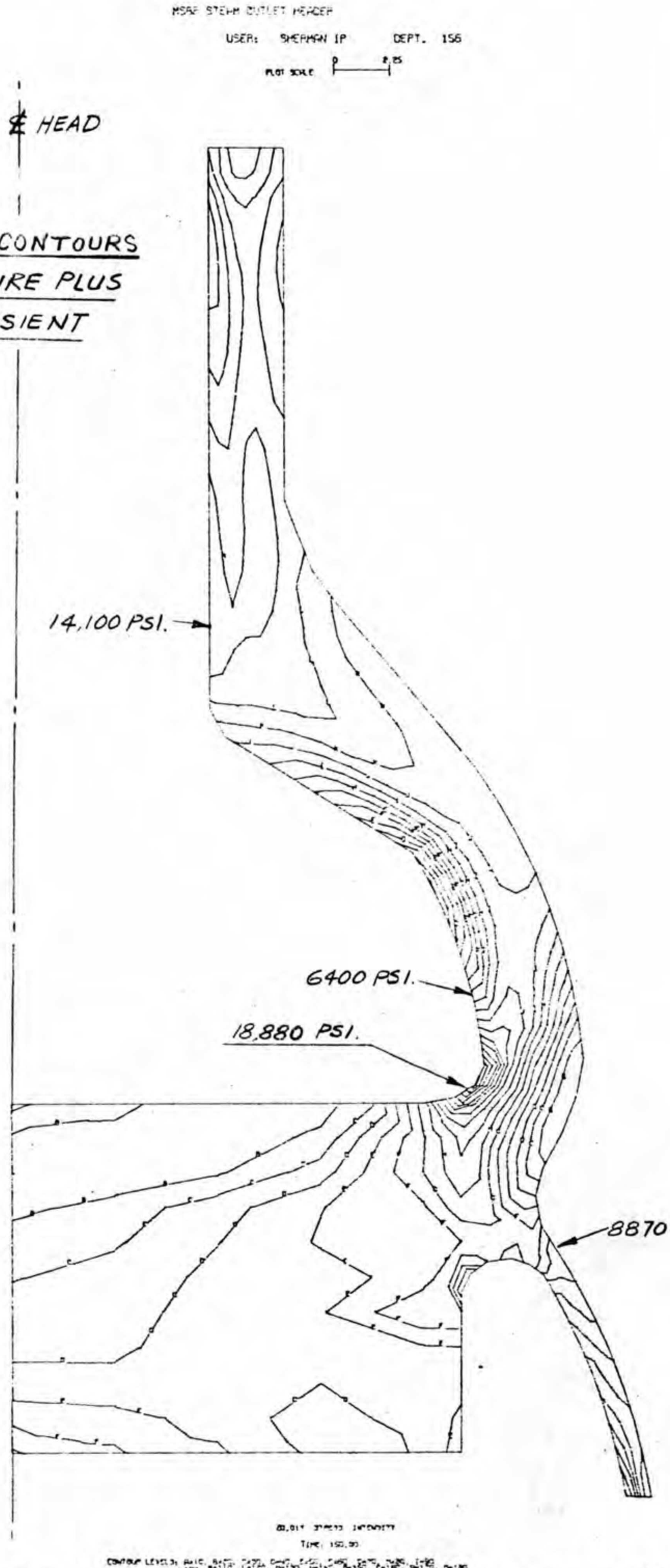

FIGURE 13
STRESS INTENSITY CONTOURS
OPERATING PRESSURE PLUS
LOAD SCRAM TRANSIENT

5.2.4 SIMPLIFIED INELASTIC ANALYSIS

Inelastic strains were calculated by Bree's simplified method (Reference 3). In the Bree Analysis, it is assumed that there are a total of 200 severe thermal cycles (sum of load scrams and reactor scrams). With a 30-year design life, the time per cycle is 262,800/200 = 1314 hours.

The derivation of the creep law used is given on the next page. The Bree Analysis of Reference 3 has been computerized by Foster Wheeler. The following results were obtained (Reference: Computer Output NHJLOST):

Location	Primary Stress, ksi	Secondary Stress, ksi	Total Strain/Cycle, %	Total Strain
1-1	8.57	23.36	10^{-4}	0.02%
2-2	12.16	14.22	10^{-4}	0.02%
3-3	6.15	49.81	5×10^{-4}	0.1%
4-4	6.55	20.31	0	0
5-5	7.15	60.84	8×10^{-4}	0.16%
6-6	8.47	31.32	2×10^{-4}	0.04%
7-7	12.97	37.09	8×10^{-4}	0.16%

DERIVATION OF CREEP CONSTANTS FOR THE POWER LAW

$$\dot{\eta}_c = A\,\sigma^n$$

WHERE: $\dot{\eta}_c$ = CREEP RATE (ACCOUNTS O[illegible] FOR SECONDARY CREEP EFF[illegible]

σ = STEADY-STATE APPLIED PRIMARY LOAD.

A, n = CREEP CONSTANTS O[illegible] MATERIAL AT TEMPERATU[illegible]

REFER TO FIG. 10 OF "DATA FOR NICKEL-MOLYBDENUM-CHROMIUM-IRON ALLOY, INOR-8".

FOR TEMP. = 1100° F :

$$\dot{\eta}_c = 2 \times 10^{-8} = A\,(9.95 \times 10^{3})^{n} \qquad (1)$$

$$\dot{\eta}_c = 4 \times 10^{-7} = A\,(2 \times 10^{4})^{n} \qquad (2)$$

SOLVING (1) & (2),

$$20 = 2.01005^{n}$$

$$n = \underline{4.3}$$

$$A = \underline{1.28 \times 10^{-25}}$$

<u>FOR TEMP. = 1200 °F :</u>

$$\dot{\eta}_c = 4 \times 10^{-7} = A\,(10^4)^n$$

$$\dot{\eta}_c = 4.5 \times 10^{-5} = A\,(3 \times 10^4)^n$$

$$\frac{10^{-2}}{1.125} = \left(\frac{1}{3}\right)^n$$

$$0.00889 = 0.3334^n$$

$$n = 4.3$$

$$A = \frac{4 \times 10^{-7}}{(10^4)^{4.3}} = \underline{2.52 \times 10^{-24}}$$

<u>FOR TEMP. = 1300 °F :</u>

$$\dot{\eta}_c = 9 \times 10^{-8} = A\,(4 \times 10^3)^n$$

$$\dot{\eta}_c = 9 \times 10^{-5} = A\,(2 \times 10^4)^n$$

$$10^{-3} = \left(\frac{1}{5}\right)^n$$

$$0.001 = 0.2^n$$

$$n = 4.3$$

$$A = \frac{9 \times 10^{-5}}{(2 \times 10^4)^{4.3}} = \underline{2.88 \times 10^{-23}}$$

5.2.5 FATIGUE ANALYSIS AND CREEP FATIGUE INTERACTION

A preliminary fatigue analysis was made with the aid of Code Case 1331-4. The following results were obtained. Allowable cycles were obtained at 1100°F.

Location	S Ksi	Ref. Page	Salt	N all
1-1	33.62	C-1-5	16.81	15000
2-2	22.76	C-1-9	11.38	∞
3-3	49.81	C-1-10	24.91	2,500
4-4	20.31	C-1-11	10.16	∞
5-5	60.84	C-1-13	30.42	1,300
6-6	31.32	C-1-15	15.66	20,000
7-7	37.09	C-1-16	18.55	10,000

With only 200 severe thermal cycles, maximum fatigue damage is 200/1300 = 0.15 which occurs at location 5-5. This value is well below the allowable value of 1.0.

CREEP FATIGUE INTERACTION

Creep fatigue interaction was performed by the method described in the nozzle portion of this report. Location 7-7 proved to be the most severely loaded section, and only that section was analyzed. The section was idealized as a cylinder with 8" inside radius and 4" thickness. The following loading was applied:

$pR_m/t = p \times 8/4 = 12970 \times 3600/4000$ (refer to Appendix C-1 for source of 12,970)

solving for p, p = 5836 psi

$$\frac{E\alpha\Delta T}{2(1-\nu)} = \left.\begin{matrix} 22184 \\ -8362 \end{matrix}\right\} \quad \Delta T = \left\{\begin{matrix} 156 \\ -59 \end{matrix}\right.$$

where $E = 26.7 \times 10^6$, $\alpha = 7.43 \times 10^{-6}$

PROGRAM RESULTS

The same type of loading histogram was used for the tubesheet as was used for the inlet nozzle. There are a total of 50 cycles, each cycle consisting of 3 load scrams and 1 reactor scram. The program was run for five cycles and the strain for each remaining cycle was estimated by taking the difference in strains between the fourth and fifth cycles.

Maximum total strength = 0.432 + 45 (0.01) = 0.88%

Creep damage = 0.0135 + 45 (.0026) = 0.13

Maximum strain range = 0.381%

(Maximum temp = 1000°F)

Fatigue damage = 50/500 = 0.1

Total creep fatigue damage = 0.23<1.

Ref: Computer Run EBHJL06C

FWC FORM 172 - 4

—NOTATIONS IN THIS COLUMN INDICATE WHERE CHANGES HAVE BEEN MADE—

5.3 STRESS ANALYSIS OF THE MSBR SHELL

5.3.1 INTRODUCTION AND SUMMARY

The MSBR shell was analyzed for both pressure and thermal transient stresses. Three locations of possible high stresses were selected, and are shown in Figure 1.

At locations A and B, pressure stresses were determined by hand calculation. Temperature distributions and thermal stresses were determined using the finite element models shown in Figure 2. At location C, the finite element model shown in Figure 3 was used to determine pressure stresses, temperature distributions, and thermal stresses.

Table 1 gives a summary of the stresses obtained at the three locations. Primary stresses are due to a design pressure of 300 psi or an operating pressure of 235 psi, while primary plus secondary stress intensity ranges are due to an operating pressure of 235 psi, the severest up thermal transient, and the severest down thermal transient. Examination of Reference 1 indicates that a "Ramp Change in Load from 100% to 40% in 3 Seconds" (Load Scram) is the most severe up transient, while "Insertion of Two Safety Rods" (Reactors Scram) is the most severe down transient (Figure 4).

The stresses in Table 1 are categorized in accordance with the rules of ASME Code Case 1331-5. Although the Code Case does not place a stress limit on the primary plus secondary stress intensity range, the $3S_m$ limit was calculated for reference purposes.

The effect of the tube thermal expansion loads on the shell was calculated by hand and found to be negligible (<200 psi).

FWC FORM 172 - 4

NOTATIONS IN THIS COLUMN INDICATE WHERE CHANGES HAVE BEEN MADE

TABLE I - STRESS SUMMARY - MSBR SHELL

Location		Stress Category	Calculated Stress Intensity	Allowable
DESIGN CONDITION	A	P_m	8.2	S_o=9.5
		P_L+P_b	8.2	$1.5S_o$=14.25
	B	P_m	0.3	S_o=9.5
		P_L+P_b	0.3	$1.5S_o$=14.25
	C	P_m	8.2	S_o=9.5
		P_L+P_b	10.3	$1.5S_o$=14.25
OPERATING CONDITION	A	P_m	6.4	S_{mt}=7.5
		P_L+P_b	6.4	KS_t=7.8
		P_L+P_b+Q	38.9	$3S_m$=67.5
	B	P_m	.2	S_{mt}=7.5
		P_L+P_b	.2	KS_t=9.3
		P_L+P_b+Q	4.1	$3S_m$=67.5
	C	P_m	6.4	S_{mt}=7.5
		P_L+P_b	8.0	KS_t=7.8
		P_L+P_b+Q	45.0	$3S_m$=67.5

NOTE: All allowables are at 1150°F

See Appendix C-2 for material properties and allowables.

See Section 5.3.6 for creep fatigue interaction.

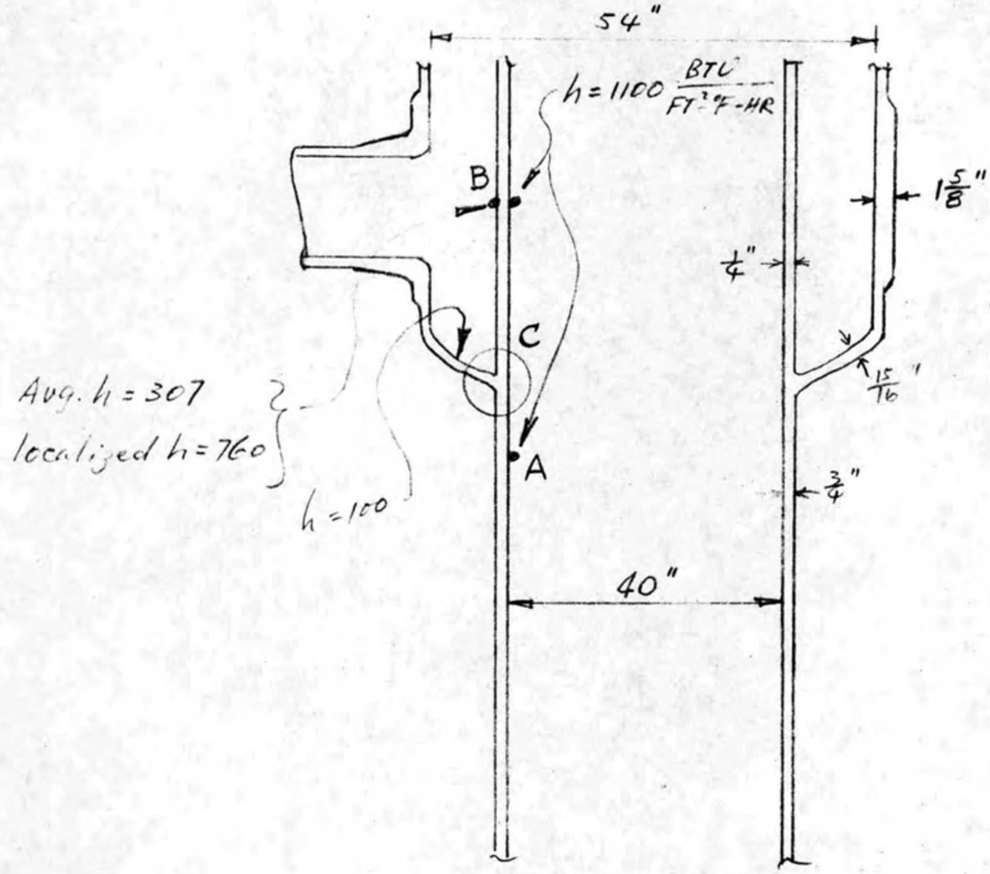
54"
h = 1100 BTU / FT² °F-HR
B
1 5/8"
1/4"
C
15/16"
Avg. h = 307
localized h = 760
A
3/4"
h = 100
40"

FIGURE 1

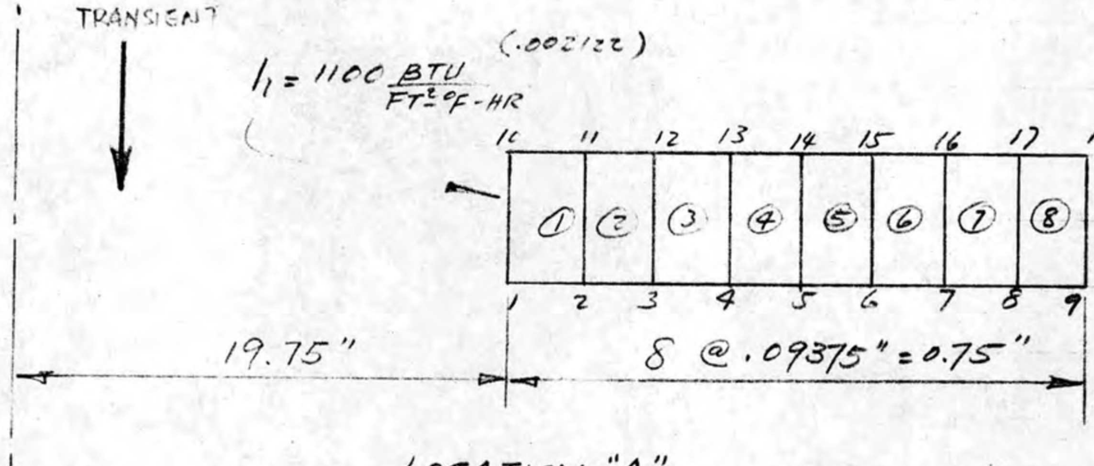

LOCATION "A"

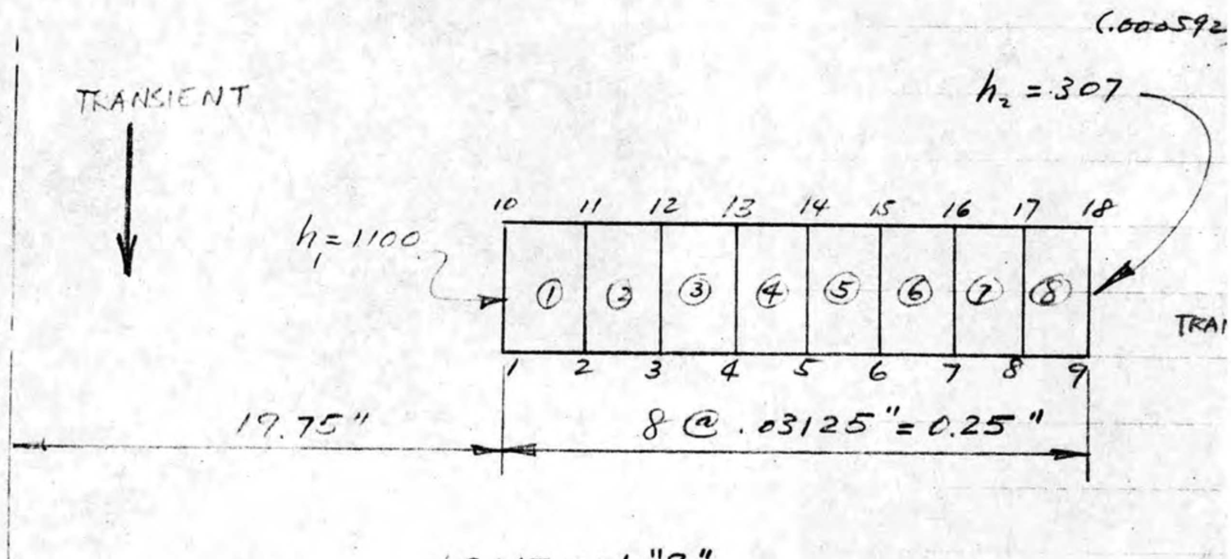

LOCATION "B"

FIGURE 2: FINITE ELEMENT MODELS

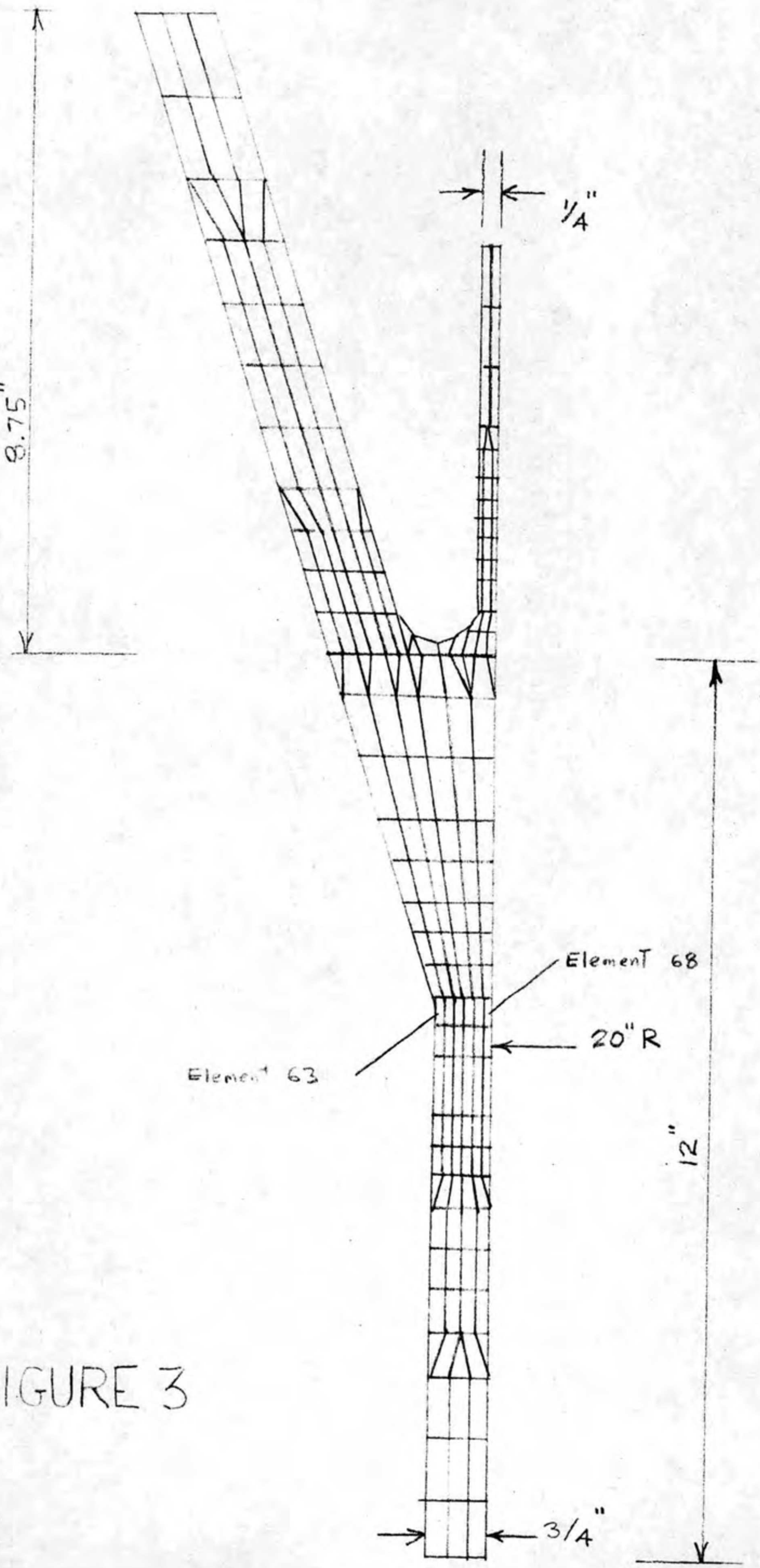

FIGURE 3

FORM (285)-47

FIGURE 4

COMBINED INLET SALT TRANSIENT DUE TO REACTOR SCRAM AND LOAD SCRAM

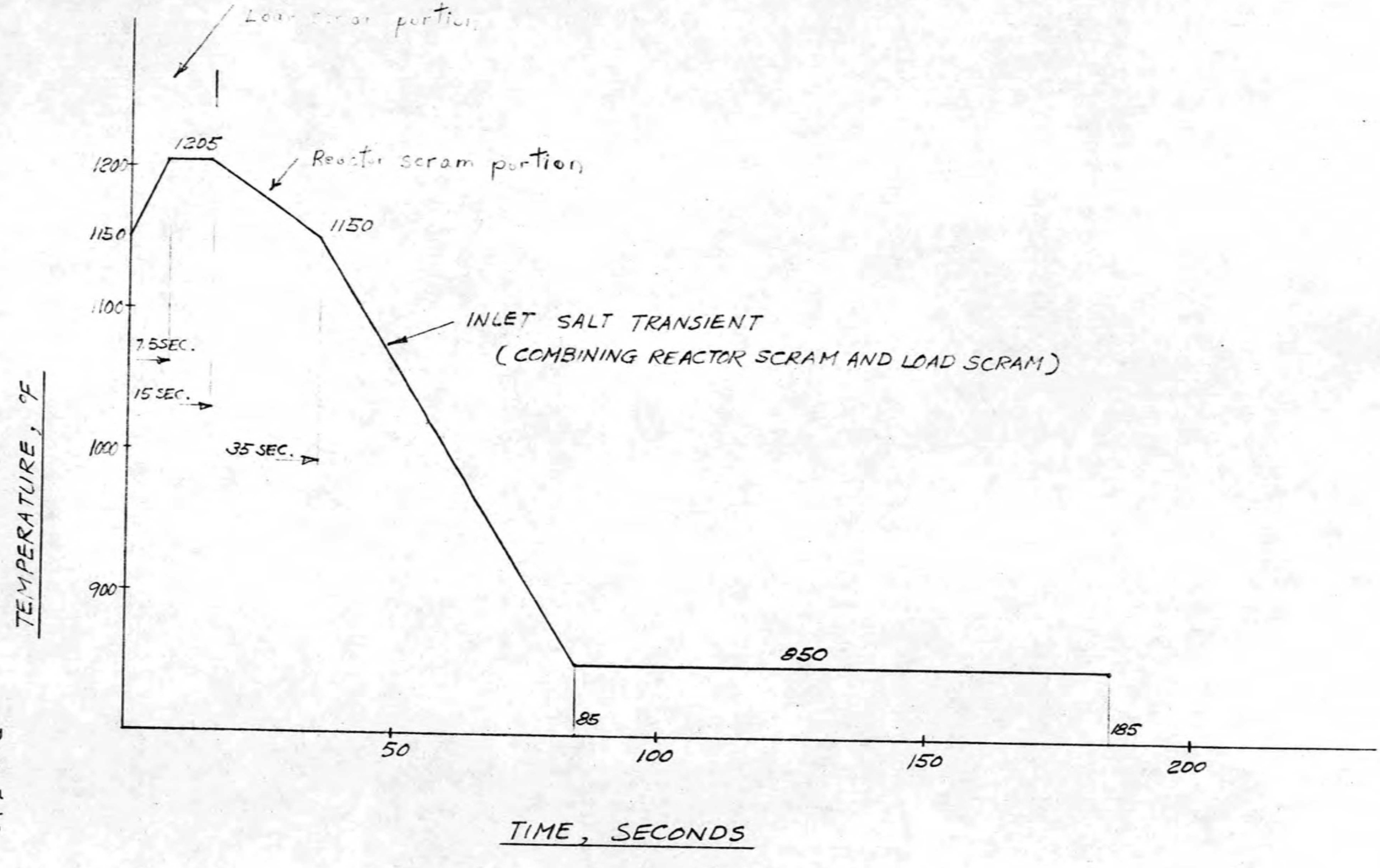

5.3.2 SHELL STRESSES AT LOCATION "A"

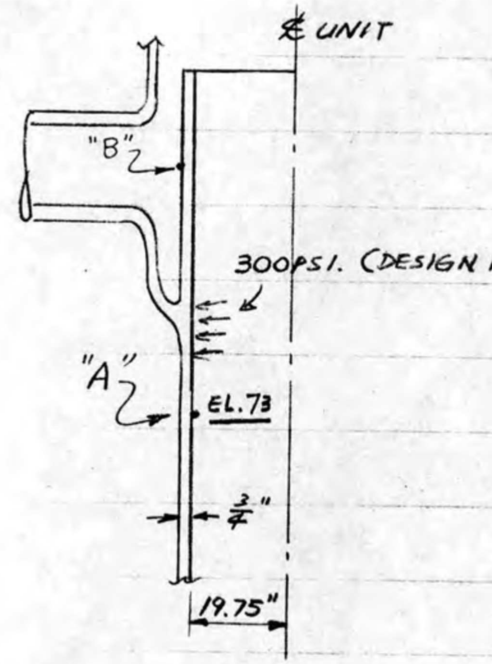

DESIGN PRESSURE STRESS

$$\sigma_Z = \frac{300 \times 19.75}{2 \times 0.75} = +3950 \text{ PSI.}$$

$$\sigma_T = 2 \times 3950 = +7900 \text{ PSI.}$$

$$\sigma_R = -300 \text{ PSI. (I.S.)}$$

SI = 8200 psi

TRANSIENT TEMPERATURE STRESSES

	σ_R	σ_Z	σ_T	σ_{RZ}	STRESS IN
① REACTOR SCRAM	90	15,800	31,690	-20	31,610
② LOAD SCRAM	-20	-3,780	-7,300	10	7,280
① + ② + OPER. PRESS.	110	19,580	38,990	-30	38,880

$$\sigma_1, \sigma_2 = \tfrac{1}{2}(19{,}580 + 110) \pm \left[\left(\frac{19{,}580 - 110}{2}\right)^2 + (-30)^2\right]^{\frac{1}{2}}$$

$$= 9845 \pm 9735$$

$$= 19{,}580,\ 110$$

$$\sigma_3 = \sigma_T = 38{,}990,$$

STRESS INTENSITY = 38,990 − 110 = 38,880 PSI.

NOTE: MAX. REACTOR SCRAM STRESS OCCURS AT END OF 85 SEC. AFTER START OF SCRAM. $\Delta T = 171°F$.
MAX. LOAD SCRAM STRESS OCCURS AT END OF 15 SEC. AFTER START OF SCRAM. $\Delta T = 38°F$.

5.3.3 SHELL STRESSES AT LOCATION "B"

DESIGN PRESSURE STRESS

$\sigma_T = \sigma_Z = 0$

$\sigma_R = -300$ PSI. (AT THE SURFACES)

TRANSIENT TEMPERATURE STRESSES

	σ_R	σ_Z	σ_T	σ_{RZ}	STRESS I
① REACTOR SCRAM	4	1538	2282	2	2278
② LOAD SCRAM	-3	-1267	-1837	-1	1833
① + ② + OP. PRESSURE	7	2805	4119	3	4112

$$\sigma_1, \sigma_2 = \frac{1}{2}(2805 + 7) \pm \left[\left(\frac{2805-7}{2}\right)^2 + (3)^2\right]^{\frac{1}{2}}$$
$$= 1406 \pm 1399$$
$$= 2805,\ 7$$
$$\sigma_3 = \sigma_T = 4119$$

STRESS INTENSITY = 4119 - 7 = 4112 PSI.

NOTE: MAX. REACTOR SCRAM STRESS OCCURS AT END OF 67 SEC. AFTER START OF SCRAM. $\Delta T = 15°F$
MAX. LOAD SCRAM STRESS OCCURS AT END OF 7.5 SEC. AFTER START OF SCRAM. $\Delta T = 12°F$

FOSTER WHEELER CORPORATION — 110 SOUTH ORANGE AVE., LIVINGSTON, N.

BY [initials] DATE 5/31/74 SUBJECT SHEET NO. 1 OF

CHKD. BY DATE JOB NO.

5.3.4 SHELL SHROUD JUNCTURE STRESSES

I PRESSURE STRESSES (MAXIMUM STRESSES AT ELEMENTS 63-68 DUE TO 300 PSI DESIGN PRESSURE)

FROM FIGURE 5 WE OBTAIN THE FOLLOWING MEMBRANE STRESSES

$\sigma_r^m = 0.0236$ KSI $\quad \sigma_z^m = 4.19$

$\sigma_t^m = 10.31$ $\quad \sigma_{rz}^m = 0.361$

PRINCIPAL STRESSES:

$\sigma_1 = 10.31$ KSI
$\sigma_2 = 4.221$
$\sigma_3 = -0.007$

MAXIMUM STRESS INTENSITY = 10.32 KSI = P_L

FROM FIGURE 5, WE OBTAIN THE MAXIMUM LINEARIZED BENDING STRESSES:

$\sigma_r^b = 0.361$ $\quad \sigma_z^b = 4.38$

$\sigma_t^b = 1.21$ $\quad \sigma_{rz}^b = 0.668$

SP 10307A

 FORM (285)-47

FOR THE DESIGN CONDITION ($p = 300$ psi)

$P_m = 8.2$ ksi $< S_o = 9.5$ ksi @ 1150°F

$P_L = 10.32 < 1.5 S_o = 14.25$ ksi

FOR THE OPERATING CONDITION ($p = 235$ psi)

$P_m = 6.43 < S_{mt} = 8.0$ ksi

$P_L = 8.07 < kS_t = 1.25 \times 8 - 0.25 \times 6.43 = 8.39$

II PRESSURE + THERMAL STRESS:
MAXIMUM STRESS INTENSITY RANGE (REF. 6)

ELEMENTS 63-68 (SEE FIG.'S 6-7; LINEARIZED STRES
ARE GIVEN BELOW

	σ_r	σ_z	σ_θ	σ_{rz}	S.I.
113 SEC.	0.11	31.78	40.78	0.61	REACTOR SCRAM
17 SEC.	-0.36	-13.62	-0.58*	-0.69	LOAD SCRAM
Range:	0.47	45.4	41.36	1.30	45.0

A value of -13.93 was previously conservatively calculated and was used in the fatigue and creep fatigue interaction.

SF 18107A

FOSTER WHEELER CORPORATION 110 SOUTH ORANGE AVE., LIVINGSTON, N

BY 9C DATE 5/28/74 SUBJECT MSBR Y- JUNCTION SHEET NO. 5 OF

CHKD. BY DATE JOB NO.

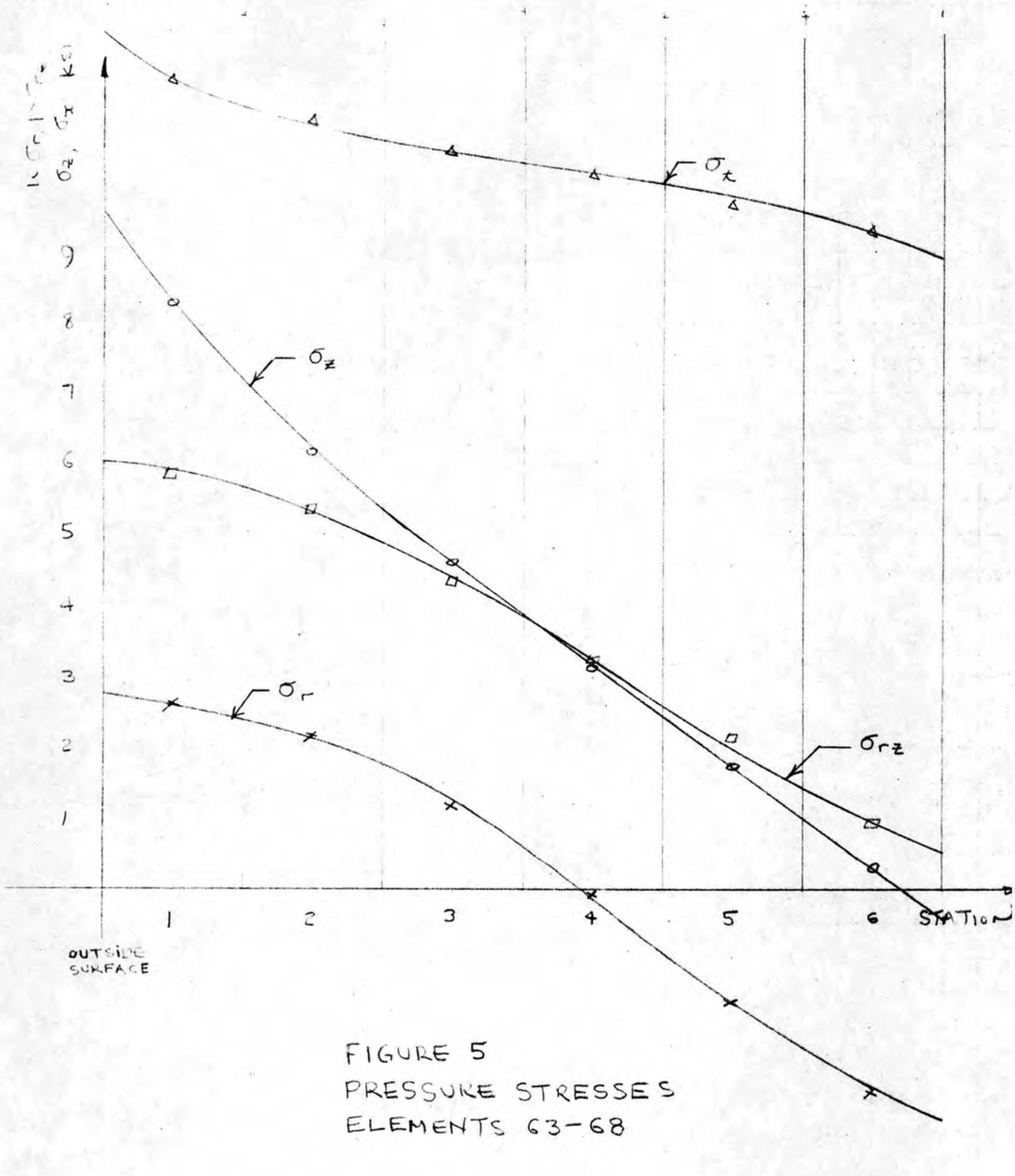

FIGURE 5
PRESSURE STRESSES
ELEMENTS 63-68

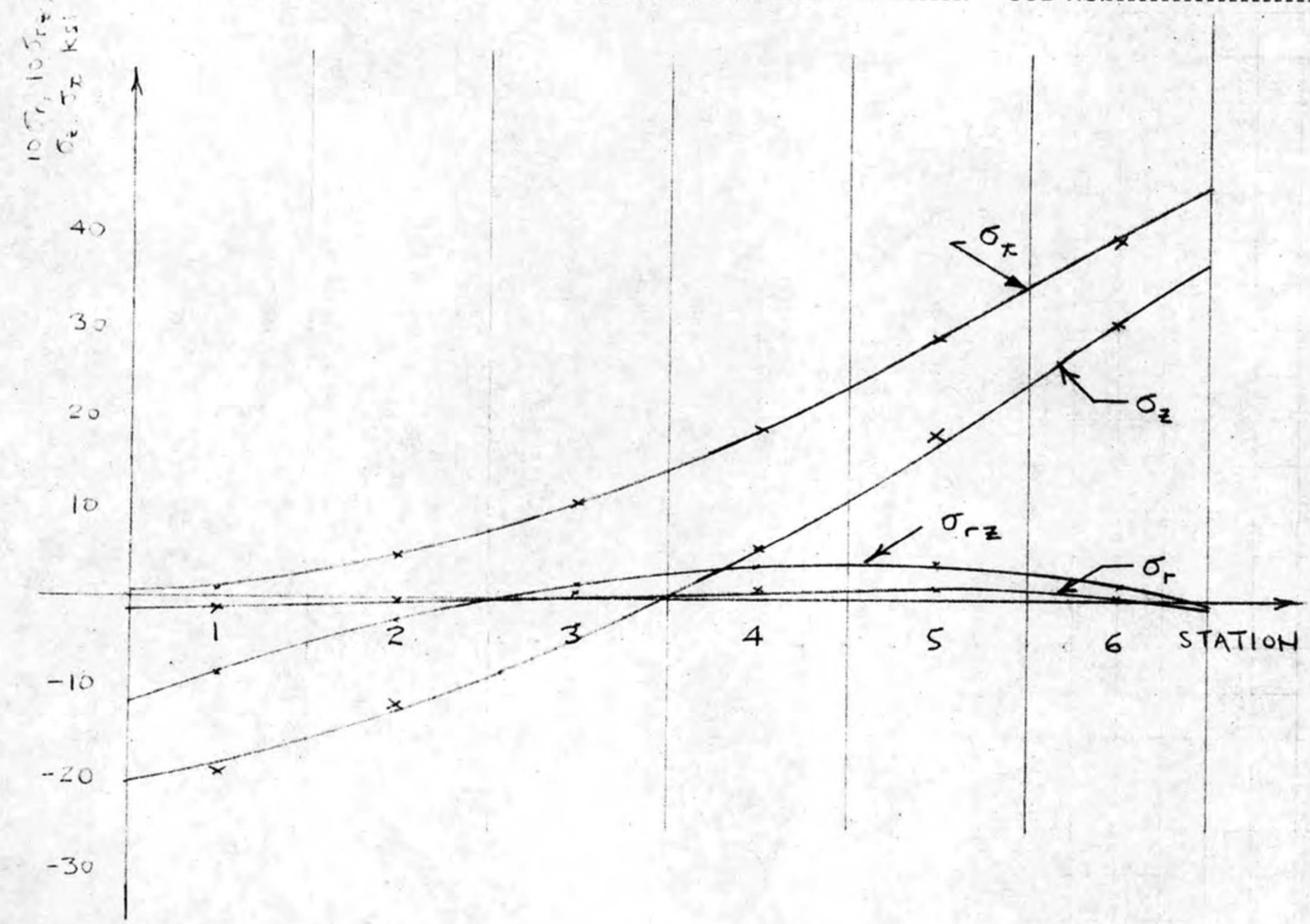

FIGURE 6
THERMAL STRESSES
ELEMENTS 63-68
TIME = 113 SECONDS

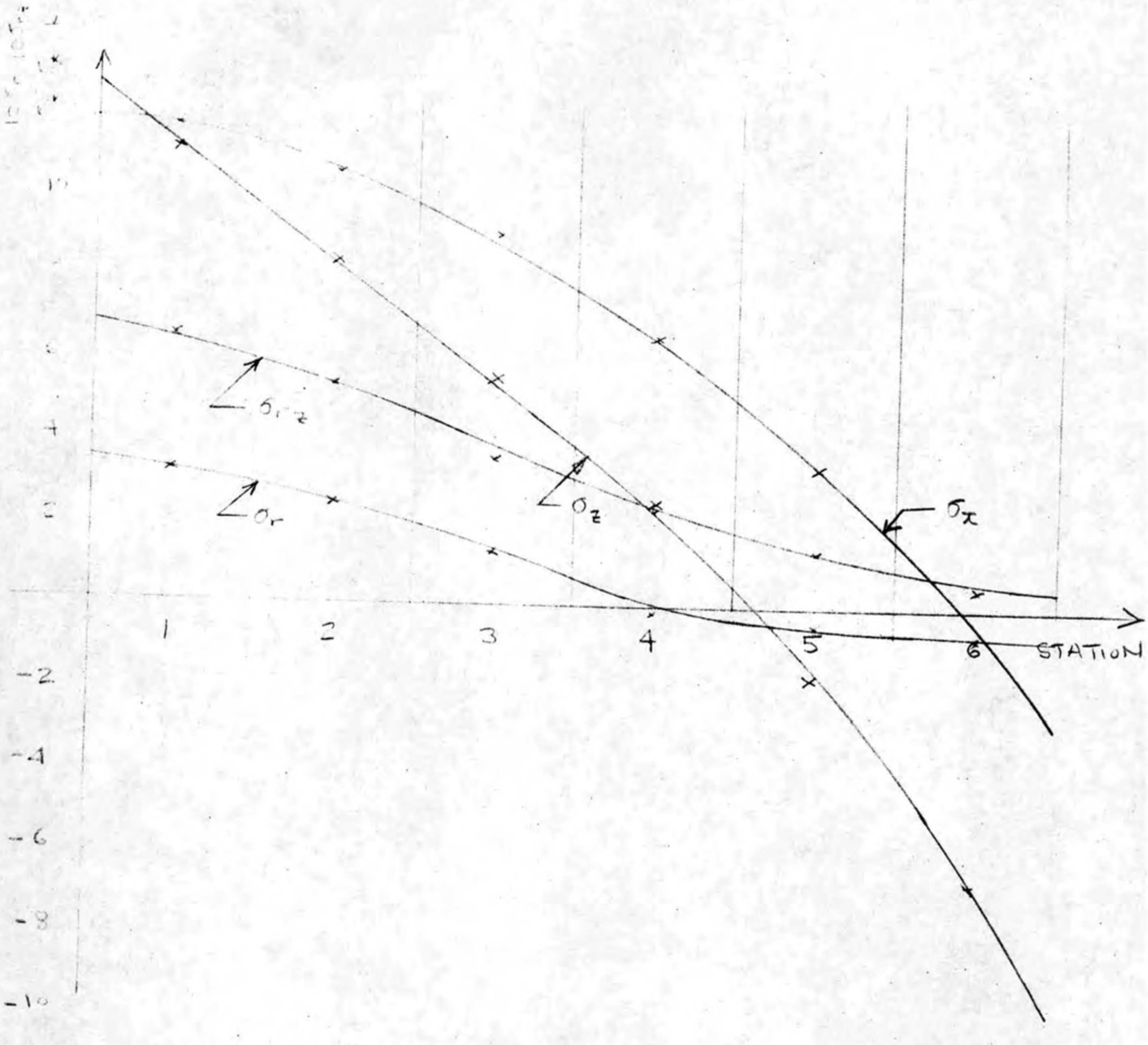

FIGURE 7
THERMAL STRESSES
ELEMENT 63-68
TIME = 17 SECONDS

5.3.5 SIMPLIFIED INELASTIC ANALYSIS

Inelastic strains were calculated by Bree's simplified method (Reference 3). In the Bree analysis, it is assumed that there are a total of 200 severe thermal cycles (sum of load scrams and reactor scrams). With a 30-year design life, the time per cycle is 262,800/200 = 1314 hours.

The derivation of the creep law used in the Bree analysis is given in the tubesheet section of this report.

The Bree analysis of Reference 3 has been computerized. The following results were obtained:

Location	Primary Stress	Secondary Stress	Strain/Cycle%	Total Strain %
A	8200	38880	$5x10^{-4}$	0.1 < 1%
B	300	4112	0	0
C	8070	55000	$8x10^{-4}$	0.16<1%

Ref.: Computer Run NHJL09J

5.3.6 FATIGUE ANALYSIS AND CREEP FATIGUE INTERACTION

A preliminary fatigue analysis was made using the fatigue curves from Code Case 1331-4. The following results were obtained:

Location	S, Ksi	Salt	N_{all}
A	38.9	19.5	6000
B	4.1	2.1	∞
C	54.3	27.2	1500

With only 200 cycles of significatn stress, maximum fatigue damage is 200/1500 = 0.13.

CREEP FATIGUE INTERACTION

Creep fatigue interaction was performed by the method described in the nozzle section of this report. The load histogram is also shown in that section. The shell shroud juncture had the highest loadings, which are given below.

$$\frac{pr}{t} = 8.07; \quad p = \frac{0.75}{20} \times 8.07 = 0.31 \text{ Ksi}$$

$$\frac{E\alpha\Delta T}{2(1-\nu)} = \begin{matrix} 40.8 \\ -13.9 \end{matrix} \qquad \Delta T = \begin{matrix} 290 \text{ F (down transient)} \\ -97 \text{ F (up transient)} \end{matrix}$$

where $E = 27.45 \times 10^6$ $\quad \alpha = 7.175 \times 10^{-6}$ (down transient)
$E = 25.8 \times 10^6$ $\quad \alpha = 7.81 \times 10^{-6}$ (up transient)

In addition, a ΔT of 20°F was applied to simulate the pressure bending stress.

PROGRAM RESULTS

There are a total of 50 cycles, each cycle consisting of 3 load scrams and 1 reactor scram. The program was run for five cycles and the strain for each of the remaining cycles was estimated by taking the difference in strains between the fourth and fifty cycles.

Maximum total strain = 0.487 + 45 (0.041) = 2.33%*

Creep damage = 0.0547 + 45 (0.0120) = 0.595

Maximum strain range = 0.3347

FWC FORM 172 - 4

NOTATIONS IN THIS COLUMN INDICATE WHERE CHANGES HAVE BEEN MADE

Fatigue damage = 50/1000 = 0.05 at 1150°F

Total creep fatigue damage = 0.645<1

Ref.: Computer Run EBHJL01C

* Some slight thickening in the area of the shell shroud juncture may be necessary to reduce the total strain below the allowable value of 2%.

5.4 STRESS ANALYSIS OF THE MSBR TUBES

5.4.1 INTRODUCTION AND SUMMARY

The MSBR tubes, constructed of Hastelloy N material, were analyzed for pressure, radial temperature gradient, and restrained thermal expansion stresses. The temperature difference between the salt and steam is greatest during the steady state condition (rather than the transient condition) and, therefore, the highest radial gradient thermal stresses occur during steady state.

Restrained thermal expansion stresses occur in the tube because of the fact that the average shell temperature is different than the average tube temperature. These stresses were calculated with the aid of the computer program STRUDL.

Table 1 gives a summary of the results. Stresses were catagorized in accordance with the rules of Code Case 1331-5. Design stresses are due to a 3600 psi design pressure and restrained thermal expansion. Operating stresses are due to a 3425 psi pressure differential, radial temperature gradients during steady state, and restrained thermal expansion. Although there is no limit on primary plus secondary stress intensity range in the Code Case, the $3S_m$ limit was calculated for reference purposes.

Natural frequencies in the bend area of the tubes, where flow induced vibrations are possible, were calculated. It was found that natural frequencies were at least 50% higher than the vortex shedding frequencies, which is satisfactory.

TABLE 1 - SUMMARY OF RESULTS - MSBR TUBES

Condition	Stress Category	Calculated Value (ksi)	Allowable (ksi)
Design	Pm	11.67	S = 11.8 @1120°F*
	P_L+P_b	11.67	$1.5S_o$=17.7
Operating	Pm	11.4	S_{mt}=11.8
	P_L+P_b	11.4	KS_t=12.2
	$(P_L+P_b+Q)_R$	29.3	$3S_m$=67.5

*Maximum average through the wall tube temperature.

See Section 5.4.6 for creep fatigue interaction.

See Appendix C-2 for material properties and allowables.

5.4.2 TUBE PRIMARY STRESSES

A) Pressure Stresses

$p = 3600$ psi (at loc. of max. T.E stresses - which are considered primary)

$r_o = 0.375 - 30(.00050) = 0.360 = b$ $\qquad t = b - a = 0.1025$

$r_i = 0.25 + 30(.00025) = 0.2575 = a$ $\qquad b + a = 0.6175$

$$\sigma_r = -p\frac{a^2(b^2 - r^2)}{r^2(b^2-a^2)} \qquad \sigma_z = p\frac{a^2}{b^2-a^2}$$

$$= \bar{\sigma}_z = \text{AVERAGE STRESS}$$

$$\sigma_t = p\frac{a^2(b^2+r^2)}{r^2(b^2-a^2)}$$

$$\bar{\sigma}_r = \frac{-1}{b-a}\int_a^b \frac{pa^2}{b^2-a^2}\left(\frac{b^2}{r^2} - 1\right)dr$$

$$= \frac{-1}{b-a}\,\frac{pa^2}{b^2-a^2}\left[-b^2 r^{-1} - r\right]_a^b$$

$$= \frac{-1}{b-a}\,\frac{pa^2}{b^2-a^2}\left[-b - b + \frac{b^2}{a} + a\right] = \frac{-pa^2}{(b-a)(b^2-a^2)}\,\frac{b^2 - 2ab + a^2}{a}$$

$$= \frac{-pa(b-a)}{b^2-a^2} = \frac{-pa}{b+a}$$

$$\bar{\sigma}_t = \frac{+1}{b-a}\,\frac{pa^2}{b^2-a^2}\left[-b^2 r^{-1} + r\right]_a^b$$

$$= \frac{+1}{b-a}\,\frac{pa^2}{b^2-a^2}\left[\frac{b^2}{a} - a\right]$$

$$= \frac{+pa}{b-a}$$

FORM (285)-47

$$\bar{\sigma}_r = \frac{-p(0.2575)}{0.6175} = -0.417\,p$$

$$\bar{\sigma}_\theta = \frac{p(0.2575)}{0.1025} = 2.512\,p$$

$$\bar{\sigma}_z = \frac{p(0.2575)^2}{0.36^2 - 0.2575^2} = 1.048\,p$$

$$\sigma_{r_{max}} = -p \quad (\text{at } r = a)$$

$$\sigma_{\theta_{max}} = p\,\frac{b^2 + a^2}{b^2 - a^2} = p\,\frac{0.1959}{0.06329} = 3.095\,p \quad (r = a)$$

$$\sigma_{z_{max}} = 1.048\,p$$

$$S_{max} = 4.095\,p = 4.095 \times 3.8 = 15.6 \text{ ksi}$$

PRIMARY MEMBRANE PRESSURE STRESSES

$$\bar{\sigma}_r = -0.417\,p$$

$$\bar{\sigma}_\theta = 2.512\,p$$

$$\bar{\sigma}_z = 1.048\,p$$

FORM (285)-47

B) TUBE THERMAL EXPANSION STRESSES

Because of the temperature difference between the tubes and shell, thermal expansion stresses will exist in the tubes. Below are tabulated tube and shell temperatures.

	Tube	Shell	ΔT
Inlet Temperature	1083	1150	67
Outlet Temperature	756	850	94
		Average ΔT =	80.5°

A STRUDL model of a typical tube was prepared (Figure 1). Applying an average temperature difference of 80.5 F between the tubes and shell, a maximum stress (at joint 29) of 6400 psi was obtained.

Reference: FWC Computer Run EBHLEVYC, July 8, 1974.

FWC FORM 172 - 4

NOTATIONS IN THIS COLUMN INDICATE WHERE CHANGES HAVE BEEN MADE

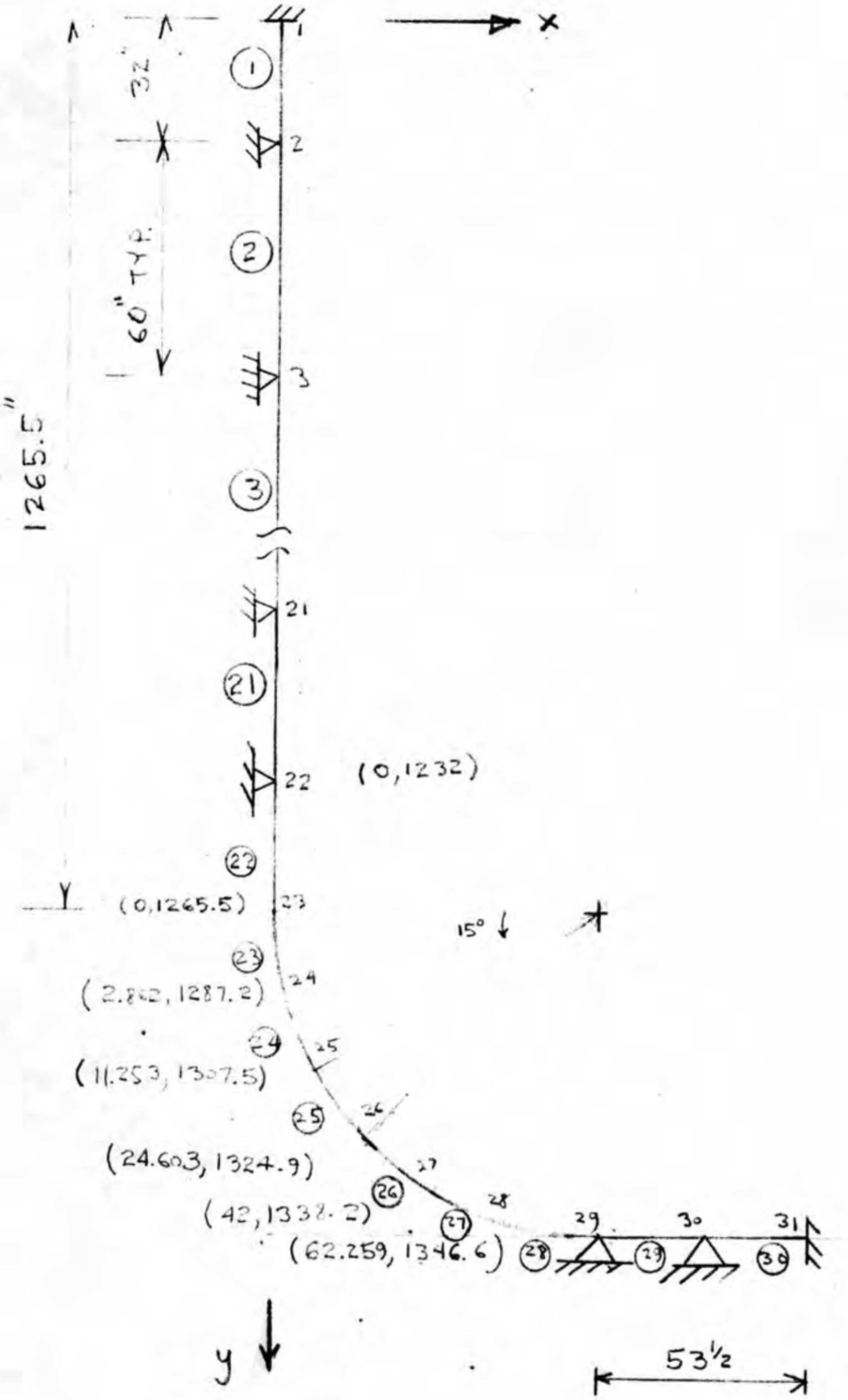

FIGURE I STRUDL MODEL FOR TUBE THERMAL EXPANSION STRESSES

DESIGN CONDITION

$\bar{\sigma}_r = -0.417 \times 3.600 = -1.5$ ksi

$\bar{\sigma}_\theta = 2.512 \times 3.600 = 9.04$

$\bar{\sigma}_z = 1.048 \times 3.600 + 6.4 = 10.17$

MAX SI = 11.67 $< S_o = 11.8$ Ksi @ 1120°F

OPERATING CONDITION $P_m = (3.6 - 0.175)(1.048 + 0.417) + 6.4 = 11.4$

(1) For full load condition, time = 3/4 × 30 years = 1.97×10^5 hrs. and maximum average tube wall temperature = 1075°F.

$P_m = 11.4 < S_{mt} = 11.8$ Ksi at 1075°F and 2×10^5 hrs.

(2) For part load condition, Time = 1/4 × 30 years = 0.66×10^5 hrs. and maximum average tube wall temperature = 1117°F.

$P_m = 11.4 < S_{mt} = 12$ Ksi at 1120°F and 0.66×10^5 hrs.

check life fraction

$$\frac{t_1}{t_{1m}} + \frac{t_2}{t_{2m}} = \frac{1.97 \times 10^5}{1 \times 10^6} + \frac{0.66 \times 10^5}{2 \times 10^5} = 0.53 < 1$$

FORM (285)-47

5.3.3 THERMAL STRESSES

STEADY STATE TUBE TEMPERATURE DISTRIBUTION

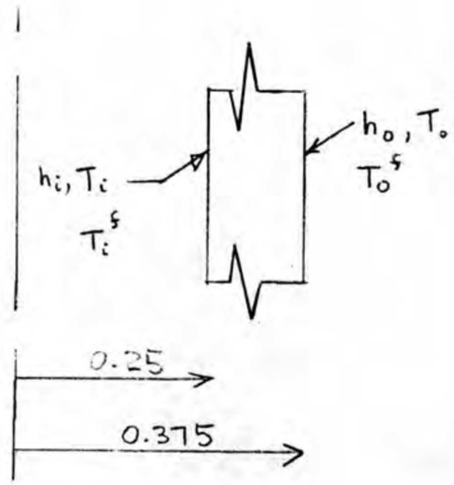

$T_i^f = 1010$ (STEAM OUTLET) $\quad K = 11.0$ @ 1080°F

$T_i^f = 700$ (STEAM INLET) $\quad K = 9.05$ @ 775°F

$T_o^f = 850$ (SODIUM OUTLET)

$T_o^f = 1150$ (SODIUM INLET)

$h_i = 4541$ (STEAM INLET - SODIUM OUTLET)

$h_i = 1439$ (STEAM OUTLET - SODIUM INLET)

$h_o = 972$ (STEAM INLET - SODIUM OUTLET)

$h_o = 1134$ (STEAM OUTLET - SODIUM INLET)

$$q = h_i(2\pi r_i)(T_i - T_i^f) = \frac{2\pi K}{\ln r_o/r_i}(T_o - T_i) = h_o(2\pi r_o)(T_o^f - T_o)$$

$$T_i - T_i^f = \frac{q}{2\pi h_i r_i}$$

$$T_o - T_i = \frac{q}{2\pi K/\ln r_o/r_i}$$

$$T_o^f - T_o = \frac{q}{2\pi h_o r_o}$$

$$T_o^f - T_i^f = q\left[\frac{1}{2\pi h_i r_i} + \frac{\ln r_o/r_i}{2\pi K} + \frac{1}{2\pi h_o r_o}\right]$$

$$q = 2\pi \left[T_o^f - T_i^f \right] \left[\frac{1}{h_i r_i} + \frac{\ln r_o/r_i}{K} + \frac{1}{h_o r_o} \right]^{-1}$$

$$T_i = T_i^f + \left[T_o^f - T_i^f \right] \left[1 + \frac{h_i r_i}{k} \ln \frac{r_o}{r_i} + \frac{h_i r_i}{h_o r_o} \right]^{-1}$$

$$T_o = T_o^f - \left[T_o^f - T_i^f \right] \left[1 + \frac{h_o r_o}{k} \ln \frac{r_o}{r_i} + \frac{h_o r_o}{h_i r_i} \right]^{-1}$$

$$T_o - T_i = \left[T_o^f - T_i^f \right] \left[1 + \frac{k}{h_i r_i \ln r_o/r_i} + \frac{k}{h_o r_o \ln r_o/r_i} \right]$$

FOR STEAM INLET - SODIUM OUTLET

$$T_i = 700 + 150 \left[1 + \frac{4541 \times 0.25/12}{9.05} \ln 1.5 + \frac{2}{3} \frac{4541}{972} \right]^{-1}$$

$T_i = 718°F$

$$T_o = 850 - 150 \left[1 + \frac{972 \times 0.375/12}{9.05} \ln 1.5 + \frac{3}{2} \frac{972}{4541} \right]^{-1}$$

$T_o = 794°F$ $T_{mean} = 756°F$

$$T_o - T_i = 150 \left[1 + \frac{9.05 \times 12}{4541 \times 0.25 \ln 1.5} + \frac{9.05 \times 12}{972 \times 0.375 \ln 1.5} \right]^{-1}$$

$T_o - T_i = 76°F$

$$\sigma = \frac{E\alpha}{2(1-\nu)} (T_o - T_i) = \frac{27.5 \times 7.09}{1.4} (76) = 10{,}600 \text{ psi}$$

FOR STEAM OUTLET - SODIUM INLET

$$T_i = 1010 + 140 \left[1 + \frac{1439 \times 0.25/12}{11.0} \ln 1.5 + \frac{2}{3} \frac{1439}{1134} \right]^{-1}$$

$T_i = 1057°F$

$$T_o = 1150 - 140 \left[1 + \frac{1134 \times 0.375/12}{11.0} \ln 1.5 + \frac{3}{2} \frac{1134}{1439} \right]^{-1}$$

$T_o = 1110°F$ $T_{mean} = 1083.5$

$$T_o - T_i = 140\left[1 + \frac{11.0 \times 12}{1439 \times 0.25 \times \ln 1.5} + \frac{11.0 \times 12}{1134 \times 0.375 \times \ln 1.5}\right]^{-1}$$

$$T_o - T_i = 52^\circ F$$

$$\sigma = \frac{E\alpha}{2(1-\nu)}(T_o - T_i) = \frac{26.3 \times 7.6}{1.4}(52) = 7420 \text{ psi}$$

5.3.4 FLOW INDUCED VIBRATION

There is a possibility of flow induced vibration only in the bend area of the tubes. The direction of possible vibration is shown in Figure 2. Supports have been provided as shown, to increase the natural frequency to 50% above the vortex shedding, and minimize the possibility of vibration.

The natural frequency is calculated below.

Tube Natural Frequency

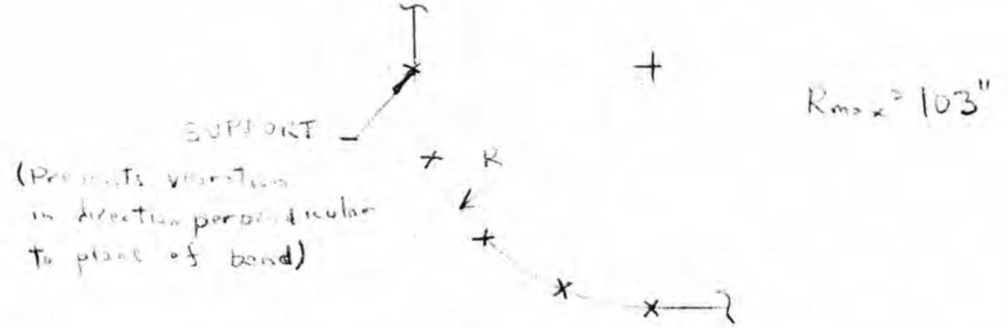

Figure 2: Tube and Supports in Bend Area

$$K_1 = \sqrt{\frac{EIg}{\mu}} = \sqrt{\frac{26.3\times10^6\times0.01246\times386.4}{0.0778}} = 40.34\times10^3$$

L = SPAN LENGTH $= 103\times\pi/8 = 40.45$

FOR A SIMPLY SUPPORTED BEAM

$\omega = \frac{\pi}{2L^2} K_1 = 38.7$ cps

FOR A FIXED, FIXED BEAM

$\omega = 2.236\times38.7 = 86.5$ cps

USE AVERAGE

$\omega = \frac{1}{2}(38.7 + 86.5) = 62.6$

MAX VORTEX SHEDDING FREQUENCY = 40 CPS

∴ NATURAL FREQUENCY IS MORE THAN 50% HIGHER THAN VORTEX SHEDDING FREQUENCY, AND FLOW INDUCED VIBRATION SHOULD BE MINIMAL.

5.3.5 SIMPLFIED INELASTIC ANALYSIS

Inelastic strains were calculated by Bree's simplified method (see Chapter VI of the LMFBR Piping Design Guide). In the Bree analysis, it is assumed that there are a total of 200 severe thermal cycles (sum of load scrams and reactor scrams). With a 30-year design life, the time per cycle is 262,800/200 = 1314 hours.

The derivation of the creep law used in the Bree analysis is given in the tubesheet report.

The Bree analysis has been computerized by Foster Wheeler, and the following results were obtained.

P_m	$P_L P_b + Q)_R$	ϵ/cycle %	ϵ %
11.4 ksi	11.4+10.6 = 22.0	3×10^{-4}	0.06< 1%

Ref: Computer Run NHJL07P
In computer run, input data is conservative.

5.3.6 FATIGUE ANALYSIS

A preliminary fatigue analysis was made with the aid of Code Case 1331-4. With a stress range of 22.0 Ksi, or an alternating stress of 11.0 Ksi, the Code Case gives an infinite number of allowable cycles. Thus, fatigue should be no problem.

CREEP FATIGUE INTERACTION

Creep fatigue interaction was performed by the method described in the nozzle portion of the report. An internal pressure differential of 3425 psi was applied for the 30-year life of the unit. The steady state radial temperature gradient is 52°F. In addition, a 28 F radial ΔT was applied to simulate the tube thermal expansion stresses. During the transient conditions, the radial temperature gradients in the tubes are milder.

PROGRAM RESULTS

Maximum total strain = 0.65%

Creep damage = 0.095

Maximum strain range = 0.258%

Fatigue damage = 0.05 (Maximum temperature = 1100 F)

Total creep fatigue damage = 0.15 < 1.0

Ref: Computer run EBHJL01C

5.5 TUBE RUPTURE ANALYSES

Tube rupture effect analyses were performed by the Gulf General Atomics Company. Detailed descriptions of the analyses are contained in Reference (8) which is included in its original form in Appendix C-3 of this report.

The analyses covered two areas of concern: the effect of a tube rupture on the shell cylinder and the adjacent tube. The effect of a tube rupture on the shell was examined by modeling the shell in a state of plane strain loaded by internal pressure of varying profile. Numerical calculations were done by using the finite difference code system, PISCES, developed by Physics International Company. The bilinear stress-strain relation of Hastelloy N at 850°F was used. The results indicate a maximum stress of 42,900 psi which is well above the yield strength (27,600 psi), but only one-half the ultimate strength (85,500 psi) of the shell material. It also predicted an increase of 3.6" (or 9%) in the diameter of the shell.

The effect of a tube rupture on the adjacent tube was examined by modeling the adjacent tube as a lumped-mass continuous beam with an appropriate elastic-plastic moment-curvature diagram derived from the stress-strain curve of the tube material (Hastelloy N at 850°). The loads acting on the beam model consisted of a transverse inertial force and the resistive force of the molten-salt. The results indicate that the ultimate strength is not exceeded and, therefore, the adjacent tube would not rupture. However, a deflection of 24.5" was calculated which was about 40 percent of the length of the span between two consecutive supports.

As indicated in Reference (8), the conclusion reached concerning the shell response due to a tube rupture was conservative in that the applied pressure was chosen as an upper bound of the data available on ruptures. The assumption of a plane strain state was also conservative in that the pressure load resulting from the tube rupture was assumed to act along the entire axis of the shell. However, for a more accurate prediction, much knowledge concerning the pressure profile is needed experimentally and analytically. On the other hand, the analysis concerning the effect of a tube rupture on the adjacent tube is incomplete. Due to the extremely large deflection calculated from the beam model, it is felt that the applied loads have to be reexamined and large deformation theory should be considered. In the presence of large deflections, the analysis should also include the interaction of adjacent tubes, and perhaps the associated problems of instability.

5.6 REFERENCES

1. Foster Wheeler Computer Program R1015 by R. E. Nickell, revised by M. B. Hsu.

2. Hybrid Computer Simulation of the MSBR by O. W. Burke, ORNL-TM-3767.

3. LMFBR Piping Design Guide by C. F. Braun & Company.

4. Bases for Design of MSBR Systems for Temperatures to 1300 F, ORNL-73-1-23.

5. Tubesheet computer runs EBMSBR2A (pressure), EBMSBREC (steady state temperature), EBMSBRCF-1 (load reduction transient), EBMSBRCF-2 (reactor scram transient)

6. Shell computer runs, EBMSBR2C-1 (Pressure), EBMSBR2C-2 (thermal stress)

7. Data for Nickel - Molybdenum Chromium - Iron Alloy, Iron-8, June 1, 1961.

8. J. J. Johnson and D. A. Wesley, Tube Rupture Analysis of a Counter Flow Heat Exchanger, Gulf-GA-A 12414, Nov. 20, 1972, Prepared for Foster Wheeler Energy Corporation.

9. Nozzle computer runs - EBRS156C (pressure), EBRS156C-1 (temperature stresses)

SECTION 6

HASTELLOY N STEAM CORROSION

BY

George V. Amoruso
GEORGE V. AMORUSO

Approved by

E. D. Montrone
E. D. Montrone
Assistant Chief Metallurgist

W. R. Applett, Jr.
W. R. Applett, Jr.
Chief Metallurgist

FWC FORM 172 - 4
NOTATIONS IN THIS COLUMN INDICATE WHERE CHANGES HAVE BEEN MADE

CHARGE NO. 8-25-2431 | DOCUMENT NO. ND/74/66 | ISSUE 1 | DATE 12/16/74

TABLE OF CONTENTS

FWC FORM 172 - 4

NOTATIONS IN THIS COLUMN INDICATE WHERE CHANGES HAVE BEEN MADE

BY George V. Amoruso APPROVED

FWC FORM 172 - 4
NOTATIONS IN THIS COLUMN INDICATE WHERE CHANGES HAVE BEEN MADE

6.0 REVIEW OF HASTELLOY N STEAM CORROSION

6.1 ABSTRACT

The literature survey described herein included a review of high temperature water/steam material investigations published in Corrosion Abstracts, ASME Transactions, GEAP[1], ORNL[2], EURAEC[3] and miscellaneous technical papers concerning the corrosion behavior of various low alloy steels, ferritic and austenitic stainless steels and nickel base alloy subjected to water/steam environments at high temperatures and pressures.

Particular attention was focussed on the corrosion behavior of Hastelloy N in high temperature steam service since the alloy is the preferred material of construction for the reactor vessel, piping and primary and secondary heat transfer equipment in the Molten Salt Breeder Reactor.

The literature search included a limited evaluation of alternate alloys or combinations of alloys that could be used for the steam generator tubing in the Molten Salt Breeder Reactor.

The survey indicates that there are no single commercial alloys or combinations of tubing alloys other than those presently under investigation at the Oak Ridge National Laboratory that can satisfy the tubing requirements for long term elevated temperature strength, stability, ductility, creep and corrosion resistance.

The data indicates there are several areas which require further investigation particularly with respect to the evaluation of Hastelloy N under constant stress and new duplex tubing processes used to provide increased corrosion protection to tubing surfaces.

---

(1) General Electric Atomic Power Equipment Department Vallecitos Atomic Laboratory, San Jose, California (Studies prepared for U.S. Atomic Energy Commission under Contract AT(04-3)-189 Project Agreement 13.

(2) Oak Ridge National Laboratory, Oak Ridge, Tenn. Studies prepared for U.S. Atomic Energy Commission under Contract W 7405-eng 26.

(3) Joint Europe Atomic Energy/U.S. Atomic Energy Commission studies performed under Contract # 089-62-7 RDB.

6.2 SUMMARY

The literature survey shows there is insufficient data presently available to properly assess or predict the performance of Hastelloy N in high temperature/pressure supercritical steam environments under constant and cyclic loading conditions anticipated in Molten Salt Breeder Reactor service.

The survey shows that aside from the data accumulated in ORNL material evaluation programs conducted at two steam corrosion test facilities located at TVA Bull Run Steam Plant in Knoxville, Tenn. and the Bartow Plant of the Florida Power Corp., little data exists concerning the corrosion behavior of Hastelloy N in high temperature water/steam environments.

The published data indicates that in pure[(1)] deoxygenated ($<$ 1 ppb O_2) supercritical steam environments at temperatures of 1000°-1100°F and pressures of 3500 psi pressure, unstressed standard and modified Hastelloy N alloys containing titanium exhibit satisfactory general corrosion resistance.

The average thickness of the oxide layer formed after 15,000 hours exposure varies from .01-.04 mils. The extremely thin oxide formed is tenacious, and non spalling containing complex oxides consisting primarily of NiO_2, MoO_2, a spinel and small quantities of Cr_2O_3.

The alloy exhibits a proneness to the formation of irregular localized oxidized nodular/blister type penetrations varying from .4-.8 mil in depth which ORNL investigators have attributed to possible iron particle deposition resulting from mass transport from ferritic tubing in the system.

However, in other short term studies (2,400 hours) conducted in oxygenated (3-4 ppm) supercritical steam environments @ 1022°F and 3000 psi, the presence of pits having depths of 1.5 mils were noted after oxide layers were electrolytically removed from the surfaces of Hastelloy N test specimens indicating that larger sized nodules may have been formed as a result of higher oxygen contents in the supercritical steam.

---

(1)Pure steam as used in this text is actually high purity steam normally used in commercial once-thru boilers.

The study also showed that unstressed modified Hastelloy N compositions containing low molybdenum (12%) and iron (.05%) contents exhibit deep localized intergranular oxide penetrations up to 10 mils after 10,000 hours exposure in pure deoxygenated supercritical steam environments. Intergranular penetrations of this type have not been observed in modified alloys of similar compositions to which additions of .5%-2.1% Titanium have been added.

The published data indicates that constantly stressed Hastelloy N alloys may be prone to stress corrosion cracking in pure and impure supercritical steam environments.

Some data shows that Hastelloy N in the ground and annealed condition is relatively immune to stress corrosion cracking processes when subjected to impure steam environments containing small quantities of oxygen and sodium chloride while tube burst tests conducted by ORNL at the Bull Run Steam Plant and General Electric at the Vallecitos Atomic Laboratory indicate that constantly stressed Hastelloy N material in the as received, and machined condition is susceptible to stress corrosion cracking in pure as well as impure steam environments.

Evaluation of the published tube burst test data indicates that the erratic behavior may be due in part to the technique used to apply constant stresses to thinly machined (.010"-.020") tube wall specimens and failure to consider the effects of residual stresses induced during tube cold drawing processes and/or the effects of macro/micro residual stresses superimposed by machining operations.

Summarily, the data indicates that there is no single tubing material that can meet all prerequisite requirements to guarantee satisfactory material performance for long term service in molten salt/supercritical steam environments.

The use of duplex tubing to provide increased corrosion protection to the outside and inside surfaces of the steam generator tubing appears to be a prudent compromise requiring further consideration and test evaluation.

6.3 INTRODUCTION

A large amount of the technology incorporated in the present Molten Salt Breeder Reactor program was derived in numerous material investigations of developmental nature which were conducted during the Aircraft Nuclear Propulsion (ANP) and Molten Salt Reactor Experiment (MSRE) programs at the Oak Ridge National Laboratory (ORNL) in Oak Ridge, Tenn. during the 1950's and 1960's.

The thrust of these programs led to the development of INOR-8 (Hastelloy N) as the containment material for molten fluorides at service temperatures up to 1500°F. This alloy was also designed to meet other requirements for good oxidation resistance, moderate strength and ductility at high temperature; long term stability at service temperatures; ability to be melted and fabricated into complex shapes and ability to be joined by welding and brazing.

The satisfactory performance of the Hastelloy N alloy in the short term MSRE program led to its preferred status as the material of construction for the core vessel, heat-exchangers and the associated piping in the Molten Salt Breeder Reactor.

However it was recognized that a material with greater resistance to irradiation effects was required for those parts of the MSBR that would be subject to long term neutron irradiation during the 30 year design life.

Considerable improvement had been achieved by adding small amounts of titanium and/or hafnium or niobium to a slightly altered base material to obtain modified Hastelloy N of the range of compositions shown in Table 1.

The stress rupture life and the ductility of the modified Hastelloy N varies considerably with variations in treatment and in the amounts of some minor constituents. In general, studies had shown that irradiation also decreases the rupture life and ductility of the modified alloy, but, for irradiation fluences of about 10^{21} neutrons/cm2 (fast and thermal) at temperatures to 1380°F, its properties were about equal to the standard alloy when unirradiated.

On this basis, and on the assumption that the reactor equipment would be made of modified Hastelloy N, the extensive data on the properties of the unirradiated Hastelloy N were used in ORNL design studies for the reactor equipment. These properties are shown in Table 2.

The maximum allowables stresses shown in Tables 3 and 4 were established and reviewed by the ASME Boiler and Pressure Vessel Code Committee and stress values approved for use under Case 1315 for Unfired Pressure Vessels and under Case 1345 for Nuclear Vessels.

Since this alloy was developed exclusively for high temperature molten salt service it possessed relatively little other commercial value and was cursorily dismissed for steam tubing applications due to its high cost, relatively unattractive fabrication/drawing properties and low chromium content.

Chromium has long been recognized as the principal elemental constituent required to confer increased oxidation and corrosion resistance to alloys subjected to air and steam environments at low and particularly at elevated temperatures.

In the Molten Salt Breeder Reactor the Hastelloy N tubing must provide simultaneously maximum corrosion resistance to high temperature coolant molten fluoride salts (1150°F) on one side and supercritical steam at temperatures of 1000°F and 3800 psi pressure on the other.

A literature search was conducted to review details of pertinent high temperature water/steam material investigations in order to derive directly or indirectly fundamental data useful in evaluating the performance of Hastelloy N and to a limited extent other possible alternate steam generator tubing materials for use in the Molten Salt Breeder Reactor.

6.4 DISCUSSION

6.4.1 EARLY STUDIES

The earliest data involving the corrosion behavior of Hastelloy N in high temperature water/steam environments was found in a material investigation[1] conducted at the Battelle Memorial Institute at the request of the International Nickel Co. in early 1959. This investigation was undertaken principally to evaluate the cracking behavior of Inconel 600 reported earlier by Coriou and his coworkers[2] at the Center of Nuclear Studies at Saclay, France in 1959.

In this study which involved the use of several other nickel base alloys for comparative purposes, an annealed INOR-8 (Hastelloy N) strip specimen was stressed beyond its yield point by a three point jig shown in Figure 1 and subjected in a five liter capacity autoclave to high purity, neutral, degassed water at a temperature of 662°F for 4000 hours.

Visual examination of the stressed Hastelloy N test specimen after exposure showed the surfaces to be frosty but free of any evidence of cracking.

Earlier in 1956, W. K. Boyd and H. A. Pray[3] reported the results of an investigation which was undertaken to determine the corrosion resistance of twelve alloys (1) subjected to degassed supercritical water at temperatures ranging from 800°F-1350°F and pressures to 5000 psi.

While this investigation was concerned primarily with corrosion properties of the various alloys in the absence of applied stress, a few tests were conducted to determine the effects of constant stress(2) on two of the stainless steel alloys (316 and 347).

In this study, the constant stress samples consisted of six inch lengths of 1/2" O.D. tubing sealed in a jig (Figure 2) so that the pressure differential at temperature between the outside and inside of the tube provided a constant load, By varying the wall thicknesses of the test specimens over a 2" gauge length the desired stress levels were attained.

The concept and tube jig configuration used by Boyd and Pray to apply constant stress to evaluate material behavior served as a model for other investigators in future materials investigations.

---

(1) AMS 5616, 410, 302, 309, 310, 347, Armco 17-4PH, Armco 17-7PH, Allegheny A 286, Inconel X, Hastelloy F and Hastelloy X.

(2) Stress was 90% of stress necessary to cause rupture in 1000 hours; 15,000 psi for 316 and 12,000 psi for 347.

FWC FORM 172 - 4

NOTATIONS IN THIS COLUMN INDICATE WHERE CHANGES HAVE BEEN MADE

In a literature survey published in Jan. 1962 by C. N. Spalaris and coworkers[4] a review was made of available data concerning the corrosion behavior of ferritic, austenitic steels and nickel base alloys in order to select candidate alloys for use in high temperature nuclear superheated steam environments.

In this review, a number of alloys were recommended for further study for nuclear superheat applications. These alloys included Incoloy, Inconel, modified 300 austenitic series such as 310, 304 L types but with low nitrogen and carbon, Hastelloy X, AISI 406, and RA 330. Also recommended for preliminary screening tests because of attractive high temperature mechanical properties were Hastelloy N, Ni-o-nel (modified), IN 102, R-20, Discaloy and 17-14 Cu-Mo.

In July 1963, F. A. Comprelli, and coworkers[5] published the results of the follow up materials investigation conducted to evaluate the relative performance of various alloys in actual and simulated superheated steam environments.

The purpose of the investigation was to select sheath or cladding materials for use in the design/fabrication of fuel elements which would be subject in service to nuclear superheat environments at temperatures of 550°F to 1350°F; pressures up to 1500 psi; oxygen contents in steam up to 20 ppm; stiochiometric hydrogen, high velocity (200 ft/sec. max.) steam, containing moisture up to 1% with small amounts of solid impurities; stress levels up to the yield point (often applied cyclically) and neutron fluxes up to 10^{22} nvt accumulated total.

In this study, unstressed and constantly stressed tubular test specimens diagramically shown in Figure 3 were placed in the CL-1 superheat test facility loop shown in Figure 4 and exposed to 1050°F superheated steam containing 20 ppm oxygen and flowing past the test specimens at a velocity approximately 20 feet per second.

Additional stressed specimens coated with chloride salts deposited on surfaces were inserted into the Auxiliary Coupon Section (ACS), a low flow bleed off from the CL-1 steam supply. The specimens in this loop were exposed to 1160°F static superheated steam environments containing levels of oxygen and hydrogen similar to the CL-1 steam supply.

The Hastelloy N. tubular test specimens containing applied stresses of 19,300 and 21,850 psia were exposed in both the CL-1 and ACS corrosion test loops for up to 3000 hours. The examination after exposure showed no indications that the applied stresses exceeded the creep-rupture strength of the alloy.

However metallographic examination showed the constantly stressed specimens subjected in the CL-1 test loop @ 1050°F to flowing superheated steam exhibited localized intergranular cracking extending to a depth of 4 mls after 1000 hours exposure and a uniform scale penetration depth of .16 mils after 3000 hours exposure.

The examination of the constantly stressed specimen coated with chloride deposits prior to subjection in the ACS loop @ 1160°F static superheated steam exhibited complete intergranular penetration after 266 hours exposure and a uniform scale thickness of .4 mls after the 266 hour exposure period. Another chloride deposit coated unstressed specimen in the ACS test loop exhibited intergranular penetrations to a maximum depth of 2.5 mls after 1119 hours exposure.

The localized intergranular penetrations of the Hastelloy N specimens were attributed primarily to a highly preferential oxidation mechanism associated with the low chromium content of the alloy rather than the applied stress. The photomicrographs illustrating the appearance of the intergranular cracking which occurred in the failed Hastelloy N specimens are shown in Figure 5.

As a result of this behavior, Hastelloy N was eliminated from further consideration as a material for Superheat Fuel Sheaths.

The final selection of candidate alloys was made and included the following alloys in order of preference: Incoloy, Inconel (at low stresses) Hastelloy X, Ni-o-nel, AISI 406 and 310 stainless steel. Other alloys eliminated from further consideration in addition to Hastelloy N were 2-1/4 Croloy and 5 Croloy Ti due to their excessive scale buildup in 1050°F steam.

A summary of the various materials investigated and the tests used to determine their relative performance is shown in Table 5.

This study established the basis for evaluating comparative material behavior in subsequent studies[6-10] which ultimately led to the selection of Incoloy 800 as the reference fuel-cladding material for use in superheat reactor (SHR) systems.

In a paper[11] published in 1963, H. J. Pessl of the General Electric Co. (HAPO) describes the results of autoclave corrosion testing of Hastelloy N and various iron and nickel base alloys after 100 days exposure to oxygenated (3-4 ppm O_2) superheated steam @ 550°C (1022°F) and 3000 psi pressure.

A graph excerpted from this paper and illustrating the relative behavior of the various materials subjected to the test environment is shown in Figure 6. The data shows that Hastelloy N test specimens exhibited an average oxide depth of penetration of approximately .16 mils and were pitted to depths of 1.5 mils.

In Nov. 1965, T. T. Claudson and R. E. Westerman of the Pacific Northwest Laboratory published[12] the results of another investigation to evaluate the corrosion resistance of several high temperature alloys including Hastelloy N for nuclear applications.

The investigation consisted essentially of subjecting ten candidate alloys to short term (100-300 hours) screening tests involving exposure at temperatures of 815°C-1150°C to low pressure water vapor (15 torrs in helium) to simulate corrosive environments in high temperature nuclear applications.

The results of the investigation which are summarized in Table 6 and graphically illustrated in Figures 7 to 9 show that the Hastelloy N alloy exhibited excellent short term high temperature corrosion behavior in an oxidizing environment.

Another paper, published in Nov. 1965 by T. T. Claudson and H. J. Pessl[13] describes the results of an investigation conducted to evaluate various iron and nickel base alloys including Hastelloy N for medium and high temperature reactor applications.

The investigation included extensive autoclave testing of selected alloys in oxygenated and deoxygenated superheated steam environments at temperatures of 1022°F and pressures of 1000, 3000 and 5000 psi for 2400 hours exposure.

This study established the following tentative grouping of alloys with increasing steam oxidation resistance:

1. Type 304, 316, 406 and 430 SS showed weight gains from about 50-300 mg/dm^2 or over .2 mils of penetration.

2. Fe-25 Cr-3Al-0.6Y, Hastelloy N, PDRL-102 and Inconel X750 showed weight gains from about 8-75 mg/dm^2 or 0.1 to 0.2 mil penetration.

3. Incoloy 800, AISI 446 SS, Hastelloy X280, Hastelloy R 235 and Fe-24 Cr-5Al showed weight gains below 15 mg/dm^2 or less than 0.1 mil penetration.

The oxygen content and the pressure of the steam appeared to affect the various alloys in different ways. While the ferritic stainless steels and the Fe-Cr-Al base alloys seemed to offer better resistance in oxygenated steam, the austenitic and martensitic stainless steels and the nickel base superalloys were more resistant to deoxygenated steam.

The weight gain data obtained for the iron and nickel base alloys in superheated steam at 1022°F and 1000 and 3000 psi pressure are summarized in Table 7 and graphically plotted in Figure 10 A. Barographs illustrating the corrosion of various alloys after 100 days exposure in deoxygenated (< 50 ppb) and oxygenated (3-4 ppm) steam @ 1022°F and 3000 psi are shown in Figure 11. Additional barographs illustrating the descaled corrosion penetrations of the various alloys after 100 days exposure in deoxygenated steam @ 1022°F and 3000 and 5000 psi pressures are shown in Figure 12.

A portion of the Hastelloy N to steam corrosion described above was reviewed and summarized by H. E. McCoy and J. R. Weir, Jr. in a report[14] published in June 1967. The summary is shown in Table 8.

6.4.2 OAK RIDGE NATIONAL LABORATORY STUDIES

6.4.2.1

GENERAL CORROSION TESTS

The need for advanced materials technology required in a proposed Molten Salt Breeder Reactor[15] led to a series of material development programs one of which involved tests to determine the compatibility of Hastelloy N in supercritical steam.

In this service, the outside surfaces of the steam generating tubing material contacts the molten coolant salt while the inside surface contacts supercritical steam having a maximum temperature and pressure of 1000°F and 3800 psi respectively. Because of the higher pressure of the steam, tube failure results in steam being forced into the coolant salt circuit with deleterious effects arising therefrom.

The ORNL material evaluation programs involving Hastelloy N and other steam generators alloys are currently being conducted at two steam corrosion test facilities located at TVA's Bull Run Steam Plant in Knoxville, Tenn. and at the Bartow Plant of the Florida Power Corp. in collaboration with Southern Nuclear Engineering (SNE) in Dunedin, Florida.

The TVA Bull Run Steam Plant Corrosion Test Loop Facility was designed primarily to evaluate the behavior of standard and modified Hastelloy N alloys and a number of other alloys in supercritical steam environments @ 1000°F and 3,500 psi pressure. The corrosion facility at Bartow was designed to evaluate (a) the corrosion behavior of weldments in conventional superheater alloys for advanced steam generator applications and (b) the general corrosion and stress corrosion cracking propensities of various steam generator alloys.

The TVA Bull Run Steam Plant[16] is a coal fired plant with a supercritical steam cycle and a power generation capability of 980 MW. The facility is located approximately 18 feet upstream from the turbine. The steam is extremely clean at this location containing < 1 ppb O_2; < 3 ppb Na; < 5 ppb Cu; < 15 ppb SiO_2; and < 6 ppb Fe.

Hydrogen is added to scavenge oxygen and the Ph is controlled at 9.40-9.45 with ammonia. The electrical conductivity in the condensed steam is less than 3×10^{-7} ohm^{-1} cm^{-1}.

In the test loop, which is schematically illustrated in Figure 13 and shown photographically in Figure 14, the steam enters the 4" diameter schedule 160 type 316 stainless steel test chamber at a rate of approximately 16-17 lbs/min. flowing longitudinally past the specimens, through the filter and the flow restricter, and into the condenser. The steam pressure is reduced to approximately 1 psig in the flow restricter. A thermocouple well was installed in the specimen holder to monitor temperature and this tube also supports the sample holder. The Grayloc flange is removable with the specimen holder. The specimens are coupons made from sheet material of 0.010", 0.020", 0.035", and 0.060" in thickness.

The corrosion test coupons are 0.5" and 2.0" with 0.1875" holes at each end for mounting on the bolts in the specimen holder. The working volume of the facility is about 2" x 2" x 2" and approximately 100 specimens were included in the first loading. This was subsequently increased to 140. The velocity of the steam across the specimens is approximately 20 ft/sec and the mass flow rate is about 1000 lb/hr.

Specimens from some commercial heats of standard air melted and vacuum melted Hastelloy N and from several two pound laboratory melts and larger commercial melts of modified Hastelloy N were included in the first loading of the facility which went on stream on 8/7/69. The results of Hastelloy N behavior in the supercritical steam corrosion tests were systematically reported by B. McNabb and H. McCoy in ORNL MSR Semiannual Progress reports.(17-26)

The authors recently published[27] a summary of the overall general corrosion data obtained for various modified and standard unstressed air melted and vacuum melted Hastelloy N alloys as well as various low alloy ferritic and maraging steels; stainless steels; and nickel base alloys which were subjected to the supercritical steam at 1000°F and 3500 psi for exposure times up to 15,000 hours.

The general corrosion data indicates that unstressed air method and vacuum melted Hastelloy N alloys are compatible with steam and exhibit corrosion rates that vary from approximately .01 to <.04 mil after 15,000 hours exposure.

The low corrosion rates are probably due to the low (< 1 ppb) oxygen content of the superheated steam at the Bull Run Steam Plant Facility. It was noted that several specimens of similar heats exposed at 1100°F for 15,000 hrs. in the Bartow Plant Facility exhibited slightly higher corrosion rates which were equivalent to oxide penetration depths of .1 mil.

The previously reported work of Claudson and Pessl[13] conducted @ 1050°F and 3000 psi pressure for 2400 hours showed that the Hastelloy N exhibited rates of .08 mil in deoxygenated (< 50 ppb) steam and .16 mil in oxygenated (3-4 ppm) steam and pits extending to depths of 1.5 mils.

The chemical composition and pertinent fabrication data for all alloys tested is shown in Table 9 while the weight change data recorded for all alloys exposed to supercritical steam at temperatures of 1000°F and pressures of 3,500 psi are shown in Tables 10 to 21 inclusive.

Graphs illustrating (a) the weight changes of several heats of Hastelloy N and several alloys of Hastelloy N modified with titanium are shown in Figures 15 A, B; (b) the corrosion of various modified compositions of Hastelloy N exposed to supercritical steam @ 1000°F and 3,500 psi and similar alloys exposed to air at 1000°F are shown in Figures 16 A, B; (c) the effect of surface finish on the corrosion of Hastelloy N and the effects of cold work on the corrosion of Hastelloy N and type 201 stainless steel in steam at 1000 psi and 3,500 psi are shown in Figures 17 and 18 respectively.

LOW ALLOY FERRITE STEELS

For comparative purposes, the evaluation included exposure of five low-alloy ferritic steels containing chromium contents varying from 1.1% to 8.7% to supercritical steam @ 1000°F and 3,500 psi for 14,000 hours. The data which is graphically illustrated in Figures 19A, B, indicate the maximum and minimum weight changes for this group of alloys may vary at any given time by only a factor of 2.

The oxidation behavior of similar alloys in air is quite different and is graphically illustrated in Figure 20. The data shows that in an air environment, approximately 8% chromium is required to prevent spalling of the oxide.

STAINLESS STEELS/NICKEL BASE ALLOYS

A graph illustrating the general corrosion of the Croloys (1-9%Cr) and several stainless steel and nickel base alloys is shown in Figure 21.

METALLOGRAPHIC EXAMINATION

A photomacrograph illustrating the appearance of the surface of a typical Hastelloy N specimen exposed to supercritical steam for 4,000 hours is shown in Figure 22. A photomicrograph illustrating the chemical composition of surface and matrix constituents of a standard Hastelloy N alloy exposed for 10,000 hours to supercritical steam is shown in Figure 23A. The high iron content detected in oxide nodules was attributed to iron mass transport from low-alloy ferritic steel piping in the steam unit. Composite photomicrographs shown in Figure 23B illustrate the cross sectional appearances of nodule blisters and intergranular penetrations observed in several Hastelloy N alloys. It will be noted that deep intergranular penetration occurs in a modified Hastelloy N alloy having low molybdenum (12%) and iron (.05%) content while no penetrations exist in a similar alloy having 2.1% Titanium added.

The investigators indicate that the addition of concentrations as low as 0.5% Titanium prevent the deep intergranular penetrations observed in Hastelloy N alloys containing low molybdenum (12%) and iron (.05%) contents.

6.4.2.2

TUBE BURST TESTS

The earlier work of Comprelli and coworkers[5] indicated that Hastelloy N exhibited a propensity to intergranular cracking when exposed to superheated steam environments in the constantly stressed condition below the yield point. In addition the results of preliminary studies conducted by J. Hammond at the Bartow plant indicated the alloy appeared to be susceptible to stress corrosion cracking when subjected to impure oxygenated steam environments containing small quantities of sodium chloride.

Since steam generator tubing is constantly stressed during unit operation, knowledge of Hastelloy N tubing material behavior in the stressed condition is essential.

In early 1971, after 6000 hours of operation, the sample chamber of the Bull Run Steam Plant Corrosion Test Loop was removed for modification to facilitate tests to observe the behavior of constantly stressed Hastelloy N specimens subjected to supercritical steam environments at temperatures of 1000°F and pressures of 3,500 psi. A schematic of the modified specimen chamber is shown in Figure 24.

The constant stress tubular burst specimens were double-walled with an annulus between the walls into which the inner tube would burst during the test. The annulus was connected to the steam condenser by a capillary tube and a thermocouple attached to the capillary to sense failure by an increase in temperature when steam is introduced into the annulus as a result of specimen failure.

The wall thicknesses of the tube specimen were machined to obtain the desired stress levels. The outer thick wall of the double walled specimen was designed so that it would not collapse into the annulus during operation in the 3,500 psi steam.

Two of the group of four Hastelloy N tube burst test specimens failed prematurely. The highest stressed specimens (77,000 psi; 010" wall thickness) failed in one (1) hour and the next highest stressed specimen (52,500 psi; 0.015" wall thickness) failed in 3.7 hours.

These specimens which were removed after 1000 hours exposure were stressed considerably above the yield stress (40,000 psi) at 1000°F. The subsequent metallurgical examination of the failed specimen surfaces discounted causes of failure due to the presence of flaws, poor machining of gage sections or inaccuracies in measurement of wall thicknesses.

A photograph of the two tube burst specimens and a photomicrograph illustrating the cracking initiating from the inside surfaces (steam side) of one of the failed specimens are shown in Figures 25A, B.

The two failed tubular test specimens were subsequently replaced by two similar type tube specimens stressed @ 56,000 psi (0.014" wall) and 50,000 psi (0.016" wall).

Subsequently, four additional tube burst specimens were installed in the test facility in order to increase the rate of data accumulation. The specimen design was identical to the other double-wall tube burst specimens except that the annulus between the tubes was not connected to the outside of the chamber by capillary tubing for indication of failure. Internal diametral strains were measured periodically and rupture times estimated by comparison with the instrumented tests.

One of the specimens with the highest stress (58,000 psi) failed sometime during the first 1000 hours of exposure. A small crack developed in the inner tube and pressurized the annulus between the tubes. When the plant steam pressure was reduced, the pressure in the annular region collapsed the tube, as shown in Figure 26. The specimen had a hairline crack extending almost the entire length of the reduced section of the tube wall. Numerous cracks formed on the inside and outside surfaces of the tube.

Examination of the plant records at the Bull Run Plant indicated that failure could have occurred when a pressure excursion to 3750 psig momentarily occurred, and as a result the pressure dropped to zero in about thirty (30) minutes. This 3750 psig would have been equivalent to a stress of 62,000 psi on the specimen. Assuming this was the case, the failure occurred after 792 hours exposure. The appearances of the numerous intergranular cracks formed in the failed sample are shown in Figure 27.

In the semiannual progress report[23] period ending 8/31/72, B. McNabb and H. McCoy indicated that ten instrumented tube burst specimens were in test at stresses varying from 28,000 to 72,000 psi (specimen wall thicknesses varying from 0.0108" to 0.0302").

Three additional specimens stressed at 66,000, 56,000 and 55,300 psi had failed at 4.0, 27.4 and 99.7 hours, respectively. The investigators reported that the two more highly stressed specimens had failed with considerable deformation while the latter specimen failed with less deformation.

The examination of the fractures showed that the specimen having the highest stress level exhibited the most ductile fracture, being almost shear while the specimen at the intermediate stress level had a mixed shear and intergranular fracture characteristic of high temperature failure.

The scatter in stress rupture data for tubes tested in argon/steam environments led to the conduct of additional tests to determine if flaws could be the cause of the scatter. Control specimens were ultrasonically inspected and compared with an electrical-discharge machined flaw 1 mil deep and 62 mils long.

Of forty-two specimens inspected eleven gave indications equal to or greater than the standard. Specimen wall machined thicknesses ranged from 0.011" to .020". With an applied pressure of 3500 psi, a decrease of 1 mil in the wall thickness would increase the stress in a 0.020" wall machined specimen by approximately 2000 psi and 6000 psi on a .011" wall machined specimen.

A control tube burst test specimen was also tested at 1000°F at a constant stress of 40,300 psig in argon with an argon internal pressure of 3500 psig. This specimen failed after 565.2 hours which was considerably less than a similar specimen exposed to steam still in test after over 7000 hours.

The erratic behavior observed in test specimens was believed to be due in part to the presence of undetected flaws in the thinly machined tube walls and, as a consequence, no definite conclusions were drawn regarding the effects of pure steam on the stress rupture properties of Hastelloy N tubing material.

A photograph of the three Hastelloy N tube burst specimens which failed after short time exposure in the supercritical steam environment is shown in Figure 28 while photomicrographs taken of the failure areas of each of the specimens are shown in Figure 29. Photomicrographs illustrating the failure of the Hastelloy N specimen tested in argon @ 1000°F are shown in Figure 30. The investigators indicated the specimen was not ultrasonically inspected prior to testing and that the numerous cracks observed on specimen inside surfaces may have been present before testing.

A summary of the compiled tube burst test data is shown in Table 21.

6.4.2.3

DUPLEX TUBING TESTS

Tests were also conducted at the Oak Ridge National Laboratory to evaluate the properties of duplex tubing for steam generator service. The duplex tubing which was designed to provide each side of the tubing with increased corrosion resistance for the molten fluoride supercritical steam service was made by coextruding a Nickel 280 sleeve over a wrought Incoloy 800 tube. (The Nickel 280 alloy is pure nickel with .05% Al_2O_3 added for grain size control required for long term elevated temperature service).

The study also included an evaluation of the mechanical and tube burst properties of the duplex tubing and individual components as well as auxiliary tests to evaluate the corrosion behavior of the Nickel 280 alloy alone in supercritical steam environments @ 1000°F and 3500 psi pressure.

A twelve inch piece of 0.75 inch diameter tubing was tensile tested @ 25°C at a displacement rate of 0.05 in/min. The test results indicated that the 0.2% offset yield stress was 37,600 psi; the ultimate tensile stress was 70,780 psi and the elongation, 50.5% in 2". The room temperature results indicated that in the tensile type test Nickel 280 and Incoloy 800 components contribute equally to material strength.

A tube burst specimen was also tested @ 1000°F in an argon atmosphere with an argon internal pressure and ruptured in 3263 hours.

The results indicated that the Nickel 280 clad contributed little to the strength of the tubing in this type test. (The rupture life of 3263 hours for a stress of 46,000 psi @ 1000°F is in agreement with data published in Inco Technical Bulletin (T-40) for the Incoloy 800 alloy).

A photograph illustrating the dye checked appearance of the failed duplex Nickel 280/Incoloy 800 tube burst specimen is shown in Figure 31A. A photomicrograph of the Nickel 280 cladding illustrating the extent and depth of cracking in the outer portions of the nickel clad is shown in Figure 31B.

A photomicrograph illustrating the cracking occurring on the inner Incoloy 800 tube and extending on through the Nickel 280 clad is shown in Figure 32A. (The interface between the two materials was metallurgically sound and the Incoloy alloy was not cracked around the circumference as was the Nickel 280 clad).

The nature of the profuse and preferential longitudinal cracking in the Nickel 280 clad material led to the conduct of additional mechanical tests to determine if the prior working direction influenced the cracking behavior.

Specimens from a Nickel 280 alloy sheet were cut longitudinally and transversely to the rolling direction and creep tested at temperatures of 1000°F and pressures of 2000 psi in argon. A plot of the percent elongation v.s. time for specimens tested in the as received condition is shown in Figure 32B. The data shows that the longitudinal specimen is slightly stronger with a longer rupture life and lower minimum creep rate. However, fracture strains were high for both specimens.

To observe the compatibility of Nickel 280 with steam in the event of a leak, sheet specimens were exposed to the supercritical steam @ 1000°F and 3500 psi for 2000 hours.

The specimens gained approximately 75 mg/cm^2 and appeared to be about completely oxidized indicating that Nickel 280 is not compatible with steam under the supercritical steam environments. A photograph of the oxidized specimen is shown in Figure 33.

Additional tube burst tests were conducted on the duplex tubing at 1000°F in an argon atmosphere with argon internal pressure. One specimen with a pressure corresponding to a stress of 46,000 psi on the Incoloy 800 (or 28,720 psi for the entire wall) ruptured at 3,263 hours with a diametral strain of 3.04%. The Nickel 280 clad exterior was cracked profusely.

Another tube burst specimen was stressed at 40,000 psi on the Incoloy 800 and was discontinued at 7075 hours with a diametral strain of 1.14%. The dye checked appearance of this clad specimen is shown in Figure 34. A photomicrograph illustrating the appearance of the cracking which occurs at relatively low diametral strain is shown in Figure 35.

A graph illustrating several creep curves for Nickel 280 sheet at 1000°F in argon is shown in Figure 36. The data indicates there is no clear cut effect of rolling direction or creep properties, as the longitudinal specimen had longer rupture times at the two higher stresses and the transverse specimen had a longer rupture life at 15,000 psi.

All the sheet specimens had rupture strains greater than 20% indicating much greater ductility than that shown by the Nickel 280 on the duplex tubing.

Generally, the data indicates that the duplex tubing can be produced with a nickel layer that possesses good ductility.

6.4.3 CRITICAL REVIEW OF STEAM GENERATOR TUBING MATERIALS

The literature search included a critical review of alternate alloys for possible use as steam generator tubing in Molten Salt Breeder Reactor service. This involved a study of fundamental selection criteria and review of all commercial and experimental alloys used in the previously cited material investigations as well as others described in the referenced literature. 1-108.

This also included technical discussions with tubing manufacturers regarding the selection and usage of commercial steam generator tubing materials; the behavior of various iron and nickel base alloys subject to long term exposure to high temperature supercritical and molten salt environments; and the new duplex tubing fabrication processes developed for special applications requiring increased corrosion protection for both the inside and outside surfaces of tubing.

6.4.3.1

DESIGN REQUIREMENTS AND CRITERIA

The steam generator is based on a 30 year plant life and the use of tubing having a minimum I.D. of 0.375" and corrosion allowances of 0.5 mil/yr. on the salt side and 0.25 mil/yr. on the steam side.

The design operational conditions to which the tubing will be subjected in service are summarized below:

	Coolant Salt	Water/Steam
Inlet temperature, °F	1150	700
Outlet temperature, °F	850	1000
Flow rate, lb/hr.	15,280,000	2,517,000
Inlet pressure, psia	235	3800
Outlet pressure, psia	175	3600
Maximum pressure drop,psi	60	200

The coolant salt consists of sodium fluoroborate and sodium fluoride salts having a eutectic composition of 92-8 mole % ($NaBF_4$-NaF). The phase diagram shown below illustrates a liquidus temperature of 384°C (723°F) indicating the coolant system must operate above approximately 750°F.

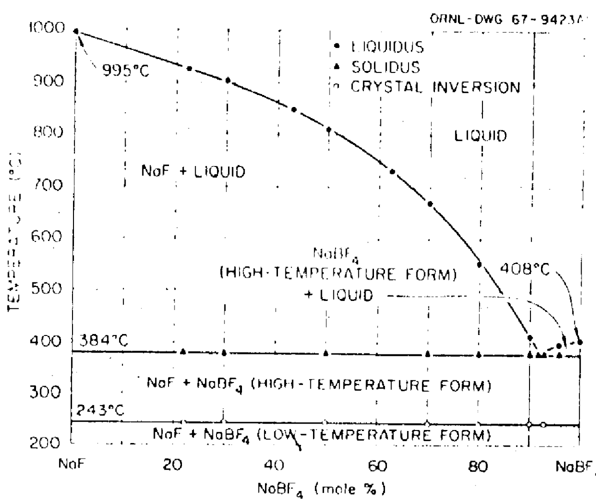

Two-Fluid MSBR Coolant Salt – The System NaF-$NaBF_4$.

6.4.3.2

CORROSION RESISTANCE TO MOLTEN FLUORIDE SALTS

The best known alloy to contain molten fluoride salts at temperatures up to 1500°F is Hastelloy N. This alloy which was specifically developed for high temperature molten fluoride service by ORNL as part of the ANP program conducted during the mid 1950's possesses long term high temperature strength, thermal stability, ductility, creep resistance and satisfactory tube fabrication/joining properties.

In the early screening stages of alloy development nickel base alloys were found to be the most promising and the commercial nickel-chromium group received the most attention. However the alloys were subject to selective chromium depletion processes which resulted in the formation of subsurface voids illustrated in Figure 37.

The corrosion mechanism consists of oxidation of alloy constituents to their fluoride salts which are soluble in the melt and therefore do not form passivating protective films. This electrochemical type attack is limited only by the thermodynamic potential for the oxidation reaction and is more selective for chromium since it is the least noble element in the alloy.

The possible corrosion reactions are expressed in the equations below:

$$2HF + Cr \rightleftharpoons H_2 + CrF_2$$

$$NiF_2 + Cr \rightleftharpoons Ni + CrF_2$$

$$FeF_2 + Cr \rightleftharpoons Ni + CrF_2$$

The relative thermodynamic stabilities of the fluoride composites are shown in Table 22 and illustrate that molybdenum and nickel constituents are more stable and more resistant to molten salt attack at high temperatures.

In related developmental studies, Manley and coworkers[28] reported that while chromium in the newly developed alloy was undesirable because of fused fluoride corrosion, the addition of at least 6% chromium was required for oxidation resistance for long time service at temperatures above 650°C (1200°F). The increased oxidation resistance conferred by 6-8% chromium to an 80-20 Ni-Mo alloy is shown in Figure 38A. Also shown in Figure 38B is a list of a number of alloys melted in the course of developing the Hastelloy N (INOR-8). A comprehensive review of the work conducted by ORNL and other participating laboratories which led to the development of the Hastelloy N alloy was published[29] in 1969 by H. E. McCoy.

The results of corrosion tests obtained by ORNL in continuing studies involving the behavior of Hastelloy N and other materials subjected to various types of fuel, blanket, fertile fissile and coolant molten salts for various exposure times, temperatures, velocities, Δt's in natural thermal convection loops (NCL) and forced circulating loops (FCL) are described in referenced ORNL MSR semiannual progress reports 30-38 and further discussion is beyond the scope of present study.

Table 23 shows the status of the MSR program thermal convection loops (NCL) as of 8/31/72.

Summarily the results of the continuing investigation indicate that the Hastelloy N alloy is the most suitable material for high temperature molten salt service having average corrosion rates of several tenths of a mil/yr.

The corrosion rate of the Hastelloy N material is increased when the coolant salt ($NaBF_4$-NaF, 92-8 mole %) is contaminated by the presence of impurities particularly oxygen and moisture which results in the formation of HF. However, analytical techniques are being used to determine and monitor the oxygen and water impurity levels while other techniques are being developed to remove these impurities from the coolant salt.

The corrosion reactions in the impure sodium fluoroborate salt mixture have not been well established but they are reasonably expressed by the following equations:

$H_2O + NaBF_4 \rightleftharpoons NaBF_3OH + HF$,

$NaBF_3OH \rightleftharpoons NaBOF_2 + HF$,

$6HF + 2Cr + 6\ NaF \rightleftharpoons 2Na_3CrF_6 + 3H_2$ (and similar reactions with nickel and iron),

$3O_2 + 4Cr \rightleftharpoons 2Cr_2O_3$,

$Cr_2O_3 + 3NaBF_4 + 6NaF \rightleftharpoons 2Na_3CrF_6 + 3NaBOF_2$,

$FeF_2 + Cr \rightleftharpoons CrF_2 + Fe$ (and similar reactions with nickel and molybdenum fluorides).

Graphs illustrating the relative corrosion resistance of various alloys in a $LIF-BeF_2-THF_4-UF_4$ molten salt are shown in Figure 39.

6.4.3.3

CORROSION RESISTANCE TO SUPERCRITICAL STEAM

The best commercial alloy found for the supercritical steam service is Incoloy 800. This alloy when exposed to superheated steam at temperatures of 1050°-1100°F forms a tenacious uniform and predictable oxide scale and possesses high temperature strength, ductility, creep resistance and thermal stability required for long term high temperature/pressure steam service.

The alloy has been widely used for commercial steam generating applications particularly where increased strength and resistance to stress corrosion cracking processes are required. The maximum allowable stresses shown for the Incoloy 800 alloy in Table 25 were established and reviewed by the ASME Boiler and Pressure Vessel Code Committee and the stress values approved for use on 4/29/74 under Code Case 1592 for Nuclear Vessels.

Also shown in Table 24 for comparison purposes, are the maximum allowable design stresses for 304 SS, 316 SS and 2 1/4Cr-1 Mo alloys. A graph illustrating manufacturers data on the relative strengths of Inconel 600, Incoloy 800 and Inconel 625 alloys are shown for comparison purposes in Figure 40.

6.4.4 CRITICAL REVIEW OF HASTELLOY N AND DUPLEX TUBING

6.4.4.1 HASTELLOY N

The dilemma concerning the use of Hastelloy N in the MSBR application is largely based on the fact that it has no prior commercial use in steam generating applications and that the present nuclear application requires the use of tubing that will be subjected to steam side service conditions substantially more severe than those previously encountered in conventional power plant operations.

The recent work published by J. P. Hammond et al[39] indicates that the surface condition and prior heat treatment has a pronounced effect upon the stress corrosion cracking proclivity of welded and non welded U-bend specimens subjected to impure, oxygenated steam environments containing small quantities of NaCl introduced during cyclic operation from saturated temperatures @ 544°F to superheat temperatures of 800-900°F.

A photograph of the U-bend specimen holder with mounted specimens and two schematics illustrating specimens/environmental conditions during cyclic testing and the high pressure chloride SCC facility at the Bartow Florida Plant are shown in Figures 41 A, B, C.

In these tests Hammond observed that the ground specimen surface condition promoted the highest susceptibility to cracking in a number of alloys including Hastelloy N while none of the ground and properly annealed Hastelloy N specimens failed in the severe test environment.

These results which are summarized in the Table 25 indicate that the stress corrosion cracking susceptibility of the Hastelloy N material may be reduced or eliminated by proper annealing treatment prior to use. (The actual data as excerpted from references 26 and 39 are shown in Tables 26 and 27 respectively).

The relieval of high levels of residual stress existing in as received material may provide additional insight as to the behavior of the Hastelloy N tubing material used by Comprelli[5] at GEAP and H. McCoy at ORNL in their constantly stressed tube burst tests.

In addition, it appears that the concept of machining Hastelloy N specimen tube walls to thicknesses as low as .010" to obtain required stress values should be reevaluated to assess the effects of the magnitude and distribution of macro/micro residual stresses superimposed by the machining operations. The magnitude of these stresses can be determined by X-ray diffraction techniques.

6.4.4.2 DUPLEX TUBING

The use of duplex tubing to provide increased corrosion protection to the outside and inside surfaces of the steam generator tubing appears to be a prudent compromize requiring further consideration and test evaluation.

In the duplex tube fabrication process developed by Huntington Alloys in Huntington, West Virginia, a Nickel 270 clad (pure nickel containing <.01%C) sleeve made by powdered metallurgy techniques is placed over a section of wrought Incoloy 800 tubing. The composite is then sintered, coextruded and subjected to conventional cold drawing tube processing operations to obtain required cladding thicknesses ranging from .010-.050" over final size Incoloy 800 tubing. The duplex tubing section lengths vary from 85-120 feet in length depending upon the draw bench limitation of the mill.

The duplex tubing design strength is based on the ASME Code approved strength levels for Incoloy 800 material since the Nickel 270 clad does not contribute significantly to the strength of the duplex tube.

The vendor recommends that the duplex tubing can be welded by conventional standard welding practices using Inconel 82 filler metal for the Incoloy 800 tube weldments and Inconel 61 for the Nickel 270 clad weldments.

However, on the basis of the previously cited studies conducted by J. Hammond and coworkers[39] at the Bartow Corrosion Test Facility it may be prudent to consider for test purposes the use of duplex tube test specimens containing Incoloy 800 tube weldments made from Inco A welding rod and/or combinations of Inco A welding rod and Inconel 82 filler metal since this combination appears to be more resistant to stress corrosion cracking processes when exposed to impure, oxygenated, supersaturated/superheated steam environments containing sodium chloride salts.

A vendor photograph illustrating a similar commercial duplex tube composite consisting of a sintered nickel shell on a Monel alloy 400 extrusion billet is shown in Figure 42. Also shown are cross sections of the clad tube sections at various processing stages.

Photomacrographs illustrating the transverse appearances of experimental Nickel 270 and Nickel 280 claddings over wrought Incoloy 800 tube sections are shown in Figure 43 in the unetched and macroetched conditions.

Photomicrographs taken of transverse sections of coextruded duplex tube sections illustrating the microstructural appearance in the interfacial areas of the sound metallurgical bond between the Nickel 270 and 280 claddings on Incoloy 800 tube sections are shown in Figures 44 and 45.

6.5 CONCLUSIONS/RECOMMENDATIONS

On the basis of the literature survey described herein the following conclusions and recommendations are made:

1. There is insufficient published data to properly assess or predict the performance of Hastelloy N in high temperature/pressure supercritical steam environments under constant and cyclic loading conditions encountered in Molten Salt Breeder Reactors.

2. There is no known single commercial tubing alloy that can simultaneously provide the required long term corrosion resistance to molten fluoride salts on one side and supercritical steam on the other.

3. Standard and modified compositions of Hastelloy N provide the best corrosion resistance to molten fluoride salts than all other alloys. The corrosion resistance depends essentially on the following:

a) alloy composition.
b) coolant salt temperature and velocity.
c) coolant salt impurity levels particularly oxygen and water contents.

4. Published data concerning the performance of Hastelloy N tubing in commercial steam generating power plant applications is non existent.

5. Unstressed standard and modified Hastelloy N alloy compositions exhibit satisfactory general corrosion behavior in pure deoxygenated (<1 ppb) supercritical' steam environments @ 1000°F and 3500 psi.

a) The oxide formed is a thin, tenacious non spalling type containing complex oxides consisting primarily of NiO_2, MoO_2, a spinel and small quantities of Cr_2O_3.

b) The average depth of oxide penetration varies from .01-.04 mil after 15,000 hrs. exposure. In oxygenated (3-4 ppm) environments @ 1022°F and 3000 psi, oxide depths of penetration of .16 mils were reported after 2400 hrs. exposure.

c) Hastelloy N alloys exhibit higher corrosion rates in steam with increasing surface roughness.

d) The corrosion resistance of standard Hastelloy N alloys is improved by the presence of .5-.6% Si.

e) The surfaces of standard Hastelloy N alloys are prone to the formation of localized nodular type intergranular penetrations possibly initiated and/or accelerated by iron particle deposition.

f) Nodule depths of .4-.8 mils reported after 10,000 hours in deoxygenated (<1 ppb) supercritical steam environments.

g) Pit depths of 1.5 mils were reported after 2,400 hours in oxygenated (3-4 ppm) supercritical steam environments.

h) Modified Hastelloy N compositions containing low Mo (12%) and Fe (.05%) contents exhibit deep localized intergranular oxide penetrations up to 10 mils after 10,000 hours exposure in pure deoxygenated (<1 ppb) supercritical steam environments. The intergranular penetrations are absent in similarly exposed modified Hastelloy N compositions containing .5%-2.1% Ti.

6. Material investigation indicates that the corrosion behavior of stressed standard and modified compositions of Hastelloy N under supercritical steam generating conditions is uncertain.

a) The alloy in the as received and stressed condition is prone to stress corrosion cracking processes when subjected to pure and impure supercritical steam environments containing small quantities of oxygen and NaCl.

b) The Hastelloy N alloy in the properly annealed condition exhibits immunity to stress corrosion cracking in impure supersaturated/superheated steam environments in the welded and non welded conditions.

7. The use of duplex tubing to provide increased corrosion protection to the outside and inside surfaces of the steam generator tubing appears promising and requires additional testing/evaluation.

8. Due to uncertainties of material performance under cyclic loading conditions, it is recommended that a cooperative test program be considered to evaluate the performance of Hastelloy N tubing material under commercial high temperature/pressure steam service conditions. The program should include the incorporation of selected sections of Hastelloy N tubing in the superheater sections of several commercial boilers.

REFERENCES

1. STRESS CORROSION OF NICKEL-CHROMIUM ALLOYS IN 350°C HIGH PURITY WATER, Warren E. Berry, W. Stiegelmeyer and F. Fink. Special report prepared by Battelle Memorial Institute for the International Nickel Co., 9/22/61.

2. STRESS CORROSION CRACKING OF INCONEL IN HIGH-TEMPERATURE WATER, H. Coriou, R. Grall, M. LeGall and S. Vettier, 3e Colloque De Metallurgie sur la Corrosion (1959), North Holland Publishing Co. (1960), pp 161-169.

3. CORROSION OF STAINLESS STEELS IN SUPERCRITICAL WATER, W. K. Boyd and H. A. Pray. Corrosion 1956, 375t-384t.

4. MATERIALS FOR NUCLEAR SUPERHEATED APPLICATIONS, C. N. Spalaris, F. A. Comprelli, D. L. Douglass and M. B. Reynolds. AEC Project Agreement #13 Contract AT(04-3)-189 GEAP 3875, Jan. 1962.

5. MATERIALS FOR SUPERHEATED FUEL SHEATHS-RELATIVE PERFORMANCE OF ALLOYS IN SUPERHEATED STEAM ENVIRONMENTS, F. A. Comprelli, D. F. MacMillian and C. N. Spalaris, AEC Project Agreement #13 Contract AT(04-3)-189, GEAP 4351, July 1963.

6. GENERAL CORROSION OF INCOLOY 800 IN SIMULATED SUPERHEATED REACTOR ENVIRONMENT, W. L. Pearl, E. G. Brush, G. G. Gaul and G. P. Wozadlo, GEAP 4495, March 1964.

7. INCOLOY 800 FOR NUCLEAR FUEL SHEATHS (A MONOGRAPH), C. N. SPALARIS, GEAP 4633, July 1964

8. STABILITY OF HIGH-NICKEL ALLOYS IN SUPERHEATED STEAM, F. A. Comprelli, U. E. Wolff, GEAP 4745, Nov. 1964.

9. GENERAL CORROSION OF MATERIALS FOR NUCLEAR SUPERHEATED APPLICATIONS, W. L. Pearl, E. G. Brush, G. G. Gaul, G. P. Wozadlo, GEAP 4760, March 1965.

10. GENERAL CORROSION OF INCONEL ALLOY 625 IN SIMULATED SUPERHEATED REACTOR ENVIRONMENT. W. L. Pearl, E. G. Brush, G. G. Gaul, and S. Leistikow, Nuclear Applications, Vol. 3, No. 7., p 418-432; July 1967, BTR.

11. EFFECTS OF EXPOSURE TO SUPERHEATER - OXYGENATED STEAM OF 550°C (1022°F) AND 1000 - 3000 PSI PRESSURE UPON IRON AND NICKEL BASE ALLOYS, H. J. Pessl - TID, 7674; Proceedings of the Nuclear Superheat Meeting No. 8 3/20, 21, 22, 1963 Idaho Falls, Idaho.

12. AN EVALUATION OF THE CORROSION RESISTANCE OF SEVERAL HIGH TEMPERATURE ALLOYS FOR NUCLEAR APPLICATIONS, T. T. Claudson, R. E. Westerman, P. 26(1965) Nov. Contract AT (45-1)-1830. BNWL 155.

13. EVALUATION OF IRON-AND-NICKEL-BASE ALLOYS FOR MEDIUM AND HIGH TEMPERATURE REACTOR APPLICATIONS, T. T. Claudson, H. J. Pessl, p. 60, (1965) November. Contract AT(45-1)-1830. BNWL 154.

14. MATERIALS DEVELOPMENT FOR MOLTEN SALT BREEDER REACTORS, H. E. McCoy, J. R. Weir, Contract W-7405-eng 26, Oak Ridge National Laboratory Report ORNL-TM-1854, June 1967.

15. DESIGN STUDIES OF 1000 Mu(e) MOLTEN-SALT BREEDER REACTOR; ORNL 3996 (8/66), P. R. Kasten, E. S. Betlis, and R. C. Robertson.

16. Tennessee Valley Authority, The Bull Run Plant, TVA Technical Report 28, Knoxville, Tenn., 1967.

17. MOLTEN SALT REACTOR PROGRAM, PERIOD ENDING 8/31/69, Contract W-74-5-eng 26 Oak Ridge National Laboratory Report, ORNL 4449, 8/31/69.

18. MOLTEN SALT REACTOR PROGRAM SEMIANNUAL PROGRESS REPORT, PERIOD ENDING 2/28/70, Contract W-7405-eng 26, Oak Ridge National Laboratory Report, ORNL 4548, 8/70.

19. FUELS AND MATERIALS DEVELOPMENT PROGRAM QUARTERLY PROGRESS REPORT PERIOD ENDING 3/31/70 (Advanced Materials In Steam Generators pp 275-280), Oak Ridge National Laboratory Report, ORNL 4560, 3/31/70.

20. METALS AND CERAMICS ANNUAL PROGRESS REPORT PERIOD ENDING 6/30/70, Contract W-7405-eng 26, Oak Ridge National Laboratory Report ORNL 4570, 10/70.

21. MOLTEN SALT REACTOR PROGRAM SEMIANNUAL PROGRESS REPORT PERIOD ENDING 2/28/71, Contract W-7405-eng 26, Oak Ridge National Laboratory Report, ORNL 4676, 2/28/71.

22. MOLTEN SALT REACTOR PROGRAM SEMIANNUAL PROGRESS REPORT PERIOD ENDING 8/31/71, Contract W-7405-eng 26, Oak Ridge National Laboratory Report ORNL 4728, 8/31/71.

24. CORROSION AND MASS TRANSFER CHARACTERISTICS OF Na BF_4-NaF (92-8 mole %) IN HASTELLOY N, J. W. Koger, Contract W-7405-eng 26, Oak Ridge National Laboratory Report ORNL-TM-3866, 10/72.

25. MOLTEN SALT REACTOR PROGRAM SEMIANNUAL PROGRESS REPORT, PERIOD ENDING 2/29/72, Contract W-7405-eng 26, H. E. McCoy, J. R. Weir, Oak Ridge National Laboratory Report ORNL 4782, 2/29/72.

26. FUELS AND MATERIALS DEVELOPMENT PROGRAM QUARTERLY PROGRESS REPORT PERIOD ENDING 12/31/72, Contract W-7405-eng 26 Oak Ridge National Laboratory ORNL-TM-4105, 12/31/72.

27. CORROSION OF SEVERAL IRON AND NICKEL BASE ALLOYS IN SUPER-CRITICAL STEAM AT 1000°F, H. E. McCoy and B. McNabb, 8/74, ORNL-TM 4552.

28. METALLURGICAL PROBLEMS IN MOLTEN FLORIDE SYSTEMS, W. D. Manly, J. H. Cools, J. H. DeVan, D. A. Douglas, H. Inouye, P. Patriarca, T. K. Roche, and J. L. Scott, Geneva Conference Paper (1958) p/1990, Reprinted from "Progress in Nuclear Energy, Series IV, Vol 2 - Technology, Engineering and Safety.

29. THE INOR-8 STORY, H. E. McCoy, Review, Fall 1969, ORNL pp 35 - 49.

30. METALS AND CERAMICS DIVISION ANNUAL PROGRESS REPORT FOR PERIOD ENDING 6/30/67, Contract W-7405-eng 26 Oak Ridge National Laboratory Report ORNL 4170, June 30, 1967.

31. MATERIALS DEVELOPMENT FOR MOLTEN SALT BREEDER REACTORS, H. E. McCoy, J. R. Weir, Contract W-7405-eng 26, Oak Ridge National Laboratory Report ORNL-TM-1854, June 1967.

32. MOLTEN SALT REACTOR PROGRAM, SEMIANNUAL PROGRESS REPORT FOR PERIOD ENDING 8/31/67, H. E. McCoy, Contract W-7405-eng 26, Oak Ridge National Laboratory Report ORNL 4191, Aug. 31, 1967.

33. AN EVALUATION OF THE MOLTEN SALT REACTOR EXPERIMENT HASTELLOY IN SURVEILLANCE SPECIMENS-FIRST GROUP, H. E. McCoy, Contract W-7405-eng 26 Oak Ridge National Laboratory Report ORNL-TM-1997, Nov. 1967.

34. TWO FLUID MOLTEN SALT BREEDER REACTOR DESIGN STUDY STATUS AS OF 1/1/68, Contract W-7405-eng 26, Oak Ridge National Laboratory Report ORNL 4528, 1/1/68.

35. MOLTEN SALT REACTOR PROGRAM, PERIOD ENDING 2/29/68, Contract W-7405-eng 26, Oak Ridge National Laboratory Report ORNL 4254, Feb. 29, 1968.

36. MOLTEN SALT REACTOR PROGRAM, PERIOD ENDING 8/31/68, Contract W-7405-eng 26, Oak Ridge National Laboratory Report ORNL 4344, 8/31/68.

37. MOLTEN SALT REACTOR PROGRAM, PERIOD ENDING 2/28/69, Contract W-7405-eng 26, Oak Ridge National Laboratory Report, ORNL 4396, 2/28/69.

38. MOLTEN SALT REACTOR PROGRAM, PERIOD ENDING 8/31/69, Contract W-74-5-eng 26, Oak Ridge National Laboratory Report, ORNL 4449, 8/31/69.

39. CHLORIDE STRESS-CORROSION OF STEAM GENERATOR MATERIALS AND POST-TEST ANALYSIS OF AN INCOLOY 800 LOOP by J. P. Hammond, P. Patriarca and G. M. Slaughter of ORNL and W. A. Maxwell of SNE. Paper 51 presented at NACE Conference 3/74, Chicago, Ill.

40. CORROSION STUDIES IN WATER AND VAPOR AT HIGH TEMPERATURES, Contract 089-62-7 RDB Quarterly Report 1, 6/16-9/30/62, 10/62, EURAEC 474.

41. STUDIES OF STEEL CORROSION IN HIGH TEMPERATURE WATER AND STEAM. Quarterly Report No. 2 Oct. 1 to Dec. 31, 1962, Societe d'Etudes, de Recherches et d'Applications pour l'Industrie, Jan. 30, 1963. Work performed under U.S.-Euratom Joint Res. and Dev. Program. A Translation. 1/30/62, EURAEC 552.

42. DEVELOPMENT OF NIOBIUM-BASE ALLOYS FOR USE IN A NUCLEAR SUPERHEATER. Quarterly Progress Report. January-March 1963. John A. DeMastry, Arthur A. Bauer and Frank A. Rough. Battelle Memorial Inst. April 1, 1963. Work performed under U.S.-Euratom Joint Res. & Dev. Program, Contract W-7405-eng 92, 12 pp. 4/1/63 EURAEC-626.

43. CORROSION TESTS IN STEAM. Quarterly Report No. 8, January-March 1964. Work performed under US-Euratom Joint Res. and Dev. Program, 27 pp (1964), Contract 067-62-4-RDF, 5/64, EURAEC-1062.

FWC FORM 172 - 4 — NOTATIONS IN THIS COLUMN INDICATE WHERE CHANGES HAVE BEEN MADE

44. STUDIES ON CORROSION OF STEELS IN HIGH-TEMPERATURE WATER AND STEAM. Quarterly Report No. 9, July-Sept. 1964. Euratom Joint Res. and Dev. Program, 48 pp (1964), Contract 089-62-7 RDB, 10/30/64, EURAEC-1237.

45. DEVELOPMENT OF NIOBIUM ALLOYS RESISTANT TO SUPERHEATED STEAM. Robert D. Koester, John A. DeMastry, Warren E. Berry, Arthur A. Bauer, Frank A. Rough, Battelle Memorial Inst., Columbus, Ohio. Work performed under United States-Euratom Joint Res. and Dev. Program, 44 pp (1964), Contract W-7405-eng 92, 11/11/64 EURAEC-1285.

46. CORROSION STUDIES ON STEELS IN WATER AND STEAM AT HIGH TEMPERATURE. Quarterly Progress Report No. 10, Oct.-Dec. 1964. Euratom Joint Res. and Dev. Program, 82 p., Contract 089-62-7 RDB, Jan. 1965, EURAEC-1308.

47. STUDIES OF STEEL CORROSION IN HIGH TEMPERATURE WATER AND STEAM, Contract 089-62-7 RDB, Quarterly Report 13 7/1-10/31/65; 11/26/65, EURAEC-1500.

48. DYNAMIC CORROSION TESTS ON CARBON AND STAINLESS STEELS IN PRESSURIZED WATER. M. Warzee, P. de Dorlodot, J. Waty, CFSTI, Contract 089-62-7-RDB (EUR-2688) 12/6/65, EURAEC-1546.

49. STUDIES OF STEEL CORROSION IN HIGH TEMPERATURE WATER AND STEAM, Societe d'Etudes, de Recherches et d'Applications pour l'Industrie, Contract 089-62-7 RDB; 31 p. Dec. 1965, EURAEC-1581.

50. STUDIES OF STEEL CORROSION IN HIGH TEMPERATURE WATER AND STEAM, Societe d'Etudes, Contract 087-66-ITEEB (RD). (EUR-2838) Dep. mn CFSTI (In Belgium), Apr. 1966, EURAEC-1625.

51. CORROSION OF STAINLESS STEELS IN HIGH TEMPERATURE WATER AND STEAM. M. Warzee, W. R. Ruston, P. deDorlodot, J. Hennaut, J. - PH Berge; (Societe d'Etudes, de Recherches et d'Applications pour l'Industrie, Brussels (Belgium), Contract 089-62-7-RDB, 14 p. (EUR-2857. e; CONF-660514-3); Feb. 1966, EURAEC-1665.

52. STUDIES OF STEEL CORROSION IN HIGH TEMPERATURE WATER AND STEAM, Quarterly Report No. 15, 4/16/30/66; 7/25/66, EURAEC-1689.

53. STUDIES OF STEEL CORROSION IN HIGH TEMPERATURE WATER AND STEAM, Societe d'Etudes, de Recherches et d'Applications pour l'Industrie, Brussels (Belgium), (EUR-3304) 10/30/66, Contract 087-66-1 TEEB(RD), 89 p EURAEC-1744.

54. BEHAVIOR OF STAINLESS STEELS IN SUPERHEATED STEAM. G. Chaudron; Contract 059-65-7-TEEB(RB); 18 p (EUR-3306); Quarterly Report #5, 7/1-9/30/66; EURAEC-1749.

55. INFLUENCE OF SURFACE TREATMENT ON CORROSION OR CARBON AND STAINLESS STEELS IN HIGH TEMPERATURE WATER AND STEAM, PART II. CORROSION EVALUATION THROUGH DETERMINATION OF THE HYDROGEN FORMED IN THE REACTION. C. Sonnen, M. Warzee, (Societe d'Etudes, de Recherches et d'Applications pour l'Industrie, Brussels (Belgium); Contract 089-62-7 RD-B; 35 p; (EUR-3319) Dep. mn CFSTI Dec. 1966, EURAEC 1764.

56. BEHAVIOR OF STAINLESS STEELS IN SUPERHEATED STEAM. G. Chaudron; Contract 059-65-1 TEEB(RD): 18 p (EUR-3345); Quarterly Report #16 10/1-12/31/66, EURAEC-1804.

57. STUDIES OF STEEL CORROSION IN HIGH TEMPERATURE WATER AND STEAM. Societe d'Etudes, Contract 087-1-TEEB(RD); 102 p (EUR-3361); May 1967, EURAEC-1850.

58. CORROSION OF STAINLESS STEEL AND HIGH NICKEL CONTENT ALLOYS IN HIGH-TEMPERATURE SUPERHEATED STEAM. M. Warzee; C. Sonnen; J. Cremer; Ph. Berge; (Societe d'Etudes, (Belgium); Contract 087-1-TEEB(RD), 74 p. (EUR-3387); July 1967, EURAEC-1895.

59. OXIDATION OF SUPERHEATED MATERIALS IN STEAM: AUSTENITIC STAINLESS STEEL, J. Board, G.Holyfield; J. Dalley (Atomic Power Constructions Ltd., Hounslow, Eng.) pp 163-173 of Journees Internationales d'Etude sur l'Oxydation des Metaux Brussels, Societe d'Etudes de Recherches et d'Applications pour l'Industrie, (1965).

60. NEW STUDIES OF THE ISOTHERMAL CORROSION OF INCOLOY 800 BY SUPER-HEATED STEAM. S. Leistikow, Kernforschungszentrum, Karlsruhe (West Germany) 5 p (1971) March.

61. INVESTIGATIONS OF THE CORROSION BEHAVIOR OF AUSTENITIC CrNi STEELS AND NICKEL ALLOYS IN SUPERHEATED STEAM. S.Leistikow, 32 p (1972) (KFK-1463) (N72-25534) EUR FNR 954.

62. INFLUENCE OF COLD WORK ON THE CORROSION RESISTANCE OF AUSTENITIC CrNi STEELS IN SUPERHEATED STEAM. 2. STATIC AUTOCLAVE STUDIES ON INCOLOY 800 IN DIFFERENT GRAIN SIZES. S. LEISTIKOW, E. Pott. (Kernforschungszentrum, Karlsruhe (West Germany). Institut fuer Material und Festkocrperforschung). 28 pp Dec. 1972 (KFK-1681). UERFNR 1061.

63. INFLUENCE OF COLD WORK ON THE CORROSION RESISTANCE OF AUSTENITIC CrNi STEELS IN SUPERHEATED STEAM. Part 3. STATIC AUTOCLAVE INVESTIGATIONS ON MATERIAL 1.4301 (x 5 CrNi 18.9). S. Leistikow, E. Pott and W. Volz. (Kernforschungszentrum, Karlsruhe (West Germany). Institut fuer Material and Festkoerperforschung). 34 pp March 1973, EURFNR 1087.

64. WATERSIDE CORROSION IN ADVANCED DESIGNS OF NUCLEAR STEAM GENERATORS, R. Garnsey, B. Hearn, G. M. W. Mann. Journal of the British Nuclear Energy Society, Vol II (1972) p. 65-70.

65. METALLURGICAL PROBLEMS IN MOLTEN FLUORIDE SYSTEMS, W. D. Manly, J. H. Cools, J. H. DeVan, D. A. Doublas, H. Inouye, P. Patriarca, T. K. Roche and J. L. Scott. Pergamon Press reprinted from "Progress in Nuclear Energy". Series IV, Vol 2-Technology, Engineering and Safety, Geneva Conference Paper (1958) P/1990 pp 164-179.

66. PROBLEMS DE CORROSION POSES PAR L'EMPLOI DES ACIERS DANS LA CONSTRUCTION DES GENERATEURS DE VAPEUR POUR REACTEURS NUCLEAIRES, H. Coriou, R. Darras, L. Grall, O. Konovalt-schikoff, M. Pelras, J. Sannier, R. Teraube. Fourth International Conference on the Peaceful Uses of Atomic Energy, Geneva, Switzerland, Sept. 6-16/71.

67. MATERIALS FOR LIQUID METAL FAST BREEDER REACTORS VESSELS, PIPING, INTERVALS AND CLASSING, S. H. Bush, 5/24/72. Conf. 7211104 Pacific Northwest Lab. Div. of Battelle Memorial Institute.

68. RELATION OF TUBE MANUFACTURING VARIABLES TO CORROSION AND CORROSION RELEASE RATES OF A NI-CR-FE ALLOY IN SIMULATED P.W.R. PRIMARY WATER, G. C. Bodine Jr., J. W. Carter, Paper #53 NACE 1974.

69. PWR WATER: VARYING CHEMISTRY AND "HOT" CONTAMINANTS. W. D. Fletcher, Industrial Water Engineering. (1971) March.

70. CORROSION IN WATER-COOLED NUCLEAR POWER REACTORS. P. J. Shirvington, Australasian Corrosion Engineering (1971) Jan-Feb.

71. STAINLESS STEEL REACTOR PRESSURE VESSELS, 27786, P. J. Karnoski, Jr., (Brown and Root, Inc., Houston, Tex.), W. J. Fretague, U. Potapovs, and L. E. Steele, Nucl. Eng. Design, II, 347-67 (1970) April.

72. OXIDATION RESISTANCE OF SOME STAINLESS STEELS AND NICKEL-BASED ALLOYS IN HIGH-TEMPERATURE WATER AND STEAM, S. Jansson, W. Huebner, G. Oestberg, M. Pourbaix, Brit. Corros. J., Vol. 4, 21-31 (1969) Jan.

73. NEW DEVELOPMENTS IN MATERIALS FOR MOLTEN-SALT REACTORS, H. E. McCoy, R. L. Beatty, W. H. Cook, R. E. Gehlbach, C. R. Kennedy, J. W. Koger, A. P. Litman, C. E. Sessions and J. R. Weir, Nucl. Appl. Technol., Vol. 8, 156-69 (1970) Feb.

74. CORROSION BEHAVIOR OF STAINLESS STEEL IN HIGH-TEMPERATURE WATER AND STEAM. T. Maekawa, and M. Kagawa, Nippon Kinzoku Gakkaishi, Vol. 31, 1213-19 (1967) Oct. (In Japanese).

75. STRESS CORROSION CRACKING OF STAINLESS STEELS AND NICKEL BASE ALLOYS IN CHLORIDE CONTAINING WATER AND STEAM AT 200-300°C; W.Hubner, M. DePourbaix, and G. Ostberg, Paper presented at the 4th International Congress on Metallic Corrosion, Amsterdam, The Netherlands (1969) Sept.

76. STUDY OF SEVERAL HIGH TEMPERATURE CORROSION PHENOMENA OF AUSTENITIC IRON-CHROME-NICKEL ALLOYS IN WATER AND SUPER-HEATED STEAM. H. Coriou, L. Grail, and M. Pelras, Presented at the 4th International Congress on Metallic Corrosion, Amsterdam, Netherlands, Sept. 7-14 (1969) Order from NACE, 2400 West Loop South, Houston, Tex. 77027.

77. CORROSION AND FAILURE CHARACTERISTICS OF ZIRCONIUM ALLOYS IN HIGH-PRESSURE STEAM IN THE TEMPERATURE RANGE 400 TO 500°C A. B. Johnson, Jr., 25 p (1969) Sept. Contract AT(45-1)-1830 CONF-681105-2 CFSTI From Application-Related Phenomenon of Zirconium and Hafnium Symposium, Philadelphia, Pa.

78. EFFECT OF SOME ENVIRONMENTAL CONDITIONS ON STRESS CORROSION BEHAVIOR OF NI-CR-FE ALLOYS IN PRESSURIZED WATER. H. R. Copson and G. Economy; Corrosion 24(3), (1968).

79. MECHANISMS OF SENSITIZATION AND STABILIZATION OF INCOLOY NICKEL IRON-CHROMIUM ALLOY 825, E. L. Raymond; Corrosion, 24(6), (1968).

80. THE RESISTANCE OF VARIOUS IRON-CHROMIUM-NICKEL AUSTENITIC ALLOYS AND AN IRON-40 PERCENT ALUMINUM ALLOY TO SUPERHEATED STEAM. H. Coriou, L. Grall, C. Maniev and M. Pelras (A.T.B Metallurgie, 6(2), 79-85, 1966.

81. CORROSION OF INCOLOY 800 AND NICKEL BASE ALLOY WELDMENTS IN STEAM. J. P. Hammond (Oak Ridge National Lab., TN); O. Patriarca, G. M. Slaughter, W. A. Maxwell and J. Weld (N.Y.); Vol. 52, No. 6, pp 268s-280s (1973) June.

82. FLUORIDE SALT CORROSION AND MASS TRANSFER IN HIGH TEMPERATURE DYNAMIC SYSTEMS, J. W. Koger, Corrosion, Vol. 29, No. 3 (1974).

83. STRESS CORROSION CRACKING OF SENSITIZED STAINLESS STEEL IN OXYGENATED HIGH TEMPERATURE WATER, Warren E. Berry, Earl L. White, and Walter K. Boyd, Corrosion, Vol. 29, No. 12, (1973).

84. THE INTERGRANULAR STRESS CORROSION CRACKING OF NICKEL ALLOYS IN PRESSURIZED WATER. J. Weber and P. Sury (Sulzer Brothers, Ltd., Winterthur, Switzerland). Presented at Corrosion/74.

85. STEAM GENERATOR AND HEAT EXCHANGER MATERIALS. (ORNL-TM-4105), pp. 2.1-2.52 (1973) May.

86. INFLUENCE OF COLD WORK ON THE CORROSION RESISTANCE OF AUSTENITIC Cr-Ni STEELS IN SUPERHEATED STEAM. Part 3. STATIC AUTOCLAVE INVESTIGATIONS ON MATERIAL 1.4301 (x 5 CrNi 18.9). S. Leistikow, E. Pott, and W. Volz. (Kernforschungszentrum, Karlsruhe (West Germany). Institut fuer Material and Festkoerperforschung). 34 pp. (1973) March. Dep.

87. INVESTIGATION INTO THE HOT STEAM CORROSION OF WELDED INCOLOY 800 PLATE. S. Leistikow and W. Scheibe. Werkstoffe u. Korrosion Vol. 24, p. 269-273 (1973).

88. RELATION OF TUBE MANUFACTURING VARIABLES TO CORROSION AND CORROSION PRODUCT RELEASE RATES OF A NiCrFe ALLOY IN SIMILATED PWR PRIMARY WATER, G. C. BODINE, JR., J. W. Carter, Paper # 53 NACE, 1974.

89. CORROSION OF ADVANCED STEAM GENERATOR ALLOY WELDMENTS IN 1100 AND 1200°F (595 AND 650 C) STEAM. J. P. Hammond, P. Patriarca, G. M. Slaughter, and W. A. Maxwell, Proceedings of the 26th Conference of the National Association of Corrosion Engineers, Philadelphia, Pa., March 2-6, 1970, pp 277-91, Houston, Texas, National Association of Corrosion Engineers (1970) (CONF-700324-1) Paper No. 46.

90. GENERAL CORROSION OF STAINLESS STEELS AND NICKEL BASE ALLOYS EXPOSED ISOTHERMALLY IN SUPERHEATED STEAM. G. P. Wozadlo and W. I. Pearl, Corrosion 21, No. 11 (1965) Nov.

91. NUCLEAR SUPERHEATED PROJECT TWENTY-SECOND QUARTERLY REPORT, NOV. 1964 - JAN. 1965. W. L. Fiock, General Electric Co., San Jose, Calif., Atomic Power Equipment Dept., 163 p. (1965) Feb. Contract AT(04-3)-189.

92. CORROSION-RATE-LAW CONSIDERATIONS IN SUPERHEATED STEAM. E. G. Brush, Nucl. Appl., 1, 246-51 (1965) June.

93. CORROSION OF CARBON STEEL IN SIMULATED BOILING WATER AND SUPERHEATED REACTOR ENVIRONMENTS. W. L. Pearl and G. P. Wozadlo, Corrosion, 21 No. 8(1965) August.

94. CORROSION OF STEELS AND NICKEL ALLOYS IN SUPERHEATED STEAM. W. E. Ruther and S. Greenberg, Journal of the Electrochemical Society, 3, No. 10, 1116-1121 (1965) Oct.

95. MATERIALS FOR BOILING WATER AND SUPERHEATED STEAM NUCLEAR POWER REACTORS. W. R. Smith, Sr., Materials Research and Standards, 4 No. 4, 170-174 (1964) April.

96. ZIRCONIUM ALLOYS FOR USE IN SUPERHEATED STEAM. S.Greenberg, J. Nuclear Materials, 4, No. 3, 334-335 (1961) August/ September.

97. TESTING STEAM GENERATOR MATERIALS FOR PRESSURIZED WATER REACTOR PLANTS, John W. McGrew, Corrosion, 18, No. 1, 27t-32t (1962) Jan.

98. STUDIES OF STEEL CORROSION IN HIGH TEMPERATURE WATER AND STEAM. Quarterly Report No. 6, Oct.-Dec. 1963. Euratom Joint Research and Development Program, 70 pp (1964) Jan. Contract 089 62-7 RDB, Order from OTS.

99. STRESS CORROSION CRACKING OF AUSTENITIC STAINLESS STEEL IN SUPERCRITICAL STEAM. P. P. Snowden, Monthly Technical Bulletin of International Combustion Ltd., IV 17, Jan. 1963 pp 39-45.

100. CORROSION BEHAVIOR OF STEELS AND NICKEL ALLOYS IN SUPER-HEATED STEAM. W. E. Ruther, R. R. Schlueter, R. H. Lee, R. K. Hart, Presented at NACE 21st Conference in St. Louis, Missouri 3/14-19/65.

101. REVIEW ARTICLE, THE AQUEOUS CORROSION OF REACTOR METALS, J. N. Wanklyn and P. J. Jones. UKAEA Metallurgy Division, Atomic Energy Research Establishment, Harwell, Didcot, Berks, U. K. Received 12 March 1962.

102. METALLURGICAL EVALUATION OF SUPERHEATER TUBE ALLOYS AFTER SIX-MONTHS EXPOSURE AT TEMPERATURES OF 1100° to 1500°F., C. L. Clark, J. J. B. Rutherford, A. B. Wilder, M. A. Cordovi, Journal of Engineering for Power, Jan. 1960, pp 35-67.

103. METALLURGICAL EVALUATION OF SUPERHEATER TUBE ALLOYS AFTER 12 AND 18 MONTHS EXPOSURE TO STEAM AT 1200, 1350, AND 1500°F. C. L. Clark, J. J. B. Rutherford, A. B. Wilder, M. A. Cordovi, Transactions of ASME, July 1962 pp 258-288.

104. EFFECT OF ALLOY COMPOSITION ON STRESS CORROSION CRACKING OF FE-CR-NI BASE ALLOYS, R. W. Staehle, J. J. Royuela, T. L. Raredon, E. Serrate, R. V. Farrae, Corrosion, Nov. 1970 451-486.

105. SCALING BEHAVIOR OF SUPERHEATER TUBE ALLOYS IN ASME HIGH TEMPERATURE STEAM RESEARCH TESTS AT 1100-1500°F; F. Eberle, C. H. Anderson; Journal of Engineering for Power, July 1962 pp 223-257.

106. CORROSION PROBLEMS IN NUCLEAR REACTOR POWER STATIONS, W. Z. Friend, Reprint, Vol. XVIII Proceedings of the American Power Conference, 1956.

107. STUDY OF SEVERAL HIGH TEMPERATURE CORROSION PHENOMENA OF AUSTENITIC IRON-CHROM-NICKEL ALLOYS IN WATER AND SUPER-HEATED STEAM. H. Coriou, L. Grall and M. Pebras, Presented at 4th International Congress on Metallic Corrosion, Amsterdam, Netherlands, Sept. 7-14 (1964).

108. PROBLEMES DE CORROSION POSES PAR L'EMPLOI DES ACIERS DANS LA CONSTRUCTION DES GENERATEURS DE VAPEUR POUR REACTEURS NUCLEAIRES. H. Coriou, R. Darras, L. Grall, O. Konovaltschikoff, M. Pelras, J. Sannier and R. Teraube, Presented at 4th U.N. International Conference on the Peaceful Uses of Atomic Energy, Geneva, Switzerland, Sept. 6-16, 1971.

Table 1 Nominal Chemical Composition of Hastelloy N

Element	Standard Alloy[11] (Much as Used in MSRE) (wt %)[a]	Modified Alloy[9] Recommended for MSBR's (wt %)
Nickel	Balance	Balance
Molybdenum	15–18	12
Chromium	6–8	7
Iron	5	0–4
Manganese	1	0.2–0.5
Silicon	1	0.1 max
Boron	0.01	0.001 max
Titanium		0.5–1.0
Hafnium or Niobium		0–2
Copper	0.35	} 0.35 (total for Copper through Aluminum + Titanium)
Cobalt	0.2	
Phosphorus	0.015	
Sulfur	0.02	
Carbon	0.04–0.08	
Tungsten	0.5	
Aluminum + Titanium	0.5	

[a]Single values are maximum percentages unless otherwise specified.

Table 2 Physical Properties of Hastelloy N

	80°F	500°F	1000°F	1300°F	1500°F
Density, lb/in.^{3}	0.320[a]				
Density, lb/ft^3	553.0				
Thermal conductivity, Btu hr^{-1} ft^{-1} °F^{-1}	6.0	7.8	10.4	12.6	14.1
Specific heat, Btu lb^{-1} °F^{-1}	0.098	0.104	0.115[a]	0.136	0.153
Coefficient of thermal expansion per °F[b]	5.7×10^{-6}	7.0×10^{-6}	8.6×10^{-6}	9.5×10^{-6}	9.9×10^{-6}
Modulus of elasticity, lb/in.^{2}	31×10^6	29×10^6	27×10^6	25×10^6	24×10^6
Electrical resistance, microhm-cm	120.5[a]	123.7	125.8	126.0[a]	124.1[a]
Approximate tensile strength, psi	115,000	106,000	95,000	75,000	55,000
[illegible]	25,000	20,000	17,000	3500	
[illegible]	[illegible]	7700	6600	2500	
Melting temperature, °F[c]			2470–2555		

[a]Taken directly from ref. 10. All other values found from interpolation of plots of ref. 10 data. See this reference for more precise information.

[b]Average coefficient of expansion over 212 to 1832°F range is 8.6×10^{-6} per °F.

[c]Ref. 11.

FW. FORM 172 - 4

NOTATIONS IN THIS COLUMN INDICATE WHERE CHANGES HAVE BEEN MADE

BY	APPROVED	PAGE 6-43

ASME BOILER AND VESSEL CODE
CODE CASE: 1315-2
SECTION VIII

Table 3—Maximum Allowable Stress Values

Metal Temperatures Not Exceeding Deg. F.	Maximum Allowable Stress Values, psi	
	All Material Other Than Bolting	Bolting
100	25,000	10,000
200	24,000	9,300
300	23,000	8,600
400	21,000	8,000
500	20,000	7,700
600	20,000	7,500
700	19,000	7,200
800	18,000	7,000
900	18,000	6,800
1000	17,000	6,600
1100	13,000	6,000
1200	6,000	6,000
1300	3,500	3,500

Table 4

Design Stress Intensity Values, S_m, in ksi

Temperature	
100	26.7
200	25.3
300	24.2
400	23.3
500	22.6
600	21.9
650	21.6
700	21.3
750	21.1
800	20.7

NOTE: Design stress intensity values are based on lesser of:
(1) ⅓ Specified Minimum Tensile Strength
(2) ⅓ Tensile Strength @ Temperature
(3) ⅔ Specified Minimum Yield Strength
(4) ⅔ Yield Strength @ Temperature

ASME BOILER AND VESSEL CODE
CODE CASE: 1345-2
SECTION III
APPROVED 3/9/72

TABLE 5

MATERIALS INVESTIGATED AND TESTS USED TO DETERMINE RELATIVE PERFORMANCE

Material	Irradiations	Uniform Corrosion at 1050 F		Corrosion With Salts	Tensile Properties	Structure
	6×10^{19} nvt 700-800 F	Unstressed	Constantly Stressed 0.1% Creep in 1000 Hrs.	1075-1100 F 70 μ gm. $Cl^-/in.^2$	Effect of Exposure	Microstructural Changes
304	No deleterious effects	Normal scale growth	Some intergranular stress ruptures	Intergranular failures, stress-accelerated	Not tested	Not tested
Incoloy	No deleterious effects	Normal scale growth	No failures, normal scale	Normal scale formation	Reduction in ductility to 20%. Recovery after 3000 hours.	Sensitization and microstructural instability
Inconel	Not tested	Normal scale growth	Intergranular penetrations, stress ruptures	Intergranular failures, stress-accelerated	Slight changes in strength and ductility	Complete sensitization
310	Not tested	Normal scale growth	Normal scale formation	Embrittlement because of sigma phase. Normal scale.	Not tested	Not tested
316	No deleterious effects	Not tested	Not tested	Not tested	Not tested	Not tested
330	No deleterious effects	Not tested	Intergranular attack	Intergranular failure	Not tested	Not tested
347	No deleterious effects	Not tested	Normal scale formation	Not tested	Not tested	Not tested
AISI 406	Loss in uniform elongation from 11.4% to 4.4%	Large oxide layer formation	Large oxide layer formation	Large oxide formation, stress-rupture failure	No effect up to 2000 hours	No visible changes
Hastelloy-X	Not tested	Normal oxide layer formation	Normal scale formation	Normal scale formation	Reduction in ductility from 42% to 10% in 5200 hours	Continuous intergranular precipitate network
Hastelloy-N	Not tested	Not tested	Intergranular failure	Intergranular failure	Not tested	Not tested
Ni-O-Nel	Not tested	Normal scale growth	Normal scale formation	Normal scale formation	Slowly decreasing ductility after 2000 hours	Intergranular precipitate network
2¼ Croloy	Not tested	Not tested	Excessive scale formation	Excessive scale formation	Not tested	Not tested
5 Croloy Ti	Not tested	Not tested	Excessive scale formation	Excessive scale formation	Not tested	Not tested

TABLE 6

AVERAGE WEIGHT GAINS FOR ALLOYS EXPOSED TO 15 TORR WATER VAPOR AT 815, 1030, AND 1150 °C FOR 100, 200, AND 300 hr

Alloy	Test Temperature, °C	Time, hr	Average Weight Change, mg/cm^2
Inconel 600	815	100	+ 0.1201
		200	+ 0.1617
		300	+ 0.1782
	930	100	+ 0.3464
		200	+ 0.4952
		300	+ 0.5552
	1038	100	+ 0.9133
		200	+ 1.2931
		300	+ 1.4600
Inconel 625	815	100	+ 0.1650
		200	+ 0.2244
		300	+ 0.2600
	930	100	+ [illegible]
		200	+ 0.8790
		300	+ 1.1004
	1038	100	+ 2.4905
		200	+ 3.3270
		300	+ 4.196
Inconel 702	815	100	+ 0.2561
		200	+ 0.3838
		300	+ 0.4896
	930	100	+ 1.1436
		200	+ 1.5732
		300	+ 1.8232
	1038	100	+ 1.7439
		200	+ 1.5241
		300	+ 1.7000
Inconel 718	815	100	+ 0.2869
		200	+ 0.3832
		300	+ 0.4013
	930	100	+ 0.9886
		200	+ 1.3872
		300	+ 1.6162
	1038	100	- 3.7936
		200	- 5.0674
		300	- 13.8400
Incoloy 800	815	100	+ 0.3478
		200	+ 0.4887
		300	+ 0.5327
	930	100	+ 0.8788
		200	+ 1.2563
		300	+ 1.4634
	1038	100	+ 1.5593
		200	+ 1.8669
		300	+ 2.3700
Hastelloy C	815	100	+ 0.1029
		200	+ 0.1194
		300	+ 0.1362
	930	100	+ 0.2750
		200	+ 0.3792
		300	+ 0.4592
	1038	100	+ 0.5733
		200	+ 0.6229
		300	+ 0.7010
Hastelloy N	815	100	+ 0.0331
		200	+ 0.1023
		300	+ 0.1037
	930	100	+ 0.2570
		200	+ 0.2262
		300	+ 0.3153
	1038	100	+ 0.5276
		200	+ 0.6205
		300	+ 0.7650
Hastelloy R-235	815	100	+ 0.7130
		200	+ 0.8013
		300	+ 0.9343
	930	100	+ 2.1750
		200	+ 3.0357
		300	+ 3.5573
	1038	100	+ 3.8658
		200	+ 4.7407
		300	+ 6.9150
Hastelloy X-28	815	100	+ 0.0840
		200	+ 0.0993
		300	+ 0.0905
	930	100	+ 0.3025
		200	+ 0.4191
		300	+ [illegible]
	1038	100	+ 0.6701
		200	+ 0.9012
		300	+ 0.903
Haynes 25	815	100	+ 0.1793
		200	+ 0.2147
		300	+ 0.2461
	930	100	+ 0.5122
		200	+ 0.7398
		300	+ 0.7506
	1038	100	+ 0.8255
		200	+ 0.9939
		300	+ 1.0470

NUCLEAR DEPARTMENT
FOSTER WHEELER ENERGY CORPORATION
LIVINGSTON, N. J.

CHARGE NO. 8-25-2431
DOCUMENT NO. ND/74/66
ISSUE 1
DATE 12/16/74

TABLE 7

WEIGHT GAIN OF IRON- AND NICKEL- BASE ALLOYS IN SUPERHEATED STEAM, mg/dm^2.
AT 550 °C (1022 °F) AND 1000 OR 3000 psi PRESSURE

ALLOY EXPOSURE HOURS	72	[illegible]	[illegible]	138	174	262	235	340	599	678	720	984	1062
PRESSURE, psi	1000	3000	3000	1000	3000	3000	1000	3000	3000	3000	1000	3000	3000
ASTM A 212-B	260.0			305.0			730.0			915.0			
AISI 304 SS	62.0	64.9		78.0	4.0		117.0	121.0		160.0	219.0		220.0**
AISI 439 SS	(141.)	124.0		(160.)	1 6.0		(209.)	177.0		193.0	(226.)		240.0
AISI 446 SS	3.2	5.3		4.1	7.6		6.3	9.4		10.6	5.7		11.0
FERRAL		124.0			1 6.0			250.0		342.0			583.0
AISI 406 SS (AL)	(155.)	121.0		(186.)	1 8.0		(259.)	167.0		185.0	(280.)		219.0
AISI 406 SS (Carp.)		45.0			[illegible]		[illegible]			143.0			190.0
* AISI 406 SS (Carp.) Wa		143.0			[illegible]		212.0			247.0			310.0
Fe-24CR-5.6 AL		2.2			3.5			5.0		10.0			(56.)
Fe-25CR-3 Al-0.6Y		22.0			[illegible]4.0			43.0		52.0			73.0
Hastelloy X-280			4.5			6.0			9.0			13.0	
Hastelloy N		8.0			12.0			16.0		51.0			57.0
Inconel X		9.0			11.0			14.0		18.0			26.0
Incoloy			6.4			3.4			11.0			14.0	
PDRL-102		8.5			10.5			12.4		31.0			42.0

* Weldrawn
304-L SS

BY

APPROVED

Table 8. Summary of Data on the Corrosion of Hastelloy N in Steam

Environment and Test Conditions	Test Results: Weight Gain (mg/cm^2)		Test Results: Oxide Penetration (mil)	
	Hastelloy N	Type 304L Stainless Steel	Hastelloy N	Type 304L Stainless Steel
Superheated steam, 1022°F, 3000 psi, 1062 hr	0.57	2.20		
Deoxygenated steam,				
932°F, 3000 psi, 2400 hr			0.08	3.3
932°F, 5000 psi, 2400 hr			0.04	0.14
(< 50 ppb), 1022°F, 3000 psi, 2400 hr			0.08	0.33
Oxygenated steam, (3 to 4 ppm), 1022°F, 3000 psi, 2400 hr			0.15	0.37
Helium plus 15 torrs water vapor, 1500°F, 300 hr, ~1 atm pressure	0.109			

Table 9. Chemical Analyses of Test Materials

Alloy	Concentration, wt %																			
	Ni	Mo	Cr	Fe	Mn	C	Si	P	S	Cu	Co	V	W	Al	Ti	B	Nb	Hf	Zr	Other
Armco Iron*				Bal.	0.017	0.012		0.005	0.025											
Low-alloy Ferritic																				
1.1 Cr	0.25	0.49	1.1	Bal.	0.42		0.64				<0.05	<0.02	<0.05	<0.05	<0.02					
1.9 Cr	0.20	0.54	1.9	Bal.	0.46		0.17													
2.0 Cr	0.32	0.88	2.0	Bal.	0.40		0.25													
4.2 Cr	0.36	0.47	4.2	Bal.	0.40		0.35													
8.7 Cr	0.35	0.97	8.7	Bal.	0.44		0.50													
12-5-3 Maraging	12.7	2.80	5.1	Bal.	0.05		0.10							~0.3						
Stainless Steels																				
Type 502*		0.5	5.0	Bal.		0.1														
17-7 PH	7.10		17.0	Bal.		0.07								1.15						
Type 201	5.23		16.55	Bal.	7.28	0.076	0.54	0.34	0.006											0.059 N
Type 304*	8.0		18.0	Bal.		0.03														
Type 309*	13.5		23.0	Bal.		0.2														
Type 310*	20.5		25.0	Bal.		0.25	1.5													
Type 316	13.01	2.8	17.0	Bal.	1.74	0.027	0.65	0.016	0.017	0.10	0.15									
Type 321*	10.5		18.0	Bal.		0.08									0.4					
Type 347*	11.0		18.0	Bal.		0.08											0.4			0.4 TA
Type 406			13.0	Bal.		0.15								4.0						
Type 410*			12.5	Bal.		0.15														
Type 446*			25.0	Bal.		0.20														0.25 N
Ni-280	Bal.	0.0002	0.002	0.003	<0.0001	0.34	0.005			<0.001	0.002	<0.0001	<0.0001	0.03	<0.0001		<0.0001		<0.0001	
Monel*	60			3.5	3.5	0.5				23				0.5						
Copper*								0.02		9949										
Inconel 600	78.0		14.5	7.0		0.05														
Inconel 601	60.5		23.0	14.1	0.5	0.05	0.25		0.007	0.25				1.35						
Inconel 718	53.0	3.0	18.0			0.05								0.50	1.0		5.0			
Incoloy 800	31.3		20.1	46.2	0.84	0.04	0.38		0.008	0.50				0.24	0.36					
Hastelloy B	Bal.	27.0	<0.2	5.2	0.96		0.3			0.01	0.48	0.2		<0.05	<0.01				<0.05	
Hastelloy C	Bal.	16.0	16.0	5.8	0.75		0.48			0.01	1.2	0.1	5.0	0.2	<0.01				<0.05	
Hastelloy S	Bal.	14.7	14.5	0.90	0.04	0.007	<0.01				0.22			0.2						0.01 B
Hastelloy W	60.0	25.0	5.0	5.5		0.08					1.0	0.30								
Hastelloy X		8.6	22.0	19.0	0.64		0.60			0.02	2.0	0.05	0.5	0.2	<0.01				<0.05	
Haynes Alloy 25	10.0	0.5	20.0	1.4	1.0	0.1	0.7	0.015	0.01	0.02	Bal.	<0.02	15.2	0.1	0.02				<0.05	
Haynes Alloy 188	22.0		22.0	3.0	1.25	0.15					Bal.		15.0							
Rene 62	Bal.	9.0	15.0	22.0	0.25	0.05	0.25							1.25	2.5		2.25		0.01	
Hastelloy N Modifications																				
185	Bal.	11.0	5.9	3.8	0.46	0.05	0.10				<0.03		<0.1	<0.05	0.91			<0.1	0.98	
186	Bal.	10.0	5.4	3.5	0.45	0.05	0.09				<0.03		<0.1	0.84	0.88			<0.1	<0.05	
188	Bal.	13.0	7.3	4.5	0.49	0.05	0.15				<0.03		<0.1	0.95	<0.02			1.1	<0.05	
231	Bal.	12.0	7.0	4.2	0.03	0.05	0.12				<0.03			<0.05	<0.02		<0.05	1.3	<0.05	1.2 Y
232	Bal.	13.0	8.0	4.5	<0.02	0.05	0.12				<0.03			<0.05	<0.02		<0.05	1.2	<0.05	
234	Bal.	16.0	7.2	4.0	<0.02	0.05	0.13				<0.03			<0.05	<0.02		<0.05	<0.1	<0.05	
236	Bal.	11.0	7.0	4.0	0.5	0.05	0.13				<0.03			1.0	<0.02		<0.05	<0.05	0.5	
237	Bal.	12.0	6.7	4.3	0.49	0.05	0.13				<0.03			<0.05	0.04		1.03	<0.1	<0.05	
2477	Bal.	16.2	7.0	4.2	0.055	0.057	0.047	0.008	0.004	0.01	0.05	<0.01	0.03	0.02	0.03	0.0002	<0.0005	<0.001	<0.001	
5065	Bal.	16.5	7.1	4.0	0.55	0.07	0.58	0.005	0.004	0.007	0.05	0.20	0.1	<0.03	<0.01	0.001	<0.05	<0.1	<0.1	
5067	Bal.	17.2	7.4	4.0	0.48	0.06	0.43	0.005	0.007	0.01	0.09	0.30	0.6	0.01	0.01	0.004				
5085	Bal.	17.0	7.0	3.6	0.64	0.06	0.65	0.004	0.003	0.01	0.15	0.20	0.07	0.05	<0.01	0.004	<0.05		<0.002	
21541	Bal.	11.6	7.3	0.04	0.16	0.05	0.017	0.001	0.002	0.01	<0.10	<0.10	1.98	0.03	0.005	0.0007			<0.005	
21542	Bal.	12.1	7.21	0.041	0.16	0.06	0.014	0.001	0.004	0.01	<0.10	<0.10	2.05	<0.10	<0.10	0.0005	0.96		<0.005	
21543	Bal.	12.4	7.31	0.038	0.08	0.05	0.019	<0.001	0.004	0.01	<0.10	<0.10	<0.10	<0.02	<0.003	0.0002	0.70		<0.005	
21544	Bal.	12.6	7.3	<0.10	0.13	0.06	<0.03	<0.01	0.003	0.01	<0.10	<0.10	<0.10	<0.10	<0.10	0.0005			0.44	
21545	Bal.	12.0	7.18	0.034	0.29	0.05	0.015	0.001	<0.002	0.01	<0.10	<0.10	<0.10	0.02	0.49	0.00007			0.01	
21546	Bal.	12.3	7.29	0.046	0.16	0.05	0.009	0.001	<0.002	0.01	<0.10	<0.10	<0.10	0.02	0.10	0.0002			0.005	
21554	Bal.	12.4	7.39	0.097	0.16	0.065	0.01	0.004	<0.002					0.03	0.003	0.0002			0.35	
21555	Bal.	12.4	7.18	0.065	0.16	0.052	0.008	0.003	<0.002					0.02	0.003	0.0007			0.05	
M1566	Bal.	16.0	7.5	5.0	0.5	0.06					0.5									
68688	Bal.	13.8	7.91	4.98	0.52	0.079	0.38	0.042	<0.002	0.023	0.08				0.013	0.0002	<0.05	<0.05	<0.05	
68689	Bal.	13.7	7.6	4.8	0.47	0.081	0.53	0.01	<0.002	0.02	0.075				0.36	0.0002	<0.05	<0.05	<0.05	
69344	Bal.	13.0	7.4	4.0	0.56	0.109	0.5	0.001	0.004	0.03	0.06	<0.01	<0.01	0.24	0.77	0.00001	1.7	<0.01	0.001	
69345	Bal.	13.0	7.5	4.0	0.52	0.078	0.5	0.001	0.01	0.02	0.07	<0.01	0.03	0.27	1.05	0.00006	<0.01	0.92	0.3	
69641	Bal.	13.9	6.9	0.30	0.35	0.06	0.02	0.001	0.003	0.01	<0.03	0.02		<0.03	1.30	0.0001	<0.05	0.70	0.01	
69648	Bal.	12.8	6.9	0.30	0.24	0.04	0.05	0.001	0.003	0.02	<0.03	0.10		<0.05	0.92	0.00008	1.95	0.08	0.02	
69714	Bal.	12.4	8.0	0.10	0.35	0.012	<0.05	0.001	0.004	0.05	0.05	<0.01	0.01	0.17	0.80	0.00001	1.6	<0.01	<0.01	
70727	Bal.	11.7	7.5	0.05	0.37	0.04	<0.05	0.004	0.001	<0.01	<0.01	<0.01	0.01	<0.03	2.1	0.00006	<0.1	<0.01	<0.01	
70785	Bal.	12.2	7.0	0.16	0.27	0.057	0.09	0.002	0.004	0.02	0.03	0.003	0.003	0.14	1.1	0.002	0.097	<0.003	0.01	
70786	Bal.	12.2	7.2	0.41	0.48	0.044	0.08	0.002	0.01	0.02	0.05	0.008	0.003	0.13	0.82	0.0005	0.62	0.003	0.06	
70787	Bal.	12.5	7.0	0.18	0.43	0.041	0.09	0.002	0.004	0.02	0.05	0.003	0.003	0.17	0.90	0.0005	0.12	0.77	0.07	
70788	Bal.	12.5	7.2	0.43	0.43	0.027	0.10	0.002	0.004	0.02	<0.02	0.008	0.003	0.18	1.36	0.0005	0.67	0.30	0.01	
70795	Bal.	13.0	7.8	0.04	0.63	0.054	0.03	<0.005	0.005	0.003	0.005	0.001	<0.005	0.06	1.49	0.002	0.005	0.42	0.017	
70796	Bal.	12.4	7.3	0.05	0.64	0.043	0.02	<0.005	0.005	0.003	0.005	0.002	<0.005	0.10	0.04	0.0005	0.04	0.75	0.024	
70797	Bal.	12.5	7.0	0.29	0.38	0.055	0.02	<0.005	0.003	0.003	0.005	0.002	<0.005	0.07	0.59	0.0002	0.98	0.75	0.035	
70798	Bal.	12.8	7.5	0.26	0.53	0.038	0.02	0.002	0.005	0.003	0.005	0.003	<0.005	0.07	0.71	0.0001	0.94	0.32	0.011	
70835	Bal.	12.1	7.8	0.68	0.58	0.053	0.05	0.001	0.004	0.005	0.10	<0.01	<0.01	0.10	0.71	0.002	2.6	<0.01	<0.005	
71114	Bal.	12.5	7.14	0.062	0.02	0.05	0.026	0.002	0.005	0.007	0.07			0.07	1.75	0.002			<0.03	
71583	Bal.	12.4	7.35	0.13	0.03	0.05	0.055	0.002	0.004	0.015	0.10			0.2	1.44				<0.03	
72115	Bal.	11.9	7.03	0.07	0.07	0.091	0.09	0.003	0.002							<0.001		0.72	0.2	
72503	Bal.	12.9	6.79	0.32	0.01	0.066	0.01	0.0008	0.002					0.1	1.94	<0.001				
72604	Bal.	11.5	6.69	0.07	0.07	0.09	0.09	0.003	0.003							<0.001		0.30	0.02	

*Nominal composition, all others are actual analyses

All the alloys up to "Hastelloy N modifications" were commercial production heats. Heats 185 through 237 were 2-lb laboratory melts. Hastelloy N heats 21541 through 72604 were small 50- to 100-lb melts that were vacuum melted and fabricated by commercial vendors. Hastelloy N heats 2477, 5065, 5067, 5085 and M/566 were large commercial heats of standard Hastelloy N.

All alloys were rolled to 0.035-in.-thick sheet. The rolling was done cold with intermediate anneals for stress relief; the finish of the exposed sample surface was generally typical of cold-rolled sheet. Samples 1/2 in. wide x 2 in. long x 0.035 in. thick were sheared, cleaned, and annealed in argon for 1 hr at 1700°F (the low-alloy ferritic steels), 1 hr at 1900°F (the stainless steels), or 1 hr at 2150°F (all other alloys).

Table 10. Weight Change Data for Specimens of Low-Alloy Ferritic and Maraging Steels

Alloy	Specimen	Area (cm^2)	Weight Gain, mg/cm^2 at Various Times in hr										
			670	1000	2000	2482	4000	4482	6000	8000	10,000	13,000	14,000
Cr 1.1[a]	172	13.6924		3.14	3.78			5.12	6.00	6.47	6.80		9.12
	173	13.6444		3.21									
	205	13.6221	2.31			4.22	4.96		5.37	5.60	6.22	7.74	
Cr 1.9[a]	202	13.5654	3.97			6.30	7.98						
	208	13.6392	4.28			7.95	8.53		8.89	8.89	9.78	11.71	
	163	13.6274		4.94									
	164	13.6355		4.93	5.98			7.57	8.90	9.31	9.81		12.03
Cr 2.0[a]	166	13.6369		3.93									
	167	13.6287		3.40	4.32			5.80	6.93	7.37	7.63		9.60
	203	13.5638	2.90			4.63	5.91						
	209	13.5759	2.73			4.51	5.77		6.08	6.53	7.31	8.96	
Cr 4.2[a]	204	13.5999	3.76			6.14	7.74		8.07	8.64	9.97	11.88	
	169	13.6329		3.98	5.13			6.83	7.97	8.48	8.96		10.41
	170	13.5955		4.49	6.89								
Cr 8.7[a]	175	13.6411		3.77									
	176	13.6668		3.73	4.56			5.98	7.03	7.43	7.68		
	206	13.6558	2.74			5.81	6.27		6.27	6.57	7.29	8.79	
12-5-3[b]	207	13.5928	3.97			6.61	8.91		9.73	10.22	11.33	13.99	
	178	13.5173		6.33									
	179	13.4833		6.16	7.37			9.48	11.04	11.77	12.13		15.48

[a]Low-alloy ferritic steel annealed 1 hr at 1700°F in argon.

[b]12-5-3 maraging steel annealed 1 hr at 1500°F in argon.

Table 11. Weight Change Data for Specimens of Stainless Steels

Stainless Steel Type	Specimen	Condition[a]	Area (cm^2)	Weight Gain, mg/cm^2 at Various Times in hr				
				1000	2000	3000	4000	5000
502	372	Annealed	13.7092	3.71	4.77	5.43	6.05	
502	373	Annealed	13.0605	3.29	4.23	4.95	5.49	
17-7PH	374	Annealed	13.9202	0.50	0.66	0.83	0.98	
17-7PH	375	Annealed	13.8598	0.33	0.51	0.67	0.84	
201	352	Annealed	13.5782	0.71	1.16	1.81	2.20	
201	353	Annealed	13.5727	0.81	1.35	2.08	2.49	
201	354	Cold worked 50%	13.6137	0.04	0.04	0.07	0.04	
201	355	Cold worked 50%	13.7611	0.03	0.03	0.05	0.03	
304	349	As received	13.6554	0.79	1.11	1.25	1.47	1.64
309	359	Annealed	13.7911	1.60	2.05	2.53	2.72	
309	360	Annealed	13.4095	1.69	2.06	2.48	2.67	
310	361	Annealed	13.5377	0.57	0.91	1.10	1.20	
310	362	Annealed	13.5377	0.83	1.10	1.29	1.40	
316	363	Annealed	13.5893	1.34	1.71	2.07	2.39	
316	364	Annealed	13.1245	1.44	1.87	2.27	2.61	
316	365	Cold worked 50%	13.5512	0.52	0.66	0.85	1.00	
321	366	Annealed	13.4699	0.75	1.05	1.39	1.69	
321	367	Annealed	13.4320	0.67	0.93	1.22	1.47	
347	334	Annealed	13.2688	0.67	1.05	1.17	1.33	1.42
347	335	Annealed	13.3337	0.55	0.78	0.92	1.09	1.19
406	368	Annealed	13.7580	1.56	1.92	2.28	2.51	
406	369	Annealed	13.6301	1.25	1.54	1.86	2.09	
410	336	Annealed 1700°F	13.7768	2.39	2.80	3.03	3.48	3.80
410	337	Annealed 1700°F	13.5450	2.53	3.03	3.22	3.68	4.02
446	370	Annealed	12.8269	1.03	1.30	1.58	1.77	
446	371	Annealed	14.0554	1.52	1.82	2.03	2.16	

[a] Annealed 1 hr in argon at 1900°F unless otherwise specified.

CHARGE NO. 8-25-2431
DOCUMENT NO. ND/74/66
ISSUE 1
DATE 12/16/74

NUCLEAR DEPARTMENT
FOSTER WHEELER ENERGY CORPORATION
LIVINGSTON, N. J.

Table 12. Weight Change Data for Specimens of Nickel 280 Annealed 1 hr in Argon at 1470°F

Specimen	Area (cm^2)	Weight Gain, mg/cm^2 at 400 hr	Weight Gain, mg/cm^2 at 1518 hr
266	13.8262	4.44	54.43
267	13.8262	3.33	77.11
268	13.9680	4.30	72.95
269	13.7880	5.25	75.29

Table 13. Weight Change Data for Specimens of Various Metals and Alloys

Material	Specimen	Condition[a]	Area (cm^2)	Weight Gain, mg/cm^2 at Various Times in hr 1000	2000	3000	4000	5000	6000	9000
Armco Iron	356	Annealed 1700°F	13.6683	4.44	5.52	7.06	8.06			
	357	Annealed 1700°F	13.6241	4.33	5.37	6.88	7.87			
	358	Cold worked 50%	13.7063	4.66	5.68	7.22	8.24			
Monel	332	Annealed 1470°F	13.6301	0.62	2.81	7.89	12.96	17.28		
	333	Annealed 1470°F	13.6301	1.19	4.59	9.50	14.42	18.54		
Copper	466	Annealed 1470°F	13.5783	0.34	−0.13					
	467	Annealed 1470°F	13.5554	0.22	−0.18					
Inconel 600	388	Annealed 2150°F	13.5130	0.26	0.30	0.41	0.46			
	389	Annealed 2150°F	13.5265	0.24	0.27	0.37	0.43			
Inconel 601	316	Annealed 2150°F	13.7337	0.06	0.11	0.17	0.17	0.19	0.25	0.36
	317	Annealed 2150°F	13.7611	0.07	0.12	0.20	0.22	0.24	0.31	0.40
	468	Cold worked 50%	13.7546	0.21						
Inconel 718	390	Annealed 2150°F	13.5644	0.05	0.01		0.01			
	391	Annealed 2150°F	13.7195	0.05	0.01	−0.01				
	412	Cold worked 50%	13.3954	0.12	0.13	0.15	0.18			

[a] Annealed 1 hr in argon at the indicated temperature.

CHARGE NO. 8-25-2431
DOCUMENT NO. ND/74/66
ISSUE 1
DATE 12/16/74

NUCLEAR DEPARTMENT
FOSTER WHEELER ENERGY CORPORATION
LIVINGSTON, N. J.

NUCLEAR DEPARTMENT
FOSTER WHEELER ENERGY CORPORATION
LIVINGSTON, N. J.

Table 14. Weight Change Data for Specimens of Incoloy 800 and Hastelloys B and C

Alloy	Specimen	Condition[a]	Area (cm^2)	Weight Gain, mg/cm^2 at Various Times in hr						
				1000	2000	4482	6000	8000	10,000	13,000
Incoloy 800	198	Annealed 1900°F	13.6339	0.50	0.80	0.95				
	199	Annealed 1900°F	13.6200	0.41	0.71	0.81	0.81	0.84	0.90	0.92
	200	Annealed 1900°F	13.6350	0.42	0.68	0.81	0.71	0.75	0.83	0.80
	201	Annealed 1900°F	13.5310	0.51	0.81					
	469	Cold worked 50%	13.8543	0.17						
Hastelloy B	376	Annealed 2150°F	12.6206	0.10	0.11	0.16	0.19			
	377	Annealed 2150°F	13.6480	0.12	0.16	0.21	0.25			
	407	Cold worked 50%	13.3631	0.16	0.29	0.49	0.62			
Hastelloy C	378	Annealed 2150°F	13.5241	0.06	0.08	0.10	0.13			
	379	Annealed 2150°F	13.5621	0.04	0.06	0.07	0.08			
	408	Cold worked 50%	13.6220	0.15	0.17	0.21	0.21			

[a]Annealed 1 hr in argon at the indicated temperature.

Table 15. Weight Change Data for Specimens of Various Superalloys

Alloy	Specimen	Condition[a]	Area (cm^2)	Weight Gain, mg/cm^2 at Various Times in hr			
				1000	2000	3000	4000
Hastelloy S	417	Annealed	13.7229	0.09	0.14	0.15	
	418	Annealed	13.7229	0.09	0.12	0.15	
Hastelloy W	380	Annealed	12.8533	0.04	0.05	0.09	0.10
	381	Annealed	13.2794	0.04	0.06	0.09	0.07
	409	Cold worked 50%	13.3134	0.11	0.16	0.20	0.23
Hastelloy X	382	Annealed	13.8476	0.06	0.06	0.09	0.11
	383	Annealed	13.7953	0.04	0.04	0.05	0.05
	410	Cold worked 50%	13.7063	0.12	0.14	0.17	0.21
Haynes 25	384	Annealed	13.4209	0.03	0.01	0.10	0.16
	385	Annealed	13.5889	0.07	0.08	0.18	0.23
Haynes 188	386	Annealed	13.2926	0.03	0.01	0.05	0.08
	387	Annealed	14.0295	0.04	0.04	0.07	0.11
	413	Cold worked 50%	13.7684	0.23	0.27	0.30	0.33
Rene 62	392	Annealed	13.6678	0.18	0.16	0.19	0.22
	393	Annealed	13.8791	0.15	0.14	0.17	0.18
	411	Cold worked	13.7580	0.15	0.16	0.20	0.24

[a] Anneals are for 1 hr in argon at 2150°F.

CHARGE NO. 8-25-2431
DOCUMENT NO. ND/74/66
ISSUE 1
DATE 12/16/74

NUCLEAR DEPARTMENT
FOSTER WHEELER ENERGY CORPORATION
LIVINGSTON, N. J.

Table 16. Weight Change Data for Specimens of Modified Hastelloy N Laboratory Heats[a]

Heat	Specimen	Area (cm^2)	Weight Gain, mg/cm^2 at Various Times in hr						
			1000	2000	4482	6000	8000	10,000	15,000
185	87	13.6149	0.14						
185	88	13.6431	0.21	0.29	0.49	0.54	0.59	0.65	0.74
185	89	13.6603	0.20	0.32					
185	90	13.6048	0.12	0.24	0.41	0.55	0.53	0.58	
186	91	13.5903	0.21	0.24					
186	92	13.6285	0.12	0.21	0.36	0.49	0.48	0.59	
188	37	13.6213	0.29	0.40	0.62	0.57	0.68	0.71	0.78
188	38	13.5819	0.09	0.19	0.32	0.32	0.40	0.46	
231	35	13.6267	0.12	0.21	0.28	0.29			
231	36	13.6386	0.26	0.43					
231	105	12.5198	0.27	0.38	0.58	0.62	0.65	0.69	0.72
232	103	13.5416	0.18	0.22	0.39	0.43	0.44	0.47	0.55
232	104	13.5230	0.21	0.24	0.39	0.46	0.47	0.50	
236	101	13.6424	0.11	0.17	0.35	0.41	0.45	0.52	0.60
236	102	13.6070	0.18	0.26	0.43	0.46	0.49	0.54	
237	99	13.6422	0.10	0.15	0.24	0.28	0.29	0.33	0.38
237	100	13.6359	0.10	0.14	0.23	0.32	0.26	0.32	

[a]Annealed 1 hr in argon at 2150°F.

Table 17. Weight Change Data for Specimens of Standard Hastelloy N Large Commercial Heats

Heat	Specimen	Condition[a]	Thickness (in.)	Area (cm^2)	Weight Gain, mg/cm^2 at Various Times in hr						
					1000	2000	4482	6000	8000	10,000	15,000
2477	23		0.035	13.6662	0.15	0.21	0.34	0.33	0.38	0.41	0.48
2477	24		0.035	13.5224	0.13	0.25					
2477	55		0.010	12.9177	0.07	0.12	0.22	0.26	0.23	0.27	0.29
2477	56		0.010	12.7622	0.09	0.14	0.24	0.29			
2477	57		0.010	12.6151	0.10	0.17					
2477	58		0.010	12.4519	0.07	0.13	0.18	0.26	0.22	0.26	
2477	59		0.010	12.7940	0.07	0.09	0.25	0.26			
2477	60		0.010	12.6220	0.11	0.13					
2477	61	Cold worked 50%	0.010	12.6409	0.13	0.15	0.27	0.31	0.36	0.42	0.50
2477	62	Cold worked 50%	0.010	12.9948	0.15	0.18					
2477	63	Cold worked 50%	0.010	12.9303	0.13	0.20	0.33	0.39			
2477	64	Cold worked 50%	0.010	12.5853	0.10	0.17	0.28	0.36	0.36	0.45	0.52
5065	1		0.010	12.5543	0.14	0.20	0.29	0.32	0.29	0.33	
5065	2		0.010	12.5932	0.10	0.14	0.33	0.28	0.30	0.33	0.36
5065	3		0.020	12.9448	0.15	0.20	0.30	0.32	0.35	0.37	0.41
5065	4		0.020	12.9558	0.14	0.22	0.33	0.35	0.33	0.36	0.41
5065	5		0.035	13.4914	0.16	0.22	0.33	0.33	0.33	0.36	0.39
5065	6		0.035	13.5692	0.15	0.22	0.34	0.35	0.37	0.41	0.45
5065	7		0.060	14.5614	0.14	0.24	0.36	0.40	0.41	0.45	0.55
5065	8		0.060	14.5693	0.14	0.21	0.33	0.36	0.38	0.42	0.47
5065	9		0.035	13.5302	0.18	0.22	0.33	0.33	0.33	0.34	0.38
5065	10		0.035	13.6351	0.15	0.22	0.31	0.32	0.37	0.40	0.43
5065	11	Abraded	0.035	13.5960	0.29	0.40	0.56	0.60	0.63	0.70	0.81
5065	12	Abraded	0.035	13.5079	0.25	0.39	0.55	0.60	0.64	0.69	0.78
5065	13	Electropolished	0.035	13.3979	0.04	0.08	0.13	0.16	0.14	0.18	0.22
5065	14	Electropolished	0.035	13.2262	0.03	0.09	0.15	0.15	0.18	0.22	0.29
5065	15		0.010	12.5496	0.08	0.37	0.29	0.29			
5065	16		0.010	12.5359	0.07	0.18					
5065	17		0.010	12.5742	0.14	0.22	0.34	0.32			
5067	18		0.035	13.3301	0.14	0.22	0.30	0.31			
5065	19		0.010	12.4907	0.10	0.22	0.26	0.34			
5067	20		0.035	13.3419	0.12	0.21	0.30	0.30	0.31	0.35	0.40
5067	67		0.035	13.2601	0.12	0.20					
5067	68		0.035	13.1974	0.06	0.11	0.23	0.28	0.26	0.32	
5085	21		0.035	13.6078	0.12	0.23	0.32	0.32	0.32	0.37	0.44
5085	22		0.035	13.5278	0.13	0.18	0.34	0.34			
5085	65		0.035	13.7014	0.11	0.17	0.34	0.36	0.37	0.43	
5085	66		0.035	13.5821	0.13	0.18					
M1566	394		0.035	13.6297	0.09	0.09	0.15[b]	0.18[c]			
M1566	395		0.035	13.6678	0.11	0.12	0.17[b]	0.22[c]			

[a] Unless otherwise specified, annealed 1 hr at 2150°F in argon, tested with the surface in the as-rolled condition.

[b] 3000 hr.

[c] 4000 hr.

Table 18. Weight Change Data for Specimens of Modified Hastelloy N Commercial Heats[a]

Heat	Specimen	Area (cm^2)	Weight Gain, mg/cm^2 at Various Times in hr						
			1000	2000	4482	6000	8000	10,000	14,000
21545	27	13.4661	0.19						
21545	28	13.4492	0.25	0.34	0.42	0.43	0.43	0.48	
21545	97	13.3940	0.13	0.22					
21545	98	13.4485	0.15	0.19	0.34	0.42			
21546	25	13.5637	0.23	0.31	0.40	0.37	0.41	0.44	
21546	26	13.5364	0.18						
21546	95	13.6380	0.23	0.29	0.40	0.45			
21546	96	13.5981	0.25	0.31					
21554	83	13.5252	0.21	0.31	0.49	0.59			
21554	84	13.5208	0.22	0.33					
21554	85	13.5629	0.19	0.28	0.43	0.56	0.52	0.60	
21554	86	13.5674	0.27						
21555	79	13.4514	0.25						
21555	80	13.5829	0.13	0.22	0.35	0.46			
21555	81	13.5219	0.11	0.18	0.29	0.35	0.36	0.41	
21555	82	13.4692	0.29	0.39					
68688	75	13.6022	0.12	0.18					
68688	76	13.5285	0.10	0.14	0.24	0.33			
68688	77	13.5245	0.04	0.13	0.24	0.30	0.27	0.33	
68688	78	13.5056	0.10						
68688	194	13.1127	−0.01	0.13	0.25	0.19	0.19	0.24	0.26[b]
68689	71	13.2735	0.12	0.18	0.31	0.41			
68689	72	13.5373	0.10	0.18	0.30	0.41	0.40	0.44	
68689	73	13.4412	0.13	0.19					
68689	74	13.4479	0.14						
68689	195	12.9800	0.03	0.13	0.25	0.17	0.18	0.26	0.29[b]
69641	160	13.4860	0.10						
69641	161	13.5752	0.09	0.12	0.24	0.22	0.25	0.39	0.40
69641	196	13.5937	0.04	0.17	0.18	0.21	0.27	0.32	0.38
69648	157	13.5881	0.12	0.14	0.26	0.34	0.32	0.36	0.52
69648	158	13.5307	0.10						
69648	197	13.6013	0.03	0.18	0.26	0.24	0.29	0.36	0.45

[a]Annealed 1 hr in argon at 2150°F

[b]13,000 hr.

Table 19. Weight Change Data for Specimens of Modified Hastelloy N Commercial Heats[a]

Heat	Specimen	Area (cm^2)	Weight Gain, mg/cm^2 at Various Times in hr						
			1000	2000	3000	4000	5000	6000	9000
21541	314	13.6926	0.12	0.14	0.19	0.22	0.18	0.20	0.26
21541	315	13.7063	0.11	0.18	0.20	0.23	0.20	0.20	0.30
21542	312	13.6926	0.02	0.06	0.09	0.13	0.12	0.12	0.18
21542	313	13.8022	0.10	0.12	0.16	0.17	0.16	0.19	0.21
21543	310	13.7611	0.09	0.12	0.15	0.15	0.14	0.15	0.22
21543	311	13.7748	0.12	0.14	0.17	0.19	0.16	0.17	0.24
21544	308	13.7200	0.24	0.35	0.36	0.31	0.19	0.23	0.36
21544	309	13.7959	0.17	0.26	0.31	0.36	0.28	0.27	0.41
21545	343	13.4363	0.19	0.25	0.27	0.31	0.31		
21546	344	13.6956	0.27	0.34	0.34	0.39	0.41		
21554	345	13.6301	0.13	0.17	0.20	0.27	0.31		
21555	346	13.3827	0.07	0.12	0.13	0.19	0.25		
70727	342	14.1173	−0.05	−0.04	−0.05	−0.03	−0.03		
70785	306	13.7337	0.05	0.11	0.17	0.23	0.18	0.19	0.30
70785	307	13.7063	0.12	0.12	0.18	0.20	0.21	0.23	0.26
70786	304	13.7063	0.07	0.11	0.16	0.20	0.20	0.20	0.33
70786	305	13.7474	0.09	0.09	0.14	0.15	0.17	0.21	0.33
70787	302	13.7337	0.10	0.15	0.24	0.25	0.27	0.28	0.44
70787	303	13.6926	0.07	0.15	0.23	0.26	0.23	0.25	0.38
70788	300	13.7337	0.09	0.10	0.15	0.15	0.17	0.18	0.30
70788	301	13.7885	0.01	0.01	0.06	0.05	0.07	0.08	0.18
70795	298	13.6515	0.03	0.08	0.14	0.20	0.18	0.18	0.27
70795	299	13.6789	0.01	0.06	0.08	0.16	0.16	0.16	0.28
70796	296	13.8323	0.06	0.10	0.17	0.20	0.15	0.13	0.25
70796	297	13.8296	0.09	0.12	0.17	0.23	0.13	0.12	0.28
70797	294	13.7666	0.03	0.04	0.09	0.14	0.12	0.12	0.19
70797	295	13.7611	0.04	0.07	0.10	0.13	0.13	0.12	0.20
70798	292	13.7081	0.03	0.03	0.09	0.12	0.09	0.09	0.16

Table 19. (Continued)

Heat	Specimen	Area (cm^2)	Weight Gain, mg/cm^2 at Various Times in hr						
			1000	2000	3000	4000	5000	6000	9000
70798	293	13.6877	0.04	0.08	0.12	0.16	0.15	0.15	0.25
70835	290	13.9187	0.05	0.02	0.06	0.08	0.07	0.07	0.09
70835	291	13.7819	0.04	0.04	0.09	0.09	0.09	0.08	0.14
71114	338	13.7502	0.10	0.17	0.17	0.23	0.28		
71114	339	13.4699	0.10	0.15	0.15	0.20	0.23		
71583	340	13.6410	0.08	0.11	0.13	0.20	0.25		
71583	341	13.5512	0.08	0.13	0.15	0.21	0.26		
72115	396	13.7987	0.18	0.23	0.34	0.44			
72115	397	13.7606	0.17	0.20	0.31	0.41			
72115	414[b]	13.7200	0.18	0.29	0.42	0.51			
72503	398	13.8469	0.12	0.14	0.22	0.27			
72503	399	13.9060	0.11	0.12	0.20	0.27			
72503	415[b]	13.7870	0.04	0.02	0.02	0.04			
72604	400	14.0059	0.39	0.40	0.47	0.54			
72604	401	13.9300	0.34	0.34	0.39	0.46			
72604	416	12.4655	0.15	0.23	0.36	0.44			

[a]Unless otherwise specified, annealed 1 hr at 2150°F in argon.

[b]Cold worked 50%.

Table 20. Weight Change Data for Specimens of Modified Hastelloy N Commercial Heats[a]

Heat	Specimen	Area (cm^2)	Weight Gain, mg/cm^2 at Various Times in hr						
			1812	3330	4330	5330	6330	8330	12,330
69344	258	13.6713	0.21	0.17	0.19	0.21	0.23	0.22	0.26
69344	259	13.6708	0.12	0.20	0.24	0.21	0.25	0.25	0.28
69345	260	13.6722	0.18	0.13	0.16	0.20	0.26	0.21	0.26
69345	261	13.6106	0.15	0.20	0.19	0.19	0.23	0.21	0.26
69714	262	13.6283	0.16	0.22	0.20	0.21	0.23	0.24	0.31
69714	263	13.6248	0.16	0.20	0.18	0.21	0.30	0.28	0.34
70727	264	13.6558	0.19	0.24	0.27	0.29	0.39	0.37	
70727	265	13.6675	0.19	0.20	0.18	0.20	0.27	0.26	0.33

[a] Annealed 1 hr at 2150°F in argon.

TABLE 21

SUMMARY OF TUBE BURST TEST DATA

Date of Placement (1)	Heat No.	Stress (PSI)	Diametral Strain %	Exposure Time (Hrs)	Failure (Hrs)	Machined Tube Wall Thickness (Inches)
2/28/71	N25095*	77,000	-	1,000	1	0.010
2/28/71	N25095*	52,500	-	1,000	3.7	0.015
2/28/71	N15095	40,250	0.71	5,000	None	-
2/28/71	N15095	28,000	0.19	5,000	None	0.0302*
8/31/71	N25101	56,000	0.57	4,000	None	0.014
8/31/71	N25101	50,000	0.33	4,000	None	0.016
2/29/72	N15095	58,000	-	1,000	792*	-
2/29/72	N15095	53,000	0.25	1,000	None	-
2/29/72	N15095	42,502	0.24	1,000	None	-
2/29/72	N15095	42,400	0.14	1,000	None	-
(2)	-	72,000*	-	-	-	0.0108*
(2)	-	66,000	-	1,000	4.0	-
(2)	-	56,000	-	1,000	27.4	-
(2)	-	55,300	-	1,000	99.7	-

* Date Inferred

(1) ORNL 4676 Molten Salt Reactor Program, Semiannual Progress Report Period Ending, 2/28/71.
ORNL 4728 Molten Salt Reactor Program, Semiannual Progress Report Period Ending, 8/31/71.
ORNL 4782 Molten Salt Reactor Program, Semiannual Progress Report Period Ending, 2/29/72.
ORNL 4832 Molten Salt Reactor Program, Semiannual Progress Report Period Ending, 8/31/72.

(2) Between 2/29/72 and 8/31/72.

	Element	Most Stable Fluoride Compound	Stability*
Structural Metals	chromium	CrF_2	72
	iron	FeF_2	66
	nickel	NiF_2	59
	molybdenum	MoF_2	57
Carrier Salts	lithium	LiF	120
	sodium	NaF	110
	potassium	KF	108
	beryllium	BeF_2	103
	zirconium	ZrF_4	92
	boron	BF_3	86
Active Salts	uranium	UF_4	92
		UF_3	93
	thorium	ThF_4	99

*Negative standard free energy of formation @ 800°C.

Table 22. Relative thermodynamic stabilities of fluoride compounds.

NOTATIONS IN THIS COLUMN INDICATE WHERE CHANGES HAVE BEEN MADE

Table 23. Status of MSR program thermal-convection loops through August 31, 1972

Loop No.	Loop material	Specimens	Salt type	Salt composition (mole %)	Max. temp. (°C)	ΔT (°C)	Operating time (hr)
1258	Type 304L stainless steel	Type 304L stainless steel[a,b]	Fuel	$LiF-BeF_2-ZrF_4-UF_4-ThF_4$ (70-23-5-1-1)	688	100	79,367
NCL-13A	Hastelloy N	Hastelloy N; Ti-modified Hastelloy N controls[b,c]	Coolant	$NaBF_4-NaF$ (92-8) plus tritium additions	607	125	33,579
NCL-14	Hastelloy N	Ti-modified Hastelloy N[b,c]	Cooland	$NaBF_4-NaF$ (92-8)	607	150	42,154
NCL-15A	Hastelloy N	Ti-modified Hastelloy N; Hastelloy N controls[b,c]	Blanket	$LiF-BeF_2-ThF_4$(73-2-25)	677	55	35,416
NCL-16	Hastelloy N	Ti-modified Hastelloy N; Hastelloy N controls[b,c]	Fuel	$LiF-BeF_2-UF_4$ (65.5-34.0-0.5)	704	170	37,942[d]
NCL-16A	Hastelloy N	Hastelloy N, one Te-coated Hastelloy N[b,c]	Fuel	$LiF-BeF_2-UF_4$ (65.5-34.0-0.5)	704	170	1,729
NCL-17	Hastelloy N	Hastelloy N; Ti-modified Hastelloy N controls[b,c]	Coolant	$NaBF_4-NaF$ (92-8) plus steam additions	607	100	27,817
NCL-18A	Hastelloy N	Hastelloy N[b,c]	Fertile-fissile	$LiF-BeF_2-ThF_4-UF_4$ (68-20-11.7-0.3)	704	170	672
NCL-19A	Hastelloy N	Hastelloy N; Ti-modified Hastelloy N controls[b,c]	Fertile-fissile	$LiF-BeF_2-ThF_4-UF_4$ (68-20-11.7-0.3) plus bismuth in melybdenum hot finger	704	170	22,203
NCL-20	Hastelloy N	Hastelloy N; Ti-modified Hastelloy N controls[b,c]	Coolant	$NaBF_4-NaF$ (92-8)	687	250	19,928[e]
NCL-20A	Hastelloy N	Hastelloy N; Ti-modified Hastelloy N controls[b,c]	Coolant	$NaBF_4-NaF$ (92-8)	687	250	1,682
NCL-21	Hastelloy N	Hastelloy N[b,c]	MSRE fuel	$LiF-BeF_2-ZrF_4-UF_4$ (65.4-29.1-5.0-0.5)	650	110	9,793
NCL-22	Type 316 stainless steel	Type 316 stainless steel[b,c]	Fertile-fissil	$LiF-BeF_2-ThF_4-UF_4$ (68-20-11.7-0.3)	650	110	342

FWC FORM 172 - 4

CHARGE NO. 8-25-2431	DOCUMENT NO. ND/74/66	ISSUE 1	DATE 12/16/74

WHERE CHANGES HAVE BEEN MADE

Table 24A.

S_o – Maximum Allowable Stress Intensity (ksi)
(For Design Condition Calculations)

Temp. °F	304 SS	316 SS	Ni-Fe-Cr Alloy 800H (Solution Annealed)	2¼ Cr - 1 Mo
700				15.0
750				15.0
800	15.1	15.8	15.3	15.0
850	14.9	15.7	15.1	14.4
900	14.6	15.5	14.8	13.1
950	14.3	15.4	14.6	11.0
1000	13.7	15.3	14.4	7.8
1050	12.1	14.5	13.7	5.8
1100	9.7	12.4	13.5	4.2
1150	7.7	9.8	11.2	3.0
1200	6.0	7.4	8.4	1.6
1250	4.7	5.4	6.9	
1300	3.7	4.1	5.4	
1350	2.9	3.0	4.5	
1400	2.3	2.2	3.6	
1450	1.8	1.7		
1500	1.4	1.2		

Table 24B.

Ni-Fe-Cr (Alloy 800H), S_{mt} Allowable Stress Intensity Values, ksi

Temp. °F	1 hr	10 hr	30 hr	100 hr	300 hr	1000 hr	3000 hr	10,000 hr	30,000 hr	100,000 hr	300,000 hr
850	15.1	15.1	15.1	15.1	15.1	15.1	15.1	15.1	15.1	15.1	15.1
900	14.8	14.8	15.8	14.8	14.8	14.8	14.8	14.8	14.8	14.8	14.8
950	14.6	14.6	14.6	14.6	14.6	14.6	14.6	14.6	14.6	14.6	14.6
1000	14.4	14.4	14.4	14.4	14.4	14.4	14.4	14.4	14.4	14.4	14.4
1050	14.3	14.3	14.3	14.3	14.3	14.3	14.3	14.3	14.3	14.3	13.4
1100	14.1	14.1	14.1	14.1	14.1	14.1	14.1	14.1	13.6	11.7	10.3
1150	13.9	13.9	13.9	13.9	13.9	13.9	13.9	12.0	10.5	9.1	8.0
1200	13.8	13.8	13.8	13.8	13.8	12.5	10.9	9.4	8.2	7.2	6.4
1250	13.5	13.5	13.5	13.3	11.5	9.8	8.6	7.5	6.6	5.8	5.1
1300	13.2	13.2	12.4	10.5	9.1	7.9	6.9	6.0	5.3	4.6	4.1
1350	12.0	11.4	9.9	8.4	7.4	6.4	5.6	4.9	4.3	3.7	3.3
1400	11.6	9.2	8.0	6.8	6.0	5.2	4.6	4.0	3.5	3.0	2.6

Table 24C.

Ni-Fe-Cr (Alloy 800H) S_t – Allowable Stress Intensity Values ksi

Temp. °F	1 hr	10 hr	30 hr	100 hr	300 hr	1000 hr	3,000 hr	10,000 hr	30,000 hr	100,000 hr	300,000 hr
850	20.0	20.0	20.0	20.0	20.0	20.0	20.0	20.0	20.0	20.0	20.0
900	19.8	19.8	19.8	19.8	19.8	19.8	19.8	19.8	19.8	19.7	19.6
950	19.6	19.6	19.6	19.6	19.6	19.6	19.6	19.5	19.3	19.2	19.1
1000	19.4	19.4	19.4	19.4	19.4	19.3	19.1	18.9	18.6	18.5	17.0
1050	19.3	19.3	19.3	19.3	19.3	18.9	18.7	18.4	17.4	15.3	13.4
1100	19.1	19.1	19.0	18.6	18.4	18.0	17.8	15.7	13.6	11.7	10.3
1150	18.6	18.5	18.4	18.1	17.7	16.3	14.0	12.0	10.5	9.1	8.0
1200	18.2	17.6	17.3	16.6	14.7	12.5	10.9	9.4	8.2	7.2	6.4
1250	17.7	16.6	15.8	13.3	11.5	9.8	8.6	7.5	6.6	5.8	5.1
1300	16.6	14.5	12.4	10.5	9.1	7.9	6.9	6.0	5.3	4.6	4.1
1350	14.9	11.4	9.9	8.4	7.4	6.4	5.6	4.9	4.3	3.7	3.3
1400	12.6	9.2	8.0	6.8	6.0	5.2	4.6	4.0	3.5	3.0	2.6

TABLE 25

PERFORMANCE OF HASTELLOY N SPECIMENS IN HIGH PRESSURE CHLORIDE SCC FACILITY*

Alloy	Specimen Type Weld	Specimen Type Non Weld	Specimen Condition	No. of Specimens	No. of Failures
Hastelloy N	✓	-	AR(1)	3	3
Hastelloy N	✓	-	Ground(2) Annealed	3	0
Hastelloy N	-	✓	Ground	3	3
Hastelloy N	-	✓	AR(1)	3	3
Hastelloy N	-	✓	Anneal 1(3)	3	0
Hastelloy N	-	✓	Anneal 2(3)	3	3
Hastelloy N	-	✓	Anneal 3(3)	3	0
Hastelloy N	-	✓	Anneal 4(3)	3	0

*Compiled from data reported in Ref. 39

(1) AR - As Received, Solution Annealed 2150°F.

(2) Annealed in accordance with supplier of alloy.

(3) Anneal 1 - Ground and heated 1 hour at 2150°F; air cooled.
Anneal 2 - Ground and heated 10 min. at 1600°F; air cooled.
Anneal 3 - Ground and heated 1 hour at 1600°F; air cooled.
Anneal 4 - Ground and heated 6 hours at 1600°F; air cooled.

TABLE 26

Preliminary Results for Run 9 in the Chloride Injection Loop

Exposure consisted of 10 weeks of thermal cycling between the superheated (700°F) and saturated (540°C) states, holding 24 hr at the latter 3 times per week; 7 ppm O was injected continuously and 7 ppm NaCl during the 540°C sojourns.

Group	Materials[a]	Material Conditions[b]	Results[c]
1	Inconel 625 and Inconel 625 welded with itself.	As-furnished. As-furnished and welded. Ground and welded. Ground, welded, and annealed. As-furnished, welded, and pickled.	No cracking either at top or bottom location.
2	Hastelloy X and Hastelloy X welded with itself.	As-furnished. As-furnished and welded. Ground and welded. Ground, welded, and annealed. As-furnished, welded, and pickled.	No cracking either at top or bottom location.
3	Hastelloy N and Hastelloy N welded with itself.	As-furnished. As-furnished and welded. Ground and welded. Ground, welded, and annealed. As-furnished, welded, and pickled.	All cracked to varying degrees except for those of ground, welded, and annealed condition.
4	Inconel 600 and Inconel 600 welded with Inconel 82.	As-furnished. As-furnished and welded. Ground and welded. Ground, welded, and annealed. As-furnished, welded, and pickled.	No cracking except for one suspect specimen of the welded and pickled group located at the upper position.
5	Incoloy 800 and Incoloy 800 welded with Inconel 82.	As-furnished. As-furnished and welded. Ground and welded. Ground, welded, and annealed. As-furnished, welded, and pickled.	No cracking either at top or bottom location.
6	Type 316 stainless steel and type 316 stainless steel welded with itself.	As-furnished. As-furnished and welded. Ground and welded. Ground, welded, and annealed. As-furnished, welded, and pickled.	No cracking except for one suspect specimen of the welded and pickled group located at the bottom location.
7	Type 304 stainless steel and type 304 stainless steel welded with type 308.	As-furnished. As-furnished and welded. Ground and welded. Ground, welded, and annealed. As-furnished, welded, and pickled.	No cracking except for one suspect specimen of the welded and pickled group at the bottom position.
8	26 Cr–1 Mo-Ti (electron-beam melted) welded with itself.	Ground and welded. Ground, welded, and pickled.	All cracked severely within 4 weeks.
9	18 Cr–2 Mo-Ti steel and 18 Cr–2 Mo steel welded with itself.	As-furnished. As-furnished and welded. Ground and welded. Ground, welded, and annealed optimumly.	No cracking either at top or bottom location.

TABLE 26
(Cont'd)

Group	Materials[a]	Material Conditions[b]	Results[c]
10	Super 12 Cr steel (HT-9) and super 12 Cr steel welded with itself.	As-furnished. Ground, welded, and annealed optimumly. Ground, welded, and annealed in temper brittleness range.	All cracked severely within 4 weeks of those annealed in the temper brittleness range.
11	9 Cr–1 Mo steel and 9 Cr–1 Mo steel welded with itself.	As-furnished. As-furnished and welded. Ground and welded. Ground, welded, and annealed optimumly. Ground, welded, and annealed in temper brittleness range.	All cracked severely within 4 weeks of those as-furnished and welded and those ground and welded.
12	9 Cr–1 Mo–Ti steel and 9 Cr–1 Mo-Ti steel welded with itself.	Ground, welded, and annealed in temper brittleness range.	No cracking either at top or bottom location.
13	5 Cr–1/2 Mo steel and 5 Cr–1/2 Mo steel welded with itself.	As-furnished. As-furnished and welded. Ground and welded. Ground, welded, and annealed optimumly.	No cracking either at top or bottom location.
14	5 Cr–1/2 Mo Ti steel and 5 Cr–1/2 Mo–Ti welded with itself.	As-furnished. As-furnished and welded. Ground and welded. Ground, welded, and annealed optimumly. Ground, welded, and annealed in temper brittleness range.	No cracking except one in the ground and welded conditions each at top and bottom location; one in ground and welded conditions at bottom location.
15	2 1/4 Cr–1 Mo steel and 2 1/4 Cr–1 Mo steel welded with itself.	As-furnished. As-furnished and welded. Ground and welded. Ground, welded, and annealed optimumly.	No cracking either at top or bottom location.
16	2 1/4 Cr–1 Mo–Nb steel (HT8X6) and 2 1/4 Cr–1 Mo–Nb welded with itself.	As-furnished. As-furnished and welded. Ground and welded. Ground, welded, and annealed optimumly. Ground, welded, and annealed in temper brittleness range.	No cracking either at top or bottom location except for ground and welded condition for which two cracked severely in 2 weeks at top position and one at bottom position.

[a]Specimens were of the C-configuration type prepared from 3/4-in.-OD × 1/16-in.-wall tubing. They were strained 0.88% on the bore side incident to mounting.

[b]The Inconels, Hastelloys, Incoloy 800, and 300 series stainless steels were annealed by heating 10 min at 1800°F and rapid cooling; 26 Cr–1 Mo, 18 Cr–2 Mo-Ti, and super 12 Cr were annealed optimumly by heating 45 min at 1400°F and 5 Cr–1 Mo, 5 Cr–1/2 Mo-Ti, 2 1/4 Cr–1 Mo, and 2 1/4 Cr–1 Mo-Nb were annealed optimumly by heating 45 min at 1350°F (all cooled 80°F/hr); super 12 Cr, 9 Cr–1 Mo-Ti, and 9 Cr–1 Mo were exposed to the upper temper brittleness range by heating 45 min at 1000°F and 5 Cr–1/2 Mo-Ti and 2 1/4 Cr–1 Mo-Nb were exposed to the upper temper brittleness range by heating 45 min at 900°F (all cooled 80°F/hr). The Inconels, Hastelloys, Incoloy 800, and 300 series stainless steels that were welded and pickled were heated in air 10 min at 2200°F just prior to pickling to simulate a loss of purge gas (welding) incident.

[c]Specimens were tested in triplicate for each surface condition and location in the autoclaves.

TABLE 27

Cracking Results on Stress Corrosion Cracking Specimens Tested in Runs 6 Through 8

Specimen Group No.[a]	Base Metal	Filler Metal[b]	Surface Condition[c]	Number of Failures	Crack Initiation Time[d] (weeks)	Crack Size, in. Initial[e]	Crack Size, in. Final	Crack Location[f]
1	Type 304 SS[g]	Type 308 SS	Ground	3 of 3	1–2	1/2	1/2	HAZ into WD
			Ground	3 of 3	6	1/2	1/2	HAZ into WD
			Ground and annealed	6 of 6	11	1/2	1/2	HAZ into WD
			Ground, annealed, and pickled	3 of 3	3–10	1/2	1/2	BM, HAZ into WD
2	Type 410 SS[g,h]	Type 410 SS	Ground	0 of 6				
			Ground and annealed	0 of 3				
			Ground, annealed, and pickled	0 of 6				
3	Incoloy 800[g]	Inconel 82	Ground	3 of 3	1–7	1/16–3/16	7/16	HAZ into FL
			Ground	3 of 3	6	1/16	1/8–1/4	HAZ, HAZ into FL
			Ground and annealed	1 of 3	7	3/16	1/4	HAZ into FL
			Ground and annealed	3 of 3	6–12	1/16–1/8	1/4	HAZ
			Ground, annealed, and pickled	1 of 3	6	1/16	1/8	HAZ
4	Inconel 600[g]	Inconel 82	Ground	2 of 3	1–4	1/8–3/16	3/8–7/16	HAZ
			Ground	2 of 3	5–12	1/16–1/8	1/8–5/16	HAZ
			Ground and annealed	0 of 6				
			Ground, annealed, and pickled	0 of 3				
5	Inconel 625[g]	Inconel 625	Ground	0 of 6				
			Ground and annealed	0 of 6				
			Ground, annealed, and pickled	0 of 3				
6	IN-102[g]	IN-102	Ground	3 of 3	2–5	1/2	1/2	HAZ into WD
			Ground	3 of 3	8–16	1/16–1/8	1/16–1/8	HAZ into WD
			Ground and annealed	3 of 6	5–12	1/8–1/4	1/4	HAZ and WD
7	Hastelloy X[g]	Hastelloy X	Ground	3 of 3	1	1/4–5/16	1/2	HAZ into WD, WD
			Ground	3 of 3	1–6	1/8–1/4	1/4–1/2	HAZ into WD, WD
			Ground and annealed	0 of 6				
			Ground, annealed, and pickled	0 of 3				
8	Hastelloy N[g]	Hastelloy N	Ground	3 of 3	4–11	1/2	1/2	HAZ into WD, WD
			Ground and annealed	0 of 3				
9	Type 304 SS[i]	No weld	Ground	3 of 6	3–9	1/32–1/8	1/16–1/4	E, (many)
			Ground and solution annealed	6 of 6	3–18	1/64–1/8	1/64–1/8	E, I (many, superficial)
10	Type 304N SS[i]	No weld	Ground	6 of 6	5–9	1/64–3/16	1/32–1/4	E,I (many, superficial)
			Ground and solution annealed	3 of 6	18	1/16–3/16	1/16–3/16	
11	18-18-2 SS[i]	No weld	Ground	3 of 3	8	1/4–1/2	1/2	
			Ground and solution annealed	3 of 3	6–8	1/16–1/2	7/16–1/2	E
12	18-3 Mn[i]	No weld	Ground	3 of 3	5–16	1/8–3/8	3/8–1/2	E
			As received	3 of 3	5–18	1/16–5/16	1/16–1/2	E, I
13	X20-6[i]	No weld	Ground	3 of 3	18	1/64–1/16	1/64–5/16	E (many)
			As received	3 of 3	18	1/64–1/16	1/64–1/16	E (many)
14	26 Cr-1 Mo[i] (EB melted)	No weld	Ground	3 of 3	1–2	1/2	1/2	
			As received	3 of 3	2–4	1/2	1/2	
15	Type 410 SS[i]	No weld	Ground	0 of 3				
			Ground and annealed	0 of 3				
			Ground, annealed, and pickled	0 of 3				
16	Super 12 Cr[j] (HT-9)	No weld	Ground	0 of 3				
			Ground and annealed	0 of 3				
17	9 Cr-1 Mo[k] (SA-213T9)	No weld	Ground	0 of 3				
			Ground and annealed	0 of 3				
18	5 Cr-1/2 Mo[k] (SA-213T5)	No weld	Ground	0 of 3				
			Ground and annealed	0 of 3				
19	2 1/4 Cr-1 Mo[g] (SA-213T22)	No weld	Ground	0 of 3				
			Ground and annealed	0 of 3				
20	Incoloy 800[i]	No weld	Ground	3 of 3	16–18	1/16–5/32	5/32–3/8	E, I
			Ground	3 of 3	16	1/8–3/16	1/8–3/16	I, E
			Ground and annealed	1 of 6	16	1/16	1/16	E
21	20 Cr-45 Ni-5 Mn[i]	No weld	Ground	3 of 3	1–15	3/16–1/4	1/4–1/2	E
			Ground and annealed	3 of 3	4–16	1/32–1/8	1/32–7/32	E, I
22	Inconel 600[i]	No weld	Ground	1 of 3	16	3/32	3/32	E
			Ground and annealed	0 of 3				
			As received	1 of 3	5	1/8	5/16	E
23	Inconel 601[i]	No weld	Ground	0 of 6				
			Ground and annealed	0 of 6				
24	Inconel 625[i]	No weld	Ground	0 of 6				
			Ground and annealed	0 of 6				

(Continued)

TABLE 27
(Cont'd)

Specimen Group No.[a]	Base Metal	Filler Metal[b]	Surface Condition[c]	Number of Failures	Crack Initiation Time[d] (weeks)	Crack Size, in. Initial[e]	Crack Size, in. Final	Crack Location[f]
25	Inconel 690[i] (10 Fe–60 Ni–30 Cr)	No weld	Ground	0 of 3				
			As received	0 of 3				
26	36 Fe–32 Ni–32 Cr[i]	No weld	Microduplexed and ground (100 mesh)	0 of 3				
			Microduplexed	0 of 3				
			Macroduplexed and ground (100 mesh)	0 of 3				
			Macroduplexed	0 of 3				
27	Incoloy 809E (19 Fe–44 Ni–37 Cr)	No weld	Microduplexed and ground (100 mesh)	0 of 3				
			Microduplexed	0 of 3				
			Macroduplexed and ground (100 mesh)	0 of 3				
			Macroduplexed	0 of 3				
28	Hastelloy X[i]	No weld	Ground	0 of 3				
			As received	2 of 3	12	1/16–3/32	1/16–3/32	E (several)
29	Hastelloy C-276[i]	No weld	Ground	0 of 3				
			As received	0 of 3				
30	Hastelloy G[i]	No weld	Ground	0 of 3				
			As received	0 of 3				
31	Hastelloy N[i]	No weld	Ground	3 of 3	1	1/2	1/2	(Many smaller ones)
			As received	3 of 3	1–2	1/2	1/2	
			Anneal 1	0 of 3				
			Anneal 2	3 of 3	7–14	1/16–1/8	1/4–1/2	E
			Anneal 3	0 of 3				
			Anneal 4	0 of 3				

[a]Specimens measured 3 1/4 × 1/2 × 1/16 in. and were bent to a 1/2-in. radius (6.2% maximum strain) incident to mounting.

[b]Weldments were prepared by an automated gas tungsten-arc process.

[c]Ground = surfaces ground on a 100-mesh-grit belt.

Ground and annealed = ground on 100-mesh belt and heated 10 min at 1800°F and cooled 100°F/min except for ferritic steels, which were ground and heated just below their lower critical temperature (1400°F for type 410 SS, super 12 Cr, and 9 Cr-1 Mo steel, and 1350°F for 5 Cr-1/2 Mo and 2 1/4 Cr-1 Mo) for 1 hr and gas cooled.

(Continued)

Ground, annealed, and pickled = given the preceeding treatment and then pickled by the procedure recommended by supplier of alloy.

Ground and solution annealed = ground and heated 1/2 hr at 1950°F and cooled rapidly.

As received = solution annealed (2150°F for Hastelloy S, G, and N; 2050°F for Hastelloy C-276; 1950°F for 18–3 Mn, 1900°F for X20-6; 1850°F for Inconel 600, and 1725°F for Inconel 690) or normalized and tempered for ferritic alloys (except annealed at 1450°F and water quenched for 26 Cr-1 Mo).

Anneal 1 = ground and heated 1 hr at 2150°F, air cooled; and Anneal 2 = ground and heated 10 min at 1600°F, air cooled; Anneal 3 = ground and heated 1 hr at 1600°F, air cooled; Anneal 4 = ground and heated 6 hr at 1600°F, air cooled.

Microduplexed = annealed at 1750°F and air cooled for 32 Cr–32 Ni–36 Fe alloy and at 1800°F and air cooled for 37 Cr–44 Ni–19 Fe alloy (5-μm and 3-μm grain sizes, respectively).

Macroduplexed = heated at 2300°F and water quenched plus annealed at 1750°F and air cooled for 32 Cr–32 Ni–36 Fe alloy and heated at 2300°F and water quenched plus annealed at 1800°F and air cooled for 37 Cr–44 Ni–19 Fe alloy (300-μm and 100-μm grain sizes, respectively).

[d]Crack distance in a lateral direction at the time first observed (specimens were inspected at one-week intervals).

[e]Crack distance in a lateral direction at the termination of test (after 16 or 18 weeks).

[f]HAZ = heat affected zone, WD = weld deposit, BM = base metal, FL = fusion line, E = edge of specimen, and I = inside.

[g]Hot-rolled and descaled plate stock of 1/2-in. thickness.

[h]In preparing weldment, 400°F preheating (continued through multipass welding) and a 1250°F postweld treatment was employed.

[i]Annealed sheet or strip stock of 1/16-in. thickness.

[j]Prepared as 1/16-in. strip by hot flattening a tube, austenitizing at 1925°F (air cooled), tempering at 1435°F (air cooled), and machining.

[k]Furnished by supplier of tubes as special strip sample (annealed).

[l]Prepared as 1/16-in. strip by hot flattening a tube, and solution annealing at 1750°F (water quench).

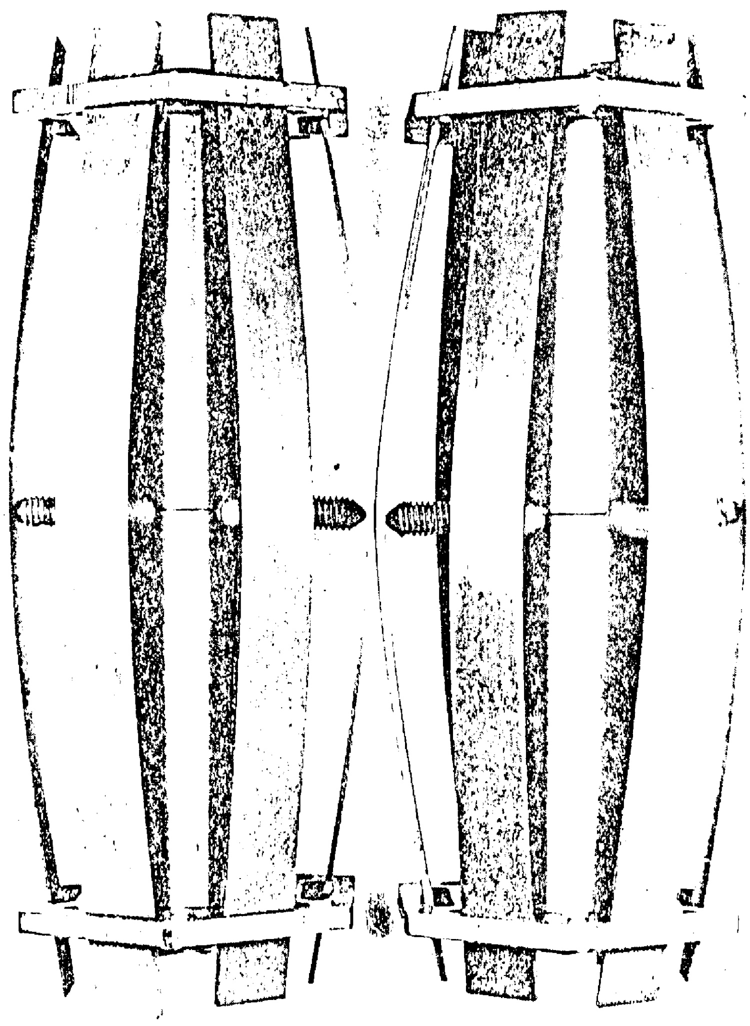

1X C1454

FIGURE 1 APPEARANCE OF TYPICAL SPECIMENS STRESSED BY 3-POINT LOADING (BATTELLE JIGS) AND EXPOSED 4000 HOURS TO 350°C WATER

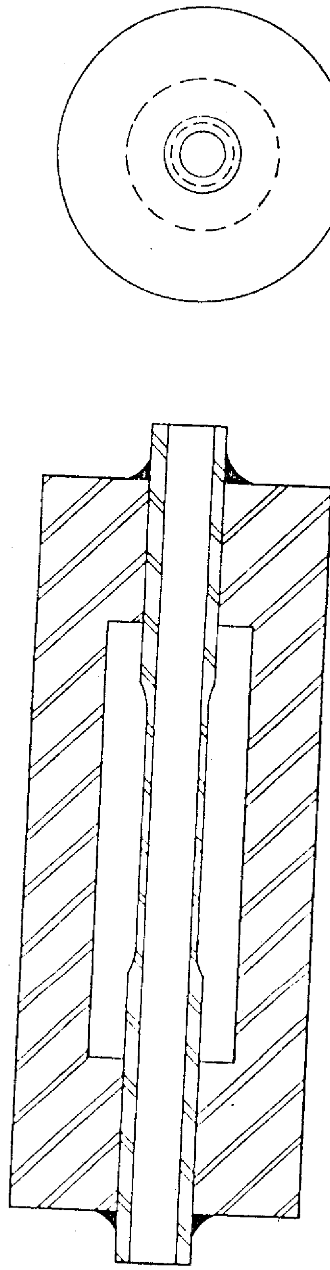

Figure 2 —Jig for stress-corrosion test.

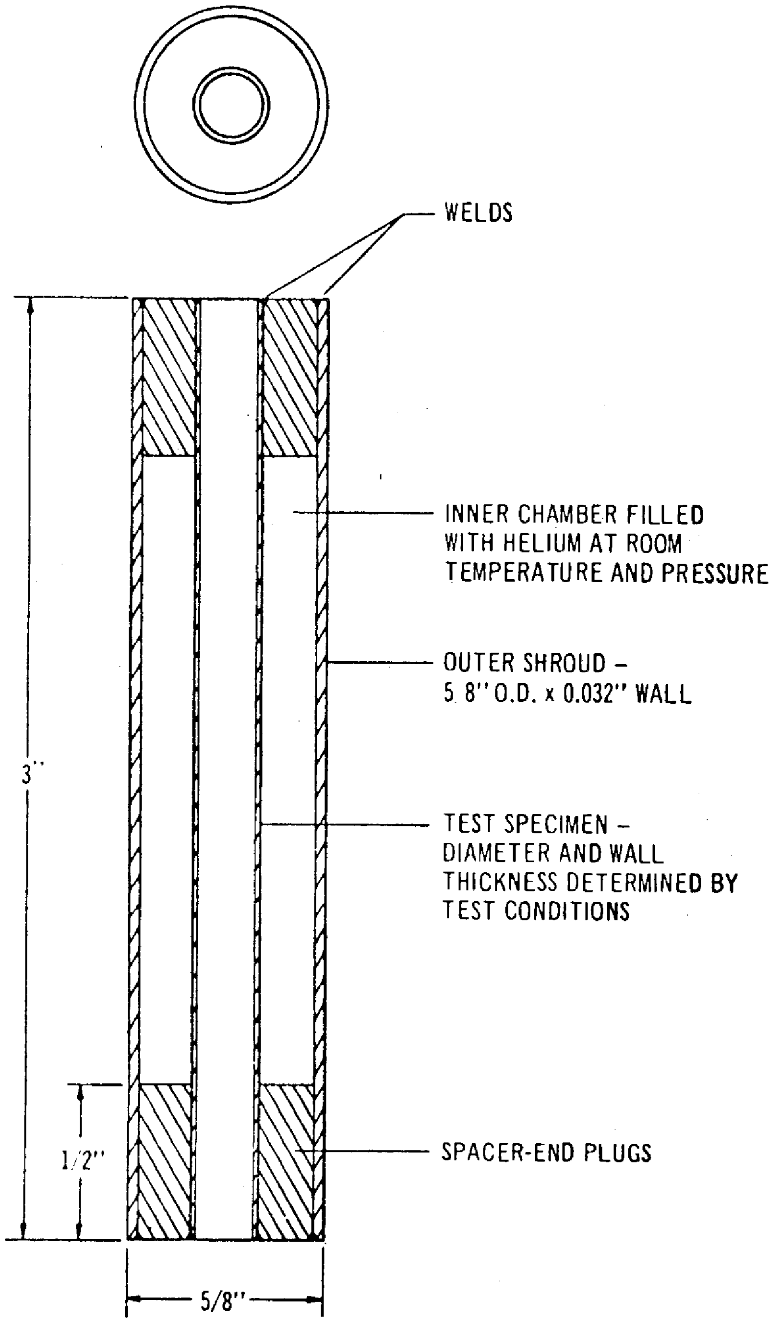

Figure 3. Constantly Stressed Coupon

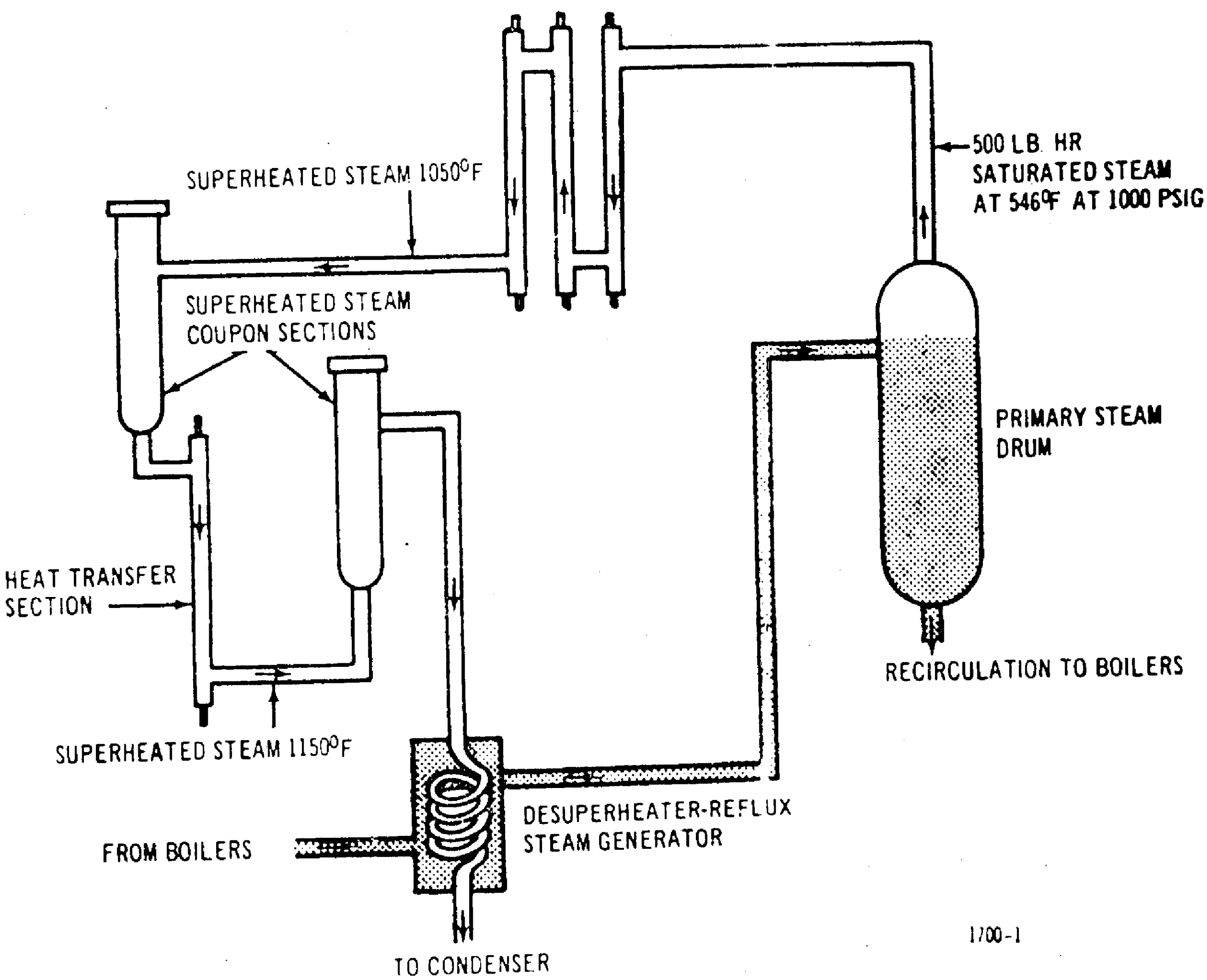

Figure 4 Superheat Corrosion Facility

CHARGE

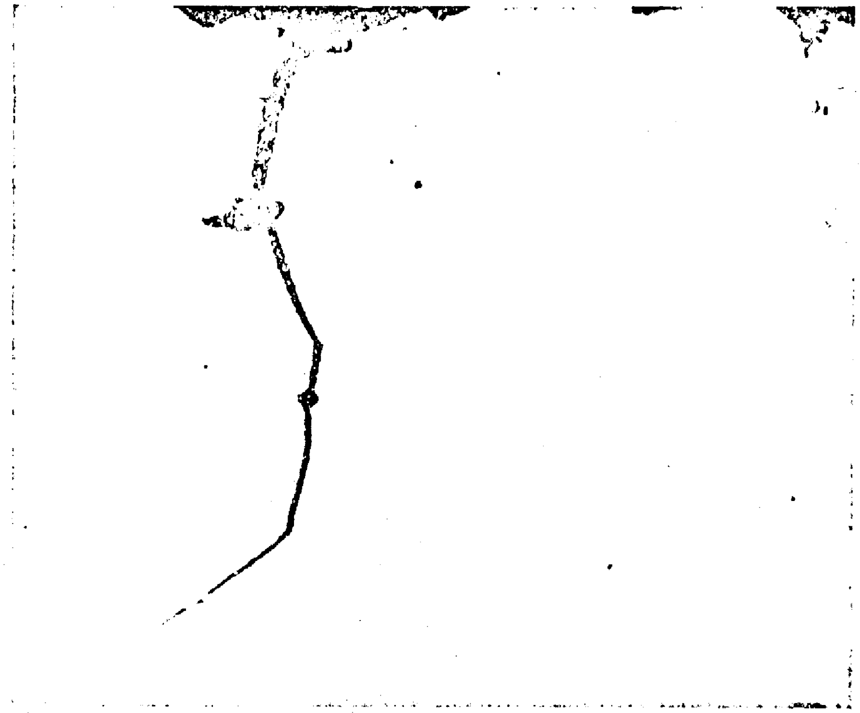

750X

Hastelloy-N Exposed For 1000 Hours In Steam At 1050 F

500X

Figure 5 Hastelloy-N Exposed For 266 Hours In ACS At 1160 F

CORROSION OF IRON-AND NICKEL-BASE ALLOYS EXPOSED 100 DAYS IN OXYGENATED STEAM (3 to 4 ppm O_2) of 550 C (1022 F) AND 3000 psi PRESSURE. Samples Cathodically Descaled in Molten Electrolyte of 60 w/o NaOH and 40 w/o Na_2CO_3 at 560 C (1040 F)

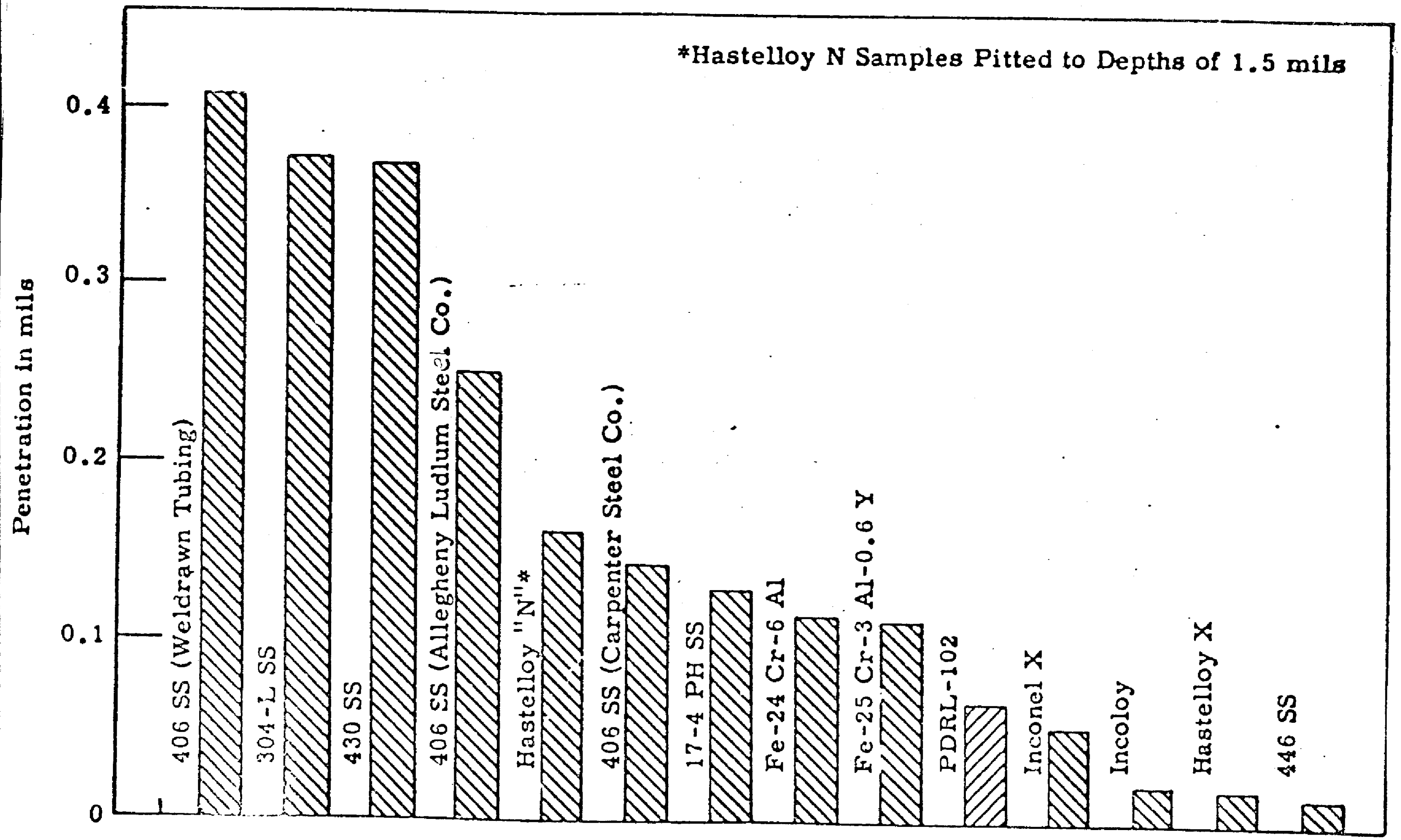

FIGURE 6

APPROVED

BY

CI

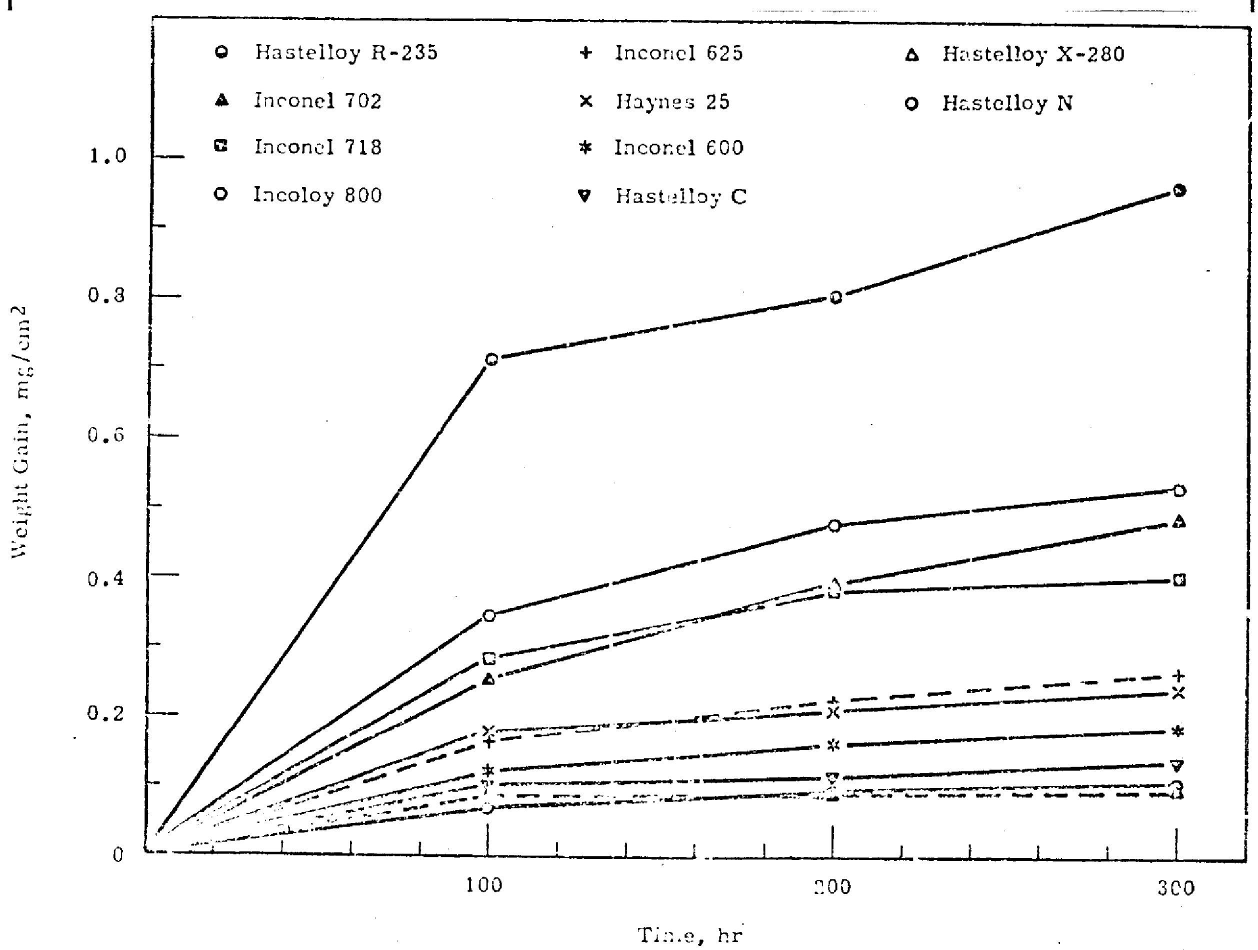

FIGURE 7

Oxidation of High Temperature Alloys Exposed to 15 Torr Water Vapor in Helium Flowing at 1 ft^3/min at 815 °C

CHARGE NO. 8-25-2431	DOCUMENT NO. ND/74/66	ISSUE 1	DATE 12/16/74

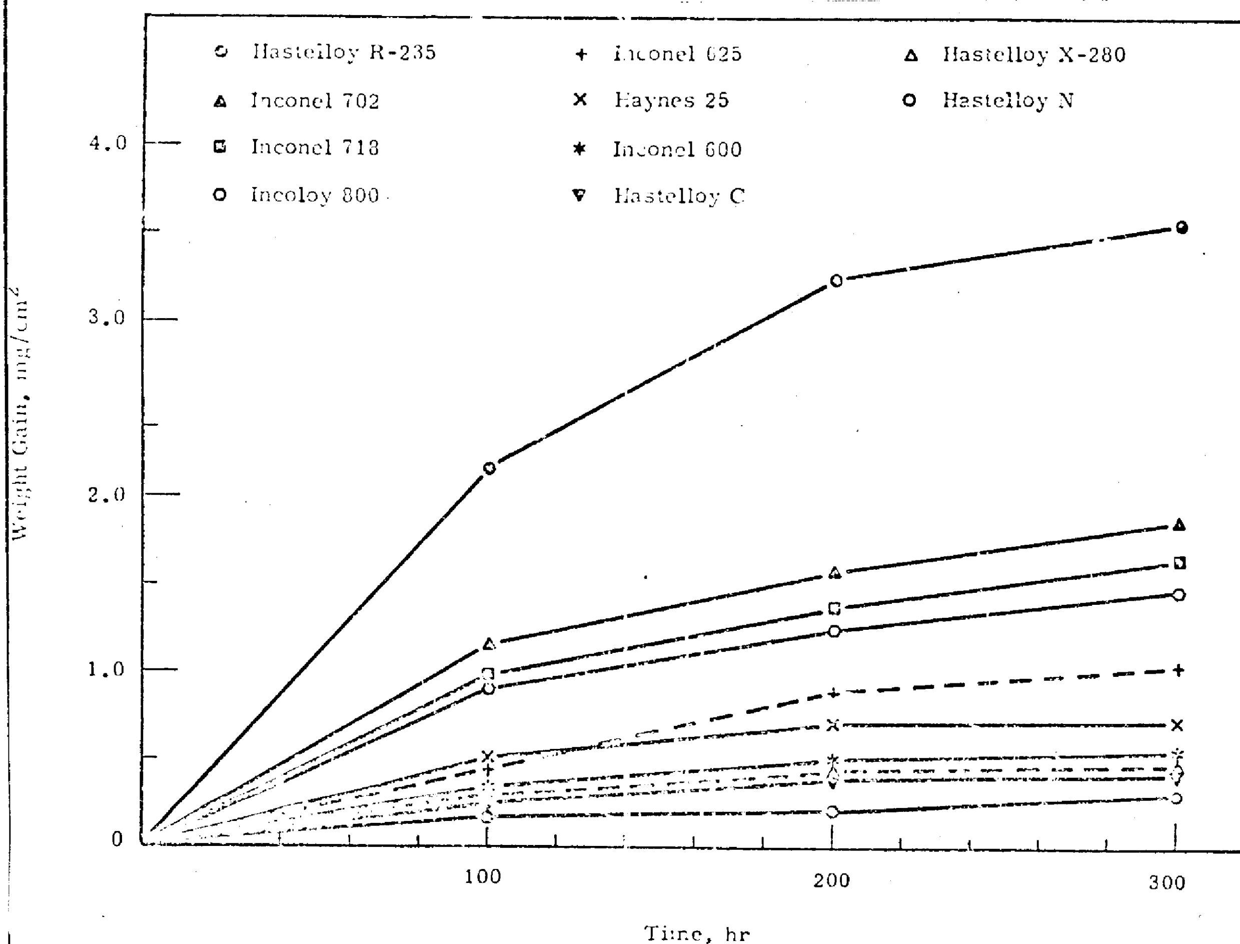

FIGURE 8

Oxidation of High Temperature Alloys Exposed to 15 Torr Water Vapor in Helium Flowing at 1 ft^3/min at 930 °C

FWC FORM 172 - 4

NOTATIONS IN THIS COLUMN INDICATE WHERE CHANGES HAVE BEEN MADE

BY

APPROVED

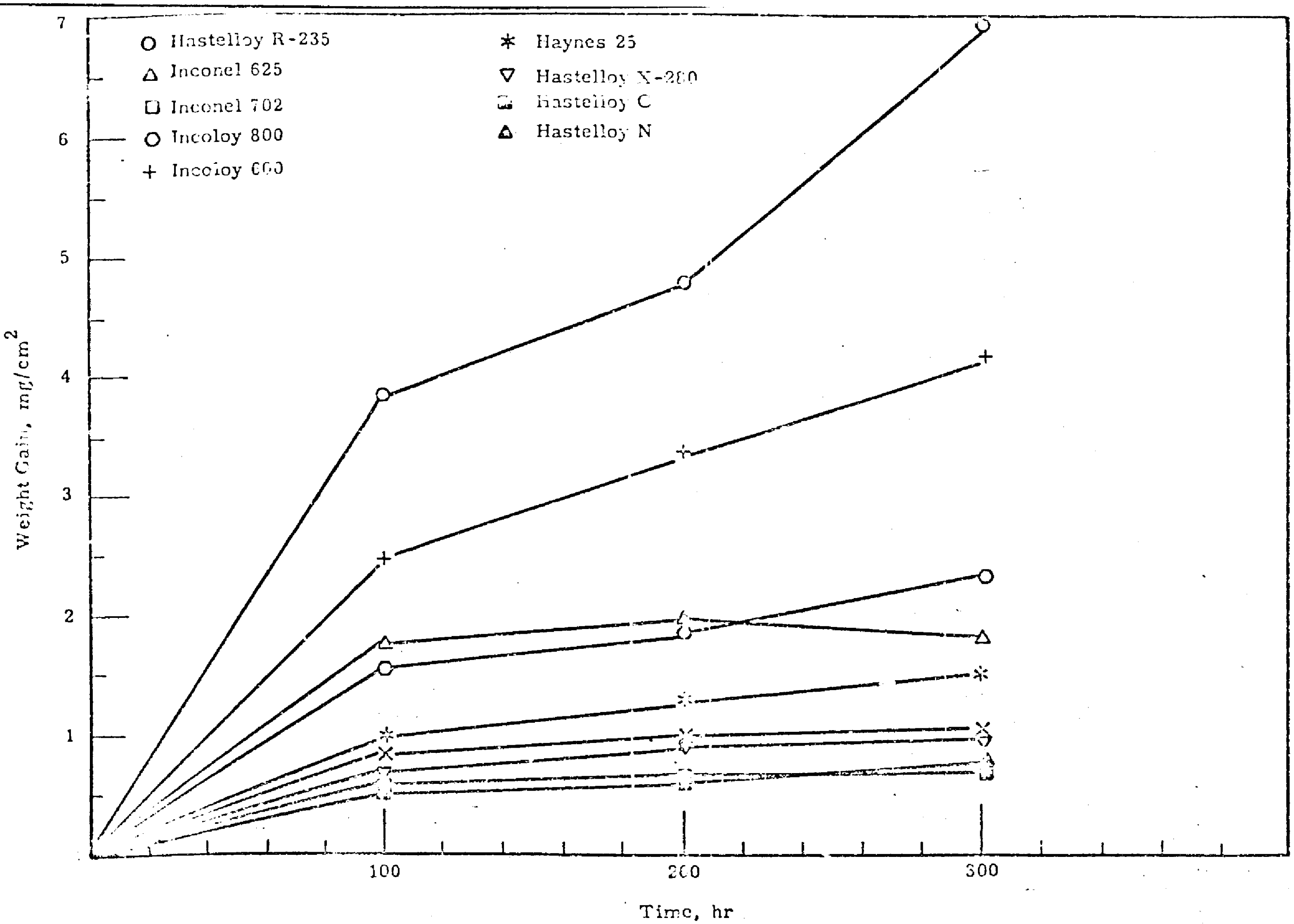

FIGURE 9

Oxidation of High Temperature Alloys Exposed to 15 Torr Water Vapor in Helium Flowing at 1 ft^3/min at 1038 °C

NUCLEAR DEPARTMENT
FOSTER WHEELER ENERGY CORPORATION
LIVINGSTON, N. J.

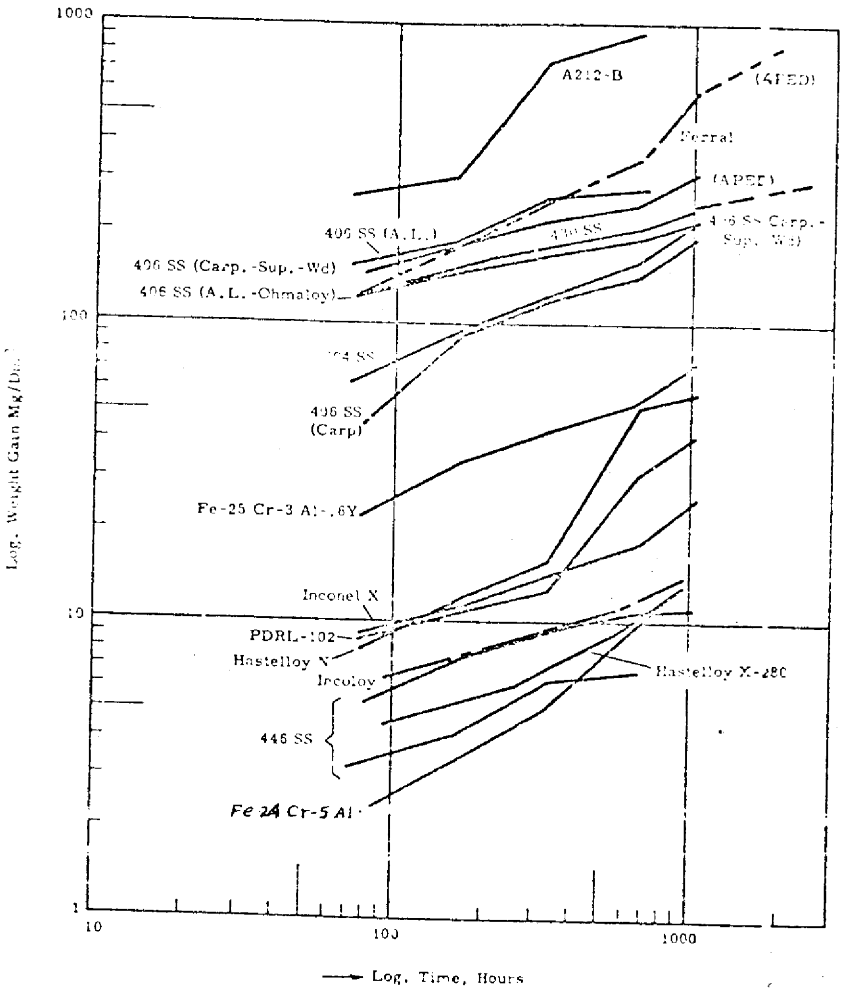

FIGURE 10A

Weight Gain of Iron- and Nickel-Base Alloys in Superheated Steam of 550 °C and (1000), 3000 psi Pressure (mg/dm^2)

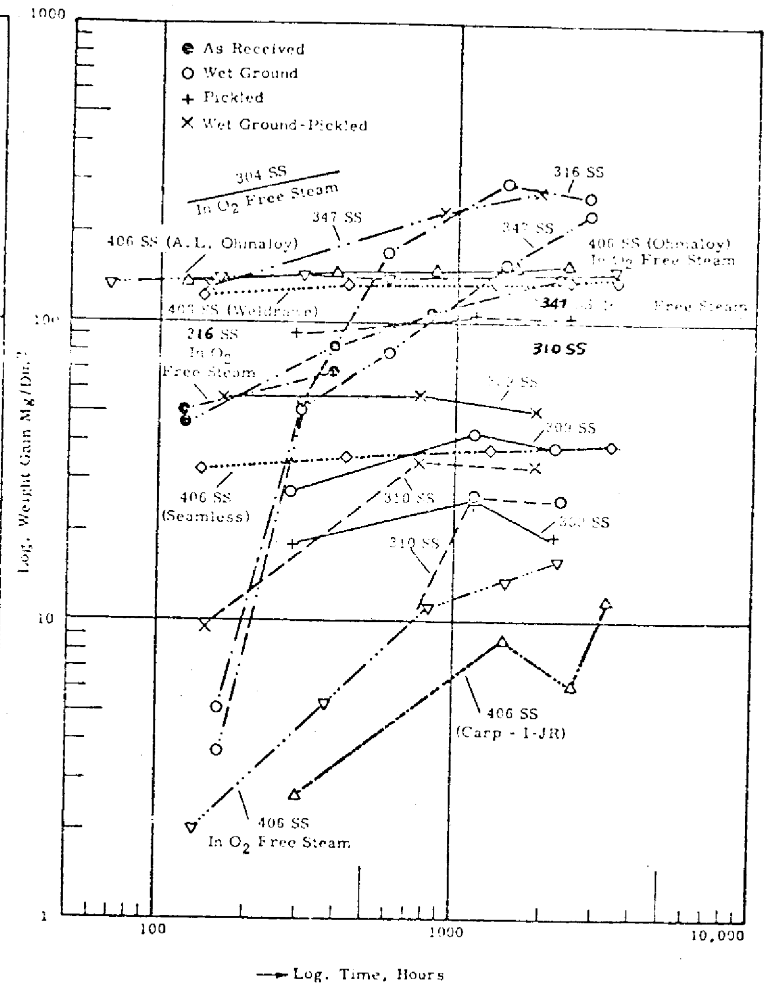

FIGURE 10 B

Weight Gain of Iron- and Nickel-Base Alloys in Oxygenated, and Oxygen Free, Superheated Stearr of 650 °C and 600 psi Pressure (mg/dm^2)

CHARGE NO. 8-25-2431
DOCUMENT NO. ND/74/66
ISSUE 1
DATE 12/16/74

NUCLEAR DEPARTMENT
FOSTER WHEELER ENERGY CORPORATION
LIVINGSTON, N. J.

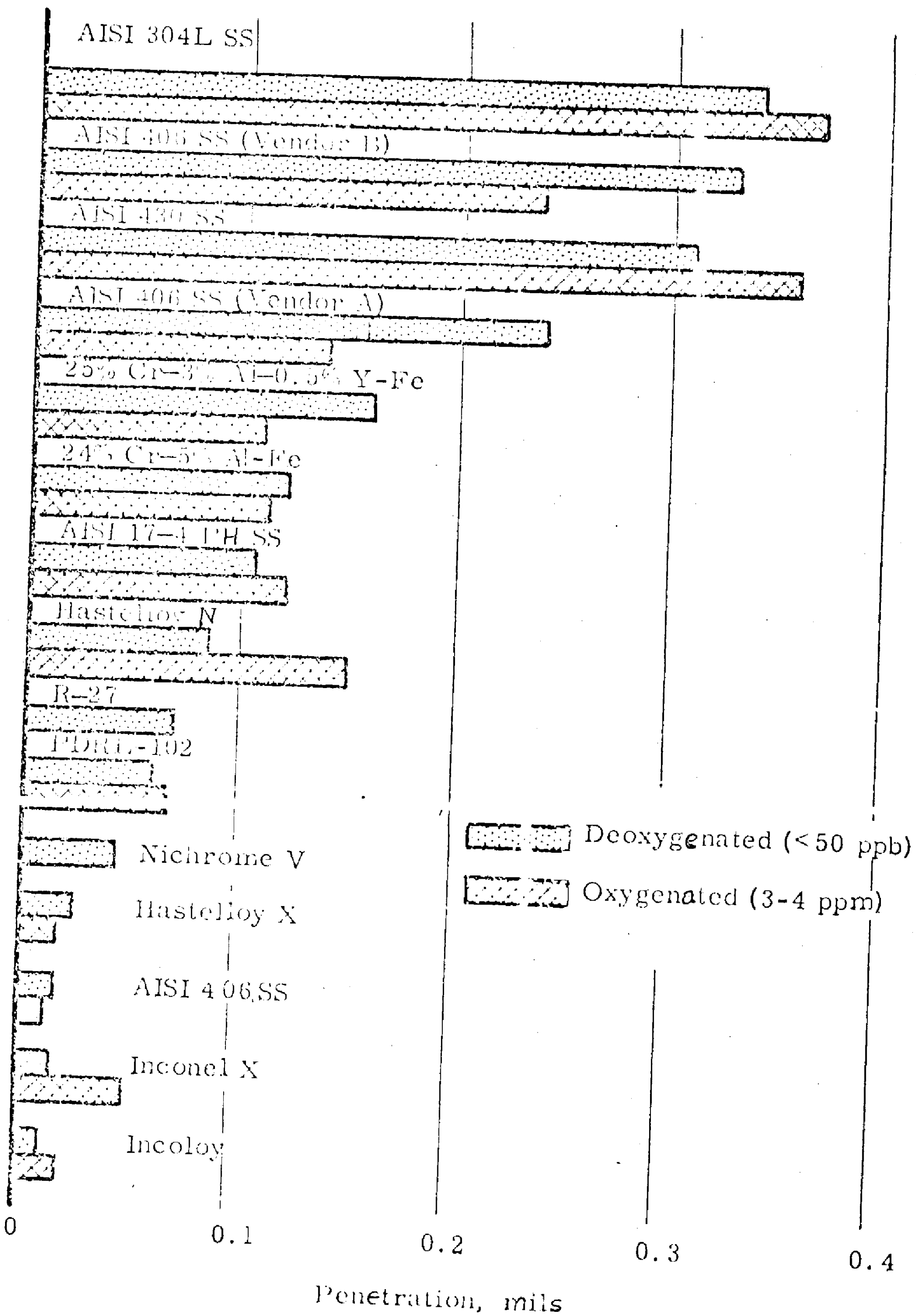

FIGURE 11

Corrosion of Various Alloys
Following 100 Days in 550 °C - 3000 psi Steam

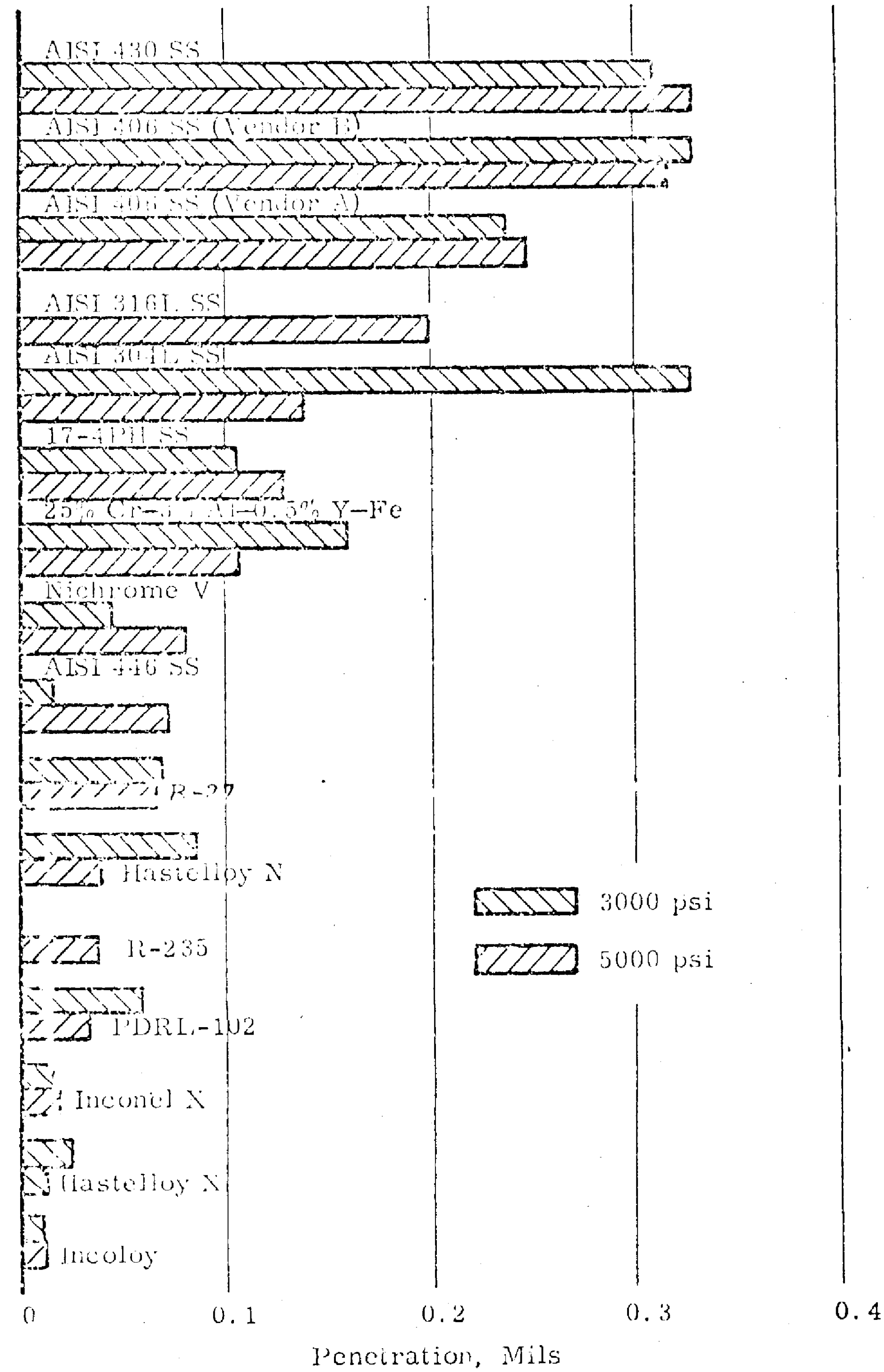

FIGURE 12

Descaled Corrosion Penetrations of Various Alloys
Following 100 Days in 3000 psi and 5000 psi 500 °C Deoxygenated Steam

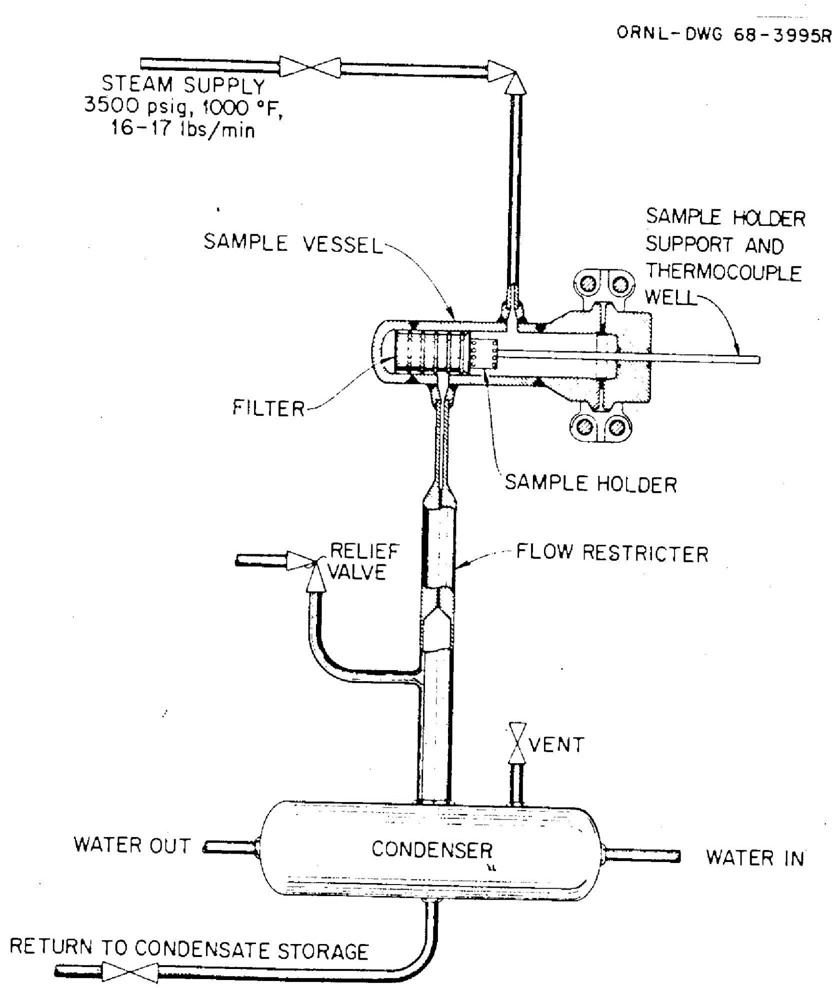

Fig. 13 Steam Corrosion Facility at Bull Run Steam Plant.

to steam. These cannot be viewed as control tests, but comparisons of the behavior in air and steam are useful in some instances.

CHARGE NO. 8-25-2431	DOCUMENT NO. ND/74/66	ISSUE 1	DATE 12/16/74

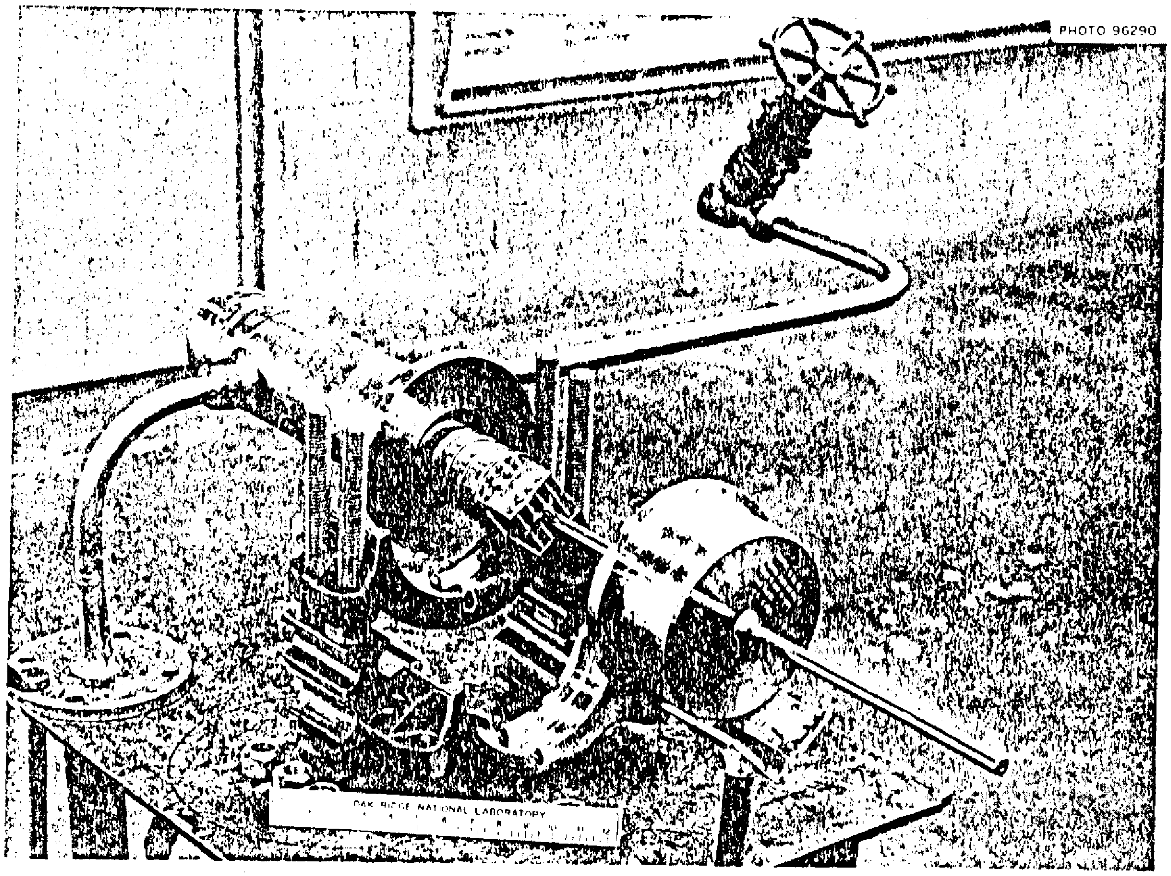

Fig. 14 Photograph of the Steam Corrosion Facility Before Installation. The valve ties into the steam supply. The flange has been unbolted to allow removal of the sample holder and the filter.

FWC FORM 172 - 4

NOTATIONS IN THIS COLUMN INDICATE WHERE CHANGES HAVE BEEN MADE

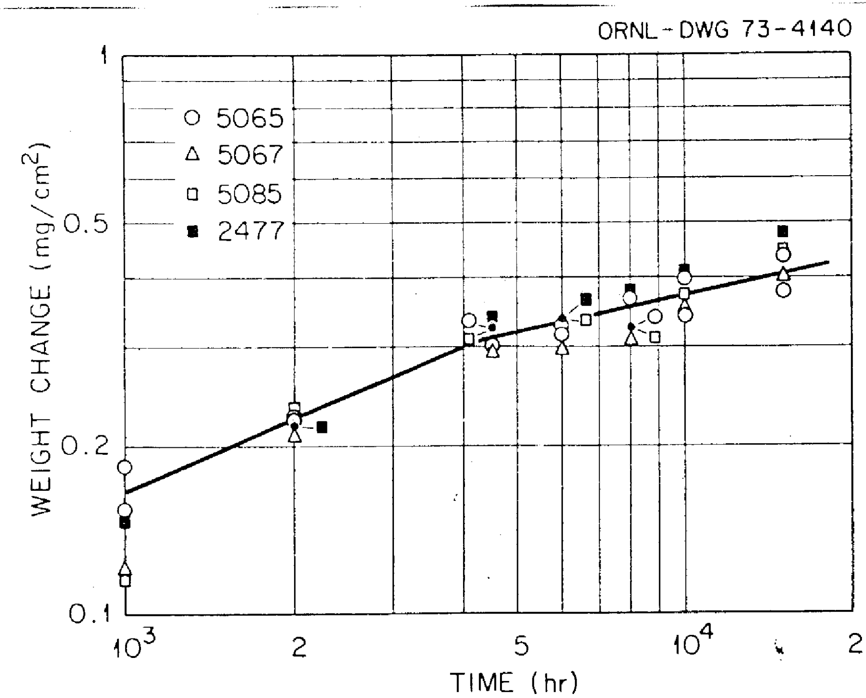

Fig. 15A Weight Changes of Several Heats of Hastelloy N Exposed to Supercritical Steam at 1000°F and 3500 psi.

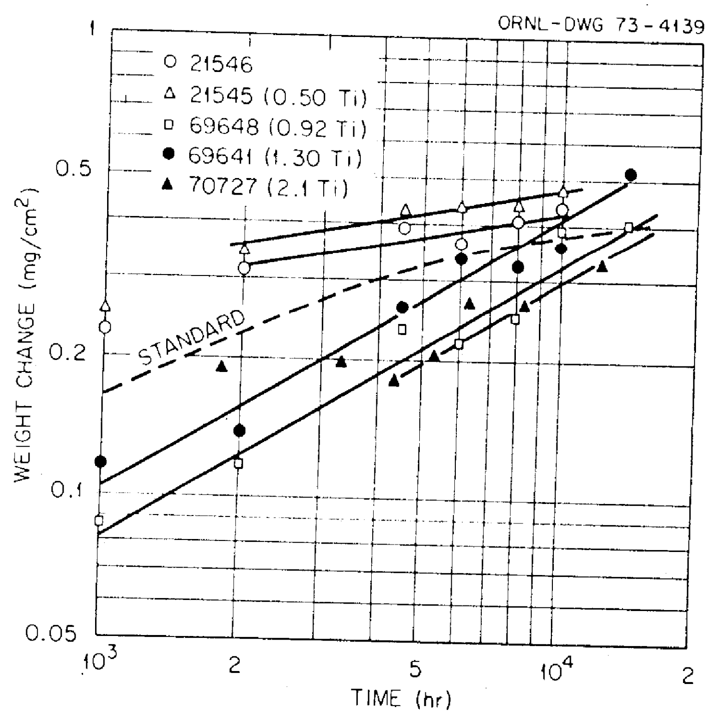

Fig. 15B Weight Changes of Several Alloys of Hastelloy N Modified with Titanium and Exposed to Supercritical Steam at 1000°F and 3500 psi

CHARGE NO. 8-25-2431	DOCUMENT NO. ND/74/66	ISSUE 1	DATE 12/16/74

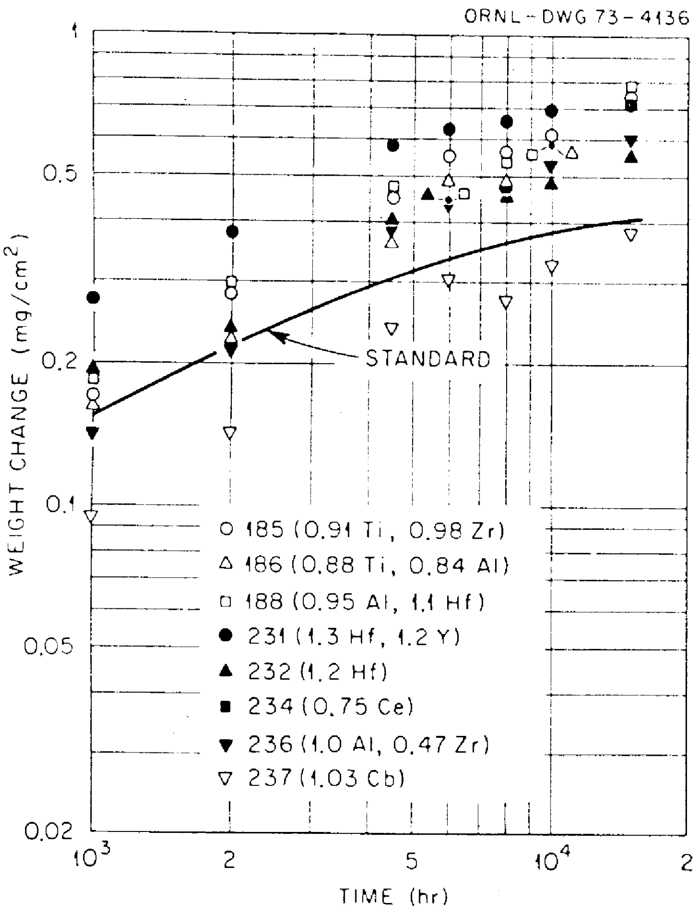

Fig. 16A Corrosion of Various Modified Compositions of Hastelloy N in Steam at 1000°F and 3500 psi.

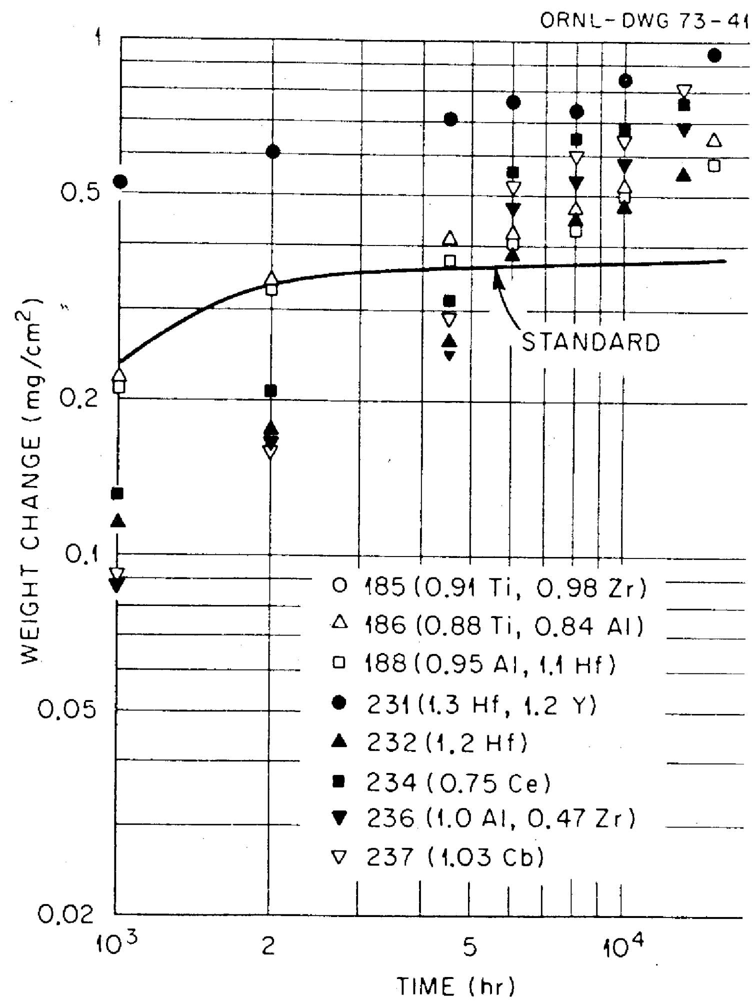

Fig. 16B Corrosion of Various Modified Compositions of Hastelloy N in Air at 1000°F.

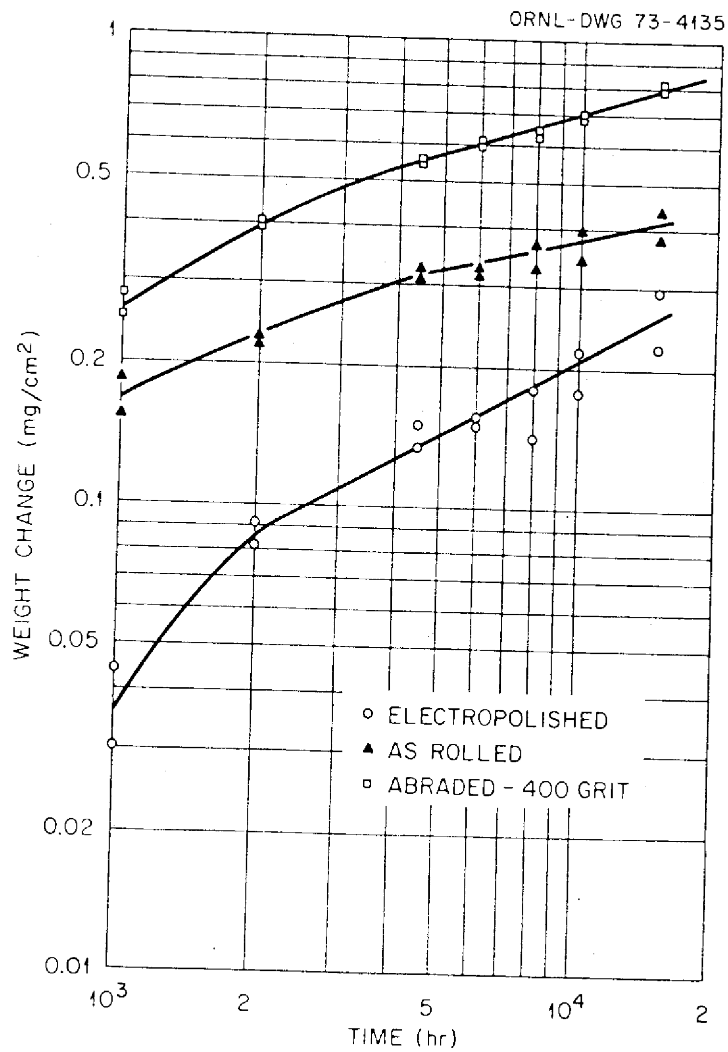

Fig. 17 Effect of Surface Finish on the Corrosion of Hastelloy N (Heat 5065) in Steam at 1000°F and 3500 psi.

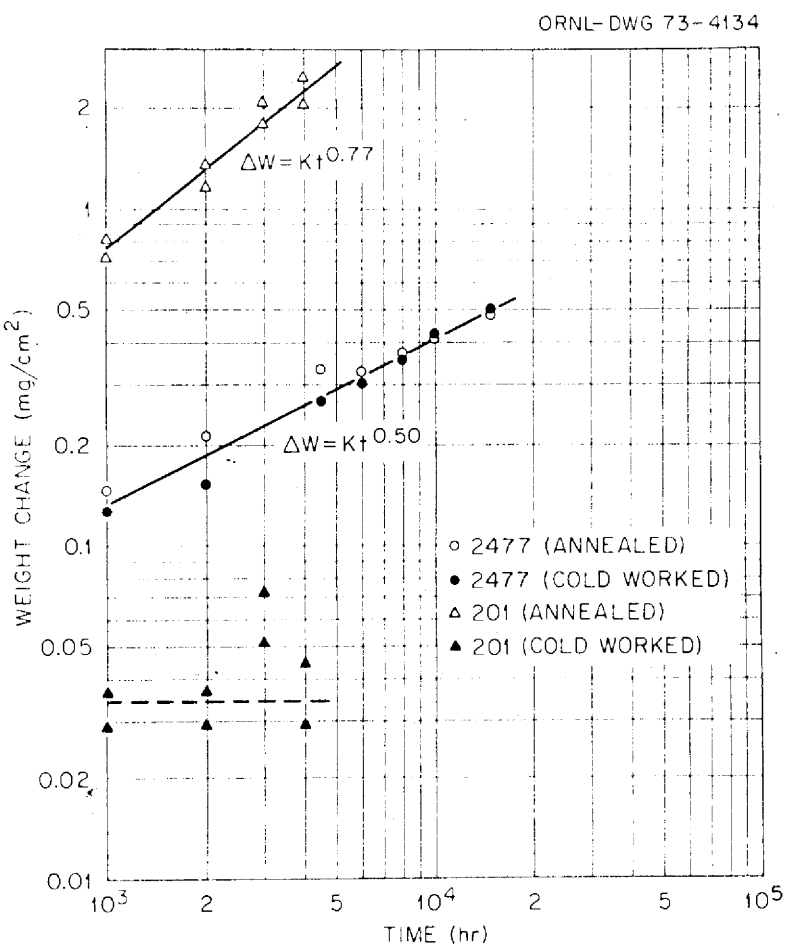

Fig. 18 Effect of Cold Work on the Corrosion of Hastelloy N (Heat 2477) and Type 201 Stainless Steel in Steam at 1000°F and 3500 psi.

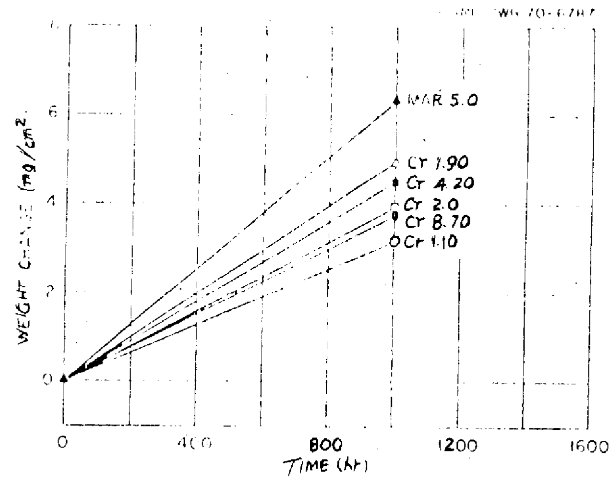

Fig. 19A Oxidation of Chromium Steels in a Steam Environment at 538°C and 3500 psi. The chromium concentration is shown by each symbol

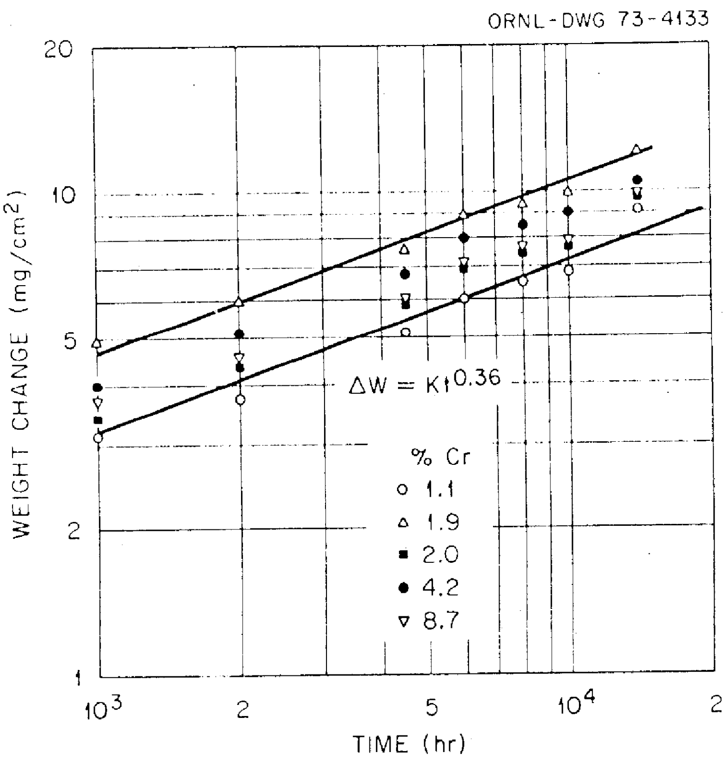

Fig. 19B Weight Changes of Low-Alloy Ferritic Steels in Supercritical Steam at 1000°F and 3500 psi.

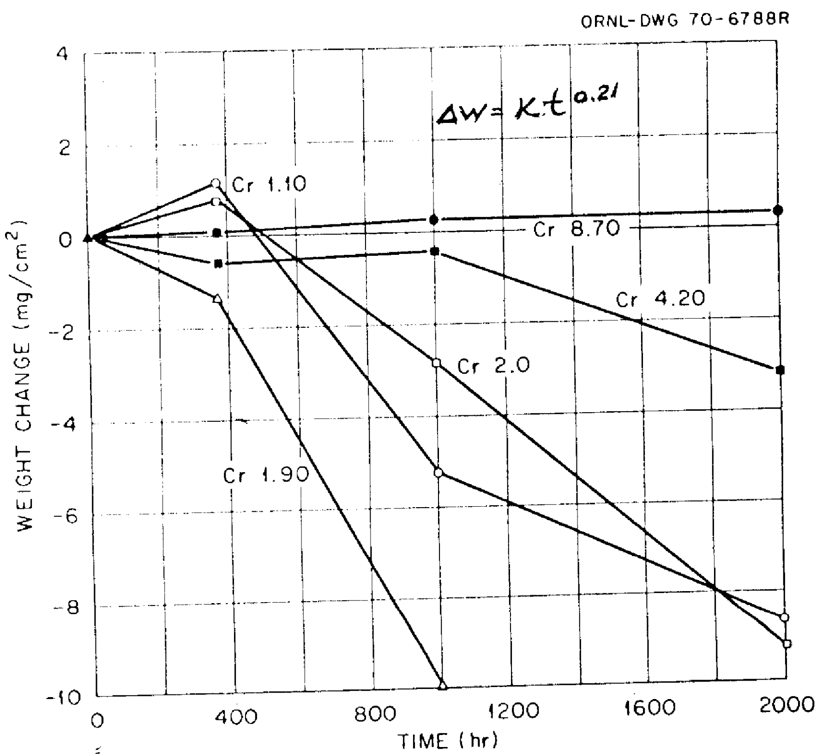

Fig. 20 Oxidation of chromium steels in air at 1000°F. The chromium concentration is shown for each curve.

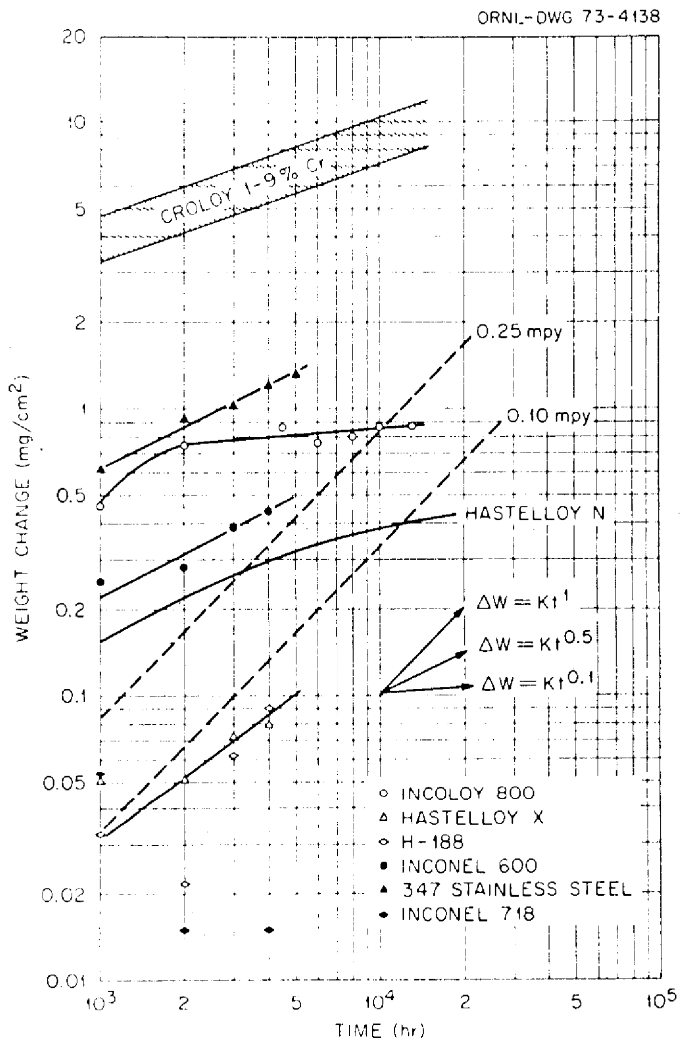

Fig. 21 Corrosion of Several Alloys in Steam at 1000°F and 3500

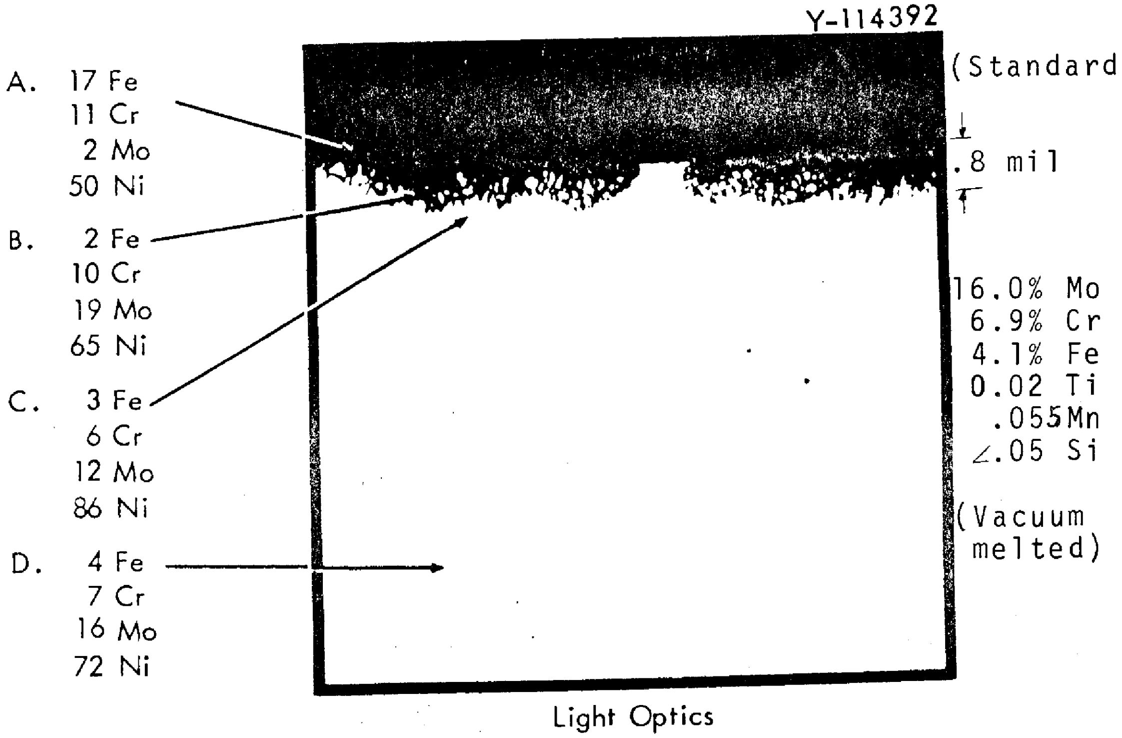

Fig. 23A Photomicrograph of Hastelloy N (Heat 2477) Oxidized in Steam at 1000°F and 3500 psi for 10,000 hr. The results of electron microprobe analysis are shown at the left. 500×.

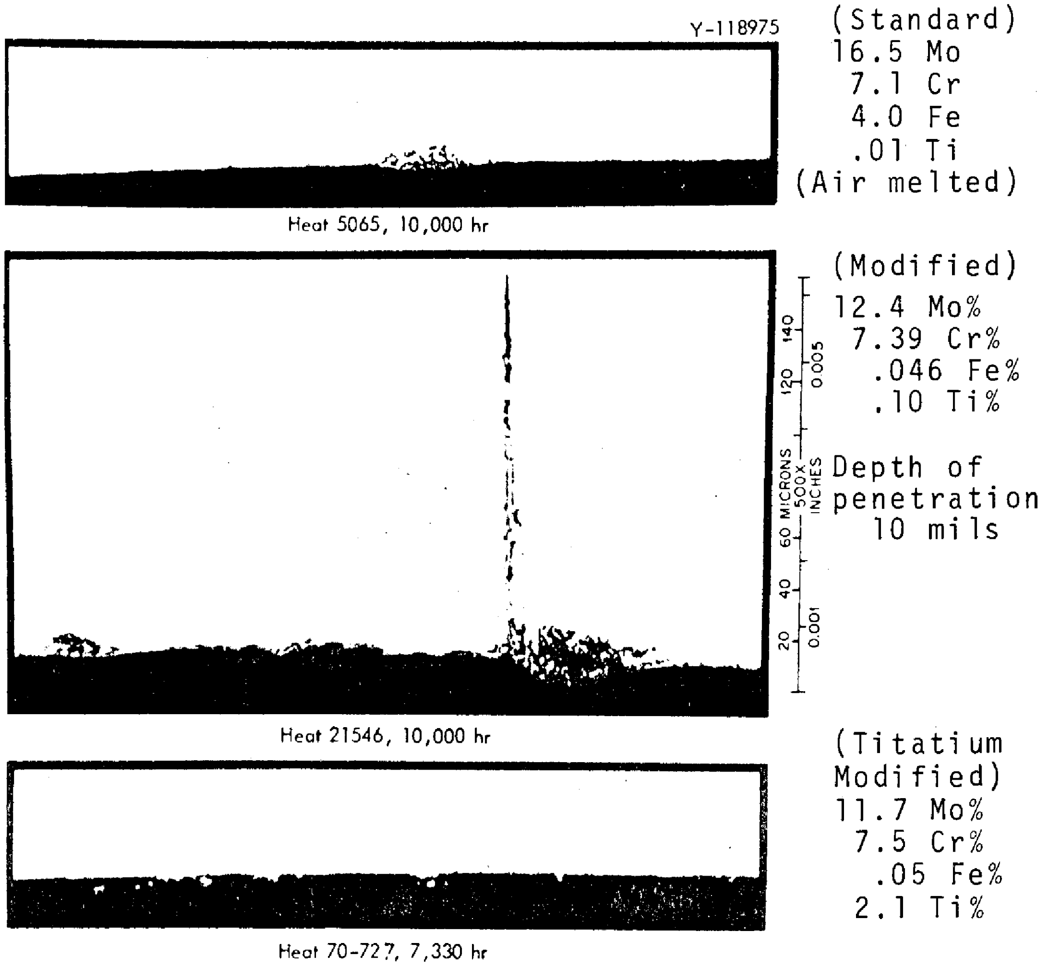

Fig. 23B Photomicrograph of Three Hastelloy N Specimens Following Exposure to Steam at 1000°F and 3500 psi.

Compositions of several heats of standard and modified Hastelloy N

Alloy No.	Mo	Cr	Fe	Mn	C	Si	Cu	Co	V	W	Al	Ti	B	Cb	Hf	Zr	Mg
	Concentration (%)																
5065	16.0	7.1	4.0	0.55	0.06	0.57	0.01	0.07	0.23	0.1	<0.03	<0.01	0.001	<0.05	<0.1	<0.1	0.02
2477	16.0	6.9	4.1	0.055	0.057	0.047	0.01	0.05	<0.01	0.03	0.03	0.02	0.0002	<0.0005	<0.001	<0.001	<0.005
21546	12.3	7.3	0.046	0.16	0.05	0.009	0.01	<0.10	<0.10	<0.10	0.02	0.10	0.0002			0.005	
70727	13.0	7.4	0.05	0.37	0.044	<0.05	<0.01	<0.01	<0.01	<0.01	<0.03	2.1	0.00006	<0.01	<0.01	<0.001	0.015

BY	APPROVED	

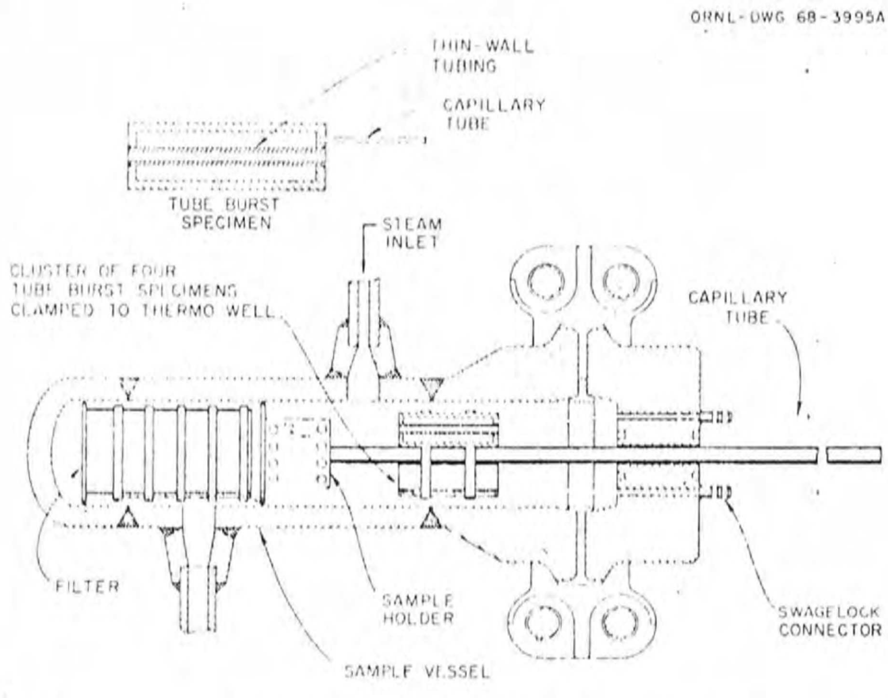

Fig. 24 Schematic of steam corrosion facility at Bull Run Steam Plant showing modifications for dynamically stressed tubes.

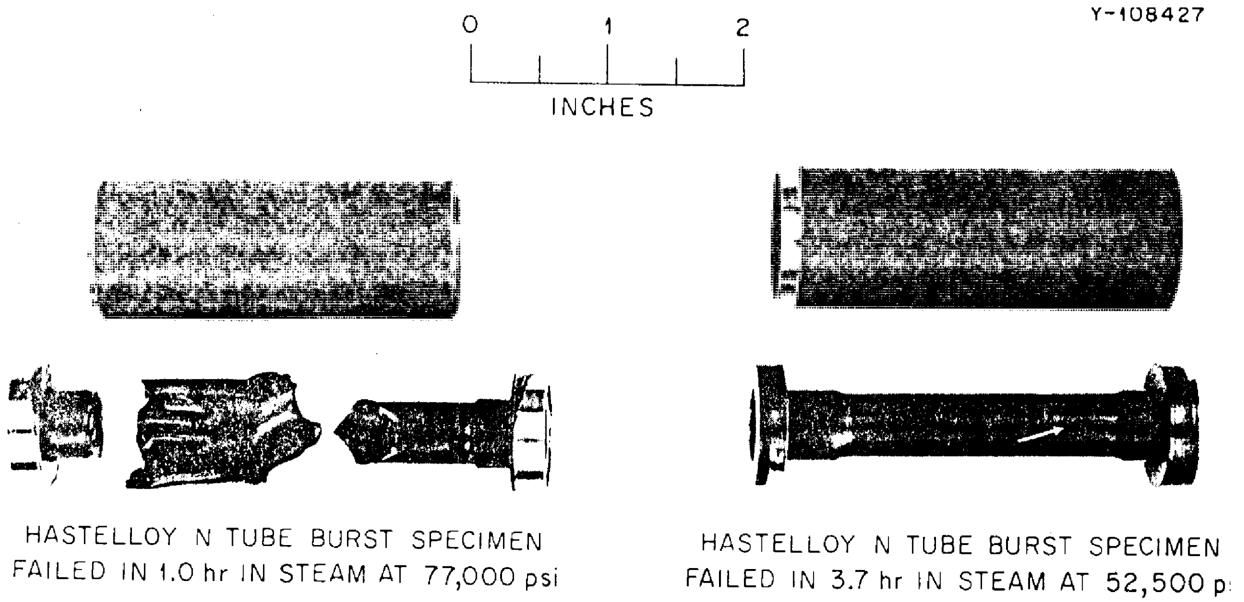

Fig. 25A Hastelloy N tube burst specimens removed from the Bull Run Steam Plant after failure. The small tube in the te section was exposed to steam at 538°C and 3500 psi.

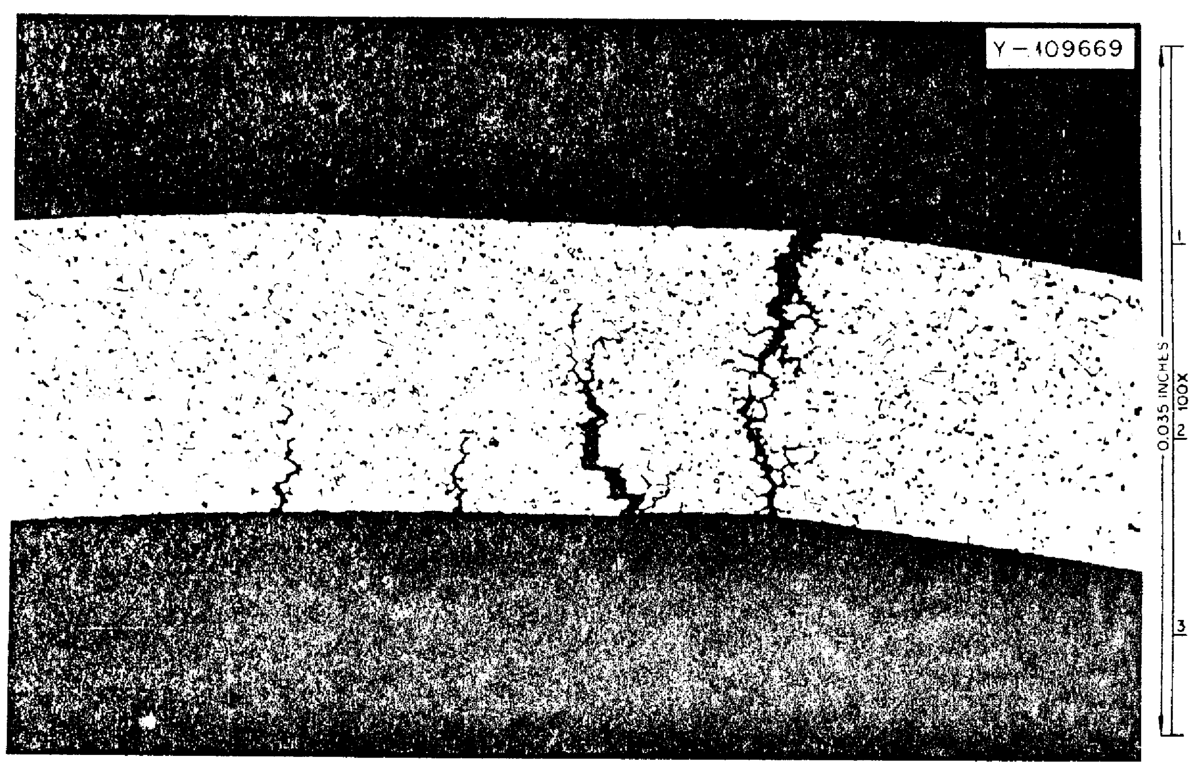

Fig. 25B. Photomicrograph of Hastelloy N tube burst specimen. Failure occurred after exposure to steam for 3.7 hr at 52,500 psi at 538°C. Steam was on the inside of the tube.

Y-111910

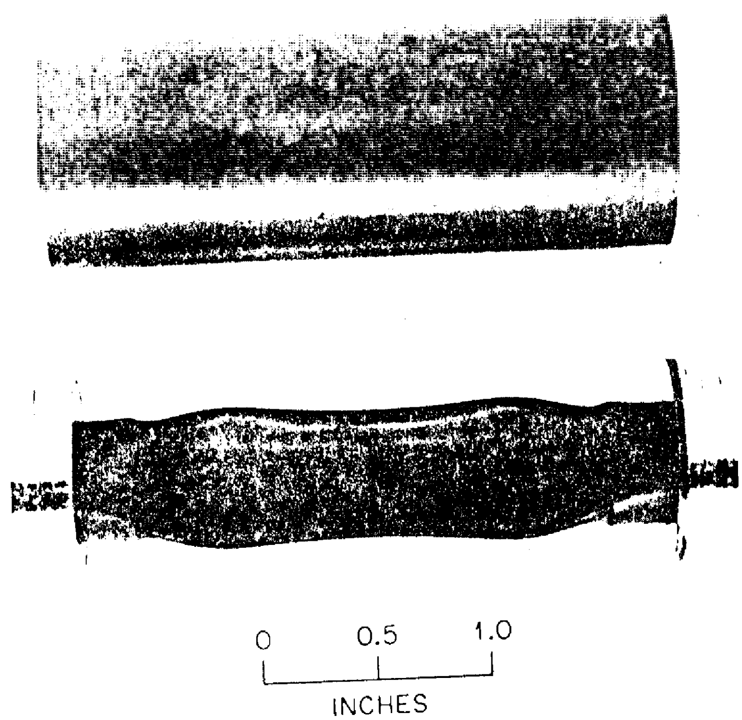

Fig. 26 Photograph of tube-burst sample that was stressed at 58,000 psi in steam at 538°C and failed in <1000 hr. The smaller tube was initially pressurized, failed, and pressurized the annular region, and the smaller tube was collapsed when the plant steam pressure decreased rapidly.

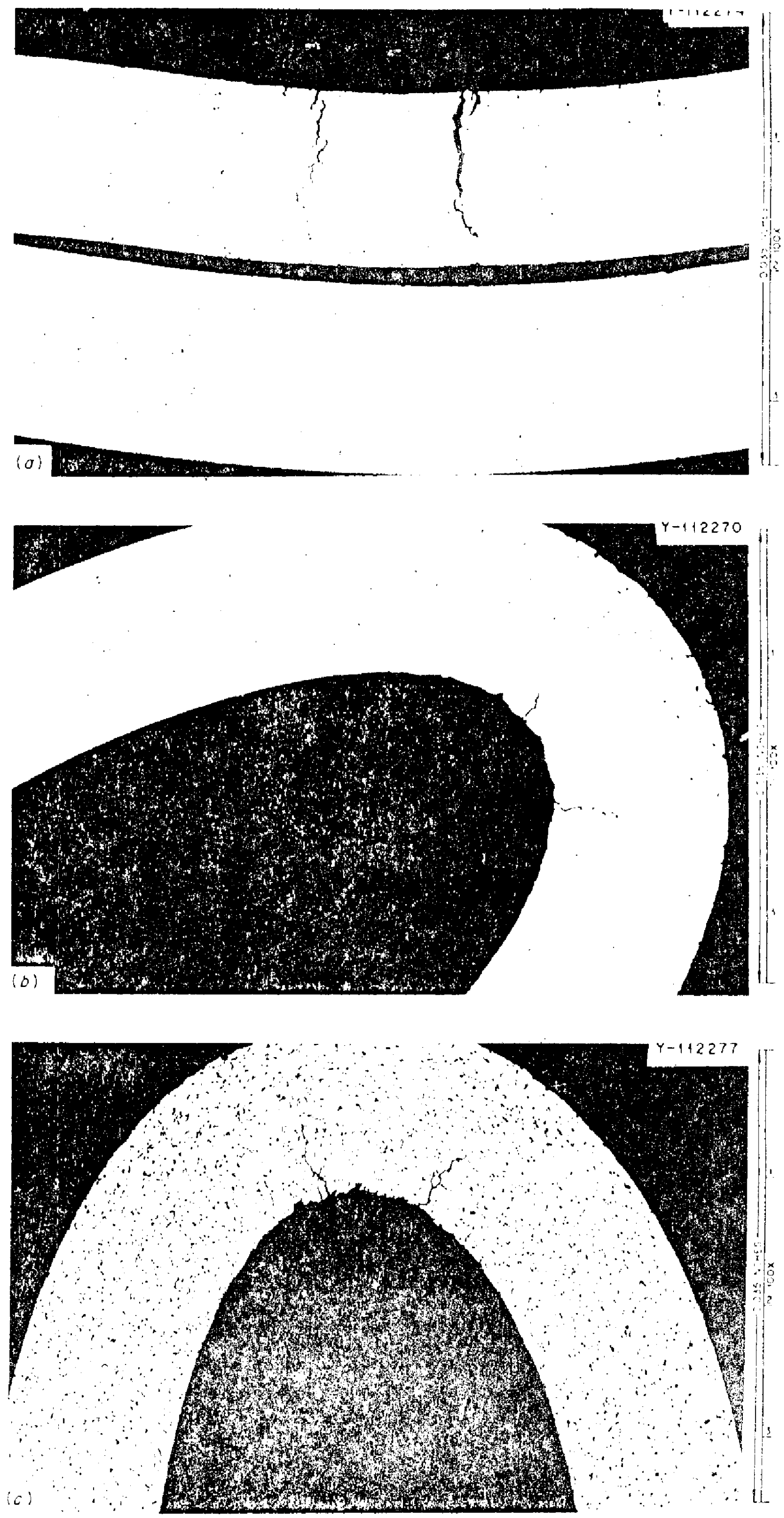

Fig. 27 . Photomicrographs of the inner tube shown in Fig. 14.30. Intergranular fractures occurred on both sides of the tube because of the unusual loading sequence. (*a*) Cracks from the OD, (*b*) cracks from the ID, (*c*) cracks from the ID. Etched with glyceria regia. Reduced 33%.

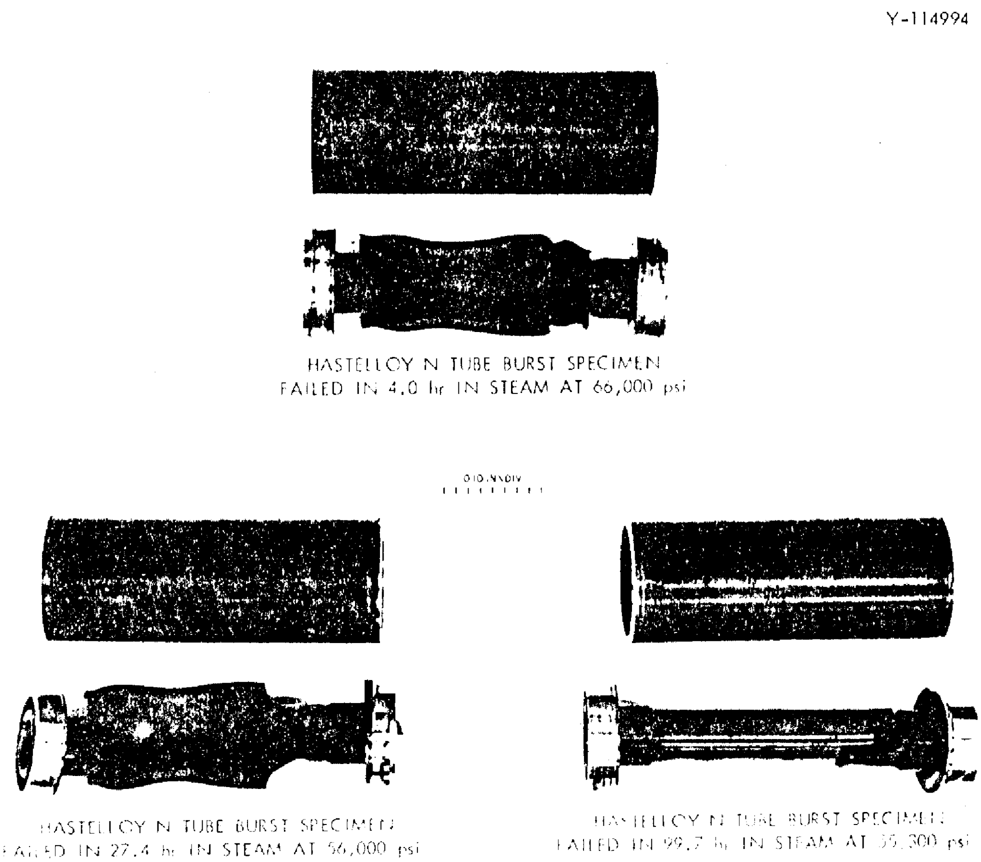

Fig. 28 Photograph of Hastelloy N tube-burst specimens stressed in steam at 538°C. The inner annulus of the concentric tube assembly is exposed to the steam.

FWC FORM 172 - 4

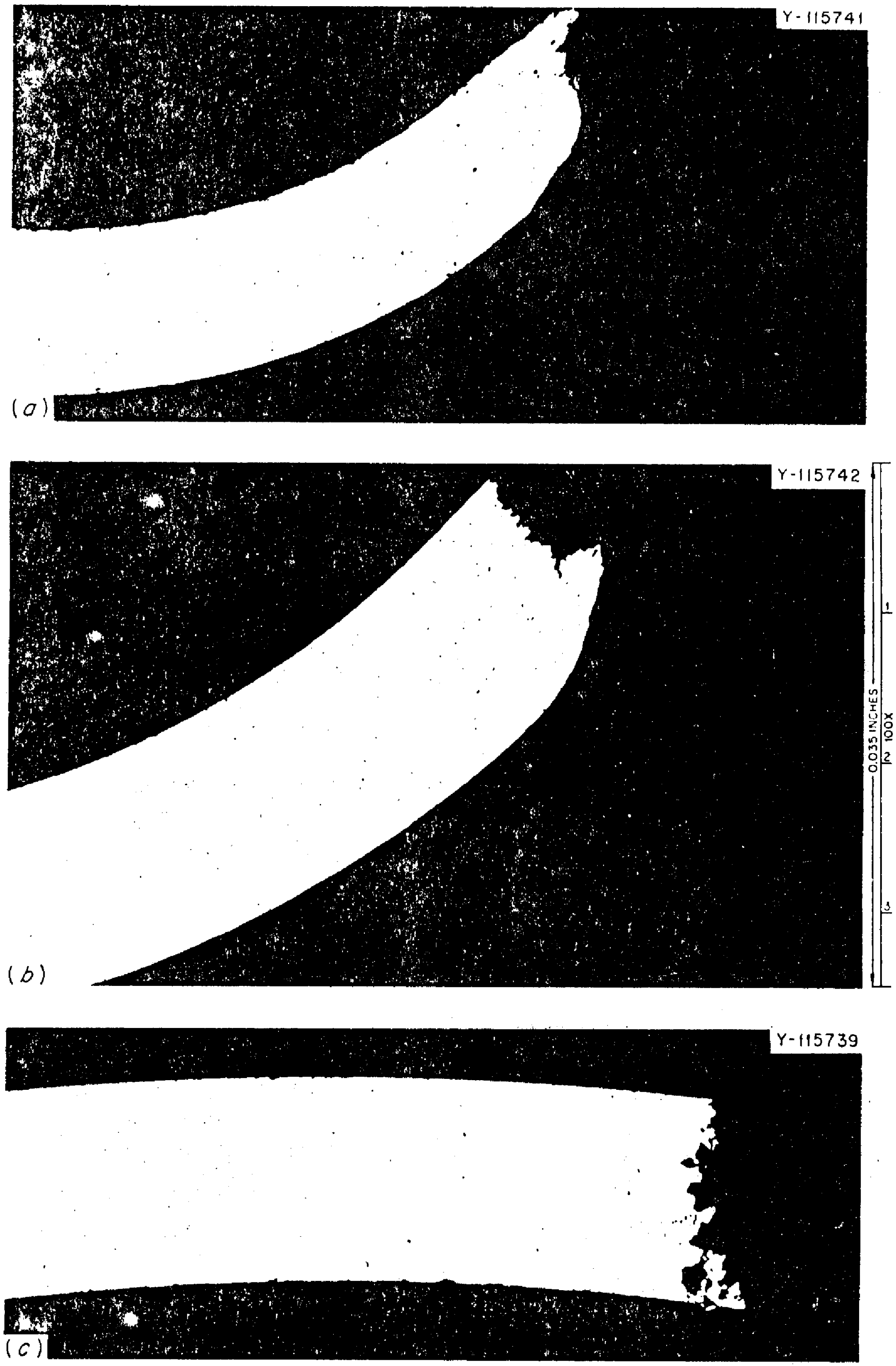

Fig. 29. Photomicrographs of the fractures of Hastelloy N tube-burst samples exposed to steam at 538°C. (*a*) Stressed at 66,000 psi and failed in 4.0 hr, (*b*) stressed at 56,000 psi and failed in 27.4 hr, and (*c*) stressed at 55,300 psi and failed in 99.7 hr. As polished.

FWC FORM 172 - 4
NOTATIONS IN THIS COLUMN INDICATE WHERE CHANGES HAVE BEEN MADE

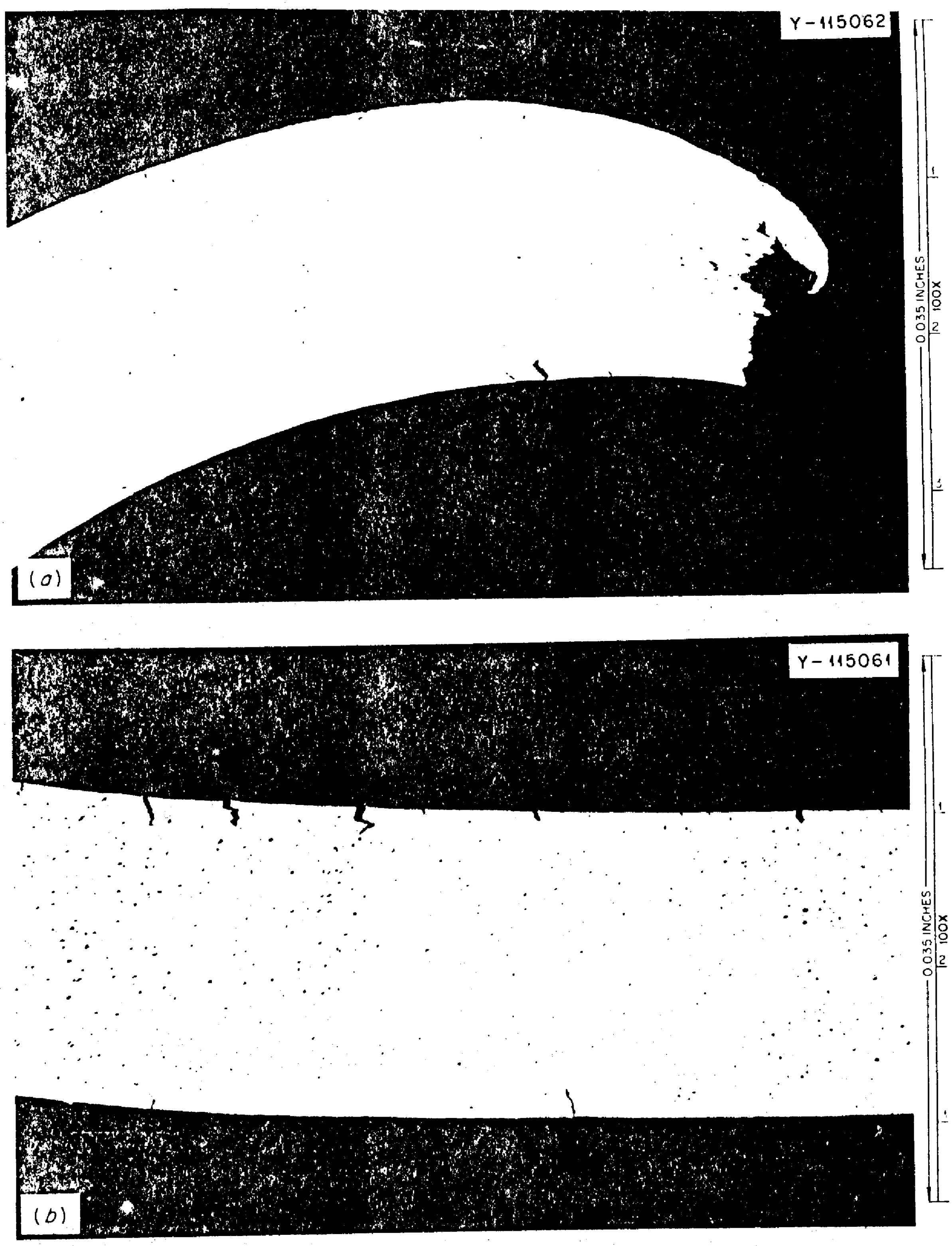

Fig. 30 Photomicrographs of a Hastelloy N sample tested in argon at 538°C and 40,300 psi and failed in 565 hr. (*a*) Fracture (*b*) Region away from fracture showing frequent cracks on the inside diameter of the tube. As polished.

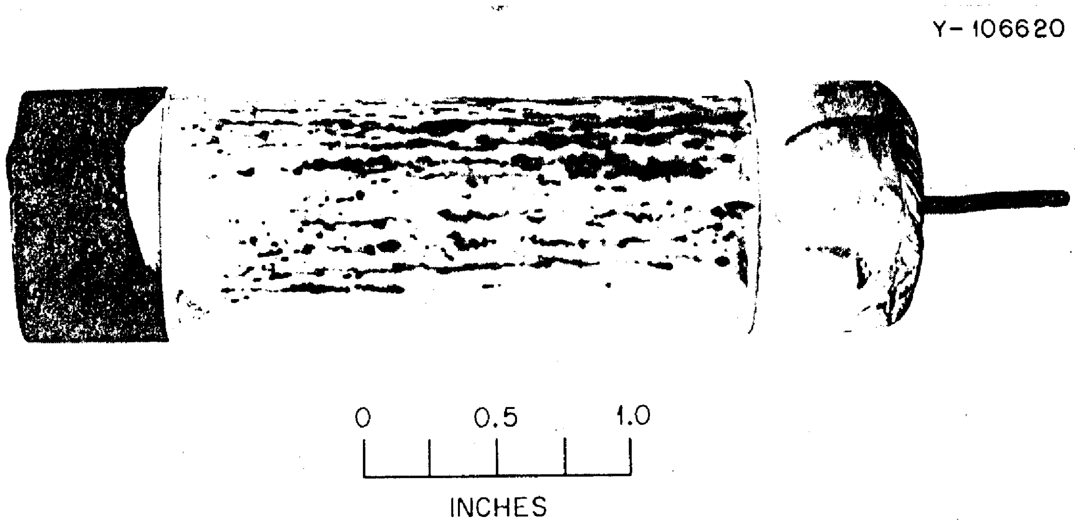

Fig. 3/A. Specimen of duplex Incoloy 800–Ni 280 tubing tested at 538°C and 46,000 psi hoop stress in the Incoloy 800. The specimen failed in 3263 hr with 2.3% diametral strain. The longitudinal markings are due to dye penetrant that was absorbed by the cracks.

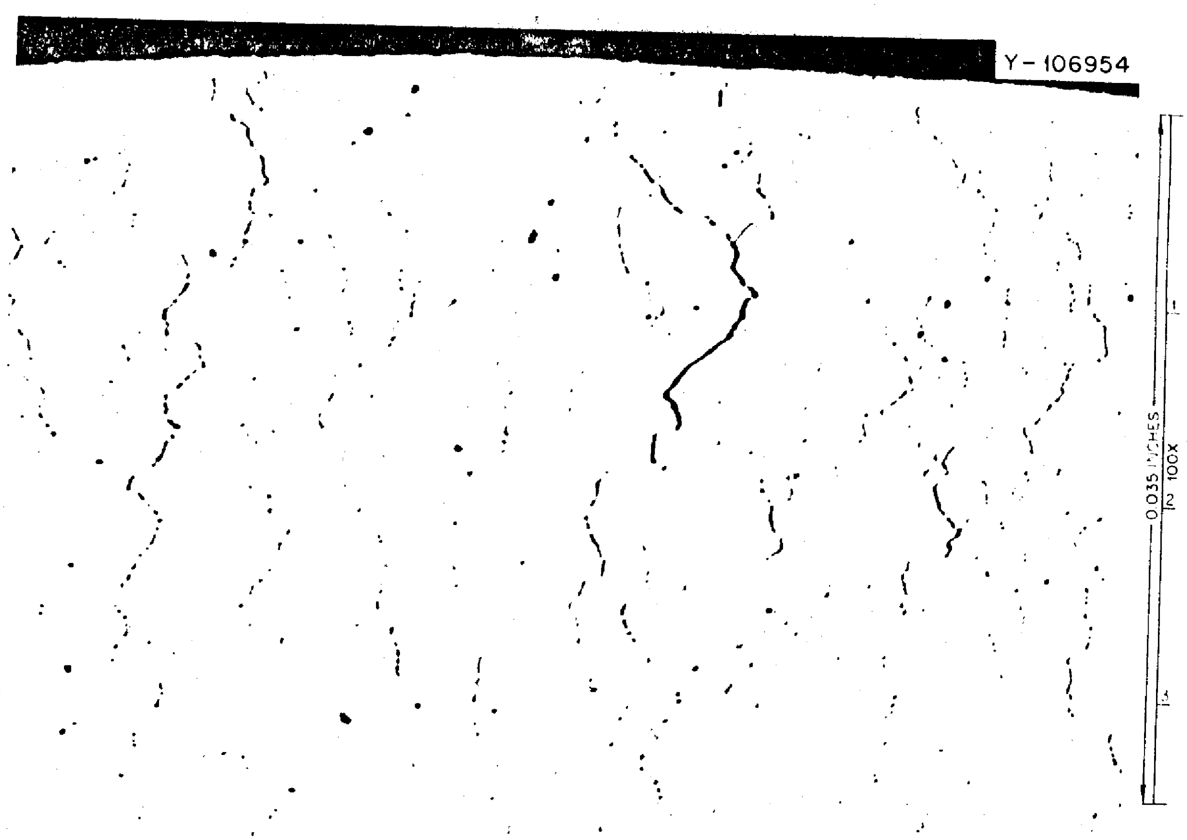

Fig. 3/B. Photomicrograph of the Ni 280 from the specimen in the previous figure. As polished.

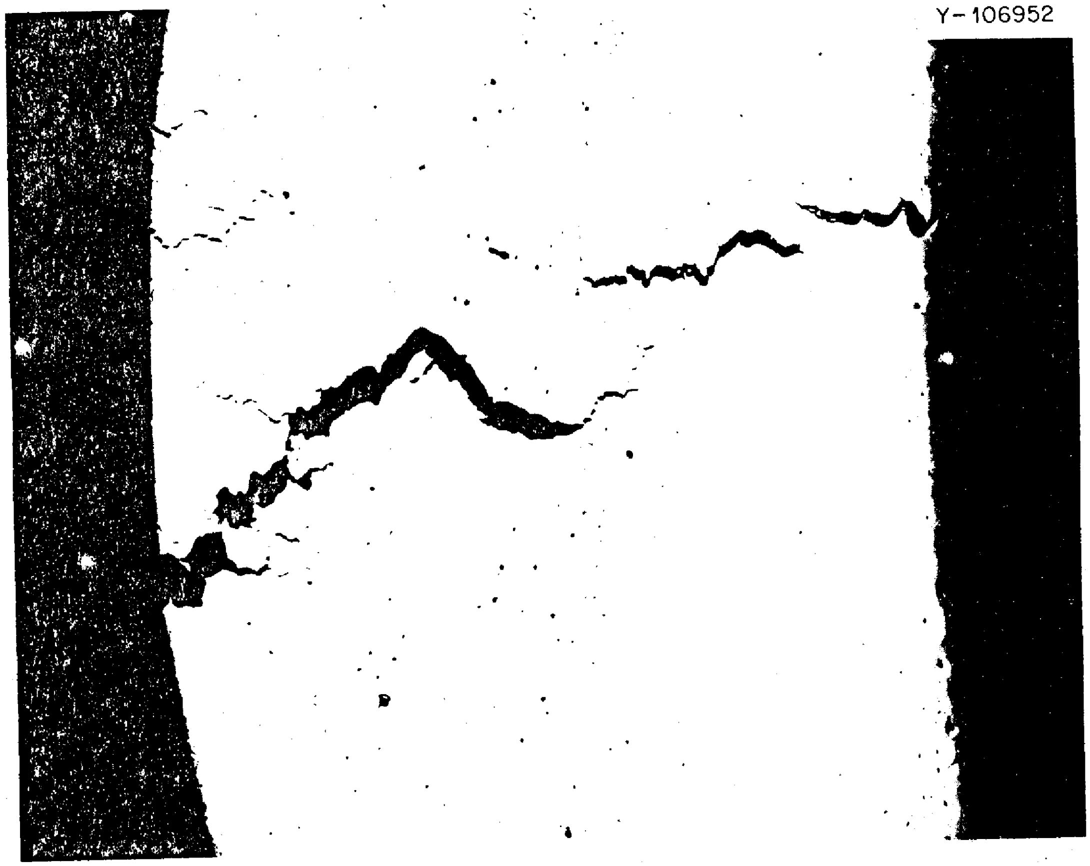

Fig. 32A Photomicrograph of the primary failure region in the tube in Fig. 13.32. Incoloy 800 is on the inside and the Ni 280 on the outside. As polished. Magnification 35X.

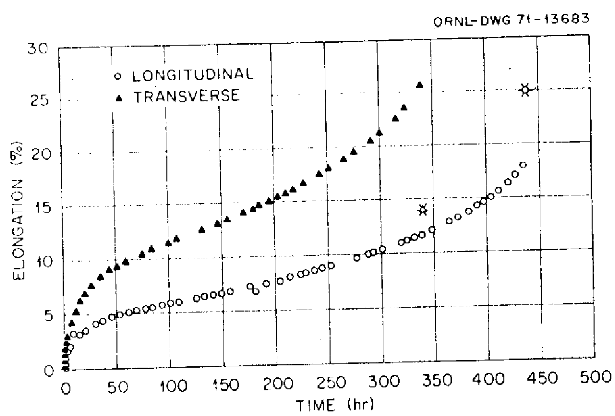

Fig. 32B Comparative creep curves of Ni 280 sheet at 538°C and 20,000 psi in an argon atmosphere. Samples taken from longitudinal and transverse orientation.

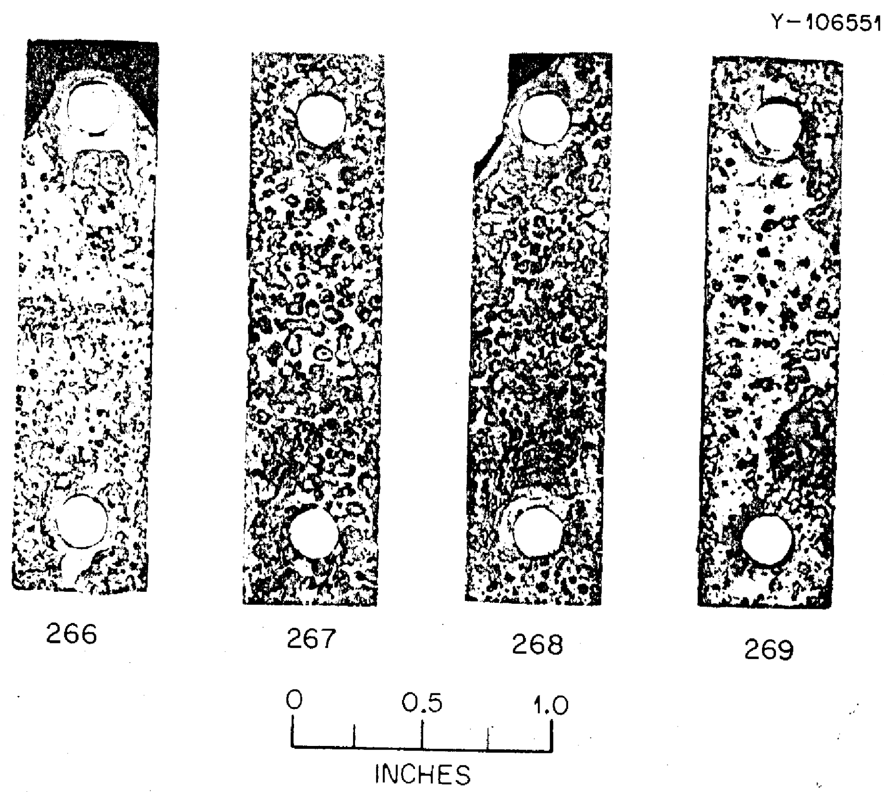

Fig. 33 . Samples of Ni 280 exposed to steam for 2000 hr at 538°C and 3500 psi.

Y-111626

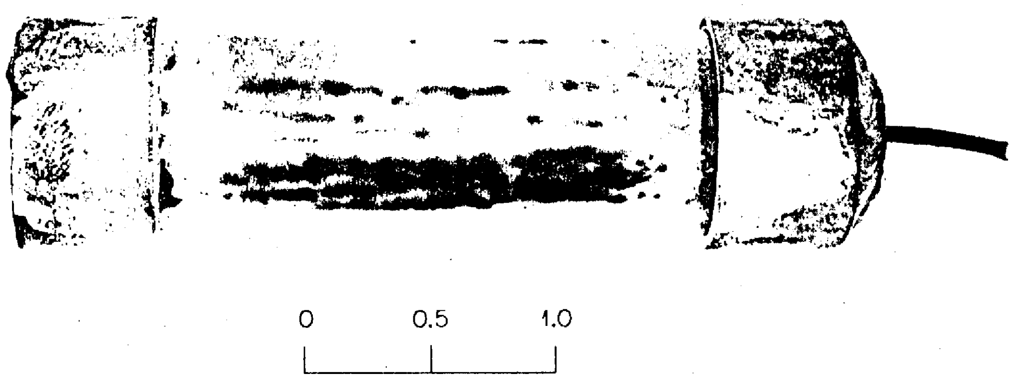

Fig. 34 Photograph of duplex tube-burst specimen discontinued after being stressed for 7075 hr at 40,000 psi at 538°C. The tube had a diametral strain of 1.14%, and the dye penetrant clearly reveals cracks in the outer nickel 280 layer.

(a)

(b)

Fig. 35 Photomicrograph of the cross section of the specimen shown in Fig. 34. The nickel 280 is on the outside, and numerous cracks are present. The Incoloy 800 is on the inside and is not cracked. As polished.

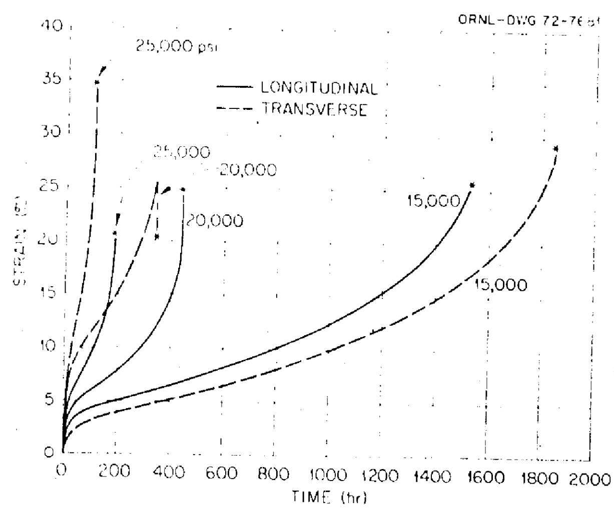

Fig. 36 . Creep curves of nickel 280 sheet at 538°C in argon.

Figure 37 Photomicrograph of a sample of INCONEL 600 (20% Ni-15% Cr-5% Fe) after exposure to fluoride salt in a pumped loop for 15,000 hours at 1300°F. Voids near the surface are formed as chromium is removed selectively by the salt.

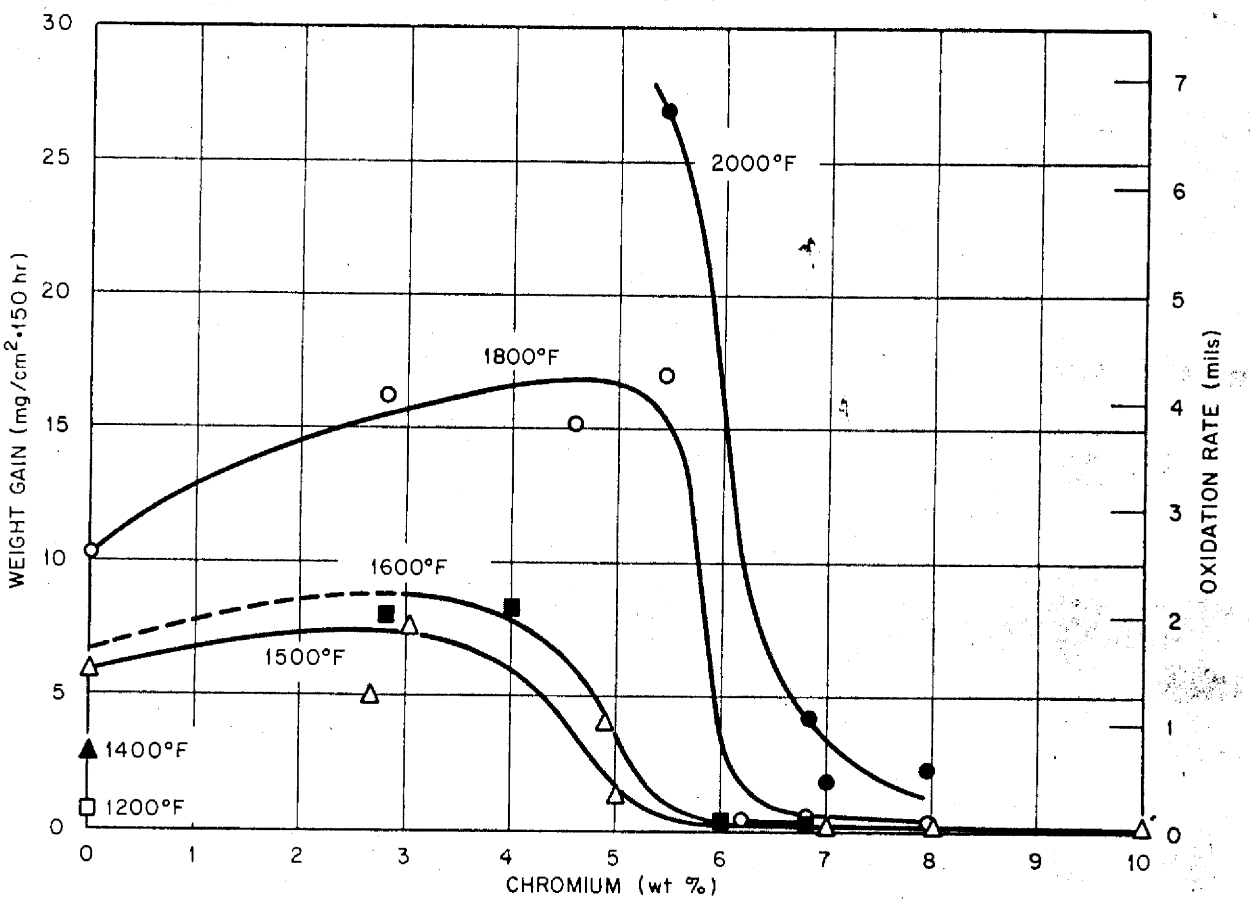

Figure 38A Variation of the rate of oxidation of an 80% Ni-20% Mo alloy with chromium content. Note the very sharp decrease in rate at chromium levels of 5 to 7%.

Alloy	Composition, % by weight (Base: Ni)						
	Mo	Cr	Fe	Ti	Al	Nb	W
INOR-1	20						
INOR-2	16	5					
INOR-3	16			1.5	1		
INOR-4	16			1.5	2		
INOR-5	15					2	2
INOR-6	16	5		1.5	1		
INOR-7	16	6			1	1	
INOR-8	16	6	5				
INOR-9	17		5			3	

FIGURE 38B Several promising nickel base alloys melted in the course of developing INOR-8.

FWC FORM 172 - 4

NOTATIONS IN THIS COLUMN INDICATE WHERE CHANGES HAVE BEEN MADE

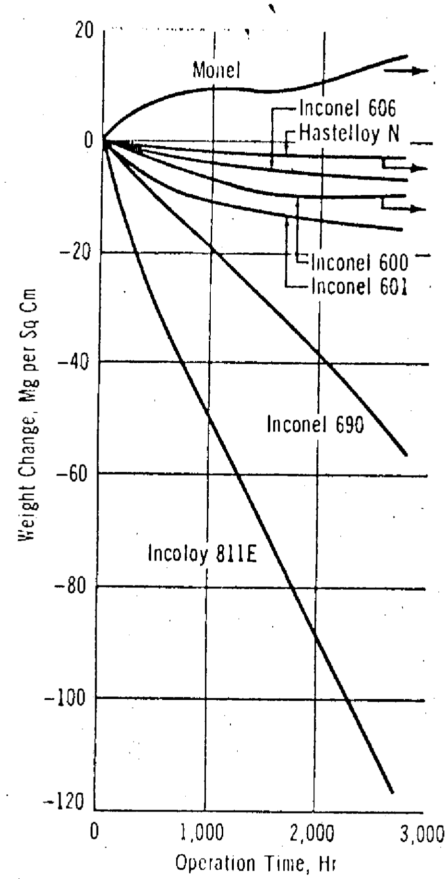

FIGURE 39

Graph illustrates the relative corrosion resistance of various alloys in LIF-BeF_2-ThF_4-UF_4 molten salt studies conducted at ORNL @ 690°C(1,275°F).

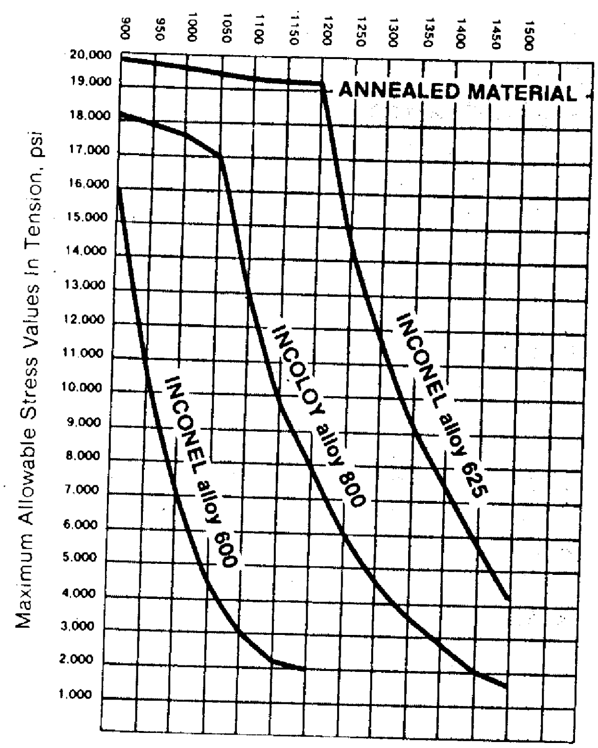

HIGH-TEMPERATURE APPLICATIONS
900 to 1500 F

FIGURE 40

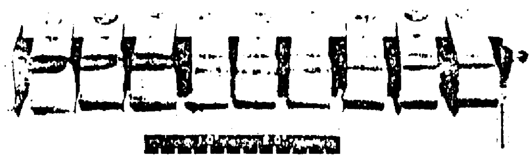

FIG 41A U-Bend SCC Specimen Holder with Mounted Specimens.

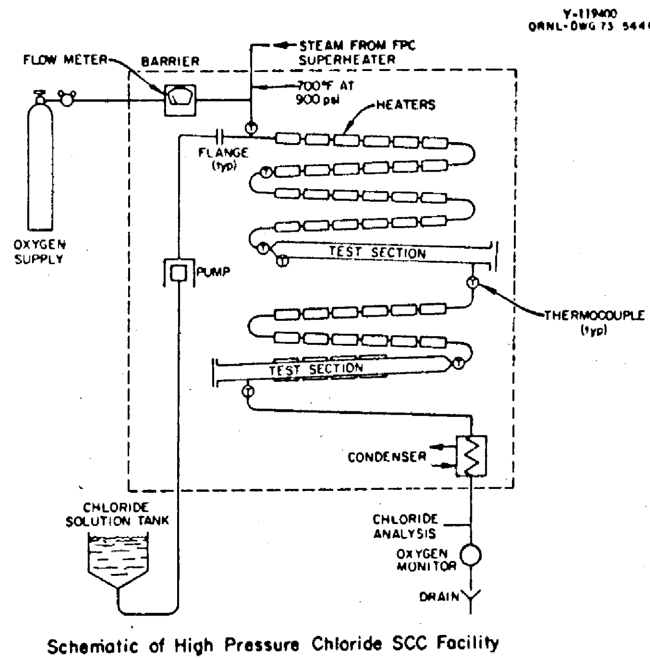

Fig. 41B Schematic of High-Pressure Chloride SCC Facility.

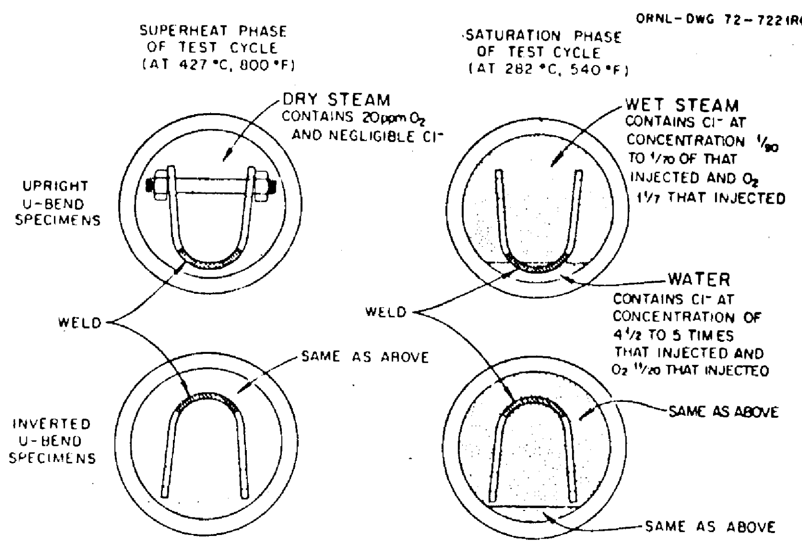

Fig. 41C Schematic Showing Specimens and Environmental Conditions During Cyclic Test. Continuous injection of 20 ppm O_2; 10 ppm Cl^- (as NaCl) injected only during saturation phase (24 hr at 540°F three times per week).

FWC FORM 172 - 4

NOTATIONS IN THIS COLUMN INDICATE WHERE CHANGES HAVE BEEN MADE

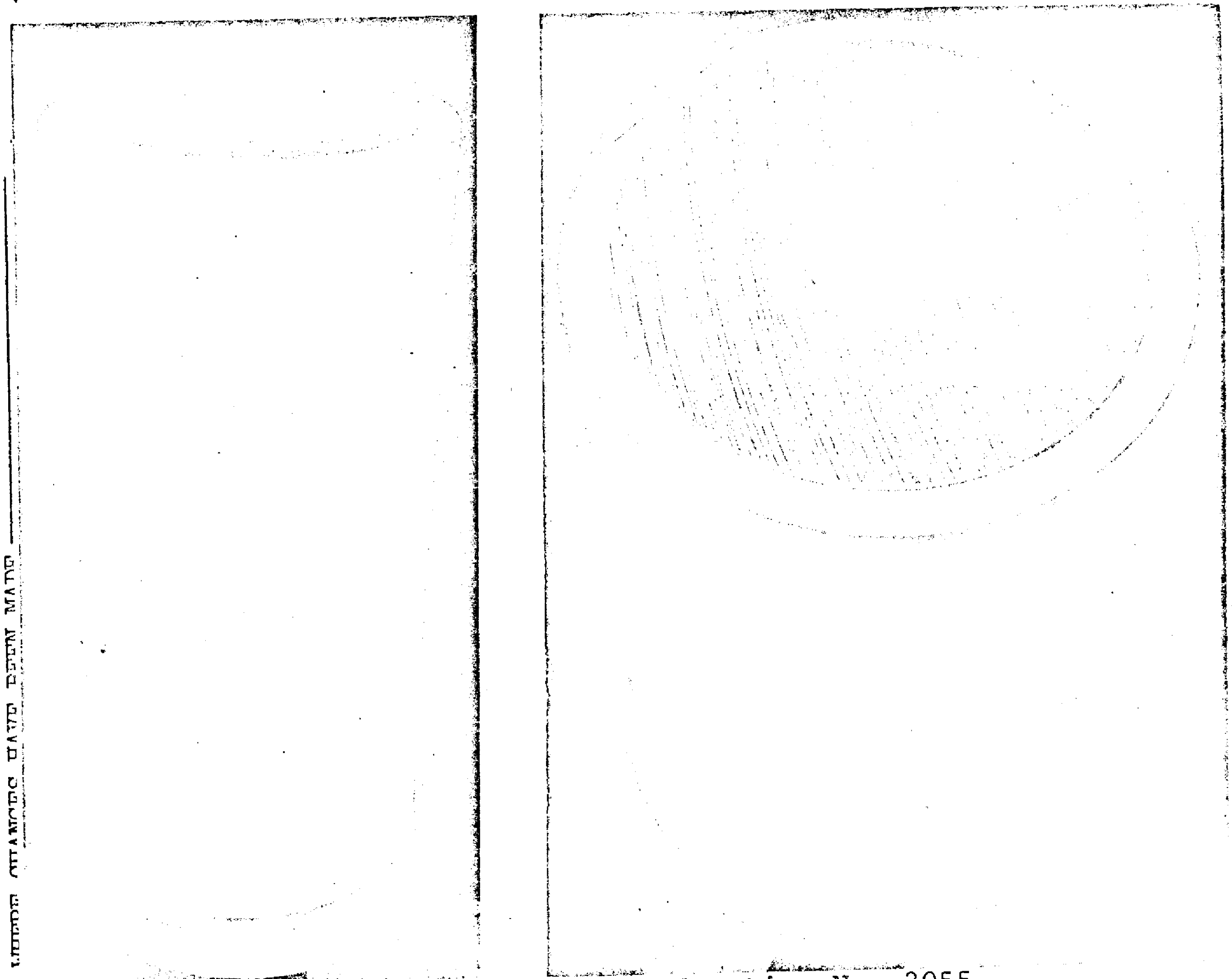

Negative No. 3055

Sintered nickel shell on MONEL alloy 400 extrusion billet.

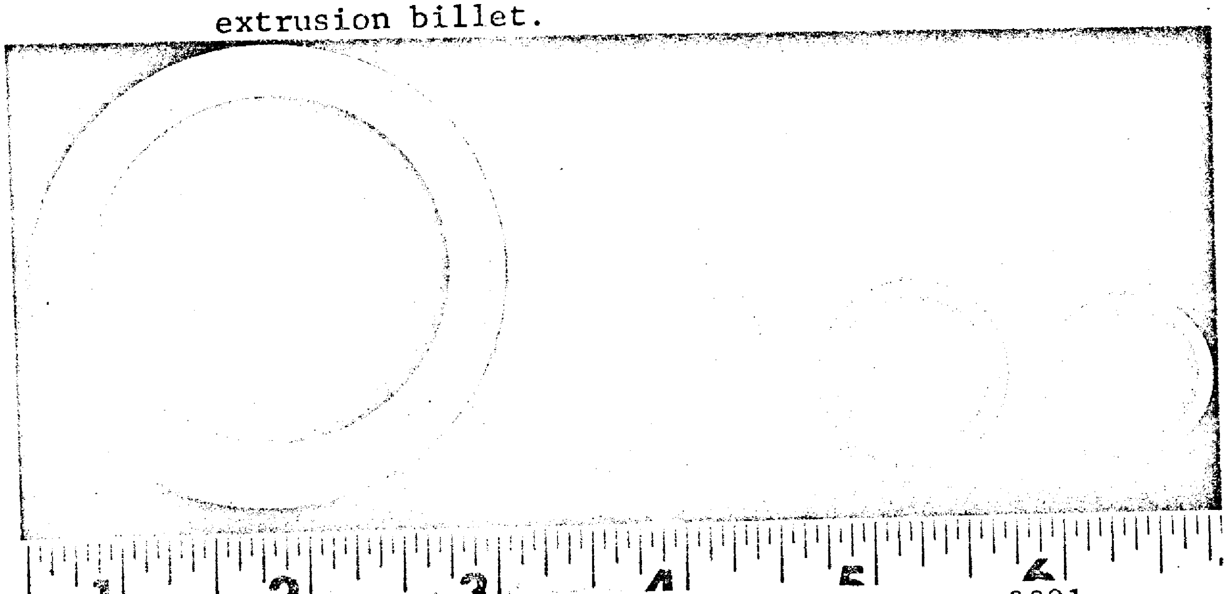

Negative No. 3091

FIGURE 42

Cross sections of nickel clad MONEL tubing at various processing steps. From left to right the samples are:

As-Extruded 2.500" O.D. x 0.312" wall
Tube reduced 1.250" O.D. x 0.095" wall
Cold Drawn 1.000" O.D. x 0.077" wall
Cold Drawn 0.875" O.D. x 0.065" wall

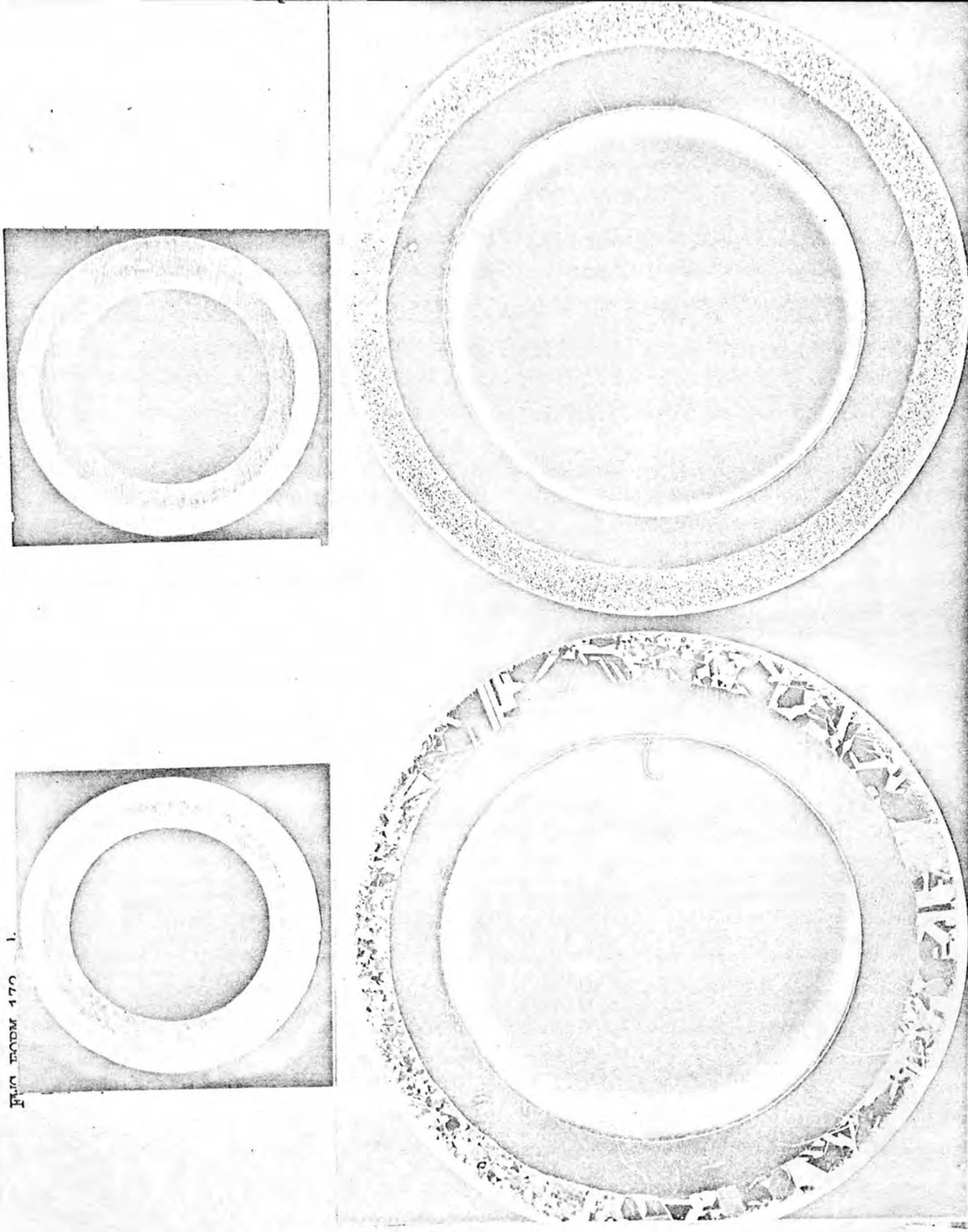

FIGURE 43

LEFT(TOP, BOTTOM) PHOTOMACROGRAPH 3X MAGNIFICATION AS RECEIVED
RIGHT(TOP,BOTTOM) PHOTOMACROGRAPH 6X MAGNIFICATION MACROETCHED

Photomacrographs at top (left and right) illustrate the appearances of clad Ni 270/Incoloy 800 tubing at different magnifications in the as received and macroetched conditions.

Photomacrographs at bottom (left and right) illustrate the appearances of clad Ni 280/Incoloy 800 tubing at different magnifications in the as received and macroetched conditions.

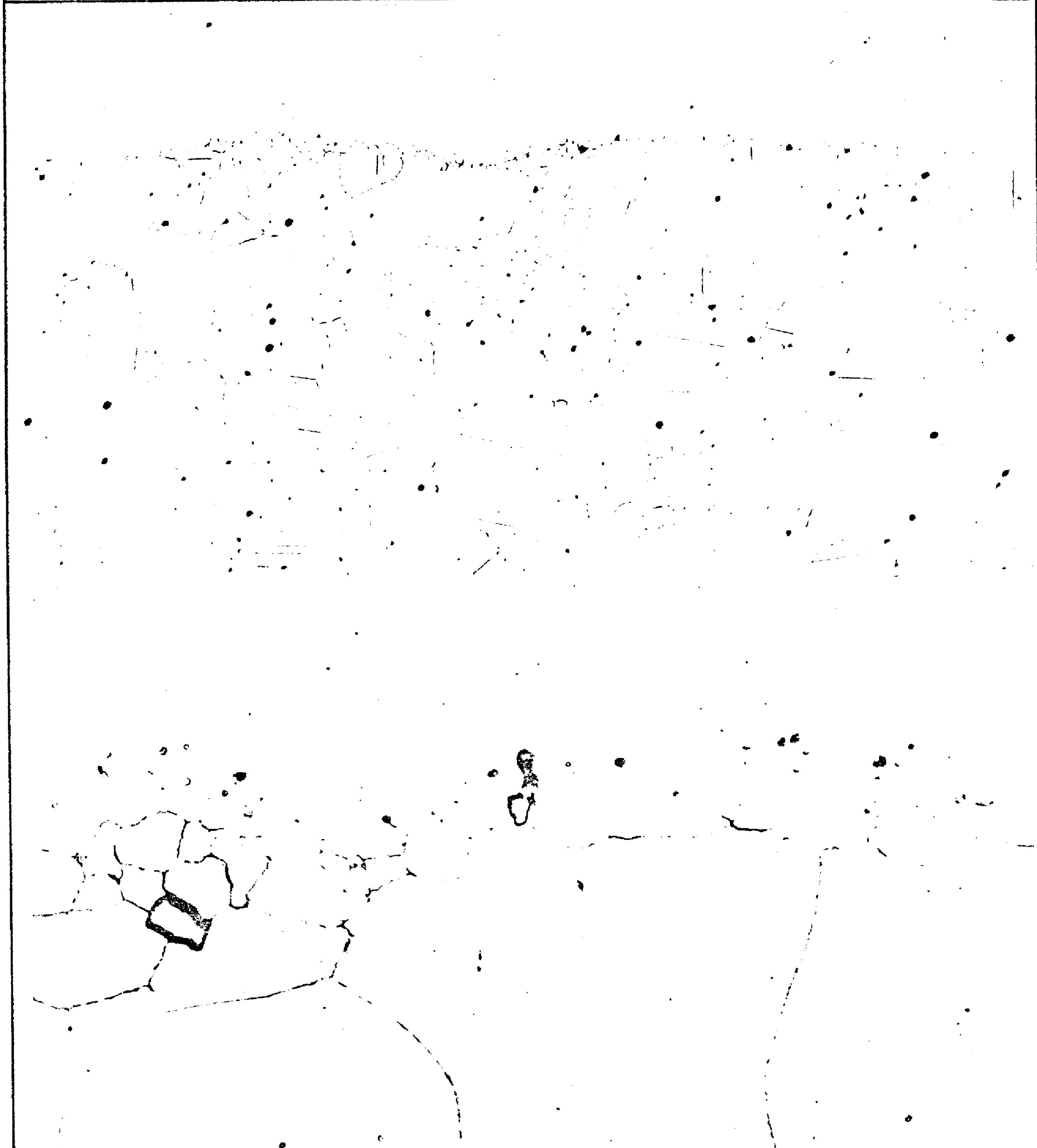

FIGURE 44

TOP: PHOTOMICROGRAPH 100X MAGNIFICATION 10% ELECT. OXALIC ACID ETCH
BOTTOM: PHOTOMICROGRAPH 1000X MAGNIFICATION 10% ELECT. OXALIC ACID ETCH

Photomicrographs taken of a transverse section illustrate the microstructural appearances of the nickel 270 clad and Incoloy 800 materials in the metallurgically bonded areas.

CHARGE NO. 8-25-2431	DOCUMENT NO. ND/74/53	ISSUE 1	DATE 12/16/74

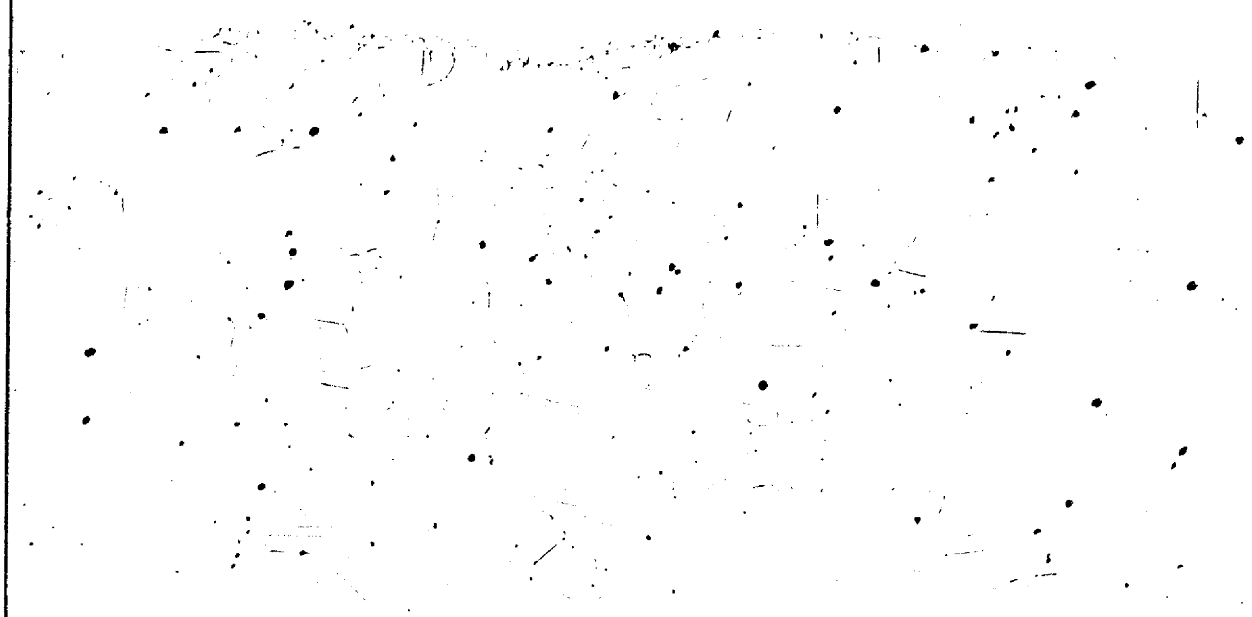

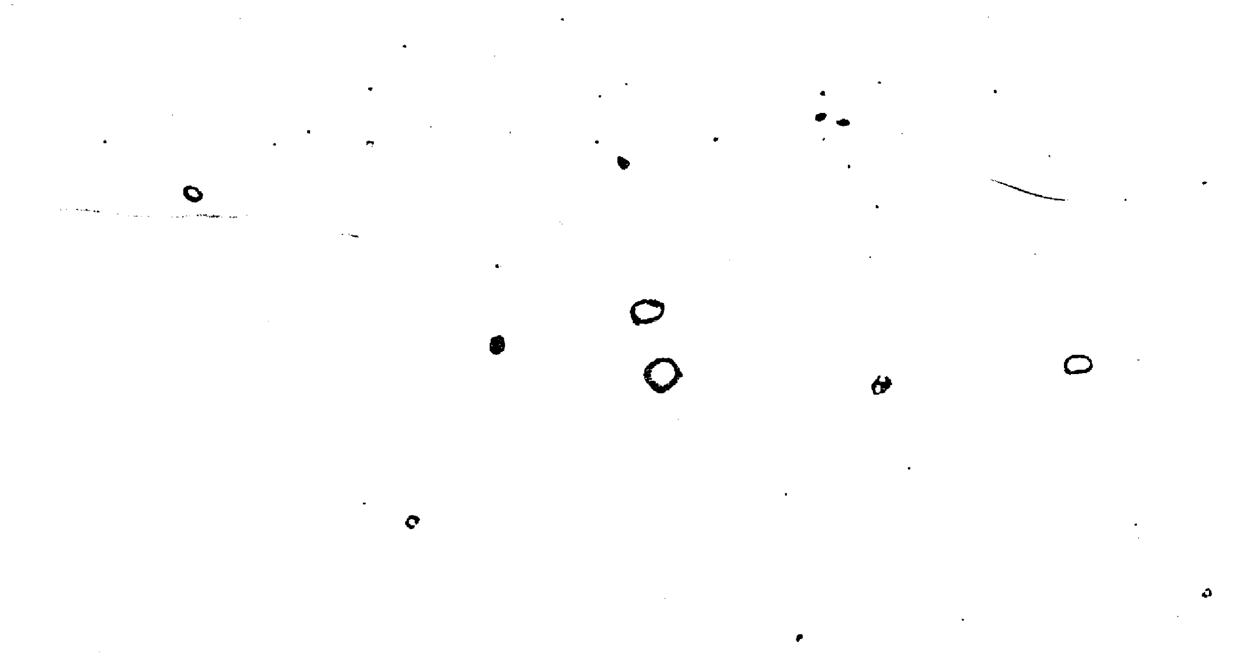

FIGURE 45

TOP: PHOTOMICROGRAPH 100X MAGNIFICATION 10% ELECT. OXALIC ACID ETCH
BOTTOM: PHOTOMICROGRAPH 1000X MAGNIFICATION 10% ELECT. OXALIC ACID ETCH

Photomicrographs taken of a transverse section illustrate the crostructural appearances of the nickel 280 clad and Incoloy 800 materials in the metallurgically bonded areas.

FWC FORM 172 - 4

NOTATIONS IN THIS COLUMN INDICATE WHERE CHANGES HAVE BEEN MADE

FWC FORM 172 - 4

NOTATIONS IN THIS COLUMN INDICATE WHERE CHANGES HAVE BEEN MADE

SECTION 7

MANUFACTURING ENGINEERING

BY

J. G. WHELLEY

Approved by

M. J. Kraje
Manager, Manufacturing Engineering

TABLE OF CONTENTS

7.0 MANUFACTURING ENGINEERING

A. The manufacturing engineering responsibility is to review the drawings of the project and determine the manufacturing feasibility of the design as it is presented; and make suggestions that will enable the product to be manufactured and assembled to all controlling codes and specifications within the ability of the shops to produce.

B. The following assumptions have been made in order to make a continuous review of the proposed steam generator.

1. The size of this unit precludes the shipment by rail, so it must be shipped by barge. This can be accomplished at our Panama City, Florida plant.

2. Our experience in internal bore welding and excellent intrepretation of the gamma ray film should allow us to mass spectrometer test the completed unit and void the requirement for helium leak testing each individual tube.

3. The ability of Foster Wheeler to develop the internal bore welding in the "5G" position is only a matter of time as demonstrated by the test welds made in our Mountaintop lab.

4. That the hastelloy-N tubes will be able to be produced by welding two short straight sections together and to bend the tubes so they are defect free.

5. There will be no cladding of the tube sheet.

6. That the radius shell section can be purchased completely fabricated except for girth seam welding by Foster Wheeler.

7. The parts of the shell will be manufactured of plates and forgings.

8. Supports at the curved portion of the shell will be made up in pieces.

9. Stress relieving will not be required.

C. The summary of the results are detailed in section 7.2 where the assembly procedure is presented.

7.1 MAINTENANCE PROCEDURE

The following is an outline for detecting the leaking tube and the procedure for plugging it.
To find the tube that is leaking, it will be necessary to remove the unit from the system.
The unit may be removed by cutting the inlet and outlet steam pipes and the salt inlet and outlet piping. The piping should be removed by cutting through the field welds that were made to seal the piping to the unit.
By pressurizing the salt side of the unit with helium and "sniffing" the tubes at the face of the tube sheet (steam/water side) the leaking tube can be found.
When the leaking tube has been identified and marked the following procedure will be used to plug the tube. This procedure starts when access to both tube sheets has been obtained. The procedure is based on the following:

1. The tube sheets are accessable to allow the insertion and welding of the plugs.

2. The unit has been decontaminated and cleaned making hands on maintenance possible.

7.1.1 Operational Procedure for Plugging the Tubesheet Tube Holes after the Leaky Tubes Have Been Identified

1. Insert expandable plugs into both ends of the failed tube to prevent foreign matter from entering the unit. These plugs must be inserted far enough to allow the various preparatory tube plugging operations to proceed. These temporary plugs are to be designed for convenient removal.

2. Plug both ends of the tubes of two adjacent rows surrounding the failed tube with expandable plugs to avoid contamination. Inventory plugs and record data. See sketch on page 7-17. for typical pattern of tubes to be plugged with expandable plugs.

3. Cover the balance of the tubesheet holes on both tubesheets with clean polyethylene and seal with tape.

4. Clean both ends of the failed tube hole, inside and adjacent surfaces with a clean stainless brush and acetone, then vacuum all surfaces clean.

5. P.T. area to be welded

6. Clean

7. Remove expandable plug prior to inserting permanent plug.

CHARGE NO 8-25-2431	DOCUMENT NO. ND/74/66	ISSUE 1	DATE 12/16/74

8. Insert permanent plug as shown on sketch
9. Weld plug complete using filler rings.
10. Inspect between each pass.
11. Clean after welding.
12. Cleanliness inspect.
13. Repeat operations 7.1.1-5 to 12 for other end of failed tube.
14. Remove plugs installed in para. 7.1.1-2 and polyethylene seal installed in para 7.1.1-3.
15. When the tube sheets have been exposed to plug a leaking tube, the rest of the tubes can be checked for errosion by the use of U.T.

    Each tube is U.T. examined at the time the unit is being assembled and the wall thickness pattern is recorded. The tubes that have been in service are reexamined by U.T. and the wall thickness pattern is recorded. The records of the in service tubes are compared to the records of the tubes at the time of unit assembly and the errosion determined by the difference in these records.

FWC FORM 172 - 4

NOTATIONS IN THIS COLUMN INDICATE WHERE CHANGES HAVE BEEN MADE

7.2 SEQUENCES OF OPERATIONS FOR MANUFACTURE OF MOLTEN SALT STEAM GENERATOR

7.2.1 Purpose

To establish a preliminary procedure for fabricating the Molten Salt Steam Generator.

7.2.2 General

Certain Assumptions were made in order to fabricate these Hastalloy "N" Steam Generators and these are:

2.1 Tube Sheets will not be clad.

2.2 Tube to Tube sheet weld will be performed in the 2g and 5g position respectively.

2.3 We can purchase the radius shell section completely fabricated except for girth seam welding by Foster Wheeler.

2.4 The parts of the shell will be made from plates and forgings.

2.5 Supports at the curved portion of shell will be made up in pieces.

2.6 Stress relieving will not be required.

7.2.3 Plan

Listed below is an index of procedures for component sub-assemblies and final assembly identifying the overall plan to fabricate the Molten Salt Steam Generator. Refer to sketches shown on Pages 7-14 and 7-15 to assist in understanding these procedures.

3.1 Straight Shell Course Subassembly "A"

3.2 Shell Section "B"

3.3 Inner Shroud Section "C"

3.4 Thermal Sleeve Forging "D"

3.5 Straight Shell Section "A" through "D" Subassembly.

3.6 Straight Shroud Section "E"

3.7 Radius Shroud Section "F"

7.2.3 Plan (continued)

3.8 Radius Shell Section "G"

3.9 Shell Section "H"

3.10 Tube Sheets "K"

3.11 Tubes "L"

3.12 Adapter Ring "M"

3.13 Steam Nozzle "N"

3.14 Bundle Assembly

7.2.3.1 Straight Shell Course Subassembly "A"

The shell sections will be made in a number of courses, each with one longitudinal seam and joined by girth seams.

1. Layout and machine the weld preparations on each of four edges in the flat.

2. Penetrant Inspect Weld Preparations.

3. Roll to required inside diameter.

4. Set up and weld longitudinal seam.

5. Dress longitudinal weld inside and outside.

6. Check circularity and reround.

7. Radiograph longitudinal seam.

8. Repeat sequences #1 through #7 as required for each course.

9. Set up for circle seam welding.

10. Weld circle seam.

11. Dress inside and outside girth seam.

12. Radiograph girth seam.

13. Repeat sequences #9 through #12 as required.

7.2.3.2 Shell Section "B"

The shell section will be made in one course with one longitudinal seam.

1. Layout and machine weld preparations on each of three edges in the flat. (Finish machine three edges.) Don't machine edge that butts to adapter ring.

2. Penetrant inspect weld preparations.

3. Roll to required inside diameter.

4. Set up and weld longitudinal seam.

5. Dress longitudinal seam inside and outside.

6. Check circularity and reround.

7. Install roundness retaining rings.

8. Machine cutout and weld groove for inlet nozzle.

9. Dress balance of weld preparation.

10. Penetrant inspect weld preparations.

11. Weld nozzle to shell.

12. Dress inside and outside weld seams.

13. Radiograph longitudinal shell seam and nozzle to shell seams welds.

14. Set up V.B.M. and machine girth seam weld preparation for "EB" insert weld @ adapter ring. It may be necessary to weld build up this section before machining.

15. Penetrant inspect girth edge preparation.

7.2.3.3 Inner Shroud Section "C"

The shroud section will be made in one course with one longitudinal seam from perforated plate.

1. Layout and machine weld preparations on each of three edges in the flat.

2. Penetrant inspect weld preparations.

3. Roll to required inside diameter.

4. Set up and weld longitudinal seam.

5. Grind longitudinal seam inside and outside.

6. Check circularity and reround.

7. Penetrant inspect longitudinal seam.

7.2.3.4 Thermal Sleeve Forging "D"

The thermal sleeve will be purchased as a rough forging.

1. Layout and identify centerlines.

2. Set up on VBM and machine to configuration.

3. Penetrant inspect weld preparations.

7.2.3.5 Straight Shell Section "A" through "D" Subassembly

1. Set up for welding of shell course subassembly to thermal sleeve forging "D".

2. Weld girth seams.

3. Radiograph inspect shell to forging girth seams.

4. Set up for welding Shell "B" to subassembly from sequence #3.

5. Weld girth seam and grind inside and outside.

6. Radiograph inspect girth seam.

7. Set up for welding inner Shroud "C" to subassembly from sequence #6.

8. Weld girth seam and grind inside.

9. Penetrant inspect shroud to forging girth seam.

7.2.3.6 Straight Shroud Section "E"

The shroud section will be fabricated as two half shells from plate.

1. Layout and machine weld preparation on each of four edges in the flat.

2. Penetrant inspect weld preparations.

3. Roll half shells to required inside diameter.

4. Trial fit the two half shells.

7.2.3.7 Radius Shroud Section "F"

The radius shroud section will be fabricated from purchased formed half elbows with all machined weld preparations.

1. Penetrant inspect weld preparations.

2. Set up for welding smaller radius half elbow sections together.

3. Weld girth seam.

4. Grind inside and outside girth seam.

5. Penetrant inspect girth seam.

6. Repeat sequences #1 through #5 as required to make complete small radius section.

7. Set up for welding subassembly from sequence #6 to half shroud "E" from #3.6.

8. Weld girth seam.

9. Grind inside and outside girth seam.

10. Penetrant inspect girth seam.

11. Repeat sequence through #10 to make up complete separate larger radius shroud section.

7.2.3.8 Radius Shell Sections "G"

The radius shell sections will be fabricated from two purchased elbows with the girth edges machined for "EB" insert welding.

1. Penetrant inspect weld preparations.

7.2.3.9 Shell Section "H"

The shell section will be made in one course with one longitudinal seam.

1. Layout and machine weld preparations on each of two edges in the flat. (Finish machine two edges - Don't machine girth seam edges.)

2. Penetrant inspect weld preparations.

3. Roll to required inside diameter.

4. Set up and weld longitudinal seam.

5. Grind longitudinal seam inside and outside.

6. Check circularity and reround.

7. Install roundness retaining rings.

8. Machine cutout and weld groove for outlet nozzle.

9. Grind balance of weld preparations.

10. Penetrant inspect weld preparations.

11. Weld nozzle to shell seam.

12. Grind inside and outside weld seams.

13. Set up on VBM and machine both girth seam weld preparations for "EB" insert welds. It may be necessary to weld build up these sections before machining.

14. Radiograph longitudinal shell seam and nozzle to shell seam welds and penetrant inspect girth edges.

7.2.3.10 Tube Sheets "K"

The tube sheets will be purchased as forgings.

1. Set up on VBM and machine both flat side surfaces and weld grooves.
2. Ultrasonic and penetrant inspect machined surfaces.
3. Layout and drill tube holes.
4. Machine spigots and counterbores.
5. Set up and machine for island removal between spigots.
6. Clean and deburr tube holes.
7. Penetrant inspect spigots and island removal areas.
8. Radiograph spigots.
9. Clean.

7.2.3.11 Tubes "L"

The tubes will be purchased in various short lengths and welded together.

1. Set up and machine ends of tubes.
2. Weld tube to tube.
3. Grind tube welds on outside diameter.
4. Penetrant inspect tube welds.
5. Radiograph tube welds.
6. Helium test straight tubes.

7. Set up bending machine for bending tubes.

8. Bend smallest radius row of tubes.

9. Trim tubes to length and machine weld prep.

10. P.T. ends and inspect.

7.2.3.12 Adapter Rings "M".

The adapter rings will be purchased as forgings and machined at final assembly after welding Handhole nozzles.

7.2.3.13 Steam Nozzles "N"

The nozzles will be purchased as forgings.

1. Set up on VBM and machine complete.

2. Penetrant inspect weld preparations.

7.2.3.14 Bundle Final Assembly

1. Set up for welding straight shell subassembly "D" to small radius shroud half "F".

2. Weld girth seam.

3. Grind girth seam.

4. Penetrant inspect girth seam.

5. Set up bundle assembly fixture and attach inlet and outlet tube sheets "K".

6. Insert guide rods through steam outlet tube sheet into shell and install full supportplates using the guide rods for alignment purposes.

7. Set up and install segmented support parts in the small radius shroud for the smallest radius row of tubes.

8. The guide rods will be attached to the longer tube leg and withdrawn as the tube is inserted into the bundle. This will insure that the tube passes through the proper hole in the support plate.

9. Thread the tube using the rod, if required, and spring the tube against tube sheets.

10. IBW weld tube to tube sheets for the smallest radius row of tubes.

11. Clean tube to tube sheet welds.

12. Radiograph inspect.

13. Install segmented support parts for assembly of the next larger radius row of tubes.

14. Repeat sequences #8 through #14 until all tubes have been installed.

15. Inspect and check bundle for cleanliness.

16. Set up and weld larger radius shroud assembly to bundle.

17. Grind welds outside.

18. Penetrant inspect longitudinal and girth welds.

19. Slide shell sections "G" and "H" over shroud.

20. Weld girth weld of the shell to thermal sleeve and shell course to shell course.

21. Grind outside girth welds.

22. Radiograph girth welds.

23. Determine finished measurement of distance between tube sheet and shell for adapter ring.

24. Set up adapter ring "M" on VBM and machine to suit.

25. Penetrant inspect weld preparations on adapter ring.

26. Slide adapter rings over tube sheet and weld adapter to tube sheets and shells.

27. Grind girth seams.

28. Radiograph girth welds.

29. Install test caps and test shell side.

30. Set up and weld steam nozzles to tube sheets.

31. Grind girth welds.

32. Penetrant inspect inside girth welds.

33. Radiograph girth welds.

34. Install test caps and test tube side.

35. Pressurize unit and prepare for shipment.

FWC FORM 172 - 4

NOTATIONS IN THIS COLUMN INDICATE WHERE CHANGES HAVE BEEN MADE

CHARGE NO 8-25-2431	DOCUMENT NO. ND/74/66	ISSUE 1	DATE 12/16/74

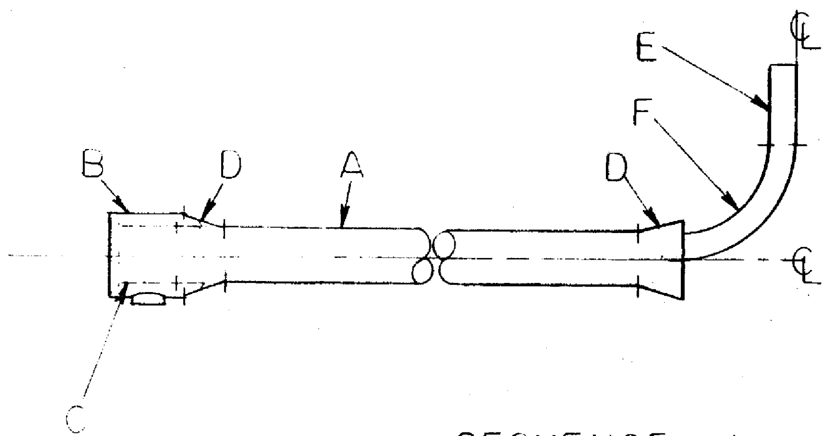

SEQUENCE — 1

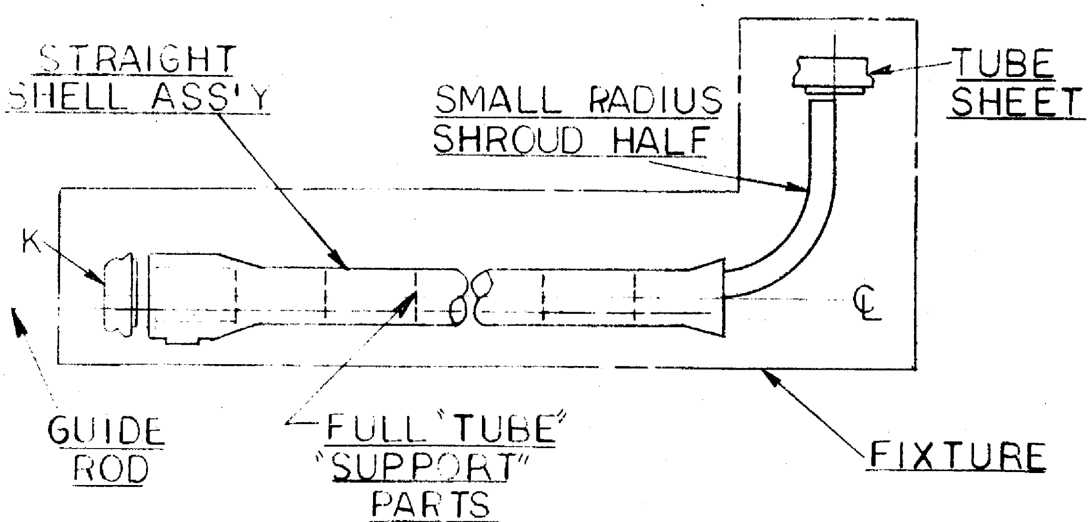

SEQUENCE-6

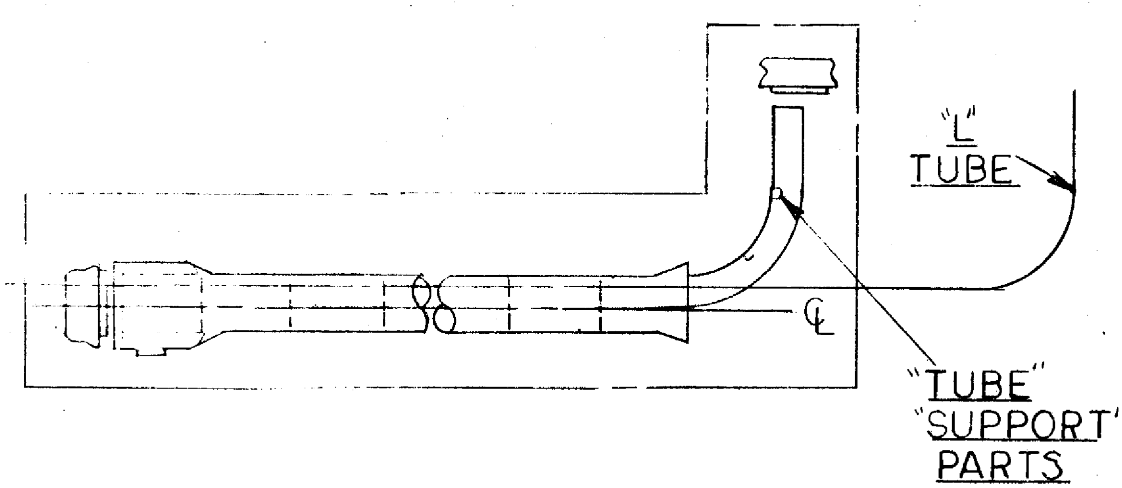

SEQUENCE-9

FWC FORM 172 - 4

NOTATIONS IN THIS COLUMN INDICATE WHERE CHANGES HAVE BEEN MADE

CHARGE NO 8-25-2431	DOCUMENT NO. ND/74/66	ISSUE 1	DATE 12/16/74

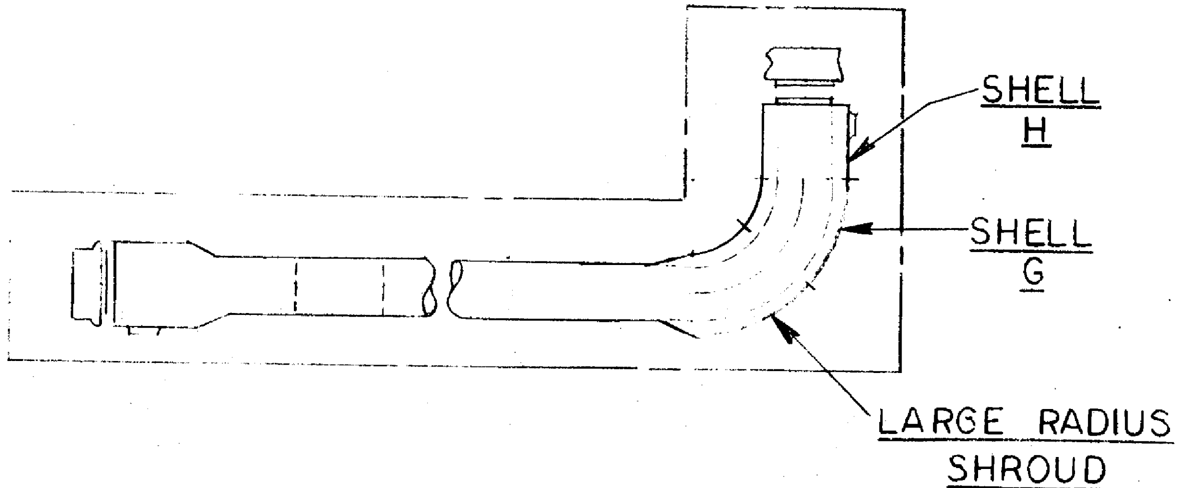

SEQUENCE-23

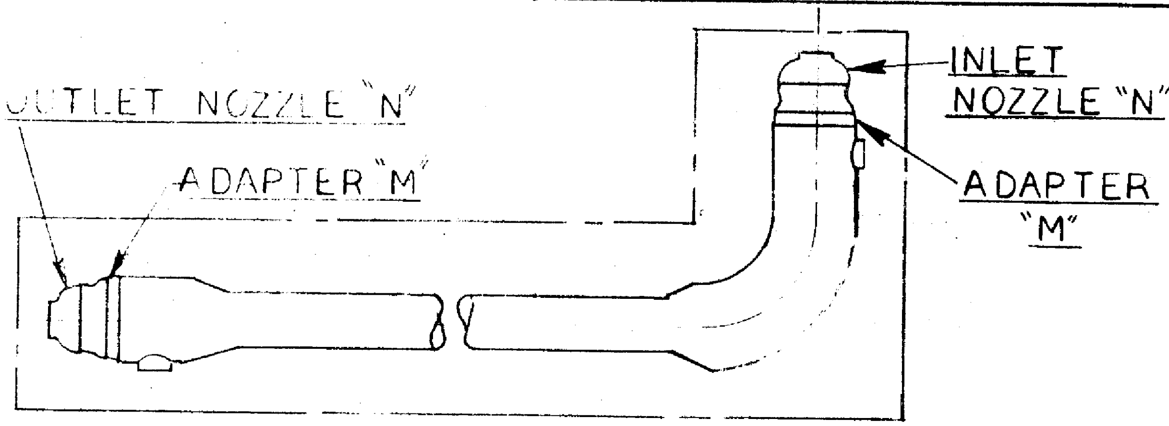

SEQUENCE-36

FWC FORM 172 - 4

NOTATIONS IN THIS COLUMN INDICATE WHERE CHANGES HAVE BEEN MADE

BY	APPROVED	PAGE 7-15 OF

SK-3

STRAIGHT SHOULDER PLUG

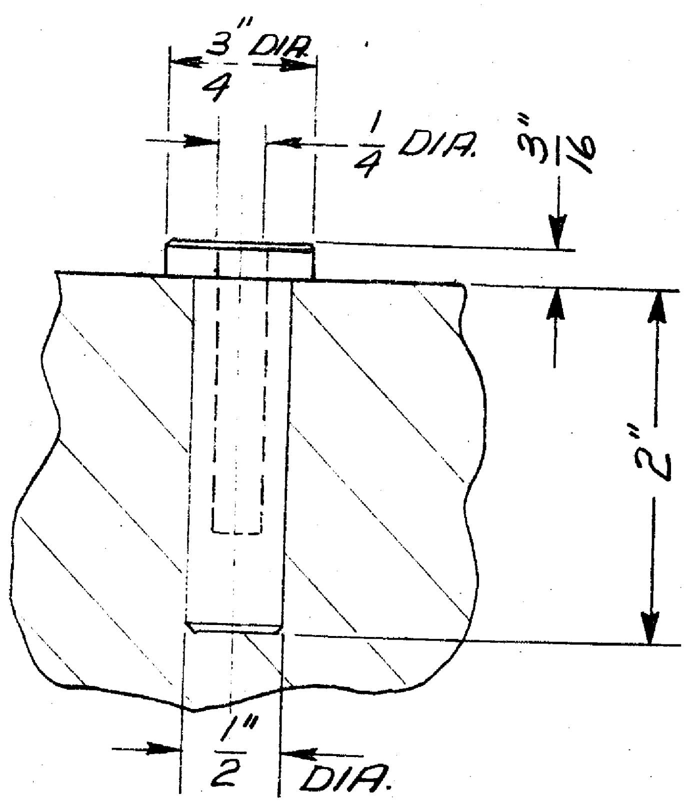

CHARGE NO 8-25-2431	DOCUMENT NO. ND/74/66	ISSUE 1	DATE 12/16/74

TYPICAL PATTERN OF TUBES TO BE PLUGGED WITH EXPANDABLE PLUGS

SK-4

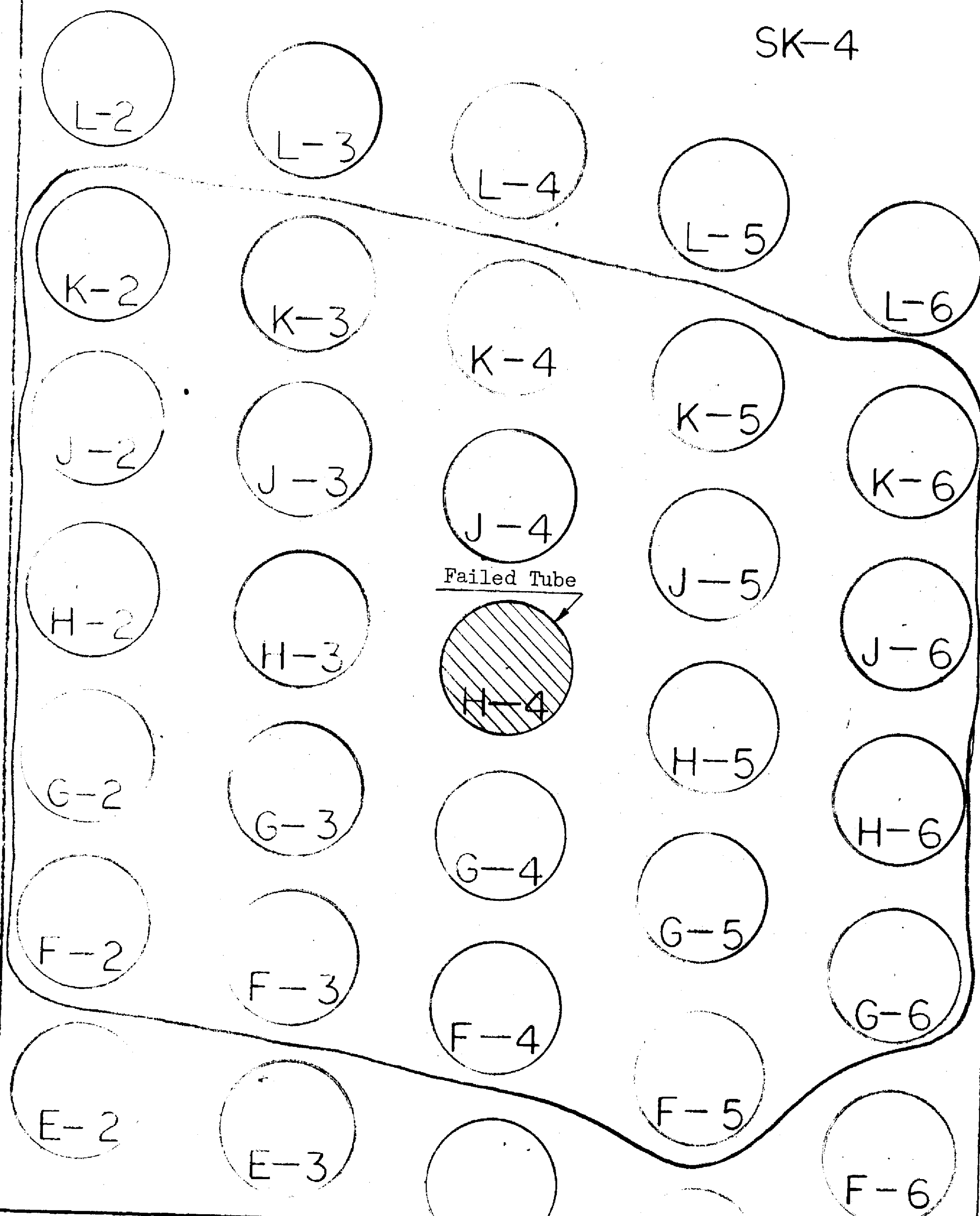

FWC FORM 172 - 4

NOTATIONS IN THIS COLUMN INDICATE WHERE CHANGES HAVE BEEN MADE

BY	APPROVED	PAGE 7-17 of

APPENDIX A

Mechanical Design Calculations

Contents:

BY C. H... DATE 1/23/74 SUBJECT Molten Salt Steam Generator SHEET NO. 1 OF 2

CHKD. BY ______ DATE ______ JOB NO. 8-25-2431

Design Conditions — Code: A.S.M.E. Sect. III 1971

Primary Side (Shell)

Design Temp.	1150°F
Design Press.	220 P.S.I.G.
Eff. %	100%
Allow. Stress	9,500 P.S.I.
I.D. Shell	39½"
Shell Mat'l	Hast. "N"

Secondary Side (Tube)

Design Temp.	1120°F
Design Press.	[illegible] P.S.I.G.
Eff. %	100%
Allow Stress	11,600 P.S.I.
No. of Tubes	~~1032~~ 1014
Tube Pitch	1⅛"
Tube Size	¾" O.D. × .125 wall
Effective Length	114 FT. 140 FT.
Tube Material	Hast. "N"

Pressure Boundaries

- (A) 16" Nozzle (typical)
- (B) Head (typical)
- (C) Tube Sheet (typical)
- (E) Shell Large O.D. (typ.)
- (F) 20" Nozzle (typical)
- (G) Shell Transition
- (H) Shell Small I.D.
- (J) Tube

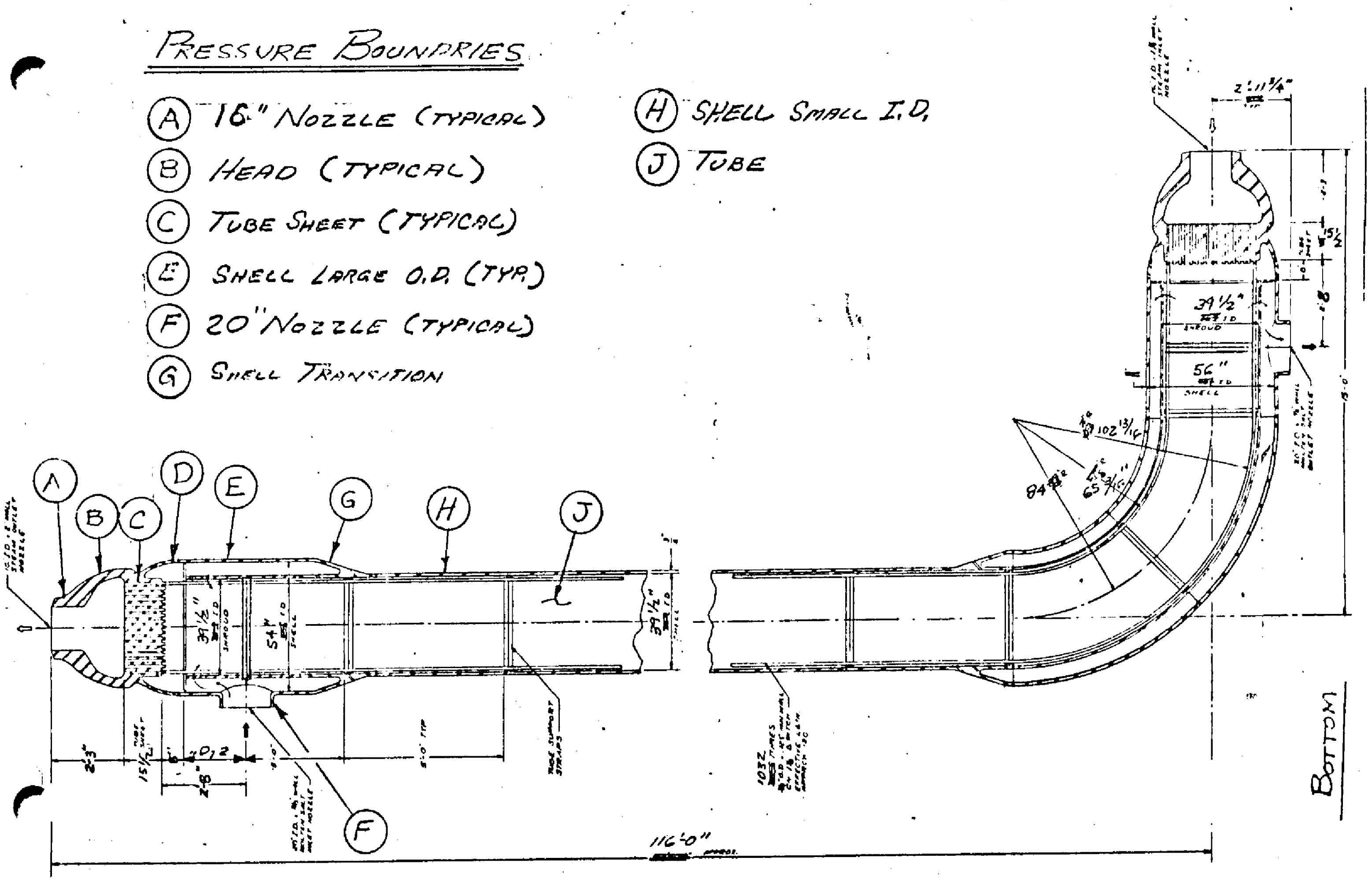

Vert. Plane

See sheet 1 for design conditions

Shell (small I.D.)

$$t = \frac{PR}{SE - 0.6P}$$

$$t = \frac{(220)(19.75)}{(9{,}500)(1.0) - (0.6)(220)}$$

$$t = \frac{4345}{9368}$$

$t = .464''$ say 1/2" PL

Head

$$t = \frac{PL}{2SE - .2P}$$

$$t = \frac{(3800)(21)}{(2)(11{,}600)(1.0) - (.2)(3800)}$$

$$t = \frac{79800}{22440}$$

$t = 3.556''$

Expanded Shell

$$t = \frac{PR}{SE - .06P}$$

$$t = \frac{(220)(28)}{(9500)(1.0) - (.6)(220)}$$

$$t = \frac{6160}{9368}$$

$t = .658''$ say 3/4" PL

ORM (2051-47

HEAD + TUBESHEET

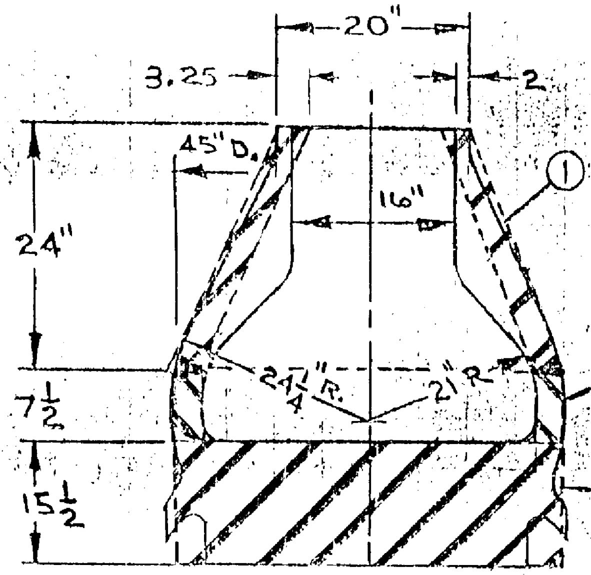

TOTAL WEIGHTS:

Solid (T.S.)	WITH Holes
11952#	9933#

① CONE: $A = 1.5708\, S\, (D + d)$

$D = 3.75$ Ft, $d = 1.666$ FT

$S =$ [triangle: 1.722, 2 Ft] $c^2 = a^2 + b^2$

$= 2.392$ Ft

$A = 20.349\ Ft^2$

Wt @ 3.25" = 134.362 #/Ft²

$W_T = (134.362)(20.349)$

$W_T = 2{,}734\#$

② RING: $A = .7854\,(D^2 - d^2)$

$= .7854\,(16.335 - 12.25)$

$= .7854\,(4.085)$

$= 3.208\ Ft^2$

Wt @ 7 1/2" = 310.065 #/Ft²

$W_T = (310.065)(3.208)$

$W_T = 995\#$

③ BAR: $A = .7854\,(D^2)$

$= .7854\,(16.335)$

$= 12.832\ Ft^2$ } solid

Wt @ 15 1/2" = 640.801 #/Ft

$W_T = (640.801)(12.832)$

$W_T = 8223\#$ solid

with tube holes

$A = 12.832 - 3.15$

$= 9.682\ Ft^2$

$W_T = (9.682)(640.801)$

$W_T = 6204\#$

FORM 12031-47

TUBESHEET EXTENSION

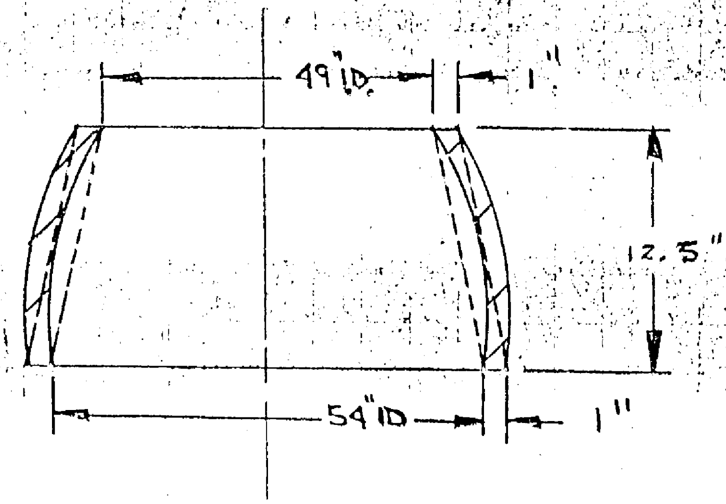

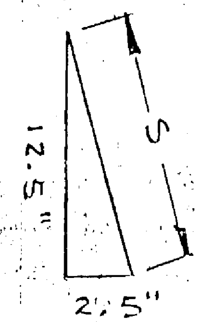

$s = \sqrt{(12.5)^2 + (2.5)^2}$

$= 12.75''$ or 1.0625 Ft

$A_{(CONE)} = 1.5708\ s\ (D + d)$

$D = 56''$ or 4.66 Ft

$d = 51''$ or 4.25 Ft

$A_{(CONE)} = (1.5708)(1.0625)(8.91)$

$= 14.87\ Ft^2$

W_T @ 1" $= 41.342\ \#/Ft^2$

$W_T = (41.342)(14.87)$

$= 615\#$

NOZZLE CYLINDER

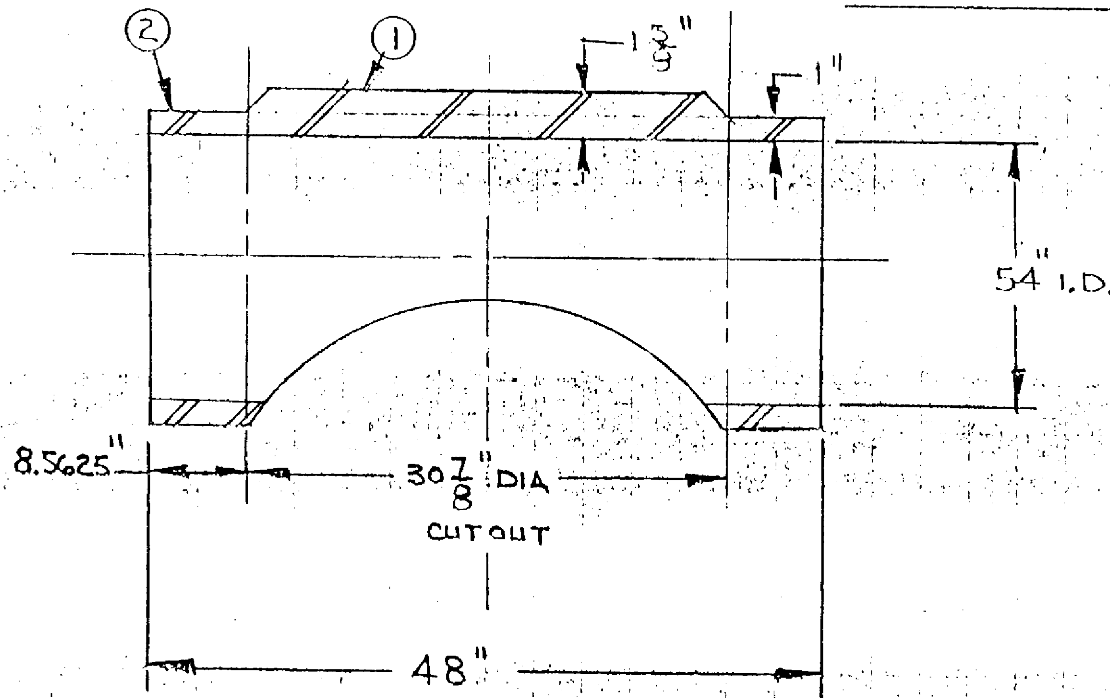

(1)

$C = \pi D = (3.1416)(55.625") = \frac{174.7515"}{12"} = 14.5626$ Ft

$A = L \times W = (2.573')(14.563') = 37.47$ Ft^2

$A_{(CUTOUT)} = \pi \frac{D^2}{4} = .7854 D^2 = (.7854)(2.573^2)$

$= 5.20$ Ft^2

$A_{(TOTAL)} = 37.47$ Ft$^2 - 5.20$ Ft$^2 = 32.27$ Ft^2

W_T @ $1\frac{5}{8} = 67.181$ #/Ft^2

$W_T = (67.181)(32.27) = 2168$ #

(2)

$C = \pi D = (3.1416)(55") = \frac{172.788"}{12} = 14.399$ Ft

$A = L \times W = (14.399$ Ft$)(.7135$ Ft$) = 10.27$ Ft^2

W_T @ 1" $= 41.342$ #/Ft^2

$W_T = (41.342)(10.27) = 425$ # ; 2×425 # $= 850$ #

$W_{T(TOTAL)} = 2168$ # $+ 850$ # $= 3018$ #

INLET / OUTLET NOZZLE

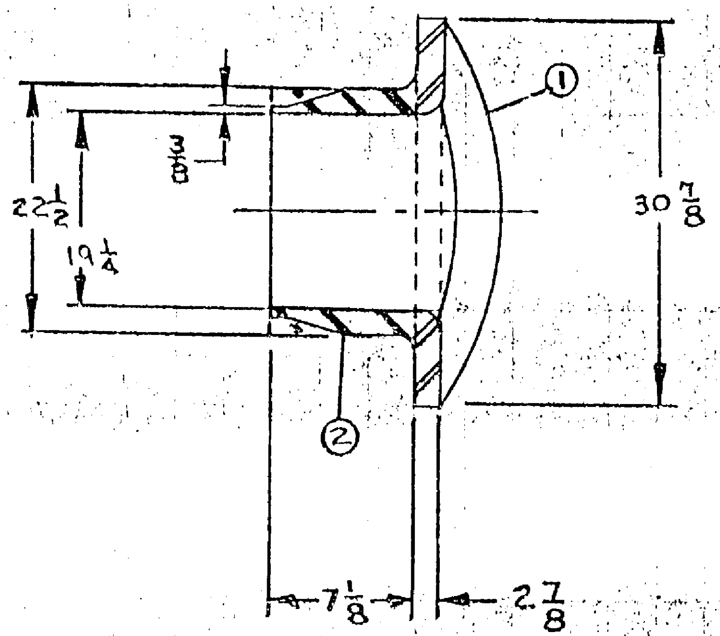

① RING :

$$A = \pi \left(\frac{D_2^2}{4} - \frac{D_1^2}{4}\right)$$
$$= \pi \left(\frac{2.573^2}{4} - \frac{1.604^2}{4}\right)$$
$$= \pi (1.012)$$
$$= 3.179\ Ft^2$$

WT. @ $2\frac{7}{8}$ = 118.859 #/Ft

WT. = (118.859)(3.179)

WT = 378 #

② CYL.

$$A = \pi \left(\frac{D_2^2}{4} - \frac{D_1^2}{4}\right)$$
$$= \pi \left(\frac{1.875^2}{4} - \frac{1.604^2}{4}\right)$$
$$= .738\ Ft^2$$

W_T @ $7\frac{1}{8}$ = 294.56 #/Ft

W_T = (294.56)(.738)

W_T = 217 #

TOTAL APPROX WT.

595 #

SHELL TRANSITION

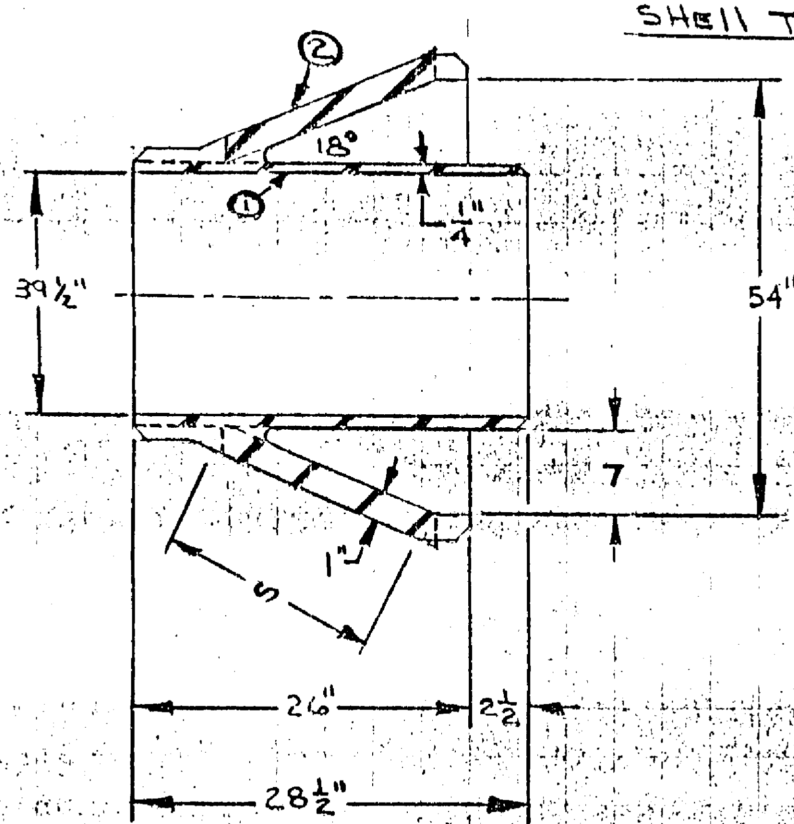

CYLENDER ①

$C = \pi D = \pi(3.33)$

$C = 10.471$ Ft

$L = 2.375$ Ft

$A = C \times L = 24.868$ Ft²

Wt @ 1/4 = 10.336 #/Ft²

Wt = (10.336)(24.868)

Wt ≈ 257 #

CONE ②

$A = 1.5708\, S\, (D + d)$

D = 56" OR 4.666 Ft

d = 42" OR 3.50 Ft

$\sin 18° = \frac{7}{S}$

$S = \frac{7}{\sin 18°} = 22.652"$

= 1.887 Ft

$A = 1.5708(1.887)(8.166) =$

A = 24.20 Ft²

Wt @ 1" = 41.342 #/Ft²

Wt ≈ (41.342)(24.2) =

Wt ≈ 1000. #

TOTAL APPROX. WT.

1257 #

FORM (285)-47

SHELL TRANSITION EXTENSION

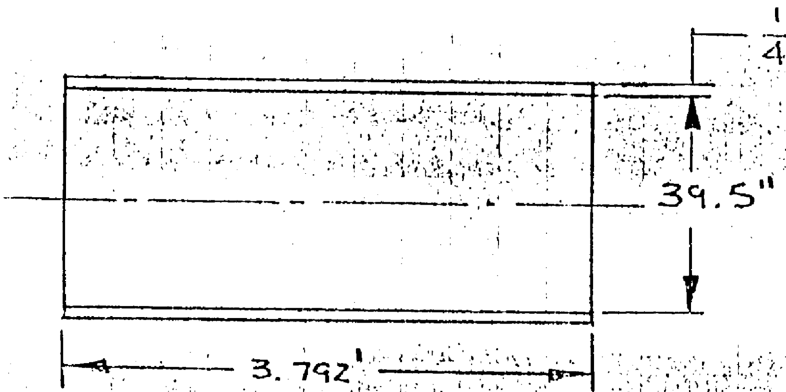

$C = \pi D = (3.1416)(3.312 \text{ Ft}) = 10.406 \text{ Ft}$

$A = L \times W = (10.406 \text{ Ft})(3.792 \text{ Ft}) = 39.459 \text{ Ft}^2$

$W_T @ \frac{1}{4}" = 10.336 \#/\text{Ft}^2$

$W_T = (10.336)(39.459) = \underline{408 \#}$

TIE ROD

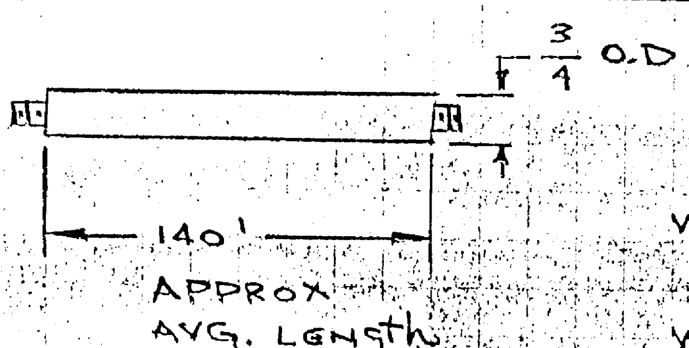

$W_T @ \frac{3}{4}" \text{DIA} = 1.51 \#/\text{Ft}$

$W_T = (1.51)(1.40)$

$= 2.11 \#/\text{Tie Rod}$

$W_T = 1,688 / 8 \text{ Tie Rods}$

FORM (285)-47

SHELL

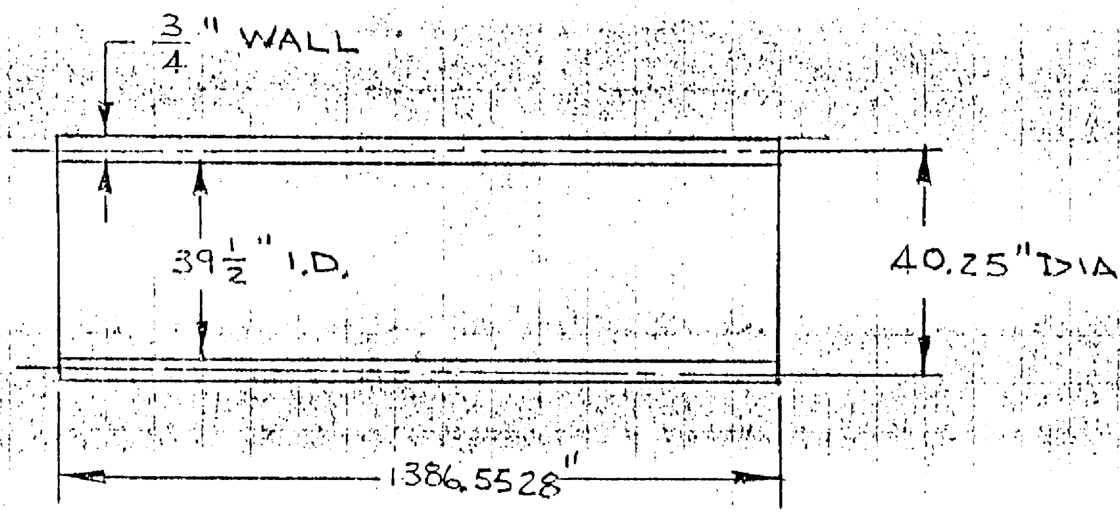

$C = \pi D = 3.1416\,(3.354') = 10.537$ Ft

$A = L \times W = 115.546$ Ft $\times$ 10.537 Ft

$A = 1217.51$ Ft^2

W_T @ 3/4" $= 31.007$ #/Ft^2

W_T (shell) $= (1217.51$ Ft$^2)(31.007$ #/Ft$^2)$

$= \underline{37{,}751\ \#}$

SHELL TRANSITION EXTENSION - 56" I.D.

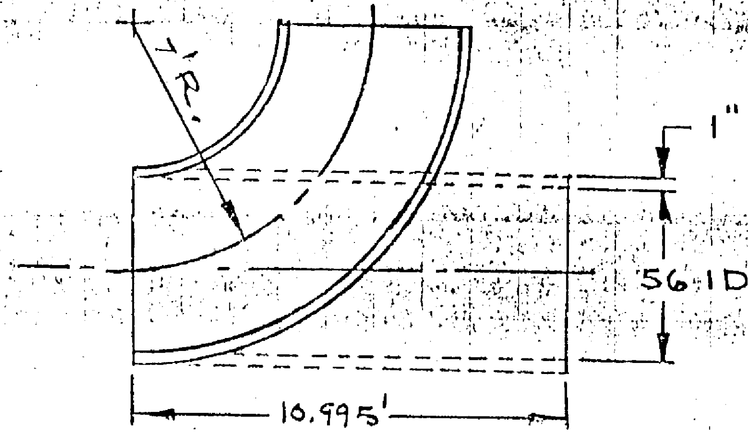

$C = \frac{\pi D}{4} = .7854\,D$

$= (.7854)(14\ Ft)$

$= 10.995$

$C = \pi D = 3.1416\left(\frac{57}{12}\right)$

$= 3.1416(4.75')$

$= 14.923\ Ft$

$A = L \times W = (14.923)(10.995)$

$= 164\ Ft^2$

W_T @ 1" $= 41.342\ \#/Ft^2$

$W_T = (41.342)(164)$

$= 6,780\ \#$

FORM (285).47

SHELL TRANSITION EXTENSION - 39½ I.D.

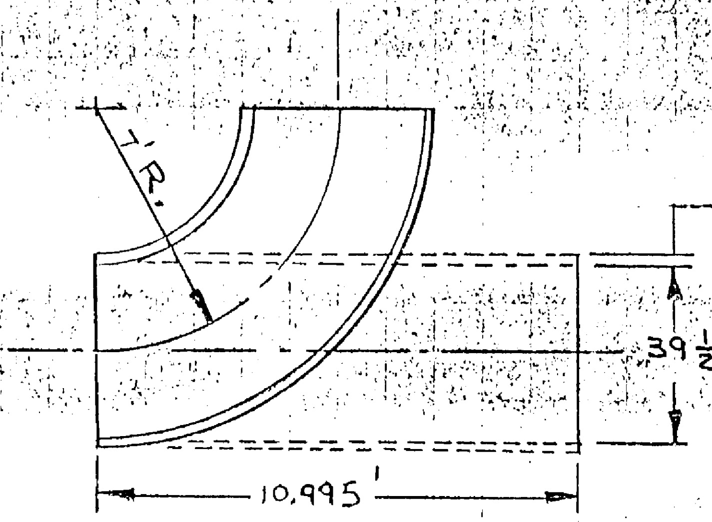

$$C = \frac{\pi D}{4} = .7854\, D = .7854\,(14') = 10.995'\ \text{Ft}$$

$$C = \pi D = 3.1416\,(3.311') = 10.40\ \text{Ft}$$

$$A = L \times W = (10.995)(10.40) = 114.35\ \text{Ft}^2$$

$$W_T @ \tfrac{1}{4}" = 10.336$$

$$W_T = (10.336)(114.35) = \underline{1{,}182^{\#}}$$

COVER PLATE

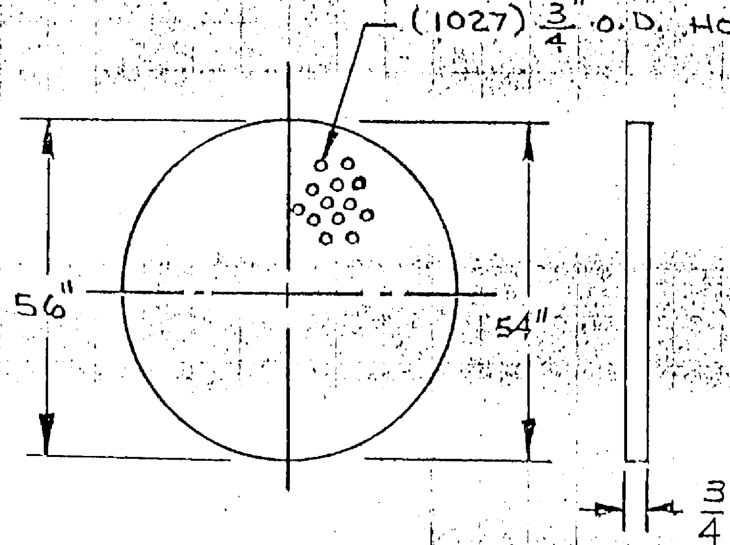

$A_{HOLE} = .7854\ D^2$

$= .7854\ (.0625\ Ft)^2$

$= .7854\ (.0039\ Ft)$

$= .0031\ Ft^2/HOLE$

$\therefore .0031 \times 1027$

$A_{HOLES} = 3.18\ Ft^2$

56" O.D.

$A = .7854\ D^2 = .7854\ (4.66')^2 = .7854\ (21.72\ Ft^2)$

$A = 17.06\ Ft^2$

$A_{TOTAL} = 17.06\ Ft^2 - 3.18\ Ft^2 = 13.88\ Ft^2$

W_T @ 3/4" = 31.007 #/Ft²

$W_T = (31.007\ \#/Ft^2)(13.88\ Ft^2) = \underline{430\ \#}$

54" O.D

$A = .7854\ D^2 = .7854\ (4.5\ Ft)^2 = .7854\ (20.25\ Ft^2)$

$A = 15.90\ Ft^2$

$A_{TOTAL} = 15.90\ Ft^2 - 3.18\ Ft^2 = 12.72\ Ft^2$

W_T @ 3/4" = 31.007 #/Ft²

$W_T = (31.007\ \#/Ft^2)(12.72\ Ft^2) = \underline{394\ \#}$

TUBE

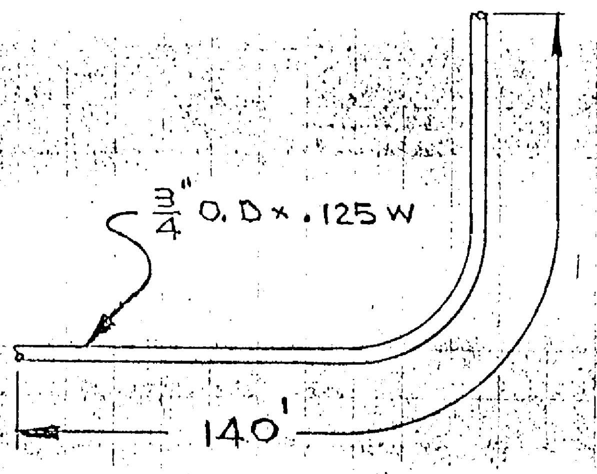

WT @ .120 WALL = .8074 #/Ft

WT = (.8074)(140)

= 113.04 # / TUBE

WT. TOTAL OF TUBES

≈ (113.04#)(1027 TUBES)

≈ 116,092 #

Tube SUPPORT PLATE (Solid)

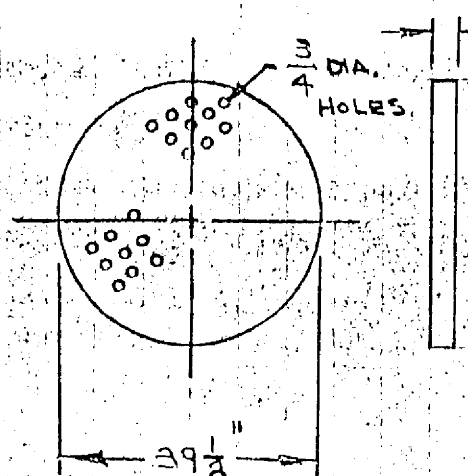

$A_{TS} = .7854\,(D^2)$

$A_{TS} = 8.35\ Ft^2$

TOTAL AREA = $A_{TUBE\ SHEET} - A_{HOLES}$

$A_H = .7854\,(D^2) = (.7854)(.0039)$

$= .0031\ Ft^2$/HOLE x 1027

$A_H = 3.18\ Ft^2$

$A_{TOTAL(TS)} = 8.35 - 3.18$

$= 5.17\ Ft^2$

WT @ 1" = 41.342 #/Ft²

WT = (5.17)(41.342)

= 214 # / TUBE SUPPORT

STRAIGHT STRIP TUBE SUPPORT

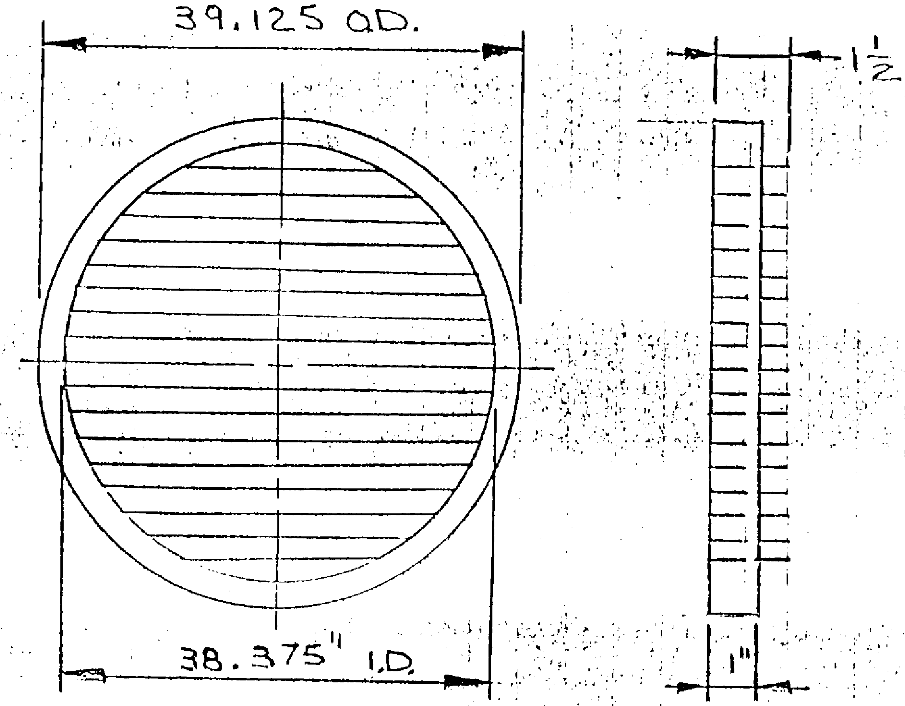

STRIP:

Length (AVG.) = 22.624

THICKNESS = .1875"

Width = 1.5"

$A_{(STRIP)} = L \times W$

$= (22.624)(1.5)$

$= 33.936 \text{ IN}^2$

or $\dfrac{33.936 \text{ IN}^2}{144 \frac{\text{IN}^2}{\text{Ft}^2}}$

$= .235 \text{ Ft}^2$

W_T @ $3/16 = 7.752$ #/Ft²

$W_T = (.235)(7.752)$

$= 2$ #/STRIP

20 STRIPS/HALF

40#/HALF

80# WHole

AREA OF RING

$A = .7854\,(D^2 - d^2)$

$= .7854\,(1530.76 \text{ IN}^2 - 1474.64 \text{ IN}^2)$

$= .7854\,(58.12)$

$= 45.647 \text{ IN}^2$ OR $\dfrac{45.647 \text{ IN}^2}{144 \frac{\text{IN}^2}{\text{Ft}^2}} = .317 \text{ Ft}^2$

$W_{T\,(Ring)}$ @ $1" = 41.342$ #/Ft²

$W_T = (41.342)(.317) = 13$ #

$W_{T\,(TOTAL)} = 93$ #

FORM (205)-47

OUTER TUBE

DESIGN TEMP.

S.S.	T.S.	
1150	700	IN
850	1000	OUT

$$\Delta t_m = \frac{\Delta t_b - \Delta t_a}{\ln(\Delta t_b / \Delta t_a)}$$

$\Delta t_a = 1150 - 1000 = 150$

$\Delta t_b = 850 - 700 = 150$

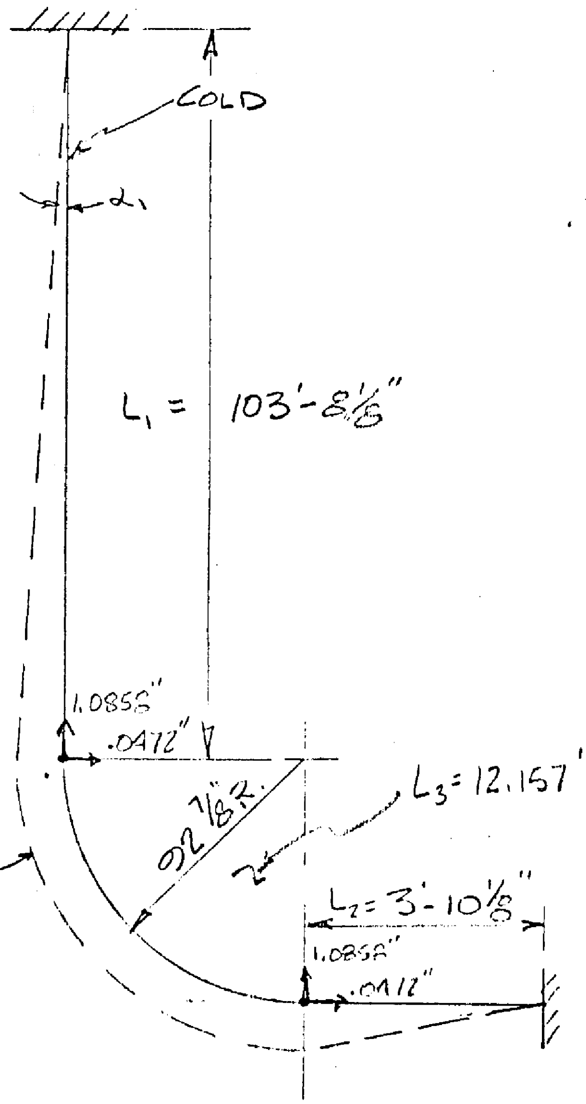

$$\Delta t_m = \frac{150 - 150}{\ln 150/150} \simeq \frac{0}{1}$$

SEE J. COX TAB. & GRAPH

HASTELLOY N TUBES & SHELL

$e\ (900 - 1150) = 7.43 \times 10^{-6}$ IN/IN/°F

TUBE EXPANSION

EACH BANK 5.7 FT LONG

SEE TAB. SHT FOR AVG ΔT FOR EACH BANK

$$7.43 \times 10^{-6} (5.7) = 4.235 \times 10^{-5}$$

BANK	AVG ΔT	EXP (FT $\times 10^{-5}$)		TOTAL EXP (IN.)
1	78.5	332.447		
2	83.35	352.987		
3	93.35	395.337		
4	103.7	439.169		
5	113.65	481.307		
6	123.0	520.905		
7	131.35	556.267		
8	137.65	582.947		
9	141.55	599.464		
10	143.0	605.605		
11	142.0	601.370		
12	138.75	587.606		
13	133.75	566.431		
14	127.65	540.597		
15	121.05	512.646		
16	114.45	484.695		
17	108.0	457.380		
18	101.95	BEND BEGINS 431.758	9.0189×10^{-2}	1.0858
19	96.9	410.371		
20	93.05	BEND ENDS 394.066	9.8533×10^{-2}	1.1824
** 21	93.05	394.066	10.2473×10^{-2}	1.2296

(1.0858 to 1.1824: .0966)

* NOTE 0 BANK @ T.S.
** NOT IN ORIG. CALCS

SP 18302A

FORM (285)

DISPLACEMENT

$$\cos \alpha_1 = \frac{103.677}{103.7675} = .99912$$

$\alpha_1 = 2^\circ - 24'$

$$x_1 = 103.677 \sin 2.4^\circ$$
$$x_1 = 3.799'$$

SINCE DISPLACEMENT X_1 HIGH ASSUME FLEXING IN L_2 SUFFICIENT FOR EXP. OF L_1 & FLEXING IN L_1 SUFFICIENT FOR EXP. OF L_2

TOTAL GROWTH BEND REGION

$$\Delta = .0966''$$

$$C_{COLD} = 2\pi R = 6.28(92.875) = 583.255''$$

$$C_{HOT} = 583.255 + 4(.0966) = 583.6414$$

$$R_{HOT} = \frac{583.6414}{2(3.14)} = 92.9365''$$

$$\Delta_R = 92.9365 - 92.875 = .0615''$$

CHECK ACTUAL DIFF. GROWTH OF INNER & OUTER TUBES

INNER $R_1 = 57\frac{7}{8}$

ASSUME $\Delta T = 95^\circ F$

OUTER $R_2 = 92\frac{7}{8}$

$C_1 = 363.455$ $\Delta L_1 = 7.13 \times 10^{-6}(95)(363.455)/4 = .064134$

$C_2 = 583.255$ $\Delta L_1 = 7.13 \times 10^{-6}(95)(583.255)/4 = .102922$

$$R_{1H} = \frac{C_{1H}}{2\pi} = \frac{363.711}{6.28} = 57.9158''$$ $\Delta_{R_1} = .0408$

$$R_{2H} = \frac{C_{2H}}{2\pi} = \frac{583.666}{6.28} = 92.9405''$$ $\Delta_{R_2} = .0655$

} .0247''

TUBE EXP. CONT'D

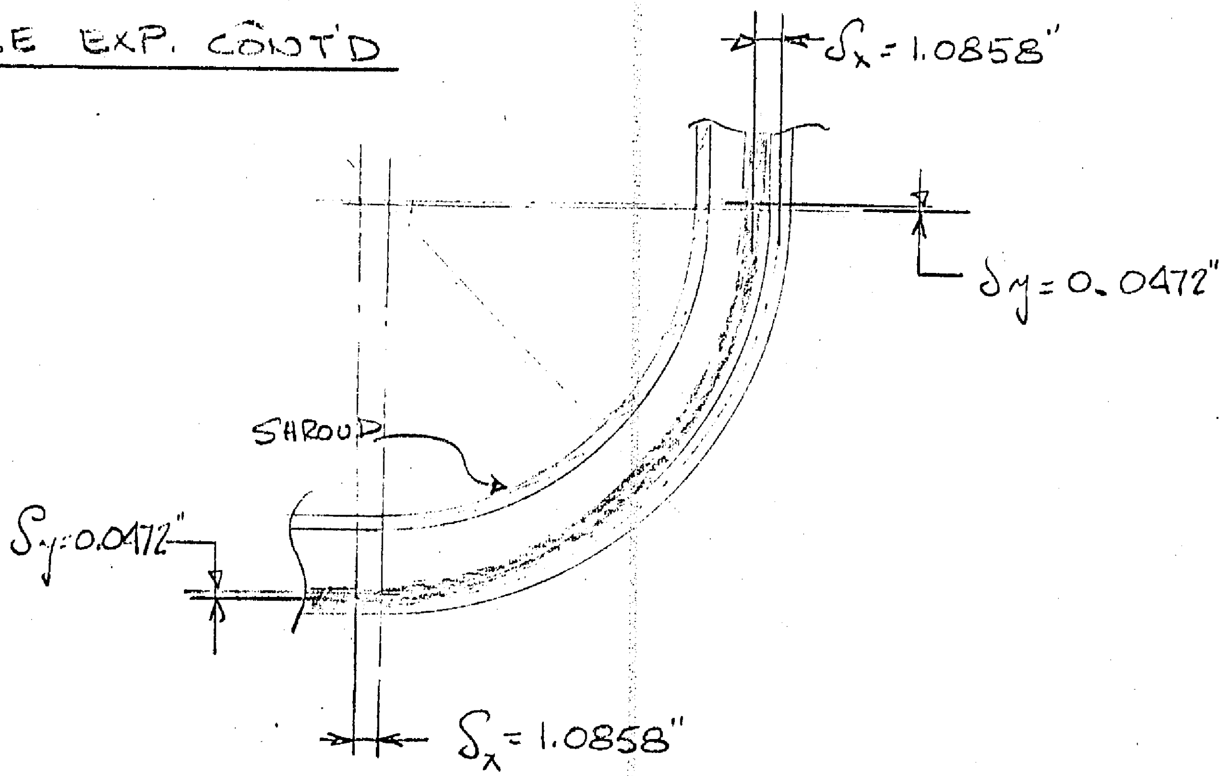

∴ UNLESS SHROUD IS MANUF. ECCENTRIC, THE MINIMUM CLEARANCE REQ'D = 1 1/16" FOR THE DIFF. EXP. OF TUBES VS SHELL.

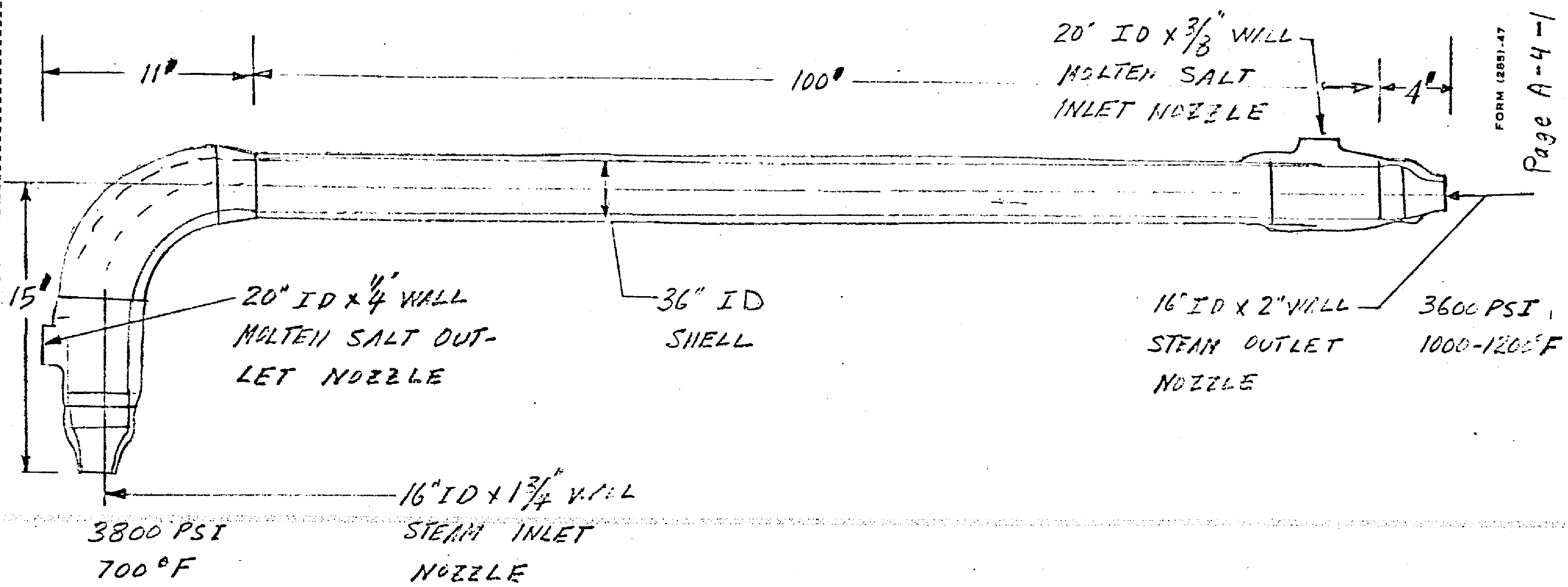

STEAM GENERATOR
GENERAL ARRANGEMENT
HOCKEY STICK DESIGN
MOLTEN SALT

$W_{MS} = 15.28 \times 10^6$ #/HR

$W_S = 2.517 \times 10^6$ #/HR

$V = \frac{W}{\rho A (3.6 \times 10^3)}$ [illegible]

ρ_S 34#/ft³ — 5#/ft³

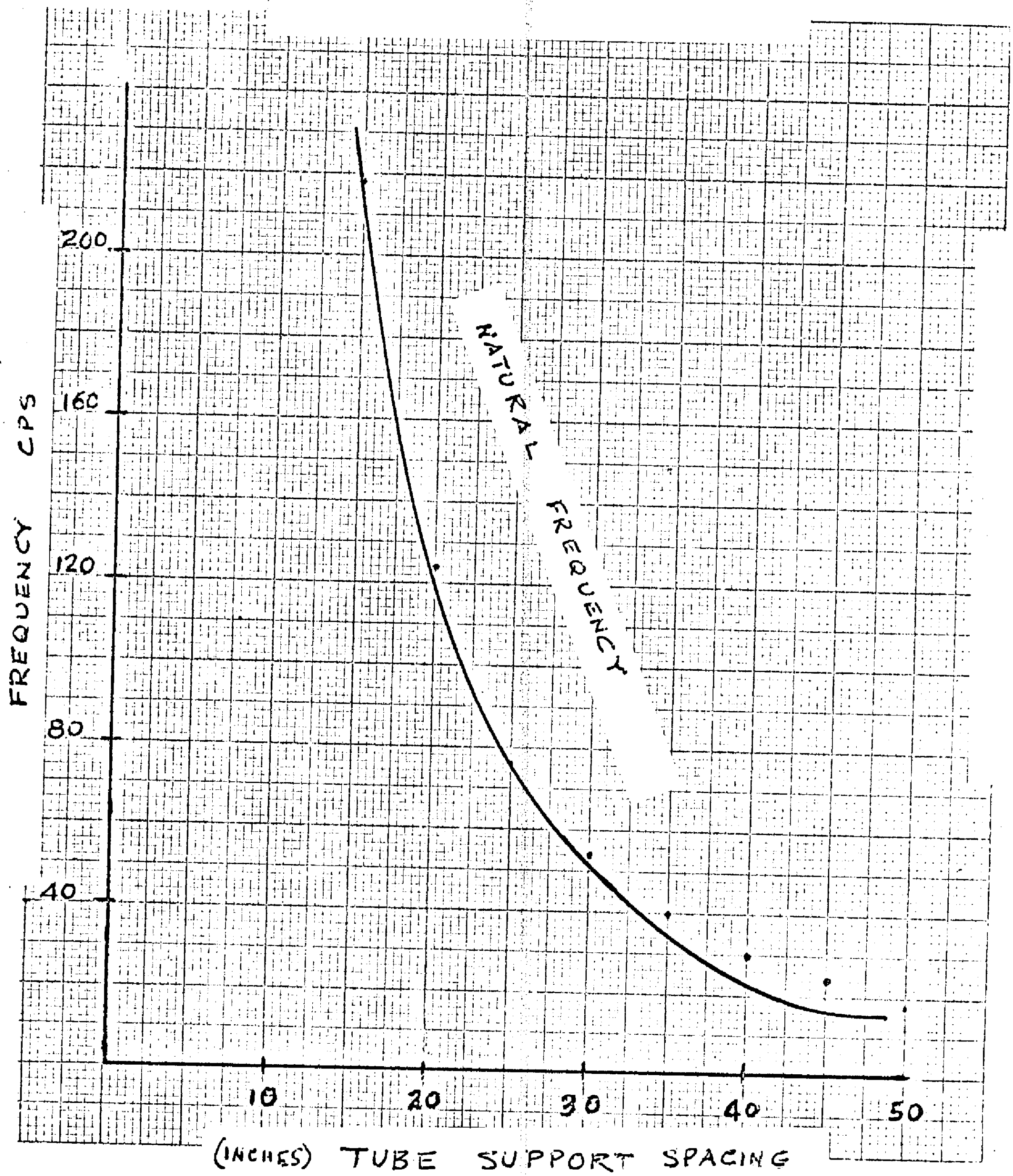
200
160
120
80
40
FREQUENCY CPS
NATURAL FREQUENCY
10
20
30
40
50
(INCHES) TUBE SUPPORT SPACING

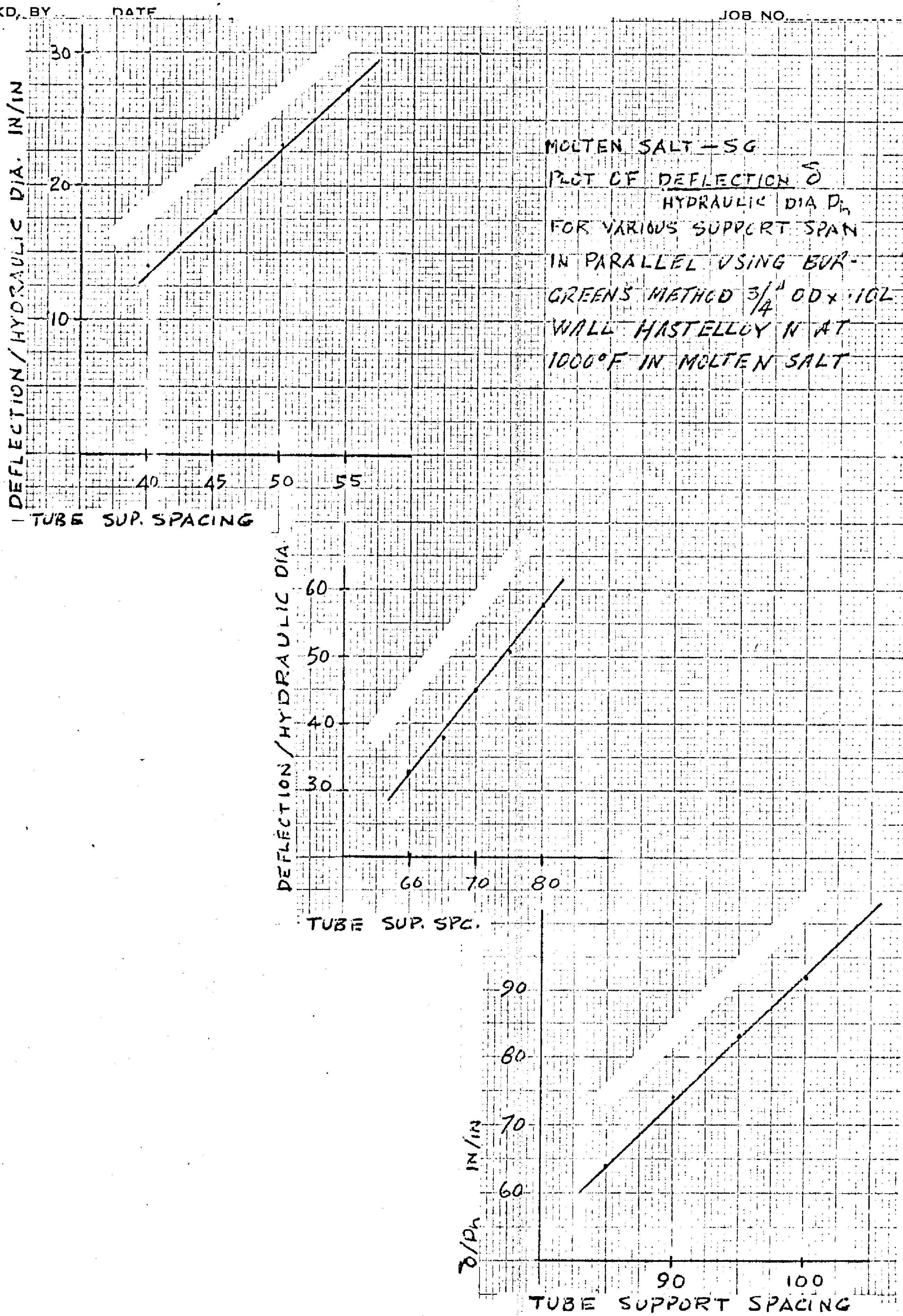
MOLTEN SALT — SG
PLOT OF DEFLECTION δ / HYDRAULIC DIA D_h
FOR VARIOUS SUPPORT SPAN
IN PARALLEL USING BURGREENS METHOD 3/4" OD × .102
WALL HASTELLOY N AT
1000°F IN MOLTEN SALT
DEFLECTION/HYDRAULIC DIA. IN/IN
30
20
10
40
45
50
55
TUBE SUP. SPACING
DEFLECTION/HYDRAULIC DIA
60
50
40
30
60
70
80
TUBE SUP. SPC.
δ/D_h IN/IN
90
80
70
60
90
100
TUBE SUPPORT SPACING

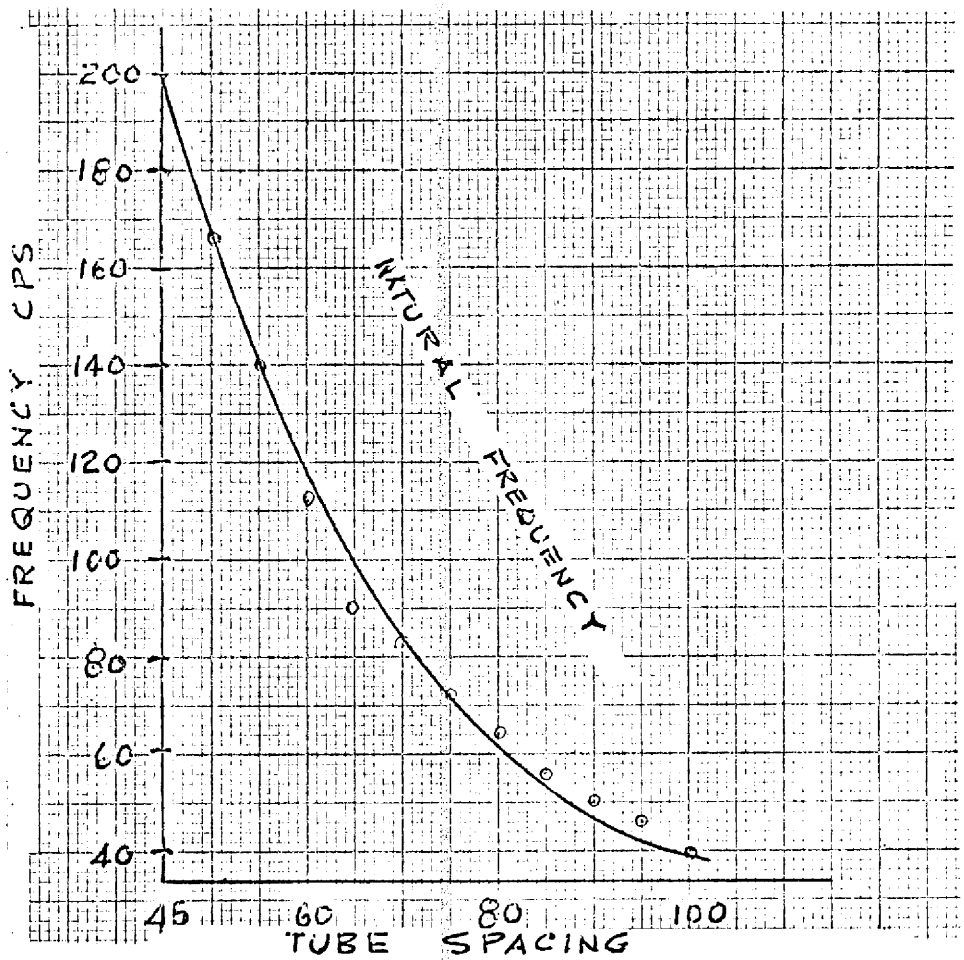
FREQUENCY CPS
200
180
160
140
120
100
80
60
40
45
60
80
100
TUBE SPACING
NATURAL FREQUENCY

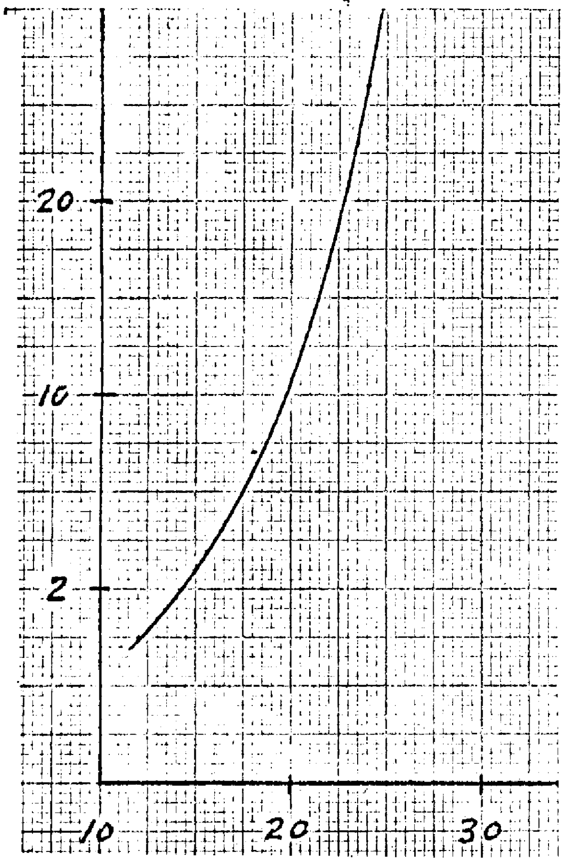

MOLTEN SALT - S G
PLOT OF DEFLECTION
δ/HYDRAULIC DIAMETER
D_L FOR VARIOUS SUP-
PORT SPAN IN PARAL-
LEL USING BURGREEN'S
METHOD AND 3/4" OD x
0.102" WALL HASTEL-
LOY N AT 1000°F
IN MOLTEN SALT

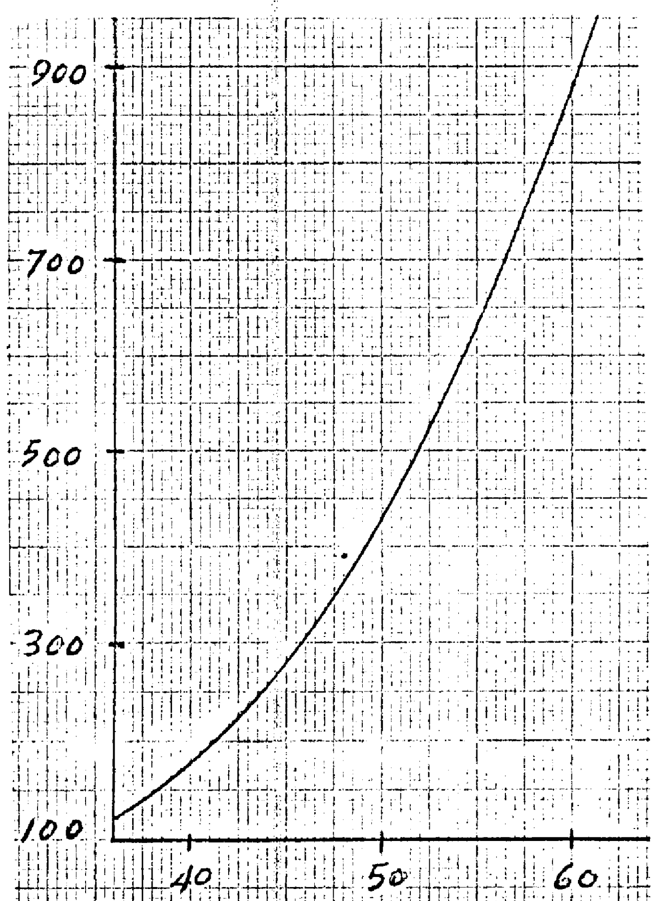

SP 16382A

FORM (285)-47

$$f_s = \frac{N_s V}{D_o}$$

$$f_s = \left(\frac{0.4}{.75/12}\right) V$$

$$f_s = 6.40\ V$$ (6.40 struck through, corrected to 4.80)

N_s = NON-DIMENSIONAL STROUHAL NUMBER

f_s = VORTEX SHEDDING FREQUENCY (CPS)

D_o = TUBE OUTSIDE DIAMETER (FT)

V = TRANSVERSE FLOW VELOCITY FT/SEC

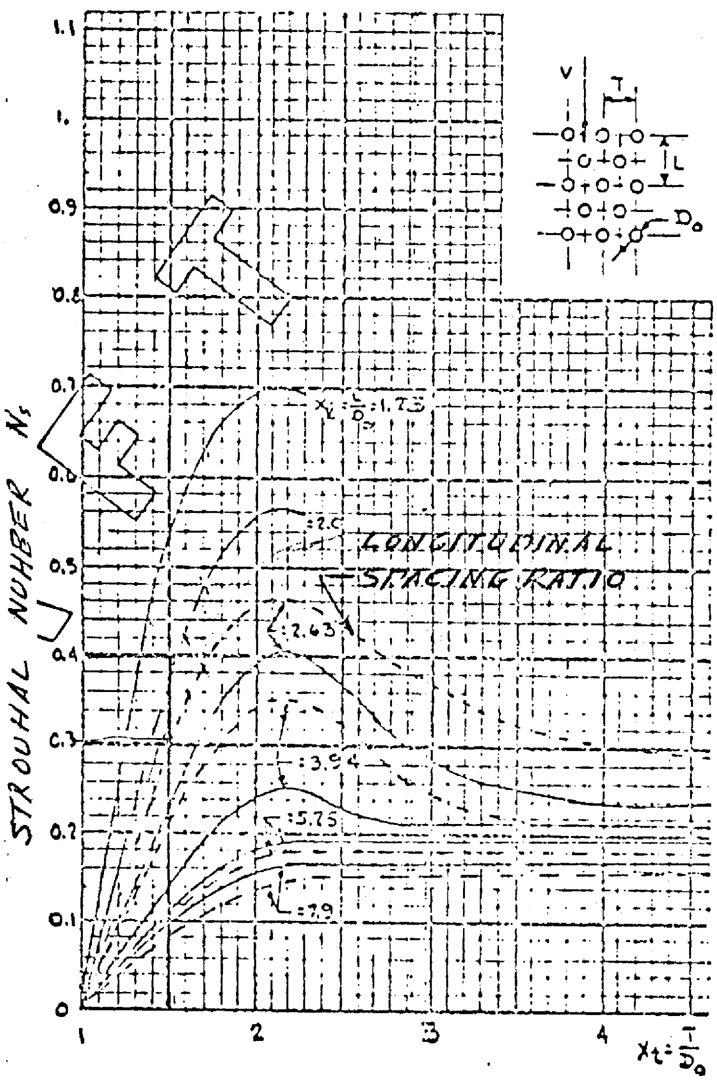

$$\chi_t = T/D_o = \frac{1.125}{0.75} = 1.50$$

$$\chi_l = L/D_o = 1.84/0.75 = 2.45$$

	f_s	N_s/D_o	V
24.0	32.0	~~6.40~~	5
48.0	64.0	4.80	10
72.0	96.0		15
96.0	128.0		20
120.0	160.0		25
144.0	192.0		30
168.0	224.0		35
192.0	256.0		40

$$f_s = \frac{N_s V}{D_o}$$

$$= \left(\frac{.03}{.75/12}\right) V$$

$$f_s = 4.8\ V$$

SP 10302A

FORM (285) 47

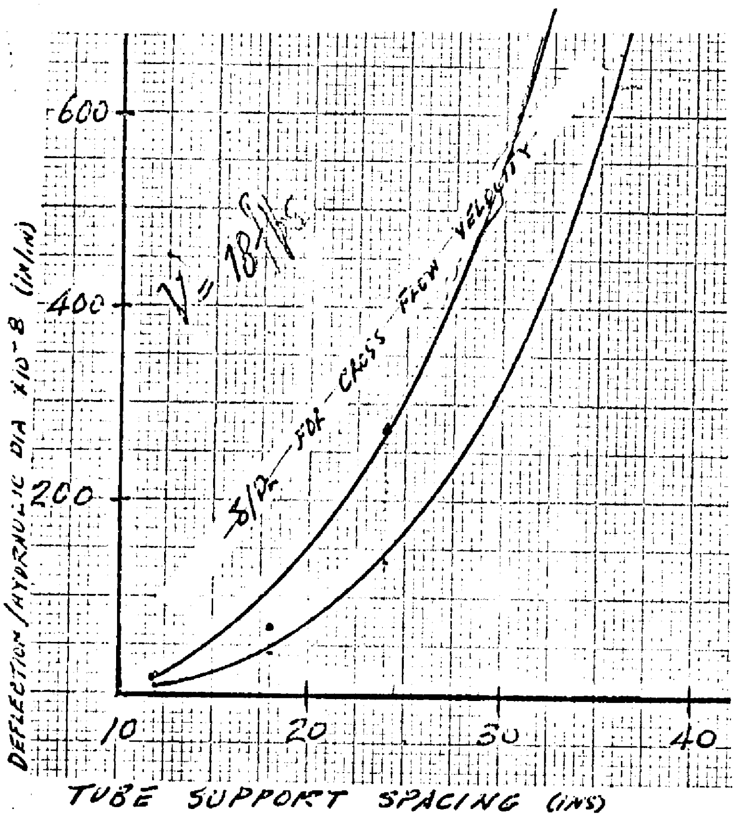

MOLTEN SALT - SG
PLOT OF DEFLECTION
δ/HYDRAULIC DIAMETER
D_h FOR VARIOUS SUPPORT
SPAN IN PARALLEL USING
BURGREEN'S METHOD AND 3/4"
OD × 0.102" WALL HASTEL-
LOY N AT 1000°F IN
MOLTEN SALT

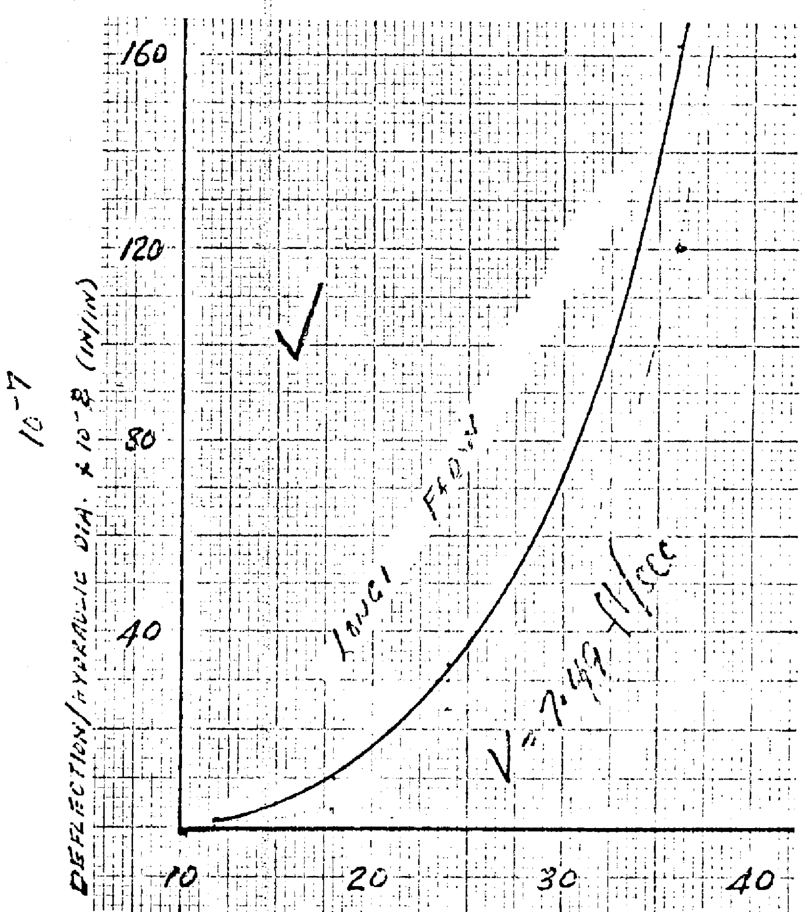

$$\left(\frac{\delta}{D_h}\right)^{1.3} = .83\times10^{-10} K_1 \, \Upsilon^{1/2} \Omega$$

FOR UNIFORM BEAM SIMPLY SUPPORTED $K_1 = 5$

$$\Upsilon = \frac{\rho V^2 L^4}{EI}$$

$$\Omega = \frac{\rho V^2}{\mu \omega}$$

$$= .83\times10^{-10} \times K_1 \left(\frac{\rho V^2 L^4}{EI}\right)^{\frac{1}{2}} \left(\frac{\rho V^2}{\mu \omega}\right)$$

$$\left[4.15\times10^{-10}\left(\frac{\rho^{3/2}}{\mu}\right)\left(\frac{1}{EI}\right)^{\frac{1}{2}} V^3\right]\frac{L^2}{\omega}$$

$$\left[4.15\times10^{-10}\left(\frac{120\sqrt{120}}{2.6}\right)\sqrt{\frac{1}{29.1\times10^4}}\,(1728)\right]\frac{L^2}{\omega} \checkmark$$

①	②	③	④	⑤	⑥	⑦	⑧
CROSS FLOW V	L	L^2	L^2/ω	f_n	$\omega = 2\pi f_n$	$\delta/D_n = C \cdot L^2/\omega$	C
12.0	12	144	0.066	347.0	2180	8.22×10^{-8}	1.245×10^{-6}
	18	324	0.334	154.0	970	41.58×10^{-8}	
	24	587	1.097	85.0	535	136.60×10^{-8}	
	36	1296	5.355	38.5	242	666.74×10^{-8}	
LONGITU. V							
7.49	12	144	0.066	347.0	2180	1.99×10^{-8}	0.3027×10^{-6}
	18	324	0.334	154.0	970	10.11×10^{-8}	
	24	587	1.097	85.0	535	33.21×10^{-8}	
	36	1296	5.355	38.5	242	162.10×10^{-8}	

1 DETERMINE TUBE VIBRATION FREQUENCY

1 $f_n = 4.944 \times 10^{-6} C \sqrt{\frac{EIg}{W_e L^4}}$

$W_e = W_t + W_c + W_a$

$f_n = 1/L^2 \cdot A$

$A = 4.944 \times 31.73 \times 1.96 \times 1.63 \times 10^2$
$= 5.0 \times 10^4$

C = TABULATED VALUE $\times 10^4$
E @ 1000°F = 26×10^6 PSI
I = INERTIA IN^4
g = 386 "/S
L = SPAN LENGTH BETWEEN SUPPORTS
W_t = TUBING WGT #/IN
W_c = INTERNAL FLUID WGT #/IN
W_a = EXTERNAL FLUID WGT #/IN

2 DETERMINE AVERAGE SHELL VELOCITY

2 $V = W / \rho A (3.6 \times 10^3)$

$= \left(\frac{15.28 \text{ \#/HR} \times 10^1}{1.2 \text{ \#/FT}^3 \times 3 \text{ FT}^2 \times 3.6 \text{ SEC/HR}} \right)$

$= 12.0$ FT/SEC

W = MASS FLOW RATE THRU. HEAT EXCHANGER SHELL #/HR
ρ = SHELL SIDE FLUID DENSITY #/FT³
A = MEAN CROSS FLOW AREA WITHIN TUBE BUNDLE BETWEEN BAFFLE WINDOWS FT²

3 DETERMINE VORTEX SHEDDING FREQUENCY

3 $f_s = N_s V / D_o$

0.3

$= \left(\frac{0.4 \times 12.0}{0.75/12} \right) =$ ~~77 C/S~~
57.6 C/S

N_s = NON-DIMENSIONAL STROUHAL NUMBER
f_s = VORTEX SHEDDING FREQUENCY C/S
V = TRANSVERSE FLOW VELOCITY FT/SEC

f_s VS $3 f_n$. ✓

SF 10302A

FORM (285)-47

$$\left(\frac{S}{l_k}\right)^{1.3} = .83\times10^{-10} K_1 \Upsilon^{\frac{1}{2}} \Omega$$

FOR UNIFORM BEAM
SIMPLY SUPPORTED
$K_1 = 5$

$$\Upsilon = \frac{\rho V^2 L^4}{EI} \qquad \Omega = \frac{\rho V^2}{\mu \omega}$$

$$= .83\times10^{-10} K_1 \left(\frac{\rho V^2 L^4}{EI}\right)^{\frac{1}{2}} \left(\frac{\rho V^2}{\mu \omega}\right)$$

$$\left[4.15\times10^{-10}\left(\frac{120\sqrt{120}}{2.6}\right)\left(\frac{1}{29.1}\times10^{-4}\right)^{\frac{1}{2}} \cdot V^3\right] \frac{L^2}{\omega}$$

$$= \left(4.15\times 5.0559\times 1.86\times 5.835\right) 10^{-8}$$

V (fps)	L (INS)	L^2 (IN²)	L^2/ω	f_n	$\omega = 2\pi f_n$	$\delta/l_k = C \cdot L^2/\omega$	C
18	12	144	0.066	347.0	2180.0	1.5×10^{-7}	2.265×10^{-6}
	18	324	0.334	154.0	970.0	7.50×10^{-7}	
	24	587	1.097	85.0	535.0	24.75×10^{-7}	
	36	1296	5.355	38.5	242.0	121.0×10^{-7}	
	48	2304	17.200	21.7	136.0	390.0×10^{-7}	
	60	3600	38.600	14.9	93.0	880.0×10^{-7}	

4.8
× 12
57.6
× 3
172.8

SP 16002A

FORM (285)-47

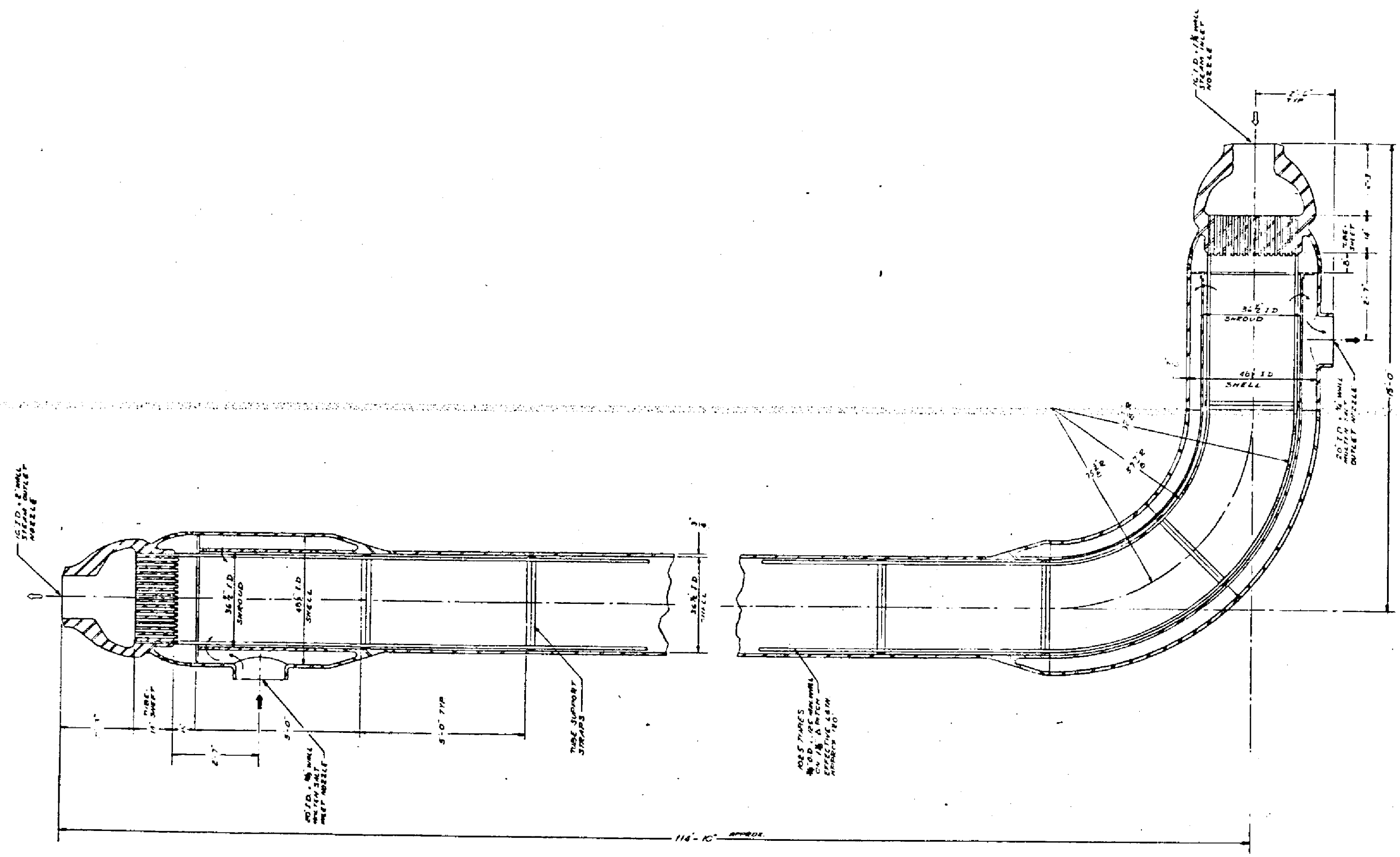

NOTES

REVISIONS

STEAM GENERATOR
GENERAL ARRANGEMENT
(HOCKEY STICK DESIGN)

MOLTEN SALT

ND-720-153

FOSTER WHEELER CORPORATION

DWG. NO.

BY Thomson DATE 5/1/72 SUBJECT TUBE BUNDLE OD VS TUBE QUANTITY FOR TUBES 3/4" TO 3" SIZE SHEET NO. 11 OF 12

CHKD. BY ______ DATE ______ JOB NO. ______

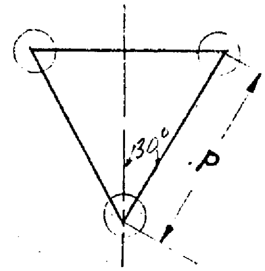

$P = 1.25\,D \qquad A = P(P \times .866) \qquad D^2\pi/4 = A$

$NA = (NP^2 \times .866) \qquad P = (D \times 1.25)^2 \times .866 \qquad D = (4/\pi\, A)^{\frac{1}{2}}$

$\text{TUBE BUNDLE DIA} = 1.05\left[N \times .866\,(1.25D)^2\, 4/\pi\right]^{\frac{1}{2}}$

$= 1.05\,N^{\frac{1}{2}} + 1.45\,D$

D	N	$N^{\frac{1}{2}}$	1.45 D	TUBE BUNDLE OD
3/4"	400	20.00	1.09	23.90
	800	28.25		32.60
	1200	34.60		39.00
	1600	40.00		46.00
	2000	45.25		52.00
1"	400	20.00	1.45	30.60
	800	28.25		42.75
	1200	34.60		53.00
	1600	40.00		61.00
	2000	45.25		69.00
1.25"	400	20.00	1.82	38.50
	800	28.25		53.00
	1200	34.60		66.00
	1600	40.00		76.50
	2000	45.25		86.50
1.50"	400	20.00	2.18	45.60
	800	28.25		64.50
	1200	34.60		79.50
	1620	40.00		91.20
	2000	45.25		104.00
2"	400	20.00	2.90	61.00
	800	28.25		86.00
	1200	34.60		106.00
	1600	40.00		122.00
	2000	45.25		138.00
3"	400	20.00	4.35	91.00
	800	28.25		128.00
	1200	34.60		159.00
	1600	40.00		182.00
	2000	45.25		207.00

SP 18382A FORM (285).47

TUBE BUNDLE OD VS TUBE QUANTITY FOR TUBES 3/4" TO 3" SIZE

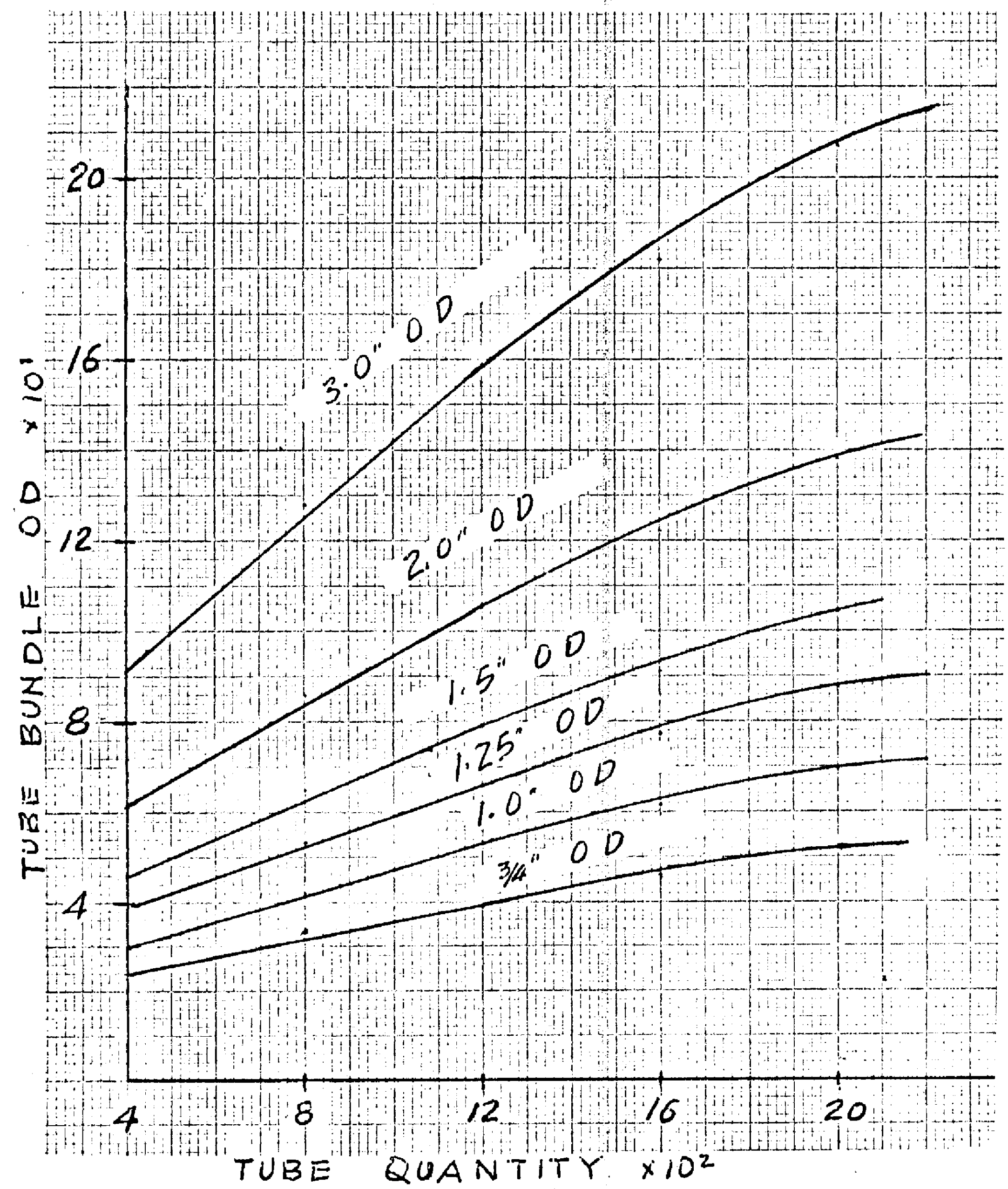

APPENDIX B

Thermal/Hydraulic Calculations

Contents:

B - 1

Objective : Calculate the inlet steam side pressure drop through nozzle and tube sheet at 100, 80, 60, 40 and 20% load conditions

Reference : (1) Engineering Department Manual, Volume I. FWC

(2) Thermal hydraulic performance computer code output

(3) Steam Generator General Arrangement,

Drawing no. ND-720-153 B. FWC

(4) 1967 ASME Steam Tables

(I) 100% load

Flow rate $\dot{m} = 2.538 \times 10^6$ lb/hr

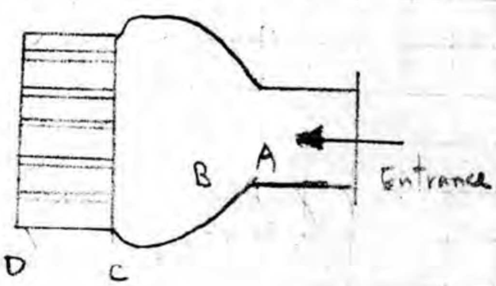

From computer code output, the temperature and pressure at point D are

$T_D = 700°F$

$P_D = 3568.8671$ psia

(a) ΔP at tube sheet

The length of tube sheet $L = 15.5'' = 1.2917$ ft

Flow cross section area $A = 1000 \times \frac{1}{4}\pi \left(\frac{0.4823}{12}\right)^2 = 1.2698$ ft^2

mass velocity $G = \frac{\dot{m}}{A} = \frac{2.538 \times 10^6}{1.2698} = 1998739.96$ lb/ft^2-hr

$= 555.2055$ lb/ft^2-sec.

FORM (203)-47

$\mu = 0.1261 \ lb/hr\text{-}ft$

$$R_e = \frac{GD}{\mu} = \frac{1998139.96 \times \frac{0.4825}{12}}{0.1261} = 637319.61$$

relative roughness $\frac{\varepsilon}{D} = \frac{0.00006}{0.4825} = 0.0001244$

From Moody's diagram $f = 0.0145$

Assume $P_c = 3769.3240$ psia

$T_c = 700°F$

$\therefore v_c = 0.0295 \ ft^3/lb$

$$\Delta P_f = f \frac{G^2}{2g} v \frac{L}{D}$$

$$= 0.0145 \times \frac{555.2055^2}{2 \times 32.2} \times 0.0295 \times \frac{1.2917}{\frac{0.4825}{12} \times 144}$$

$= 0.4569$

$\therefore P_c = 3768.8671 + 0.4569 = 3769.3240$ psia

$T_c = 700°F$

$v_c = 0.0295$

(b) Sudden Contraction

$A_2 = 1.2698 \ ft^2$

$A_1 = \frac{1}{4}\pi \left(\frac{42}{12}\right)^2 = 9.6211 \ ft$ $\qquad \frac{A_2}{A_1} = 0.1320$

FORM (288)-47

$$K_2 = 1.5 - 0.648\left(\frac{A_2}{A_1}\right) - 0.852\left(\frac{A_2}{A_1}\right)^2 \quad \text{(Ref. 1)}$$

$$= 1.5 - 0.648 \times 0.1320 - 0.852 \times 0.1320^2$$

$$= 1.3996$$

$$\Delta P_b = K_2 \cdot (V_h)_2$$

$$= 1.3996 \times \frac{1}{2g} V_c \, G^2$$

$$= 1.3996 \times \frac{1}{64.4} \times 0.0295 \times 555.2055^2 \times \frac{1}{144}$$

$$= 1.3724$$

$$\therefore \quad P_B = 3769.3240 + 1.3724 = 3770.6964 \text{ psia}$$

$$T_B = 700°F$$

(C) Sudden Expansion

$$A_1 = \frac{\pi}{4}\left(\frac{16}{12}\right)^2 = 1.3963 \text{ ft}^2$$

$$A_2 = 9.6211 \text{ ft}^2$$

$$N_2 = 2\left[1 - \frac{A_2}{A_1}\right] = 2\left[1 - \frac{9.6211}{1.3963}\right] = -11.7808$$

$$G_B = \frac{\dot m}{A_B} = \frac{2.538 \times 10^6}{9.6211 \times 3600} = 73.2764 \text{ lb/ft}^2\text{-sec}$$

$$\Delta P_c = N_2 (V_h)_2$$

$\therefore \Delta P_b = -1178.8 \times \frac{1}{64.4} \times 0.0295 \times (73.2764)^2 \times \frac{1}{144} = -0.2012$

$P_A = 3770.6964 - 0.2012 = 3770.4952$ psia

(D) Nozzle Inlet

$G = \frac{2.538 \times 10^6}{1.3963} = 1817660.96 \ \frac{lb}{hr \cdot ft^2}$

$= 504.9058 \ \frac{lb}{ft^2 \ sec}$

$Re = \frac{GD}{\mu} = \frac{1817660.96 \times \frac{16}{12}}{0.1261} = 1.922 \times 10^7$

$\frac{\varepsilon}{D} = \frac{0.00015}{16/12} = 0.0001375$

$f = 0.008$

$\Delta P_f = 0.008 \times \frac{504.9058^2}{64.4} \times 0.0295 \times \frac{1}{1.3333 \times 144} = 0.0049$

$\therefore$ Pressure at entrance $= 3770.4952 + 0.0049 = 3770.5001$

Total pressure drop $= 3770.5001 - 3768.8671$

$= 1.633$ psi ✱

(II) 80% Load

$\dot{m} = 2030400 \ lb/hr$

$T_D = 700°F$

$P_D = 3714.4229 \ psia$

$V_D = 0.0299 \ ft^3/lb$

(a) ΔP at tube sheet

$L = 1.2917 \ ft$

$$G = \frac{2030400}{1.2698} = 1598991.97 \ lb/ft^2\text{-}hr$$

$$= 444.16 \ lb/ft^2\text{-}sec$$

$$\mu = 10.8 \times 10^{-7} \times 115826.575 = 0.1251 \ lbm/hr\text{-}ft$$

$$Re = \frac{1598991.97 \times \frac{0.4825}{12}}{0.1251} = 513931.27$$

$\frac{\varepsilon}{D} = 0.0001244$

$f = 0.0149$

$$\Delta P_f = 0.0149 \times \frac{444.16^2}{64.4} \times 0.0299 \times \frac{1.2917}{\frac{0.4825}{12} \times 144} = 0.2984$$

$$\therefore P_c = 3714.4229 + 0.2984 = 3714.7213 \ psia$$

(b) Extraction

$K_2 = 1.3956$

$\Delta P_b = 1.3956 \times \frac{1}{64.4} \times 0.0297 \times 444.16^2 \times \frac{1}{144} = 0.8843$

$P_B = 3714.7213 + 0.8843 = 3715.6056$

(c) Expansion

$N_2 = -11.7808$

$G_B = \frac{2030400}{9.6211 \times 3600} = 58.6212$

$\Delta P_b = -11.7808 \times \frac{1}{64.4} \times 0.0297 \times (58.6212)^2 \times \frac{1}{144} = -0.1297$

$P_B = 3715.6056 - 0.1297 = 3715.4759$

(D) Nozzle inlet

$G = \frac{2030400}{1.3963} = 1454128.77 \ lb/ft^2\text{-}hr$

$= 403.92 \ lb/ft^2\text{-}sec$

$Re = \frac{1454128.77 \times \frac{16}{12}}{0.1251} = 15498308.23$

$\frac{\varepsilon}{D} = 0.0001375$, $f = 0.0083$

FORM (2851)-4

$$\Delta P_f = 0.0083 \times \frac{403.92^2}{64.4} \times 0.0297 \times \frac{1}{1.3333 \times 144} = 0.0033$$

$$\therefore P_{Entrance} = 3715.4759 + 0.0033 = 3715.4792$$

$$\text{Total Pressure Drop} = 3715.4792 - 3714.4229$$

$$= 1.0563 \quad //$$

(III) 60% Load

$m = 1522800$ lb/hr

$T_D = 700\ °F$

$P_D = 3673.1113$

$v_D = 0.0299$ ft³/lbm

$\mu = 10.6 \times 10^{-7} \times 115826.575 = 0.1228$ lb/hr-ft

(a) ΔP at tube sheet

$$G = \frac{1522800}{1.2698} = 1199243.98 \text{ lb/ft}^2\text{-hr}$$

$$= 333.12 \text{ lb/ft}^2\text{-sec}$$

$$Re = \frac{1199243.98 \times \frac{0.4825}{12}}{0.1228} = 392667.77$$

$$\frac{\varepsilon}{D} = 0.0001244$$

FORM (2851-47)

$\therefore f = 0.015$

$$\Delta P_f = 0.015 \times \frac{333.12^2}{64.4} \times 0.0299 \times \frac{1.2917}{\frac{0.4825}{12} \times 144} = 0.1724$$

$\therefore P_C = 3673.2837$ psia

(b) Contraction

$$\Delta P_b = 1.3996 \times \frac{1}{64.4} \times 0.0299 \times 333.12^2 \times \frac{1}{144} = 0.5008$$

$\therefore P_B = 3673.7845$ psia

(c) Expansion

$$G_{TB} = \frac{1522800}{9.6211 \times 3600} = 43.9659$$

$$\Delta P_b = -11.7808 \times \frac{1}{64.4} \times 0.0299 \times 43.9659^2 \times \frac{1}{144} = -0.0734$$

$P_A = 3673.7111$ psia.

(D) Nozzle inlet

$$G_T = \frac{1522800}{1.3963} = 1090586.58 \ \ lb/ft^2\text{-}hr$$

$$= 302.9435 \ \ lb/ft^2\text{-}sec$$

$$Re = \frac{1090586.58 \times \frac{16}{12}}{0.1228} = 11841439.52$$

FORM (208)-47

$\frac{\varepsilon}{D} = 0.0085$

$\Delta P_f = 0.0085 \times \frac{302.8435^2}{64.4} \times 0.0299 \times \frac{1}{1.3333 \times 144} = 0.0019$

$P_{entrance} = 3673.7130$ psia

Total Pressure Drop $= 3673.7130 - 3673.1113$

$= 0.6017$ psi

(IV) 40% Load

$\dot{m} = 1015200$ lb/hr

$P_D = 3639.4411$ psia

$T_D = 700$ F

$v_D = 0.0300$ ft³/lb

$\mu = 0.1216$ lb/hr-ft

(a) ΔP at tube sheet

$G_T = \frac{1015200}{1.2698} = 799485.9856$ lb/ft²-hr

$= 222.0822$ lb/ft²-sec.

$R_e = \frac{799485.9856 \times \frac{0.485}{12}}{0.1216} = 264361.85$

FORM (285)-47

$\frac{\epsilon}{D} = 0.0001244$

$f = 0.0162$

$\Delta P_f = 0.0162 \times \frac{222.0822^2}{64.4} \times 0.03 \times \frac{1.2917}{\frac{0.4825}{12} \times 144} = 0.0830$

$\therefore P_c = 3639.5241$ psia

(b) Contraction

$\Delta P_b = 1.3996 \times \frac{1}{64.4} \times 0.03 \times 222.0822^2 \times \frac{1}{144} = 0.2233$

$\therefore P_B = 3639.7474$ psia

(c) Expansion

$G_{TB} = \frac{1015200}{9.6211 \times 3600} = 29.3106$

$\Delta P_b = -11.7808 \times \frac{1}{64.4} \times 0.03 \times 29.3106^2 \times \frac{1}{144} = -0.0327$

$\therefore P_A = 3639.7147$ psia

(D) Nozzle inlet

$G = \frac{1015200}{1.3963} = 727064.38 \quad lb/ft^2\text{-}hr$

$= 201.9623 \quad lb/ft^2\text{-}sec.$

$$Re = \frac{727064.38 \times \frac{16}{12}}{0.1216} = 7972197.15$$

$$\frac{\varepsilon}{D} = 0.0000375$$

$$f = 0.0089$$

$$\Delta P_f = 0.0089 \times \frac{20.9623^2}{64.4} \times 0.03 \times \frac{1}{1.3333 \times 144} = 0.0009$$

$$P_{entrance} = 3639.7156 \text{ psia}$$

Total pressure Drop = 0.2745 psi

(V) 20% Load

$\dot{m} = 507600$ lb/hr

$P_o = 3615.4303$ psia

$T_o = 700°F$

$v_p = 0.0301$ ft³/lb

$\mu = 0.1216$ lb/ft-hr

(a) ΔP at tube sheet

$$G_T = \frac{507600}{1.2618} = 399742.9918 \; \text{lb/ft}^2\text{-hr}$$

$$= 111.0411 \; \text{lb/ft}^2\text{-sec}$$

$$Re = \frac{399742.9318 \times \frac{0.4825}{12}}{0.1216} = 132180.9252$$

$$\frac{\varepsilon}{D} = 0.0001244$$

$$f = 0.018$$

$$\Delta P_f = 0.018 \times \frac{111.0411^2}{64.4} \times 0.0301 \times \frac{1.2917}{\frac{0.4825}{12} \times 144} = 0.0231$$

$$P_c = 3615.4534 \text{ psia}$$

(b) Contraction

$$\Delta P_b = 1.3996 \times \frac{1}{64.4} \times 0.0301 \times 111.0411^2 \times \frac{1}{144} = 0.0560$$

$$P_B = 3615.5094 \text{ psia}$$

(c) Expansion

$$G_B = \frac{507600}{9.6211 \times 3600} = 14.6553$$

$$\Delta P_b = -11.7808 \times \frac{1}{64.4} \times 0.0301 \times 14.6553^2 \times \frac{1}{144} = -0.0082$$

$$P_A = 3615.5012 \text{ psia}$$

(D) Nozzle inlet

$$G = \frac{507600}{1.3963} = 363532.1922 \ \text{lb/ft}^2\text{-hr} = 100.9812 \ \text{lb/ft}^2\text{-sec}$$

FORM (2851)-47

$$R_e = \frac{363552.1922 \times \frac{16}{12}}{0.1216} = 3986098.599$$

$$\frac{\varepsilon}{D} = 0.0000575$$

$$f = 0.0095$$

$$\Delta P_f = 0.0095 \times \frac{100.3812^2}{64.4} \times 0.0501 \times \frac{1}{1.3333 \times 144} = 0.0002$$

$$P_{entrance} = 3615.5014 \text{ psia}$$

Total Pressure Drop = 0.0711 psi

FORM (285)-47

B-2

Objective: Calculate the outlet steam side pressure drop through noz and tube sheet at 100, 80, 60, 40 and 20% load conditions

Reference:
(1) Engineering Department Manual, Volume I, FWC
(2) Thermal hydraulic performance computer code output
(3) Steam Generator General Arrangement Drawing No: ND-720-153 B FWC
(4) 1967 ASME Steam Tables

(I) 100 % Load

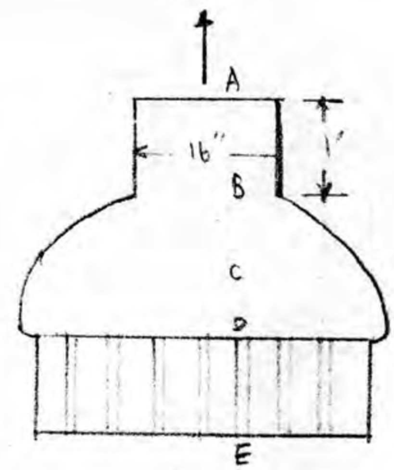

(a) ΔP at Exit nozzle ΔP_{A-B}

$P_A = 3000$ psia, $T_A = 1000\,°F$

$v_A = 0.1996\ ft^3/lb$

$\mu_A = 0.0818\ lb/hr\text{-}ft$

roughness (absolute) = 0.00006 in

$D_A = 16/12 = 1.3333$ ft

$\frac{\varepsilon}{D_A} = 0.0000375$

Area at A = $A_A = 1.3963\ ft^2$

$L_A = 1$ ft

FORM 1283

$\dot{m} = 2.538 \times 10^{6}$ lb/hr

$G_{B} = \frac{2.538 \times 10^{6}}{1.3963} = 1817660.96$ lb/hr-ft²

$= 504.9058$ lb/ft²-sec

$R_e = \frac{GD}{\mu} = 2.9896 \times 10^{7}$

$f = 0.007$

$\Delta P_f = \frac{fL}{D} \frac{1}{2g} v G^2$

$= \frac{0.007 \times 1}{1.3333} \times \frac{1}{64.4} \times 0.1996 \times 504.9058^2 \times \frac{1}{144} = 0.0288$

Due to change of elevation $\Delta P_g = \frac{1}{0.1996 \times 144} = 0.0348$

$\therefore \Delta P_{A\text{-}B} = 0.0288 + 0.0348 = 0.0636$

$\therefore P_B = 3600.0636$

$T_B = 1000°F$

$v_B = 0.1996$

(b) Extraction $\Delta P_{B\text{-}C}$

$A_C = 9.6211$ ft²

$\Delta P_{B\text{-}C} = N_2 (V_h)_2$

$N_2 = 1.5 - 0.648 \left[\frac{A_2}{A_1} \right] - 0.852 \left[\frac{A_2}{A_1} \right]^2$

$\frac{A_2}{A_1} = \frac{A_B}{A_C} = \frac{1.3963}{9.6211}$

FORM (285)

$K_2 = 1.3880$

$\Delta P_{B-C} = 1.3880 \times \frac{1}{64.4} \times 0.1996 \times 504.9058^2 \times \frac{1}{144} = 7.3416$

$P_C = 3600.0636 + 7.3416 = 3607.4052$

$T_C = 1000°F$

$\rho_C = 0.1991$

(c) Expansion ΔP_{C-D}

$G_C = \frac{2.538 \times 10^6}{9.6211 \times 3600} = 73.2764 \ lb/ft^2\text{-}sec$

$A_D = 1.2698 \ ft^2$

$\Delta P_{C-D} = K_2 \cdot (VH)_C$

$K_2 = 2\left[1 - \frac{A_2}{A_1}\right]$

$= 2\left[1 - \frac{A_C}{A_D}\right] = 2\left[1 - \frac{9.6211}{1.2698}\right] = -13.1537$

$\Delta P_{C-D} = -13.1537 \times \frac{1}{64.4} \times 0.1991 \times (73.2764)^2 \times \frac{1}{144} = -1.5164$

$\therefore \quad P_D = 3607.4052 - 1.5164 = 3605.8888$

$\rho_D = 0.1912$

(d) ΔP_{D-E} at Tube inlet

$A_{DE} = 1.2919 \ ft^2$

FORM (285)

$G_p = 1998739.96 \ \frac{lb}{ft^2\,hr}$

$= 555.2055 \ \frac{lb}{ft^2\text{-}sec}$

$D = 0.4825 = 0.0402 \ ft$

$\mu = 0.08108 \ \frac{lb}{hr\text{-}ft}$

$Re = \frac{G\,D}{\mu} = \frac{1998739.96 \times 0.0402}{0.08108} = 990988.49$

$\frac{\varepsilon}{D} = \frac{0.000005}{0.0402} = 0.0001244$

$f = 0.0137$ Assume $P_E = 3608.8699 \ \therefore v_E = 0.1990$ $v = \frac{1}{2}(0.1990 + 0.1992) = 0.1991$

$\therefore \Delta P_f = 0.0137 \times \frac{1.2917}{0.0402} \times \frac{1}{64.4} \times 0.1991 \times (555.2055)^2 \times \frac{1}{144} = 2.9133$

$\Delta P_g = \frac{1.2917}{0.1991 \times 144} = 0.0451$

ΔP_a = acceleration ΔP

$\Delta P_a = \frac{(0.1992 - 0.1990) \times \frac{555.2055^2}{64.4} \times 3}{144} = 0.0199$

$\therefore \Delta P = 2.9133 + 0.0451 + 0.0199 = 2.9783$

$P_E = 3605.8888 + 2.9783 = 3608.8671$ psia.

$T_E = 100 \ F$

$v_E = 0.1990$

Total pressure drop $\rightarrow \Delta P_{Total} = 3608.8671 - 3600$

$= 8.8671$ psi

#

(2) 80% Load

a. ΔP at Exit Nozzle ΔP_{A-B}

$P_A = 3600$ psia

$T_A = 1066$ °F

$v_A = 0.2169$ ft^3/lb

$\mu_A = 0.08455$ $lb/hr\text{-}ft$

$\dot{m} = 1885730$ lb/hr

$$G_A = \frac{1885730}{1.3963} = 1350519.23 \ lb/ft^2\text{-}hr$$

$$= 375.1442 \ lb/ft^2\text{-}sec$$

$$Re = \frac{1350519.23 \times 1.3333}{0.08455} = 2.1297 \times 10^7$$

$$\frac{\varepsilon}{D} = 0.0000375$$

$f = 0.0096$

$$\Delta P_f = \frac{0.0096 \times 1}{1.3333} \times \frac{1}{64.4} \times 0.2169 \times 375.1442^2 \times \frac{1}{144} = 0.0188$$

$$\Delta P_v = \frac{1}{0.2169 \times 144} = 0.0320$$

$\Delta P_a = 0$

$\Delta P = 0.0188 + 0.0320 = 0.0508$

$\therefore P_B = 3600.0508$ psia, $v_B = 0.2169$ ft^3/lb

(b) Extraction ΔP_{B-C}

$N_2 = 1.3880$

$\Delta P_{BC} = 1.388 \times \frac{1}{64.4} \times 0.2167 \times 395.1442^2 \times \frac{1}{144} = 4.4042$

$\therefore P_C = 3600.0508 + 4.4042 = 3604.4550$

$v_C = 0.2166$

$G_{TC} = \frac{1885730}{9.6211 \times 3600} = 54.4443 \ \ lb/ft^2\text{-}sec$

(c) Expansion ΔP_{C-D}

$N_2 = -13.1537$

$\Delta P_{CD} = -13.1537 \times \frac{1}{64.4} \times 0.2166 \times (54.4443)^2 \times \frac{1}{144} = -0.9107$

$\therefore P_D = 3604.4550 - 0.9107 = 3603.5443$

$v_D = 0.2167$

(d) ΔP_{D-E} at tube sheet

$G_D = \frac{1885730}{1.2698} = 1485060.637 \ \ lb/hr\text{-}ft^2$

$= 412.5168 \ \ lb/ft^2\text{-}sec$

$D = 0.0402$ ft

$\mu = 0.2455 \ \ lb/hr\text{-}ft$

$$R_e = \frac{1485060.839 \times 0.0402}{0.08455} = 706084.42$$

$$\frac{\varepsilon}{D} = 0.0001244$$

$$f = 0.0143$$

Assume $P_E = 3605.4887$

$$v_E = 0.2165$$

$$\therefore \bar{v} = \frac{1}{2}(v_E + v_0) = 0.2166$$

$$\Delta P_f = 0.0143 \times \frac{1.2917}{0.0402} \times \frac{1}{64.4} \times 0.2166 \times 412.5168^2 \times \frac{1}{144} = 1.8262$$

$$\Delta P_g = \frac{1.2917}{0.2166 \times 144} = 0.0414$$

$$\Delta P_a = \frac{(0.2167 - 0.2165) \times \frac{412.5168^2}{64.4} \times 3}{144} = 0.0110$$

$$\therefore \Delta P = 1.8262 + 0.0414 + 0.0110 = 1.8786$$

$$\therefore P_E = 3603.5443 + 1.8786 = 3605.4229$$

$$T_E = 1066\,^\circ F$$

$$v_E = 0.2165 \ ft^3/lb$$

Total pressure Drop $\Delta P_{total} = 3605.4229 - 3600$

$$= 5.4229 \ psi$$

FORM (285)

(III) 60% Load

(a) ΔP at Exit Nozzle ΔP_{AB}

$P_A = 3600$ psia

$T_A = 1033.7$ °F

$v_A = 0.2251$

$\mu_A = 0.08571 \ \frac{lb}{hr\text{-}ft}$

$$G_{TA} = \frac{1367220}{1.3363} = 979173.53 \ \frac{lb}{ft^2\text{-}hr}$$

$$= 271.9926 \ \frac{lb}{ft^2\text{-}sec}$$

$$Re = \frac{979173.53 \times 1.3333}{0.08571} = 1.5232 \times 10^7$$

$$\frac{e}{D} = 0.0000\,1375$$

$f = 0.008$

$$\Delta P_f = \frac{0.008 \times 1}{1.3333} \times \frac{1}{64.4} \times 0.2251 \times 271.9926^2 \times \frac{1}{144} = 0.0108$$

$$\Delta P_g = \frac{1}{0.2251 \times 144} = 0.0309$$

$\Delta P_a = 0$

$\therefore \Delta P = 0.0108 + 0.0309 = 0.0417$

$\therefore P_B = 3600.0417 \qquad v_B = 0.2251$

FORM (28

(b) Extraction ΔP_{B-C}

$N_2 = 1.3880$

$\Delta P_{BC} = 1.3880 \times \frac{1}{14.4} \times 0.2251 \times 271.9926^2 \times \frac{1}{144} = 2.4925$

$P_C = 3600.0417 + 2.4925 = 3602.5342$

$\nu_C = 0.2249$

$G_C = \frac{1367220}{9.6211 \times 3600} = 39.4740 \quad lb/ft^2\text{-sec}$

(c) Expansion ΔP_{C-D}

$N_2 = -13.1537$

$\Delta P_{CD} = -13.1537 \times \frac{1}{14.4} \times 0.2249 \times (39.4740)^2 \times \frac{1}{144} = -0.5115$

$P_D = 3602.5342 - 0.5115 = 3602.0227$

$\nu_D = 0.2250$

(D) ΔP at tube sheet

$G_D = \frac{1367220}{1.2698} = 1076720.74 \quad lb/ft^2\text{-hr}$

$= 299.0891 \quad lb/ft^2\text{-sec}$

$\mu = 0.0839$

$$R_E = \frac{1079226.04 \times 0.0402}{0.08591} = 505007.28$$

$$\frac{\epsilon}{D} = 0.001244$$

$$f = 0.015$$

Assume $P_E = 3603.7227$

$$V_E = 0.2248$$

$$V = \frac{1}{2}(V_E + V_0) = 0.2249$$

$$\Delta P_f = 0.015 \times \frac{1.2917}{0.0402} \times \frac{1}{64.4} \times 0.2249 \times 299.0891^2 \times \frac{1}{144} = 1.0456$$

$$\Delta P_g = \frac{1.2917}{0.2249 \times 144} = 0.0399$$

$$\Delta P_a = \frac{(0.2250 - 0.2248) \times \frac{299.0891^2}{64.4} \times 3}{144} = 0.0058$$

$$\Delta P = 1.0456 + 0.0399 + 0.0058 = 1.0913$$

$$P_E = 3602.0227 + 1.0913 = 3603.1140$$

$$V_E = 0.2249$$

$$\Delta P_f = 1.0458$$

$$\Delta P_g = 0.0399$$

$$\Delta P_a = 0.0029$$

$$\Delta P = 1.0886$$

$$P_E = 3602.0227 + 1.0886 = 3603.1113$$

$$V_E = 0.2249$$

∴ Total pressure Drop = 3.1113 psi ∗

IV) 40% load

$P_A = 3600$ psia

$T_A = 1106.4$ °F

$v_A = 0.2268$ ft³/lb

$\mu = 0.08571$ lb/hr-ft

$G_A = \frac{905360}{1.3963} = 648542.58$ lb/ft²-hr

$= 180.1507$ lb/ft²-sec

$Re = \frac{648542.58 \times 1.3333}{0.08571} = 1.0089 \times 10^7$

$f = 0.0085$

$\Delta P_f = \frac{0.0085 \times 1}{1.3333} \times \frac{1}{64.4} \times 0.2268 \times 180.1507^2 \times \frac{1}{144} = 0.0051$

$\Delta P_g = \frac{1}{0.2268 \times 144} = 0.0306$

$\Delta P_a = 0$

$\Delta P = 0.0051 + 0.0306 = 0.0357$

$P_B = 3600.0357$ psia

$v_B = 0.2268$ ft³/lb

FORM (28

(b) Contraction ΔP_{BC}

$N_c = 1.3880$

$$\Delta P_{BC} = 1.3880 \times \frac{1}{64.4} \times 0.2268 \times 180.1507^2 \times \frac{1}{144} = 1.1017$$

$$P_C = 3600.0357 + 1.1017 = 3601.1374$$

$$v_C = 0.2267 \ ft^3/lb$$

$$G_C = \frac{905560}{9.6211 \times 3600} = 26.1451 \ lb/sec\text{-}ft^2$$

(c) Expansion ΔP_{CD}

$N_e = -13.1537$

$$\Delta P_{CD} = -13.1537 \times \frac{1}{64.4} \times 0.2267 \times (26.1451)^2 \times \frac{1}{144} = -0.2198$$

$$P_D = 3601.1374 - 0.2198 = 3600.9176$$

$$v_D = 0.2267$$

(d) Friction in tube sheet ΔP_{DE}

$$G_D = \frac{905560}{1.2618} = 713151.6774 \ lb/ft^2\text{-}hr$$

$$= 198.0977 \ lb/ft^2\text{-}sec$$

$d = 0.08571$

$$R_e = \frac{713151.6774 \times 0.0402}{0.08571} = 334484.86$$

$\frac{\varepsilon}{D} = 0.0001244$

$f = 0.0157$

Assume $P_E = 3602.8196$

$v_E = 0.2266$

$v = \frac{1}{2}(v_E + v_D) = 0.22665$

$\Delta P_f = 0.0157 \times \frac{1.2917}{0.0402} \times \frac{1}{64.4} \times 0.22665 \times 198.0977^2 \times \frac{1}{144} = 0.4838$

$\Delta P_g = \frac{1.2917}{0.22665 \times 144} = 0.0396$

$\Delta P_a = \frac{(0.2267 - 0.2266) \times \frac{198.0977^2}{64.4} \times 3}{144} = 0.0013$

$\Delta P = 0.4838 + 0.0396 + 0.0013 = 0.5247$

Assume $P_E = 3600.9176 + 0.5247 = 3601.4423$

$v_E = 0.2267$

$v = 0.2267$

$\Delta P_f = 0.4839$

$\Delta P_g = 0.0396$

$\Delta P_a = 0$

$\Delta P = 0.5235$

$\therefore P_E = 3600.9176 + 0.5235 = 3601.4411$

$v_E = 0.2267$

Total pressure Drop $\Delta P_{total} = 1.4411$ psi *

FORM (285)-47

(V) 20% Load

$P_A = 3600$ psia

$T_A = 1088.3$ °F

$v_A = 0.2224$

$\mu = 0.08571$

(a) ΔP_{AB} at outlet nozzle

$$G_{TA} = \frac{461890}{1.3963} = 330086.66 \ \text{lb/ft}^2\text{-hr}$$

$$= 91.6907 \ \text{lb/ft}^2\text{-sec}$$

$$R_e = \frac{330086.66 \times 1.3333}{0.08571} = 5.1348 \times 10^6$$

$$\frac{\varepsilon}{D} = 0.0000373$$

$$f = 0.0093$$

$$\Delta P_f = 0.0093 \times \frac{1}{1.3333} \times \frac{1}{64.4} \times 0.2224 \times 91.6907^2 \times \frac{1}{144} = 0.0014$$

$$\Delta P_g = \frac{1}{0.2224 \times 144} = 0.0312$$

$$\Delta P_a = 0.$$

$$\therefore \Delta P = 0.0014 + 0.0312 = 0.0326$$

$$\therefore P_B = 3600.0326 \ \text{psi}$$

$$v_B = 0.2224 \ \text{ft}^3/\text{lb}$$

FORM (285)

(b) Contraction ΔP_{BC}

$N_2 = 13880$

$\Delta P_{BC} = 13880 \times \frac{1}{64.4} \times 0.2224 \times 91.6907^2 \times \frac{1}{144} = 0.2799$

$P_C = 3600.0326 + 0.2799 = 3600.3125$

$v_C = 0.2224$

$G_C = \frac{460900}{9.6211 \times 3600} = 13.3070$ lb/ft²-sec

(c) Expansion ΔP_{CD}

$N_2 = -13.1557$

$\Delta P_{CD} = -13.1537 \times \frac{1}{64.4} \times 0.2224 \times 13.3070^2 \times \frac{1}{144} = -0.0559$

$P_D = 3600.3125 - 0.0559 = 3600.2566$

$v_D = 0.2224$

(d) Friction in tube sheet ΔP_{DE}

$G_D = \frac{460900}{1.2698} = 362970.55$ lb/ft²-hr

$= 100.8252$ lb/ft²-sec

$\mu = 0.08571$

$Re = \frac{362970.55 \times 0.0402}{0.08571} = 170241.7$

FORM (285)

$\frac{\varepsilon}{D} = 0.0001244$

$f = 0.017$

Assume $P_E = 3600.5566$

$v_E = 0.2224$

$\bar{v} = 0.2224$

$\Delta P_f = 0.017 \times \frac{1.2917}{0.0402} \times \frac{1}{64.4} \times 0.2224 \times 100.8252^2 \times \frac{1}{144} = 0.1332$

$\Delta P_g = \frac{1.2917}{0.2224 \times 144} = 0.0403$

$\Delta P_a = 0$

$\Delta P = 0.1332 + 0.0403 = 0.1735$

$\therefore P_E = 3600.2566 + 0.1735 = 3600.4301$ psia

$v_E = 0.2224$ ft³/lb

Total pressure Drop $\Delta P_{Total} = 0.4301$ psi //

FORM (285).

B-3

Objective : Calculate the pressure drops of molten salt passing through tube support plates and vibration suppressors

Reference : (1) Engineering Department Manual, volume I, FWC

(2) Thermal hydraulic performance computer code output

(3) Tube support plate, Drawing no. ND-720-195

(4) Tube vibration suppressor, Drawing no. ND-740-197

(5) 1967 ASME Steam Tables

(I) 100% Load

(a) ΔP, tube support plates

Based on basic design 1000 tubes, 120 ft long. 13 tie rods

I.D. of shell = 39.5"

Clearance = $\frac{3}{32}$"

Area of Clearance $A_2 = 0.080214 \ ft^2$

Free flow area at tube support $A_1 = 0.003119 \times 1000 + A_2$

$= 3.199214 \ ft^2$

Free flow area at tube bundle

$$A = \frac{1}{4}\pi\left(\frac{39.5}{12}\right)^2 - 1000 \times \frac{1}{4}\pi\left(\frac{0.75}{12}\right)^2 - 13 \times \frac{1}{4}\pi\left(\frac{13/16}{12}\right)^2$$

$= 8.509804 - 3.067962 - 0.099986$

$= 5.341856 \ ft^2$

FORM (285)-4

$$\frac{A_1}{A} = \frac{3.199214}{5.341896} = 0.598891 = \left(\frac{D_1}{D}\right)^2$$

$$\frac{D_1}{D} = 0.774$$

$$k = 0.323$$

$$\Delta P = k \, \frac{1}{2g_c} \times \frac{1}{\rho} \, G_T^2$$

$$G_T = \frac{15.28 \times 10^6}{5.341891} = 2860407.62 \; \frac{lb}{hr\text{-}ft^2}$$

$$= 794.5577 \; \frac{lb}{ft^2\text{-}sec}$$

From the computer output, the temperature at each tube support plate is tabulated below. Location of tube support plate is measured from (leg. (vibration suppressors are included)

Location, ft	Temp. °F	Specific volume ft³/lb
2.67	856	0.0083
4.46	858	0.0083
7.21	864	0.0083
9.96	870	0.0083
12.71	874	0.0083
17.33	885	0.0084
22.33	894	0.0084
27.33	904	0.0084
32.33	918	0.0084
37.33	928	0.0084
42.33	940	0.0085
47.33	954	0.0085
52.33	968	0.0085
57.33	982	0.0085
62.33	999	0.0086
67.33	1015	0.0086
72.33	1030	0.0086
77.33	1045	0.0087
82.33	1062	0.0087
87.33	1070	0.0087
92.33	1087	0.0087
97.33	1103	0.0088
102.33	1112	0.0088
107.33	1125	0.0088
112.33	1137	0.0088
117.33	1144	0.0088

} vibration suppressors (rows 7.21–12.71)

FORM (285)-47

$\Delta P_1 = 0.375 \times \frac{1}{64.4} \times 0.0083 \times 794.5577^2 \times \frac{1}{144} = 0.1836$

$\Delta P_2 = 0.375 \times \frac{1}{64.4} \times 0.0084 \times 794.5577^2 \times \frac{1}{144} = 0.1859$

$\Delta P_3 = 0.375 \times \frac{1}{64.4} \times 0.0085 \times 794.5577^2 \times \frac{1}{144} = 0.1881$

$\Delta P_4 = 0.375 \times \frac{1}{64.4} \times 0.0086 \times 794.5577^2 \times \frac{1}{144} = 0.1903$

$\Delta P_5 = 0.375 \times \frac{1}{64.4} \times 0.0087 \times 794.5577^2 \times \frac{1}{144} = 0.1925$

$\Delta P_6 = 0.375 \times \frac{1}{64.4} \times 0.0088 \times 794.5577^2 \times \frac{1}{144} = 0.1947$

∴ Pressure drops occurred at tube support plates

$\Delta P = 2\Delta P_1 + 5\Delta P_2 + 4\Delta P_3 + 3\Delta P_4 + 4\Delta P_5 + 5\Delta P_6$

$= 4.3635$ psi

(b) ΔP. vibration suppressors

Clearance = 3/32"

ID of shell at vibration suppressors $= 39.5 - 2 \times \frac{3}{32} = 39.3125$"

Clearance area $A_2 = \frac{1}{4}\pi\left[\left(\frac{39.3125}{12}\right)^2 - \left(\frac{39.125}{12}\right)^2\right] = 0.080214$ ft²

total free flow area at tube support

$A_1 = \frac{1}{4}\pi\left[\left(\frac{39.3125}{12}\right)^2\right] - 13 \times \frac{1}{4}\pi\left(\frac{19/16}{12}\right)^2 - \text{bar area} - 1000 \times \frac{\pi}{4}\left(\frac{0.75}{12}\right)^2$

$= 8.429446 - 0.099986 - 1.865314 - 3.067962$

$= 3.395984$ ft²

FORM (28

Free flow area at tube bundle $A = 5.341886\ ft^2$

$$\frac{A_1}{A} = \frac{3.395784}{5.341886} = 0.635726 = \left(\frac{D_1}{D}\right)^2$$

$$\frac{D_1}{D} = 0.797$$

$$k = 0.28$$

$$\Delta P = k \frac{1}{2g_c} \times \frac{1}{\rho} G^2$$

$$= 0.28 \times \frac{1}{64.4} \times 0.0083 \times 794.5577^2 \times \frac{1}{144} = 0.1582$$

For 3 vibration suppressors $\Delta P = 3 \times 0.1582 = 0.4746$

∴ Total pressure drops through tube support plates and vibration suppressors

$$\Delta P_{Total} = 4.3635 + 0.4746$$

$$= 4.8381\ psi$$

(II) 80% Load

As in 100% Load case, the temperature at each tube support plates and vibration suppressor is tabulated below:

Location, ft	Temp. °F	Specific volume ft³/lb
2.67	856	0.0083
4.67	853	
7.21	865	
9.86	869	
12.97	876	
17.33	886	0.0084
22.33	900	
27.33	912	
32.33	927	
37.33	941	0.0085
42.33	956	
47.33	971	
52.33	986	
57.33	1003	0.0086
62.33	1018	
67.33	1032	
72.33	1047	0.0087
77.33	1061	
82.33	1075	
87.33	1085	
92.33	1097	
97.33	1105	0.0088
102.33	1115	
107.33	1124	
112.33	1132	
117.33	1147	

} vibration suppressors (rows 4.67–12.97)

FORM (285)-47

$$G = \frac{12606000}{5.341886 \times 3600} = 655.5101 \ \frac{lb}{ft^2 \cdot sec}$$

$$\Delta P_1 = 0.325 \times \frac{1}{64.4} \times 0.0083 \times 655.5101^2 \times \frac{1}{144} = 0.1250$$

$$\Delta P_2 = 0.325 \times \frac{1}{64.4} \times 0.0084 \times 655.5101^2 \times \frac{1}{144} = 0.1265$$

$$\Delta P_3 = 0.325 \times \frac{1}{64.4} \times 0.0085 \times 655.5101^2 \times \frac{1}{144} = 0.1280$$

$$\Delta P_4 = 0.325 \times \frac{1}{64.4} \times 0.0086 \times 655.5101^2 \times \frac{1}{144} = 0.1295$$

$$\Delta P_5 = 0.325 \times \frac{1}{64.4} \times 0.0087 \times 655.5101^2 \times \frac{1}{144} = 0.1310$$

$$\Delta P_6 = 0.325 \times \frac{1}{64.4} \times 0.0088 \times 655.5101^2 \times \frac{1}{144} = 0.1325$$

Pressure drops occurred at tube support plates

$$\Delta P = 2\Delta P_1 + 4\Delta P_2 + 4\Delta P_3 + 3\Delta P_4 + 5\Delta P_5 + 5\Delta P_6$$

$$= 2.9740$$

ΔP at vibration suppressors

$$\Delta P = 0.28 \times \frac{1}{64.4} \times 0.0083 \times 655.5101^2 \times \frac{1}{144} = 0.1077$$

$$3\Delta P = 0.1077 \times 3 = 0.3230$$

∴ Total ΔP through tube support plates and vibration suppressors

$$\Delta P_{Total} = 0.3230 + 2.9740 = 3.2970 \text{ psi}$$

FORM (285).

III) 60% Load

Location, ft	Temp. °F	Specific volume ft³/lb
2.67	861	0.0083
4.67	866	″
[illegible]	873	″
9.36	879	0.0084
[illegible]	887	″
17.33	900	″
22.33	914	″
27.33	930	″
32.33	946	0.0085
[illegible]	964	″
42.33	981	″
47.33	992	0.0086
52.33	1012	″
57.33	1031	″
62.33	1045	0.0087
67.33	1057	″
72.33	1069	″
77.33	1082	″
82.33	1090	″
87.33	1099	″
92.33	1107	0.0088
97.33	1112	″
102.33	1118	″
107.33	1123	″
112.33	1126	″
[illegible]	113[illegible]	″

} vibration suppressors (rows 873–887)

FORM (285)-47

$$G_T = \frac{9932000}{5.341856 \times 3600} = 516.4625 \quad \text{lb/ft}^2\text{-sec}$$

$$\Delta P_1 = 0.325 \times \frac{1}{64.4} \times 0.0083 \times 516.4625^2 \times \frac{1}{144} = 0.0776$$

$$\Delta P_2 = 0.325 \times \frac{1}{64.4} \times 0.0084 \times 516.4625^2 \times \frac{1}{144} = 0.0785$$

$$\Delta P_3 = 0.325 \times \frac{1}{64.4} \times 0.0085 \times 516.4625^2 \times \frac{1}{144} = 0.0795$$

$$\Delta P_4 = 0.325 \times \frac{1}{64.4} \times 0.0086 \times 516.4625^2 \times \frac{1}{144} = 0.0804$$

$$\Delta P_5 = 0.325 \times \frac{1}{64.4} \times 0.0087 \times 516.4625^2 \times \frac{1}{144} = 0.0813$$

$$\Delta P_6 = 0.325 \times \frac{1}{64.4} \times 0.0088 \times 516.4625^2 \times \frac{1}{144} = 0.0823$$

$$\Delta P = 2\Delta P_1 + 3\Delta P_2 + 3\Delta P_3 + 3\Delta P_4 + 6\Delta P_5 + 6\Delta P_6$$

$$= 1.8520$$

4 Suction Compressors

$$\Delta P_1 = 0.28 \times \frac{1}{64.4} \times 0.0083 \times 516.4625^2 \times \frac{1}{144} = 0.0668$$

$$\Delta P_2 = 0.28 \times \frac{1}{64.4} \times 0.0084 \times 516.4625^2 \times \frac{1}{144} = 0.0676$$

$$\Delta P = \Delta P_1 + 2\Delta P_2 = 0.2021$$

$$\Delta P_{Total} = 0.2021 + 1.8520 = 2.0541 \text{ psi}$$

FORM (285)-47

(IV) 40% Load

Location, ft	Temp, °F	Specific volume ft³/lb
2.67	871	0.0083
4.67	877	0.0084
7.21	885	"
9.96	893	"
12.71	897	"
17.33	921	"
22.33	940	0.0085
27.33	959	"
32.33	978	"
37.33	997	0.0086
42.33	1014	"
47.33	1033	"
52.33	1048	0.0087
57.33	1057	"
62.33	1069	"
67.33	1077	"
72.33	1087	"
77.33	1093	"
82.33	1098	"
87.33	1103	0.0088
92.33	1105	
97.33	1109	
102.33	1111	
107.33	1112	
112.33	1113	
117.33	1115	

} Vibration Suppressors (locations 7.21 – 12.71)

$$G = \frac{7258000}{5.341836 \times 3600} = 377.4149 \ \text{lb/ft}^2\text{-sec}$$

$$\Delta P_1 = 0.325 \times \frac{1}{64.4} \times 0.0083 \times 377.4149^2 \times \frac{1}{144} = 0.0414$$

$$\Delta P_2 = 0.325 \times \frac{1}{64.4} \times 0.0084 \times 377.4149^2 \times \frac{1}{144} = 0.0419$$

$$\Delta P_3 = 0.325 \times \frac{1}{64.4} \times 0.0085 \times 377.4149^2 \times \frac{1}{144} = 0.0424$$

$$\Delta P_4 = 0.325 \times \frac{1}{64.4} \times 0.0086 \times 377.4149^2 \times \frac{1}{144} = 0.0429$$

$$\Delta P_5 = 0.325 \times \frac{1}{64.4} \times 0.0087 \times 377.4149^2 \times \frac{1}{144} = 0.0434$$

$$\Delta P_6 = 0.325 \times \frac{1}{64.4} \times 0.0088 \times 377.4149^2 \times \frac{1}{144} = 0.0439$$

$$\Delta P = \Delta P_1 + 2\Delta P_2 + 3\Delta P_3 + 3\Delta P_4 + 7\Delta P_5 + 7\Delta P_6$$

$$= 0.9922$$

<u>ΔP at vibration suppressors</u>

$$\Delta P = 0.28 \times \frac{1}{64.4} \times 0.0084 \times 377.4149^2 \times \frac{1}{144} = 0.0361$$

$$3\Delta P = 0.1084$$

$$\therefore \Delta P_{total} = 0.1084 + 0.9922 = 1.1006 \ \text{psi}$$

(V) 20% Load

Location Ft	Temp. °F	Specific volume ft³/lb
2.67	900	0.0084
4.67	909	"
7.21	922	"
9.96	933	"
12.71	946	0.0085
17.33	969	"
22.33	990	0.0086
27.33	1011	"
32.33	1029	"
37.33	1044	0.0087
42.33	1056	"
47.33	1063	"
52.33	1069	"
57.33	1075	"
62.33	1078	"
67.33	1082	"
72.33	1084	"
77.33	1085	"
82.33	1087	"
87.33	1087	"
92.33	1088	"
97.33	1088	"
102.33	1088	"
107.33	1088	"
112.33	1089	
117.33	1089	

} Vibration suppressors (rows 7.21–12.71)

FORM (285)

$$G = \frac{4584000}{0.341836 \times 3600} = 238.3673 \ \frac{lb}{ft^2\text{-}sec}$$

$$\Delta P_1 = 0.325 \times \frac{1}{64.4} \times 0.0084 \times 238.3673^2 \times \frac{1}{144} = 0.0167$$

$$\Delta P_2 = 0.325 \times \frac{1}{64.4} \times 0.0085 \times 238.3673^2 \times \frac{1}{144} = 0.0169$$

$$\Delta P_3 = 0.325 \times \frac{1}{64.4} \times 0.0086 \times 238.3673^2 \times \frac{1}{144} = 0.0171$$

$$\Delta P_4 = 0.325 \times \frac{1}{64.4} \times 0.0087 \times 238.3673^2 \times \frac{1}{144} = 0.0173$$

$$\Delta P = 2\Delta P_1 + \Delta P_2 + 3\Delta P_3 + 17\Delta P_4$$

$$= 0.3957$$

<u>Vibration suppressors ΔP</u>

$$\Delta P_1 = 0.28 \times \frac{1}{64.4} \times 0.0084 \times 238.3673^2 \times \frac{1}{144} = 0.0144$$

$$\Delta P_2 = 0.28 \times \frac{1}{64.4} \times 0.0085 \times 238.3673^2 \times \frac{1}{144} = 0.0146$$

$$\Delta P = 2\Delta P_1 + \Delta P_2$$

$$= 0.0434$$

$$\therefore \Delta P_{Total} = 0.3957 + 0.0434 = 0.4391 \ psi$$

FORM (285)

B-4

Objective : Calculate the molten salt pressure drops through inlet nozzle and shrouds

Reference : (1) Engineering Department manual, volume I. FWC

(2) Thermal hydraulic performance computer code output

(3) Salt inlet/outlet nozzle. ND-722-165

(4) Internal shroud . ND-742-171

(5) 1967 ASME Steam Tables

(I) 100% Load

(a) Inlet nozzle

nozzle ID = 19.25" = 1.6042 ft

nozzle Length L = 13" - 4.25" = 8.75" = 0.7292 ft

$A_0 = \frac{1}{4}\pi(1.6042)^2 = 2.0212 \ ft^2$

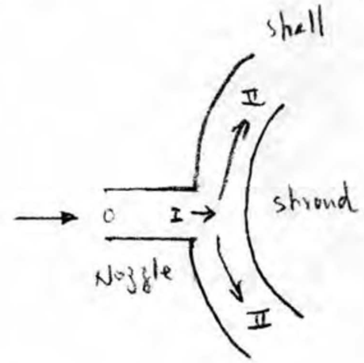

Inlet T = 1150°F

p = 235 psia

$\rho = 141.4 - 0.0247\ T(°F) = 113.0 \ lb/ft^3$

$\mu = 0.2121\ e^{\frac{4032}{T(°R)}} = 2.60 \ lb/ft\text{-}hr$

$$G_0 = \frac{1528 \times 10^6}{2.0212} = 755986543 \ lb/ft^2\text{-}hr$$

$$= 2099.9626 \ lb/ft^2\text{-}sec$$

$$R_e = \frac{GD}{\mu} = \frac{755986543 \times 1.6042}{2.60} = 4.6644 \times 10^6$$

$$\frac{\varepsilon}{D} = \frac{0.000005}{1.6042} = 0.000003$$

$f = 0.0093$

$$\therefore P_f = 0.0093 \times \frac{0.7292}{1.6042} \times \frac{1}{64.4} \times \frac{1}{113.0} \times 2099.9626^2 \times \frac{1}{144} = 0.0178$$

$$\therefore P_2 = 235 - 0.0178 = 234.9822$$

Consider horizontal spreading only

Length of shroud $L = 48'' = 4$ ft

The gap between shell and shroud $= \frac{1}{2}(54'' - 40'') = 7'' = 0.5833$ ft

$\therefore$ Area of the gap $A_{II} = 0.5833 \times 4 = 2.3333 \ ft^2$

$$W_{II} = \frac{1}{2}(1528 \times 10^6) = 764 \times 10^6 \ lb/hr$$

$$G_{II} = \frac{764 \times 10^6}{2.3333} = 327428572 \ lb/hr\text{-}ft^2$$

$$= 909.5238 \ lb/ft^2\text{-}sec$$

FORM (285)

$(h_L)_{0-1} = (V_h)_0 \left[1+0.8\left(\frac{G_1}{G_0}\right)^2 - 0.42\left(\frac{G_1}{G_0}\right) \right]$

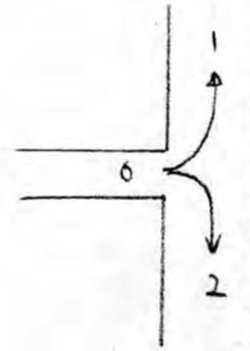

$1+0.8\left(\frac{G_1}{G_2}\right)^2 - 0.42\left(\frac{G_1}{G_0}\right)$

$= 1+0.8\left(\frac{909.5238}{2099.9626}\right)^2 - 0.42\left(\frac{909.5238}{2099.9626}\right)$

$= 0.9682$

$\therefore \Delta P_{01} = 0.9682 \times \frac{1}{64.4} \times \frac{1}{\rho} G_0^2 \times \frac{1}{144} + \frac{1}{64.4} \times \frac{1}{\rho}\left[G_{II}^2 - G_0^2\right] \times \frac{1}{144}$

$= 0.9682 \times \frac{1}{64.4} \times \frac{1}{113.0} \times 2099.9626^2 \times \frac{1}{144} + \frac{1}{64.4} \times \frac{1}{113} \times \left[909.5238^2 - 2099.9626^2\right] \times$

$= 4.0742 - 3.4188$

$= 0.6554$ psi

$\therefore P_{II} = 234.3822 - 0.6554 = 234.3268$ psia.

$De = \frac{4A}{P} = \frac{4 \times 2.3333}{2 \times (4+0.5833)} = 1.0182$ ft

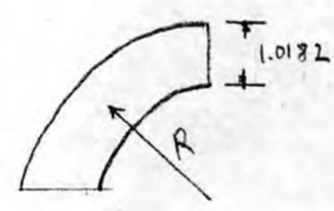

$R = \frac{1}{2}(1.0182) + \frac{20}{12}$

$= 2.1758$ ft

$\frac{R}{De} = \frac{2.1758}{1.0182} = 2.1369$

$\therefore K_b = 0.46$

$\Delta P_b = 0.46 \times \frac{1}{64.4} \times \frac{1}{113} \times 909.5238^2 \times \frac{1}{144} = 0.3631$

$R_e = \frac{G\,De}{\mu} = \frac{3274285.72 \times 1.0182}{2.6} = 1.28226 \times 10^6$

FORM (285)

$\frac{\varepsilon}{D} = \frac{0.000005}{1.0182} = 0.000004911$

$f = 0.011$

Length of arc $= \frac{1}{4}\pi R = \frac{1}{4}\pi \times 2.1758 = 1.7089$ ft

$\Delta P_f = 0.011 \times \frac{1.7089}{1.0182} \times \frac{1}{64.4} \times \frac{1}{113} \times 909.5238^2 \times \frac{1}{144} = 0.0146$

$\Delta P = 0.3777$ psi

∴ Pressure before entering shroud $= 234.3268 - 0.3777$

$= 233.9491$ psia.

(b) Shroud

1640 holes of 0.75" D

∴ Total area of holes $= 1640 \times \frac{1}{4}\pi \left(\frac{0.75}{12}\right)^2 = 5.0315$ ft^2 $= A_o$

Total area of shroud $= \pi \times \left(\frac{40}{12}\right) \times 4 = 41.8879$ ft^2 $= A_t$

$\frac{A_o}{A_t} = \frac{5.0315}{41.8879} = 0.1201 = \left(\frac{D_o}{D_t}\right)^2$

∴ $\frac{D_o}{D_t} = 0.3466$

∴ $K = 1.16$

$G_e = \frac{15.28 \times 10^6}{41.8879 \times 3600} = 101.3287$ lb/ft^2-sec

$\Delta P = 1.16 \times \frac{1}{64.4} \times \frac{1}{113} \times 101.3287^2 \times \frac{1}{144} = 0.0113$

∴ Pressure entering tube bundle $= 233.9491 - 0.0113 = 233.9378$ psia

Total pressure Drop $\Delta P_{total} = 235 - 233.9415 = 1.0622$ psi

(II) 80% Load

$T = 1142.6°F = 1602.6°R$

$P = 235$ psia

$\rho = 113.18$ lb/ft³

$\mu = 2.63$ lb/hr-ft

$$G_T = \frac{1260600}{2.0212} = 6236888.98 \ \text{lb/hr-ft}^2$$

$$= 1732.47 \ \text{lb/ft}^2\text{-sec}$$

$$Re = \frac{6236888.98 \times 1.6042}{2.63} = 3804265.13$$

$\frac{\varepsilon}{D} = 0.0002$

$f = 0.00975$

$$\Delta P_f = 0.00975 \times \frac{0.3312}{1.6042} \times \frac{1}{64.4} \times \frac{1}{113.18} \times 1732.47^2 \times \frac{1}{144} = 0.0127$$

$$P_I = 235 - 0.0127 = 234.9873$$

$$\dot{m}_I = \frac{1}{2}(1260600) = 630300$$

$$G_I = \frac{630300}{2.3333} = 270132 4.305 \ \text{lb/ft}^2\text{hr}$$

$$= 750.3679 \ \text{lb/ft}^2\text{-sec}$$

$D = 0.9682$

$\Delta P_{01} = 0.5682 \times \frac{1}{64.4} \times \frac{1}{113.18} \times 1732.47^2 \times \frac{1}{144} + \frac{1}{64.4} \times \frac{1}{113.18} \left[750.3679^2 - 1732.47^2 \right]$

$= 2.7687 - 2.3232$

$= 0.4455$

$P_{II} = 234.1873 - 0.4455 = 234.5418$

$K_b = 0.46$

$\Delta P_b = 0.46 \times \frac{1}{64.4} \times \frac{1}{113.18} \times 750.3679^2 \times \frac{1}{144} = 0.2468$

$R_e = \frac{2701574.565 \times 1.0182}{2.63} = 1.0458 \times 10^6$

$\frac{\varepsilon}{D} = 0.0000491$

$f = 0.012$

$\Delta P_f = 0.012 \times \frac{1.9083}{1.0182} \times \frac{1}{64.4} \times \frac{1}{113.18} \times 750.3679^2 \times \frac{1}{144} = 0.0108$

$\Delta P = 0.2576$

Pressure entering shroud $= 234.5418 - 0.2576 = 234.2842$

$K = 1.16$

$G_2 = \frac{12.60600}{41.8879 \times 3600} = 83.5961 \ \text{lb/ft}^2\text{-sec}$

$\Delta P = 1.16 \times \frac{1}{64.4} \times \frac{1}{113.18} \times 83.5961^2 \times \frac{1}{144} = 0.0077$

Pressure entering tube bundle $= 234.2842 - 0.0077 = 234.2765$

total pressure drop $\Delta P_{Total} = 0.7235$ psi

III) 60% Load

$T = 1132.2\,^\circ F = 1592.20\,^\circ R$

$P = 235$ psia

$\rho = 113.43$ lb/ft³

$\mu = 2.69$ lb/ft-hr

$$G_0 = \frac{973200}{0.2022} = 4813912.53 \quad \text{lb/ft}^2\text{-hr}$$

$$= 1364.98 \quad \text{lb/ft}^2\text{-sec}$$

$$R_e = \frac{4813912.53 \times 1.6042}{2.69} = 2952396.44$$

$$\frac{\varepsilon}{D} = 0.00003$$

$$f = 0.0145$$

$$\Delta P_f = 0.0145 \times \frac{0.9682}{1.6042} \times \frac{1}{64.4} \times \frac{1}{113.43} (1364.98)^2 \times \frac{1}{144} = 0.0117$$

$$P_I = 235 - 0.0117 = 234.9883 \quad \text{psia}$$

$$\dot{m}_I = \frac{1}{2} (973200) = 486600$$

$$G_I = \frac{486600}{2.2853} = 212816.12 \quad \text{lb/ft}^2\text{-hr}$$

$$= 591.1989 \quad \text{lb/ft}^2\text{-sec}$$

$$N = 0.9682$$

$$\Delta P_{01} = 0.9682 \times \frac{1}{64.4} \times \frac{1}{113.43} \times 1364.98^2 \times \frac{1}{144} + \frac{1}{64.4} \times \frac{1}{113.43} \left[591.1989^2 - 1364.98^2\right] \frac{1}{144}$$

$$= 1.7149 - 1.4390 = 0.2759 \quad \text{psi}$$

FORM (285)-47

$\therefore P_{II} = 234.9883 - 0.2759 = 234.7124$ psia

$K_t = 0.46$

$\Delta P_b = 0.46 \times \frac{1}{144} \times \frac{1}{113.43} \times 591.1989^2 \times \frac{1}{144} = 0.1528$

$Re = \frac{2128316.12 \times 1.0182}{2.67} = 811629.77$

$\frac{\varepsilon}{D} = 0.0000114411$

$f = 0.0122$

$\Delta P_f = 0.0122 \times \frac{1.7089}{1.0182} \times \frac{1}{64.4} \times \frac{1}{113.43} \times 591.1989^2 \times \frac{1}{144} = 0.0068$

$\Delta P = 0.1596$

Pressure entering shroud = 234.5528

$K = 1.16$

$G_e = \frac{9932000}{41.8879 \times 3600} = 65.8636$ lb/ft²-sec

$\Delta P = 1.16 \times \frac{1}{64.4} \times \frac{1}{113.43} \times 65.8636^2 \times \frac{1}{144} = 0.0048$

Pressure entering tube bundle = 234.5528 − 0.0048 = 234.5480

$\therefore \Delta P_{total} = 0.4520$ psi

FORM (285)

(III) [illegible]

$T = $ [illegible] $°F = $ [illegible] $°R$

$P = $ [illegible] psia

$\rho = $ [illegible] 84 lb/ft³

$\mu = $ [illegible] 94 lb/ft hr

$G = \frac{[illegible]}{[illegible]} = 3390936 \ \text{lb/ft}^2\,\text{hr}$

$= 937.4822 \ \text{lb/ft}^2\,\text{sec}$

$Re = \frac{[illegible]}{[illegible]} = 2.1[illegible]4 \times 10^6$

$\frac{\varepsilon}{D} = $ [illegible]

$f = 0.0106$ [illegible]

$\Delta P_f = 0.0106 \times \frac{[illegible]}{[illegible]} \times \frac{1}{[illegible]} \times \frac{1}{113.84} \times (937.4822)^2 \times \frac{1}{144} = 0.0045$

$P_I = $ [illegible] $- 0.0045 = 234.9955$ psia

$m_I = \frac{1}{2}$ ([illegible]) $= $ [illegible]

$G_I = \frac{[illegible]}{[illegible]} = 1555307.93 \ \text{lb/ft-hr} = 432.03 \ \text{lb/ft}^2\,\text{sec}$

$f = 0.0[illegible]$

$\Delta P_{ft} = 0.0[illegible] \times \frac{[illegible]}{[illegible]} \times \frac{1}{113.84} \times (937.4822)^2 \times \frac{1}{144} + \frac{1}{64.4} \times \frac{1}{113.84} \left[432.03^2 - 937.4822^2\right]$

$\times \frac{1}{144}$

[illegible] $= $ [illegible] 2077 psi

FORM (285)-4

$P_5 = 234.9955 - 0.2077$

$= 234.7878$

$h_1 = 246$

$\Delta P_6 = 246 \times \frac{1}{64.4} \times \frac{1}{115.86} \times 432.05^2 \times \frac{1}{144} = 0.0813$

$R_e = \frac{[illegible]}{2.74} = 577861.5038$

$\frac{\varepsilon}{D} = [illegible]$

$f = .13$

$\Delta P_7 = 0.13 \times \frac{[illegible]}{[illegible]} \times \frac{1}{64.4} \times \frac{1}{115.86} \times 432.05^2 \times \frac{1}{144} = 0.0039$

$\Delta P = 0.0852$

Pressure entering shroud = 234.7878 - 0.0852 = 234.7026

$h = 1.16$

$G_s = \frac{[illegible]}{[illegible]} = 48.1311 \ \text{lb}/\text{ft}^2\text{sec}$

$\Delta P = 1.16 \times \frac{1}{64.4} \times \frac{1}{115.84} \times 48.1311^2 \times \frac{1}{144} = 0.0025$

Pressure entering tube bundle = 234.7026 - 0.0025 = 234.7001

$\therefore \Delta P_{total} = 0.2999$ psi

FORM (285)

(E) 20% Load

$T = 1$[illegible]$ F = 1549.$[illegible]$ K$

$P = 252$ psia

$\rho = 1.1443$ lb/ft^3

$\mu = 0.086$ lb/ft hr

$$G_1 = \frac{4584000}{2.0212} = 2267959.63 \ lb/ft^2\ hr$$

$$= 629.9880 \ lb/ft^2\text{-sec}$$

$$Re = \frac{2267959.63 \times 1.612}{0.086} = 12$$[illegible]

$\frac{\varepsilon}{D} = 0.000$[illegible]

$f = 0.011$

$$\Delta P_f = 0.011 \times \frac{12.12}{1.612} \times \frac{1}{64.4} \times \frac{1}{1.1449} \times (629.9888)^2 \times \frac{1}{144} = 0.0019$$

$$P_2 = 252 - 0.0019 = 251.9981 \ \text{psia}$$

$$W_2 = \frac{1}{2}(4584000) = 2292000$$

$$G_2 = \frac{2292000}{2.0212} = $$ [illegible] $$ lb/ft^2\ hr = 272.8610 \ lb/ft^2\text{-sec}$$

$K = 0.368$

$$\Delta P_c = 0.368 \times \frac{1}{64.4} \times \frac{1}{1.1449} \times 629.9888^2 \times \frac{1}{144} + \frac{1}{64.4} \times \frac{1}{1.1449}\left[272.861^2 - 629.9888^2\right]$$

$= 0.3618 - 0.3$[illegible]

$= 0.0282$

FORM (285)

P_2 = [illegible]$.9381 - 0.0382 = 234.8399$ psia

f_t = [illegible]

ΔP_f = [illegible] $\times \frac{1}{144} \times \frac{1}{[illegible]} \times 272.8610^2 \times \frac{1}{144}$ = [illegible]323

$R_e = \frac{[illegible]}{[illegible]} = 349712.43$

$\frac{\epsilon}{D}$ = [illegible]

f = [illegible]14

ΔP_f = [illegible] $\times \frac{[illegible]}{[illegible]} \times \frac{1}{144} \times \frac{1}{[illegible]} \times 272.861^2 \times \frac{1}{144} = 0.0016$

ΔP = [illegible]339

Pressure entering throat $= 234.8399 - 0.0339 = 234.8060$

K = [illegible]

$G_T = \frac{[illegible]}{[illegible] \times [illegible]}$ = [illegible] $\frac{lb}{ft^2\,sec}$

ΔP = [illegible] $\times \frac{1}{144} \times \frac{1}{[illegible]} \times$ [illegible]$^2 \times \frac{1}{144}$ = [illegible]

Pressure entering tube bundle $= 234.8060 - 0.0010 = 234.9050$

ΔP_{total} = [illegible] psi

B-5

Objective: Calculate the molten salt pressure drops through outlet nozzle and shrouds

References: (1) Engineering Department Manual, volume I, FWC

(2) Thermal Hydraulic performance computer code output

(3) Salt inlet/outlet nozzle, ND-722-165

(4) Internal shroud, ND-742-171

(5) 1967 ASME steam Tables

(I) 100% Load

T = [illegible] °F

P = 2??.???? psia

ρ = 1?6.8?42 lb/ft³

μ = [illegible] lb/hr-ft

For [illegible] [illegible] values, consider only 1 shroud.

[illegible]

$G = \frac{[illegible]}{41.[illegible]} = 31,4?83,1404 \ \frac{lb}{ft^2\,hr}$

$= 101.[illegible] \ \frac{lb}{ft^2\text{-}sec}$

[illegible] $\times \frac{[illegible]}{[illegible]} \times \frac{[illegible]}{[illegible]} \times [illegible]^2 \times \frac{1}{144} = [illegible]$

∴ Pressure leaving shroud $P_s = 299.8997 - 0.0107 = 299.8890$

$A = \frac{1}{4}\pi\left[\left(\frac{136}{12}\right)^2 - \left(\frac{90}{12}\right)^2\right] = 8.3776 \ ft^2$

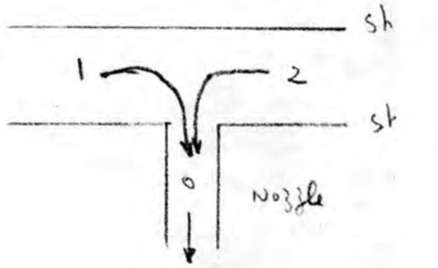

$G_1 = G_2 = \frac{\frac{1}{2}(15.28 \times 10^6)}{8.3776} = 911955.65 \ lb/ft^2 hr$

$= 253.3210 \ lb/ft^2\text{-}sec$

$G_o = \frac{15.28 \times 10^6}{2.0212} = 7559865.43 \ lb/ft^2\text{-}hr$

$= 2099.9626 \ lb/ft^2\text{-}sec$

$N = 0.3524$

$\Delta P = 0.3524 \times \frac{1}{64.4} \times \frac{1}{130.3902} \times 2099.9626^2 \times \frac{1}{144} = 3.7619$

Pressure at nozzle inlet $P_o = 299.8890 - 3.7619 = 296.1271$

$Re = \frac{7559865.43 \times 1.6042}{4.5986} = 2637243.53$

$\frac{\epsilon}{D} = 0.0000$[illegible]

$f = 0.0102$

$\Delta P_f = 0.0102 \times \frac{0.7892}{1.6042} \times \frac{1}{64.4} \times \frac{1}{130.3902} \times 2099.9626^2 \times \frac{1}{144} = 0.0183$

∴ $P_{out} = 296.1271 - 0.0183 = 296.1088$

∴ $\Delta P_{total} = 3.7909$ psi

FORM 1285

<u>(II) 80% Load</u>

$T = 858\,^\circ F$

$P = 306.9923$ psia

$\rho = 120.3309$ lb/ft³

$\mu = 4.5728$ lb/hr-ft

$G = \frac{[illegible]}{41.8879} = 291826.5179$ lb/ft²-hr

$= 81.0629$ lb/ft²-sec

$\Delta P = 1.16 \times \frac{1}{64.4} \times \frac{1}{120.3309} \times 81.0629^2 \times \frac{1}{144} = 0.0068$

$P_i = 306.9924$ psia

$G_T = \frac{[illegible]}{2.0212} = 6049892.36$ lb/ft²-hr

$= 1679.9701$ lb/ft²-sec

$\Delta P = 0.524 \times \frac{1}{64.4} \times \frac{1}{120.3309} \times 1679.9701^2 \times \frac{1}{144} = 2.4088$

$P_i = 304.5639$ psia

$R_e = \frac{6049892.36 \times 1.6042}{4.5728} = 2121682.3$

$\frac{\epsilon}{D} = $ [illegible]

$f = 0.0109$

$\Delta P_f = 0.0109 \times \frac{0.7292}{1.6042} \times \frac{1}{64.4} \times \frac{1}{120.3309} \times 1679.9701^2 \times \frac{1}{144} = 0.0123$

$\Delta P_{[illegible]} = $ [illegible]4.556

$\Delta P_{total} = 2.4279$ psi

III) 60% Load

$T = 857°F$ $\rho = 120.2321$ lb/ft³

$P = 312.9938$ psia $\mu = 4.5304$ lb/ft-hr

$$G = \frac{0.6 \times 15.28 \times 10^6}{41.8878 \times 3600} = 60.7972 \text{ lb/ft}^2\text{-sec}$$

$$\Delta P = 1.16 \times \frac{1}{64.4} \times \frac{1}{120.2321} \times 60.7972^2 \times \frac{1}{144} = 0.0038$$

$P_3 = 312.9901$ psia

$$G_T = \frac{0.6 \times 15.28 \times 10^6}{2.0212} = 4535919.258 \text{ lb/ft}^2\text{-hr}$$

$$= 1259.9776 \text{ lb/ft}^2\text{-sec}$$

$$\Delta P = 0.9524 \times \frac{1}{64.4} \times \frac{1}{120.2321} \times 1259.9776^2 \times \frac{1}{144} = 1.3561$$

$P_2 = 311.6340$ psia

$$Re = \frac{4535919.258 \times 1.6042}{4.5304} = 1.60615 \times 10^6$$

$\frac{e}{D} = 0.00003$ $f = 0.011$

$$\Delta P_4 = 0.011 \times \frac{0.7292}{1.6042} \times \frac{1}{64.4} \times \frac{1}{120.2321} \times 1259.9776^2 \times \frac{1}{144} = 0.0071$$

$\therefore P_{out} = 311.6268$ psia

$\Delta P_{total} = 1.3670$ psi

[illegible] 4% Load

$T = 365\ ^\circ F$ $\rho = 120.0345\ lb/ft^3$

$P =$ [illegible] psia $\mu = 4.4474\ lb/hr\text{-}ft$

$G = \dfrac{[illegible]}{41.[illegible] \times 600} = 40.5315\ lb/ft^2\text{-}sec$

$\Delta P =$ [illegible] $\times \dfrac{1}{64.4} \times \dfrac{1}{120.0345} \times 40.5315^2 \times \dfrac{1}{144} = 0.0017$

$P_1 =$ [illegible] psia

$G = \dfrac{[illegible] \times 10^6}{[illegible]} = 3023946.172\ lb/ft^2\text{-}hr$

$= 839.9850\ lb/ft^2\text{-}sec$

$\Delta P =$ [illegible] $\times \dfrac{1}{64.4} \times \dfrac{1}{120.0345} \times 839.9850^2 \times \dfrac{1}{144} = 0.6037$

$P_2 = 316.[illegible]$ psia

$Re = \dfrac{3023946.172 \times 1.642}{4.4474} = 1.0[illegible] \times 10^6$

$\dfrac{\epsilon}{D} =$ [illegible] $f = 0.0119$

$\Delta P_f =$ [illegible] $\times \dfrac{[illegible]}{1.642} \times \dfrac{1}{64.4} \times \dfrac{1}{120.0345} \times 839.9850^2 \times \dfrac{1}{144} = 0.0042$

$P_{out} = 316.[illegible]$ psia

$\Delta P_{total} = 0.60[illegible]$ psi ✓

(I) [illegible]% Load

$T = [illegible]\ ^\circ F$ $\rho = 119.3923\ lb/ft^3$

$P = 321.[illegible]$ psia $\mu = 4.1944\ lb/hr\text{-}ft$

$\tau = \frac{[illegible] \times [illegible] \times 10^6}{[illegible] \times 3600} = 20.2657\ lb/ft^2\text{-}sec$

$\Delta P = [illegible] \times \frac{1}{64.4} \times \frac{1}{119.39[illegible]} \times 20.2657^2 \times \frac{1}{144} = 0.0004$

$P_i = 321.4653$ psia

$G = \frac{[illegible] \times [illegible] \times 10^6}{[illegible]} = 1511973.085\ lb/ft^2\text{-}hr$

$= 419.9925\ lb/ft^2\text{-}sec$

$\Delta P = [illegible] \times \frac{1}{64.4} \times \frac{1}{119.3923} \times 419.9925^2 \times \frac{1}{144} = 0.1517$

$P_o = 321.3138$ psia

$Re = \frac{1511973.085 \times 1.6442}{4.4494} = 545376.4498$

$\frac{e}{D} = [illegible]$ $f = 0.013$

$\Delta P_f = [illegible] \times \frac{[illegible]}{1.6442} \times \frac{1}{64.4} \times \frac{1}{119.3923} \times 419.9925^2 \times \frac{1}{144} = 0.0009$

$P_{out} = 321.312[illegible]$ psia

$\Delta P_{total} = 0.1530$ psi

APPENDIX B-6

GULF GENERAL ATOMIC

REPORT GULF-GA-A12416

GULF GENERAL ATOMIC

Gulf-GA-A12416

FINAL REPORT

ANALYSIS OF DYNAMIC FLOW STABILITY IN STEAM GENERATORS FOR THE MOLTEN-SALT BREEDER REACTOR

by

B. E. Boyack

Prepared under
P.O. N24013
Project No. 0540.0000
for
Foster Wheeler Corporation

under
Union Carbide Corporation, Nuclear Division
Subcontract No. 91X-88070C

under
Prime Contract No. W-7405-eng-26
with the
U.S. Atomic Energy Commission

Gulf General Atomic Project 0540 November 20, 1972

GULF GENERAL ATOMIC COMPANY
P.O. BOX 81608, SAN DIEGO, CALIFORNIA 92138

LIST OF SYMBOLS

A	Cross sectional flow area of a steam generator tube, ft^2
D	Tube inside diameter, ft
f	Darcy friction factor
g	Local gravitational acceleration, ft/hr^2
g_c	Newton constant relating force and mass, $lbm\text{-}ft/lbf\text{-}hr^2$
H	Steam enthalphy, Btu/lbm
ΔH	Change in steam enthalphy, Btu/lbm
N	Number of tube segments
p	Static pressure, lbf/ft^2
$\overline{P}$	Normalized heat flow distribution
S	Complex variable replacing time
t	Time, sec
W	Mass flow rate per tube, lbm/hr
z	Spatial coordinate along axis of tube, ft

Greek Symbols

θ	Tube inclination from vertical, degree
ρ	Steam density, lbm/ft^3
ϕ	Time-dependent heat input, Btu/ft-hr
ω	Circular frequency, rad/sec

Subscripts

exit	exit from steam generator tube
inlet	inlet to steam generator tube
j	j^{th} tube segment

TABLES

1. INTRODUCTION

Design procedures for steam generators must include the analysis of instability phenomena in heated tubes. The physical damage and performance degradation associated with flow instabilities such as system control problems, mechanical vibration or thermal cycling of steam generator tubes can be serious and must be avoided or reduced to minimize their effects. Experimental prototype testing of each steam generator design is prohibitive, and the complexity of the physical phenomena precludes simulation through model testing. Consequently, analytical techniques are useful in evaluating or predicting the onset of instability phenomena for conceptual and design studies. A liquid flowing through a heated channel is susceptible to a variety of destabilizing phenomena. It is useful to categorize these phenomena at the outset in order to define the scope of this study. Following Bouré, et al. (Ref. 1), two major classifications may be defined: static instabilities and dynamic instabilities. Static instabilities include the flow excursion or Ledinegg instability, boiling crisis due to ineffective removal of heat from the heated surface, flow pattern transition instability and the compound relaxation instabilities described as bumping, geysering and chugging. The fundamental dynamic instabilities are acoustic oscillations and density wave oscillations.

The static instability of primary design importance in steam generators is the excursive instability. The criterion for onset of the flow excursion instability is well known (Ref. 1), and prediction techniques have been developed which are based on the solution of the steady-state conservation equations for mass, momentum and energy.

Dynamic instabilities are associated with the physics of wave phenomena, density waves for density wave oscillations and pressure (acoustic) waves for acoustic phenomena. In any real system, both kinds of waves are present and interact, but their velocities differ in general by one or two orders of magnitude, thus allowing one to distinguish between the two types of instabilities. The acoustic or pressure wave oscillations are characterized by a high frequency, the period being of the same order of magnitude as the time required for a pressure wave to travel through the system. Acoustic waves are not the subject of the present investigation and will not be discussed further.

Density wave oscillations are common in a variety of equipment and have been extensively studied during the past fifteen years. These are low frequency oscillations in which the period is approximately the order of magnitude of the time required for a density wave to travel through the tube. The instability can be initiated by a temporary reduction or perturbation of inlet flow to the heated channel, producing thereby an increase in the rate of enthalpy rise and a reduction in the average density. The disturbance affects the pressure drop as well as the heat transfer behavior. For certain geometrical arrangements, operating conditions, and boundary conditions, the perturbations can require appropriate phases and become self-sustaining.

Several computer codes exist which can be used to predict the onset of density wave oscillations in heated channels. Codes developed prior to 1965 were reviewed in a comprehensive testing program by Neal and Zivi (Ref. 2). The STABLE-3 code of Jones (Ref. 3) was found to be the most reliable, predicting the threshold of instability for loop experiments within 20 percent for about 70 percent of the tests. It should be noted that the study of Neal and Zivi was restricted to low quality steam systems, the highest exit quality being approximately 0.2. The STABLE-4 program, modified to permit analysis of boiling tubes with superheat and renamed DYNAM (Ref. 4), is in use at Gulf General Atomic Company (GGA). To the author's knowledge, no computer codes have previously been developed to permit analysis of forced circulation loops containing supercritical steam.

A conceptual design has been developed for a single-fluid 1000-MW(e) Molten-Salt Breeder Reactor (MSBR) power station by Oak Ridge National Laboratory (ORNL). In a single-fluid MSBR the nuclear fuel is carried in a fuel salt, a molten-salt mixture at temperatures above ∿ 930°F. Four primary shell-and-tube heat exchangers transfer heat from the fuel salt to a primary coolant salt. Also contained in the primary coolant loop are steam generators, receiving controlled flow rates of the primary coolant salt to provide 1000°F outlet steam temperatures. The steam generators operate on a supercritical pressure steam cycle which was selected because it affords a high thermal efficiency and also permits steam to be directly mixed with high pressure feedwater to raise its temperature to ∿700°F and thereby guard against freezing of the primary coolant salt in the steam generators. Foster Wheeler Corporation has been awarded a contract for the conceptual design of the steam generators for the MSBR.

For this study, the reference design proposed by the Foster Wheeler Corporation for the steam generators of a MSBR was analyzed to determine stability with respect to density wave oscillations. This report describes the method of analysis and summarizes the predicted dynamic stability characteristics of the MSBR steam generator at 100, 80, 60, 40 and 20 percent of full-rated load. Several parameters including inlet orificing, exit orificing, and pressure level have been varied to determine their overall relationship to the steam generator stability.

2. ANALYSIS

2.1 PROBLEM DESCRIPTION

The conceptual design of a steam generator for the ORNL 1000-MW(e) reference steam cycle has been developed by the Foster Wheeler Corporation. The unit, roughly the shape of an "L," is vertically oriented with molten salt flowing on the tube side and steam in the supercritical state on the tube side. Steady-state operating conditions for a single representative tube have been prepared by Foster Wheeler (Ref. 5). The steam inlet and exit conditions at the full and partial loads for which stability calculations have been made are presented in Table 2-1. The tube material is Hastelloy N having the properties outlined in Ref. 6 and reproduced here in Table 2-2. Neither the properties of the molten salt nor details of the tube layout are presented herein. The analytical technique used to predict the onset of density wave oscillations considers a representative tube only and does not explicitly require data describing overall steam generator geometry or shell-side interactions.

2.2 LITERATURE SURVEY

The prediction of the onset of density wave oscillations in heated channels or tubes containing two-phase flow has been reviewed in Ref. 1. Previous studies have included both analytical and experimental investigations to enable the prediction of the onset of the instability. As part of this investigation a literature survey was conducted for the purpose of determining if previous investigations have been conducted to investigate the onset of density wave oscillations in systems containing a fluid in the supercritical thermodynamic state. It is emphasized that the literature survey conducted was limited and should not be considered to be complete.

TABLE 2-1
STEADY-STATE OPERATING CONDITIONS FOR THE
MSBR STEAM GENERATOR REFERENCE DESIGN

	Percent of Rated Load				
	99.68	79.95	59.97	39.89	19.94
Flow Rate/Tube (lbm/hr)	2538.	1900.4	1378.1	910.6	463.1
Inlet Pressure (psi)	3730.	3690.	3658.	3632.	3613.
Exit Pressure (psi)	3599.1	3599.9	3600.	3599.7	3599.8
Inlet Enthalphy (Btu/lbm)	770.5	771.8	772.9	773.9	774.6
Exit Enthalphy (Btu/lbm)	1418.5	1466.	1490.9	1496.7	1485.

TABLE 2-2
DESIGN PROPERTIES FOR NICKEL-MOLYBDENUM-CHROMIUM-IRON ALLOY
(HASTELLOY N)

Temperature (°F)	Allowable Stress (psi)	Modulus of Elasticity (psi)	Mean Coefficient of Expansion (in./in.-°F)	Thermal Conductivity (Btu/ft-hr-°F)
		$X\ 10^{-6}$	$X\ 10^{6}$	
100	25,000	31.3		6.6
200	24,000	30.6		
300	23,000	30.0		
400	21,000	29.5	6.45	7.4
500	20,000	29.0		
600	20,000	28.5	6.76	8.3
700	19,000	28.1		
800	18,000	27.7	7.09	9.2
900	18,000	27.2		9.3
1000	17,000	26.7	7.43	10.4
1050		26.4		
1100	13,000	26.3		11.1
1150		26.1		12.1
1200	6,000	25.7	7.81	11.7

Density, 0.317 lb/in.^{3} at room temperature

Specific heat, 0.095 Btu/lb °F at room temperature;
0.139 Btu/lb °F at 1200°F

A considerable body of literature has been developed which describes the extreme property variations which occur near the critical point. A recent review has been presented by Hall (Ref. 7). As the critical point is approached large changes in density, specific heat, viscosity and thermal conductivity are observed. It is precisely these variations which have been postulated as forming the initiating agency for thermo-hydraulic flow oscillations observed during several experimental investigations.

Mechanized (computer) literature searches were obtained from two sources. The searches were conducted by the Nuclear Safety Information Center (NSIC) located at Oak Ridge National Laboratory and the Heat Transfer and Fluid Flow Service (HTFS) of the British Atomic Energy Research Establishment, Harwell. Citations of publications dealing with density wave oscillations in channels or tubes containing steam in the supercritical state were requested. Both mechanized surveys indicated that the available data are very limited.

A series of studies have been conducted at Oklahoma State University to investigate instabilities encountered during heat transfer to a supercritical fluid. Although experimental programs at Oklahoma State University have concentrated on natural circulation loops, associated literature surveys have been more broadly directed to include both forced and natural circulation test programs. Many fluids, including steam, helium, hydrogen, etc., have been considered. Cornelius (Ref. 8) has conducted an extensive review of the literature available prior to 1965 and reports that the literature contains reference to two modes of oscillations. The first is an acoustic oscillation while the second, having a frequency several orders of magnitude less than the acoustic oscillations, is attributed to a "boiling like" phenomenon. The nature of this second oscillation is clarified by Walker and Hardon (Ref. 9), who focused on the prediction of the threshold of these oscillations assuming that the "density effect" is the sole driving mechanism for the oscillations. They assumed the density effect is the consequence of the non-linear physical relationship between the enthalphy and density of the fluid. The density effect model formulated by Bouré (Ref. 10) was used to predict the flow instability threshold, and excellent agreement with experiment was obtained on a natural circulation loop with Freon-114 as the working fluid.

A similar investigation was reported by Zuber (Ref. 11) in 1966. Zuber's report contains an extensive literature survey and describes an analysis to predict the onset of oscillations in flow systems containing fluid in the supercritical state. The method also follows Bouré (Ref. 10) in that similar assumptions and formulations are used. The problem is analyzed by perturbing the inlet flow, linearizing the set of governing equations (conservation of mass, momentum and energy plus an equation of state) and integrating them along the channel to obtain the characteristic equation. Zuber describes three mechanisms which can induce thermo-hydraulic oscillations at supercritical pressures. One is caused by the variation of the heat transfer coefficient at the pseudo-critical point. The second is caused by the effects of large compressibility and the resultant low velocity of sound in the critical region. The third mechanism is caused by the large variation of flow characteristics brought about by density variations of the fluid during the heating process.

2.3 METHOD

2.3.1 General

The analysis of density wave oscillations in heated tubes can proceed along one of several paths, depending upon the type and detail of information required. A requirement for extensive information concerning the time-dependent physical processes associated with the instability would require the simultaneous solution of a coupled set of non-linear, time-dependent partial differential equations. Generally, such detail is not necessary and only an answer as to whether an instability can occur under specified operating conditions is required. If an instability is predicted, the design is adjusted to eliminate such an occurrence.

For this analysis only a yes or no answer to the question of the possible occurrence of density wave oscillations in the steam generators of the MSBR is sought. The classical method of stability analysis is employed whereby the governing equations are linearized and the behavior of the resulting equations to small perturbations is determined (Ref. 12). The mathematical model used to define steam generator instabilities is based on a single steam tube located in an array of tubes connected in parallel between headers. It is assumed that a flow perturbation might occur in this single tube while the remaining tubes operate normally. Therefore, the pressure drop across the tube under investigation will be constant since it is established by the steady flow through the remaining tubes and all are connected to common headers. In an actual steam generator it may be expected that once a reasonable magnitude flow oscillation starts in one tube, others will be affected and the mode of oscillation may be very complex owing to the many degrees of freedom in the complete system.

The question of accuracy naturally arises when linearization is performed on a set of equations to obtain a solution. In this case the linearization leads to a conservative answer from the standpoint of safe performance. The linearized analysis will predict the threshold of an instability due to a small system perturbation. In the physical case, small perturbations tend to be damped or lead to small limit cycle oscillations which are often difficult to detect without precision instrumentation.

There are several methods for determining the stability of a system described by a set of linear differential equations. A particularly useful method is based on feedback control theory, and only a small part of this highly developed field need be used for solving the problem of density wave oscillations in steam generators. The primary reasons for choosing feedback control theory are the completely systematized nature of the procedure and because the method reduces the set of partial differential equations to ordinary differential equations, a significant reduction in complexity for numerical analysis.

The steps in the solution of the density wave oscillation problem are:

1. The equations expressing the conservation of mass, momentum, and energy and the equation of state are written in terms of suitable variables.

2. The governing equations are linearized by assuming each variable to be composed of a part which is at most a function of position plus a perturbation term which is a function of position and time.

3. The Laplace transform of the equations is taken, which has the effect of transforming the original partial differential equations into ordinary differential equations by replacing the time derivative with a complex frequency variable.

4. The resulting ordinary differential equations are integrated over small increments of length by assuming the system parameters are constant over these small increments of length. It is presumed that the steady state solution for the steam generator is known since parameters from the state of equilibrium are required to determine the transient behavior. Accuracy increases as the length of the segment decreases.

5. The feedback control system representation of the steam generator is set up. For the density wave oscillation problem, the selection of input and output variables is arbitrary but certain choices of these quantities turn out to be more convenient than others. Specifically, pressure perturbations are used in this study. The feedforward and feedback transfer functions are defined, as is the open loop transfer function.

6. The magnitude and phase angle of the open loop transfer function is calculated as a function of the input variable which is assigned a magnitude of unity and frequencies ranging from zero to a value considerably above the expected frequency of density wave oscillations.

7. The values for the open loop transfer function are plotting in polar form (Nyquist diagram) and the Nyquist criterion is used as the basis for assessing stability.

2.3.2 Method Development for Molten-Salt Steam Generators

Gulf General Atomic has developed a computer code which is used for prediction of the onset of density wave oscillations in once-through steam generators containing liquid, two-phase and superheated steam. The GGA code is a modified and extended version of the series of STABLE codes developed at Knolls Atomic Power Laboratory (Ref. 3). The STABLE codes are applicable only to the analysis of boiling channels containing single-phase liquid and two-phase steam. The STABLE-IV code was extended at GGA to permit analysis of steam generators with superheated steam and the modified code designated as DYNAM (Ref. 4).

In order to use DYNAM to predict the dynamic stability characteristics of the reference design steam generators of the MSBR, a modified version of the code, hereafter referred to as the DYMSBR code, was developed. The significant elements in the modification program are described in the following sections.

2.3.3 DYMSBR Code Structure

For the purpose of this analysis, the significant features of the tube-side supercritical steam are that the fluid is compressible and can be described as consisting of a single phase. The analytical formulation of the DYNAM code permits analysis of steam generators having a single-phase liquid at the tube inlet, two-phase flow through an intermediate region of the heated tube and superheated steam at the exit. Thus, of the three flow regimes only the superheat regime is a single-phase compressible fluid.

In order to develop an orderly code structure, that portion of the DYNAM code associated with the superheat regime was extracted from DYNAM and modified to include new input and output routines. As previously indicated, the revised code was named DYMSBR and can be used to predict the dynamic stability characteristics of a steam generator using supercritical steam on the tube side.

2.3.4 Governing Equations

The equations governing the thermodynamic and hydrodynamic processes occurring in a steam generator can be derived from the principles of conservation of mass, momentum and energy. An additional equation, the equation of state, is required if a compressible fluid is being analyzed. If the time-varying flow processes are considered to be one-dimensional in space, considerable simplification of the governing equation is possible. The resultant conservation equations are presented below:

$$\frac{\partial \rho}{\partial t} + \frac{1}{A}\frac{\partial W}{\partial z} = 0 \qquad (2\text{-}1)$$

$$-\frac{\partial p}{\partial z} = \frac{1}{g_c A}\frac{\partial W}{\partial t} + \frac{1}{g_c A^2}\frac{\partial}{\partial z}\left(\frac{W^2}{\rho}\right) + \frac{f}{2 g_c D A^2}\left(\frac{W^2}{\rho}\right) + \frac{g}{g_c}\rho \cos\theta \qquad (2\text{-}2)$$

$$A \rho \frac{\partial H}{\partial t} + W\frac{\partial H}{\partial z} = \phi \qquad (2\text{-}3)$$

Equations 2-1, 2-2, and 2-3 are derived from the principles of conservation of mass, momentum and energy, respectively. The variables W, ρ, p, and H are mass flow rate per tube, density, pressure and enthalpy of the steam flow. The variables z and t are the distance along the heated tube and time, A is the tube cross-sectional area and D the tube inside diameter. The angle θ is the tube inclination from the vertical, f is the Darcy friction factor and ϕ is the heat input per unit length of tube. For this analysis the equation of state considers the density to be a function of enthalpy only, thus eliminating consideration of acoustic effects.

The procedure for deriving the final equation forms has been outlined in Section 2.2.1. The equations are first linearized, the Laplace transform is taken, and the resultant equations are integrated over small spatial increments. The final equations obtained are identical to those reported in Ref. 4. The final equation forms are algebraically complex and thus are not repeated here. The final dependent variables are the perturbation quantities for pressure, mass flow rate and density. The coefficients in the perturbation equation consist of combinations of variables which include geometry factors, tube material properties, and steady-state flow distributions. To this point analyses of channels containing superheated steam and supercritical steam are identical. However, the evaluation of the steady-state flow distributions and coefficients in the perturbation equations marks the separation of the two analyses.

2.3.5 Steady-State Flow Distributions

A steady-state solution is required for evaluation of coefficients appearing in linear perturbation forms of the governing equations. Several features of the steady-state solution require comment. Since the tube-side fluid in the steam generator is steam in the supercritical thermodynamic state, special care must be taken to insure that the evaluations of thermodynamic and transport properties are accurate. For this investigation a set of computer routines published by the ASME (Ref. 13) were used. These subroutines are based on the 1967 IFC Formulations which are described in the 1967 ASME Steam Tables (Ref. 14). The effective film coefficient for supercritical steam has been evaluated following the formulation of Ref. 15. The friction factor for supercritical steam has been evaluated using Deissler's formulation (Ref. 16).

For a given steady-state calculation the tube is divided into a number of segments. For each segment the following parameters are determined:

1. Thermodynamic properties: enthalpy, temperature, pressure, and specific volume.

2. Transport properties: viscosity, thermal conductivity, and specific heat at constant pressure.

3. Pressure drop components: elevation, friction, momentum and orifice losses.

4. Convective film coefficient, wall temperature.

The procedure for obtaining the steady-state solution is direct when mass flow rate, inlet pressure, heat flow distribution, and enthalpy at inlet and exit are specified. The enthalpy rise across the j^{th} tube segment can be calculated from

$$\Delta H_j = \frac{\overline{P}_j (H_{exit} - H_{inlet})}{N} \tag{2-4}$$

where $\overline{P}_j$ is the normalized heat flow distribution and N is the number of tube segments. To eliminate the need for an extensive iterative solution, thermodynamic and transport properties are calculated using the enthalpy at the midpoint of the j^{th} segment and the pressure at the exit of the j-1 segment. The wall temperature at the segment midpoint is calculated by an iterative procedure which begins with the evaluation of the convective film coefficient using values of wall temperature from the previous iteration. The heat transfer is calculated and compared to the known heat transfer, and, if necessary, the wall temperature adjusted to start the next iteration. Once calculated, the wall temperature is used to calculate the friction factor, permitting evaluation of the friction pressure drop across the j^{th} segment. The procedure is repeated for each segment, and the required steady-state distributions are stored for later use in calculating coefficients for the perturbation equations.

Specific parameters from the steady-state solution required for coefficient evaluation are the convective film coefficient, the derivative of the specific volume with respect to enthalpy, specific volume, pressure drop due to friction, specific heat, viscosity, thermal conductivity and enthalpy.

2.3.6 Frequency Response Analysis

As previously indicated, once the governing linear perturbation equations have been derived, a feedback control representation of the steam generator is set up. An open loop transfer function is determined which depends only on the parameters of the system (e.g., steady-state distributions, tube geometry and physical properties, etc.) and is not related to either the initial conditions or the forcing function. Since the transfer function is a complex variable quantity, the output generally differs from the input in both magnitude and phase.

A steam generator is stable if the system will return to equilibrium conditions after being perturbed by some external excitation. The stability of a system can be completely determined from the transfer function by the following rule: for a system to be stable, the transfer function cannot have infinities (poles) in the right half of the complex S-plane. It is noted that when Laplace transforms are taken of the original time-dependent partial differential equations governing the flow of supercritical steam through the steam generator, the independent variable time is replaced by the complex variable S. The utility of the transfer function methodology is based on the above rule since it is only necessary to determine the poles of the transfer function to decide if a system is stable, rather than completely finding the solution of the governing equations.

Several methods are available for determining system stability using the rule described above. The method of Nyquist is the simplest and most direct method for determining system stability. However, a description of the criterion and its relation to the transfer function representation of the system of governing perturbation equation for a steam generator is beyond the scope of this report. A simplified description of the method and its application to steam generators is given in Ref. 12. The specific application of the method to the system of equations solved in this analysis is presented in Ref. 4.

In brief, the procedure for determining system stability is as follows:

1. Let $S = i\omega$ with ω the circular frequency and make a polar plot of the open loop response as ω takes on values from $-\infty$ to $+\infty$.

2. Determine if a vector from the -1 point on the real axis to the trace of the open loop transfer function makes one or more complete revolutions as the trace of the open loop transfer function is developed.

3. The system is unstable if the vector makes one or more clockwise revolutions as ω proceeds from $-\infty$ to $+\infty$.

4. In many cases system stability can be evaluated simply by determining where the trace of the open loop transfer function crosses the real axis. If the trace crosses the real axis to the left of the -1 point the system is unstable, and if to the right of -1 the system is stable.

Example Nyquist diagrams are presented in Fig. 2-1 for the trace of the open loop transfer function and $0 < \omega < +\infty$.

It is emphasized that if there is any question about stability when determined by the above rules, the complete Nyquist criterion must be used. For each of the cases examined in this investigation, it was possible to determine system stability using the simplified procedures listed above.

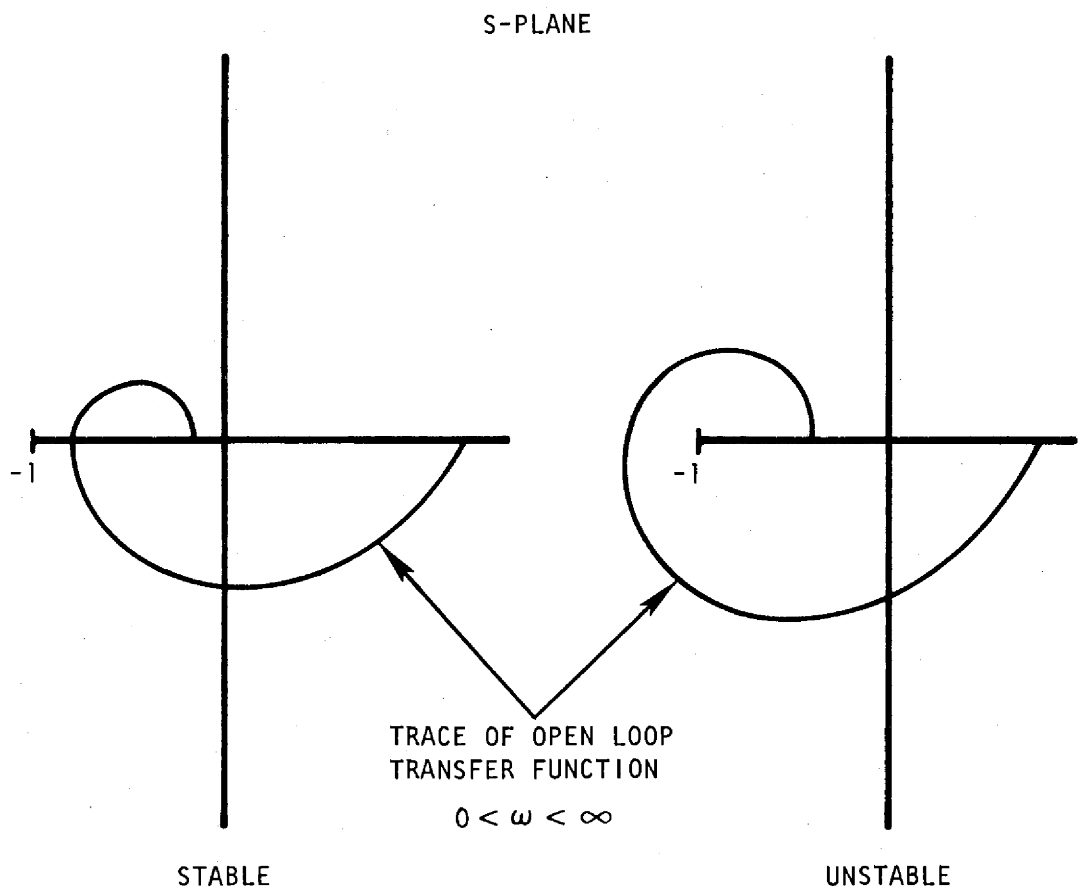

Figure 2-1. Example Nyquist diagrams for polar plots of the open loop transfer function

3. RESULTS

The stability of the reference design steam generators for the Molten Salt Breeder Reactor has been analyzed at 99.68, 79.95, 59.97, 39.89 and 19.94% of full rated load. Operating conditions and design parameters have been provided by Foster Wheeler Corporation in Refs. 5 and 6. Individual steam generator tubes are made of Hastelloy N having design properties listed in Table 2-2. Tube length is 114 ft, tube inner diameter is 0.5 in., and tube wall thickness is 0.125 in. Inlet and exit orifice pressure losses are taken equal to one velocity head or 0.85 psia at the inlet and 5.8 psia at the exit. Steady-state operating conditions for the reference design at each load rating are listed in Table 2-1. The heating distribution along the tube for each load rating is given in Ref. 5.

3.1 TUBE-SIDE DYNAMIC STABILITY AT FULL AND PART LOAD

The open loop frequency response of the reference design is presented in Tables 3-1 through 3-5 for 99.68, 79.95, 59.97, 39.89 and 19.94% of rated load, respectively. In each case the reference design is stable with respect to density wave oscillations as measured by the Nyquist stability criterion. Nyquist plots are presented in Fig. 3-1 for the reference design at 99.68 and 19.94% of rated load. It is clear that the system is highly stable as the trace of the open loop transfer function does not approach the region of the imaginary axis. Further, at reduced flow and heating rates the trace of the open loop transfer function is shifted along the real axis away from the -1 point, indicating an increase in stability at the lower flow and heat rates. However, it is emphasized that the system is very stable and that the above effects are not significant for the reference design.

TABLE 3-1
OPEN LOOP FREQUENCY RESPONSE OF REFERENCE DESIGN STEAM GENERATORS FOR AN MSBR OPERATING AT 99.68% OF RATED LOAD

Frequency (radians/sec)	Open Loop Response[a]	
	Real Part	Imaginary Part
.0000	.4105+04	.0000
.2500+00	.2650+04	.1680+00
.5000+00	.2650+04	.3360+00
.1000+01	.2650+04	.6719+00
.5000+01	.2650+04	.3360+01
.1000+02	.2650+04	.6718+01
.2500+02	.2650+04	.1678+02
.5000+02	.2652+04	.3345+02
.7500+02	.2656+04	.4989+02
.1000+03	.2660+04	.6600+02
.1500+03	.2674+04	.9681+02
.2000+03	.2691+04	.1251+03
.5000+03	.2860+04	.2143+03
.1000+04	.3109+04	.7495+02

[a] Tube length divided into 60 segments

TABLE 3-2
OPEN LOOP FREQUENCY RESPONSE OF REFERENCE DESIGN STEAM GENERATORS FOR AN MSBR OPERATING AT 79.95% OF RATED LOAD

Frequency (radians/sec)	Open Loop Response[a]	
	Real Part	Imaginary Part
.0000	.4876+04	.0000
.2500+00	.3119+04	.4114+00
.5000+00	.3119+04	.8228+00
.7500+00	.3119+04	.1234+01
.1000+01	.3119+04	.1646+01
.1500+01	.3119+04	.2468+01
.2000+01	.3119+04	.3291+01
.5000+01	.3119+04	.8227+01
.7500+01	.3119+04	.1234+02
.1000+02	.3119+04	.1645+02
.1500+02	.3120+04	.2466+02
.2000+02	.3120+04	.3287+02
.5000+02	.3128+04	.3156+02
.1000+03	.3155+04	.1589+03

[a] Tube length divided into 66 segments

TABLE 3-3
OPEN LOOP FREQUENCY RESPONSE OF REFERENCE DESIGN STEAM GENERATORS FOR AN MSBR OPERATING AT 59.97% OF RATED LOAD

Frequency (radians/sec)	Open Loop Response[a]	
	Real Part	Imaginary Part
.0000	.5698+04	.0000
.2500+00	.3533+04	.1030+01
.5000+00	.3533+04	.2059+01
.7500+00	.3533+04	.3089+01
.1000+01	.3533+04	.4119+01
.1500+01	.3533+04	.6178+01
.2000+01	.3533+04	.8237+01
.5000+01	.3533+04	.2059+02
.7500+01	.3534+04	.3088+02
.1000+02	.3534+04	.4116+02
.1500+02	.3536+04	.6169+02
.2000+02	.3538+04	.8216+02
.5000+02	.3563+04	.2026+03
.1000+03	.3647+04	.3860+03

[a] Tube length divided into 69 segments

TABLE 3-4
OPEN LOOP FREQUENCY RESPONSE OF REFERENCE DESIGN STEAM GENERATORS FOR AN MSBR OPERATING AT 39.89% OF RATED LOAD

	Open Loop Response[a]	
Frequency (radians/sec)	Real Part	Imaginary Part
.0000	.6653+04	.0000
.2500+00	.4438+04	.2058+01
.5000+00	.4438+04	.4116+01
.7500+00	.4438+04	.6174+01
.1000+01	.4438+04	.8232+01
.1500+01	.4438+04	.1235+02
.2000+01	.4438+04	.1646+02
.5000+01	.4439+04	.4115+02
.7500+01	.4440+04	.6169+02
.1000+02	.4441+04	.8219+02
.1500+02	.4446+04	.1230+03
.2000+02	.4453+04	.1636+03
.5000+02	.4530+04	.3951+03
.1000+03	.4777+04	.6997+03

[a] Tube length divided into 74 segments

TABLE 3-5
OPEN LOOP FREQUENCY RESPONSE OF REFERENCE DESIGN STEAM GENERATORS FOR AN MSBR OPERATING AT 19.94% OF RATED LOAD

Frequency (radians/sec)	Open Loop Response[(a)]	
	Real Part	Imaginary Part
.0000	.8092+04	.0000
.2500-01	.6610+04	.4106+00
.5000+00	.6610+04	.8212+01
.1000+01	.6610+04	.1642+02
.5000+01	.6614+04	.8194+02
.1000+02	.6627+04	.1628+03
.2500+02	.6716+04	.3887+03
.5000+02	.6990+04	.6602+03
.7500+02	.7331+04	.7561+03
.1000+03	.7637+04	.6931+03
.1500+03	.7964+04	.3466+03
.2000+03	.7992+04	.3425+02
.5000+03	.7626+04	-.5160+03
.1000+04	.7156+04	-.7167+03

[(a)] Tube length divided into 86 segments

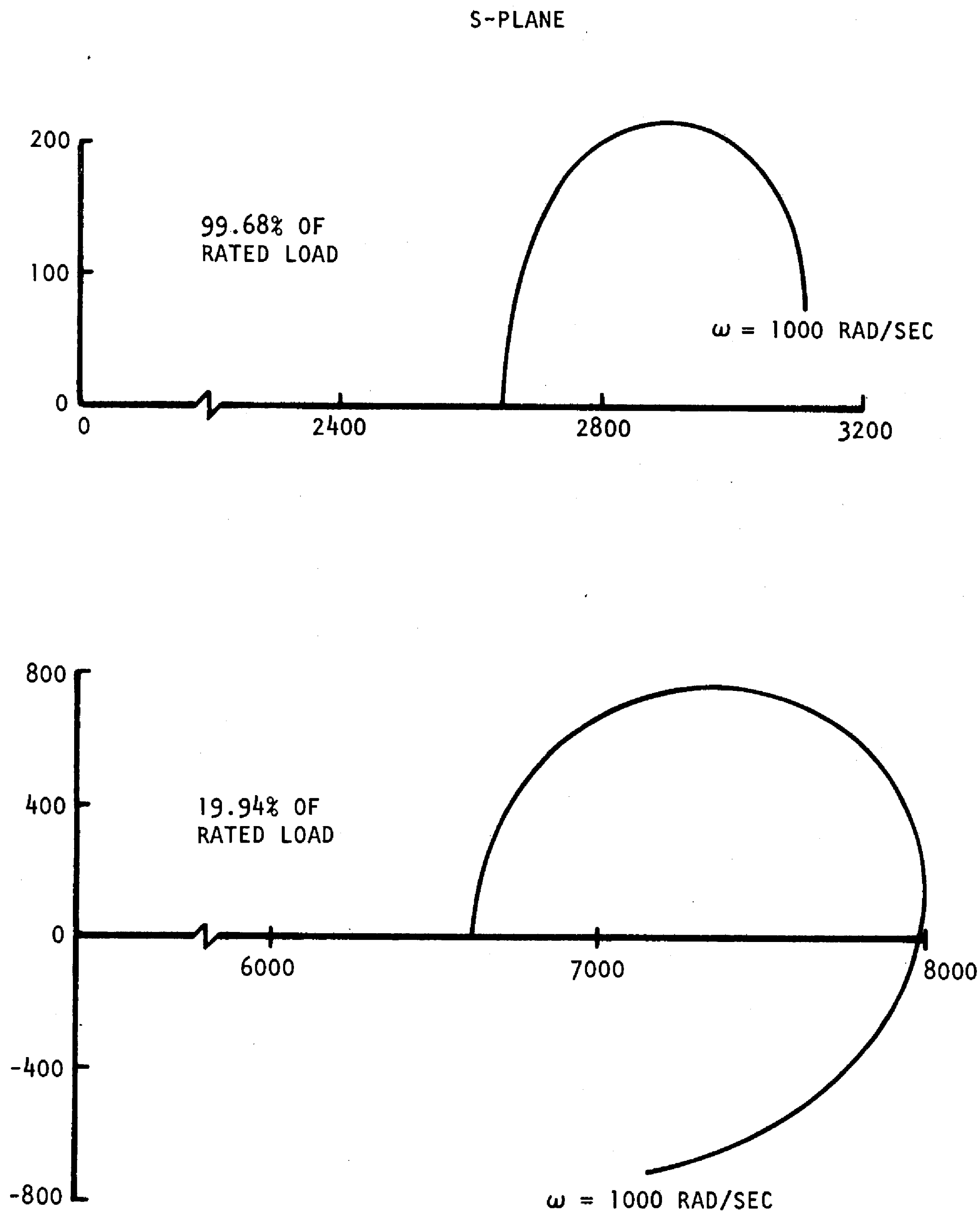

Figure 3-1. Nyquist diagrams of the open loop transfer function for MSBR steam generators, reference design

In density wave oscillations, disturbances travel with the same velocity as the fluid in contrast to acoustic type oscillations where disturbances travel with the local speed of sound in the medium. The period of a density wave oscillation in a steam tube can be roughly estimated by dividing the tube length by the mean velocity of the steam in the tube. For the full and partial loads listed above, density wave oscillations, if they exist, are estimated to have a frequency varying from approximately 0.5 radians/sec at full load to 2.0 radians/sec at 20% of full load. Thus, the frequency ranges as presented in Tables 3-1 through 3-5 clearly encompass the possible frequencies of density wave oscillations.

3.2 SUPPORTING CALCULATIONS

The accuracy of the analysis is dependent upon the number of segments into which the total tube length is divided. As the number of segments becomes large, or conversely as the length of each segment becomes very small, the accuracy of the method is expected to improve. The results reported in Section 3.1 were obtained by specifying non-uniform segment lengths identical to those reported by Foster Wheeler in Ref. 5. The total number of segments used for the 99.68, 79.95, 59.97, 39.89 and 19.94% of rated load cases were 60, 66, 69, 74, and 86, respectively. These tube divisions were determined by Foster Wheeler Corporation to yield highly accurate steady-state solutions. The effect of segment length on accuracy was investigated by examining the 99.68% of rated load case with tube length divided into 23 segments. The resultant frequency response is presented in Table 3-6. It can be seen that the effect of the larger segment length was to shift the trace of the frequency response curve along the real axis away from the -1 point. Clearly accuracy is a second-order effect when compared to the increased stability predicted as flow and heating rates decrease. Further investigation of the effect of segment

TABLE 3-6
OPEN LOOP FREQUENCY RESPONSE OF REFERENCE DESIGN STEAM GENERATORS FOR AN MSBR OPERATING AT 99.68% OF RATED LOAD. TUBE LENGTH DIVIDED INTO 23 SEGMENTS

Frequency (radians/sec)	Open Loop Response	
	Real Part	Imaginary Part
.0000	.4129+04	.0000
.2500+00	.2789+04	.1003+00
.5000+00	.2789+04	.2006+00
.7500+00	.2789+04	.3010+00
.1000+01	.2789+04	.4013+00
.1500+01	.2789+04	.6019+00
.2000+01	.2789+04	.8025+00
.5000+01	.2789+04	.2006+01
.7500+01	.2789+04	.3009+01
.1000+02	.2789+04	.4012+01
.1500+02	.2789+04	.6016+01
.2000+02	.2789+04	.8017+01
.5000+02	.2791+04	.1994+02
.1000+03	.2797+04	.3913+02

length on accuracy was not deemed necessary since the effect of increased segment length was to indicate a more stable system. Also, the segment lengths reported by Foster Wheeler (Ref. 5), and used in this study, have been found by Foster Wheeler to be adequate.

Although tube-side dynamic instabilities are not predicted for the reference design, several brief parameter studies were run to determine the effect of inlet and exit orificing and the effect of system pressure level on system stability. The results for an inlet orifice resistance coefficient K = 120 are presented in Table 3-7 and has an exit orifice resistance coefficient of K = 20 are presented in Table 3-8. The corresponding pressure decreases across the inlet and exit orifices are 102 psia and 116 psia, respectively. It can be seen that the effect of inlet orificing is to make the system less stable while the effect of the exit orificing is to make the system more stable. This trend is just opposite the observed stability trends for two-phase flows where inlet orificing tends to stabilize and exit orificing makes the system less stable. An additional calculation was made with an inlet orifice value K = 180 (a pressure decrease of approximately 153 psia), and the minimum real value of the open loop transfer function was 15.64. Although the margin of stability has been decreased by the inlet orificing, the reference design remains very stable with respect to density wave oscillations.

Zuber (Ref. 11) in his analytical investigation of thermally induced flow oscillations in the supercritical thermodynamic region predicts similar trends for two-phase and supercritical regimes. Thus, inlet orificing is reported as stabilizing the flow and frictional pressure losses and exit orificing leads to a less stable flow. Zuber further notes that his conclusions and results are new and have not yet been verified against experimental data.

TABLE 3-7
OPEN LOOP FREQUENCY RESPONSE OF REFERENCE DESIGN
AT FULL LOAD, INLET ORIFICE K=120

	Open Loop Response[a]	
Frequency (radians/sec)	Real Part	Imaginary Part
.0000	.3480+02	.0000
.2500+00	.2339+02	.8505-03
.5000+00	.2339+02	.1701-02
.7500+00	.2339+02	.2552-02
.1000+01	.2339+02	.3402-02
.1500+01	.2339+02	.5103-02
.2000+01	.2339+02	.6804-02
.5000+01	.2339+02	.1701-01
.7500+01	.2339+02	.2551-01
.1000+02	.2339+02	.3401-01
.1500+02	.2339+02	.5100-01
.2000+02	.2340+02	.6797-01
.5000+02	.2341+02	.1690-00
.1000+03	.2347+02	.3317-00

[a] Tube length divided into 23 segments

TABLE 3-8
OPEN LOOP FREQUENCY RESPONSE OF REFERENCE DESIGN
AT FULL LOAD, EXIT ORIFICE K=20

Frequency (radians/sec)	Open Loop Response[a]	
	Real Part	Imaginary Part
.0000	.8294+04	.0000
.2500+00	.5303+04	.3678+00
.5000+00	.5303+04	.7356+00
.7500+00	.5303+04	.1103+01
.1000+01	.5303+04	.1471+01
.1500+01	.5303+04	.2207+01
.2000+01	.5303+04	.2942+01
.5000+01	.5303+04	.7356+01
.7500+01	.5303+04	.1103+02
.1000+02	.5303+04	.1471+02
.1500+02	.5303+04	.2206+02
.2000+02	.5304+04	.2939+02
.5000+02	.5310+04	.7309+02
.1000+03	.5333+04	.1434+03

[a] Tube length divided into 23 segments

Finally the effect of system pressure level on the stability of the reference design was examined. It was found that the reference design was less stable at lower pressures (3530 psia) than at higher pressures (3930 psia), but that the effect was of second-order importance when compared to the effect of either orificing or reducing flow and heating rates.

4. SUMMARY AND CONCLUSION

The DYNAM computer code has been modified to permit the analysis of dynamic instabilities, specifically density wave oscillations, in the reference design steam generator for the Molten-Salt Breeder Reactor. Since the analysis is based on the solution of linear perturbation forms of the conservation equations for mass, momentum, and energy, the primary result of the analysis is to indicate by a 'yes' or 'no' result whether the reference design is stable or unstable with respect to density wave oscillations.

It is emphasized that the available experimental data and analytical studies are very limited. Thus, it has not been possible to verify the solution against either test data or other analyses.

The reference design appears to be highly stable. Analyses of the effect of inlet orificing, exit orificing, and pressure level indicate trends opposite to those observed in two-phase systems. For the reference design, increased inlet orificing and increased pressure level have been found to decrease the stability margin. Exit orificing, reduced pressure level or reduced flow and heating rates appear to increase system stability.

REFERENCES

1. Bouré, J. A., Bergles, A. E., and Tong, L. S., "A Review of Two-Phase Flow Instability," ASME paper 71-HT-42, ASME-AICHE Heat Transfer Conference, Tulsa, Oklahoma, Aug. 1971.

2. Neal, L. G., and Zivi, S. M., "The Stability of Boiling-Water Reactors," Nuc. Sci. Eng., 30, 25 (1967).

3. Jones, A. B., "Hydrodynamic Stability of a Boiling Channel," Knolls Atomic Power Laboratory reports Part I, KAPL-2170, Oct. 2, 1961; Part II, KAPL-2280, Apr. 20, 1962; Part III, KAPL-2290, June 28, 1963; Part IV, KAPL-3070, Aug. 18, 1964.

4. Efferding, L. E., "DYNAM - A Digital Computer Program for Study of Dynamic Stability of Once-Through Boiling Flow and Steam Superheat," USAEC Report GAMD-8656, Gulf General Atomic, 1968.

5. Cox, J. F., Foster Wheeler Corporation, "Full and Part-Load Operating Conditions for the Reference Design Molten-Salt Steam Generator," unpublished data.

6. Cox, J. F., Foster Wheeler Corporation, "Properties of Materials Used in Reference Design Molten-Salt Steam Generator," unpublished data.

7. Hall, W. B., "Heat Transfer Near the Critical Point," in Advances in Heat Transfer, Irvine, T. F., Jr. and Hartnett, J. P. (ed.), Academic Press, New York, 1971, p. 1.

8. Cornelius, A. J., "An Investigation of Instabilities Encountered During Heat Transfer to a Supercritical Fluid," Argonne National Laboratory Report ANL-7032, April 1965.

9. Walker, B. J., and Harden, D. G., "The Density Effect Model: Prediction and Verification of the Flow Oscillation Threshold in a Natural-Circulation Loop Operating Near the Critical Point," ASME paper 67-WA/HT-23, ASME Winter Annual Meeting, Pittsburgh, Pennsylvania, November 1967.

10. Bouré, J. A., "The Oscillatory Behavior of Heated Channels," Part I and II, French Report CEA-R 3049, Grenoble, France, 1966.

11. Zuber, N., "An Analysis of Thermally Induced Flow Oscillations in the Near-Critical and Supercritical Thermodynamic Region," National Aeronautics and Space Administration, Marshall Space Flight Center Report No. NAS 8-11422, May 25, 1966.

12. Katz, R., "The Analysis of Density Wave Oscillations in Steam Generators by Means of Feedback Control Theory," Gulf General Atomic Report Gulf-GA-A12228, Aug. 1, 1972.

13. McClintock, R. B., and Silvestri, G. J., "Formulations and Iterative Procedures for the Calculation of Properties of Steam," ASME Publication H-17, American Society of Mechanical Engineers, New York, New York, 1968.

14. Mayer, C. A., et al., "1967 ASME Steam Tables - Thermodynamic and Transport Properties of Steam Comprising Tables and Charts for Steam and Water," American Society of Mechanical Engineers, New York, New York, 1967.

15. Swenson, H. S., Carver, J. S., and Kakarala, C. R., "Heat Transfer to Supercritical Water in Smooth-Core Tubes," ASME paper 64-WA/HT-25, Winter Annual Meeting, New York, Sept. 1964.

16. Deissler, R. G., "Heat Transfer and Fluid Friction for Fully Developed Turbulent Flow of Air and Supercritical Water with Variable Fluid Properties," Transactions of the ASME, Jan. 1954, pp. 73-85.

APPENDIX C-1

TUBESHEET HEADER ASSEMBLY

STRESSES AT SECTIONS 1-1 THROUGH 7-7

TUBESHEET STRESS AT TUBESHEET CENTER (SECTION 1-1)

(FOR DESIGN PRESSURE, p=4000 PSI)

Element	σ_r	σ_T
391	-4780	-5111
72	-3822	-3826
68	-2432	-2440
440	- 418	- 439
64	435	424
60	1410	1397
56	2408	2396
52	3490	3480
48	4731	4733
344	5616	5946

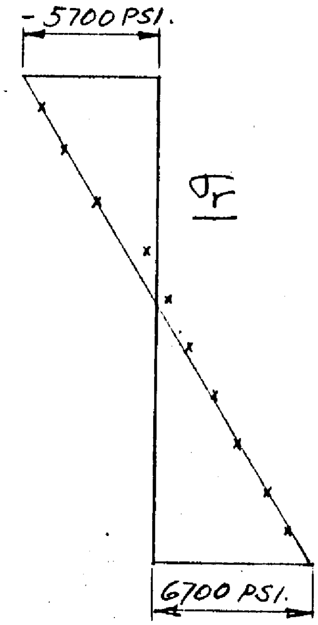

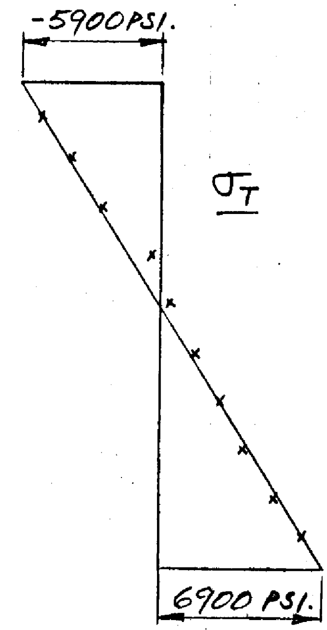

PLOT OF STRESS THROUGH TUBESHEET
(P_m+P_b)

σ_r(TOP) =-5700 psi

σ_r(BOTTOM) = 6700 psi

σ_r(AVG.) = 1/2(6700-5700) = 500 psi

σ_b = ± (5700 + 500) = ± 6200 psi

σ_T(TOP) =-5900 psi

σ_T(BOTTOM) = 6900 psi

σ_T(AVG.) = 1/2(6900-5900) = 500 psi

σ_b = ±(5900 + 500) = ± 6400 psi

(A) PRIMARY GENERAL MEMBRANE STRESS INTENSITY (SECTION 1-1)
(AT T.S. CENTER FOR DESIGN p=4000 PSI)

$$S_1 = P/h\sqrt{(\Delta P \times R/t)^2 + (\bar{\sigma}_r)^2}$$

$$S_2 = P/2h\left[\sqrt{(\Delta p \times R/t)^2 + (\bar{\sigma}_r)^2} + \bar{\sigma}_r + 2p_i h/p\right.$$

Use the larger of S_1 or S_2.

where: p/h = reciprocal of ligament eff. = 1.0/0.476 = 2.10

Δp = differential press. across plate = 4000 psi

p_i = pressure inside tube hole = 4000 psi

R = radial distance from centerline plate to section of interest = 2.063"

t = plate thickness = 14"

$\bar{\sigma}_r$ = radial stress averaged through the depth of the equivalent solid plat

= σ_r(AVG.) + h/p ((p-h) / h) p_i

= 500 + 2096

= 2596 psi

$$S_1 = 2.1\sqrt{34.74 \times 10^4 + 673.92 \times 10^4} = 5590 \text{ psi}$$

$$S_2 = 1.05\,[2662 + 2596 + 3808] = 9520 \text{ psi}$$

Maximum Average Plate Temperature $<$ 1075°F

(B) <u>PRIMARY MEMBRANE PLUS BENDING STRESS INTENSITY (SECTION 1-1)</u>
(AT T.S. CENTER FOR DESIGN p=4000 PSI)

$S = k\ p/h\ \sigma_1$

where: K = stress intensity factor

for top of t.s., $\beta = \sigma_r/\sigma_T$ = 5700/5900 = .97, K = 1.0

for bottom of t.s., β = 6700/6900 = .97, K = 1.0

$\sigma_1 = \sigma_r$ or σ_T, whichever is larger.

S = 1.0 x 2.1 x 5900 = 12,390 psi (TOP)

S = 1.0 x 2.1 x 6900 = 14,490 psi (BOTTOM)

(C) PRIMARY PLUS SECONDARY STRESS INTENSITY (SECTION 1-1)
(AT CENTER OF T.S.)

For Reactor Scram Transient Plus Operating Pressure:

$S = K\ p/h\ \sigma_1$

where K = stress intensity factor

for top of t.s., β = -520/-780 = 0.67, K = 1.015
(El. #390)
for bottom of t.s., β = 4220/4370 = 0.97, K = 1.0
(El. #343)

$\sigma_1 = \sigma_r$ or σ_T, whichever is larger.

S = 1.015 x 2.1 x 780 = 1660 psi (TOP)

S = 1.0 x 2.1 x 4370 = 9180 psi (BOTTOM)

For Load Reduction Transient plus operating pressure:

Top of T.S. (El. #390), β = (-6380) / (-6360) $\approx$ 1.0, K = 1.0

Bottom of T.S., (El. #343), β = (6710) / (6747) $\approx$ 1.0, K = 1.0

S = 1.0 x 2.1 x 6420 = 13,480 psi (TOP)

S = 1.0 x 2.1 x 6750 = 14,180 psi (BOTTOM)

S_{range} = 9.18 + 14.18 = 23.36 ksi

(D) PEAK STRESS INTENSITY
(AT CENTER OF T.S.)

FOR TRANSIENTS DUE TO REACTOR SCRAM AND LOAD CHANGE PLUS OPERATING PRESSURE.

$$S = Y_{max} \frac{P}{h} \sigma_1 + P_s$$

WHERE: Y_{max} = STRESS MULTIPLIER

P_s = PRESSURE ON THE SURFACE WHERE THE STRESS IS BEING COMPUTED

σ_1 = PRINCIPAL STRESS HAVING THE LARGER ABSOLUTE VALUE IN THE PLANE OF THE EQUIVALENT SOLID PLATE

FOR TOP OF T.S., (EL. #390) $\beta = \frac{-520 - 6380}{-780 - 6360} = \frac{6900}{7140} = 0.97$, $Y_{max} = 1.43$

FOR BOTTOM OF T.S., (EL. #343) $= \frac{4220 + 6710}{4370 + 6747} = \frac{10,930}{11,120} = 0.98$, $Y_{max} = 1.43$

S = 1.43 x 2.1 x 7140 + 3600 = 25,040 PSI (TOP)

S = 1.43 x 2.1 x 11,120 + 230 = 33,620 PSI (BOTTOM)

NOTE: FOR REACTOR SCRAM TRANSIENT ALONE PLUS OPERATING PRESSURE WE HAVE FOLLOWING RESULT:

TOP OF T.S., $\beta = \frac{-520}{-780} = 0.67$, $Y_{max.} = 1.68$

BOTTOM OF T.S., $\beta = \frac{4220}{4370} = 0.97$, $Y_{max.} = 1.43$

S = 1.68 x 2.1 x 780 + 3600 = 6350 PSI (TOP)

S = 1.43 x 2.1 x 4370 + 230 = 13,350 PSI (BOTTOM)

TUBESHEET STRESS AT OUTER RADIUS OF PERFORATED ZONE (SECTION 2-2)
(FOR DESIGN PRESSURE, p=4000 PSI ONLY)

Element	σ_r	σ_T
400	-858	-2661
75	- 91	-1119
71	145	- 217
443	1211	1476
67	991	1368
63	1349	1799
59	1295	2128
55	1091	2319
51	946	2559
353	861	2823

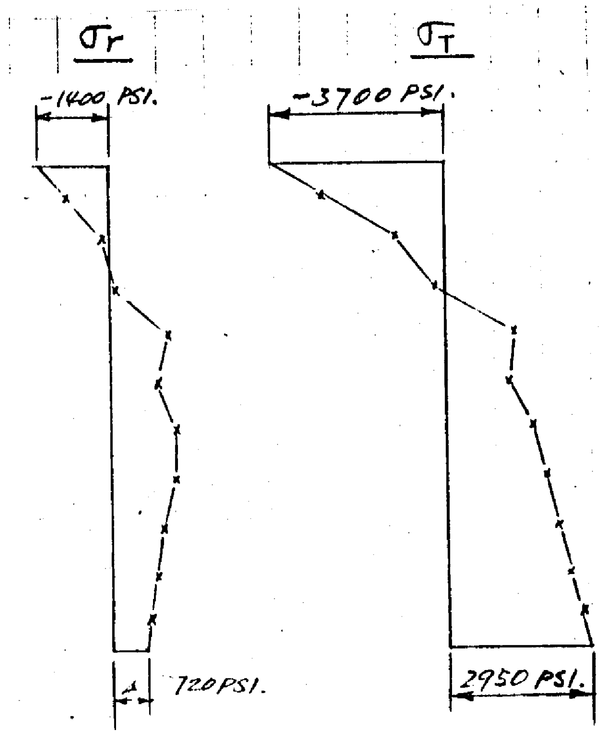

PLOT OF STRESS THROUGH TUBESHEET
$(P_m + P_B)$

σ_r(TOP) = -1400 psi

σ_r(BOTTOM) = 720 psi

σ_r(AVG.) = 694 psi

P_b = ½(1400 + 720) = ± 1060 psi

σ_T(TOP) = -3700 psi

σ_T(BOTTOM) = 2950 psi

σ_T(AVG.) = 1048 psi

P_b = ½(3700 + 2950) = ±3325 psi

Maximum Average Plate Temperature < 1075°F

(A) PRIMARY GENERAL MEMBRANE STRESS INTENSITY (EDGE OF T.S.)

$\bar{\sigma}_r = 694 + 2096 = 2790$ psi

$S_1 = 2.1\sqrt{1.7017 \times 10^7 + 778.41 \times 10^4} = 10{,}460$ psi

$S_2 = 1.05 \left[4980 + 2790 + 3808\right] = 12{,}160$ psi

(B) PRIMARY MEMBRANE PLUS BENDING STRESS INTENSITY (EDGE OF T.S.)

Top of T.S., $\beta = \sigma_r/\sigma_T = -1400/-3700 = 0.378$, K = 1.04

Bottom of T.S., $\beta = 720/2950 = 0.244$, K = 1.06

S = 1.04 x 2.1 x 3700 = 8080 psi

S = 1.06 x 2.1 x 2950 = 6570 psi

(C) PRIMARY PLUS SECONDARY STRESS INTENSITY

	Top(El. 401)	Bott(El. 354)	Top(El. 401)	Bott(El. 354)
Op.P. + R. Scram	6105	-581	3984	1524
Op.P. + Load Change	- 275	268	-2398	2592
Steady-State	506	-2272	710	-2890

LOADING CONDITION (a)   (P + R.S.)-(P+L.C.)

TOP	BOTT	TOP	BOTT
6380	-849	6382	-1068

TOP OF T.S.:

β = 6380/6382 ≈ 1.0, K=1.0

S = 1.0 x 2.1 x 6382 = 13,400 psi (TOP)

BOTTOM OF T.S.: β = -849/-1068 = 0.79   K = 1.01

S = 1.01 x 2.1 x 1068 = 2270 psi (BOTT.)

LOADING CONDITION (b)   P + R.S. + SS

TOP	BOTT	TOP	BOTT
6611	-2853	4694	-1366

TOP OF T.S.:

β = 4694/6611 = 0.704, K = 1.02

S = 1.02 x 2.1 x 6671 = 14,220 psi (TOP)

BOTTOM OF T.S.:

β = -1368/-2853 = 0.40   K = 1.03

S = 1.03 x 2.1 x 2853 = 6170 psi (BOTT)

LOADING CONDITION (c)   P + R.S.

TOP OF T.S.:

β = 3984/6105 = 0.65, K = 1.015

S = 1.015 x 2.1 x 6105 = 13,010 psi (TOP)

BOTTOM OF T.S.:

β = -581/1524 = -0.38, K = 1.45

S = 1.45 x 2.1 x 1524 = 4640 psi (BOTT)

PEAK STRESS INTENSITY
(at edge of tube sheet)

For transients due to reactor scram and load change plus operating pressure.

For top of T.S., β = 1.0: Ymax = 1.43

For bottom of T.S., β = 0.79: Ymax = 1.50

$S = Y_{max}\left(\frac{P}{h}\right)\sigma_1 + Ps$

S = 1.43 x 2.1 x 6380 + 3600 = 22760 (Top)

S = 1.50 x 2.1 x 6382 + 230 = 20333 (Bottom)

SECTION 3-3 PRIMARY MEMBRANE

Element	σ_r	σ_z	σ_T	σ_{rz}
364	71	-1578	2085	419
365	-846	-3897	891	1537
366	-1269	-3658	779	2490
367	-1626	-5858	-236	3100
368	-2664	-7190	-1144	4141
Avg.	-1267	-4436	475	2337

$\sigma_1 = -28$

$\sigma_2 = -5676$ $\quad S = 6150 = P_L$ (Assume Also P_m)

$\sigma_3 = 475$

PRIMARY PLUS SECONDARY STRESSES

ELEMENT 364	σ_r	σ_z	σ_T	σ_{rz}
1) OP. P. + R.S.	8645	3879	-6760	-5997
2) OP. P. + L.S.	-1546	-2398	3543	1572
3) S.S.	11710	6986	-11540	-9174

CONDITION (a) (1) - (2)

	σ_r	σ_z	σ_T	σ_{rz}
	10191	6277	-10303	-7569

$\sigma_1 = 16052$ $\quad \sigma_2 = 416$ $\quad \sigma_3 = -10303$

S = 26360

CONDITION (b) (1) + (3)

	σ_r	σ_z	σ_T	σ_{rz}
	20355	10865	-18300	-15171

$\sigma_1 = 31506$ $\quad \sigma_2 = -286$ $\quad \sigma_3 = -18300$

S = 49,810

Maximum Temperature $< 1150^\circ F$

SECTION 4-4 PRIMARY STRESSES

Element	σ_r	σ_z	σ_T	σ_{rz}
384	-406	2027	-404	5013
385	-1098	4791	198	4467
386	-1847	4450	-205	2831
387	-1185	3698	84	2929
388	-1107	1144	-795	792
389	+106	-508	-684	534
Avg.	-922	2600	-301	2761

$\sigma_1 = 4114$ $\sigma_2 = -2436$ $\sigma_3 = -301$

S = 6550

SECTION 4-4 PRIMARY PLUS SECONDARY STRESSES

	σ_r	σ_z	σ_T	σ_{rz}
1 OP. P + R.S.	-678	1254	-11140	5264
2 OP. P + L.S.	-609	4377	1948	3974
3 S.S.	1363	1302	-1071	1141

Condition (a) (1) - (2)

-69	-3123	-13088	1290

$\sigma_1 = -3595$ $\sigma_2 = 403$ $\sigma_3 = -13088$

S = 13490

Condition (b) (1) + (3)

685	2556	-12211	6405

$\sigma_1 = 8094$ $\sigma_2 = 4852$ $\sigma_3 = 12211$

S = 20,310

Maximum Temperature $<$ 1000°F

PRIMARY LOCAL MEMBRANE STRESS SECTION 5-5

El.	σ_R	σ_z	σ_T	σ_{Rz}
420	5492	24660	7066	10250
421	3636	14480	3449	5126
422	2891	9002	1611	3000
423	1821	6679	689	1186
424	2126	4590	102	2404
425	1397	3811	- 240	460
426	1116	1778	- 931	850
427	379	- 684	-1821	253
428	81	- 2693	-2446	- 264
AVG.	+2104	+6847	+ 831	+ 2585

$$\sigma_1, \sigma_2 = \tfrac{1}{2}(2104 + 6847) \pm \left[((6847-2104)/2)^2 + 2585^2\right]^{\frac{1}{2}}$$

$$= 4476 \pm 3508$$

$$= 7984,\ 968$$

$$\sigma_3 = \sigma_T = 831$$

Stress intensity, S = 7984 - 831 = 7150 psi

Maximum Temperature $< 1000^{\circ}F$

SECTION 5-5 PRIMARY PLUS SECONDARY STRESSES

		σ_r	σ_z	σ_T	σ_{rz}
1	OP. P. + R.S.	41110	21020	20320	24,430
2	OP. P. + L.S.	9040	4640	-240	8420
3	S.S.	5603	3397	1374	3874

Condition (a) (1) - (2)

32070	16380	20560	16010

$\sigma_1 = 41,054$ $\sigma_2 = 6396$ $\sigma_3 = 20560$

S = 34,658

Condition (b) (1) + (3)

46713	24417	21694	28304

$\sigma_1 = 65985$ $\sigma_2 = 5145$ $\sigma_3 = 21694$

S = 60,840

PRIMARY GENERAL MEMBRANE STRESS SECTION 6-6

El.	σ_R	σ_z	σ_T	σ_{Rz}
108	-2550	4667	3805	-3214
109	-2236	5248	3990	-2946
110	-1773	5621	4166	-2696
111	-1271	5840	4320	-2485
112	- 748	5974	4469	-2344
113	- 214	6070	4623	-2291
114	317	6165	4788	-2336
115	833	6300	4971	-2477
AVG.	- 955	5736	4392	-2599

$$\sigma_1, \sigma_2 = \tfrac{1}{2}(5736 - 955) \pm \left[(5736 + 955/2)^2 + (-2599)^2\right]^{\frac{1}{2}}$$

$$= 2391 \pm 4236$$

$$= 6627, -1845$$

$$\sigma_3 = \sigma_T = 4392$$

Stress Intensity, S = 6627 + 1845 = 8470 psi (Section A-A)

Maximum Temperature $< 1000^\circ F$

Stresses due to R.S. and L.S. alone are given below:

	σ_r	σ_z	σ_T	σ_{rz}	SI
R.S.	3670	11130	23330	-5020	22184
L.S.	-1370	- 4150	- 8800	1860	8362

SECTION 6-6 PRIMARY PLUS SECONDARY STRESSES

		σ_r	σ_z	σ_T	σ_{rz}
1	OP. P. + R.S.	-1311	24810	19120	-6673
2	OP. P. + L.S.	-3568	1139	-5242	-561
3	S.S.	98	1968	-262	-354

Condition (a) (1) - (2)

2257	23671	24362	-6112

σ_1 = 25293 σ_2 = 635 σ_3 = 24362

SI = 24658

Condition (b) (1) + (3)

-1213	26778	18858	-7027

σ_1 = 28444 σ_2 = -2878 σ_3 = 18858

SI = 31322

SECTION 7-7 PRIMARY STRESSES

Element	σ_r	σ_z	σ_T	σ_{rz}
180	-3144	-3264	13090	-333
181	-2059	-2809	12320	-475
182	-1129	-2265	11710	-687
183	-369	-1656	11200	-917
184	221	-991	10760	-1125
185	639	-281	10360	-1279
186	887	468	9962	-1353
187	964	1267	9571	-1328
Avg.	-499	-1191	11122	-937

$\sigma_1 = 154$

$\sigma_2 = 1844$ S = 12970

$\sigma_3 = 11,122$

Maximum Operating Temperature < 1000°F

SECTION 7-7 PRIMARY PLUS SECONDARY STRESSES

	σ_r	σ_z	σ_T	σ_{rz}	SI
1 O.P. + R.S.	843	8181	35140	-5325	37090
2 O.P. + L.S.	-4228	-7165	2680	1576	
3 S.S.	-19	-50	-189	24	

Condition (a) (1) - (2)

5071	15346	32460	-6901

$\sigma_1 = 18,812$ $\sigma_2 = 1606$ $\sigma_3 = 32460$

S = 30,850

Condition (b) does not control

Condition (c) S = 37,090 (max.)

SECTION 8-8

Primary stresses (due to design pressure of 4000 psi)

Element	σ_r	σ_z	σ_T	σ_{rz}
332	-3629	4515	12300	-3.6
333	-2941	4501	11620	11.1
334	-2331	4495	11020	20.2
335	-1788	4490	10500	24.4
336	-1305	4485	10040	24.0
337	-874	448-	9627	19.5
338	-492	4476	9259	11.2
Average	-1908	4491	10623	Negligible

$\sigma_1 = -1908$

$\sigma_2 = 4491$ S = 12531 psi

$\sigma_3 = 10623$

APPENDIX C-2

HASTELLOY N MATERIAL PROPERTIES

A) ALLOWABLE STRESSES (REFERENCE 4)

Temp.	S_t 0 hr	S_t 10 hr	S_t 10^2 hr	S_t 10^3 hr	S_t 10^4 hr	S_t 10^5 hr	S_mt 10 hr	S_mt 10^2 hr	S_mt 10^3 hr	S_mt 10^4 hr	S_mt 10^5 hr	S_o	S_m
70	26,600											25,000	26,600
400	26,600											21,000	26,600
600	26,600											20,000	26,600
800	25,200											18,000	25,200
1000	23,850											17,000	23,850
1100	22,950	48,000	34,000	24,000	17,160	12,000	22,950	-	-	17,160	12,000	13,000	22,950
1200	22,050	34,670	24,000	16,000	12,000	7,260	22,050	-	16,000	12,000	7,260	6,000	22,050
1300	19,300	24,000	16,000	10,000	6,250	3,500	19,300	16,000	10,000	6,250	3,500	3,500	19,300
1400	16,600	12,000	7,670	5,070	3,330	2,000	12,000	7,670	5,070	3,330	2,000		16,600

B) OTHER PROPERTIES (REFERENCE 7)

Temperature (°F)	Modulus of Elasticity (psi)	Mean Coefficient of Expansion in./in.-°F (70° - T)	Thermal Conductivity (Btu/ft-hr-°F)
	X 10^{-6}	X 10^{6}	
100	31.3		6.6
200	30.6		
300	30.0		
400	29.5	6.45	7.4
500	29.0		
600	28.5	6.76	8.3
700	28.1		
800	27.7	7.09	9.2
900	27.2		9.3
1000	26.7	7.43	10.4
1050	26.4		
1100	26.3		11.1
1150	26.1		12.1
1200	25.7	7.81	11.7

Density, 0.317 lb/in.^{3} at room temperature.

Specific heat, 0.095 Btu/lb °F at room temperature;
0.139 Btu/lb °F at 1200°F.

APPENDIX C-3

GULF GENERAL ATOMIC

REPORT GULF-GA-A 12414

GULF GENERAL ATOMIC

Gulf-GA-A12414

FINAL REPORT

TUBE RUPTURE ANALYSIS OF A COUNTERFLOW HEAT EXCHANGER

by

J. J. Johnson and D. A. Wesley

Prepared under
P.O. N24013
Project No. 0540.0000
for
Foster Wheeler Corporation

under
Union Carbide Corporation, Nuclear Division
Subcontract No. 91X-88070C

under
Prime Contract No. W-7405-eng-26
with the
U.S. Atomic Energy Commission

Gulf General Atomic Project 0540 November 20, 1972

GULF GENERAL ATOMIC COMPANY
P.O. BOX 81608, SAN DIEGO, CALIFORNIA 92138

ABSTRACT

The structural integrity of a counterflow heat exchanger subjected to a steam tube failure was examined. The scope of the investigation was limited to two areas of concern. The effect of the burst on the containment vessel was treated as a plane strain problem, and the results indicated that the shell could withstand the accident without failure. Stresses well above the yield strength of the shell result, however, and an increase in the diameter of the shell of the order of 4.0 inches may be anticipated for the worst case of failure of a tube immediately adjacent to the shell.

The integrity of a tube adjacent to the ruptured tube was considered using a discrete method of analysis modeling the tube as a continuous beam. The results obtained for the response of the adjacent tube indicate that although very large beam deformations are predicted, rupture will not occur, even for the very conservative assumption of no support from surrounding tubes. While this is physically an unrealistic case, it may be considered an upper bound on maximum tube response.

CONTENTS

LIST OF FIGURES

1. INTRODUCTION

A history and general description of the molten-salt breeder reactor are contained in Refs. 1 and 2 along with numerous references to more detailed information on the individual components and the development of new materials for their construction. The purpose of this study was to evaluate the structural integrity of one such component under a specified accident condition. This involved investigation of the effects of a tube rupture on a counterflow heat exchanger. The vessel is a cylindrical shell 114.83 feet in height, 41 inches in outside diameter, and .75 inch wall thickness. It contains 1032 tubes of .75 inch outside diameter and .125 inch wall thickness which are supported by tube sheets at 5 foot intervals (Ref. 6). The shell-side fluid is molten-salt and the tube-side fluid is supercritical steam. The inlet and outlet conditions of the steam and molten-salt are specified in Ref. 3. Both the shell and tubes are constructed of a nickel-base alloy, Hastelloy N, with temperature dependent material properties specified in Refs. 3-6.

The rigorous treatment of a steam tube burst on the structural integrity of its containment vessel and the adjacent tubes is a complex hydrodynamic problem. A mechanized literature survey obtained from the Nuclear Safety Information Center at Oak Ridge, Tennessee, and one performed by the authors verified the lack of completely general solution techniques available for the indicated problem. Since inadequate time was available to develop methods of analysis, it was concluded that the problem must be simplified considerably and its solution sought by an appropriate available technique. The basic philosophy of all such idealizations is to model the phenomena as accurately as possible, using a conservative representation of the problem where necessary. This allows one to qualitatively discuss the results with a reasonable degree of confidence.

The scope of this investigation was limited to two areas of concern. These were the effects of a tube rupture on the structural integrity of the shell and the integrity of an adjacent tube. The shell was treated as a plane strain problem using the PISCES 2DL computer code. This is a finite-difference program which is capable of treating hydrodynamic/structural shock problems. The response of a tube adjacent to the rupture was obtained from a lumped-mass model of a continuous beam. Due to reduction of effort allowed, the treatment of effects of adjoining tubes was not included, either in the overall beam response of the tube or the localized response due to impact, nor was any consideration of scattering of the wave possible. The analysis and models are discussed in detail in subsequent sections.

2. ANALYSIS

2.1 EFFECT OF A TUBE RUPTURE ON THE SHELL

2.1.1 General Remarks

The rupture of a tube adjacent to the wall of the shell was studied by considering a typical transverse section through the shell and analyzing it as a plane strain problem. Average values of temperature, 850°F, pressure in the steam, 3700 psi, and pressure in the molten-salt, 206 psi, were assumed. This assumption removes the longitudinal flow of the molten-salt from consideration, which is reasonable in the time span being considered. The problem was subsequently analyzed using a hydrodynamic computer code named PISCES 2DL.

A series of computer programs identified by the name PISCES have been developed by the Physics International Company (Ref. 7) and are marketed through the Control Data Corporation. The program PISCES 2DL is a two-dimensional hydrodynamic code which utilizes the Lagrangian formulation (Refs. 8 and 9) with a finite-difference approach. The programs contain specific provisions for treating shocks and they allow fluid-solid interaction, a wide variety of equations of state, and non-linear stress-strain models. The standard elastic-plastic model in PISCES is bi-linear and uses the von Mises yield criterion with a Prandtl-Reuss flow rule. This model was used in the present study for the idealized stress-strain curve of Hastelloy N at 850°F shown in Fig. 1.

The actual computer runs were made at Lawrence Berkeley Laboratory at a considerable reduction in cost over the Control Data Corporation's version. The computer models were established after consultation with the staff of Physics International Company since they were most familiar with the capabilities and restrictions of the code.

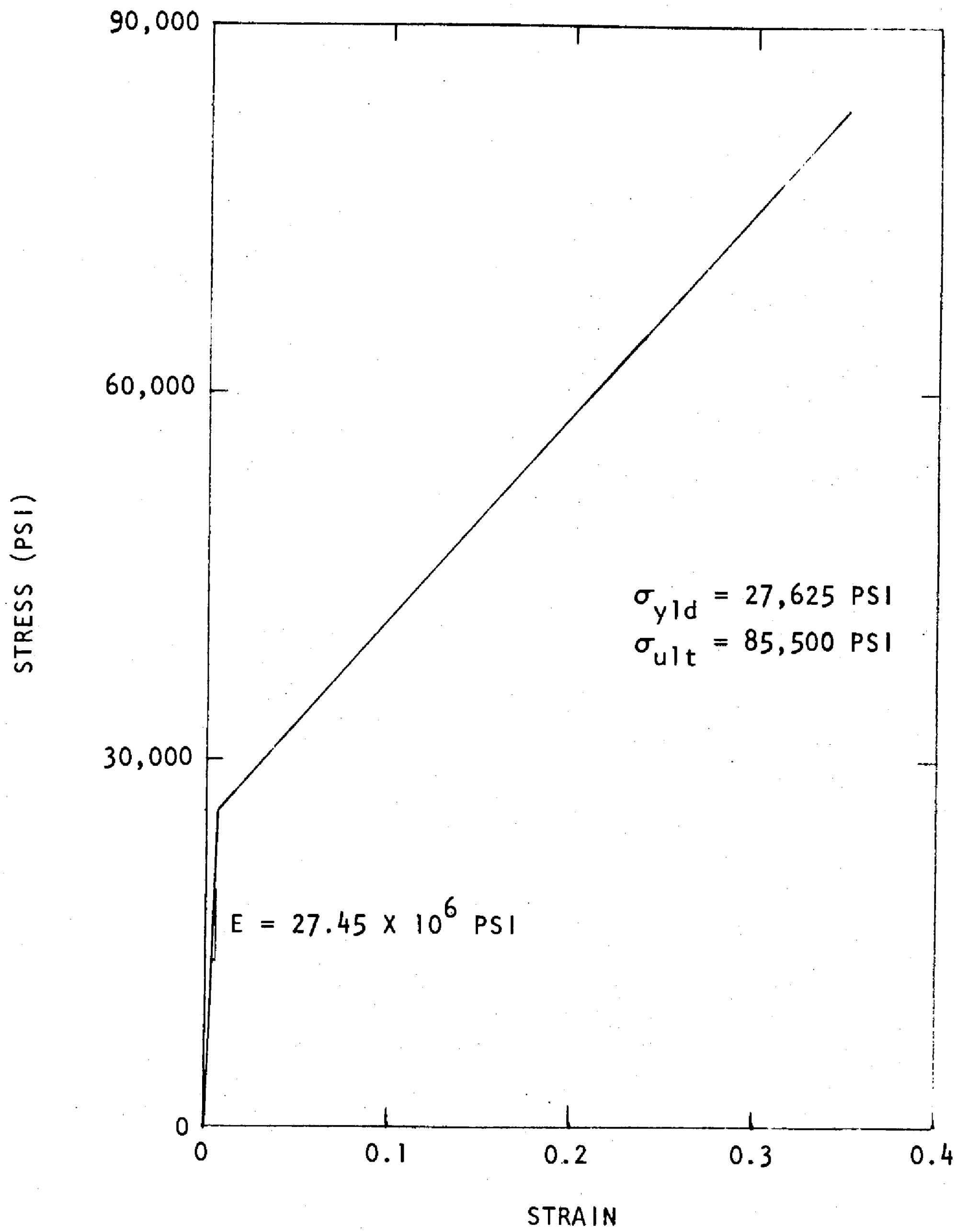

Fig. 1. Idealized stress-strain curve for Hastelloy N at 850°F

2.1.2 Models of the Problem

2.1.2.1 Model I. The first attempt at modeling the shell included the molten-salt, four steam zones (modeling the steam as an ideal gas), and four artificially dense zones (representing the tube) to direct the flow of steam. An overall view of the grid is shown in Fig. 2 and an enlargement of the area containing the steam and artifically dense zones is shown in Fig. 3. Several runs were made with this model for varying boundary conditions in the steam. An accurate representation of the problem was not possible using this configuration and an increase in the number of zones near the rupture was indicated. Although this refinement would not significantly increase the total number of zones, the corresponding reduction in the time step necessary to assure convergence made it economically infeasible. Also, an initial increase in resolution of the mesh at the rupture did not guarantee the solution and a further reduction may have been necessary.

2.1.2.2 Model II. The alternative to this situation was to model the shell excluding the molten-salt and the directed flow of steam from the tube. The disturbance then had to be applied to the shell as a pressure distribution with a specified time and spatial variation.

Quantitative results on tube ruptures are infrequent in the literature. A comprehensive study was recently completed by Eiber et al. of Battelle Columbus Laboratories, Columbus, Ohio (Ref. 10) in which a series of experiments were performed on cylindrical pressure vessels with through-wall and surface flaws to investigate the many facets of a rupture. The failure reported by Eiber propagated along the length of the vessel in contrast to the mode of failure specified by Foster Wheeler Corporation (Ref. 12), i.e., a "fish mouth" type opening in the tube. This difference may be attributed to several factors such as the initiation of failure in the tube and the fact that the tube is a thick-walled cylinder compared to the thin-walled cylinders tested by Eiber.

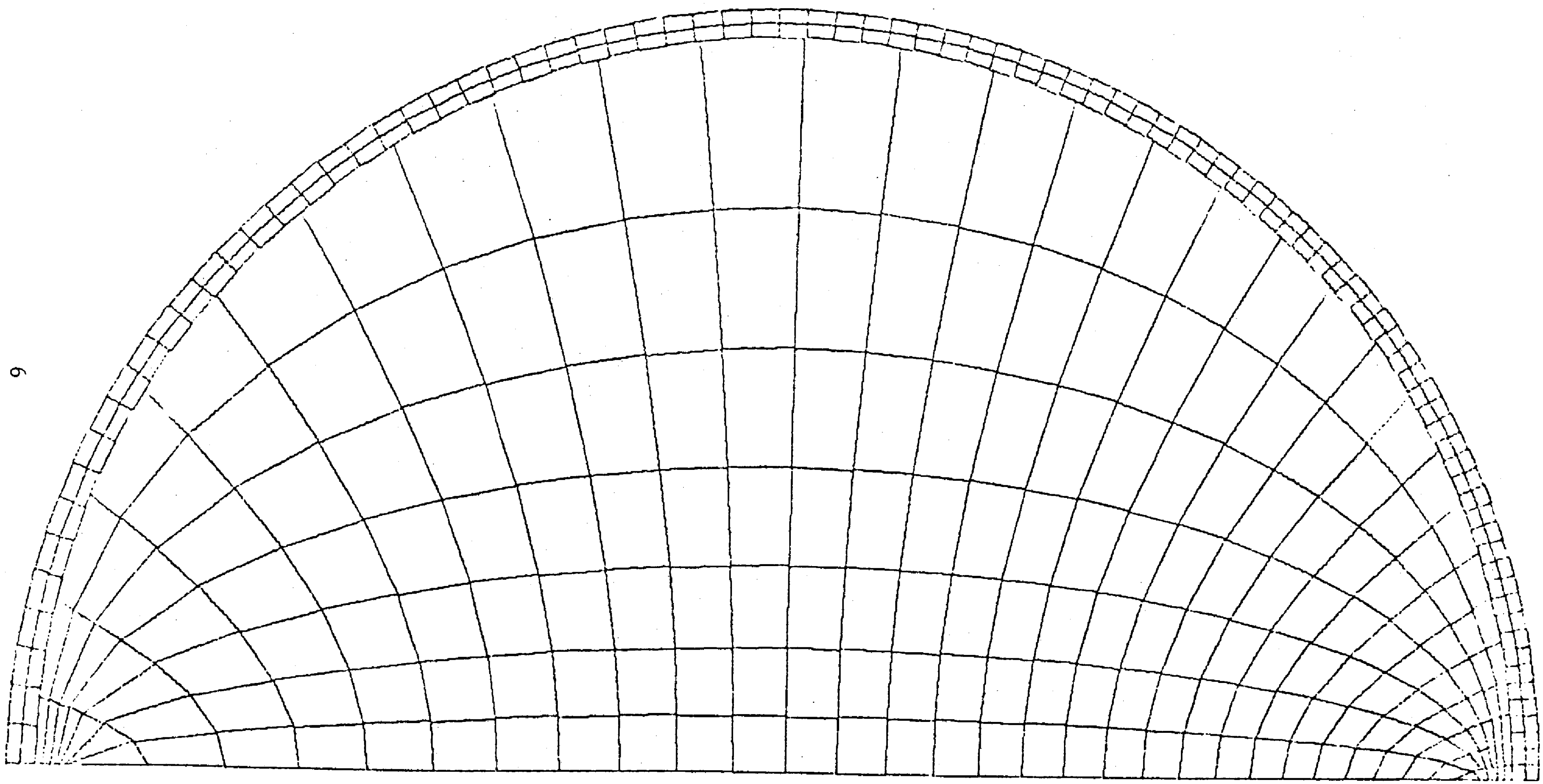

Fig. 2. Grid plot of Model I for the shell analysis

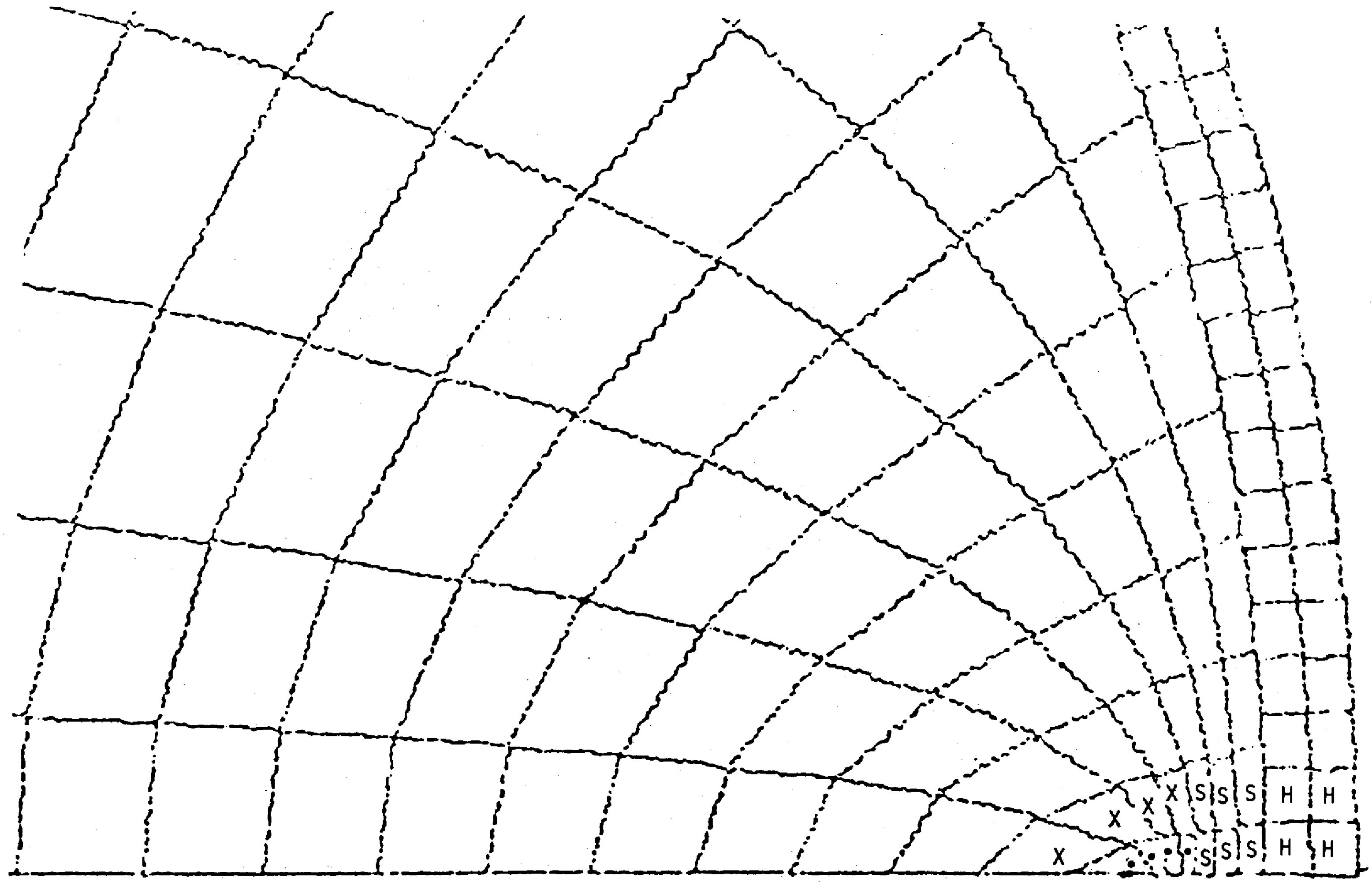

X - ARTIFICIALLY DENSE ZONE

• - STEAM ZONE

S - MOLTEN-SALT ZONE

H - HASTELLOY N ZONE

Fig. 3. Enlarged grid plot of tube rupture area of Model I

The pressure-time history shown in Fig. 4 was selected for the present study. The initial tube pressure was allowed to act for 1.5 milliseconds to reflect the aforementioned discrepancy in the mode of failure. The final pressure was estimated from the results of a shock tube analysis assuming interaction of two fluids with the pressure and other properties of the molten-salt and steam, respectively (Ref. 16). The basic pulse shape and duration are consistent with the measurements made by Eiber as well as those utilized by Gulf General Atomic (Ref. 11) for the analysis of a double-ended steam tube failure. In both cases, the pressure profile of Fig. 4 is an upper bound.

The source of the disturbance is assumed to act at a point 19.175 inches from the center of the shell, Fig. 5, which corresponds to the inside edge of the tube nearest the wall (Ref. 6). The disturbance is naturally modified as it travels through the molten-salt and interacts with the shell. Two phenomena define the character of the pulse experienced by the shell: divergence of the wave as it travels through the salt, and reflection of the disturbance at the interface of the shell and molten-salt. In close proximity to the source, the impedence difference of the molten-salt and shell governs the definition of the disturbance. As the distance from the source increases, spherical divergence plays an increasingly important role.

It is not difficult to verify that the shell is a relatively fixed surface compared to the molten-salt; i.e., a reflected wave of amplitude approaching the amplitude of the incident wave would be generated upon normal incidence (Ref. 13). The maximum amplitude of the reflected disturbance is thus equal to the amplitude of the incident disturbance and occurs at a fixed boundary. This value was conservatively assumed in the present case. This magnification of the pulse due to reflection decreases rapidly as one proceeds along the shell due to the rapidly decreasing angle of incidence.

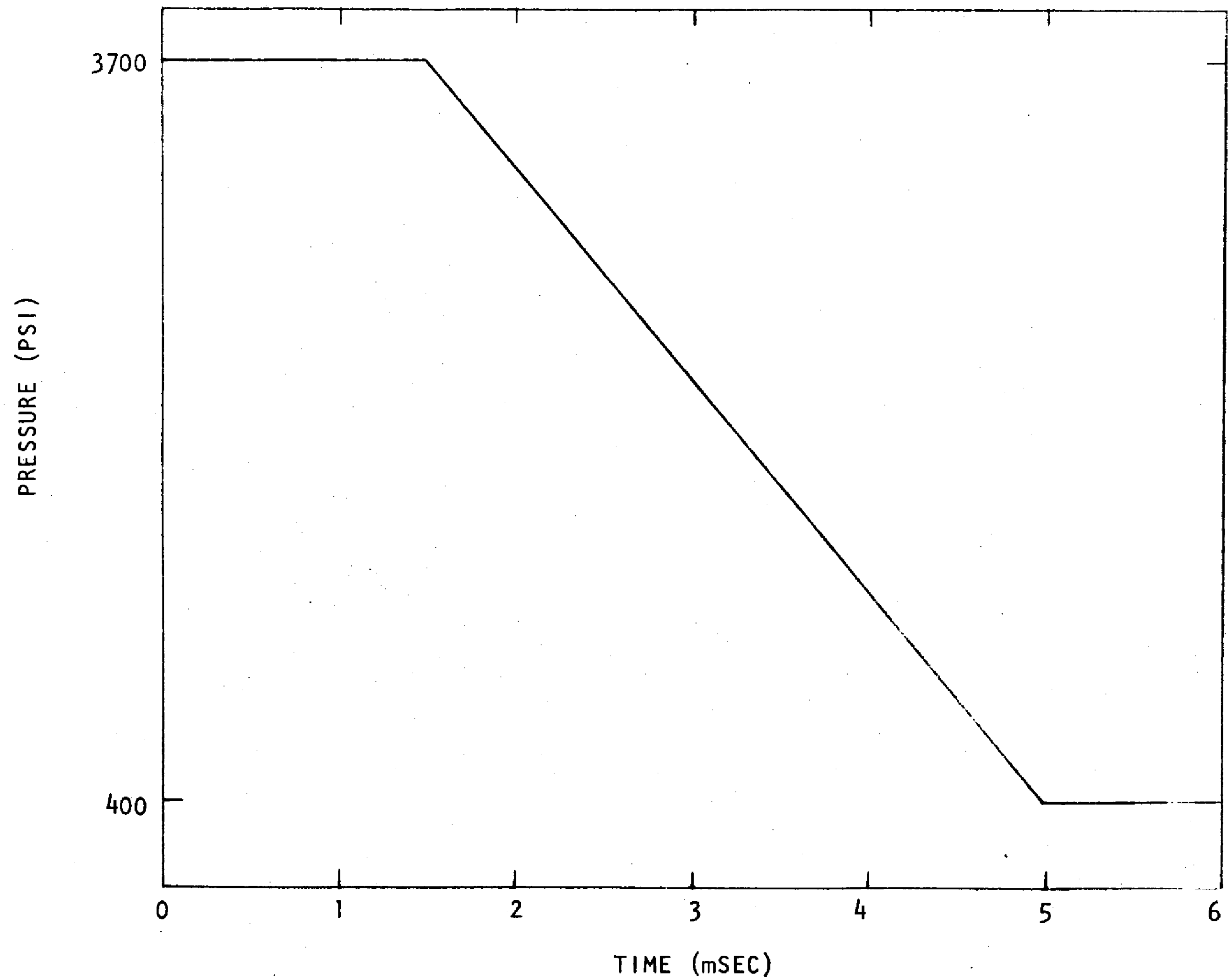

Fig. 4. Pressure-time history of the steam after tube rupture

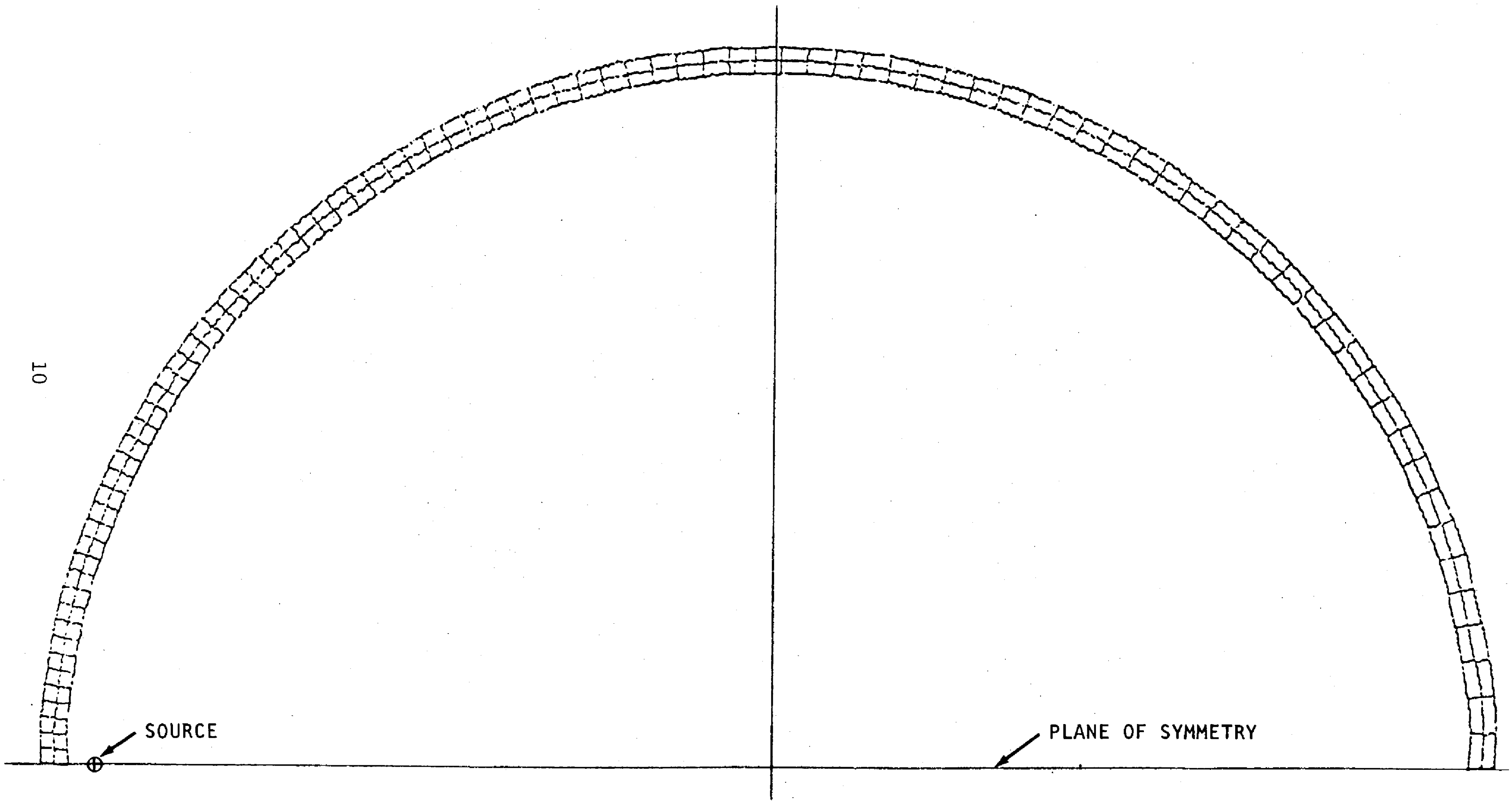

Fig. 5. Grid plot for Model II of the shell analysis

The effect of spherical divergence is two-fold: the disturbance is "spread out" in time, i.e., an increasing rise time with increasing distance from the source, and a decrease in the magnitude of the disturbance occurs (Ref. 13).

Several one-dimensional runs were made with PISCES 1DL (Refs. 14 and 15) in both spherical and plane symmetry to verify and quantify the preceding observations. The results obtained led to the pressure profiles shown in Fig. 6 with the corresponding zones of application depicted in Fig. 7. The duration of the maximum pressure corresponds to the travel time of a signal through the thickness of the shell. At points more remote from the source, the rise time of the disturbance was assumed to increase as the square of its distance from the source and subsequently follow the pressure profile of Fig. 5. The loadings were time lagged by the travel time through the molten-salt.

The results of this analysis are discussed in Section 3.1.

2.2 EFFECT OF A TUBE RUPTURE ON AN ADJACENT TUBE

In addition to the treatment of the shell, the effect of a tube rupture on an adjacent tube was considered. Those properties deemed important to the phenomena were studied and modeled appropriately. In the present case, the elastic-plastic properties of the tube together with the presence of the molten-salt are necessary to accurately represent the physical problem. Thus, as in the previous case, a discrete method of analysis was required.

The tube was modeled as a beam, continuous over four supports, and divided into a discrete number of elements with concentrated mass and stiffness properties. The solution technique used is described by Biggs (Ref. 17). In general, at each time step, an element is acted on by the applied load, shearing forces (derived from the moments at the ends of the segment), an inertial force, and a drag force which approximately represents the resistive force of the molten-salt. The acceleration of the mass is then determined from the equation of motion and integrated to obtain the velocity and displacement of the mass. The moments are determined from a moment-curvature

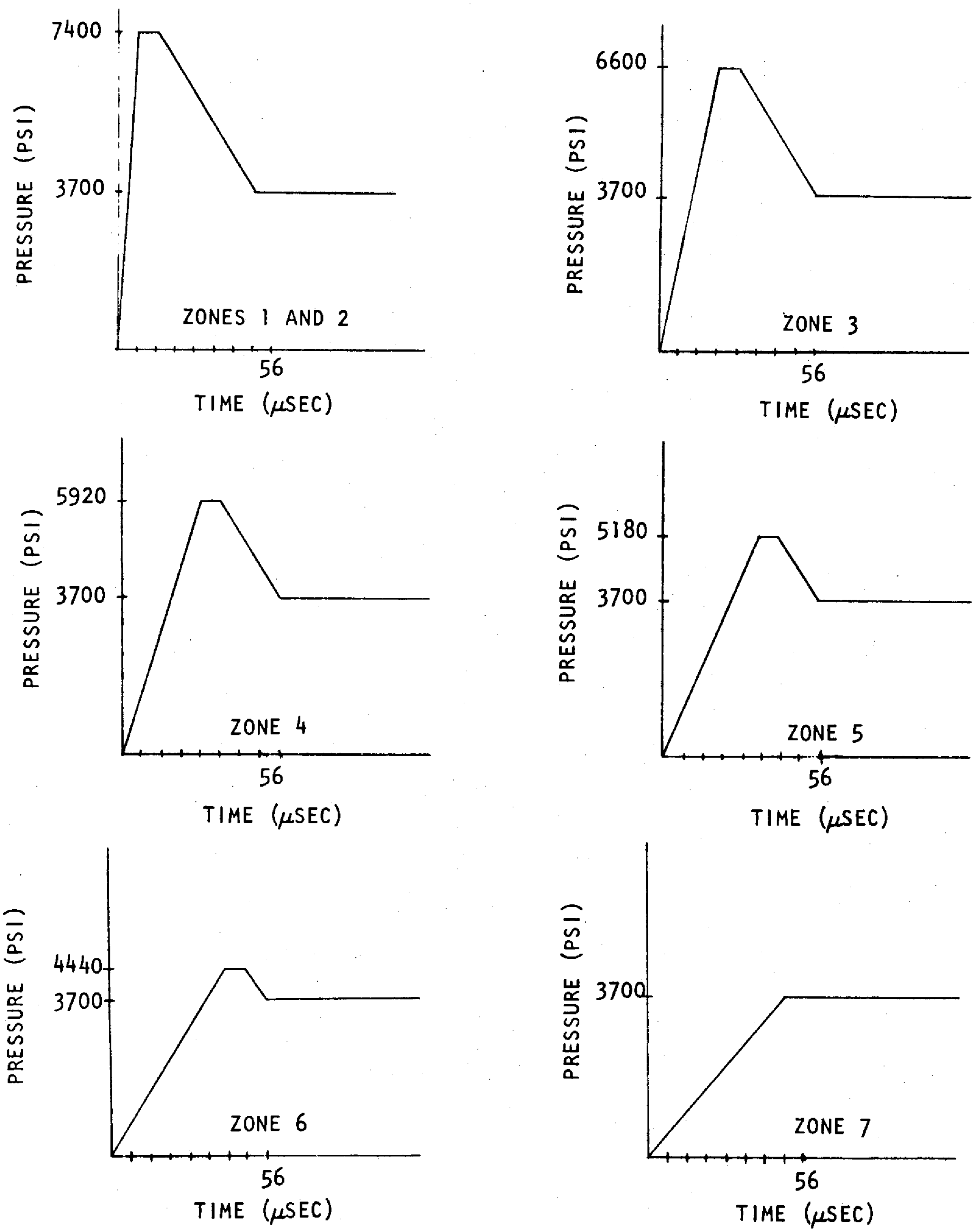

Fig. 6. Pressure profiles applied to the shell. Zone numbers refer to Fig. 7. The pressure profiles follow Fig. 4 for times exceeding 56 sec.

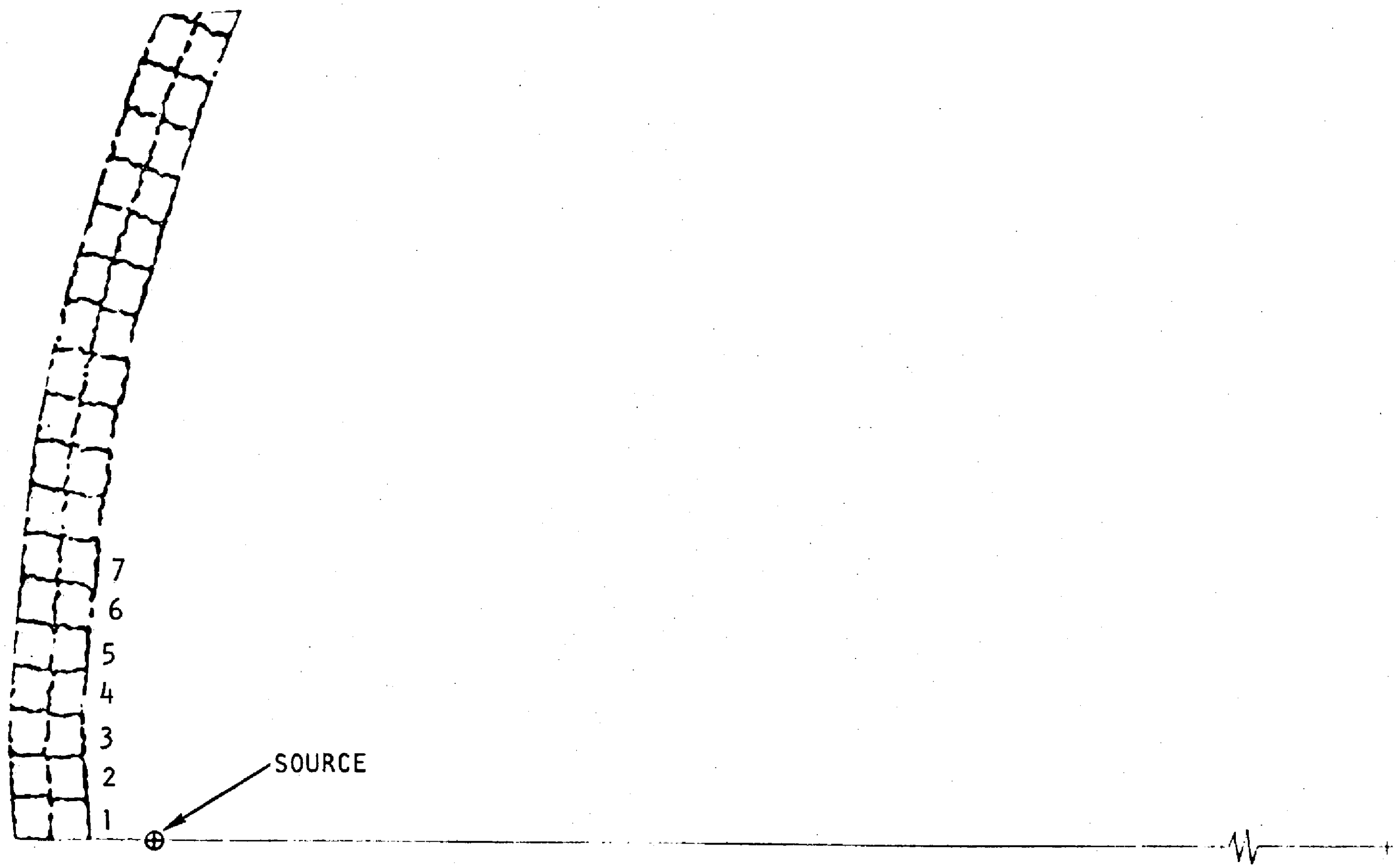

Fig. 7. Zones of application of the pressure profiles - Model II of the shell analysis

relation where the curvature is defined as the second central difference of the displacements. An elastic-plastic moment-curvature diagram was derived for the tube from the stress-strain diagram of Fig. 1 assuming a linear distribution of strain through the cross section of the tube. The result is shown in Fig. 8. The drag force was defined as in Ref. 18 with a minimum value of the drag coefficient assumed ($C_D = 1.0$). Several loading cases were considered.

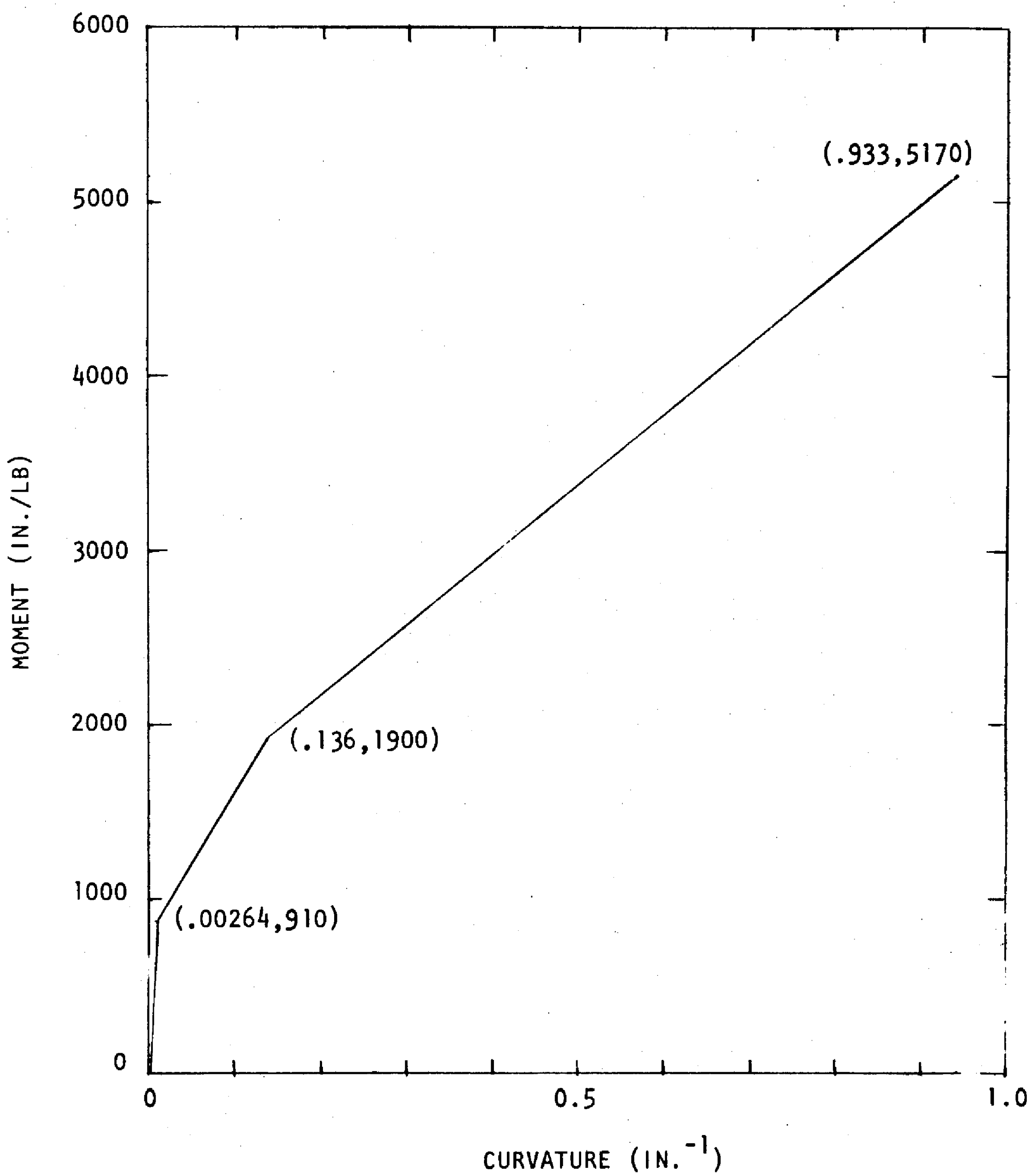

Fig. 8. Idealized moment-curvature relationship of a tube

3. RESULTS AND DISCUSSION

3.1 EFFECT OF A TUBE RUPTURE ON THE SHELL

The pressure profile discussed in the previous section was applied to the shell and the solution obtained for 1.5 milliseconds. Effective stress-time histories are plotted in Figs. 9-12 for the first four zones along the circumference of the shell. The maximum stress (42,900 psi) occurs at 1.5 milliseconds and is one-half the ultimate strength of Hastelloy N at 850°F. The computer solution was terminated at this point for several reasons. The initial disturbance has made over two complete circumferential transits of the shell and the remaining pressurization of the shell is slow in comparison. At 1.5 milliseconds, the pressure profile of Fig. 5 begins to decrease, approaching a quasi-static pressurization of the shell at a considerably smaller pressure.

Grid plots of the shell at various times in the solution are depicted in Figs. 13-20. Figure 21 is a computer plotted time history of the circumferential stress in the first zone of the shell. An increase in the diameter of the shell of 3.6 inches has occurred at 1.5 milliseconds.

3.2 EFFECT OF A TUBE RUPTURE ON AN ADJACENT TUBE

Several loading cases were considered for both a single span, simply supported beam and a three span continuous beam. The model and loading case reported here are shown in Fig. 22. A plot of the maximum moment-time history for the beam is shown in Fig. 23. The simple tube model considered would not rupture. However, the results of the analysis exceed the applicability of beam theory because very large deformations occur; e.g., a maximum mid-span deflection of 24.5 inches was calculated. Furthermore, the geometry of the heat exchanger also limits the applicability of the model,

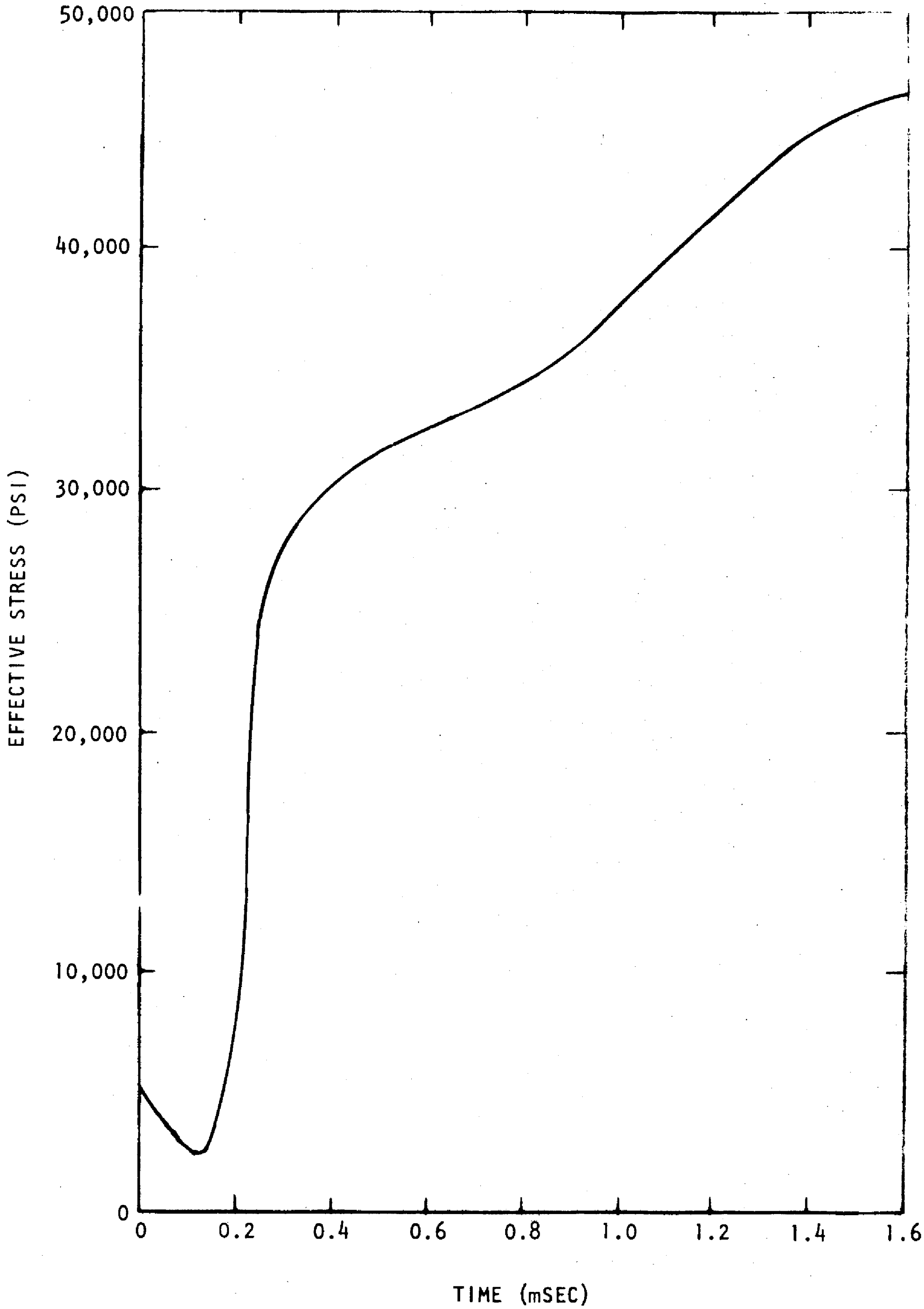

Fig. 9. Effective stress-time history in Zone 1

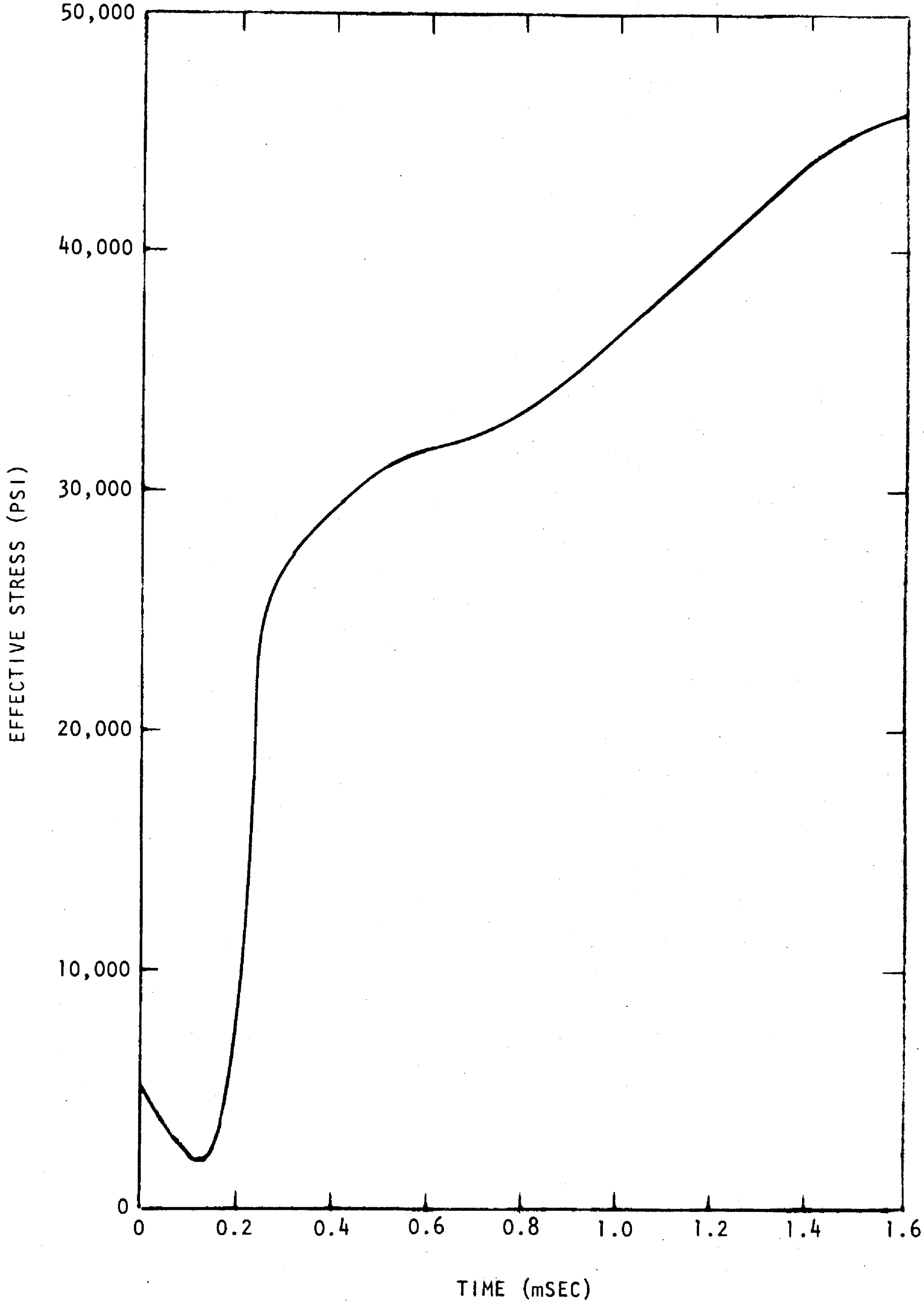

Fig. 10. Effective stress-time history in Zone 2

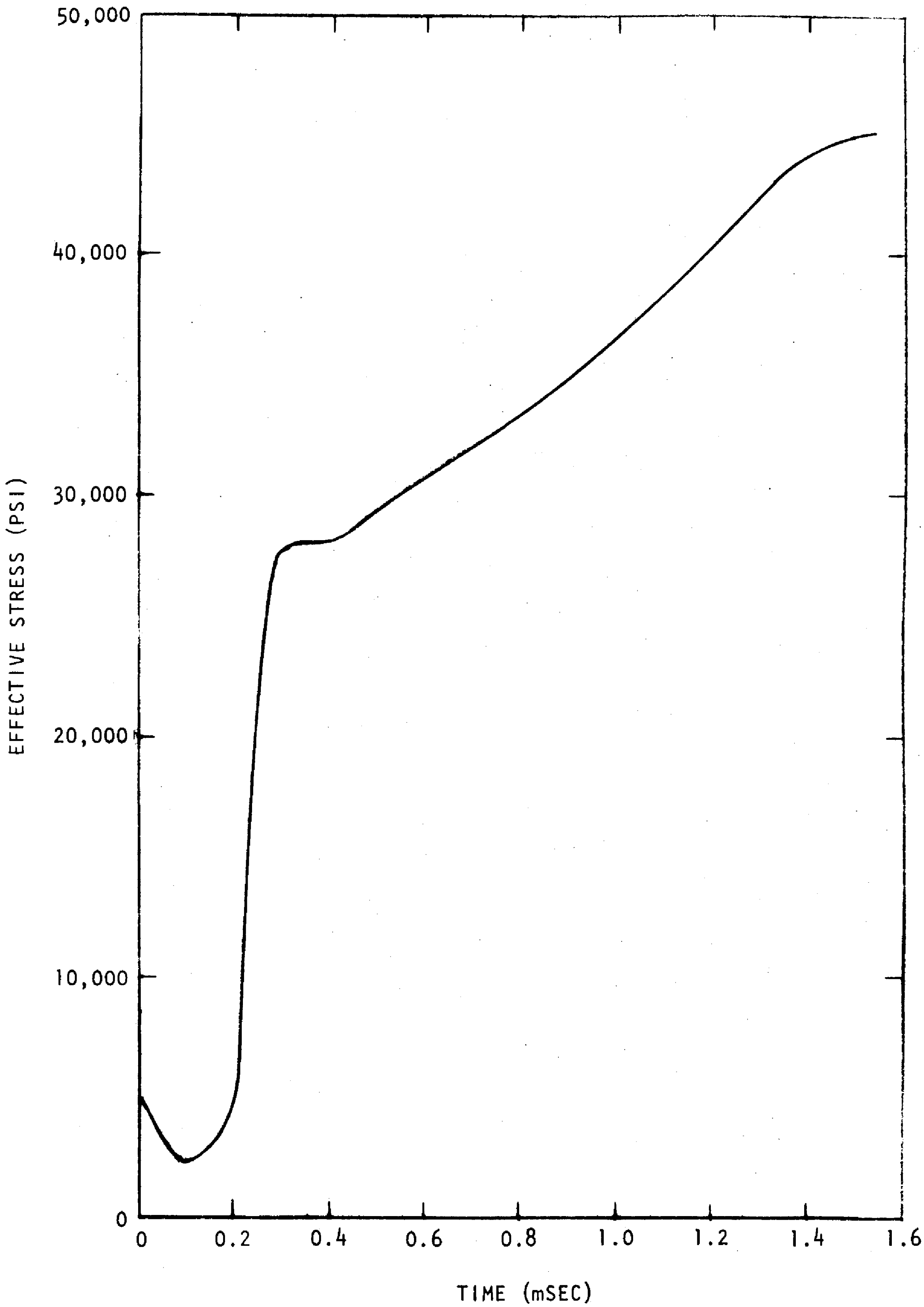

Fig. 11. Effective stress-time history in Zone 3

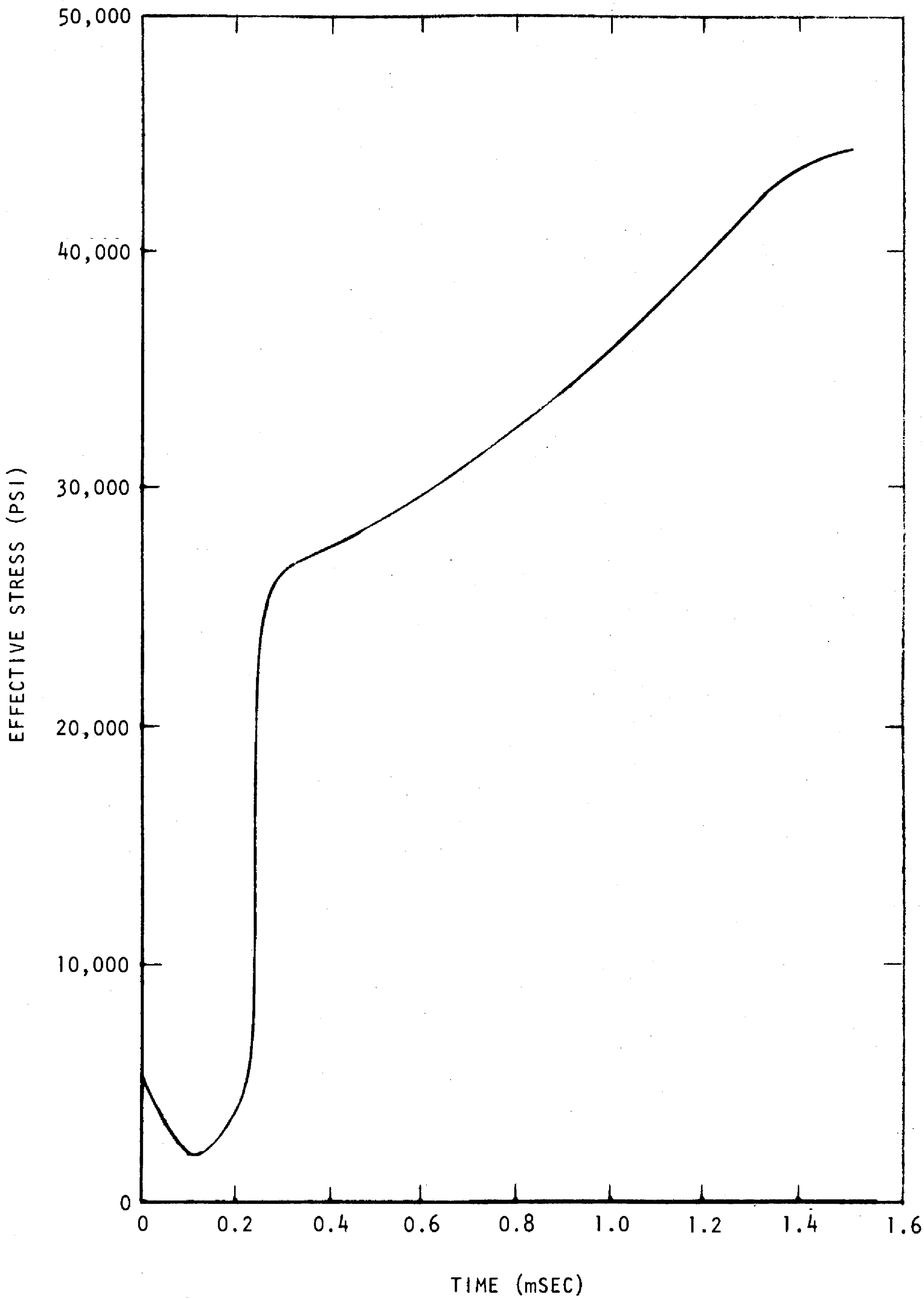

Fig. 12. Effective stress-time history in Zone 4

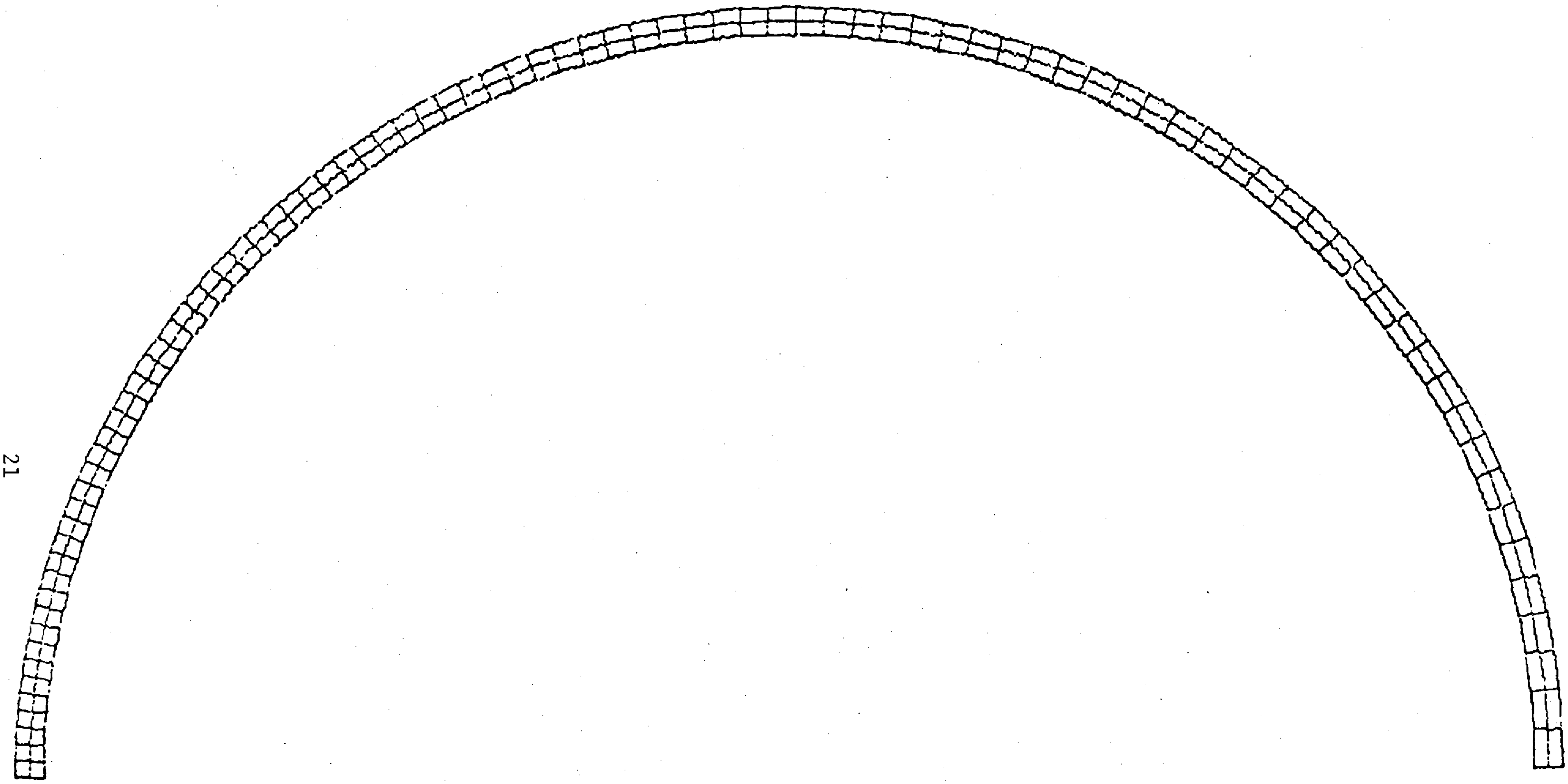

Fig. 13. Grid plot of the shell, time = 0 seconds

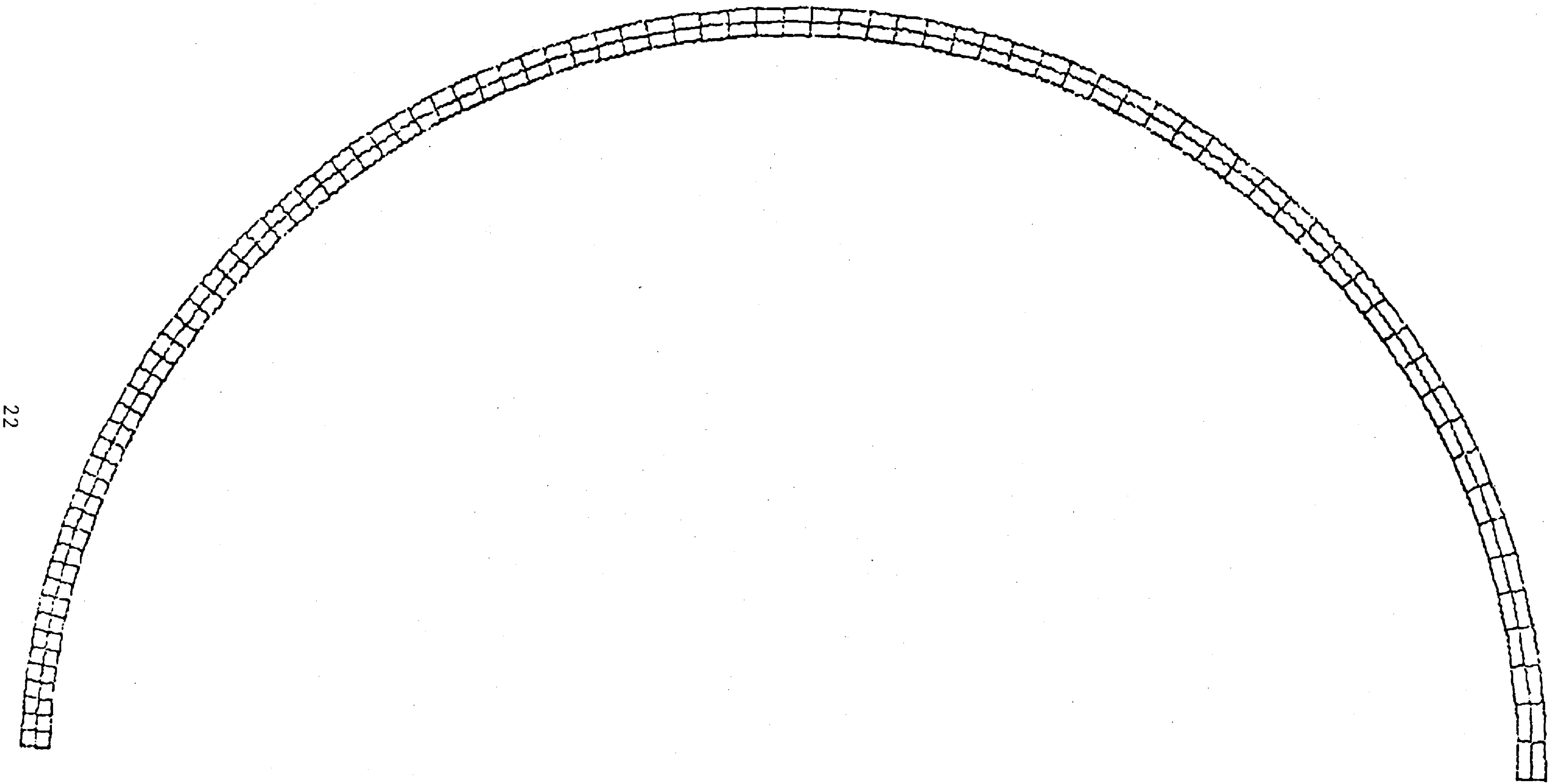

Fig. 14. Grid plot of the shell, time = 50 μsec

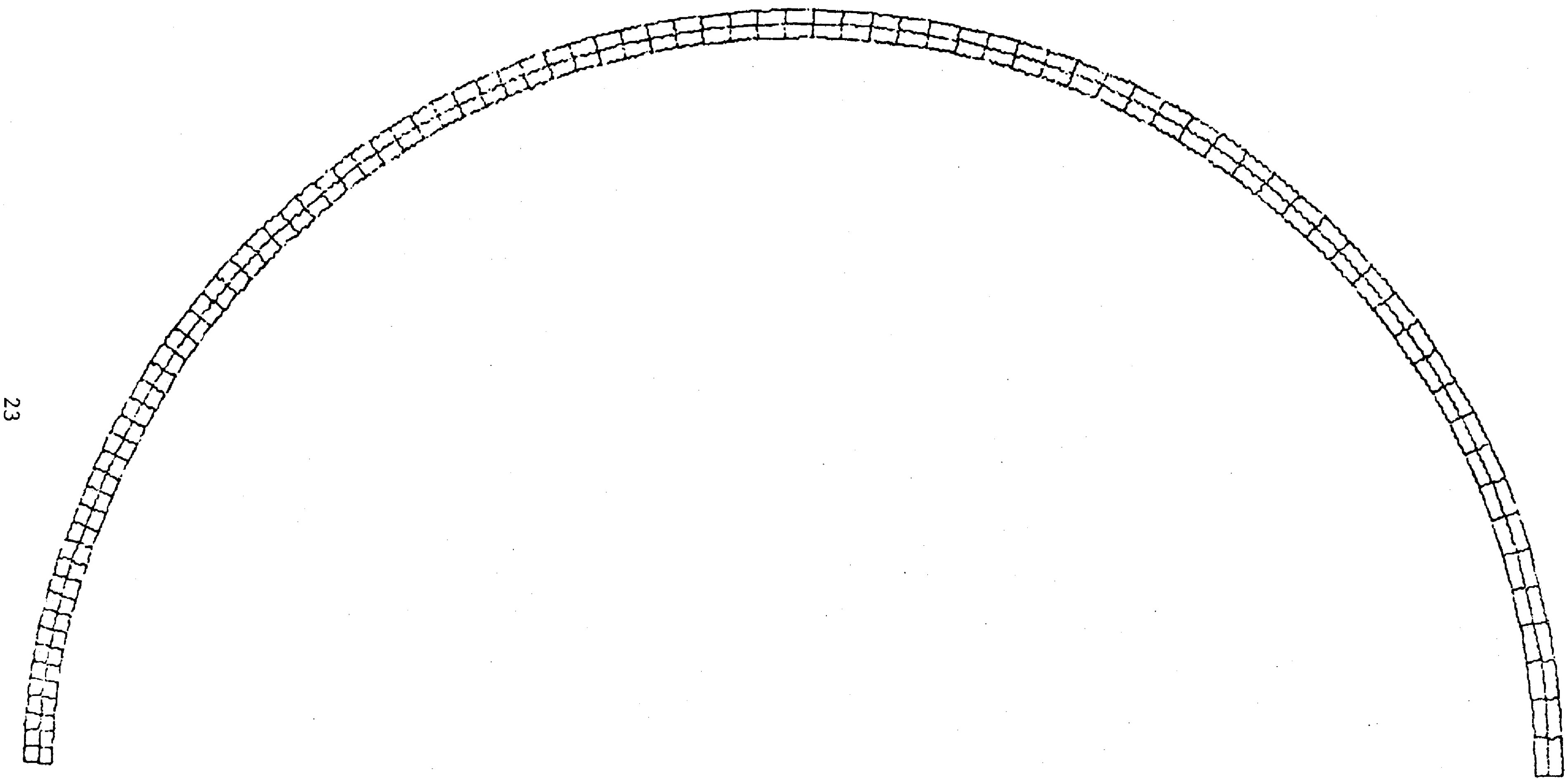

Fig. 15. Grid plot of the shell, time = 254 μsec

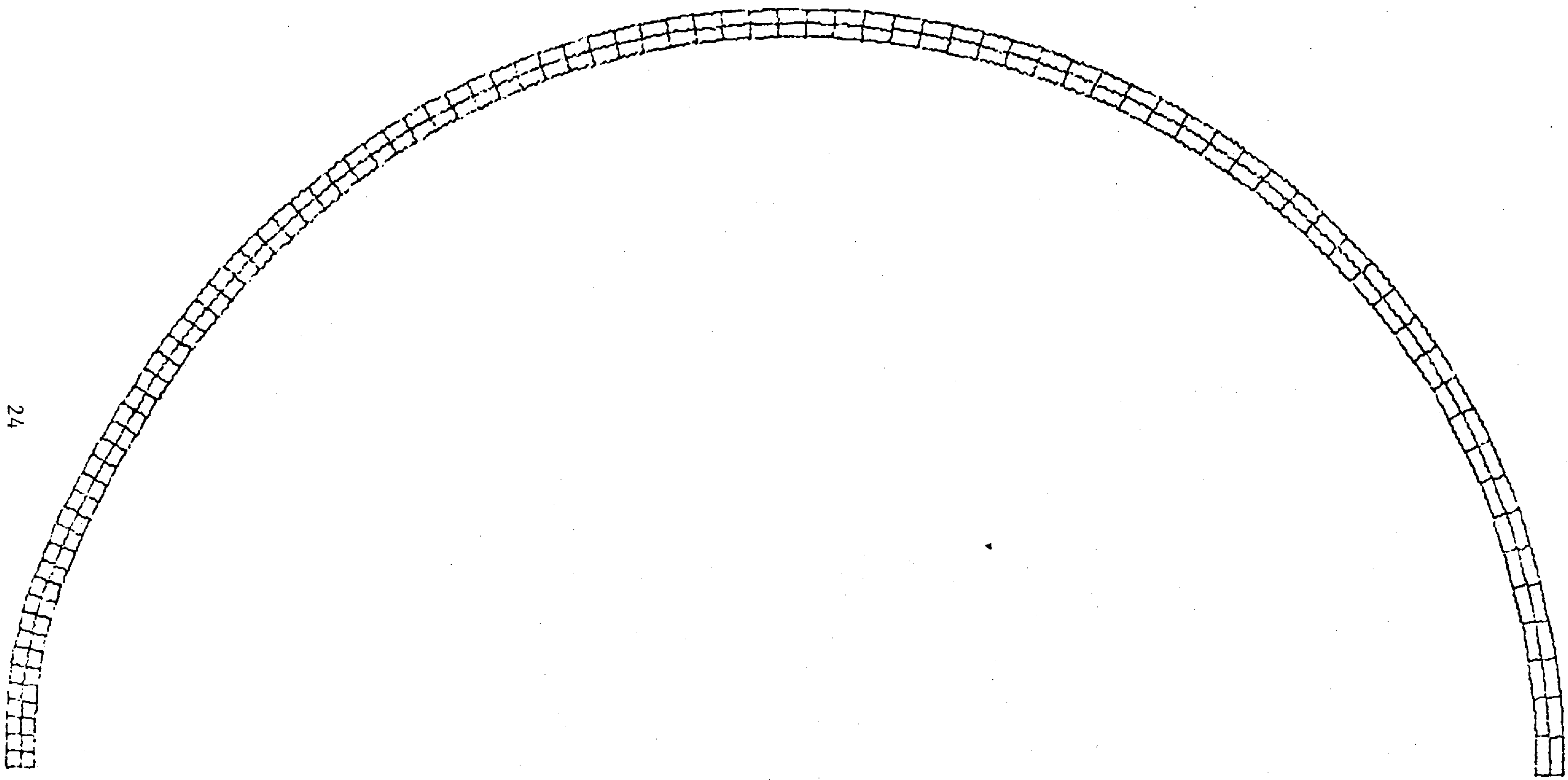

Fig. 16. Grid plot of the shell, time = 551 μsec

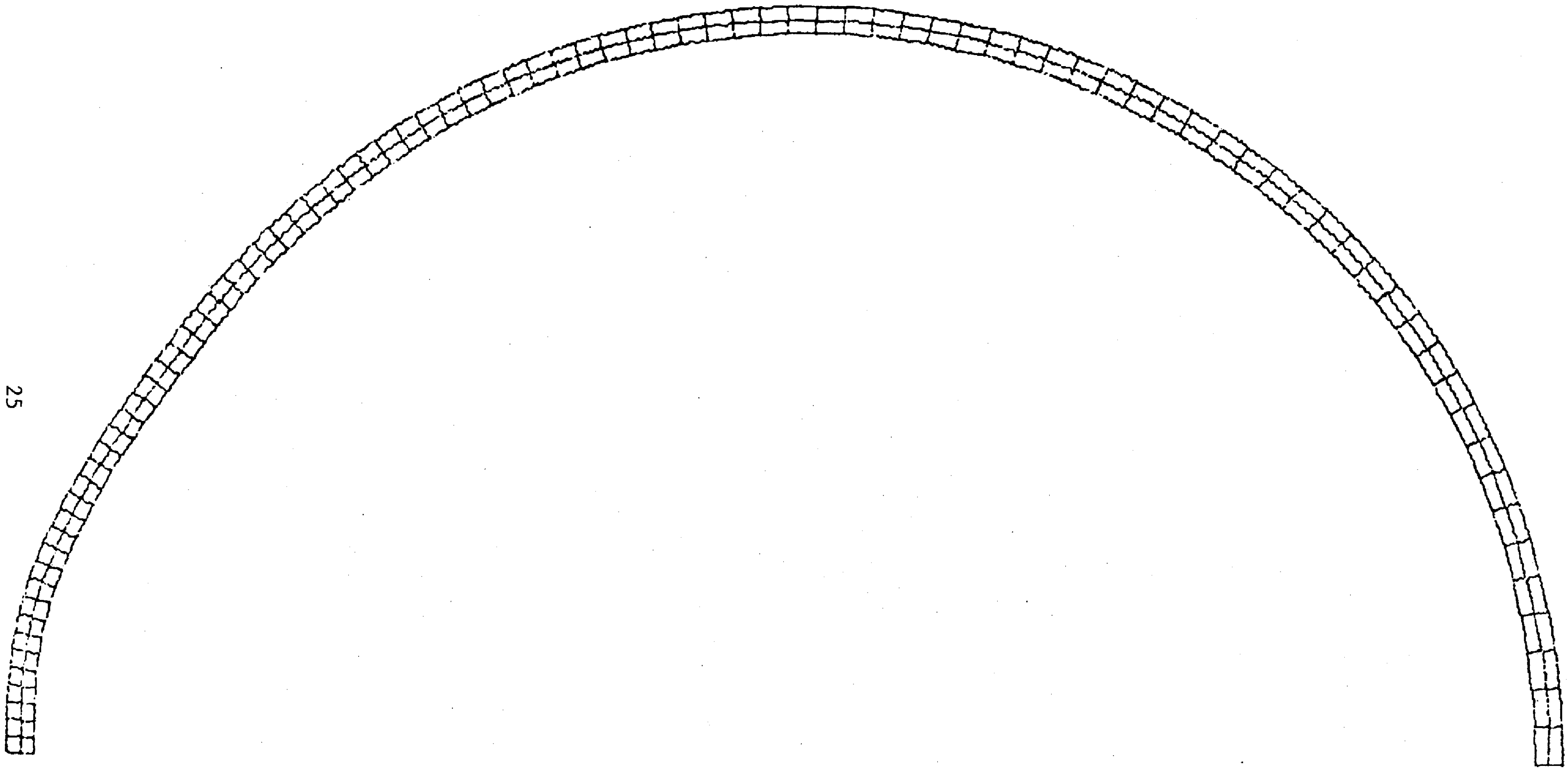

Fig. 17. Grid plot of the shell, time = 754 μsec

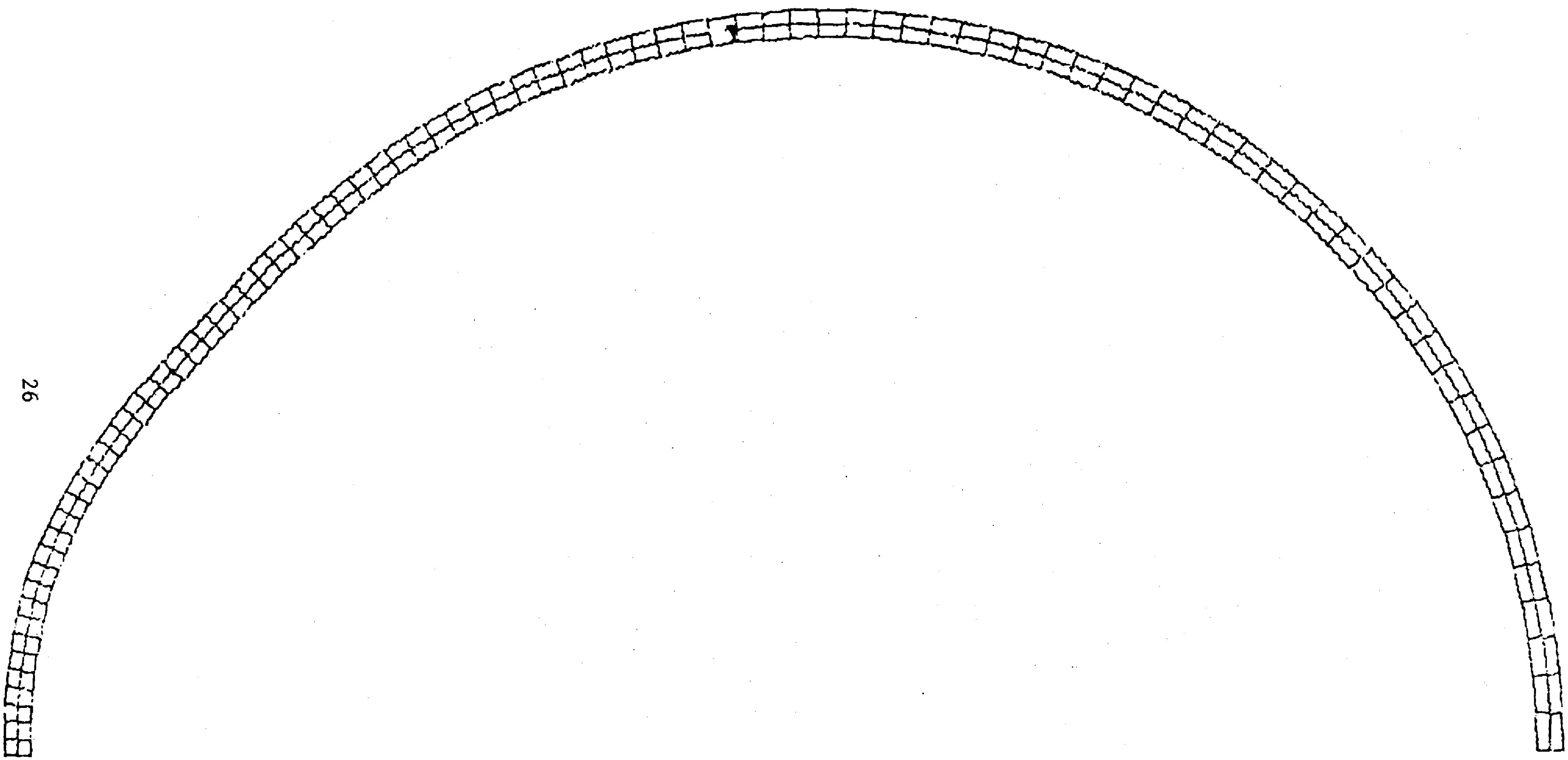

Fig. 18. Grid plot of the shell, time = 1 millisec

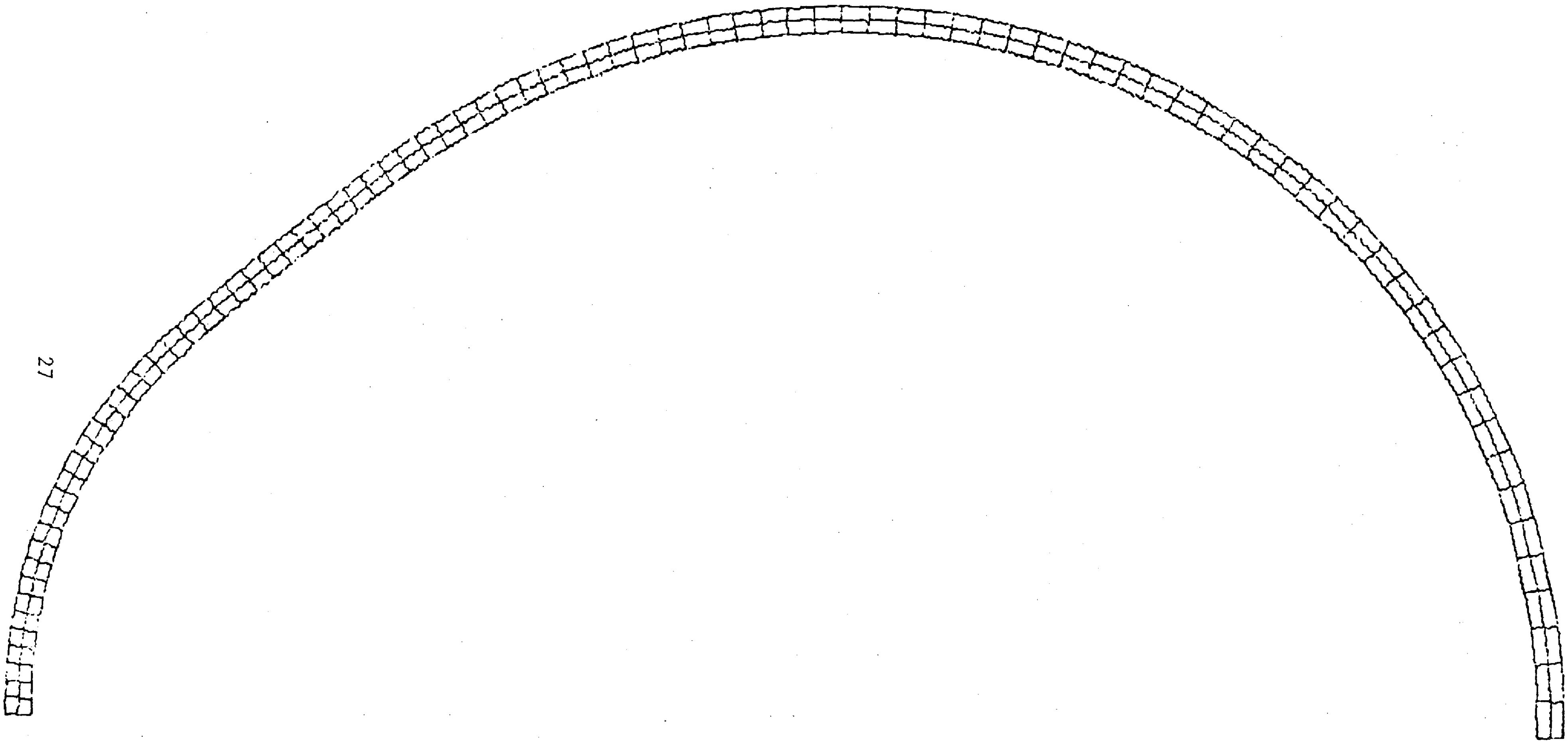

Fig. 19. Grid plot of the shell, time = 1.25 millisec

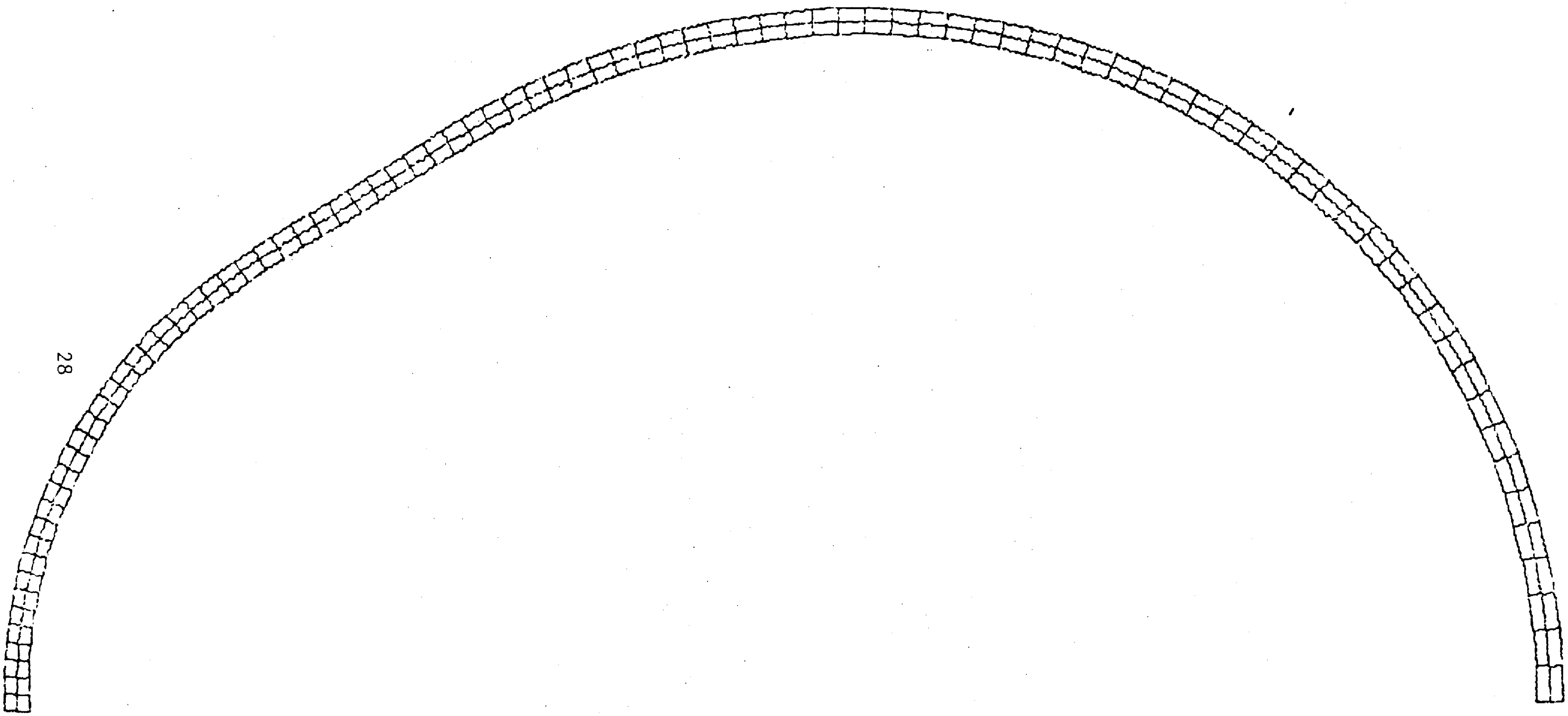

Fig. 20. Grid plot of the shell, time = 1.5 millisec

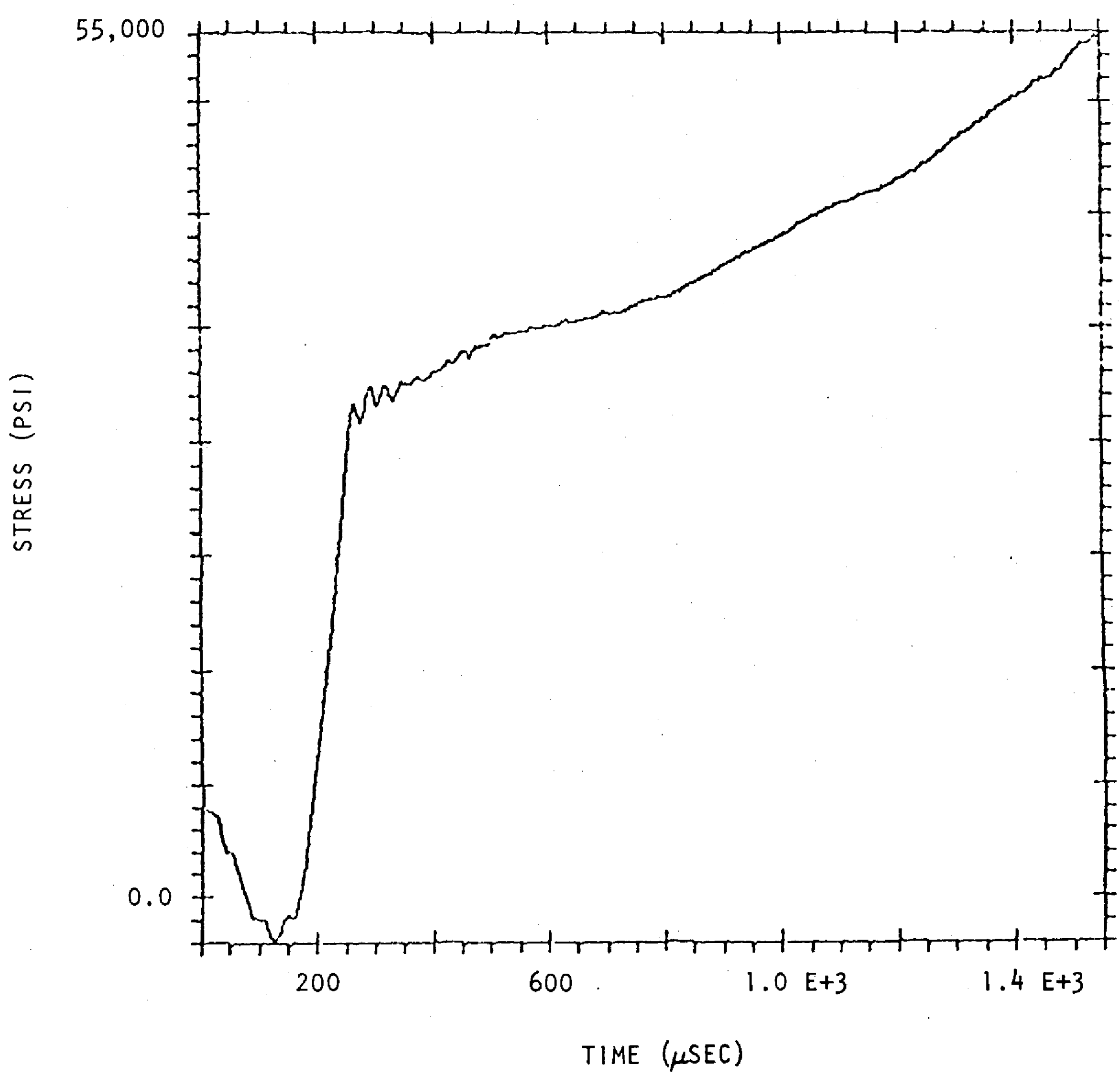

Fig. 21. Circumferential stress-time history in Zone 1

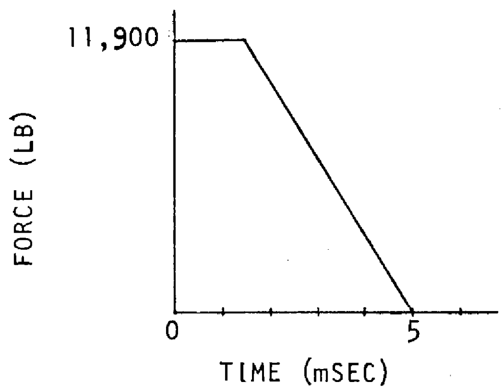

(a) Force applied to Node 22

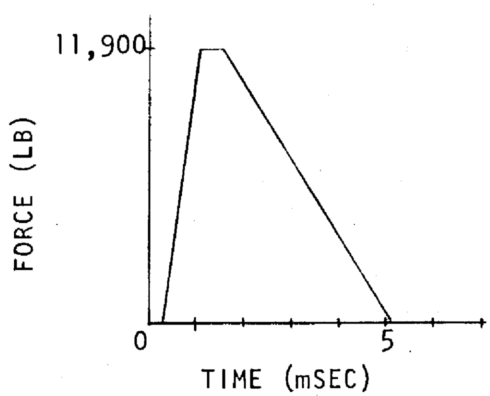

(b) Force applied to Nodes 21 and 23. Time lagged with a rise time of 0.2 milliseconds.

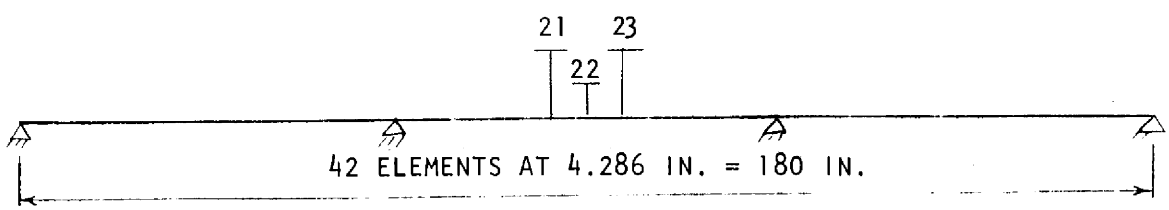

(c) Model of tube

Fig. 22. Model and loading of a tube adjacent to the rupture

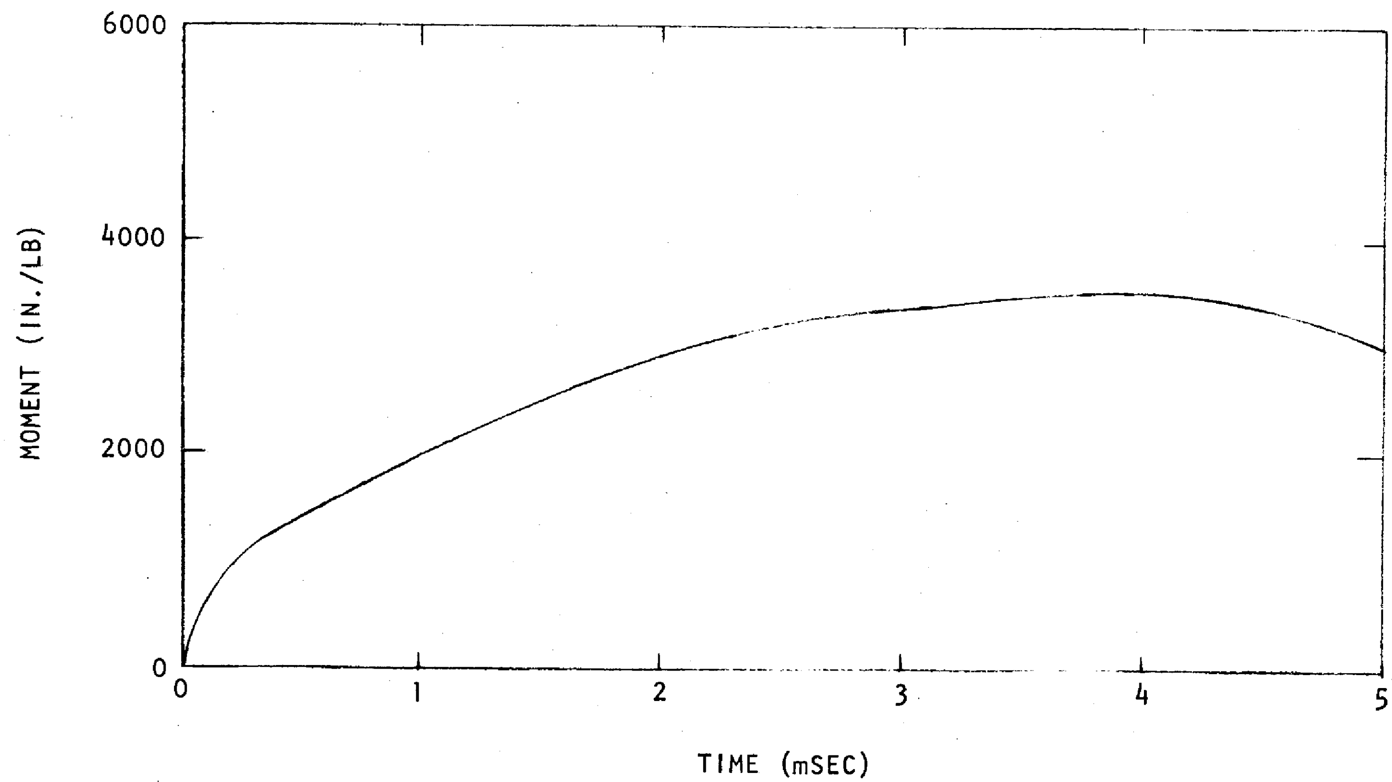

Fig. 23. Maximum moment-time history in the tube

since after a very small amount of deformation, the tube would hit another tube. This would increase its resistance to deformation (at least until the combination of the pressure disturbance and impact loading of the adjacent tubes results in essentially equal velocities). Also, localized stress concentration at the points of impact would occur. Inadequate time was available to consider these facets of the problem.

4. CONCLUSIONS

The analysis of a counterflow heat exchanger under a specified accident condition, i.e., a steam tube rupture, was performed in this investigation. The results of the analysis indicate that the containment vessel will not fail due to a tube failure. The analysis was a conservative one in several regards. The applied load was chosen as an upper bound of the data available on ruptures and, due to the idealization of the shell in two dimensions, was assumed to act along the entire axis of the shell. This latter assumption neglects the increase in strength due to axial stresses in the region of the rupture.

The results of the analysis of a tube adjacent to the rupture are less conclusive. A more sophisticated analysis is required including the interaction of several tubes and perhaps large deformation considerations. However, several observations can be made from the results of the present analysis. The most significant one concerns the amount of deformation sustained by the tube without failure. This is due to the stress-strain relation of Hastelloy N and is an essential factor in this and any subsequent analysis. Similarly, the effect of the molten-salt must be included in the analysis.

Scattering of the disturbance, while not investigated, is believed to be a beneficial effect reducing the intensity of the disturbance. Inadequate time did not permit a detailed consideration of the phenomenon.

This investigation identified the need for greater research and understanding of the mechanisms of failure and related phenomena, e.g., a measure of rupture area and pressure as a function of time. Only after such research is completed will more sophisticated and accurate methods of analysis be available.

REFERENCES

1. Nuclear Applications & Technology 8, 2, 105-219 (February 1970).

2. Robertson, R. C., ed., Conceptual Design Study of a Single-Fluid Molten-Salt Breeder Reactor, ORNL-4541 (June 1971).

3. Cox, J. F., Foster Wheeler Corporation, "Basic Information - Reference Design Molten-Salt Steam Generator," unpublished data.

4. Cox, J. F., Foster Wheeler Corporation, "Properties of Materials Used in the Reference Design Molten-Salt Steam Generator," unpublished data.

5. Cox, J. F., Foster Wheeler Corporation, "Bulk Modulus of Molten-Salt and High Temperature Properties of Hastelloy N," unpublished data.

6. Cox, J. F., Foster Wheeler Corporation, "Final Drawings Steam Generator," unpublished data.

7. Physics International Company, An Introduction to the PISCES System of Continuum Mechanics Codes (October 1971).

8. Physics International Company, PISCES 2DL-General Description and Finite-Difference Equations (1972).

9. Physics International Company, PISCES 2DL - Input Manual (1972).

10. Eiber, R. J., et al., "Investigation of the Initiation and Extent of Ductile Pipe Rupture," Battelle Columbus Laboratories Report BMI-1908 (June 1971).

11. Jones, D. J., (Gulf General Atomic), private communication.

12. Cox, J. F., Foster Wheeler Corporation, "Specification of Rupture Area in a Tube," unpublished data.

REFERENCES (Continued)

13. Ewing, W. M., W. S. Jardetzky and F. Press, Elastic Waves in Layered Media, McGraw-Hill Book Company, New York, 1957.

14. Physics International Company, PISCES 1DL - General Description and Finite-Difference Equations (1971).

15. Physics International Company, PISCES 1DL - Input Manual (1971).

16. Liepmann, H. W. and A. Roshko, Elements of Gasdynamics, John Wiley and Sons, New York, 1962.

17. Biggs, J. M., Introduction to Structural Dynamics, McGraw-Hill Book Co., New York, 1964, pp. 192-195.

18. Daily, J. W., and D. R. F. Harleman, Fluid Dynamics, Addison-Wesley Publishing Co., Reading, Mass., 1966, pp. 376-385.